Com SIS

Computer Science and Information Systems

Volume 20, Number 4, September 2023

Contents

ISSN: 2406-1018 (Online)

Computer Science and Information Systems

Vol 20, No 4, September 2023

Com SIS

Computer Science and Information Systems

Published by ComSIS Consortium

Volume 20, Number 4
September 2023

ComSIS is an international journal published by the ComSIS Consortium

ComSIS Editorial Office:
University of Novi Sad, Faculty of Sciences,
Department of Mathematics and Informatics
Trg Dositeja Obradovića 4, 21000 Novi Sad, Serbia
Phone: +381 21 458 888; **Fax:** +381 21 6350 458
www.comsis.org; Email: comsis@uns.ac.rs

Volume 20, Number 4, 2023
Novi Sad

Computer Science and Information Systems

ISSN: 2406-1018 (Online)

The ComSIS journal is sponsored by:

Ministry of Education, Science and Technological Development of the Republic of Serbia
http://www.mpn.gov.rs/

ComSIS

Computer Science and Information Systems

AIMS AND SCOPE

Computer Science and Information Systems (ComSIS) is an international refereed journal, published in Serbia. The objective of ComSIS is to communicate important research and development results in the areas of computer science, software engineering, and information systems.

We publish original papers of lasting value covering both theoretical foundations of computer science and commercial, industrial, or educational aspects that provide new insights into design and implementation of software and information systems. In addition to wide-scope regular issues, ComSIS also includes special issues covering specific topics in all areas of computer science and information systems.

ComSIS publishes invited and regular papers in English. Papers that pass a strict reviewing procedure are accepted for publishing. ComSIS is published semiannually.

Indexing Information

ComSIS is covered or selected for coverage in the following:

- Science Citation Index (also known as SciSearch) and Journal Citation Reports / Science Edition by Thomson Reuters, with 2022 two-year impact factor 1.4,
- Computer Science Bibliography, University of Trier (DBLP),
- EMBASE (Elsevier),
- Scopus (Elsevier),
- Summon (Serials Solutions),
- EBSCO bibliographic databases,
- IET bibliographic database Inspec,
- FIZ Karlsruhe bibliographic database io-port,
- Index of Information Systems Journals (Deakin University, Australia),
- Directory of Open Access Journals (DOAJ),
- Google Scholar,
- Journal Bibliometric Report of the Center for Evaluation in Education and Science (CEON/CEES) in cooperation with the National Library of Serbia, for the Serbian Ministry of Education and Science,
- Serbian Citation Index (SCIndeks),
- doiSerbia.

Information for Contributors

The Editors will be pleased to receive contributions from all parts of the world. An electronic version (LaTeX), or three hard-copies of the manuscript written in English, intended for publication and prepared as described in "Manuscript Requirements" (which may be downloaded from http://www.comsis.org), along with a cover letter containing the corresponding author's details should be sent to official journal e-mail.

Criteria for Acceptance

Criteria for acceptance will be appropriateness to the field of Journal, as described in the Aims and Scope, taking into account the merit of the content and presentation. The number of pages of submitted articles is limited to 20 (using the appropriate LaTeX template).

Manuscripts will be refereed in the manner customary with scientific journals before being accepted for publication.

Copyright and Use Agreement

Computer Science and Information Systems

Volume 20, Number 4, September 2023

CONTENTS

Special Section: Management of Digital EcoSystems – Recent Trends, and Open Issues

Special Section: Soft/edge computing for imaging and remote sensing applications

Computer Science and Information Systems 20(4): i–ii https://doi.org/10.2298/CSIS230400iI

Editorial

Mirjana Ivanović, Miloš Radovanović, and Vladimir Kurbalija

University of Novi Sad, Faculty of Sciences
Novi Sad, Serbia
{mira,radacha,kurba}@dmi.uns.ac.rs

This fourth and final issue of Computer Science and Information Systems for 2023 consists of 13 regular articles, and two special sections: "Digital Ecosystems – State of the Art and Challenges" (4 articles), and "Soft/Edge Computing for Imaging and Remote Sensing Applications." We thank the guest editors of the special sections, as well as all our authors and reviewers, whose hard work and enthusiasm made possible the publication of the current issue, as well as the our journal in general.

The first regular article, "M^2F^2-RCNN: Multi-Functional Faster RCNN Based on Multi-Scale Feature Fusion for Region Search in Remote Sensing Images," by Shoulin Yin et al. combines a feature extraction network based on ResNet50, a path aggregation network with a convolution block attention module (CBAM), RoIAlign, and an improved non maximum suppression to build an improved RCNN model for regio search in remote sensing images.

In the second regular article, "SRDF_DAG: An Efficient End-to-End RDF Data Management when Graph Exploration Meets Spatial Processing," Houssameddine Yousfi et al. propose new strategies to support spatial operators within a particular TripleStore that relies on graph fragmentation and exploration and guarantees a good compromise between scalability and performance.

Eyad Kannout et al., in "Towards Addressing Item Cold-Start Problem in Collaborative Filtering by Embedding Agglomerative Clustering and FP-Growth into the Recommendation System" introduce a frequent pattern mining framework for recommender systems (FPRS) – a novel approach to address the items' cold-start problem by employing several strategies to combine collaborative and content-based filtering methods with frequent items mining and agglomerative clustering techniques.

The article "Sentence Embedding Approach Using LSTM: Auto-Encoder for Discussion Threads Summarization" by Abdul Wali Khan et al. introduces the LSTM autoencoder as a sentence embedding technique to improve the performance of an automated discussion thread summarizing system (DTS) for online discussion forums.

In "PARSAT: Fuzzy Logic for Adaptive Spatial Ability Training in an Augmented Reality System," Christos Papakostas et al. present a novel adaptive augmented reality training system that teaches the knowledge domain of technical drawing. The novelty of the system is that it proposes using fuzzy sets to represent the students' knowledge levels more accurately in the adaptive augmented reality training system.

"Explaining Deep Residual Networks Predictions with Symplectic Adjoint Method," by Xia Lei et al., proposes a provably faithful explanation for ResNet using a surrogate explainable model, a neural ordinary differential equation network (Neural ODE). First, ResNets are proved to converge to a Neural ODE and the Neural ODE is regarded as a surrogate model to explain the decision-making attribution of the ResNets. Then, the

decision feature and the explanation map of inputs belonging to the target class for Neural ODE are generated via the symplectic adjoint method.

Hai Bang Truong and Van Cuong Tran, in "A Framework for Fake News Detection Based on the Wisdom of Crowds and the Ensemble Learning Model" propose an ensemble classification model to detect fake news based on exploiting the wisdom of crowds. The social interactions and the user's credibility are mined to automatically detect fake news on Twitter without considering news content. The proposed method extracts the features from a Twitter dataset and then a voting ensemble classifier is used to determine whether news is fake or real.

"Deep Learning-Based Sentiment Classification in Amharic Using Multi-Lingual Datasets" authored by Senait Gebremichael Tesfagergish et al. examines various deep learning methods such as CNN, LSTM, FFNN, BiLSTM, and transformers, as well as memory-based methods like cosine similarity, to perform sentiment classification using the word or sentence embedding techniques.

In "Heart Sounds Classification using Adaptive Wavelet Threshold and 1D LDCNN," Jianqiang Hu et al. present an automated heart sound classification method using adaptive wavelet threshold and 1D LDCNN (One-dimensional Lightweight Deep Convolutional Neural Net21 work). The method exploits WT (Wavelet Transform) with an adaptive threshold to de-noise heart sound signals (HSSs), and uses 1D LDCNN to realize automatic feature extraction and classification for de-noised heart sounds.

Abdulaziz Anorboev et al., in "Ensemble of Top3 Prediction of Image Pixel Interval Method Using Deep Learning," propose a multi-step strategy to improve image categorization accuracy with less data. The approach constructs numerous datasets from a single dataset by separating images into pixel intervals based on the type of dataset. Then, the model is trained using both the original and newly constructed datasets.

In their article "Intrusion Detection Model of Internet of Things Based on Deep Learning," Yan Wang et al. introduce a hybrid parallel intrusion detection model based on deep learning called HPIDM, featuring a three-layer parallel neural network structure. The model combines stacked LSTM neural networks with convolutional neural networks (CNNs) and the SK Net self-attentive mechanism, allowing HPIDM to effectively learn temporal and spatial features of traffic data.

"BI-FERH: Blockchain-IoT Based Framework for Securing Smart Hotel" by Quanlong Guan et al. proposes a blockchain-IoT based framework for securing smart hotels (BI-FERH) to enhance the security of hotel information systems. The high performance BI-FERH architecture takes advantage of real-time data transmission capabilities offered by IoT devices. Sensitive data generated by IoT devices is protected in BI-FERH, enhancing tamper-proof capabilities.

Finally, "Digital Remote Work Influencing Public Administration Employees Satisfaction in Public Health Complex Contexts" authored by Maria Sousa et al. studies the question of whether digital remote work in times of COVID-19 influenced the satisfaction of public administration employees. An online survey was conducted in the Portuguese public administration for a sample of 70 individuals, producing various interesting conclusions.

Computer Science and Information Systems 20(4): iii–v https://doi.org/10.2298/CSIS230400iiiI

Guest Editorial: Management of Digital EcoSystems – Recent Trends, and Open Issues

Mirjana Ivanović[1], Richard Chbeir[2], Ernesto Damiani[3], Yannis Manolopoulos[4], and Claudio Silvestri[5]

[1] University of Novi Sad, Serbia, mira@dmi.uns.ac.rs
[2] University of Pau and the Adour Region, Anglet, France, richard.chbeir@univ-pau.fr
[3] Khalifa University, Abu Dhabi, UAE, ernesto.damiani@ku.ac.ae
[4] Open University of Cyprus, Nicosia, Cyprus, manolopo@csd.auth.gr
[5] Claudio Silvestri, Ca' Foscari University of Venice, Italy, silvestri@unive.it

Nowadays modern, technically, and technologically highly progressed society and the rapid development of numerous ICT disciplines bring new smart, intelligent, interconnected socio-technological components and services in everyday life. One of the new concepts and challenging paradigms is digital ecosystem. It represents a group of interconnected information technology resources within a functional unit. Digital ecosystems consist of a wide range of participants and components like suppliers, customers, but also applications, third-party data service providers and all numerous supportive respective technologies. The ecosystem's success is highly dependent on interoperability.

Digital ecosystems are frequently supported by market share leaders and they are quickly influencing changes in various industries, cyber-physical systems, business processes, healthcare and other domains. Some characteristic technical, legal, and business-related difficulties found in digital ecosystems as well as service orchestration, customer engagement, and data management are significant research and practical challenges.

In today's ICT supported world numerous entities are engaged in all forms of interactions mimicking the social world of humans. It influences different producers of data (the Web, Internet of Things, Sensors, etc.), consumers of data (end users, applications, systems, etc.), networking capabilities to ensure data transfer and sharing, data-enabled services, processes (including AI and big data), deployment infrastructures (e.g., cloud computing), processing capabilities, visualization, and reporting facilities. Services underpinning such ecosystems also must satisfy non-functional requirements such as performance, security, and data privacy.

This special section contains revised and extended versions of papers presented at the 14th International Conference on ManagEment of Digital EcoSystems (MEDES 2022), which was held in Venice, Italy during the period October 20th to 21st. The conference aim was to explore the manifold challenges and issues related to web technologies and resource management of Digital Ecosystems, and how current approaches and technologies can be evolved and adapted to this end. Ten papers have been selected for the present section, whereas after standard reviewing procedure of ComSIS Journal four papers have been accepted to be published in this section.

The aim of this special section is to share the experiences in some of recently interesting and challenging trends and issues of digital ecosystems but also to help stakeholders and researchers in academia and industries to gain insights into digital ecosystems potential in practice.

The first paper entitled "DG_Summ: A schema-driven approach for personalized summarizing heterogeneous data graphs" by Amal Beldi et al. contributes to the area of modelling data graphs. The focus is on summarizing data from multiple sources using a schema-driven approach and visualizing the summary graph adjusted to the needs of users. Authors pointed out challenges and importance of identifying trends in the processing of vast amounts of data in different domains and considered graph summarization as an effective framework aiming to facilitate the identification of structure and meaning in modelling data graphs in medical domain. The problem of graph summarization has been recently intensively studied and many approaches for static contexts are proposed to summarize the graph. However, these approaches are computationally prohibitive and do not scale to large graphs in terms of both structure and content. An additional problem is that there is no proposed framework which provide summarization of mixed sources with the goal of creating a dynamic, syntactic, and semantic data summary. The innovative approach proposed by authors is promising and can be useful for researchers in other domains as well.

The second paper entitled "A faceted discovery model architecture for cyber-physical systems in the web of things" by Juan Alberto Llopis et al. presents a discovery model architecture for cyber-physical systems based on the web of things. The approach is based on proactive discovery, recommendation, federation, and query expansion. As a consequence of intensive research efforts in this area, more complex cyber-physical systems are being developed and integrated with web technologies, supporting smart city scenarios with thousands of devices available to be discovered online. For successful realization some capabilities related to locating, registering, and consulting devices must be provided to adapt to the continuous changes in cyber-physical systems. Authors considered an example scenario where the proposed architecture has been implemented with different topologies using edge computing facilities. The obtained results show that the capabilities of the discovery model architecture facilitate the discovery of cyber-physical systems in different smart environments.

The third paper entitled "Systematic exploitation of parallel task execution in business processes" by Konstantinos Varvoutas et al. is focused on business process re-engineering/ optimization as a core element of business process management (BPM). Authors proposed a novel approach which considers resource allocation and model modifications in a combined manner, where an initially suboptimal resource allocation can lead to better overall process executions. The main contributions are: (1) a variant of the representation of processes as Refined Process Structure Trees with a view to enabling novel resource allocation-driven task re-ordering and parallelization, and (2) to introduce a resource allocation paradigm that assigns tasks to resources taking into account the re-sequencing opportunities. The presented results, based on experimental cases, show significant improvements, and decrease in cycle time.

The last paper entitled "Ownership protection system for partial areas on image data using Ethereum blockchain" by Natsuki Fujiwara and Shohei Yokoyama proposes a novel method that utilizes blockchain to protect the ownership of specific regions within image data. They considered various values that are assigned to each region of image based on its importance. Particular regions are individually encrypted protecting their privacy. Nonfungible tokens (NFTs) are used to protect the key image and to manage the ownership of each object on the image data. The ownership NFT and the key NFT are verified to

match by the judgment function. Adopted method allows different values to be assigned to different parts of an image, facilitating the transfer and sharing of ownership.

We gratefully acknowledge all the hard work and enthusiasm of authors, without whom this special section would not have been possible. In addition, we appreciate for the careful study of the selected papers and the constructive comments made by the:

– Djamal Benslimane, Claude Bernard Lyon 1 University, France
– Richard Chbeir, University of Pau and the Adour Region, Anglet, France
– Marco Comuzzi, Ulsan National Institute of Science and Technology, Ulsan, Republic of Korea
– Gayo Diallo, University of Bordeaux, Bordeaux Cedex, France
– Allel Hadjali, Computer Science at Engineer School ENSMA, Poitiers, France.
– Masaharu Hirota, Okayama University of Science, Okayama, Japan
– Hiroshi Ishikawa, Waseda University, Tokyo, Japan
– Jana Koehler, University of Applied Sciences and Arts, Lucerne, Switzerland
– Anastas Misev, Ss. Cyril and Methodius University, Skopje, North Macedonia
– Srdjan Skrbic, University of Novi Sad, Novi Sad, Serbia
– Michael Vassilakopoulos, University of Thessaly, Volos, Greece

Finally, we hope that readers will enjoy the content of this special section, and that it will inspire them for high quality research in this modern and attractive area.

Computer Science and Information Systems 20(4): vii–x https://doi.org/10.2298/CSIS230400viiL

Guest Editorial: Soft/edge computing for imaging and remote sensing applications

Hang Li[1] and Mirjana Ivanovic[2]

[1] Software College, Shenyang Normal University, 253 Huanghe Bei Dajie, Huanggu District, Liaoning Province, 110034 China, lihang@synu.edu.cn
[2] University of Novi Sad, Faculty of Sciences, Serbia, mira@dmi.uns.ac.rs

Recently, soft/edge computing paradigm has been developed and it is evolving as a new branch of computing and communication technologies. This new approach integrates the existing computing environment with the digital technologies by creating a new revolution in the emerging communication technologies like Internet of Things (IoT) and cyber–physical systems. Moreover, soft/edge based communication integrates the artificial intelligence technologies to intelligently investigate, collect, process and store the huge amount of data generated by IoT applications. Edge/soft computing plays a significant role to enhance the potential of data analytics and decision-making process with the reduced amount of delay.

Remote sensing and imaging, as one of the sources for big data, are generating earth-observation data and analysis results daily from the platforms of satellites, manned/unmanned aircrafts, and ground-based structures. These different kinds of remote-sensing data include SAR - synthetic aperture radar, multi-spectral optical data and hyper-spectral optical data. Those data sets comprise different spectral bandwidths (dimensionality), spatial resolutions, and radiometric resolutions. The increasing growth of remote sensing data and geoscience research pushes earth sciences strongly and poses great challenges to data science for remote sensing big data, including collection, storage, management, analysis and interpretation.

This Special Issue is expected to bring together experts from different research areas to discover and realize the values of soft/edge computing in various remote sensing areas. This Special Issue is intended to present the current theoretical and methodological research and state-of-the-art techniques and application of imaging and remote sensing big data in the area of soft/edge computing. The aim of this special Issue is to share the experiences in processing imaging and remote sensing with large volumes and variant modes, and intelligent interpretation with advance soft/edge computing algorithms. We expect that these research results will provide a necessary effort towards the incorporation of this soft/edge computing technology into the imaging and remote sensing field and also to help stakeholders and researchers in academia, governments, and industries to gain insights into the potential of using soft/edge computing techniques and concepts in imaging and remote-sensing applications.

This special issue received 36 submissions where the corresponding authors were majorly counted by the deadline for manuscript submission with an open call-for-paper period of 5 months. All these submissions are considered significant in the field, but however, only one-third of them passed the pre-screening procedure by guest editors. The qualified papers then went through double-blinded peer review based on a strict and rigorous review policy. After a totally three-round reviews, 8 papers were accepted for publication. A quick overview to the papers in this issue can be revealed below, and we expect

the content may draw attentions from public readers, and furthermore, prompt the society development.

The first paper entitled "Generative Adversarial Network Based on LSTM and Convolutional Block Attention Module for Industrial Smoke Image Recognition" by Dahai Li et al. In this paper, a low-cost data enhancement method is used to effectively reduce the difference in the pixel field of the image. The smoke image is input into the LSTM in generator and encoded as a hidden layer vector. This hidden layer vector is then entered into the discriminator. Meanwhile, a convolutional block attention module is integrated into the discriminator to improve the feature self-extraction ability of the discriminator model, so as to improve the performance of the whole smoke image recognition network. Experiments are carried out on real diversified industrial smoke scene data, and the results show that the proposed method achieves better image classification and recognition effect. In particular, the F scores are all above 89%, which is the best among all the results.

The second paper entitled "A Novel Feature Fusion Model Based on Non-subsampled Shear-wave Transform for Retinal Blood Vessel Segmentation" by Fan Zhang et al. proposes a new feature fusion model based on non-subsampled shear-wave transform for retinal blood vessel segmentation. The contrast between blood vessels and background is enhanced by pre-processing. The vascular contour features and detailed features are extracted under the multi-scale framework, and then the image is postprocessed. The fundus images are decomposed into low frequency sub-band and high frequency sub-band by non-subsampled shear-wave transform. The two feature images are fused by regional definition weighting and guided filtering respectively, and the vascular detection image is obtained by calculating the maximum value of the corresponding pixels at each scale. Finally, the Otsu method is used for segmentation. Results: The experimental results on DRIVE data set show that the proposed method can accurately segment the vascular contour while retaining a large number of small vascular branches with high accuracy. The main conclusion is that the proposed method has a high accuracy and can perform vascular segmentation well on the premise of ensuring sensitivity.

The third paper entitled "LUN-BiSeNetV2: A Lightweight Unstructured Network Based on BiSeNetV2 for Road Scene Segmentation" by Yachao Zhang et al. proposes a road scene segmentation method based on a lightweight unstructured network based on BiSeNetV2. The network contains backbone segmentation network and BiSeNetV2 network. The Mobilenetv2 network is used in the backbone network to replace the Xception feature extraction network in the decoder. In addition, grouping convolution is used to replace common convolution in Mobilenetv2 network. And it selects the batch specification layer to reduce the number of parameters, without affecting the accuracy and improving the efficiency of segmentation.

The fourth paper entitled "A Novel Multilevel Stacked SqueezeNet Model for Handwritten Chinese Character Recognition" by Yuankun Du et al. proposes a novel multilevel stacked SqueezeNet model for handwritten Chinese characters recognition.

"Deep Adversarial Neural Network Model Based on Information Fusion for Music Sentiment Analysis" by Wenwen Chen et al. proposes a new model that combines deep adversarial neural network model based on information fusion for music sentiment analysis. Firstly, the information of music text sequence is captured by the bidirectional short and long time memory network. Then the sequence information is updated according to the tree structure of dependency syntactic tree. Further, the relative distance and syntac-

tic distance position information are embedded into the music text sequence. Thirdly, the adversarial training is used to expand the alignment boundary of the field distribution and effectively alleviate the problem of fuzzy features leading to misclassification.

The sixth paper entitled "A Novel Single Shot-multibox Detector Based on Multiple Gaussian Mixture Model for Urban Fire Smoke Detection" by Hao Han et al. proposes a novel single shot-multibox detector based on a multiple Gaussian mixture model for urban fire smoke detection. Multiple Gaussian models are used to represent the features of each pixel in the moving object image. The Gaussian mixture model is updated based on the principle that each pixel in the image is regarded as a background point if it matches the Gaussian mixture model. Otherwise, if it matches the Gaussian mixture model, it is regarded as the foreground point. By updating the foreground model and calculating the short-term stability index, the detection effect of moving objects is improved. By determining the relationship between Gaussian distribution and pixel, a new parameter is set to construct the background model to eliminate the influence caused by illumination mutation. Aiming at the problems of smoke detection efficiency and network over-fitting, authors presented an InceptionV3-feature fusion single shot-multibox detector.

The seventh paper "Anti-aliasing Filter Based on Whale Parameter Optimization Method for Feature Extraction and Recognition of Dance Motor Imagery EEG" by Tianliang Huang et al. proposes a new model for the feature extraction and recognition of dance motor imagery EEG, which makes full use of the advantage of anti-aliasing filter based on whale parameter optimization method. The anti-aliasing filter is used for preprocessing, and the filtered signal is extracted by two-dimensional empirical wavelet transform. The extracted feature is input to the robust support matrix machine to complete pattern recognition. In pattern recognition process, an improved whale algorithm is used to dynamically adjust the optimal parameters of individual subjects. Experiments are carried out on two public data sets to verify that anti-aliasing filter-based preprocessing can improve signal feature discrimination. The improved whale algorithm can find the optimal parameters of robust support matrix machine classification for individuals. This presented method can improve the recognition rate of dance motion image.

The last paper is "Heterogenous-view Occluded Expression Data Recognition Based on Cycle-Consistent Adversarial Network and K-SVD Dictionary Learning Under Intelligent Cooperative Robot Environment" by Yu Jiang et al. and it proposes a cycle-consistent adversarial network and K-SVD dictionary learning method for occluded expression recognition in education management under robot environment. Firstly, the new method uses the cyclic-consistent generation adversarial network as the skeleton model, which can generate the un-occluded expression image without the need of paired data sets. Meanwhile, in order to improve the discriminant ability and image generation ability of the network, a multi-scale discriminator is used to construct the discriminant network. Then, the least squares and cyclic sensing loss are used to strengthen the constraints on the network model and improve the image quality. By subtracting the error matrix from the test sample, a clear image of the expression classification stage can be recovered. The clear image samples are decomposed into identity features and expression features by using the collaborative representation of two dictionaries.

The first guest editor would like to thank Prof. Mirjana Ivanović, the editor-in chief of ComSIS, for her support during the preparation of this special section in the journal.

Finally, we gratefully acknowledge all the hard work and enthusiasm of authors and reviewers, without whom the special section would not have been possible.

Computer Science and Information Systems 20(4):1289–1310 https://doi.org/10.2298/CSIS230315054Y

M^2F^2-RCNN: Multi-functional Faster RCNN Based on Multi-scale Feature Fusion for Region Search in Remote Sensing Images

Shoulin Yin[1], Liguo Wang[2], Qunming Wang[3], Mirjana Ivanović[4], and Jinghui Yang[5]

[1] College of Information and Communication Engineering, Harbin Engineering University
Harbin, 150001 China
yslin@hit.edu.cn
[2] College of Information and Communications Engineering, Dalian Minzu University
Dalian, 116000 China
wangliguo@hrbeu.edu.cn
[3] College of Surveying and Geo-Informatics, Tongji University
Shanghai, 200092 China
111wqm@163.com
[4] Faculty of Sciences, University of Novi Sad
21000 Novi Sad, Serbia
mira@dmi.uns.ac.rs
[5] School of Information Engineering, China University of Geosciences
Beijing, 100083, China
yang06081102@163.com

Abstract. In order to realize fast and accurate search of sensitive regions in remote sensing images, we propose a multi-functional faster RCNN based on multi-scale feature fusion model for region search. The feature extraction network is based on ResNet50 and the dilated residual blocks are utilized for multi-layer and multi-scale feature fusion. We add a path aggregation network with a convolution block attention module (CBAM) attention mechanism in the backbone network to improve the efficiency of feature extraction. Then, the extracted feature map is processed, and RoIAlign is used to improve the pooling operation of regions of interest and it can improve the calculation speed. In the classification stage, an improved non-maximum suppression is used to improve the classification accuracy of the sensitive region. Finally, we conduct cross validation experiments on Google Earth dataset and the DOTA dataset. Meanwhile, the comparison experiments with the state-of-the-art methods also prove the high efficiency of the proposed method in region search ability.

Keywords: remote sensing images, region search, multi-functional faster RCNN, multi-scale feature fusion, convolution block attention module.

1. Introduction

Region search is widely used in automatic driving, video, image index and remote sensing etc. With the rapid development of deep learning, regional convolutional neural network (RCNN)-based algorithms [1-3] have transformed the traditional manual feature extraction into feature learning, which plays an important role in the field of remote sensing

images processing. In order to quickly obtain useful information from massive remote sensing images, region search has a high application value. Rapid detection of sensitive areas through remote sensing images is of great significance for improving military operational efficiency, civil route planning, safety search and rescue, etc [4,5].

RCNN algorithm adopts selective search(SS) [6] to extract 1000 2000 suggestion bounding boxes from remote sensing images. It adds 16 pixels around each candidate box as the border of the average pixel value. Then it subtracts the average pixel value of the suggestion box from all candidate box pixels, and inputs the results into AlexNet network for feature extraction. Then support vector machine (SVM) classification is used to determine the category of candidate boxes. And the non-maximum suppression (NMS) algorithm is adopted to reduce the number of redundant candidate boxes [7]. Finally, the remaining candidate boxes are modified through the detection box regression model to correct the final position.

The training stage of RCNN is limited to the selection of candidate boxes. The existing problems are summarized as follows:

1. When RCNN reads the image information, it needs to fix the image size, but cutting the image will lead to the loss of the image information.
2. CNN needs to calculate the candidate boxes in each region, and repeated feature extraction will bring huge computational waste.

Compared with RCNN algorithm, Fast RCNN algorithm only extracts the features of each image once, and shares the extracted features in the calculation process to improve the speed of training and testing. In view of the problem that fast RCNN cannot achieve real-time detection and end-to-end training test, Ren et al. [8] proposed faster RCNN algorithm, using regional proposal network (RPN) to replace selective search (SS) algorithm, which could effectively extract the candidate regions in the original image. Different from the aforementioned detection algorithms based on proposal regions, Redmon et al. [9] proposed a YOLO (You Only Look Once) detection algorithm based on regression. The framework abandoned the preset candidate box strategy, regarded the detection task as a regression problem, and directly carried out border regression and category determination in the output layer, which could meet the real-time detection requirements, but the detection accuracy was low. In order to give equal consideration to detection speed and accuracy, Liu et al. [10] proposed the Single Shot MultiBox Detector (SSD) framework, integrating the idea of preset candidate boxes and YOLO. It conducted multi-layer detection through feature pyramid simultaneously to improve detection accuracy. However, the detection effect of small objects was not satisfactory.

The imaging characteristics of remote sensing images are different from those of natural scenes commonly captured by digital cameras. Remote sensing images are mainly shot at high altitude, covering a wide range of ground objects, complex image background, dense target distribution and small size. And the image quality of remote sensing is not as good as that of digital camera [11,12]. If the existing deep learning detection frameworks are directly applied to remote sensing image for region detection, the detection accuracy cannot be the same as that of natural scene image. At present, a large number of scholars have improved the deep learning detection frameworks and applied them to the detection of sensitive areas in remote sensing images. Based on the RCNN model and the cascade AdaBoost algorithm, Tang et al. [13] proposed a coarse-to-fine object region recognition

algorithm, which reduced the amount of computation and improved the detection accuracy of high-resolution remote sensing images. Based on faster-RCNN, Wu et al. [14] proposed a target detection algorithm based on feature fusion combined with soft judgment, which improved the detection accuracy of small target areas. Li et al. [15] overcame the defect of losing small target information in deep feature by integrating shallow feature with deep feature after up-sampling, and improved the fast detection accuracy of target region in aerial remote sensing images. Cui et al. [16] optimized RPN according to the aspect ratio characteristics of the target region. Meanwhile, the online difficult sample mining method was adopted to balance positive and negative samples, which improved the performance of the model algorithm. Aiming at the uncertainty of the direction of the target region in remote sensing images, Pazhani et al. [17] integrated the rotating region network into the Fast RCNN, introduced the convolution layer in front of the fully connected layer of the network, reduced the dimension of the feature map. It improved the performance of the classifier, and achieved better detection results. Based on the YOLO-V2 detection framework, Anuar et al. [18] introduced the transfer learning strategy to improve the detection accuracy of high-resolution remote sensing image regions in small samples, but the detection accuracy of small targets was not high. Based on the SSD detection framework, ResNet50 was used to replace the front-facing network VGG16, and the target detection was carried out on the aerial data set [19]. The detection effect was significantly improved, but the error was also relatively large. Aiming at the problem of low detection accuracy of small targets in complex scenes, Chen et al. [20] proposed MultDet, a lightweight multi-scale feature fusion detection framework, which improved the characterization ability of small scale aircraft targets and realized high-precision detection of aircraft targets.

Previous researches on remote sensing image target region extraction mainly rely on the basic features of the image, such as spectrum, shape, contour, texture, color, shadow, etc. For example, Zheng et al.[21] proposed an object-based Markov Random field (OMRF) model for building extraction. The model constructed a weighted region adjacency map based on region size and edge feature information. Then it used OMRF with a region penalty term to achieve accurate building area extraction. Mag et al. [22] proposed a region extraction method based on saliency analysis, which extracted multi-scale texture and edge features of remote sensing images by Fourier transform and adaptive wavelet. Wang et al. [23] used Extended multi-resolution segmentation (EMRS) and back-propagation (BP) network to extract building areas. EMRS was used to represent multi-scale spatial resolution features, and BP network was used to classify pixels with different building areas. Ni et al. [24] proposed a local competitive super-pixel segmentation method, which could effectively integrate spatial resolution and multi-scale features of remote sensing images, and completed accurate extraction of building areas. Zhu et al. [25] proposed a building extraction method based on mixed sparse representation, which divided remote sensing images into subgraph combinations with different components, then used sparse representation to express different subgraph features. Finally, support vector machine was adopted to complete the extraction of building areas. The target region extraction methods based on the above basic features have achieved a certain effect. However, due to the lack of extraction of deep semantic features and global spatial features in remote sensing images, the segmentation and extraction results still have some problems, such as boundary information loss and incomplete shape structure.

In summary, this paper collects remote sensing image data sets from Google Earth, DOTA data sources, and then establishes a typical region target data sets of remote sensing images by manual annotation. Therefore, we propose a multi-functional faster RCNN based on multi-scale feature fusion model for region search. The stages of region search method are as follows. Firstly, the feature extraction network is based on ResNet50 and the dilated residual blocks are utilized for multi-layer and multi-scale feature fusion. Then, a path aggregation network with a convolution block attention module (CBAM) attention mechanism is added in the backbone network to improve the efficiency of feature extraction. Thirdly, the extracted feature map is processed, and RoIAlign is used to improve the pooling operation of regions of interest and it can improve the calculation speed. Finally, in the classification stage, an improved non-maximum suppression is used to improve the classification accuracy of the sensitive region. Meanwhile, abundant experiments also show the effectiveness of the proposed method.

The structure of this paper is as follows. In section 2, the related works are introduced including Faster-RCNN, RPN. Section 3 detailed states the proposed method for region search in remote sensing images. Rich experiments are shown in section 4. A conclusion is shown in section 5.

2. Related Works

In recent years, deep learning [26,27] has made new progress, and convolutional neural network (CNN) has been applied to target region detection. Since the appearance of the image classification competition based on the large image database ImageNet, various deep learning detection algorithms have been proposed successively, which are mainly divided into One-stage and Two-stage. Herein, YOLO-v3 [28] is a representative algorithm in One-stage. The representative algorithms in the two-stage method are Faster RCNN and other algorithms. RCNN-based algorithms have been developed from Faster RCNN to Mask RCNN. By using RoIAlign, a mask branch is added to achieve the detection and segmentation at the instance level. One-stage algorithm is superior to Two-stage algorithm in detection speed, but it is lower that two-stage algorithm in terms of accuracy. However, these mainstream target detection algorithms aim at the image of the natural scene, without considering the directivity of the target and other features.

Deep learning has achieved great success in detecting the target region in natural scenes. Therefore, a large number of researches on remote sensing image target region detection [29,30] based on deep learning continue to emerge. An important characteristic of the target region to be detected in remote sensing images is the uncertainty of its direction and shape. In addition, most target regions in remote sensing images are densely distributed, so the horizontal box method may also affect the results of non-maximum suppression (NMS) after detection, resulting in poor detection effect. In reference [31], a text detection algorithm based on the rotating region was proposed. The algorithm firstly used the region proposal network to generate horizontal candidate boxes, and then used the features after multi-scale pooling to predict slanted text boxes. In reference [32], Region Proposal Network (RPN) in Faster R-CNN network was improved and it added rotation information, so that the RPN network could directly generate an angled prediction box for multi-directional text detection.

2.1. Faster-RCNN

Faster RCNN is a region-based convolutional neural network framework, which mainly consists of four parts: feature extraction layer, RPN layer, ROI Pooling layer and detection subnetwork, as shown in Figure 1. Feature extraction layer extracts features of input images through convolutional neural networks. The candidate region generation network carries out convolution operation on the obtained image feature map to generate the candidate frame that may contain the object. The region of interest (ROI) pooling layer [33] converts the region feature maps corresponding to different candidate boxes into feature maps with the same size. The detection network identifies the target in the ROI and corrects the position of the candidate box to get the final detection result.

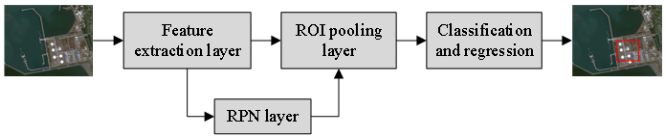

Fig. 1. Structure of Faster RCNN

2.2. Region Proposal Network (RPN)

RPN is a full convolutional network, which reduces the number of candidate boxes in the detection process and improves the detection efficiency of Faster RCNN. It can be seen from Figure 2 that RPN network mainly has two branches: one is the classification layer, which is used to classify positive and negative samples, and the other is the regression layer, which is used to regress the candidate box position of positive samples. The RPN network implementation process is as follows. A 3×3 sliding window is used to slide the feature graph (suppose the size is $N \times 60 \times 60$), and each pixel of the feature graph is traversed to generate a low-dimensional feature graph ($256 \times 60 \times 60$). In addition, k predefined candidate boxes are generated at each pixel position on the feature graph. Then two 1×1 convolution operations are performed on the low-dimensional feature graphs. $2k$ probability values and $4k$ candidate box offsets are obtained at each pixel. Finally, combined with the pre-defined candidate boxes, post-processing operations such as cross boundary clipping, small candidate box removal and Non-Maximum Suppression (NMS) are carried out to obtain the ROI candidate boxes.

The training of RPN network adopts multi-task loss function, as shown in Equation (1):

$$L(p_i, t_i) = \frac{1}{N_{cls}} L_{cls}(p_i, p_i^*) + \frac{\lambda}{N_{reg}} \sum_i p_i^* L_{reg}(t_i, t_i^*). \tag{1}$$

Where i is the index value of anchor. p_i and t_i are the $i - th$ anchor containing the probability value of the target and four coordinate values corresponding to anchor respectively. N_{cls} and N_{reg} are standardized constants. λ is the equilibrium coefficient.

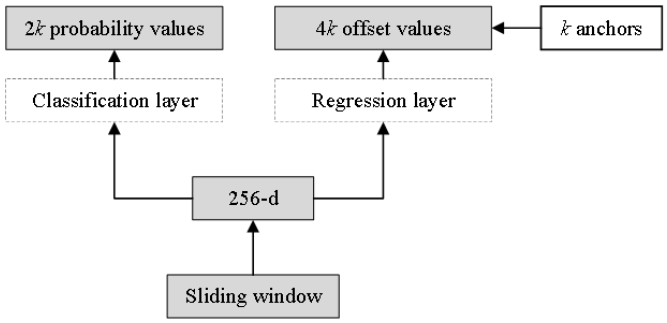

Fig. 2. RPN structure

When anchor is a positive sample, $p_i^* = 1$, otherwise $p_i^* = 0$. t_i^* is the coordinate value of the real region corresponding to the positive sample. L_{cls} and L_{reg} are the classification loss function and the regression loss function respectively. The expressions are as follows:

$$L_{cls}(p_i, p_i^*) = -log[p_i p_i^* + (1 - p_i)(1 - p_i^*)]. \tag{2}$$

$$L_{reg}(t_i, t_i^*) = R(t_i - t_i^*). \tag{3}$$

Where R is Smooth L1 function, reflecting the robustness of the function, it is defined as follows.

$$R(x) = \begin{cases} 0.5x^2 & |x| \leq 1 \\ |x| - 0.5 & |x| > 1 \end{cases} \tag{4}$$

3. Proposed M^{2}F^2-RCNN for Region Search

Considering the detection application requirements of remote sensing satellite image, this paper adopts the Faster RCNN framework with higher detection accuracy as the basic prototype. The proposed M^{2}F^2-RCNN region search model in this paper is shown in Figure 3.

Our contributions are mainly in the following three aspects:

1. In the basic network stage, we construct a feature pyramid network to perform multi-scale feature fusion. We added path aggregation network with Convolution Block Attention Module (CBAM) to improve feature extraction efficiency.
2. RoIalign is used to replace RoI pooling, and a convolution layer is added into the classification network to improve the classification efficiency.
3. A new non-maximum suppression algorithm is improved to the overlap problem of large amount of similar candidate boxes.

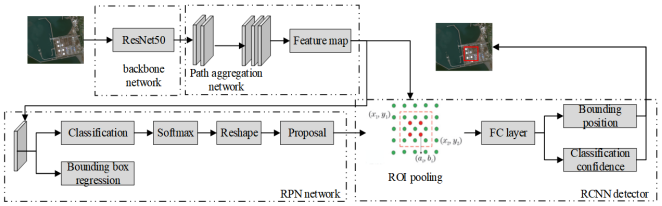

Fig. 3. M^{2}F^2-RCNN structure

3.1. Multi-scale Feature Fusion

Compared with the original feature extraction layer VGG, ResNet50 has a deeper network layer and can extract deeper and more abstract features [34]. Moreover, the residual structure of ResNet50 is conducive to solving the problems of gradient dispersion and gradient explosion when the network performance is not significantly improved. Therefore, ResNet50 is selected as the basic feature extraction network in this paper. Table 1 shows the Resnet50 network structure. In Table 1, two multiplied numbers indicate the size of the convolution kernel. The next number is the number of convolution kernels. In the case of conv1, 7×7 means the size of the convolution kernel and 64 means the number of convolution kernel. The matrix represents the residual block, and the number in the matrix represents the composition of the residual block. Taking conv3 as an example, conv3 is composed of 4 residual blocks, each of which is composed of 128 convolution kernels with 1×1 size, 128 convolution kernels with 3×3 size, and 512 convolution kernels with 1×1 size. The step size in convolution kernel with 3×3 size in the first residual block is 2, and the rest step size is 1.

Table 1. Structure of ResNet50

Layer	Structure
Convolutional layer (conv1)	7×7, 64, step size=2
Pooling layer	3×3, step size=1
Convolutional layer (conv2)	$\begin{matrix} 1 \times 1 & 64 \\ 3 \times 3 & 64 \\ 1 \times 1 & 256 \end{matrix} \times 3$, step size=2
Convolutional layer (conv3)	$\begin{matrix} 1 \times 1 & 128 \\ 3 \times 3 & 128 \\ 1 \times 1 & 512 \end{matrix} \times 4$, step size=2
Convolutional layer (conv4)	$\begin{matrix} 1 \times 1 & 256 \\ 3 \times 3 & 256 \\ 1 \times 1 & 1024 \end{matrix} \times 6$, step size=2
Convolutional layer (conv5)	$\begin{matrix} 1 \times 1 & 512 \\ 3 \times 3 & 512 \\ 1 \times 1 & 2048 \end{matrix} \times 3$, step size=2

However, if it directly uses Convl-5 as the feature extraction layer in the Faster RCNN structure, it cannot significantly improve the model detection accuracy. In order to solve

the problem that the feature extraction layer is deepened and the detection accuracy is not significantly improved, It considered conv5 and the full connection layer as the final detection subnetwork based on the structure of Networks on Convolutional Feature Maps (NoCs). The specific structure is shown in Figure 4. Moving conv5 to the detection network can improve the classifier performance and thus improve the overall detection accuracy.

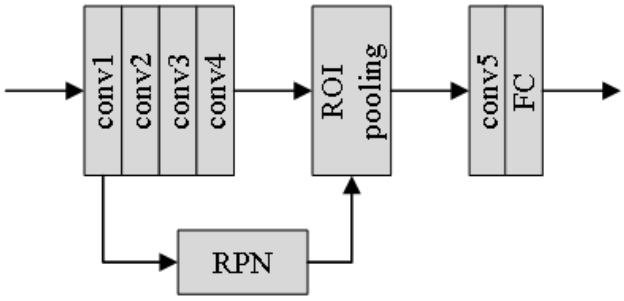

Fig. 4. ResNet50 with Faster RCNN

Figure 5(a) is the original residual block in Resnet50. The dilated residual blocks in FIG. 5(b) and 5(c) are the structures formed by introducing the dilated convolution with expansion rate 4. With the same spatial resolution, the dilated residuals can enlarge the receptive field of the deep network, which is conducive to extracting the deep semantic information of the target. In the experiment, a feature fusion model is designed by using the dilated residual block. The specific structure is shown in Figure 5(d).

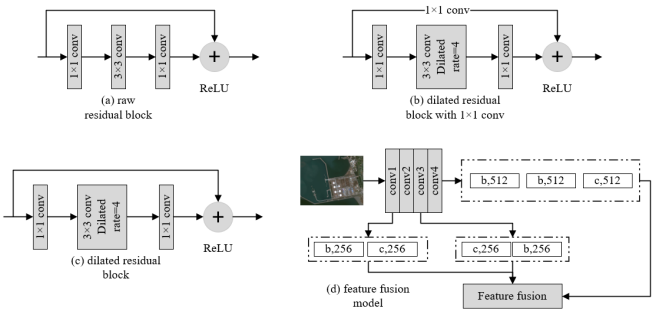

Fig. 5. Feature fusion process

Firstly, because conv5 in the original ResNet50 is moved to the detection network, the feature extraction layer only has the first four layers and the network depth is shallow. So after conv4 layer, the dilated residual block with 1×1 convolution layer mapping (Figure 5(b)) is used once time, and then the dilated residual block with 1×1 convolution

layer mapping (Figure 5(c)) is used twice as the new fifth layer in the feature extraction network. The combination of dilated residuals ensures that the spatial resolution of fifth layer is consistent with conv4, which can reduce the loss of feature information. In order to reduce the amount of computation and memory consumption, the channel number of the residual block is set to 512. Secondly, due to the large area size in the remote sensing image, the spatial resolution decreases and the semantic information of small targets is seriously lost after down-sampling. Hence, the features generated by convl, conv3 and the new fifth layer are fused to make full use of the deep semantic information under low spatial resolution and the shallow geometric, textural information under high spatial resolution. However, although the shallow feature retains high spatial resolution and abundant small target information, the shallow information is too shallow, and the directly fusion of shallow feature and deep feature cannot significantly improve the regional detection accuracy. Therefore, before feature fusion, a structure consistent with the fifth layer is introduced after the features of convl and conv3. The number of residual block channels is set to 256. To fully learn the target information under high spatial resolution, improve the positioning accuracy of large targets, and enhance the detection ability of the network model, the down-sampled shallow features and the up-sampled deep features are fused, so the improved feature extraction network is obtained.

The resolution of remote sensing image is too large, resulting in many small target areas. However, Faster RCNN uses part of the VGG Net network layer as shallow feature extractor to extract basic features such as points and edges of targets. Therefore, the detection effect of small target region is not good. In this paper, ResNet50 is selected as the basic feature extraction network, and multi-scale features are added to enhance the detection ability of small target regions. The ResNet solves the degradation problem when the traditional network is deepened, and the deepest network can reach 152 layers. Compared with traditional networks, deep residual networks have better generalization ability and lower complexity. ResNet is deeper than the VGG network. It is able to learn detailed features in the image. ResNet adds a batch normalization layer between the convolution and pooling layers to speed up training, while residuals are used to make training the depth model easier. Residual network introduces a learning framework based on residual blocks. The input can be propagated forward faster through cross-layer connections.

Faster RCNN is only classified according to the output features of the last layer in the basic network, which requires less computing and less memory. However, the features of the last layer belong to the high-level features, so the network is not expressive enough for small-scale targets. Generally, the high level features of convolutional neural networks are characterized by low resolution and high level semantic information. In contrast, low-level features are characterized by high resolution, low-level semantic information. By combining high level features with low level features, semantic information at multiple scales can be utilized at the same time. According to the idea of reference [19], feature pyramid is added to feature extraction in this paper to improve the final detection effect, as shown in Figure 6. The feature extraction process forms a bottom-up path, a top-down path and a horizontal connection. Formally, for the ROI with width w and height h, it is assumed that k is the reference value, representing the number of feature layers. k is the number of feature levels corresponding to the ROI. The formula assigned to the feature pyramid is:

$$k = [k_0 + b(\sqrt{wh}/224)]. \tag{5}$$

The feed-forward calculation of convolutional neural network is a bottom-up path. The basic network in this paper uses the characteristics of each residual block to activate the output corresponding to the output of different convolutional layers. It has different step sizes, which can deal with small targets region well. Compared with the feature extracted only by the last convolutional layer, this structure can utilize more high-level semantic information. For the small target region, the operation on the larger feature map increases the resolution of the feature map, so that more useful information about the small target region can be obtained.

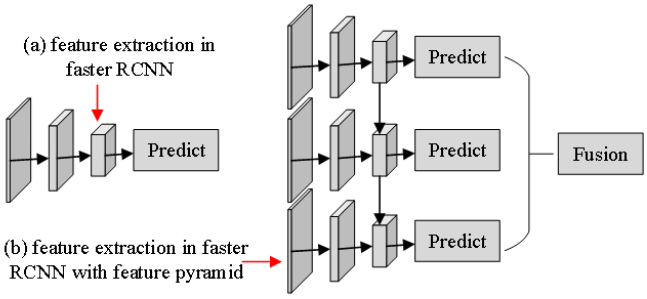

Fig. 6. Multi-scale feature extraction process

In remote sensing images, there is a large scale difference between different regions, and region targets with different scales have different features, so feature maps of different scales should be used for detection. In the underlying feature map, there are more details and the location of region targets is clear, which is suitable for detecting region targets with small scale. In the top-level feature map, the semantic information is rich, which is suitable for the detection of large scale region targets. However, the Faster RCNN model only uses the top-level feature map for target detection. The top-level feature map has rich semantic information but less detailed information after multiple sub-sampling operations, so the detection effect for small targets is not ideal.

In 2017, Lin et al. [36] proposed Feature Pyramid Network (FPN). FPN network fuses multi-scale feature maps and uses the fused feature maps for target detection. In this way, details in the underlying feature map can be fully utilized. However, the structure of FPN network is relatively concise, which leads to two shortcomings of FPN network for complex target detection tasks. Firstly, the FPN network uses the nearest neighbor interpolation algorithm with low precision to realize the up-sampling operation. The loss of the top layer information in the downward transmission process is too large, resulting in less semantic information fusion in the feature graph near the bottom. Secondly, the feature fusion path of FPN network is top-down, and a large number of details in the bottom feature map cannot be fused in the top feature map. As a result, the contour information

between overlapping regions cannot be effectively extracted when the target detection is carried out on the top feature map.

To solve the above problems in FPN networks, a path aggregation network with Convolution Block Attention Module (PACBAM) is proposed in this paper aiming to enhance the fusion effect between feature maps with different scales. Figure 7 shows the PACBAM network structure. The dimensions of feature map F1, F2, F3 and F4 are $336 \times 192 \times 256$, $168 \times 96 \times 512$, $84 \times 48 \times 1024$ and $21 \times 12 \times 2048$, respectively. The PACBAM network first convolves the four feature graphs with 1×1 to unify them into 256-channel. The bilinear interpolation algorithm is used to realize the double up-sampling operation of the feature graph, and the up-sampled feature graph is added from top to bottom to realize the first fusion of the feature graph. The convolution kernel with the step size of 2 and the size of 3×3 is used for down-sampling of the fused feature graph. The sub-sampled feature maps are added from bottom to top to realize the second fusion of feature maps. PACBAM network adopts bilinear interpolation to realize the up-sampling operation of feature graph. The bilinear interpolation carries out linear interpolation in two directions respectively, and the pixel value information of four pixel points around the target point can be utilized. The nearest neighbor interpolation only selects the nearest pixel as the pixel value of the target point. Bilinear interpolation reduces the information loss in the process of feature graph transmission and improves the up-sampling accuracy. In addition, PACBAM network adds a bottom-up feature fusion path on the basis of FPN network to realize multiple fusion of multi-scale feature maps, so that the details of the bottom layer can be better transferred to the top layer feature map.

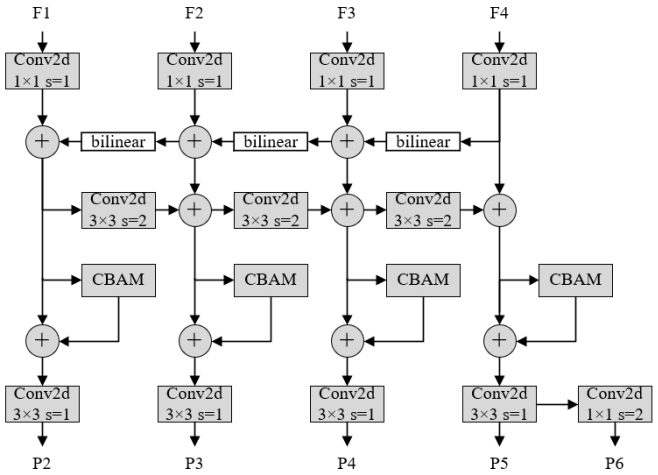

Fig. 7. MPACBAM network

The feature graphs that have been fused twice are weighted using CBAM attention mechanism, which helps to obtain the feature information that contributes more to the detection results. CBAM includes a channel attention module and a spatial attention module. Its structure is shown in Figure 8.

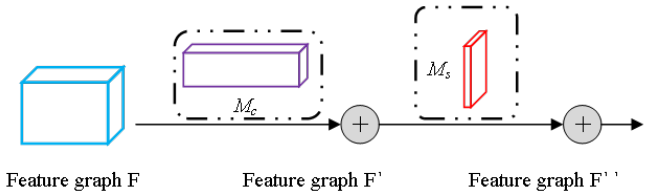

Fig. 8. CBAM structure

Here M_c is the weight of channel attention, M_s is the weight of space attention.

The channel attention module focuses on the real content of the target to be detected. The specific calculation method is as follows.

$$M_c(F') = \sigma(MLP(AvgPool(F) + MLP(MaxPool(F)))). \tag{6}$$

Where $M_c(F')$ is the channel attention weight. σ is the Sigmoid function. MLP denotes multilayer perceptron. $AvgPool$ and $MaxPool$ are global average pooling and maximum pooling, respectively. F represents the input feature graph.

Spatial attention module focuses on the location information of the target to be detected, which can reduce the interference of background information. The specific calculation method is:

$$M_s(F'') = \sigma(f^{7\times7}([AvgPool(F'); MaxPool(F')])). \tag{7}$$

Where $M(F'')$ is the weight of spatial attention. $f^{7\times7}$ means that the convolution kernel size is 7×7. F' represents the feature map weighted by channel attention.

The weighted feature graph is convolved with a convolution kernel with step size of 1 and size of 3×3, and a total of 4 feature graphs from P2 to P5 are obtained. The P6 feature map is obtained by the maximum pooled up-sampling operation with the step size of 2 on the P5 feature map. Finally, there are 5 feature maps from P2 to P6.

3.2. Pooling Layer of Region of Interest

The RoI Pooling layer proposed in Fast R-CNN can significantly accelerate training and testing and improve the detection accuracy. For boxes with different sizes, RoI Pooling can also obtain feature maps with fixed sizes. Floating point rounding occurs when the image reaches the feature mapping through the convolutional network to obtain the position of the candidate frame and when the RoI Pooling is applied to the position of each small grid. These two quantifications are likely to lead to the deviation of the position of the candidate box. First, the continuous coordinates (x_1, y_1) and (x_2, y_2) of ROI should be integer quantized. Let downward rounding and upward rounding of coordinate component x be $floor(x)$ and $cell(x)$ respectively. The discrete eigenvalues w_{ij} on the feature graph are calculated by summative operation, and the nearest neighbor sampling operation is carried out. Quantization will result in a mismatch between the image and the

feature map. The calculation formula of ROI pooling result $r_{pooling}(x_1, y_1, x_2, y_2)$ on the feature map is:

$$r_{pooling}(x_1, y_1, x_2, y_2) = \frac{\sum_{i=floor(x_1)}^{cell(x_2)} \sum_{i=floor(y_1)}^{cell(y_2)} w_{ij}}{(cell(x_2) - floor(x_1) + 1) \times (cell(y_2) - floor(y_1) + 1)}. \tag{8}$$

The RoIAlign Pooling method is proposed in Mask R-CNN algorithm, which can effectively reduce the errors generated by RoI Pooling quantization operation. RoIAlign takes no quantization and uses bilinear interpolation to convert pixel values on the image to floating point numbers, thus converting the entire feature aggregation processing into a continuous operation. In order to eliminate the quantization error of RoI Pooling discretization, the center point obtained by bilinear interpolation operation within the range from the point to the top, bottom, left and right discretization points of $N = 4$. We use formula (3) to operate each successive point (a_i, b_i) once. Bounding box is the corresponding region of ROI region on the feature graph, so the pooling result of ROI region align can be expressed as:

$$r_{align}(x_1, y_1, x_2, y_2) = \sum_{i=1}^{N} f(a_i, b_i)/N. \tag{9}$$

Where $f(\cdot)$ represents the eigenvalue of the feature graph. N is the number of feature points.

The connection model of fully connected layer of convolutional neural network is different from that of convolutional layer and pooling layer, which contains a large number of parameters. According to the study of reference [21], fully connection layer is easy to lead to over-fitting, thus reducing the generalization ability of the network. The main idea of improving the classification network is to reduce the number of parameters in the full connection layer to reduce the computation and prevent over-fitting. Therefore, this paper modifies the classification network, as shown in the dotted line box at the classification network in Figure 2. A convolution layer is added before the fully connected layer to reduce the number of parameters in the feature graph and make the classifier more powerful. In this paper, 3×3 convolution kernel is used. Small convolution kernel cannot only realize the function of large convolution kernel, but also reduce the number of parameters and speed up the calculation. In addition, this operation can prevent the over-fitting phenomenon caused by the large dimension of the fused feature, and reduce the feature size by 1/2, which is convenient for the subsequent calculation.

3.3. Bounding Box Optimization with Improved NMS

The NMS algorithm is widely used in edge and target detection. It can solve the problem that a large number of candidate boxes overlap when the target is surrounded by a large number of candidate boxes during classification. The steps of the NMS algorithm are as follows:

1. Sorting all the candidate boxes according to their score and selecting the candidate box with the highest score.

2. Comparing the remaining candidate boxes with the candidate box (highest score) in turn. If the overlap area between the two boxes is greater than a certain threshold, the box will be deleted.
3. Repeat step 2 by selecting the highest score box from the unprocessed candidate box (one that does not overlap the highest scoring box), leaving only the target in the optimal box.

In object detection process, the NMS algorithm can be understood as a process of scoring boundary boxes, and its linear weighting function can be expressed as:

$$s_i^{NMS} = \begin{cases} s_i^{NMS}, X_{IoU}(M, b_i) < N_t \\ 0, X_{IoU}(M, b_i) > N_t \end{cases} \tag{10}$$

Where s_i^{NMS} is the IOU corresponding to the $i - th$ prediction box. N_t indicates the suppression threshold. b_i indicates the $i - th$ prediction box to be filtered. M is the boundary box with the maximum score. X_{IOU} is the union of the intersection ratio of the predicted boundary frame area A and the actual boundary frame area B, which can be expressed as:

$$X_{IOU} = \frac{A \cap B}{A \cup B}. \tag{11}$$

As can be seen from the preceding steps, the original prediction box will be deleted when detecting the same type of objects with a large amount of overlap. As shown in Figure 9, the detection result should output two boxes, i.e. 0.75 and 0.90. However, the traditional NMS algorithm may delete the solid box with low confidence. As a result, the confidence level of the box with a confidence level of 0.75 becomes 0.00 or 0.35. The detected actual output has two boxes. If the IOU of the solid and dotted boxes on the NMS is greater than the threshold and the score of the solid boxes is low, so the IOU will be deleted. As a result, only the targets in the dotted box can be detected, reducing the recall rate of the targets. In order to solve this problem, the Soft-NMS algorithm is used to replace the NMS, and the score can be recursively scored according to the current score, instead of directly deleting the adjacent boxes with lower scores. When the same type of objects are highly overlapped, the situation of deleting the prediction boxes by mistake is reduced. Soft-NMS algorithm does not need to introduce any hyperparameters in the training stage. The hyperparameters used to adjust the Soft-NMS algorithm only occur during the test or demonstration phase and do not increase the computational complexity. The procedure of the Soft-NMS algorithm is as follows:

1. Grouping tags according to different types to predict all candidate regions in different tags.
2. All boxes in each category are denoted as E, and the set of filtered boxes are denoted as D. a) Select box M with the highest score and add it to D; b) Calculate the overlap area between the remaining frame and M. If it is larger than the set threshold N, it will be discarded; otherwise, it will be retained; c) If all boxes obtained in step b) are empty, return to Step 2), otherwise continue to perform step a);
3. After the above process is completed, it keeps all categories in the collection of valid boxes.

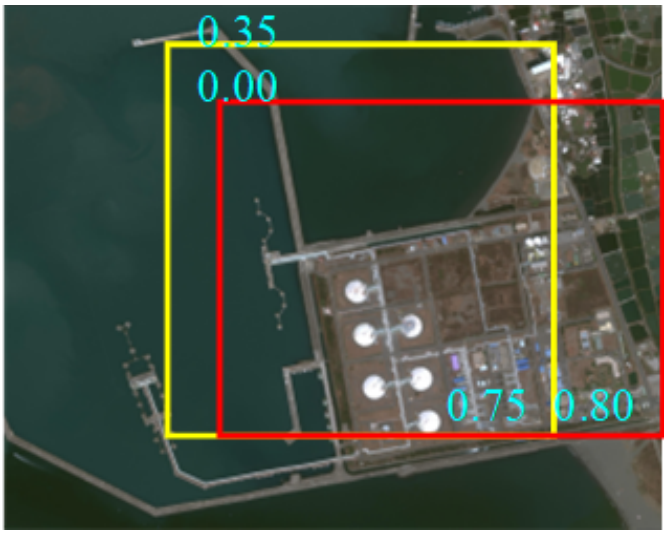

Fig. 9. NMS process

The linear weighting function in Soft-NMS can be expressed as:

$$s_i^{Soft} = \begin{cases} s_i^{Soft}, X_{IoU}(M, b_i) < N_t \\ s_i^{Soft}[1 - X_{IoU}(M, b_i)], X_{IoU}(M, b_i) > N_t \end{cases} \tag{12}$$

Where s_i^{Soft} is the classification score corresponding to the $i - th$ prediction box. Reference [37] compared the mAP of Soft-NMS and NMS under different thresholds with the same data. The results showed that the best effect was achieved when the IOU was set between 0.45 and 0.70, so the IOU value was set as 0.70 in the next experiment.

4. Experiments and Analysis

4.1. Procedure of Experiment

This paper builds a deep learning framework based on MATLAB2017a, and the relevant configuration of the test platform is Intel(R)Xeon(R) 2.30GHz CPU, NVIDIA Tesla 1060 GPU. The optimizer is stochastic gradient descent (SGD) algorithm. Initial learning rate is 5×10^{-3}, momentum factor is 0.9. Decay learning rate is 8×10^{-4}. Iteration number is 7000, batch size is 4, epoch number is 20. In RPN networks, the threshold of Soft-NMS is 0.3. The number of prediction boxes retained by each image after being suppressed by Soft-NMS is 2000.

4.2. Datasets

Different from natural images, remote sensing images have different target sizes and directions. The background environment is also complex. This paper collects and compares

a variety of remote sensing data sets, and analyzes their advantages and disadvantages. Considering that the data quality of DOTA data set is high, with the highest resolution of 4000×4000 pixels, and it contains up to 15 categories. The samples are more balanced than other data sets, and the scale changes greatly, so it is taken as the data set of the experiment. At the same time, part of the data is collected from Google Earth and marked by roLabellmg tool to provide data for the experimental test. There are 3000 images in the sample set, including 1500 training samples, 500 verification samples and 500 test samples.

The positive sample threshold of IoU is set at 0.7 and the negative sample threshold is set at 0.3 to maintain a certain ratio of positive and negative samples. When the IoU between anchor and GT(ground truth) is greater than 0.7, the anchor is considered as a positive sample. When IoU is less than 0.3, the anchor is considered as a negative sample. The IoU of anchor is within the (0.3,0.7). The IoU threshold of the NMS is set to 0.7.

4.3. Evaluation Index

Precision, Recall and Average Precision (AP) values under different IOU thresholds are used as evaluation indicators. Accuracy is the ratio of the number of target regions correctly detected by the model to the total number identified as target regions in the test set. Recall rate is the ratio of the target area correctly detected by the model to the total number of samples in the target area in the test set. AP value is a comprehensive evaluation index, which is determined by the area under P-R curve drawn by Precision and Recall. The calculation formula of each index is as follows:

$$Precision = \frac{TP}{TP + FP}. \tag{13}$$

$$Recall = \frac{TP}{TP + FN}. \tag{14}$$

$$AP = \int_0^1 P(r)dr. \tag{15}$$

Where FN is the target sample wrongly considered as the background. TP represents the correctly identified target sample. FP represents the background sample of the misjudged target. r represents the Recall value, and $P(r)$ represents the Precision value corresponding to the r value.

4.4. Training Data Analysis

The model training results are shown in Table 2 and Figure 10, where the mAP is used to test the training effect of the model, and mAP represents the comprehensive detection accuracy of the model. With the increase of the iteration number, the mAP curve grows smoothly. The reason is that the sample quantity of the last iteration in each Epoch is less than that of the previous iterations, and the sample representativeness of the last

iteration is poor, which slightly changes the iteration direction of the model and leads to the larger loss value. With the increase of the iteration number, the distance between the model training result and the global optimal solution gradually decreases. At this time, the decrease of the iteration number of samples will not significantly change the direction of iteration. This phenomenon will not affect the final training result of the model. After 150 network iterations, the model gradually converges, with mAP tending to 0.68.

Table 2. The comparison of mAP with iterations

Iteration number	mAP
50	0.55
100	0.65
150	0.68
200	0.68
250	0.68
300	0.68

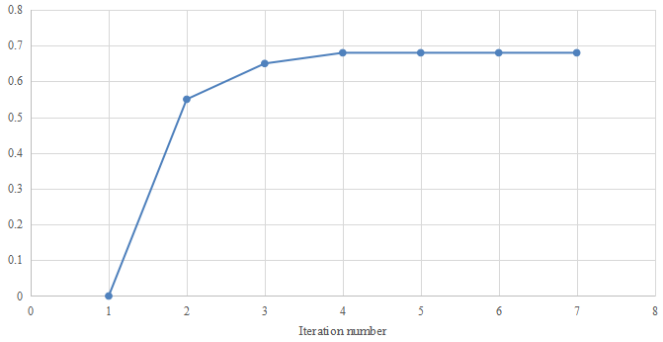

Fig. 10. The curve of loss value and average accuracy with the number of iterations

4.5. Comparison of Pooling Methods

Table 3 shows the detection results of five types of targets by two pooling methods. It can be seen that, compared with RoI Pooling method, the detection accuracy of RoIAlign pooling method is increased by 3%. Because there are a large number of small and medium targets in remote sensing images and they are very dense, RoIAlign reduces pixel deviation during pooling, so the detection rate is improved to a certain extent compared with RoI pooling method. In addition, this paper also calculates the test time of the two methods, testing multiple images from the DOTA data set for testing, and calculates the average detection time of the two methods.

Table 3. AP comparison with different pooling methods/%

Method	small-vehicle	large-vehicle	Plane
RoIPooling	60.1	83.2	89.6
RoIAlign	65.5	86.5	92.7

4.6. Comparison with different State-of-the-art methods

In this paper, the training model of the M^2F^2-RCNN is used to carry out relevant tests on the DOTA data set, including small vehicle, large vehicle, Plane. Table 5 shows the values of Precision, Recall and AP.

Table 4. AP results with M^2F^2-RCNN

Object	Precision/%	Recall/%	AP/%
small-vehicle	78.3	83.6	65.5
large-vehicle	89.7	84.5	86.5
Plane	91.7	93.4	92.7

Table 4 shows the results of target recognition on DOTA data set by the M^2F^2-RCNN in this paper. It can be seen that large vehicle and plane have good recognition effect, with an average accuracy of more than 85%. On the other hand, the identification effect of small vehicle is poor, with an average accuracy of 65.5%. The reason is that large vehicle and plane have significant shape, color and texture features, and the environment is relatively simple, it is relatively easy to identify. However, Bridges are generally located in areas with dense ground objects, with a large length-width ratio and a small number of plane in the data set, so it is difficult to detect.

In order to demonstrate the effectiveness of the M^2F^2-RCNN, other advanced methods are used for comparison. The models used are AOR [38], HASS [39], EAN [40] and OSHP [41], and the results are shown in Table 5.

Table 5. AP results with different methods/%

Object	AOR	HASS	EAN	OSHP	M^2F^2-RCNN
small vehicle	58.2	58.7	59.5	63.7	65.5
large vehicle	75.6	78.2	81.7	83.6	86.5
Plane	80.9	82.1	84.7	85.2	92.7

Table 5 shows that compared with AOR, HASS, EAN and OSHP, the M^2F^2-RCNN is greatly improved in AP. M^2F^2-RCNN in Table 5 has higher AP values than other methods. For large vehicle, AP of M^2F^2-RCNN is 92.27%, which is higher than that of AOR (75.6%), HASS (78.2%), EAN (81.7%) and OSHP (83.6%). Looking through the data of the whole table, it is not difficult to find that the proposed scheme can effectively detect the region, and the results are satisfactory.

5. Conclusions

For the problems existing in the Faster RCNN algorithm in region detection, we propose M^2F^2-RCNN model. Firstly, the feature extraction network is based on ResNet50 and the dilated residual blocks are utilized for multi-layer and multi-scale feature fusion. Then, a path aggregation network with a convolution block attention module (CBAM) attention mechanism is added in the backbone network to improve the efficiency of feature extraction. Thirdly, the extracted feature map is processed, and RoIAlign is used to improve the pooling operation of regions of interest and it can improve the calculation speed. Finally, in the classification stage, an improved non-maximum suppression is used to improve the classification accuracy of the sensitive region. The experimental results show that the M^2F^2-RCNN can get better detection results. Future work will apply this theme in practical engineering. How to use deep learning technology to realize the rapid detection of remote sensing image is still the focus of future research.

Acknowledgments. This work was supported in part by the National Natural Science Foundation of China under Grant 62071084 and National Natural Science Foundation of China under Grant 62001434. Also supported by Talents Project of the State Ethnic Affairs Commission.

References

1. Wang Z, Li P, Cui Y, et al. "Automatic Detection of Individual Trees in Forests Based on Airborne LiDAR Data with a Tree Region-Based Convolutional Neural Network (RCNN)," *Remote Sensing,* 2023, 15(4): 1024.
2. Seetharaman K, Mahendran T. Leaf Disease Detection in Banana Plant using Gabor Extraction and Region-Based Convolution Neural Network (RCNN)[J]. Journal of The Institution of Engineers (India): Series A, 2022, 103(2): 501-507.
3. Y. Yuan, Z. Xu and G. Lu, "SPEDCCNN: Spatial Pyramid-Oriented Encoder-Decoder Cascade Convolution Neural Network for Crop Disease Leaf Segmentation," IEEE Access, vol. 9, pp. 14849-14866, 2021, doi: 10.1109/ACCESS.2021.3052769.
4. Yanmaz E. Joint or decoupled optimization: Multi-UAV path planning for search and rescue[J]. Ad Hoc Networks, 2023, 138: 103018.
5. Teng, L., Qiao, Y. BiSeNet-oriented context attention model for image semantic segmentation. Computer Science and Information Systems, vol. 19, no. 3, pp. 1409-1426. (2022), https://doi.org/10.2298/CSIS220321040T.
6. Uijlings J R R, Van De Sande K E A, Gevers T, et al. Selective search for object recognition[J]. International journal of computer vision, 2013, 104: 154-171.
7. Tang X, Xie X, Hao K, et al. A line-segment-based non-maximum suppression method for accurate object detection[J]. Knowledge-Based Systems, 2022, 251: 108885.
8. Ren S, He K, Girshick R, et al. Faster r-cnn: Towards real-time object detection with region proposal networks[J]. Advances in neural information processing systems, 2015, 28.
9. Redmon J, Divvala S, Girshick R, et al. You only look once: Unified, real-time object detection[C]//Proceedings of the IEEE conference on computer vision and pattern recognition. 2016: 779-788.
10. Liu W, Anguelov D, Erhan D, et al. Ssd: Single shot multibox detector[C] Computer Vision CECCV 2016: 14th European Conference, Amsterdam, The Netherlands, October 11-14, 2016, Proceedings, Part I 14. Springer International Publishing, 2016: 21-37.

11. Karim, Shahid, Geng Tong, Jinyang Li, Akeel Qadir, Umar Farooq, and Yiting Yu. "Current Advances and Future Perspectives of Image Fusion: A Comprehensive Review." Information Fusion, Vol. 90, pp.185-217, February 2023.
12. S. Yin, L. Wang, M. Shafiq, L. Teng, A. A. Laghari and M. F. Khan, "G2Grad-CAMRL: An Object Detection and Interpretation Model Based on Gradient-weighted Class Activation Mapping and Reinforcement Learning in Remote Sensing Images," in IEEE Journal of Selected Topics in Applied Earth Observations and Remote Sensing, 2023. doi: 10.1109/JSTARS.2023.3241405.
13. Tang C, Wu J, Hou Y, et al. A spectral and spatial approach of coarse-to-fine blurred image region detection[J]. IEEE Signal Processing Letters, 2016, 23(11): 1652-1656.
14. Wu D, Cao L, Zhou P, et al. Infrared Small-Target Detection Based on Radiation Characteristics with a Multimodal Feature Fusion Network[J]. Remote Sensing, 2022, 14(15): 3570.
15. Li Z, Wang H, Zhong H, et al. Self-attention module and FPN-based remote sensing image target detection[J]. Arabian Journal of Geosciences, 2021, 14: 1-18.
16. Cui Z, Leng J, Liu Y, et al. SKNet: Detecting rotated ships as keypoints in optical remote sensing images[J]. IEEE Transactions on Geoscience and Remote Sensing, 2021, 59(10): 8826-8840.
17. Pazhani A A J, Vasanthanayaki C. Object detection in satellite images by faster R-CNN incorporated with enhanced ROI pooling (FrRNet-ERoI) framework[J]. Earth Science Informatics, 2022, 15(1): 553-561.
18. Anuar M M, Halin A A, Perumal T, et al. Aerial imagery paddy seedlings inspection using deep learning[J]. Remote Sensing, 2022, 14(2): 274.
19. Gao, Y., Wu, H., Wu, X., Li, Z., Zhao, X.: Human Action Recognition Based on Skeleton Features. Computer Science and Information Systems, Vol. 14, No. 3, 537-550. (2017), https://doi.org/10.2298/CSIS220131067G
20. Chen L, Yang Y, Wang Z, et al. Underwater Target Detection Lightweight Algorithm Based on Multi-Scale Feature Fusion[J]. Journal of Marine Science and Engineering, 2023, 11(2): 320.
21. Zheng C, Wang L. Semantic segmentation of remote sensing imagery using object-based Markov random field model with regional penalties[J]. IEEE Journal of Selected Topics in Applied Earth Observations and Remote Sensing, 2014, 8(5): 1924-1935.
22. Ma F, Gao F, Wang J, et al. A novel biologically-inspired target detection method based on saliency analysis for synthetic aperture radar (SAR) imagery[J]. Neurocomputing, 2020, 402: 66-79.
23. Wang Z, Xu N, Wang B, et al. Urban building extraction from high-resolution remote sensing imagery based on multi-scale recurrent conditional generative adversarial network[J]. GIScience & Remote Sensing, 2022, 59(1): 861-884.
24. Ni K, Zhao Y, Wu Y. SAR Image Segmentation Based on Super-Pixel and Kernel-Improved CV Model[C]//IGARSS 2022-2022 IEEE International Geoscience and Remote Sensing Symposium. IEEE, 2022: 3476-3479.
25. Zhu Z, Yin H, Chai Y, et al. A novel multi-modality image fusion method based on image decomposition and sparse representation[J]. Information Sciences, 2018, 432: 516-529.
26. Liguo Wang, Yin Shoulin, Hashem Alyami, et al. "A novel deep learning-based single shot multibox detector model for object detection in optical remote sensing images," *Geoscience Data Journal,* (2022). https://doi.org/10.1002/gdj3.162
27. Karnyoto, A. S., Sun, C., Liu, B., Wang, X.: Transfer Learning and GRU-CRF Augmentation for Covid-19 Fake News Detection. Computer Science and Information Systems, Vol. 19, No. 2, 639-658. (2022), https://doi.org/10.2298/CSIS210501053K
28. Farhadi A, Redmon J. Yolov3: An incremental improvement[C]//Computer vision and pattern recognition. Berlin/Heidelberg, Germany: Springer, 2018, 1804: 1-6.
29. Luo S, Yu J, Xi Y, et al. Aircraft target detection in remote sensing images based on improved YOLOv5[J]. Ieee Access, 2022, 10: 5184-5192.
30. Zhang K, Shen H. Multi-stage feature enhancement pyramid network for detecting objects in optical remote sensing images[J]. Remote Sensing, 2022, 14(3): 579.

31. Ma J, Shao W, Ye H, et al. Arbitrary-oriented scene text detection via rotation proposals[J]. IEEE transactions on multimedia, 2018, 20(11): 3111-3122.
32. Wang K, Du S, Liu C, et al. Interior attention-aware network for infrared small target detection[J]. IEEE Transactions on Geoscience and Remote Sensing, 2022, 60: 1-13.
33. Singhal S, Passricha V, Sharma P, et al. Multi-level region-of-interest CNNs for end to end speech recognition[J]. Journal of Ambient Intelligence and Humanized Computing, 2019, 10: 4615-4624.
34. Theckedath D, Sedamkar R R. Detecting affect states using VGG16, ResNet50 and SE-ResNet50 networks[J]. SN Computer Science, 2020, 1: 1-7.
35. Sun M, Zhao H, Li J. Road crack detection network under noise based on feature pyramid structure with feature enhancement (road crack detection under noise)[J]. IET Image Processing, 2022, 16(3): 809-822.
36. Lin T Y, Doll P, Girshick R, et al. Feature pyramid networks for object detection[C]//Proceedings of the IEEE conference on computer vision and pattern recognition. 2017: 2117-2125.
37. Addis A A, Tian W, Acheampong K N, et al. Small-Scale and Occluded Pedestrian Detection Using Multi Mapping Feature Extraction Function and Modified Soft-NMS[J]. Computational Intelligence and Neuroscience: CIN, 2022, 2022.
38. Hou Y, Yang Q, Li L, et al. Detection and Recognition Algorithm of Arbitrary-Oriented Oil Replenishment Target in Remote Sensing Image[J]. Sensors, 2023, 23(2): 767.
39. Lv N, Zhang Z, Li C, et al. A hybrid-attention semantic segmentation network for remote sensing interpretation in land-use surveillance[J]. International Journal of Machine Learning and Cybernetics, 2023, 14(2): 395-406.
40. Xiong W, Xiong Z, Cui Y. An explainable attention network for fine-grained ship classification using remote-sensing images[J]. IEEE Transactions on Geoscience and Remote Sensing, 2022, 60: 1-14.
41. Chen J, Li Z, Peng C, et al. UAV Image Stitching Based on Optimal Seam and Half-Projective Warp[J]. Remote Sensing, 2022, 14(5): 1068.

Shoulin Yin received the B.S. and M.S. degrees in image processing from Software College, Shenyang Normal University, Shenyang, China, in 2013 and 2015, respectively. He is currently a PHD with School of Information and Communication Engineering, Harbin Engineering University. He has published more than 20 technical articles in scientific journals and conference proceedings. His research interests include image fusion, object detection, and image recognition. Email:yslin@hit.edu.com.

Liguo Wang received his M.A. degree in 2002 and Ph.D. degree in signal and information processing in 2005 from Harbin Institute of Technology, Harbin, China. He held postdoctoral research position from 2006 to 2008 in the College of Information and Communications Engineering, Harbin Engineering University. He is currently a Professor with Information and Communications Engineering, Dalian Minzu University, Dalian, China. His research interests are remote sensing image processing and machine learning. He has published three books, 27 patents, and more than 200 papers in journals and conference proceedings. Email: wangliguo@hrbeu.edu.cn.

Qunming Wang received the Ph.D. degree from The Hong Kong Polytechnic University, Hong Kong, in 2015. He is currently a Professor with the College of Surveying and Geo-Informatics, Tongji University, Shanghai, China. From 2017 to 2018, he was a

Lecturer (Assistant Professor) with Lancaster Environment Centre, Lancaster University, Lancaster, U.K., where he is currently a Visiting Professor. His 3-year Ph.D. study was supported by the hypercompetitive Hong Kong Ph.D. Fellowship and his Ph.D. thesis was awarded as the Outstanding Thesis in the Faculty. He has authored or coauthored more than 70 peer-reviewed articles in international journals such as Remote Sensing of Environment, IEEE Transactions on Geoscience and Remote Sensing, and ISPRS Journal of Photogrammetry and Remote Sensing. His research interests include remote sensing, image processing, and geostatistics. Prof. Wang is an Editorial Board Member for Remote Sensing of Environment, and serves as an Associate Editor for Science of Remote Sensing (sister journal of Remote Sensing of Environment) and Photogrammetric Engineering & Remote Sensing. He was an Associate Editor for Computers and Geosciences (2017-2020).

Mirjana Ivanovic (Member, IEEE) has been a Full Professor with the Faculty of Sciences, University of Novi Sad, Serbia, since 2002. She has also been a member of the University Council for informatics for more than 10 years. She has authored or coauthored 13 textbooks, 13 edited proceedings, 3 monographs, and of more than 440 research articles on multi-agent systems, e-learning and web-based learning, applications of intelligent techniques (CBR, data and web mining), software engineering education, and most of which are published in international journals and proceedings of high-quality international conferences. She is/was a member of program committees of more than 200 international conferences and general chair and program committee chair of numerous international conferences. Also, she has been an invited speaker at several international conferences and a visiting lecturer in Australia, Thailand, and China. As a leader and researcher, she has participated in numerous international projects. She is currently an Editor-in-Chief of Computer Science and Information Systems Journal.

Jinghui Yang received the B.S., M.S., and Ph.D. degrees from Harbin Engineering University, Harbin, China, in 2010, 2013, and 2016, respectively. She is currently an associate professor with the School of Information Engineering, China University of Geosciences, Beijing, China. Her research interests include hyperspectral imagery, remote sensing, pattern recognition, and signal processing.

Received: March 20, 2023; Accepted: June 22, 2023.

Computer Science and Information Systems20(4):1311–1341 https://doi.org/10.2298/CSIS230225046Y

SRDF_QDAG: An Efficient End-to-End RDF Data Management when Graph Exploration Meets Spatial Processing

Houssameddine Yousfi[1,2], Amin Mesmoudi[3], Allel Hadjali[1], Houcine Matallah[2], and Seif-Eddine Benkabou[3]

[1] LIAS, ENSMA Engineering School
1 avenue Clément Ader, 86961 Futuroscope Chasseneuil Cedex, France
{houssameddine.yousfi, allel.hadjali}@ensma.fr
[2] LRIT, Science Faculty
University Abu Bekr Belkaid, Tlemcen, Algeria
{houssameddine.yousfi, houcine.matallah}@univ-tlemcen.dz
[3] LIAS, University of Poitiers
15 rue de l'Hôtel Dieu 86073 POITIERS Cedex 9, France
{amin.mesmoudi, seif.eddine.benkabou}@univ-poitiers.fr

Abstract. The popularity of RDF has led to the creation of several datasets (e.g., Yago, DBPedia) with different natures (graph, temporal, spatial). Different extensions have also been proposed for SPARQL language to provide appropriate processing. The best known is **GeoSparql**, that allows the integration of a set of spatial operators. In this paper, we propose new strategies to support such operators within a particular TripleStore, named RDF_QDAG, that relies on graph fragmentation and exploration and guarantees a good compromise between scalability and performance. Our proposal covers the different TripleStore components (Storage, evaluation, optimization). We evaluated our proposal using spatial queries with real RDF data, and we also compared performance with the latest version of a popular commercial TripleStore. The first results demonstrate the relevance of our proposal and how to achieve an average gain of performance of 28% by choosing the right evaluation strategies to use. Based on these results, we proposed to extend the RDF_QDAG optimizer to dynamically select the evaluation strategy to use depending on the query. Then, we show also that our proposal yields the best strategy for most queries.

Keywords: RDF, Graph Data, Spatial Data, TripleStore, Graph exploration, Optimization.

1. Introduction

Since Google popularized the use of the term Knowledge Graph to designate all knowledge used by its search engine, the number of this type of dataset has not stopped increasing. Knowledge Graphs (KG) are labeled and directed multi-graphs that encode information in the form of entities and relationships relevant to a specific domain or organization. KGs are effective tools for capturing and organizing a large amount of structured and

multi-relational data that can be explored using query mechanisms. Given these characteristics, KGs become the backbone of the Web and existing information systems in different academic fields and industrial applications. Their power comes from their ability to extend the existing knowledge without affecting the previous ones.

Following this large gain in popularity of knowledge graphs, the need for a standard data representation format has become obvious. This is especially in the context of the semantic Web due to its vision of globally accessible and linked data on the internet. In order to meet that need, RDF (Resource Definition Framework) has been proposed as the main standard for the semantic Web. In RDF format, Data are represented logically by a graph-based structure. The advantage of such a representation relies on the fact that it is schema-less, making it flexible and easy to adopt in different application domains. Moreover, such flexibility makes RDF more suitable for fast changing data where normalization is not possible or impractical due to the frequent changes to the underlying schema.

RDF Data is structured using the concept of triples $< subject, predicate, object >$ where the object can be a literal of predetermined types (string, double, ...) or it can be the subject of another triple leading to a graph structure. In the context of RDF data, SPARQL has been proposed as a query language. Since RDF is a graph representation of data, the query is composed mainly of a sub-graph where some subjects, predicates, or objects are replaced with variables. This sub-graph is called a basic graph pattern (BGP). Answering a SPARQL query is equivalent to finding sub-graphs that match the query pattern. On top of the basic graph pattern (BGP) matching, it is possible to run filters on variables such as Boolean expressions and regular expressions. The standard W3C norm of SPARQL does not provide the possibility to express spatial filters. However, many extensions have been proposed to improve the expressiveness of SPARQL, making it able to express spatial filters. The most known extensions are GeoSparql [4] and stSparql [19].

Many attempts have been proposed to implement OGC GeoSPARQL [4] by the community. Such implementation is a hard task since it requires changes on many levels of the triples store (storage, indexing, evaluation engine and optimizer). The changes also depend on the type and architecture of the Triplestore. For example, strategies that work on a Triplestore based on a single table strategy (eg. 3-Store[14]) may not work on another based on property table (eg. Jena[36]).

Some of the existing Triplestores are capable of answering Spatial-RDF queries with variant capabilities. Most of them are based on the relational model, whereas, others are based on single table or fact strategies. Nevertheless, all the previously mentioned approaches suffer from a high number of joins, which leads to performance and scalability problems. Recently in [17], the RDF_QDAG Triplestore was proposed. It relies on graph fragmentation and exploration, making it able to offer a better performance and scalability compromise. In this work, we take advantage of such capabilities and expand the system to be able to handle spatial data without the loss of this trade-off. The proposed extensions are, to the best of our knowledge, the first that provide spatial-RDF data processing in a graph exploration system. We managed throw the proposed approaches to achieve an average gain of performance estimated at 28%.

In this paper, we discuss the extension of RDF_QDAG in order to add the support of spatial operators and filters proposed in GeoSPARQL. The contributions of this paper can be summarized as follows:

- Two evaluation approaches for spatial-RDF data (Spatial-First and BGP-First) are proposed.
- An existing spatial indexing approach [22] is adapted to be compatible with the graph exploration logic in RDF_QDAG triplestore. This indexing approach is used in the Spatial First strategies.
- The effect of the query evaluation strategies and the optimization techniques on the performance of RDF_QDAG, is studied in depth.
- An optimizer capable of selecting the best available evaluation strategy based on the query and statistics about the RDF and spatial data, is developed.
- Finally, an extensive experimental evaluation of the proposed approaches is conducted and compared with a well known and used commercial Triplestore.

The rest of this paper is organized as follows. First, we provide a comprehensive review of related work in section 2. Then, we state the basic concepts in section 3. After that, we explain the proposed query evaluation strategies with the help of running examples in section 4. In section 5, we address the optimization issue and establish the basis of an optimizer capable of choosing the best evaluation strategy based on the available statistics and metadata. To validate the proposed approaches, in section 6, we discuss the results of the experimental validation performed. Finally, we conclude the paper and list some future perspectives.

2. Related Work

In this section, we provide a critical review of main related work. We have divided this review in three parts: (i) work related to RDF data processing ; (ii) work related to Spatial data processing ; and (iii) work related to Spatial-RDF data processing.

2.1. RDF Data Processing

One can summarize the approaches dedicated to RDF data processing w.r.t. to their storage strategies of data. Four families of approaches can be distinguished (see Table 1 for a comparison):

1. The most intuitive way to store RDF data is by using a single big relational table that contains tree columns corresponding to the subject, predicate and object. This strategy is known as the single table strategy.
2. A second alternative storage option is the binary table. In this approach, for each property, the system stores a binary table containing the subject and the object. This approach is widely used for salable distributed systems [9].
3. The third approach is called ”Property table”. Indeed, subjects with common proprieties are grouped and stored in a large horizontal table. Each column in the table corresponds to a property.
4. In the fourth approach, RDF data is modeled and stored in its native graph form. Subjects and objects are considered as nodes, while properties are considered as labelled edges.

Table 1. Comparison of different storage strategies for RDF data, including examples of triplestores that utilize each strategy, their advantages and disadvantages.

Storage Strategy	Triplestore Examples	Advantages	Disadvantages
Single Table	Oracle, Sesame [8], 3-Store [14]	Intuitive	Large number of self joins needed for queries
Binary Table	SW-Store [3], C-store [35]	Suitable for distributed systems	Loss in performance with multiple properties, many tables needed for updates
Property Table	Jena [36], DB2RDF [5], 4store [15]	Efficient for queries with star patterns	Difficulties with chain queries, storage overhead due to null values, does not allow multiple values for the same property
Native Graph Form	Trinity [38], gStore, RDF_QDAG [17, 39]	Stores RDF data in its native form	N/A

As for the Triplestore RDF_QDAG [17], it stores RDF data in a graph form and it answers the queries using a graph exploration. For an efficient exploration, RDF_QDAG uses a combination of data partitioning and indexing techniques. First, the graph is partitioned in many fragments called Graph Fragments ($\mathcal{GF}$ for short). Each $\mathcal{GF}$ is then indexed using a clustered B+Tree. Similar to some existing works, RDF_QDAG keeps a separate dictionary of string values. The indices store only IDs rather than the strings. For more efficiency, RDF_QDAG makes use of two different orders SPO and OPS to store indices.

2.2. Spatial Data Processing

In this section, we focus on storing and indexing techniques of spatial data. Hereafter, the principle of each technique is presented (see also Table 2 for a comparison).

1. Grid files [29]: Partition the space into stripes alongside each dimension. The width of a strip can be variable and the number of stripes may differ for each dimension.
2. Kd-trees and kdb-trees [27][33]: Tree based structures that store data entries in the leafs. Each node in the Kd-tree splits the space along side one dimension (X for example) constructing two children. Each child node splits the space in the other dimension (Y in this case). We keep cycling throw dimensions on each layer until we reach the leafs.
3. Quad-trees [32][28]: They work as follows: each node recursively divide the space into four quadrants until each bucket (leaf node) has less objects then a given maximum capacity. During update operations, as soon as a bucket exceeds the given capacity threshold, a split operation is triggered.
4. R-trees [13, 18]: They rely on object grouping based on the construction of MBRs (Minimum Bounding Rectangles). To get a tree like structure, we keep grouping recursively MBRs inside each others to construct higher levels until we get one root for the tree. Properties are considered as labelled edges.

The processing of Big spatial data covers various domains and applications, including distributed computing frameworks, spatial data analysis and modeling, and spatial data quality. Notable contributions to this field include the work of Lee et al.[21], which provides an overview of the challenges and opportunities of processing Big spatial data. In addition, distributed computing frameworks such as SpatialHadoop[10] and GeoSpark[37] have been introduced for processing large-scale spatial data. More domain-specific approaches have also been proposed, such as Astroide[6], a scalable Spark-based processing engine for Big astronomical data, and the work of Papadopoulos et al.[25], which focuses on the challenges and opportunities of using Big data processing techniques for climate change research. Together, these works demonstrate the importance and impact of Big data processing for spatial data analysis and management.

Table 2. Storing and indexing techniques of spatial data.

Technique	Advantages	Limits
Grid files [29]	Good performance in certain applications.	Performance can be severely affected by a high number of dimensions. High cost of Balancing, Splitting or re-sizing a single cell Unsuited then for highly skewed data.
Kd-trees and kdb-trees [27][33]	Built efficiently in time complexity $O(n \log n)$. Offer efficient nearness search with time complexity $O(\log n)$	Hard to balance because the direction of split is different for each level
Quad-trees [32][28]	Good performance in nearness queries and KNN joins	Many empty nodes are stored in the form of chains (which can be solved by the external balanced regular (x-BR) trees). Unsuited for secondary storage due to low fan-out
R-trees [13, 18]	Lighter memory footprint. Rely on object grouping and not space partitioning	To answer a query, multiple sub-trees needs to be considered

2.3. Spatial-RDF data processing

In order to represent geographical linked data for the semantic Web, the Open Geospatial Consortium has proposed GeoSPARQL [4] as a norm that extends classic SPARQL. Many Triplestores have subsequently been subsequently extended to support the processing of this new standard. The spatial extension of RDF stores extensively depends on the storage model and the query evaluation engine.

For instance Strabon [20], an extension of Sesame [8], supports spatial data. It stores data in PostGIS. It implements a propriety table approach, where each table is indexed using SO and OS indices. Spatial data are saved on a separate relational table. This later is indexed using an R-tree [13]. The query optimizer extension of Strabon is simple. It relies on heuristics to push down spatial filters. Since Strabon is based on an old RDF store (i.e., Sesame), it lacks many optimization techniques used in modern Triplestores.

Table 3. Overview of different spatial extensions of RDF Triplestores.

Extension	Underlying system	RDF Storage	Spatial storage
Strabon [20]	Sesame [8]	Triple table in PostgreSQL	R-tree
Brodt et al. [7]	RDF-3X[24]	Heavy indexing	R-Tree
Geo-Store [34]	RDF-3X[24]	Heavy indexing	Grid file
Virtuoso [2]	RDBMS	N/A	N/A
Oracle	N/A	N/A	N/A
GraphDB [1]	N/A	N/A	N/A

Brodt et al. [7] extended RDF-3X [24] to support spatial data. In this work, the range selection operation is the only spatial operation supported leading to very limited extension. Moreover, the spatial filtering is also limited to either at the beginning of the query evaluation or at the end of the query. Geo-Store [34] is another spatial extension of RDF-3X. Geo-Store relies on a grid file to index the spatial data. The Hilbert space-filling curve is used to establish a global order for each cell on the grid. Each spatial object will be pared in the order of the cell that it resides in. An additional triple is added to the data graph in the following form: $< o, hasPosition, gridPosition >$. The additional triple leads to an additional join step while processing the queries. Note also that spatial RDF queries are also supported by many commercial systems, such as Oracle, Virtuoso [2], and GraphDB [1]. However, details about their internal design are inaccessible.

3. Background and Preliminaries

This section introduces the principle of Spatial DataBase Management Systems (SDBMS), some main formal definitions related to RDF graph management and an overview of the architecture of the RDF_QDAG Triplestore.

3.1. SDBMS Systems: A refresher

SDBMS systems are database systems that support spatial data types in their models, their query languages and provide efficient ways to process spatial operations [12]. The term spatial data types refers to every data object that contains coordinates in some multi-dimensional metric space. SDBMSs are considered as the basis of Geographic Information Systems (GIS) and many computer-assisted design systems (CADs).

Spatial information can be represented in two different ways: Raster or Vector [30]. Raster data refer to an array or a matrix where each cell (pixel) represents a rectangular region. Vectors represent object features in the form of geometric shapes. In this work, we focus on vector representation.

In addition to storing spatial data, SDBMs need to perform spatial operations to answer queries. Spatial queries can be categorized into nearness queries, region queries and join queries. Nearness queries allow to find objects close to a certain point. While region queries aim at finding objects that reside fully or partially in a certain region. Finally, the join queries are operations that allow to filter the Cartesian product of two datasets based

on a given condition (i.e., Boolean expression). In the case where the condition implies a spatial operation, this join is called a spatial join.

In most geographic information systems, we rarely find only spatial data. We generally find other plane standard data types (i.e strings, doubles ...). These data types also need to be stored, queried and updated. A common way SDBMS fulfill this need is by using the relational model. The combination of the relational model with the spatial data has been well studied in the literature [11, 31]. However, combining spatial data with graph model has been little studied. The advantage of using a graph model is the ability to store data without passing by a schema, giving more flexibility for the information systems.

3.2. RDF graph formalisation

In this work, we propose a system capable of handling Spatial and graph data represented by means of RDF format. Data in RDF are represented using triples called SPO triples (subject, property, object). Subjects are identified by a Uniform Resource Identifier (URI). The property represents the relationship between the subject and the object. The object of a triple can be either the subject of another triple or just a simple data value called a literal. Following this format, we can represent data as a graph where the nodes are subjects/objects and the edges are the proprieties. Below, we provide some formal definitions on RDF graph necessary for the reading of the next sections.

Definition 1. *(RDF graph) An RDF graph is a four-tuple* $G = \langle V, L_V, E, L_E \rangle$*, where*

1. V *Is a collection of vertices that correspond to all subjects and objects in RDF data. The set* V *can be divided into* V_l *and* V_e *where* V_l *is the set of literal vertices and* V_e *is the set of entity vertices.*
2. L_V *is the set of vertex labels. The label of a vertex* $u \in V_l$ *is its literal value, and the label of a vertex* $u \in V_e$ *is its corresponding URI.*
3. $E = \overrightarrow{u_1, u_2}$ *is a collection of directed edges that connect the corresponding subject and objects.*
4. L_E *is a collection of edge labels. Given an edge* $e \in E$*, its edge label is its corresponding property.*

To query RDF data, we use SPARQL [26]. It is a query language that expresses queries using a basic graph pattern (BGP) containing variables. The answer to the query is the mappings of the variables where a sub graph from the data matches the graph pattern of the query. Filters can be added to the query in order to express some conditions on the graph elements. The following is a formal definition of a SPARQL query:

Definition 2. *(Query graph) A query graph is a five-tuple* $Q = \langle V^Q, L_V^Q, E^Q, L_E^Q, FL \rangle$*, where*

1. $V^Q = V_e^Q \cup V_l^Q \cup V_p^Q$ *is a collection of vertices that correspond to all subjects and objects in a SPARQL query, where* V_p^Q *is a collection of parameter vertices, and* V_e^Q *and* V_l^Q *are collections of entity vertices and literal vertices in the query graph* Q *respectively.*
2. L_V^Q *is a collection of vertex labels in* Q*. A vertex* $v \in V_p^Q$ *has no label, while that of a vertex* $v \in V_l^Q$ *is its literal value and that of a vertex* $v \in V_e^Q$ *is its corresponding URI.*

3. *E^Q is a collection of edges that correspond to properties in a SPARQL query. L_E^Q are the edge labels in E^Q.*
4. *FL are constraint filters, such as a wildcard constraint or a spatial constraint.*

When storing spatial data using the RDF format, spatial information is stored in the literals. As a consequence, to express spatial operations, it is necessary to use spatial functions in the filter part of the query. There are many extensions to the SPARQL language to support spatial filters. Here, we rely on the GeoSPARQL standard [4] defined by the Open Geospatial Consortium (OGC). It extends both RDF and SPARQL to express spatial information and queries. See also stSPARQL [19] for a similar set of features.

3.3. Architectural overview of RDF_QDAG

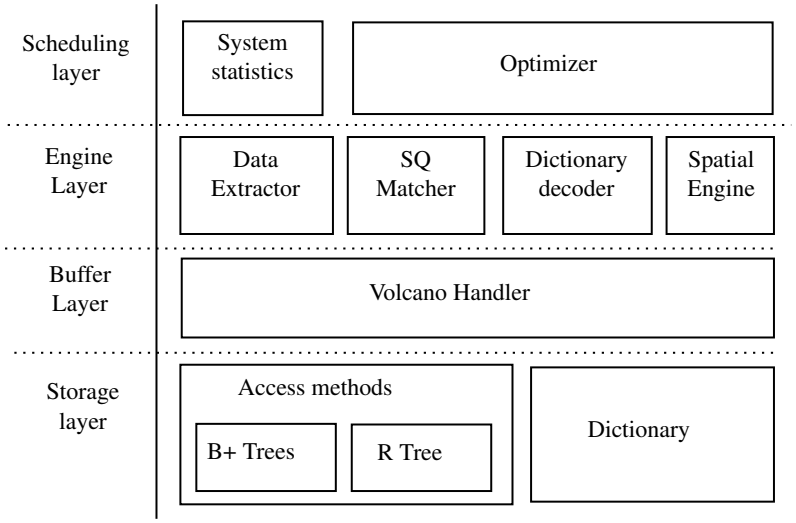

Fig. 1. Architectural overview of RDF_QDAG

RDF_QDAG [17] is composed of several layers. Each layer contains many components, as shown in figure 1. In this section, we present the overall architecture of the system and we detail the process of query evaluation.

Data storage The storage layer in RDF_QDAG is responsible for efficiently storing and accessing different types of data, mainly Graph and Spatial data. We note that data in RDF_QDAG support many native data types such as Strings, Integers, Doubles and more. To efficiently query all types of data, RDF_QDAG uses mainly three access methods B+tree, R-tree and a Dictionary.

The main storage of the graph data is the B+Tree. In order for the graph to be stored without losing the semantics that relies in the edges of the graph (Predicates in case of RDF), the graph should be partitioned into graph fragments while taking the connectivity

between them into account. The ideal graph partitioning strategy is the one that maximizes inter-partition connectivity and minimizes intra-partition connectivity.

Each graph fragment is a grouping of Data Stars. Data stars extend the notion of tuple in the relational model. We define data stars formally as:

Definition 3. *(Data Star) Given a node x (named data star head) in a RDF graph G, a Data Star $DS(x)$ is the set of either triples sharing the same subject x, or the same object x. We name Forward Data Star and Backward Data Star the sets $\overrightarrow{DS}(x) = \{(x,p,o)|\exists_{p,o} : (x,p,o) \in G\}$ and $\overleftarrow{DS}(x) = \{(s,p,x)|\exists_{s,p} : (s,p,x) \in G\}$ respectively.*

If we compare the notion of data star with the notion of tuple, the primary key of a tuple corresponds to the head x of a data star $DS(x)$. RDF_QDAG groups similar data stars into sets called *Graph Fragments* using characteristic sets [23]

Each subject s in the graph G has a characteristic set defined as $\overrightarrow{cs}(s) = \{p|\exists_o : (s,p,o) \in G\}$. Similarly, for objects, $\overleftarrow{cs}(o) = \{p|\exists_s : (s,p,o) \in G\}$. A forward graph fragment $\overrightarrow{Gf}$ groups forward data stars with the same characteristic set. The backward graph fragments $\overleftarrow{Gf}$ are formed identically. The formal definition of this concept is given in definition 4

Definition 4. *(Graph Fragment) A Graph Fragment is a set of Data Stars. It is named a Forward Graph Fragment $\overrightarrow{Gf}$ if it groups Forward Data Stars such that:*

$$\overrightarrow{Gf} = \{\overrightarrow{DS}(x)|\forall_{i \neq j} \overrightarrow{cs}(x_i) = \overrightarrow{cs}(x_j)\}.$$

Likewise, a Backward Graph Fragment $\overleftarrow{Gf}$ is defined as

$$\overleftarrow{Gf} = \{\overleftarrow{DS}(x)|\forall_{i \neq j} \overleftarrow{cs}(x_i) = \overleftarrow{cs}(x_j)\}.$$

Once the graph is partitioned into graph fragments, each fragment is loaded into an index. The index used in the case of RDF_QDAG is a B+tree. The efficiency of this type of index is well studied for this type of graph data [17]. Also compression techniques are used to optimize the space usage for storage and the number of pages loaded into the buffers while evaluating queries.

In the context of optimizing space usage, Subject and Object of the graph that are of type String or URI are replaced with an ID. Otherwise, the size of the fragments will be significant. Especially since the values of subjects/objects may figure many times in the fragments. However, this technique necessitates a dictionary to store $< value, ID >$ combinations. Moreover, an additional encoding and decoding step is required to evaluate each query.

The third and the last access method is a spatial access method (namely R-tree) that we added in the context of this work as an extension of RDF_QDAG to support spatial queries. More details on spatial indexing are in section 4.

Scheduling Layer The main component of the scheduling layer is the optimizer. The optimizer has the role of selecting the best execution plan for a given query. This process

is divided into two steps: (i) plan enumeration and (ii) cost estimation. The plan with the lowest estimated cost is the one chosen by the optimizer for evaluation.

The nature of the plan depends on the system design. In classical systems, a plan can be considered as a sequence of join operations on triple patterns. However, in RDF_QDAG, the notion of data star is proposed as an equivalent of tuple in the relational model. In a similar fashion, the notion of a star query is proposed. Indeed, triple patterns with the same Subject or Object are grouped together as a forward or a backward data star.

Definition 5. *(Query Star) Let Q be the SPARQL query graph. A Forward Query Star $\overrightarrow{QS}(x)$ is the set of triple patterns such that $\overrightarrow{QS}(x) = \{(x,p,o)|\exists_{p,o} : (x,p,o) \in Q\}$, x is named the head of the Query Star. Likewise, a Backward Query Star $\overleftarrow{QS}(x)$ is $\overleftarrow{QS}(x) = \{(s,p,x)|\exists_{s,p} : (s,p,x) \in Q\}$. We use $\overrightarrow{QS}, \overleftarrow{QS}$ to denote the set of forward and backward query stars and qs to denote indistinctly a forward and backward query star.*

An execution plan is an order function applied on a set of Query Stars and Filter Unites. The function denotes the order in which the mappings for each Query Star will be found and the order in which the filter unit will be evaluated

Definition 6. *(Execution Plan) . We denote by $\mathcal{P} = [QS_1, QS_2, Fu_1(p_1,p_2), ..., QS_n]$ the plan formed by executing QS_1, then QS_2, then evaluating the filter unit $Fu_1(p_1,p_2)$ which requires the mappings of p_1 and p_2 parameters.*

Engine Layer The engine layer is the layer responsible of evaluating the query. More precisely, it is responsible of evaluating the optimal plan provided by the optimizer.

The evaluation of a Query Star consists of finding matches between the variables of the Query Star and the nodes of the data graph. For each triple in the star, we seek the set of mappings, that satisfies it. Next, we merge the mappings related to the triples to build the Query Star matches.

Definition 7. *(Star Query Evaluation) The evaluation of a Query Star $QS(x)$ against the graph G is formally defined as follows:*

$$[\![QS(x)]\!]_G := \{[\![tp_1]\!]_G \bowtie [\![tp_2]\!]_G \bowtie ... \bowtie [\![tp_n]\!]_G | n = card(QS(x))\}$$

where:

$$[\![tp_i]\!]_G \bowtie [\![tp_j]\!]_G = \{\mu_l \cup \mu_r | \mu_l \in [\![tp_i]\!]_G \text{ and } \mu_r \in [\![tp_j]\!]_G, \mu_l \sim \mu_r \text{ and } \mu_l(tp_i) \neq \mu_r(tp_j)\}$$

We denote that a mapping μ is a function $V_p^Q \rightarrow V^G$. Given two mappings μ_1 and μ_2, $\mu_1 \sim \mu_2 \Rightarrow \mu_1(?x) = \mu_2(?x)$.

Based on the previous definitions, we can determine the evaluation of a query using the set of query stars, as follows:

Definition 8. *(Query Evaluation) Given a set of stars, $\{qs_1, qs_2, ..., qs_n\}$,that cover the query, $Triples_q(qs_1) \cup Triples_q(qs_2) \cup ... \cup Triples_q(qs_n) = Triplets(q)$, the evaluation of the BGP part of the query q using the set of query stars is defined as follows:*

$[\![q]\!]_G = \{\mu : \forall \mu \in [\![qs_1]\!]_G \bowtie [\![qs_2]\!]_G \bowtie ... \bowtie [\![qs_n]\!]_G \}$

We can also set the query BGP evaluation based on fragments, as follows:

$[\![q_g]\!]_G = \{\mu : \forall \mu \in \bigcup_{Gf \models qs_1} [\![qs_1]\!]_{Gf} \bowtie \bigcup_{Gf \models qs_2} [\![qs_2]\!]_{Gf} \bowtie ... \bowtie \bigcup_{Gf \models qs_n} [\![qs_n]\!]_{Gf}\}$
Where $Gf \models qs$ *iff* $cs(qs) \subset cs(Gf)$

The full evaluation of the query is the evaluation of the BGP part and the filters FL *and it is defined as follows*

$[\![q_g]\!]_G = \{\mu : \forall \mu \in [\![qs_1]\!]_G \bowtie [\![qs_2]\!]_G \bowtie ... \bowtie [\![qs_n]\!]_G | \mu \models FL\}$

```
SELECT ?p
WHERE {
?p <hasArea> ?a .
?p <isLocatedIn> ?l .
?l <hasGeometry> ?g .
};
```

Listing 1.1. Example of simple RDF query (Q_1)

An execution plan $\mathcal{P}$ is called an Acceptable Execution Plan if it fulfills the following conditions:

1. *Coverage:* All nodes and predicates of the given query are *covered* by the set of Query Stars of the plan.In the case of Query Q_1 the execution plan $[\overleftarrow{?l}, \overrightarrow{?p}]$ is not an acceptable plan since it does not cover the edge $< hasGeometry >$ and the variable $?g$.
2. *Instantiated head:* This condition guarantees that for a plan $\mathcal{P} = [QS_1, ... , QS_n]$, $\forall_{i>1} QS$, the head of the QS_i must be already instantiated. We use this condition to avoid to a Cartesian product when mappings are exchanged between two star queries. For example, in the case of Query Q_1 the execution plan $[\overleftarrow{?l}, \overleftarrow{?g}, \overrightarrow{?p}]$ is not an acceptable plan since the mapping of $?g$ is not yet available for the second $\overleftarrow{?g}$ to be evaluated. In this case the instantiated head condition is not satisfied.

The formal definition of an Acceptable Plan is given in Proposition 9.

Definition 9. *(Acceptable Plan)* $\mathcal{AP}$ *Let us consider* Q *as a given query,* $\overrightarrow{QS}$ *and* $\overleftarrow{QS}$ *as the sets of forward and backward graph star queries respectively,* T *has the set of triple patterns and the following functions:*

- *Tr:* $Q \cup \overrightarrow{QS} \cup \overleftarrow{QS} \rightarrow T$ *It returns the set triple patterns of a query star or a query.*
- *Nd:* $\overrightarrow{QS} \cup \overleftarrow{QS} \rightarrow V$ *It returns the nodes of a query star (subject or object).*
- *Head:* $\overrightarrow{QS} \cup \overleftarrow{QS} \rightarrow V$ *a function that returns the head of a query star.*

An ***acceptable plan*** $\mathcal{AP}$ *is a tuple* $< X, f >$ *where* $X \subset \overrightarrow{QS} \cup \overleftarrow{QS}$ *and* $f : X \rightarrow \{1...|X|\}$ *is the query stars order function such that:*

1. $\bigcup_{QS \in X} Tr(QS) = Tr(Q)$
2. $\forall i \in \{2...|X|\}, Head(f^{-1}(i)) \in \bigcup_{j=1}^{i-1} Nd(f^{-1}(j))$

4. Query Evaluation Strategies

In this section, we present two evaluation strategies for Geo-SPARQL queries which are implemented in RDF_QDAG. In order to better illustrate those strategies, we show the processing of the example query Q2 on the dataset D1.

```
PREFIX gv: <http://geovocab.org/geometry#>
PREFIX ogis: <http://www.opengis.net/ont/geosparql#>

select ?g
where {
    ?o type "cultural".
    ?o gv:geometry ?p.
    ?p ogis:asWKT ?g.
    FILTER( bif:st_intersects(
        bif:st_geomfromtext( "POLYGON((7 43, 8 43,
        8 44, 7 44, 7 43))" ), ?g ) )
};
```

Listing 1.2. Example of spatial selection query (Q_2)

Table 4. Example of RDF triples (dataset D1).

Subject	Predicate	Object
Tennis Championship	hostedIn	Paris
Tennis Championship	type	Sports
Tennis Championship	geometry	G1
G1	asWKT	Point(2.34 48.85)
Festival of Lights	hostedIn	Lyon
Festival of Lights	type	Cultural
Festival of Lights	geometry	G2
G2	asWKT	Poit(4.846 45.75)
Film Festival	hostedIn	Cannes
Film Festival	Type	Cultural
Film Festival	geometry	G3
G3	asWKT	Point(7.012 43.55)

It is worth noticing that the existing formal framework for query plan and query evaluation do not take the filters into consideration. Previous contributions have focused on the graph matching aspect of the query evaluation. The filters were considered as an implementation detail. However, to introduce support for spatial filters, the existing formal definitions need to be extended to consider the spatial operators used in the filter clause of the query.

As we mentioned in definition 2, the Filter function FL is a truth function. We then express this function in a conjunctive normal form. We also introduce the concept of filter units as the operands of the mentioned conjunction.

Definition 10. *(Filter Unit)*

Let P be a subset of query parameters $P \in \mathcal{P}(V_p^Q)$. and qs_p the parameters of the star query qs. A filter is a truth function $FL : [\![q_g]\!]_G \rightarrow \{0,1\}$. Filter function can be expressed as a conjunction of operands. We name each operand a filter unit Fu.

$$FL = Fu_1 \wedge Fu_2 \wedge ... \wedge Fu_n$$

Using this concept of filter units Fu, one can see that the definition of an execution plan is extended. In the previous definition, the execution plan is a sequence of star query evaluation. While this is sufficient to perform the graph matching, it is not enough to consider the filters. In the new definition of the plan, we consider two types of operators: the classical star query evaluation and the new filter unit evaluation.

Definition 11. *(Execution Plan - extended definition) .Let $\mathcal{P}$ be a tuple $< X, f >$ where $X \subset \overrightarrow{QS} \cup \overleftarrow{QS} \cup FL$ and $f : X \rightarrow \{1...|X|\}$ is the query stars order function.*

We denote by $\mathcal{P} = [QS_1, QS_2, Fu_1(p_1, p_2), ..., QS_n]$ the plan formed by executing QS_1, then QS_2, then evaluating the filter unit $Fu_1(p_1, p_2)$ which requires the mappings parameters p_1 and p_2.

As mentioned before, to ensure a graph exploration logic, not all plans are acceptable. An execution plan is considered acceptable if, starting from the second star query, the head of the star is already instantiated. In a similar fashion, the position of the filter unit is critical. We can execute a filter unit only if the mappings for the parameters of the filter units are already available. On this principle, we extend the definition of an acceptable plan using the following condition:

Definition 12. *(Instantiated filter unit parameter) Let consider the function Param: $FU \rightarrow V_p$ a function that returns the parameters of a Filter Unit. An acceptable plan $\mathcal{AP}$ is a tuple $< X, f >$ where $X \subset \overrightarrow{QS} \cup \overleftarrow{QS} \cup FL$ and $f : X \rightarrow \{1...|X|\}$ is the query stars order function such as $\forall i \in \{2...|X|\}, Param(f^{-1}(i)) \in \bigcup_{j=1}^{i-1} Nd(f^{-1}(j))$.*

To provide a better explanation of the concept of an acceptable plan, let's consider query Q_2, which contains the following star queries in the BGP: $\overleftarrow{?g}$, $\overrightarrow{?p}$, $\overleftarrow{?p}$, $\overrightarrow{?o}$, and $\overleftarrow{?o}$. The filter function consists of a single filter unit, $Fu(?g) =?g \neg DC"POLYGON((-100...20))"$. There are many possible execution plans for this query, but not all of them are acceptable. For example, the plan $[\overrightarrow{?o}, \overleftarrow{?g}, Fu(?g)]$ is not acceptable because we need mappings of $?g$ to be able to evaluate $\overleftarrow{?g}$. The existence of such mappings is mandatory for all star queries except the first one. This is an example of a plan that does not satisfy the instantiated head condition explained in Section 3. Additionally, the plan $[\overrightarrow{?o}, Fu(?g), \overrightarrow{?p}]$ is not acceptable because, after evaluating $\overrightarrow{?o}$, the mappings of $?g$ are not yet available to process the spatial filter $Fu(?g)$. In this case, the condition of instantiated filter unit condition (definition 12) is not satisfied.

An example of an acceptable plan of the query $Q2$ is $[\overrightarrow{?o}, \overrightarrow{?p}, Fu(?g)]$ or $[\overleftarrow{?g}, Fu(?g), \overleftarrow{?p}]$. To evaluate acceptable plans, two strategies are discussed: BGP-First strategy and Spatial-First strategy.

4.1. BGP-First strategy

This strategy consists of finding matches for the graph pattern first, before proceeding to run the filter on the results of the matching process. An example of a plan where this strategy can be considered is the following $AP_1 = [\overrightarrow{?o}, \overrightarrow{?p}, Fu(?g)]$.

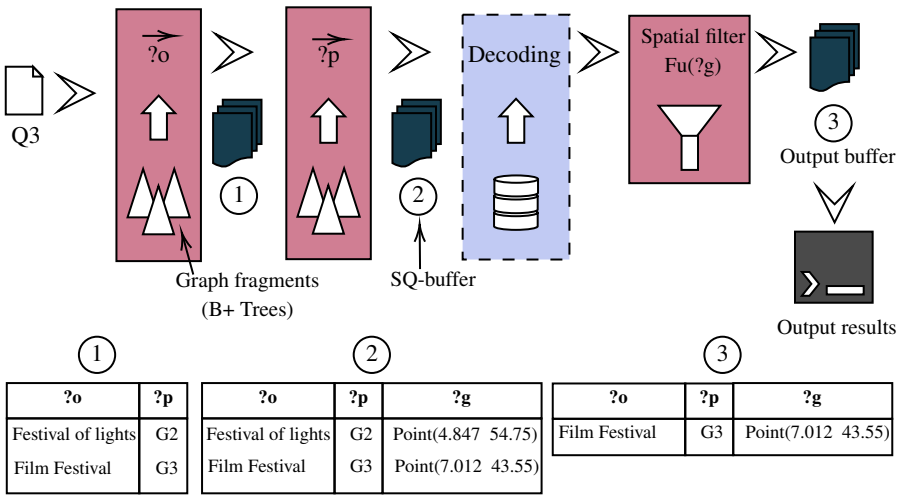

?o	?p
Festival of lights	G2
Film Festival	G3

?o	?p	?g
Festival of lights	G2	Point(4.847 54.75)
Film Festival	G3	Point(7.012 43.55)

?o	?p	?g
Film Festival	G3	Point(7.012 43.55)

Fig. 2. The execution of an BGP-First plan

The sequence of star queries and filter units listed in the logical execution plan does not consider implementation details. Therefore, we illustrate the full execution in figure 2. First, the graph matching part of the query is evaluated. Appropriate graph fragments are considered for evaluating each star query. Data in each fragment is stored in a B+tree in order to efficiently retrieve it from the disk. Once the information needed is retrieved, it is placed in a buffer, named SQ-buffer, so it can be used by the following operator in the plan.

The same logic is applied to spatial values. The true objects shapes can be significantly large depending on the geometry of the object (values describing Polygons are larger than values describing points for example) and on the resolution used to represent the object. To keep the size of the database low, and to maintain system performance, true shapes are stored in the dictionary.

Once the shapes are retrieved from the dictionary, the filter function FL is evaluated. In the case of $Q2$, the filter function is composed of a single filter unit $Fu(?g)$. This latter is evaluated in two steps (filter and refine). The Algorithm 1 is an example of an intersection filter without any loss of generalization to other region connection calculus operations. In the filter step, only MBRs of the shapes are considered (line 4) to significantly reduce the search space. The refining step considers the full geometry (line 11 and 12) hence, it is computationally expensive. However, it is necessary to eliminate false positives from the previous step.

Algorithm 1: Intersection Filter (L, Qb, Q)

Data: M: List of mappings;
s: Spatial object;
use_true_shape: flag to use true shape;
Result: Q: The set of mappings that intersect s

$Q \leftarrow \emptyset$;
for $m \in M$ **do**
  $(MBR(m), m) \leftarrow decode(m)$;
  if $MBR(m) \neg DCMBR(s)$ **then**
    add m to Q;
    continue;
  if m *is a point* **then**
    continue;
  if $use\_true\_shape = false$ **then**
    continue ;
  $GEO_m \leftarrow$ parseGeometry(m);
  if $GEO_m \neg DCs$ **then**
    add m to Q;
end
return Q;

4.2. Spatial-First strategy

The BGP-First strategy presented above can answer spatial-RDF queries and can be easily integrated into the execution model of RDF_QDAG. However, it has some limitations that we discuss in this section. In this section, we introduce the second proposed strategy Spatial-First.

When we consider the same example query $Q2$ with the same dataset $D1$, one can observe that multiple valid plans can be run to answer the query. We can list a few of them as an example: $[\overrightarrow{?o}, \overrightarrow{?p}, Fu(?g)]$, $[\overleftarrow{cultural}, \overrightarrow{?o}, \overrightarrow{?p}, Fu(?g)]$, $[\overleftarrow{?p}, \overrightarrow{?p}, Fu(?g), \overrightarrow{?o}]$. All the listed plans have a common problem. Since the filter unit relies on the execution of the previous query stars, values of the geometry need to be obtained from the dictionary. As a result, it is impossible to use any spatial access method to speed up the spatial filter evaluation.

In the Spatial-First strategy, we try to take advantage of a spatial access method. To do so, we can only consider execution plans that start with the spatial filter. In the case of query $Q2$, the plan we consider is the following $[Fu(?g), \overleftarrow{?g}, \overleftarrow{?p}, \overrightarrow{?o}]$. As before, the spatial filter is run using two steps. However, this time, the filtering step can benefit from the spatial index.

The structure of the spatial index we use is an R-tree with some modifications for better integration with RDF_QDAG. The R-tree stores only object approximations in the form of MBRs with the necessary information to continue the graph exploration. This ensures the efficiency of the first step of the spatial filter by minimizing the number of pages. The page size in the index is 16 Kb. The structure of the pages is demonstrated in the figure 3.

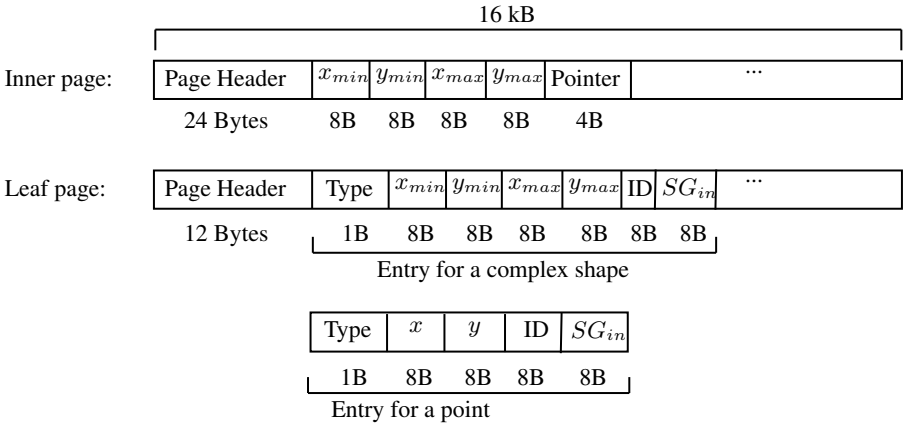

Fig. 3. The structure of index pages and entries

For inner pages, we save 24 bytes as page header. The rest is filled with inner entries where each entry is composed of an MBR (4 X 8 bytes) as a key and pointer to the appropriate page (4 bytes). An inner page can have up to 454 entries.

As for the leaf pages, we keep two types of entries: Points and MBRs. The MBRs are generally approximations of complex geometries. A point is represented by two coordinates (x, y) and an MBR is represented by four $(x_{min}, y_{min}, x_{max}, y_{max})$. On the leaf page, we save 12 bytes as page header, the rest is filled with leaf entries. For each entry, we store the object type in 1 byte, then we store the key, which is a point/MBR in 2*8/4*8 bytes, respectively, the object id in 8 bytes and the inward pointing fragment ID also in 8 bytes. The fragment ID is used to continue with the graph exploration. A leaf page can hold from 334 to 496 entries depending on the object types.

In the example shown in figure 4, only geometries $?g$ where $MBR(?g)\ \neg DC\ MBR(q)$ are returned after the exploration of the index. The next operator in the plan is standard graph exploration matchings.

At the end of the evaluation, the decoding operation is performed to replace object IDs with the true value. The same is applied to spatial data where MBR approximation is replaced using the true geometries. Once the full shapes are available (true geometries) the refining step can be performed in the same way as in the BGP-First strategy.

5. Optimization Techniques

In this section, we present details about some optimization techniques that we propose to further improve execution time for both proposed strategies.

5.1. Query scheduling

A typical DBMS can answer the same query using different execution plans. All the plans provide the same results, however, the cost of execution for each plan is different. The

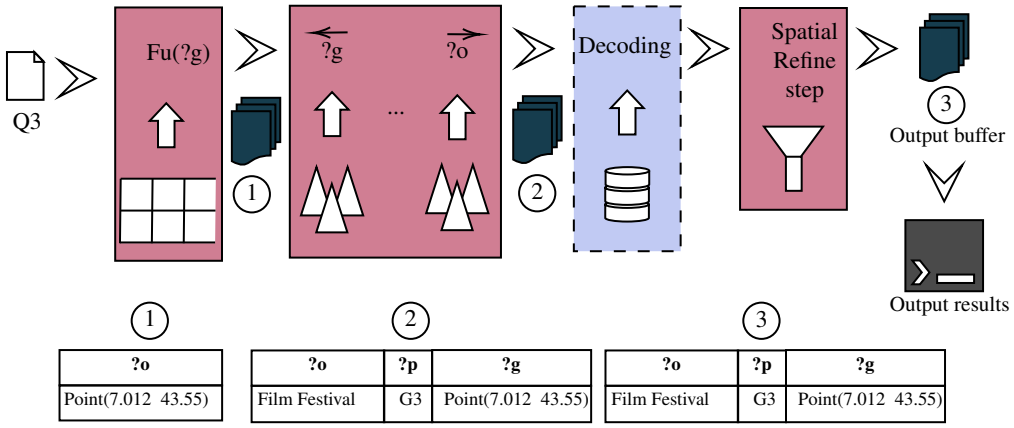

Fig. 4. Execution of Spatial-First strategy

same logic applies for RDF_QDAG. In the case of the latter, an execution plan is a sequence of SQ and Filter units. Since the execution time can vary significantly from a plan to another, it is important to choose the best execution plan for a given query.

A traditional approach to select the best plan is to use two steps: plan enumeration and cost estimation. In the plan enumeration step, we list all the possible execution plans. However the number of execution plans can be very significant, so enumerating all the plans is either not possible or not efficient. Many DBMS use a heuristic approach to enumerate only the most promising plans. In the cost estimation step, we estimate the cost of executing each plan to select the plan with the lowest possible cost. This is generally done using dynamic programming since many plans share some parts between each other and it is not reasonable to recalculate the cost of the same plan segment multiple times.

RDF_QDAG uses the GOFast approach for the optimization [39]. In this approach, both the enumeration and estimation are performed in parallel. In order to do so, authors rely on a branch and bound algorithm. They start by constructing a tree where each node represents the accumulated cost of all previous operations and the edges represent plan operations. Naturally, the cost in the root is 0. The algorithm starts by estimating the cost of all possible first operations, then it expands on the operation with the lowest cost. GoFast continues on expanding the branch with the least cost until it gets a full execution plan.

Estimation in GoFast is based on the statistics collected for each graph fragment. The statistics also make it possible to reflect the interaction.

The existing GOFast optimization does not take into account the filters since the majority of the cost is caused by the graph exploration. However, this is not the case for the spatial filters since the cost of comparing complex shapes is high. On top of that, the use of an additional access method (R-tree) must be accounted for calculating the cost. Consequently, we extend the existing logic in order to take into account the cost of filter units. The cost of a plan is mainly the sum of cost of all star queries (both normal and spatial ones):

$$Cost(\mathcal{P}) = \sum_{qs \in \mathcal{P}} Cost(qs) \tag{1}$$

The estimation of the cost of star query is already part of RDF_QDAG system, however we changed it to be calculated in terms of triples not in terms of data stars. We opted for this change since the number of data star did not show (see appendix) a correlation with the choice of the best plan in the case of spatial queries contrary to the number of triples.

To estimate the full cost of the plan, for each part of the execution plan, two estimations needs to be done: estimation of the input and estimation of the number of results. This is necessary since the estimation of the cost of part of the plan depends on the number of results of the previous parts.

Estimation of the Number of Spatial Objects The estimation of the cost of a star query is already detailed in previous work [39], we will detail only the cost of the filter unit. In the case of an BGP-First plan, no spatial access method is used. In the case of Spatial-First plan, the cost of fu is the number of spatial objects that needs to be retrieved from the index:

$$Cost(fu) = SOC(Q) \tag{2}$$

$SOC(Q)$ is the number of spatial objects estimated using the spatial index. We can do this by taking advantage of the shallow depth of an R-tree. Indeed, since the fan-out is high, the depth is low (generally 4 to 5 layers maximum). In the estimation phase, we scan only the top layers of the R-Tree without loading the leaf layer. Naturally, we count only pointers where the attached key satisfies the filter. To calculate the number of objects ($SOC(Q)$) we simply multiply the number of leaf pages that satisfy the query by the average number of objects in a page. This assumption is based on the fact that most of the pages are close to 100% fill rate since the index is loaded using STR [22] and no updates are performed later. The only limitation of this estimation is the fact that not all objects in the leaf pages satisfy the query.

Estimation of spatial filter results .

The estimation of the number of results after the filter is necessary for the rest of the process. The number of objects $SOC(Q)$ can be considered as an estimation of the number of results since it is an estimation of objects where the MBR satisfies the spatial filter. However, to be able to continue calculating the cost with the GOFast approach for the rest of the plan, the total number of objects is insufficient. We need to calculate an estimation of the number of objects for each fragment.

The cost of a plan $\mathcal{P}$ is calculated in terms of the number of triples that need to be retrieved from the disk since the disk cost is the most important cost of the query. The cost of a particular plan is the sum of the cost of all star queries sq_i that compose the plan (equation 1). The cost of a star query is the number of triples retrieved from the relevant fragments fg_j:

$$Cost(qs) = \sum_{fg_j \in sq} Input\_Tr(fg_j, sq) \tag{3}$$

In the case of the first star query, no previous input is needed. As a consequence, the number of triples retrieved from a particular fragment fg_j is simply the number of triples in the fragment that satisfy the predicates of the star query:

$$Input\_Tr(fg_j, sq_1) = \#triples(fg_i, prd(sq_1)) \tag{4}$$

However for the rest of the star queries, the number of triples retrieved from a particular fragment fg_j is calculated using:

- $\#tripls(fg_j, pred(sq_i))$: the number of triples that satisfy the predicates of the star query sq_i
- $Input\_Ds(fg_j, sq_i)$: the number of data stars considered as in input
- $dist(fg_j)$: the number of data stars in the fragment fg_j

The formula for calculating the number of triples retrieved in case $i > 1$ is the following:

$$Input\_Tr(fg_i, sq_i) = \frac{\#triples(fg_i, pred(sqi)) * Input\_Ds(fg_)}{dist(fg_j)} \tag{5}$$

Detailed calculation of $Input_Ds(fg_j, sq_i)$ and $dist(fg_j)$ is found in Zouaghi et al[39] since we did not change it. As for the number of triples retrieved from a particular fragment it is the sum of all triples in the fragment where the predicate is the same as one of the star query predicates:

$$\#triples(fg_i, prd(sq_1)) = \sum_{P_j \in Pred(sq_i)} count(pj, fg) \tag{6}$$

In the case of Spatial-First plan, the number of triples is identical to the number of spatial objects estimated for each fragment :

$$Input\_tr(fg_i, SQ_1) = \#releventObject(fg_j/Q) \tag{7}$$

The number of spatial objects estimated for each fragment is estimated based on the selectivity of the spatial query as follows:

$$\#releventObject(fgj/Q) = size\_of(fg_j) * S\_select \tag{8}$$

Where $size\_of(fg_j)$ is the total number of triples in the fragmentfg_j and the spatial selectivity (S_select) is calculated as follows:

$$S\_select = \frac{SOC(Q)}{total\_spatial} \tag{9}$$

Where $total\_spatial$ is the total number of spatial objects stored in the index.

On top of the estimation of the number of relevant triples to read from disk, GoFast optimizer also relies on the number of results produced by each star query $outpu\_DS_{sqi}$ defined in [39] as follows:

$$output\_DS_{qs_i} = \{(Gf_j, p_i, k'') | p_i \in edges(qs_i) \wedge k'' = NDS_{p_i}\} \tag{10}$$

Where NDS_{p_i} is the number of data stars heads relevant to the predicate pi

However, we had to change the calculation of NDS_{p_i} to take into account the spatial filters. The new formula is the following:

$$NDS_{p_i} = \begin{cases} 1 & , if\ e.node\ is\ const \\ \frac{k'}{dist(Gf_j)} * dist\_NE(p_i, Gf_j) * S\_select & , otherwise \end{cases} \quad (11)$$

Where $dist\_NE(p_i, Gf_j)$ is the number of distinct nodes linked to the data star head in fg_j with respect to the predicate p_i.

With both estimations of the number of spatial objects and the spatial filter results, the GoFast optimizer can choose the best execution plan for Spatial-RDF queries.

5.2. Spatial pruning

Earlier, we proposed two execution strategies, "BGP-First" and "Spatial-First", of which only the latter can benefit from a spatial access method. The "BGP-first" strategy lacks spatial awareness at the beginning of the process, which means that it misses opportunities to reduce the search space based on spatial constraints. To address this issue, we propose a new optimization technique called "Spatial pruning".

As discussed in section 3, the initial RDF graph is partitioned into graph fragments $\mathcal{GF}$ for indexing and storage. When evaluating a query, only the necessary fragments are considered based on the characteristic sets of each fragment. However, when a query contains a spatial filter, many fragments that are considered due to their characteristic sets do not contribute to the final results. This is because the spatial filter in the query eliminates all the graph patterns produced by these fragments since they are connected to spatial objects that do not satisfy the filter.

To eliminate fragments that do not contribute to the results earlier in the process, we associate each graph fragment to an MBR such as all spatial objects connected to the fragment are situated inside this MBR. When processing the query, the optimizer do not choose fragment based on the graph part only, but also based on the spatial filter. If the MBR of a fragment ($MBR(Fg)$) satisfies the filter, it can contain the results. However, if the MBR does not satisfy the filter, it is immediately pruned and not considered while evaluating the query.

The proposed algorithm 2 operates on a set of star queries specified in a query plan. The algorithm iterates through each star query in the plan (line 3). For each star query, the relevant fragments are obtained based on the characteristic set (line 4). These fragments are then linked to the fragments of the previous star query using the function LinkToPreviousFragments() (line 5). If the current star query does not contain a spatial filter (line 6), the algorithm proceeds to the next star query (line 7). However, if the current star query contains a spatial filter (line 6), the algorithm loops through each fragment while testing the intersection of the fragment's Minimum Bounding Rectangle (MBR) with the query (line 9). If there is no intersection between the fragment's MBR and the query (line 10), the fragment and all fragments linked to it are removed from further consideration (line 11).

Algorithm 2: Spatial pruning

Data: $\mathcal{P}$: Execution Plan
$\mathcal{GF}$: Set of graph fragments
$SF : Gf_s \rightarrow MBR(Gf_s)$: List of spatial fragments MBRs
Result: Gfs : qs $\rightarrow \mathcal{GF}_{Sq} | \mathcal{GF}_{Sq} \subseteq \mathcal{GF}$:Set of fragment for each Sq

```
Gfs ← [];
QS ← getQSList(P);
for sq_i ∈ QS do
    CurrentFGs ← getCurrentFragments(sq_i);
    LinkToPreviousFragments(Gfs, CurrentGfs);
    if isSpatialFilter(qs_i) = false then
        continue;
    for fg_i ∈ CurrentFGs do
        MBR_fgi ← SF.getMBR(fg_i);
        if MBR_fgi ¬DCs then
            Gfs.removeAllFGsConnectedTo(fg_i);
    end
end
return Gfs;
```

6. Experimental evaluation

In this section we discuss several experimental results on the various approaches and optimisation techniques mentioned in the previous section. We also compare our proposed solution with a well-known commercial Triplestore Virtuoso.

6.1. Experimental setup and methodology

We perform several experiments on RDF_QDAG after integrating the approach and techniques proposed in this paper. RDF_QDAG is a project developed using Java and C++. The storage and access methods are developed using C++ and compiled using GCC version 7.5.0. The engine and optimizer are implemented using Java 11 and built using maven 3.8.6. For the run environment, we used Open JDK version 11.0.16. The system can be downloaded as a Docker image, which includes all necessary dependencies. The image is available on Docker Hub at https://hub.docker.com/r/qdag/rdf_qdag. In addition, a live demo of the system is provided on our project website at https://qdag.lias-lab.fr/.

All experiments were run on a machine equipped with Intel Xeon (Skylake, IBRS) @ 10x 2.295GHz and 64 GB of RAM and an SSD running Ubuntu 18.04 bionic with linux kernel x86_64 Linux 4.15.0-194-generic.

For the evaluation, we used the YAGO [16] knowledge base. YAGO is a real world data-set that contains more than 234 million facts on which 4 million are spatial objects.

All experiments are performed on a fresh install of the operating system. We clear page cache, dentry and inode cache before each query. Execution time is calculated from the submission of the query to the end of writing the results into an output file.

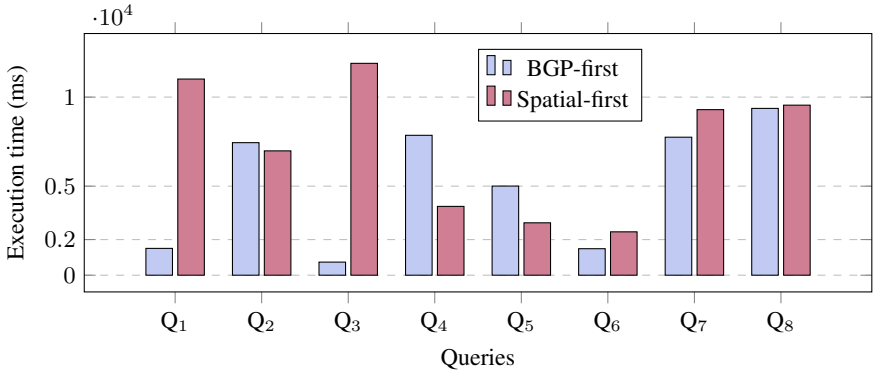

Fig. 5. Execution time (nanoseconds) of queries using both strategies BGP-first and Spatial-first.

Table 5. Execution time of queries on YAGO

Query	Best BGP-First plan			Best Spatial-First plan		
	Plan ID	**Execution time (ms)**	**# Triples**	**Plan ID**	**Execution Time (ms)**	**# Triples**
Q1	1	1506	**32503**	5	11014	463841
Q2	4	7442	238414	6	6981	**144671**
Q3	4	735	**4377**	5	11896	699942
Q4	3	7855	217526	2	3864	**91326**
Q5	4	5005	205310	6	2942	**60374**
Q6	1	1488	**10639**	3	2435	38092
Q7	3	7749	217526	2	9296	**56272**
Q8	1	9366	**369054**	3	9548	438063

6.2. Effect of evaluation strategies

To study the effect of evaluation strategies on the execution time, we ran several queries on the YAGO data-set.

The results of the execution time for queries using the BGP-First and Spatial-first strategies are shown in figure 5. Neither approach consistently outperforms the other, as demonstrated by the varying performance in queries Q_4, Q_2, and Q_5, where the Spatial-first approach is superior, and the remaining queries, in which BGP-first performs better.

To further investigate the factors contributing to the varying performance of each approach, we analyzed intermediary results in both the spatial and graph parts of the queries to extract the total number of triples loaded from the disk. The total number of triples is displayed in table 5. The results in the table show a clear correlation between the choice of the best execution strategy and the number of triples fetched from the disk. In each query, the strategy with the lowest number of triples is the best-performing one. This observation has motivated the improvements of the optimizer and the cost model proposed in section 5.

6.3. Effect of Scheduling

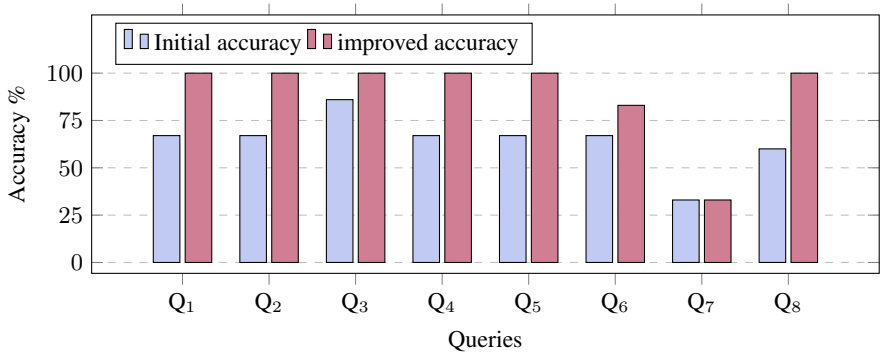

Fig. 6. Initial accuracy and the improved accuracy of the optimizer.

To select the best execution plan and execution strategy, we extended the GoFast optimizer to be able to estimate the cost and number of results of spatial filters. As far as experimental validation goes, we propose to compare the improved version of GoFast with the existing one. For that, we use the accuracy of the best plan prediction as a performance metric. The accuracy of the optimizer for a given query is calculated as follows:

$$A = \frac{\#plans - Rank\_plan}{\#plans - 1} \tag{12}$$

The primary function of an optimizer is to select the optimal execution plan for a given query. To accomplish this, the optimizer assigns a rank to each candidate plan based on an estimation of its cost. The accuracy of the optimizer is measured in terms of the rank

of the true best plan. Specifically, the accuracy is calculated as the proportion of the true best plan's rank among all the candidate plans. A higher rank for the true best plan corresponds to a higher accuracy, with an accuracy of 100% indicating that the optimizer has successfully identified the true best plan as the top-ranked plan. Conversely, an accuracy of 0% would indicate that the optimizer ranked the true best plan as the worst among the candidates.

The figure 6 shows the initial accuracy of Go-Fast and the improved accuracy. As we can notice, the optimizer after the proposed improvements provides a better prediction of the best execution plan. It can find the actual best execution plan for the all of the test queries except $Q6$ and $Q7$. Moreover, even for the latter queries, it provides the same or better accuracy than the original optimizer. This is due to a better estimation of the cost of the spatial filters.

The accuracy of both approaches is plotted in the figure 6. However, more detailed results are in the Appendix where we list the results of estimation of each plan compared to the true cost. We will refer to values form the detailed tables to better explain the results. The accuracy on queries $Q6$ and $Q7$ demonstrates that there is still room for improvement for the optimizer. In $Q6$, the improved optimizer chooses the second best execution plan performing better then the old approach, which choose the third best plan. This is due to the error of estimation. The best plan for $Q6$ is the plan $\mathcal{P}1$ with a real cost of 10639, followed by the plan $\mathcal{P}7$ with a real cost of 7338. The results of the estimation proposed a cost of 9894 for $P1$ and 7338 for $P7$ leading to the choice of $P7$ as the best plan.

We can notice the same problem with the query $Q7$ where the cost of $P3$ is 217526 however it is estimated to be 194145. The gap between the real cost and the estimation is due to the number of objects eliminated with the refinement step in the spatial filter. In the refinement step true shapes are considered and in the case of $Q7$ many objects do not satisfy the spatial filter despite that there MBR approximations do satisfy the latter. On top of that, the number of acceptable plans is very low for $Q7$ (only four acceptable plans, meaning that each error is amplified when using the accuracy metric leading to 33% accuracy.

6.4. Effect of Encoding

As we mentioned in section 3, RDF_QDAG stores data in three types of files: spatial index, graph fragments and dictionary files. The description of a spatial object in a vector format can be long, for example the map of a state or a river. For efficiency, we store the full resolution shape definition in the dictionary. The full value will be replaced by an ID in the graph fragments and with an approximation (MBR) in the spatial index.

For the storage of the spatial object, we have mainly two options: The Well Known Text format (WKT) and the Well Known Binary format (WKB). RDF_QDAG is capable of outputting both representations, however, for the storage format, we experimented with both representations to determine the best encoding format for the system.

In Figure 7, we show the effect of the encoding format on the performance of the queries. We can clearly notice that the WKB encoding outperforms the WKT one for all queries. This is due to the different sizes of the two encoding formats. WKB is generally more compact than WKT, which leads to less I/O cost. On top of that, deserializing the WKB format is more efficient than parsing the WKT format. For RDF_QDAG system, if

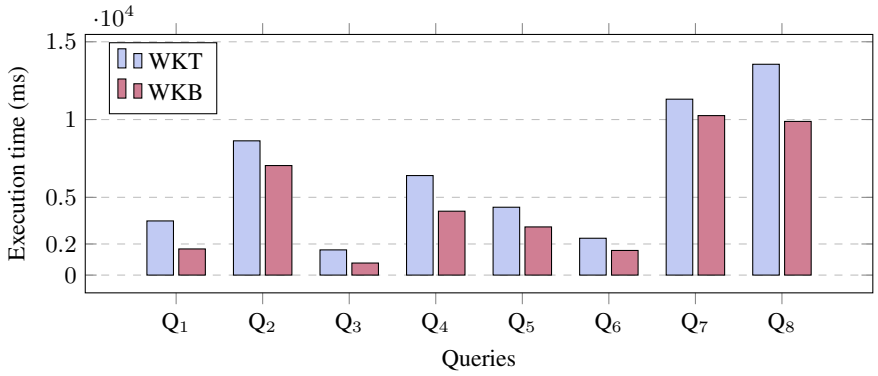

Fig. 7. Execution time (ms) of queries using WKT and WKB.

the user requests an output of the WKT format, it is more efficient to deserialize the WKB stored and convert it to WKT than to parse the WKT format.

6.5. Effect of Spatial Pruning

In figure 8, we compare the execution time of queries with and without spatial pruning. As demonstrated in the figure, the spatial pruning improves performance for most of the queries. This is due to the decreasing size of the search space. However, this is not the case of all queries, since the number of pruned fragments depends on the query and can vary form one to another. This is the case of query Q_2 where no fragment is pruned. More so, the overhead of evaluating the fragments for pruning can be negligible, as demonstrated with the same query (Q_2).

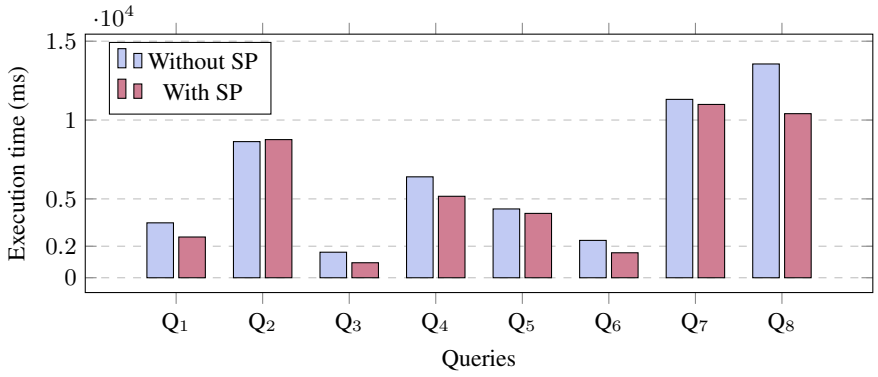

Fig. 8. Execution time (ms) of queries with and without Spatial Pruning.

6.6. Comparison against Virtuoso

After the optimization techniques applied to improve the performance of RDF_QDAG, we compare it with a commercial Triplestore Virtuoso. We choose Virtuoso since it is a stable and wildly used Triplestore. On top of that it is one of the few Triplestores capable of answering spatial-rdf queries since it support the GeoSPARQL norm proposed by the Open Geospatial Consortium. As for the other solutions (e.g., GraphDB and Strabon) we where unable to load the dataset due to stability issues in the mentioned systems.

The figure 9 depicts the execution times of queries run on both Virtuoso and RDF_QDAG. For RDF_QDAG, we plot the execution time of two different runs, one without any optimization technique used (WKT) the other one with the optimization techniques proposed and studied in previous sections (WKB+SP). We can notice that the WKT approach outperforms Virtuoso in some queries like Q_1 and Q_5. However, on most of the queries,Virtuoso still had better performace leading to a better total execution time of 47 seconds for Virtuoso compared to 52 seconds for WKT. On the other hand, after applying the proposed optimization techniques (WKT+SP), RDF_QDAG outperforms Virtuoso on all of the test queries without exception and has a better total execution time leading to an improvement of 28% on average.

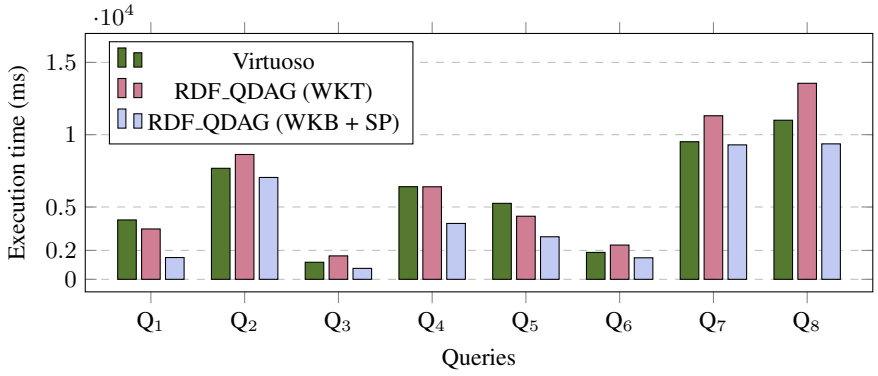

Fig. 9. Compression of execution time between Virtuoso and RDF_QDAG.

7. Conclusion

In this paper, we addressed the evaluation of spatial RDF queries issue in the setting of a graph exploration-based system, known as RDF_QDAG. To enhance the system's capability to answer such queries, we proposed an extension that integrates spatial awareness into the system's storage layer, evaluation engine and optimization process. More specifically, we proposed the use of an R-tree data structure, which is adapted to better fit the system, as well as the integration of the evaluation of spatial filters into the execution plans. Additionally, we introduced two evaluation strategies, namely, BGP-First and Spatial-First, for the execution engine. In terms of optimization, we presented a cost model that considers the cost of spatial operations in order to optimize the selection of execution plans.

Furthermore, we proposed a spatial pruning technique to further improve performance by reducing the search space.

On the other hand, we validated our proposed extension to RDF_QDAG through an experimental setup using a real-world dataset (i.e., YAGO). Our results indicated that the use of optimization techniques such as WKB encoding and spatial pruning improve the performance of the system. We also evaluated the proposed execution strategies of BGP-First and Spatial-First, and found that each strategy had advantages and limitations depending on the query being executed. To address this, we developed a cost model to determine the most suitable strategy for each query. Our results also indicated that the proposed cost model enables the system to better predict the best execution plan compared to the existing one.

In future work, we plan to continue improving the optimizer, particularly, for queries involving complex geometrical shapes in order to enhance its ability to predict the best execution plan. To achieve this, we plan to explore the use of machine learning techniques to integrate feedback from RDF_QDAG query evaluation. Additionally, we intend to extend the system by incorporating support for temporal constraints, enabling it to answer spatio-temporal queries. This could involve adapting the existing cost model, introducing new data structures and indices, and devising new evaluation strategies. The goal is to improve the efficiency and accuracy of spatio-temporal query processing.

References

1. Graphdb. https://graphdb.ontotext.com/, accessed: 2021-10-18
2. Virtuoso. https://virtuoso.openlinksw.com/, accessed: 2021-10-18
3. Abadi, D.J., Marcus, A., Madden, S.R., Hollenbach, K.: Sw-store: a vertically partitioned dbms for semantic web data management. The VLDB Journal 18(2), 385–406 (2009)
4. Battle, R., Kolas, D.: Enabling the geospatial semantic web with parliament and geosparql. Semantic Web 3(4), 355–370 (2012)
5. Bornea, M.A., Dolby, J., Kementsietsidis, A., Srinivas, K., Dantressangle, P., Udrea, O., Bhattacharjee, B.: Building an efficient rdf store over a relational database. In: Proceedings of the 2013 ACM SIGMOD International Conference on Management of Data. pp. 121–132 (2013)
6. Brahem, M., Zeitouni, K., Yeh, L.: Astroide: a unified astronomical big data processing engine over spark. IEEE Transactions on Big Data 6(3), 477–491 (2018)
7. Brodt, A., Nicklas, D., Mitschang, B.: Deep integration of spatial query processing into native rdf triple stores. In: Proceedings of the 18th SIGSPATIAL International Conference on Advances in Geographic Information Systems. pp. 33–42 (2010)
8. Broekstra, J., Kampman, A., Van Harmelen, F.: Sesame: An architecture for storing and querying rdf data and schema information (2001)
9. Chawla, T., Singh, G., Pilli, E.S., Govil, M.C.: Storage, partitioning, indexing and retrieval in big rdf frameworks: A survey. Computer Science Review 38, 100309 (2020)
10. Eldawy, A., Mokbel, M.F.: Spatialhadoop: A mapreduce framework for spatial data. In: 2015 IEEE 31st ICDE conference. pp. 1352–1363. IEEE (2015)
11. Ester, M., Kriegel, H.P., Sander, J.: Spatial data mining: A database approach. In: SSD. vol. 97, pp. 47–66. Citeseer (1997)
12. Güting, R.H.: An introduction to spatial database systems. The VLDB Journal—The Inter. Journal on Very Large Data Bases 3(4), 357–399 (1994)
13. Guttman, A.: R-trees: a dynamic index structure for spatial searching, vol. 14. ACM (1984)
14. Harris, S., Gibbins, N.: 3store: Efficient bulk rdf storage. 1st International Workshop on Practical and Scalable Semantic Systems (PSSS'03), Sanibel Island, Florida pp. 1–15 (2003)

15. Harris, S., Lamb, N., Shadbolt, N., et al.: 4store: The design and implementation of a clustered rdf store. In: 5th International Workshop on Scalable Semantic Web Knowledge Base Systems (SSWS2009). vol. 94 (2009)
16. Hoffart, J., Suchanek, F.M., Berberich, K., Weikum, G.: Yago2: A spatially and temporally enhanced knowledge base from wikipedia. Artificial intelligence 194, 28–61 (2013)
17. Khelil, A., Mesmoudi, A., Galicia, J., Bellatreche, L., Hacid, M.S., Coquery, E.: Combining graph exploration and fragmentation for scalable rdf query processing. Information Systems Frontiers 23(1), 165–183 (2021)
18. Kim, K., Cha, S.K., Kwon, K.: Optimizing multidimensional index trees for main memory access. In: ACM SIGMOD Record. vol. 30, pp. 139–150. ACM (2001)
19. Koubarakis, M., Kyzirakos, K.: Modeling and querying metadata in the semantic sensor web: The model strdf and the query language stsparql. In: Extended Semantic Web Conference. pp. 425–439. Springer (2010)
20. Kyzirakos, K., Karpathiotakis, M., Koubarakis, M.: Strabon: A semantic geospatial dbms. In: International Semantic Web Conference. pp. 295–311. Springer (2012)
21. Lee, J.G., Kang, M.: Geospatial big data: challenges and opportunities. Big Data Research 2(2), 74–81 (2015)
22. Leutenegger, S.T., Lopez, M.A., Edgington, J.: Str: A simple and efficient algorithm for r-tree packing. In: 13th ICDE conf. pp. 497–506. IEEE (1997)
23. Neumann, T., Moerkotte, G.: Characteristic sets: Accurate cardinality estimation for rdf queries with multiple joins. In: 2011 IEEE 27th International Conference on Data Engineering. pp. 984–994. IEEE (2011)
24. Neumann, T., Weikum, G.: Rdf-3x: a risc-style engine for rdf. Proceedings of the VLDB Endowment 1(1), 647–659 (2008)
25. Papadopoulos, T., Balta, M.E.: Climate change and big data analytics: Challenges and opportunities. International Journal of Information Management 63, 102448 (2022)
26. Pérez, J., Arenas, M., Gutierrez, C.: Semantics and complexity of sparql. ACM Transactions on Database Systems (TODS) 34(3), 1–45 (2009)
27. Robinson, J.T.: The kdb-tree: a search structure for large multidimensional dynamic indexes. In: Proc. of the 1981 ACM SIGMOD inter. conf. on Management of data. pp. 10–18. ACM (1981)
28. Roumelis, G., Vassilakopoulos, M., Corral, A.: Nearest neighbor algorithms using xbr-trees. In: 2011 15th Panhellenic Conference on Informatics. pp. 51–55. IEEE (2011)
29. Šidlauskas, D., Šaltenis, S., Christiansen, C.W., Johansen, J.M., Šaulys, D.: Trees or grids?: indexing moving objects in main memory. In: Proc. of the 17th ACM SIGSPATIAL inter. conf. on Advances in Geographic Info. Syst. pp. 236–245. ACM (2009)
30. Silberschatz, A., Korth, H.F., Sudarshan, S., et al.: Database system concepts, vol. 4. McGraw-Hill New York (1997)
31. Stolze, K.: Sql/mm spatial: The standard to manage spatial data in a relational database system. In: BTW 2003–Datenbanksysteme fur Business, Technologie und Web, Tagungsband der 10. BTW Konferenz. Gesellschaft für Informatik eV (2003)
32. Tang, M., Yu, Y., Aref, W., Mahmood, A., Malluhi, Q., Ouzzani, M.: In-memory distributed spatial query processing and optimization. Tech. rep., Purdue technical report (2016)
33. Wald, I., Havran, V.: On building fast kd-trees for ray tracing, and on doing that in o (n log n). In: 2006 IEEE Symposium on Interactive Ray Tracing. pp. 61–69. IEEE (2006)
34. Wang, C.J., Ku, W.S., Chen, H.: Geo-store: a spatially-augmented sparql query evaluation system. In: Proceedings of the 20th International Conference on Advances in Geographic Information Systems. pp. 562–565 (2012)
35. Weiss, C., Karras, P., Bernstein, A.: Hexastore: sextuple indexing for semantic web data management. Proceedings of the VLDB Endowment 1(1), 1008–1019 (2008)
36. Wilkinson, K., Sayers, C., Kuno, H.A., Reynolds, D., et al.: Efficient rdf storage and retrieval in jena2. In: SWDB. vol. 3, pp. 131–150. Citeseer (2003)

37. Yu, J., Wu, J., Sarwat, M.: Geospark: A cluster computing framework for processing large-scale spatial data. In: Proc. of the 23rd SIGSPATIAL Inter. Conf. on Advances in Geographic Info. Syst. p. 70. ACM (2015)
38. Zeng, K., Yang, J., Wang, H., Shao, B., Wang, Z.: A distributed graph engine for web scale rdf data. Proceedings of the VLDB Endowment 6(4), 265–276 (2013)
39. Zouaghi, I., Mesmoudi, A., Galicia, J., Bellatreche, L., Aguili, T.: Gofast: Graph-based optimization for efficient and scalable query evaluation. Information Systems 99, 101738 (2021)

Houssameddine Yousfi is a PhD student in Computer science at the university of Tlemcen, Algeria and the National Engineering School for Mechanics and Aerotechnics (ISAE-ENSMA), Poitiers, France. He is a member of the Laboratory LRIT and the laboratory LIAS. The areas of his scientific interest focus on database management systems, spatial and graph data management and Massively Parallel Processing (MPP) frameworks.

Amin Mesmoudi is an associate professor at the University of Poitiers. He is also a member of the Data Engineering team at the LIAS laboratory. He holds a PhD from the Claude Bernard (Lyon 1) University. His research interests are related to large-scale data persistence, including partitioning, indexing, and compression, as well as data exploitation. He is particularly interested in designing new evaluation and optimization techniques to support Massively Parallel Processing (MPP) frameworks.

Allel Hadjali is currently Full Professor in Computer Science at the National Engineering School for Mechanics and Aerotechnics (ISAE-ENSMA), Poitiers, France. He is a member of the Data and Model Engineering research team of the Laboratory of Computer Science and Automatic Control for Systems (LIAS). His research interests are Massive Data Exploitation and Analysis, Extraction, Recommendation and Explainabiliy in Learning Machine Models. The complete list of his publications is available in http://www.lias-lab.fr/members/allelhadjali.

Houcine Matallah is currently the Head of the Computer Science Department at the University of Tlemcen. He is also a member of the faculty's council and scientific committee. As a member of the LRIT laboratory, his research focuses on database management systems, including NoSQL and New SQL systems, as well as the challenges of Big Data.

Seif-Eddine Benkabou received his M.Sc. and Ph.D. degrees from the University of Lyon, Villeurbanne, France, in 2014 and 2018, respectively. He is currently an Assistant Professor at the University of Poitiers, Poitiers, France. His main research area is unsupervised machine learning, with a focus on outlier detection from temporal data."

Received: February 25, 2023; Accepted: June 10, 2023.

Appendix

Appendix 1: Results of estimation of each plan for the different queries considered

For all of the following tables, the best execution plan is highlighted in bold.

Table 6. Results of estimation of Q_1

Plan ID	Plan	# DS	# Triples	Initial position	New position
0	[$\overrightarrow{?c}$,$Fu(?g)$, $\overleftarrow{?c}$, $\overrightarrow{?p}$]	4774913	4775175	7	7
1	**[$\overrightarrow{?p}$, $\overrightarrow{?c}$,$Fu(?g)$]**	**5943.0**	**29657.0**	**3**	**1**
2	[$\overleftarrow{?c}$, $\overrightarrow{?c}$, $Fu(?g)$, $\overrightarrow{?p}$]	5595	54502	1	2
3	[$\overleftarrow{?c}$, $\overrightarrow{?p}$, $\overrightarrow{?c}$,$Fu(?g)$]	5720	54627	2	3
4	[$\overleftarrow{?f}$, $\overrightarrow{?p}$, $\overrightarrow{?c}$,$Fu(?g)$]	286682	859297	5	4
5	[$Fu(?g)$,$\overleftarrow{?g}$, $\overleftarrow{?c}$, $\overrightarrow{?p}$]	437395	446318	6	5
6	[$\overleftarrow{?n}$, $\overrightarrow{?p}$, $\overrightarrow{?c}$,$Fu(?g)$]	83750	857355	4	6

Table 7. Results of estimation of Q_2

Plan ID	Plan	# DS	# Triples	Initial position	New position
0	[$\overrightarrow{?c}$,$Fu(?g)$, $\overleftarrow{?c}$, $\overrightarrow{?p}$]	4775880.0	4777965.0	7	7
1	[$\overrightarrow{?p}$, $\overrightarrow{?c}$,$Fu(?g)$]	165958.0	493909.0	4	4
2	[$\overleftarrow{?a}$, $\overrightarrow{?p}$, $\overrightarrow{?c}$,$Fu(?g)$]	243796.0	1321696.0	5	6
3	[$\overleftarrow{?b}$, $\overrightarrow{?p}$, $\overrightarrow{?c}$,$Fu(?g)$]	389065.0	1154313.0	6	5
4	[$\overleftarrow{?c}$, $\overrightarrow{?c}$,$Fu(?g)$, $\overrightarrow{?p}$]	14421.0	192320.0	1	2
5	[$\overleftarrow{?c}$, $\overrightarrow{?p}$, $\overrightarrow{?c}$,$Fu(?g)$]	16412.0	194311.0	2	3
6	**[$Fu(?g)$,$\overleftarrow{?g}$, $\overleftarrow{?c}$, $\overrightarrow{?p}$]**	**104914.0**	**129598.0**	**3**	**1**

Table 8. Results of estimation of Q_3

Plan ID	Plan	# DS	# Triples	Initial position	New position
0	[$\overrightarrow{?a}$, $\overleftarrow{?a}$, $\overrightarrow{?w}$, $\overrightarrow{?l}$,$Fu(?g)$]	7231.0	7388.0	4	4
1	[$\overrightarrow{?l}$,$Fu(?g)$, $\overleftarrow{?l}$, $\overleftarrow{?w}$, $\overleftarrow{?a}$]	4774850.0	4774858.0	8	8
2	[$\overrightarrow{?p}$, $\overrightarrow{?a}$, $\overrightarrow{?w}$, $\overrightarrow{?l}$,$Fu(?g)$]	5447.0	5676.0	3	2
3	[$\overrightarrow{?w}$, $\overrightarrow{?l}$,$Fu(?g)$, $\overleftarrow{?w}$, $\overleftarrow{?a}$]	669919.0	1252615.0	7	7
4	**[$\overleftarrow{?a}$, $\overrightarrow{?a}$, $\overrightarrow{?w}$, $\overrightarrow{?l}$,$Fu(?g)$]**	**4231.0**	**5492.0**	**2**	**1**
5	[$Fu(?g)$,$\overleftarrow{?g}$, $\overleftarrow{?l}$, $\overleftarrow{?w}$, $\overleftarrow{?a}$]	441052.0	702586.0	6	5
6	[$\overleftarrow{?l}$, $\overrightarrow{?l}$,$Fu(?g)$, $\overleftarrow{?w}$, $\overleftarrow{?a}$]	59251.0	1250718.0	5	6
7	[$\overleftarrow{?w}$, $\overrightarrow{?a}$, $\overrightarrow{?w}$, $\overrightarrow{?l}$,$Fu(?g)$]	3245.0	7045.0	1	3

Table 9. Results of estimation of Q_4

Plan ID	Plan	# DS	# Triples	Initial position	New position
0	[$\overrightarrow{?e}$, $\overrightarrow{?l}$,$Fu(?g)$]	201726.0	208424.0	3	3
1	[$\overrightarrow{?l}$,$Fu(?g)$, $\overleftarrow{?l}$]	4774844.0	4774844.0	4	4
2	**[$Fu(?g)$,$\overleftarrow{?g}$, $\overleftarrow{?l}$]**	**74903.0**	**98141.0**	**2**	**1**
3	[$\overleftarrow{?l}$, $\overrightarrow{?l}$,$Fu(?g)$]	17716.0	194145.0	1	2

Table 10. Results of estimation of Q_5

Plan ID	Plan	# DS	# Triples	Initial position	New position
0	[$\overrightarrow{?c}$, $\overleftarrow{?c}$, $\overrightarrow{?p}$,$Fu(?g)$]	4775880.0	4777965.0	7	7
1	[$\overrightarrow{?p}$,$Fu(?g)$, $\overrightarrow{?c}$]	165958.0	493909.0	4	4
2	[$\overleftarrow{?a}$, $\overrightarrow{?p}$,$Fu(?g)$, $\overrightarrow{?c}$]	243796.0	1321696.0	5	5
3	[$\overleftarrow{?b}$, $\overrightarrow{?p}$,$Fu(?g)$, $\overrightarrow{?c}$]	389065.0	1154313.0	6	6
4	[$\overleftarrow{?c}$, $\overrightarrow{?c}$, $\overrightarrow{?p}$,$Fu(?g)$]	14421.0	192320.0	1	2
5	[$\overleftarrow{?c}$, $\overrightarrow{?p}$,$Fu(?g)$, $\overrightarrow{?c}$]	16412.0	194311.0	2	3
6	**[**$Fu(?g)$**,** $\overleftarrow{?g}$**,** $\overleftarrow{?c}$**,** $\overrightarrow{?p}$**]**	**51616.0**	**75701.0**	**3**	**1**

Table 11. Results of estimation of Q_6

Plan ID	Plan	# DS	# Triples	Initial position	New position
0	[$\overrightarrow{?l}$,$Fu(?g)$, $\overleftarrow{?l}$, $\overleftarrow{?u}$, $\overrightarrow{?p}$]	4774894.0	4774981.0	7	7
1	**[**$\overrightarrow{?p}$**,** $\overrightarrow{?u}$**,** $\overrightarrow{?l}$**,**$Fu(?g)$**]**	**5901.0**	**9894.0**	**3**	**2**
2	[$\overrightarrow{?u}$, $\overrightarrow{?l}$,$Fu(?g)$, $\overrightarrow{?u}$, $\overrightarrow{?p}$]	669962.0	1252701.0	6	6
3	[$Fu(?g)$,$\overleftarrow{?g}$, $\overleftarrow{?l}$, $\overleftarrow{?u}$, $\overrightarrow{?p}$]	30958.0	250625.0	5	4
4	[$\overleftarrow{?l}$, $\overrightarrow{?l}$,$Fu(?g)$, $\overleftarrow{?u}$, $\overrightarrow{?p}$]	59295.0	1250841.0	4	5
5	[$\overleftarrow{?u}$, $\overrightarrow{?p}$, $\overrightarrow{?u}$, $\overrightarrow{?l}$,$Fu(?g)$]	5192.0	32596.0	2	3
6	[$\overleftarrow{?w}$, $\overrightarrow{?p}$, $\overrightarrow{?u}$, $\overrightarrow{?l}$,$Fu(?g)$]	3394.0	7338.0	1	1

Table 12. Results of estimation of Q_7

Plan ID	Plan	# DS	# Triples	Initial position	New position
0	[$\overrightarrow{?e}$, $\overrightarrow{?l}$,$Fu(?g)$]	201726.0	208424.0	2	2
1	[$\overrightarrow{?l}$,$Fu(?g)$, $\overleftarrow{?l}$]	4774844.0	4774844.0	4	3
2	[$Fu(?g)$,$\overleftarrow{?g}$, $\overleftarrow{?l}$]	270889.0	297661.0	3	4
3	**[**$\overleftarrow{?l}$**,** $\overrightarrow{?l}$**,**$Fu(?g)$**]**	**17716.0**	**194145.0**	**1**	**1**

Table 13. Results of estimation of Q_8

Plan ID	Plan	# DS	# Triples	Initial position	New position
0	[$\overrightarrow{?l}$,$Fu(?g)$, $\overleftarrow{?l}$, $\overrightarrow{?p}$]	4775053.0	4775546.0	6	6
1	**[**$\overrightarrow{?p}$**,** $\overrightarrow{?l}$**,**$Fu(?g)$**]**	**105462.0**	**339654.0**	**3**	**1**
2	[$\overleftarrow{?a}$, $\overrightarrow{?p}$, $\overrightarrow{?l}$,$Fu(?g)$]	134597.0	469582.0	4	3
3	[$Fu(?g)$,$\overleftarrow{?g}$, $\overleftarrow{?l}$, $\overrightarrow{?p}$]	186351.0	420618.0	5	2
4	[$\overleftarrow{?l}$, $\overrightarrow{?l}$,$Fu(?g)$, $\overrightarrow{?p}$]	59454.0	1251406.0	1	4
5	[$\overleftarrow{?l}$, $\overrightarrow{?p}$, $\overrightarrow{?l}$,$Fu(?g)$]	59857.0	1251809.0	2	5

Computer Science and Information Systems 20(4):1343–1366 https://doi.org/10.2298/CSIS221116052K

Towards Addressing Item Cold-Start Problem in Collaborative Filtering by Embedding Agglomerative Clustering and FP-Growth into the Recommendation System ⋆

Eyad Kannout, Michał Grodzki, and Marek Grzegorowski

Institute of Informatics, University of Warsaw
Banacha 2, Warsaw, Poland
{eyad.kannout,m.grzegorowski}@mimuw.edu.pl,
m.grodzki@students.mimuw.edu.pl

Abstract. This paper introduces a frequent pattern mining framework for recommender systems (FPRS) - a novel approach to address the items' cold-start problem. This difficulty occurs when a new item hits the system, and properly handling such a situation is one of the key success factors of any deployment. The article proposes several strategies to combine collaborative and content-based filtering methods with frequent items mining and agglomerative clustering techniques to mitigate the cold-start problem in recommender systems. The experiments evaluated the developed methods against several quality metrics on three benchmark datasets. The conducted study confirmed usefulness of FPRS in providing apt outcomes even for cold items. The presented solution can be integrated with many different approaches and further extended to make up a complete and standalone RS.

Keywords: recommendation system, cold-start problem, frequent pattern mining, quality of recommendations.

1. Introduction

Many modern businesses undergo digital transformation, moving their offerings online, which allows for providing broadly available and more advanced products and services to customers or users [53, 74]. This trend has led to an overwhelming amount of content and the high velocity of new items reaching the systems daily. Finding the object of interest has become very time-consuming for many people, especially after moving most e-commerce to automated remote channels without qualified human advisors [2, 22, 78]. Viable solutions to this problem are recommender systems (RS), which leverage the rating history and possibly some other information, such as users' demographics or items' characteristics [57, 59].

Recommender systems are indispensable in allowing customers to find a desired product or service [69]. The quality of RS is mainly impacted by the density of the historical user-item interactions and may encounter some significant difficulties due to particular data characteristics related to volume, limited content analysis, sparsity of data, or cold

⋆ This is an extended version of the paper "Utilizing Frequent Pattern Mining for Solving Cold-Start Problem in Recommender Systems" [35] published at the FedCSIS'22 conference.

items [5, 73]. The last one is particularly challenging, having broad interest among researchers and practitioners [79, 86]. This difficulty occurs when a new item hits the system, and an RS attempts to generate recommendations with very scarce and insufficient historical ratings available [63]. Many state-of-the-art recommendation algorithms may generate unreliable recommendations for such cases since they cannot learn the preference embedding of these new items [42].

In this study, we present a particular take on the challenge of devising more effective and efficient recommendation techniques with specific attention to the problems of the sparsity of interactions and cold items. The developed Frequent Pattern mining framework for Recommender Systems (FPRS) is based on the popularity approaches extended by the FP-growth algorithm to generate frequent patterns based on items' characteristics and by adding an agglomerative clustering step into the developed pipeline [6, 38]. This way, we better reflect and leverage content-based similarities between new items, even for the partially incomplete data. The agglomerative clustering methods allow us to tune the number and size of clusters dynamically.

The developed method creates a kind of platform incorporating several strategies, which is a distinguishing feature of this approach compared to the methods reported in the literature, typically reporting one universal system. We believe that, in practical applications, the observed differences between the analyzed problems and datasets are significant. A single solution may be ineffective depending on the quality measure of choice or data characteristics. Hence, data scientists need to operate with a whole toolset and adjust it to the particular case.

Compared to our former research on utilizing frequent pattern mining for solving the cold-start problem in recommender systems [35], this study is focused on the problems of the sparsity of interactions and cold items. In this regard, we significantly extended the formerly developed strategies to better reflect and leverage content-based similarities between new items, even for the partially incomplete data. We also included new datasets for the evaluation procedure to give a more versatile assessment of our method and conducted a broad review of research efforts related to the discussed problem. The main contributions of this paper are as follows:

1. An extended version of *frequent pattern mining framework for recommender systems* (FPRS) - a hybrid recommender system that utilizes the FP-growth algorithm to produce frequent itemsets based on the ratings in the user-item matrix.
2. A novel approach to utilize the items' features to extract particular patterns based on the features selected and agglomerative clustering to mitigate the sparsity issue.
3. New strategies to mitigate the cold-start problem by using the discovered patterns to properly assess users' interest in new items.
4. An empirical evaluation of the proposed approach against two state-of-the-art models that are designed for the cold-start recommender system. The experiments are conducted on well-established benchmark datasets. Namely, MovieLens 100K, MovieLens 1M, and LDOS-CoMoDa.

The remainder of this paper is organized as follows. Section 2 describes and reviews major research efforts on the cold-start problem in the domain of recommender systems. In Section 3, we provide background information for collaborative filtering and frequent pattern mining. In Section 4, we present a novel frequent pattern mining model (FPRS)

that utilizes the ratings in user-item rating matrix to discover the frequent itemsets associated with selected users/items features. Section 5 evaluates and compares the proposed model with a baseline solution. In Section 6, we discuss the limitations of FPRS and possible future research directions. Finally, in Section 7, we summarise the study.

2. Related Works

Recommender systems (RS) predict the utility of an item to a user and suggest the best items concerning the user's preferences, where the items may represent movies, books, restaurants, or any other things [33, 62]. The aforementioned capability of RSs makes those techniques especially useful in broad areas of applications like eCommerce, online marketing, social networks, price-comparison services, or even energy market [29, 32, 48, 83]. RS may also incorporate several extensions, like context awareness, action recommendations, prescriptions, or some techniques derived from game theory [20, 65, 69].

There are many taxonomies for RS [8]. The most common approaches refer to content-based or collaboration-based techniques, and their various hybridizations [30, 37, 78]. Collaborative Filtering (CF) is one of the most widely used and successful techniques, with excellent results in a wide range of applications in many fields [8], hence is particularly interesting in our research and further reviewed in detail in Section 3.1. Despite the noticeable decline in their popularity in favor of collaborative systems, content-based techniques are still widely used because of handling the so-called cold-start problem [35, 64]. Because of the significantly different characteristics of those approaches, it is advisable to construct hybridizations of both [1], as further discussed in our study.

A typical RS consists of three main elements: a user model (established by analyzing the users' interests and preferences), an item model (based on its characteristics), and the recommendation algorithm that is a key constituent. There are many reported approaches to implementing the recommendation algorithm by the specific adoption of machine learning (ML) models like deep neural networks or factorization machines (FM) [50, 60, 80]. Building RS on top of the state-of-the-art ML models leveraged the quality of recommendation results, improving user satisfaction and profits in e-commerce [46, 54, 83]. At the same time, however, we may observe the known problems with ML related to the data sparsity, the latency of prediction returned by complex models, and foremost, the scalability and unfairness of recommendations for new users or items that is often referred to as the *cold-start* problem [31, 35, 87].

Solving scalability issues is one of the most common tasks when deploying big-scale recommender systems [5, 16, 67]. Especially as the number of users and items significantly grows over time, it is essential for RS to handle requests without appreciable latency. This problem is particularly challenging for memory-based methods like k-nearest neighbors. However, in the case of web-scale recommendation tasks like social media, the Internet of Things (IoT), or various e-commerce applications, it is a hot topic also for model-based techniques, especially considering more complex and deep models [10, 75]. Some RS suffer from over-specialization (sometimes referred to as a serendipity problem). It is observed when the RS produces recommendations with minimal novelty, i.e., all of the same kind [39]. Recently, there is also an increasing interest in privacy awareness and explainability of recommendations [4, 14, 61]. Another aspect that is particularly noticeable for collaborative filtering is related to the sparsity of user-item interactions [40].

Together with the growing amount of items available for the recommendations, the quality of CF-based methods may be impacted by an insufficient number of items rated by each user [55]. One of the possibilities to address this issue is to rally on auxiliary data or additional information sources such as user/item profiles or user reviews on items [28]. Some approaches aim to resolve the data sparsity problem by generating data (e.g., purchasees) from machine learning models of auxiliary feedback, or from the nearest neighbors with a set of purchased items in multiple dimensions [25]. Other popular approaches apply selected clustering methods, often referring to notions of similarity [19,82]. In [85], the authors use user clustering to reconstruct the user-item bipartite network such that the network density is significantly improved. The recommendations on this dense network thus can achieve much higher accuracy than on the original sparse one. In [44], the density-based clustering algorithm is used for coping with the sparsity problem. In [81], the authors employ a granular computing model to realize the nearest neighbor clustering and a covering rough granular computing model for the collaborative filtering recommendation algorithm. The application of granular methods [21], selected approaches to clustering, and various similarity measures seem to be an exciting research direction, yielding promising results [41]. From our perspective, agglomerative clustering methods are particularly interesting. They allow us to utilize various notions of similarity (e.g., the Jaccard coefficient) and manage the number and size of clusters [71].

Agglomerative clustering algorithms create a hierarchy of data clusters by starting from singleton groupings (clusters containing a single element) and iteratively merging the closest groups into a bigger cluster [15]. This process ends when all data instances are merged into a single cluster, hence, is often referred to as a bottom-up approach. To measure the proximity (dissimilarity) between groups, agglomerative clustering algorithms employ so-called linkage functions like *single linkage* or *complete linkage*. The first one defines the dissimilarity between two groups as the smallest distance between any two instances from those groups. Analogically, the second function asserts the proximity of groups as the largest distance between any two instances [71].

Cold-start problem occurs whenever a RS tries to generate recommendations for either a new user who signed up recently to the system without having any rating records available yet or when a new item is added to the system without any rating given to that item so far. Most state-of-the-art recommendation algorithms generate unreliable recommendations for such cases since they cannot learn the preference embedding of these new users/items [49, 72]. In content-based filtering (CBF), it is necessary to learn user preferences in order to provide reliable recommendations. Therefore, CBF suffers from the user cold-start problem when new users who signed up recently do not have, or have very few, ratings. Hence, the quality of recommendation will be impacted by an insufficient number of rated items [13, 61]. Many studies recognize the challenge of fairness among new items' recommendations in cold systems, [79, 86, 87].

The difficulty arises due to the deficient information about new entities [76]. Therefore it has a particularly strong negative impact on collaborative methods, heavily impacting the fairness of recommendations for new users, often passing over new items [87]. Most of the attempts to deal with such a problem consider enhancing the collaborative-based methods with content-based approaches that leverage the intrinsic characteristics of the analyzed entities. For example, in [42], the authors propose hybrid recommender models that use content-based filtering and latent Dirichlet allocation (LDA)-based models. In

[78], we may find a hybrid RS that combines the singular-value decomposition-based collaborative filtering with content-based and fuzzy expert systems.

In literature, we may find many efforts to resolve the cold-start problem [11,47]. In [7], the authors aim to address the cold-start problem by extending the matrix-factorization-based methods, namely SVD, SVD++, and the NMF models, using three simple regularization differentiating functions (RDF) so that the regularization weights on different items and users are set based on their popularity. In [9], the item-side cold-start problem is addressed with the concept of weak supervision. The authors introduced a new process for identifying representative reviewers and developed a method to predict the expected preferences for new items by combining content-based filtering and the preferences of representative users. In [87], the authors formalize fairness among new items with the concepts of equal opportunity and Rawlsian Max-Min fairness and present a learnable post-processing framework with score scaling and joint-learning generative models. Zhu et al. propose a novel model designed to overcome cold start by (i) a combined separate-training and joint-training framework to overcome the error superimposition issue and improve model quality; (ii) a Randomized Training mechanism to promote the effectiveness of model learning; and (iii) a Mixture-of-Experts Transformation mechanism to provide personalized transformation functions.

There are many more techniques to dealing with the cold-start problem by combining collaborative filtering with content-based methods, including using simultaneous co-clustering [77], self-organizing maps, meta-learning [51], or Siamese neural networks [63]. There are also attempts to combine RS with various dimensionality reduction techniques [56]. Considering the discussed problem of missing or insufficient information, it seems interesting to refer to the dimensionality reduction methods based on the granularization of the attribute space [21], and particularly on resilient ML techniques [17, 23] - i.e., resistant to data deficiencies. The hybridization of soft computing techniques with collaborative and content-based methods is a wide-ranging field of research, and an interesting area for the further development of recommendation systems [3], particularly interesting for context-aware RSs [33, 43, 58].

Some approaches to dealing with cold-start refer to popularity measures, e.g., on the recent trend in users' preferences or always returning the most popular items [50, 64]. However, these may be very misleading and result in so-called popularity bias since users often differ in their preferences, which may also vary between types of products and their characteristics [87]. Hence, an additional effort to deal with biases in data is required [70]. Another interesting approach to dealing with insufficient or missing historical transactions avail additional sources of information to enhance the data representation. In particular, in [55], the authors train RSs with the Linked Open Data model based on DBpedia to find enough information about new entities. When dealing with the cold-start problem, some researchers rely on directly inquiring the users about their preferences. Such information may be collected, e.g., via survey or by asking users to select the most relevant picture related to the desired item [45]. Combining community-based knowledge with association rule mining to alleviate the cold-start problem is also bringing very promising results [76]. Referring to association rule mining (cf. [68]) and frequent pattern mining (cf. [12]) techniques to address the cold-start problem is interesting also from the perspective of speeding up the recommender systems [36]. For this reason, frequent pattern mining is particularly interesting in our research, and we review this field in detail in Section 3.2.

Most reported cases focus on alleviating cold users [11, 47]. Scenarios related to new items - without any feedback history - are investigated far less often. Whereas, having in mind the still-emerging new products and services, such approaches are in high demand and require further research attention. Additionally, we did not find in the literature any attempt to address the cold-start problem using frequent pattern mining methods. The cold-start problem is still one of the most prevailing topics deserving further attention and is particularly interesting in the context of our study [55, 63].

3. Preliminaries

In this section, we briefly summarize the academic knowledge of collaborative filtering and frequent pattern mining techniques. Then, we review some of the research literature related to addressing the cold-start problem.

3.1. Collaborative Filtering

The basic idea behind collaborative filtering (CF) is that users who have similar preferences in the past tend to behave similarly in the future. Basically, CF-based methods rely only on users' rating history to generate recommendations, meaning that the more ratings the users provide, the more accurate the recommendations become [33]. Usually, historical ratings or preferences can be acquired explicitly or implicitly. So, the CF-based methods are often distinguished by whether they operate over explicit ratings, where the users explicitly rate particular items, or implicit ratings, where the ratings are inferred from observable user activity, such as products bought, songs heard, visited pages, or any other types of information access patterns [33]. In the literature, collaborative filtering methods can be classified into two main categories: (i) memory-based techniques, and (ii) model-based techniques.

The memory-based technique directly uses the rating history, which is stored in memory, to predict the rating of items that the user has not seen before. However, the memory-based techniques can be grouped into two different classes: (i) user-based collaborative filtering, and (ii) item-based collaborative filtering. The user-based collaborative filtering, also known as k-NN collaborative filtering, works by finding the other users (neighbors) whose historical rating behavior is similar to that of the target user and then using their top-rated products to predict what the target user will like. To mathematically formulate the problem, let us assume there is a list of users $U = \{u_1, u_2, ..., u_m\}$ and a list of items $I = \{i_i, i_2, ..., i_n\}$. Then, the user-item rating matrix consists of a set of ratings $v_{i,j}$ corresponding to the rating for user i on item j. If I_i is the set of items on which user i has rated in the past, then we can define the average rating for user i as follows:

$$\overline{v}_i = \frac{1}{|I_i|} \sum_{j \in I_i} v_{i,j} \tag{1}$$

In user-based collaborative filtering, we estimate the rating of item j that has not yet rated by the target user a as follows [37]:

$$p_{a,j} = \overline{v}_a + \frac{\sum_{i=1}^{k} s(a,i)(v_{i,j} - \overline{v}_i)}{\sum_{i=1}^{k} |s(a,i)|} \tag{2}$$

where k is the number of most similar users (nearest neighbors) to a. The weights $s(a,i)$ can reflect the degree of similarity between each neighbor i and the target user a. On the other hand, item-based collaborative filtering is just an analogous procedure to the previous method. The similarity scores can also be used to generate predictions using a weighted average, similar to the procedure used in user-based collaborative filtering. Mathematically, we can predict the rating of item j that has not yet been rated by the target user a as follows [37]:

$$p_{a,j} = \frac{\sum_{i=1}^{k} s(j,i)(v_{a,i})}{\sum_{i=1}^{k} |s(j,i)|} \tag{3}$$

where k is the number of most similar items (nearest neighbors) to j that the target user a has rated in the past. Among other popular metrics, which are often used to calculate the similarity between users, or items, we may mention cosine similarity or Pearson correlation [26]. Finally, the recommendations are generated by selecting the candidate items with the highest predictions.

On the other hand, the model-based technique works by learning a predictive model using the rating history. Basically, it is based on matrix factorization, which uses the rating history to learn the latent preferences of users and items. Matrix factorization is an unsupervised learning method that is used for dimensionality reduction. One of the most popular techniques applied for dimensionality reduction is Singular Value Decomposition (SVD). Mathematically, let us assume M is the user-item rating matrix. The SVD of M is the factorization of M into three constituent matrices such that [37]:

$$M = U\Sigma V^T \tag{4}$$

where U is an orthogonal matrix representing left singular vectors of M. V is an orthogonal matrix representing right singular vectors of M. Σ is a diagonal matrix whose values σ_i are the singular values of M [37].

3.2. Frequent Pattern Mining

The basic idea of frequent pattern mining, also known as association rule mining, is to search for all relationships between elements in a given massive dataset. It helps us to discover the associations among items using every distinct transaction in large databases. The key difference between association rules mining and collaborative filtering is that in association rules mining we aim to find global or shared preferences across all users rather than finding an individual's preference like in collaborative filtering-based techniques [27].

At a basic level, association rule mining analyzes the dataset searching for frequent patterns (itemsets) using machine learning models. To define the previous problem mathematically, let $I = \{i_1, i_2, ..., i_m\}$ be an itemset and let D be a set of transactions where each transaction T is a nonempty itemset such that $T \subseteq I$. An association rule is an implication of the form $A \Rightarrow B$, where $A \subset I$, $B \subset I$, $A \neq \emptyset$, $B \neq \emptyset$, $A \cap B = \emptyset$. In the rule $A \Rightarrow B$, A is called the antecedent and B is called the consequent. Various metrics are used to identify the most important itemset and calculate their strength, such as support, confidence, and lift. Support metric is the measure that gives an idea of how frequent an

itemset is in all transactions. In other words, the support metric represents the number of transactions that contain the itemset. Equation 5 shows how we calculate the support for an association rule.

$$support(A \Rightarrow B) = P(A \cup B) \tag{5}$$

On the other hand, confidence indicates how often the rule is true. It defines the percentage of transactions containing the antecedent A that also contain the consequent B. It can be taken as the conditional probability as shown in Equation 6.

$$confidence(A \Rightarrow B) = P(B|A) = \frac{support(A \cup B)}{support(A)} \tag{6}$$

Finally, the lift is a correlation measure used to discover and exclude the weak rules that have high confidence. Equation 7 shows that the lift measure is calculated by dividing the confidence by the unconditional probability of the consequent [27].

$$lift(A \Rightarrow B) = \frac{P(A \cup B)}{P(A)P(B)} = \frac{support(A \cup B)}{support(A)support(B)} \tag{7}$$

If the lift value is equal to 1, then A and B are independent and there is no correlation between them. If the lift value is greater than 1, then A and B are positively correlated. If the lift value is less than 1, then A and B are negatively correlated.

Various algorithms exist for mining frequent itemsets, such as Apriori, AprioriTID, Apriori Hybrid, and FP-growth (Frequent pattern) [52]. In this paper, we employ the FP-growth algorithm to generate frequent itemsets. What makes FP-growth better than other algorithms is the fact that FP-growth algorithm relies on FP-tree (frequent pattern tree) data structure to store all data concisely and compactly, which greatly helps to avoid the candidate generation step. Moreover, once the FP-tree is constructed, we can directly use a recursive divide-and-conquer approach to efficiently mine the frequent itemsets without any need to scan the database over and over again like in other algorithms.

4. Frequent Pattern Mining Framework For Recommender Systems

The main problem we address in this paper is to alleviate the impact of new items cold-start in recommender systems based on collaborative filtering techniques. These methods suffer from the cold-start problem whenever a new user joins the system or a new item is added. In practice, both situations often lead to the inability to provide accurate or meaningful recommendations. To tackle the cold-start problem, we implement the Frequent Pattern mining framework for Recommender Systems (FPRS).

The FPRS framework extends the popularity-based approach by employing frequent pattern mining techniques to learn the user preferences depending on users' and items' characteristics. Fig 1 shows the high-level design which is used to develop the FPRS framework. The process of generating the recommendations consists of four stages: (i) Data Input, (ii) Data Preparation, (iii) Data Preprocessing, (iv) Frequent Pattern Mining, and (v) Recommendation Generation.

In the first stage, we enrich the user-item rating matrix by users' demographics and items' characteristics. The data preparation stage consists of two steps. In the first one, we store only the favorable reviews by filtering out every review/rating below a determined threshold. In the second step, we perform attributes analysis and check their validity for generating the recommendation. In the third stage, we apply cluster attributes with more than one value associated with the object's key. The main objective of this step is to convert multi-valued attributes into single-value ones with the cluster id so that the dataset can be split based on their values. In the analyzed case study, we applied agglomerative clustering techniques on the 'genre' since each movie can be assigned to more than one genre. After that, we split the dataset for each selected attribute. In the fourth stage, we generate frequent itemsets using the FP-Growth algorithm. Finally, we produce the recommendations in the last stage. The developed item cold-start module in the FPRS framework contains several strategies to select the features and produce recommendations. More details about these strategies will be provided later in the next section.

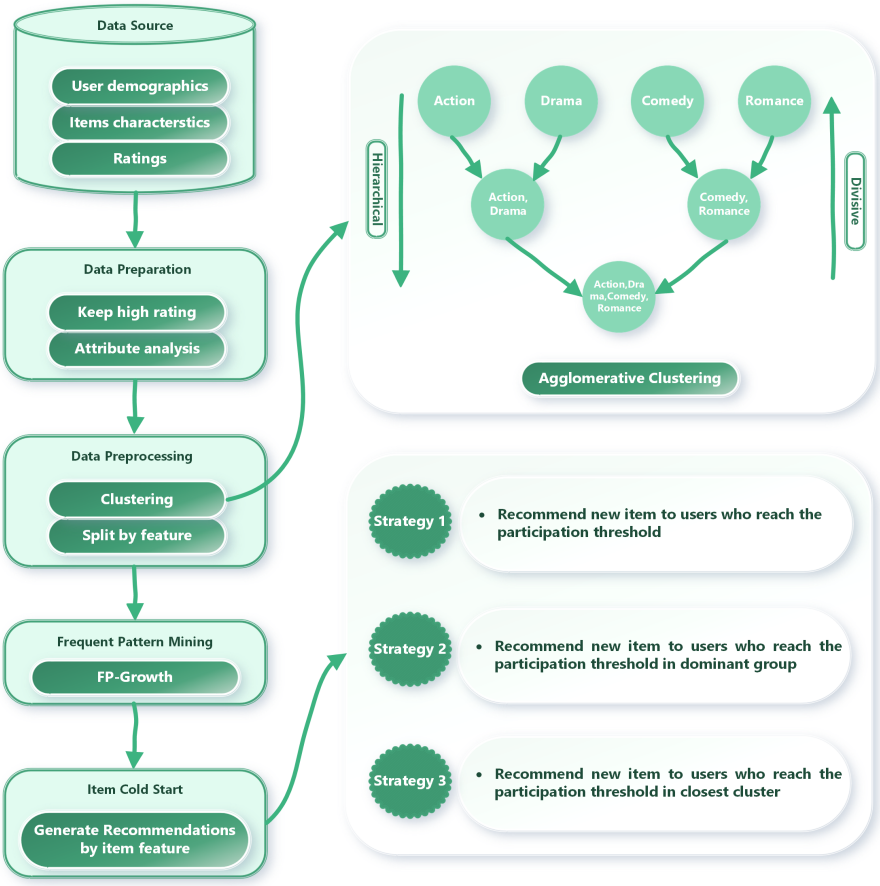

Fig. 1. Frequent Pattern Mining Framework For Recommender Systems

In the item cold-start module, we focus on generating recommendations for new items which are recently added to the system and most likely do not have, or have very few, ratings in the past. We follow multiple strategies to generate such recommendations. These strategies differ in two main factors: (i) features selected to split the data, and (ii) the way how the frequent patterns are utilized to generate the recommendations. More details about the strategies followed in the item cold-start module are provided in Strategy 1, Strategy 2, and Strategy 3.

In Strategy 1, we split the data only by items' features, while in Strategy 2. we utilize both items' and users' characteristics to split the data (cf. line 1 in both strategies). Moreover, in Strategy 1, we select the users that compose the recommendation group based on their engagement in creating the frequent itemsets (cf. line 5 in Strategy 1), whereas in Strategy 2, the representatives of recommendation group are selected based on items' features, to find the so-called dominant group, in addition to the percentage of users' engagement in creating the frequent itemsets (cf. lines 5 and 7 in Strategy 2). On the other hand, in Strategy 3, we form clusters based on the frequent 1-itemsets created by users' and items' features (cf. line 4 in Strategy 3). Then, the recommendation group for the new item is created based on the percentage of users' engagement in creating the frequent itemsets in the closest cluster (cf. line 7 in Strategy 3).

All the thresholds used in the above-described strategies are selected by objectively searching for an optimal set of values, i.e., that achieves the best performance on a given dataset. More details on how we choose these values are provided in Section 5.

Strategy 1 Item Cold-Start Module (Items Characteristics Split)

1: Split the records based on items characteristics (i.e., genre)
2: Generate frequent itemsets {support $>$ min_support}
3: Set the participation percentage threshold
4: **for each** value in genre **do**
5: Find all users who involved in creating larger than the participation threshold of frequent itemsets
6: **end for**
7: Recommend the new item based on its genre to all users found in previous step

Strategy 2 Item Cold-Start Module (Users/Items Characteristics Split)

1: Split the records based on users/items characteristics (i.e., gender and genre)
2: Generate frequent itemsets {support $>$ min_support}
3: Set the participation percentage threshold
4: **for each** value in genre **do**
5: Find the dominant gender by counting how many frequent itemsets are generated by male and female
6: **end for**
7: Recommend the new item based on its genre to all users belonging to the dominant gender who involved in creating larger than the participation threshold of frequent itemsets

Strategy 3 Item Cold-Start Module (Clustering-based)

1: Split the records based on users/items characteristics (i.e., gender and genre)
2: Generate frequent 1-itemsets {support $>$ min_support}
3: Set the participation percentage threshold
4: For each genre: assign frequent 1-itemsets created by male to one cluster and frequent 1-itemsets created by female to another cluster
5: Find the center of each cluster
6: Calculate the distance between the new item and the center of each cluster
7: Recommend the new item to all users who involved in creating larger than the participation threshold of frequent itemsets in the closest cluster

5. Evaluation Methodology

In this section, we conduct comprehensive experiments to evaluate the performance of the FPRS recommender system.

5.1. Dataset and Evaluation Measures

In our experiments, we used three datasets (MovieLens 100K, MovieLens 1M [1] and LDOS-CoMoDa [2]). MovieLens datasets were collected by the GroupLens research project at the University of Minnesota. MovieLens 100K contains 100,000 ratings given by 943 users on 1,682 movies on a scale from 1 to 5. In comparison, MovieLens 1M contains 1,000,000 ratings of approximately 3,900 movies made by 6,040 users on a scale from 1 to 5. On the other hand, LDOS-CoMoDa is a context-rich movie recommender dataset that consists of 200 users who gave 2,296 ratings for 4,138 movies in twelve pieces of contextual information describing the situation in which the user consumed the item. This dataset is collected from real user-item interactions and not from the hypothetical situation or user's memory of past interactions.

In all datasets, we combine three files (*users.data*, *items.data*, *ratings.data*) in order to join users' characteristics (e.g., demographics), items' attributes, and ratings in one dataset. The final/joined dataset contains userId, itemId, rating, gender, age, occupation, and genre attributes (cf. Table 1). Moreover, we performed further analysis of some features we used in our experiments (i.e., gender and genre) to understand the interrelation between these features and their potential impact on the obtained results. Figures 2 show the most popular movie genres among males and females for all datasets.

After preprocessing the data and removing invalid records, we split it into training and testing datasets. To properly evaluate the item cold-start module, we first find the 50 most active users. Then, we select some of the most-rated movies by those 50 users. The ratings of all those movies by all users (7,320 records in MovieLens 100K, 41,105 records in MovieLens 1M, and 126 records in CoMoDa) are considered as testing set, keeping the rest of the records in the training set. This way, we may ensure enough interactions to assess quality reliably in the testing phase. Note that all the ratings for the selected movies are removed from the training dataset, which corresponds to the item cold-start.

[1] https://grouplens.org/datasets/movielens/
[2] https://www.lucami.org/en/research/ldos-comoda-dataset/

Table 1. Selected data characteristics.

Attribute Name	Data Type	Value Range (MovieLens 100K)	Value Range (MovieLens 1M)	Value Range (LDOS-CoMoDa)
gender	Character	M-F	M-F	M-F
age	Number	Under 18-73	Under 18-56	15-63
occupation	Text	21 occupation	21 occupation	NA
genres	Text	19 genres	19 genres	25 genres

In our study, we consider a binary decision task whether a given item (i.e., a movie) is appropriate for the user. To correctly model this situation, we assume that films rated by users 3 or more are preferred by them (belong to the positive class). In contrast, those ranked lower are poorly matched to the users. Therefore, the FPRS recommender system feedback for each item is binary information: to recommend or not. Following that, in order to assess the quality of the prediction, the F_1 measure is used [66].

$$F_1 = 2 \cdot \frac{precision \cdot recall}{precision + recall} \tag{8}$$

where precision quantifies the number of correct positive recommendations made (see Equation 9), and recall quantifies the number of correct positive recommendations made out of all positive predictions that could have been made (see Equation 10).

$$Precision = \frac{TP}{TP + FP} \tag{9}$$

$$Recall = \frac{TP}{TP + FN} \tag{10}$$

Moreover, we use the accuracy metric to measure all the correctly identified cases. This measure is mostly used when all the classes are equally important.

$$Accuracy = \frac{TP + TN}{TP + FP + TN + FN} \tag{11}$$

5.2. Baseline Methods

To showcase the strengths of FPRS, we evaluate it against two baseline models designed for the cold-start recommender system. The first one [7], called regularization differentiating functions (RDF), was proposed recently to address the cold-start problem by extending the matrix factorization-based models using three simple regularization differentiating functions (RDF). In particular, these functions assign lower regularization weights to the latent factors associated with popular items and active users, and set higher regularization weights on long tail items, that were rated/viewed/purchased by few users, and less active users. The goal of this method is to enhance the MF-based models by utilizing more information revealed by popular items and active users, and make conservative predictions on long tail items and less active users. In the evaluation, we utilized the publicly available

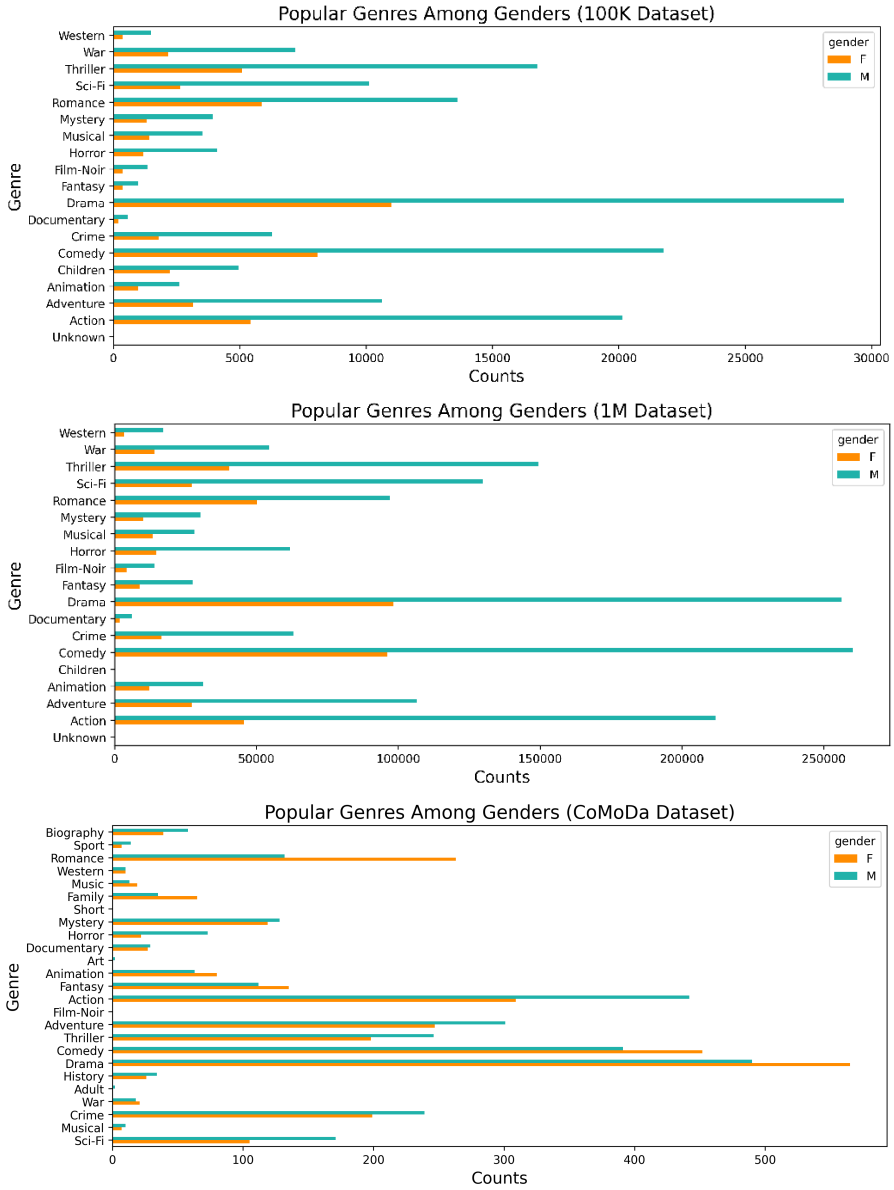

Fig. 2. Histogram of the variables (rating, genre, and gender) in MovieLens (100K and 1M) and LDOS-CoMoDa datasets.

implementation [1], provided by the authors, which integrates the proposed regularization technique with the SVD, SVD++, and the NMF models. On the other hand, in order to

[1] https://github.com/ncu-dart/rdf

demonstrate the efficiency of frequent pattern mining in RS, we build a baseline model in a similar way to the FPRS strategies, yet the FP-growth algorithm was omitted. In order to evaluate the item module of FPRS, we find the most popular (watched) genre for each user. Then each new movie is recommended to all users whose favorite genre is the same as the new movie's.

5.3. Performance Comparison and Analysis

In order to provide a fair comparison, we use precision, recall, F_1-score, and accuracy measures to compare the performance of FPRS against two RSs, namely Baseline and RDF, which are described in Section 5.2. After splitting the dataset into the training and testing sets and training the baseline and FPRS recommendation systems, we run multiple experiments to evaluate the item cold-start module.

In these experiments, we evaluated the item cold-start module in FPRS. We calculated precision, recall, F_1, and accuracy measures for the results generated by Baseline, RDF, and FPRS following all the strategies described in Section 4. The comparative summary of this evaluation is shown in Tables 2, 3, and 4. The results show that the performance of FPRS, using all strategies, is superior to Baseline and RDF solutions. However, the results differ slightly between datasets.

For MovieLens 100K, all strategies reported similar recall. Regarding precision and F_1 measures, the most successful in dealing with new items in this data appeared to be Strategy 2, which is based on both items' and users' characteristics. However, for the applications that do require high accuracy, it would be better to apply Strategy 3, which was also superior in terms of recall, F_1, and accuracy on the second dataset (i.e., MovieLens 1M). When it comes to the LDOS-CoMoDa dataset, we notice that Strategy 1 is the most successful in terms of recall and F_1 measures. Whereas, Strategy 2 achieved the highest accuracy, while strategy 3 reported the best precision. When it comes to Baseline and RDF models, they reported relatively similar F_1 scores. However, RDF outperformed Baseline in terms of recall, while Baseline achieved higher accuracy than RDF.

It is important to emphasize that there is no absolute superior strategy, but the appropriate approach should be selected based on the application's requirements. For example, when we deal with small datasets, like LDOS-CoMoDa, it is recommended to use strategies that keep enough records in the partitioned datasets to extract frequent itemsets. This is observed while evaluating FPRS using the LDOS-CoMoDa dataset (cf. Table 4). The results show that Strategy 1, which splits the data only based on items' features, is superior in terms of recall and F_1 measures.

However, selecting the appropriate evaluation measure plays an important role while choosing the proper strategy. The precision measure is focusing on the number of correct recommendations considering the mistakes made. On the other hand, the recall measure does not take into account the mistakes made since it only considers the number of correct recommendations made out of all positive predictions that could have been made (cf. Equations 9 and 10). According to the previous, the proper strategy can be selected relying on the evaluation measure that best matches the target of our application.

Finally, all strategies were evaluated at the participation threshold value of 30% and $min\_support$ value of 0.2 for MovieLens 1M and 100K. Regarding LDOS-CoMoDa, the strategies were evaluated at the participation threshold value of 20% and $min\_support$

value of 0.07. The values of the thresholds are determined based on sensitivity analysis experiments which we will be presented in Section 5.4.

Table 2. Evaluation for item cold-start (MovieLens 100k).

Strategy	Precision	Recall	F1-score	Accuracy
Baseline	0.38	0.3	0.32	0.59
RDF	0.35	0.51	0.41	0.48
Strategy 1	0.69	0.64	0.66	0.75
Strategy 2	0.79	0.62	0.69	0.84
Strategy 3	0.67	0.63	0.63	0.86

Table 3. Evaluation for item cold-start (MovieLens 1M).

Strategy	Precision	Recall	F1-score	Accuracy
Baseline	0.49	0.43	0.43	0.64
RDF	0.34	0.52	0.39	0.51
Strategy 1	0.65	0.71	0.64	0.76
Strategy 2	0.64	0.73	0.66	0.83
Strategy 3	0.6	0.79	0.66	0.86

Table 4. Evaluation for item cold-start (LDOS-CoMoDa).

Strategy	Precision	Recall	F1-score	Accuracy
Baseline	0.02	0.21	0.10	0.73
RDF	0.07	0.59	0.13	0.42
Strategy 1	0.36	0.62	0.40	0.81
Strategy 2	0.36	0.55	0.38	0.96
Strategy 3	0.4	0.21	0.26	0.86

5.4. Thresholds Sensitivity Analysis

In the FPRS model, we use some threshold values, such as $min\_support$ and $participation$ percentage, in order to extract frequent itemsets and produce relevant recommendations for new items. In this section, we conduct some experiments to show how changing those values may impact the performance of FPRS. Moreover, the output of this experiment helps to find the optimal values of these thresholds and hence to conduct fair and reliable experiments.

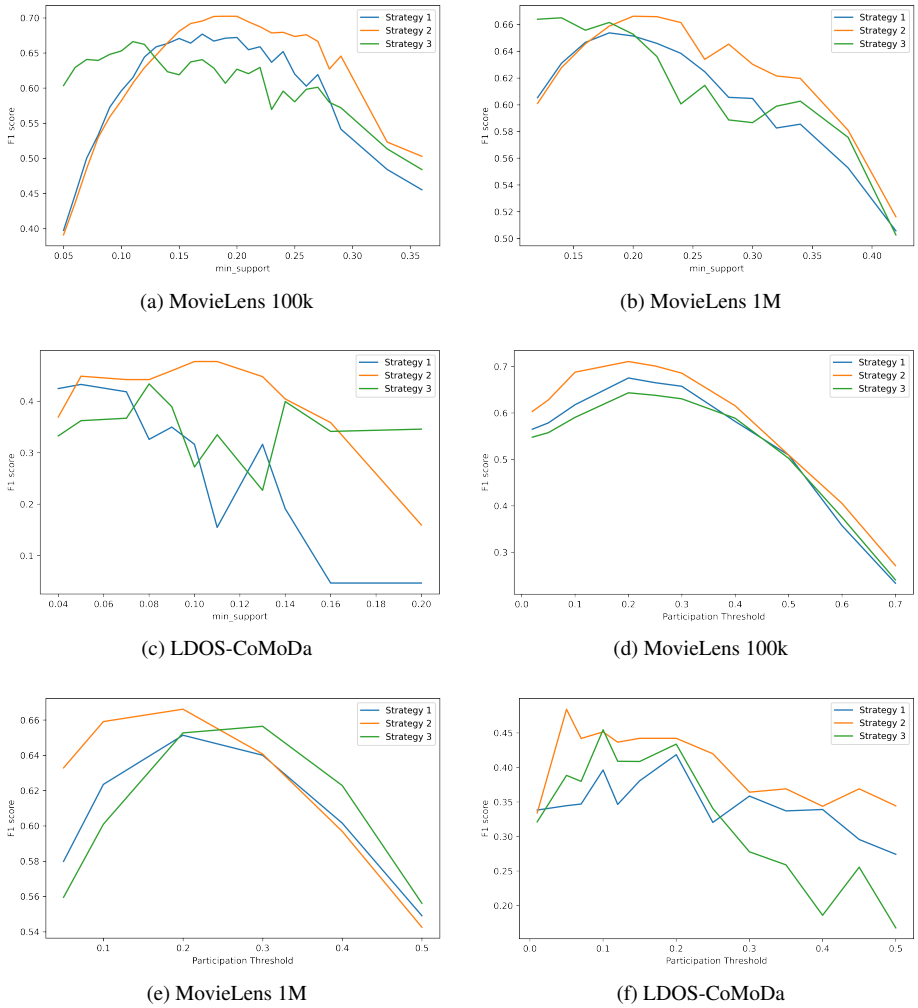

(a) MovieLens 100k

(b) MovieLens 1M

(c) LDOS-CoMoDa

(d) MovieLens 100k

(e) MovieLens 1M

(f) LDOS-CoMoDa

Fig. 3. Sensitivity analysis for min_supp and participation percentage thresholds in MovieLens (100k and 1M) and LDOS-CoMoDa.

In the first experiment, we aim to find the optimal value of min_sup threshold by evaluating FPRS (item cold-start module) using different min_sup values. Fig 3a shows how the F_1-score of FPRS is impacted by applying different values for MovieLens 100K data. Observably, the best min_supp values for all strategies used in FPRS (item cold-start module) are between 0.1 and 0.2. A similar analysis, yet regarding MovieLens 1M and LDOS-CoMoDa data, we may find in Figures 3b and 3c respectively.

In the second experiment, we search for the optimal value of the participation threshold in FPRS (item cold-start module). Figures 3d, 3e and 3f show how the F_1-score of FPRS is impacted by applying different values for all investigated datasets. Observably, the best participation threshold values for all strategies used in FPRS (item cold-start module) are between 15% and 30% for MovieLens 1M and 100K data, and it is between 5% and 20% for LDOS-CoMoDa data. Finally, it is worth noting that when we run this experiment, we use the optimal value of min_supp we found in the previous experiment.

6. Challenges, Limitations and Future Works

This section is dedicated to discussing the challenges we faced while evaluating FPRS and suggesting the best practices to overcome the revealed limitations.

One of these challenges appears when we deal with small datasets. In such scenarios, we might not be able to generate frequent patterns after splitting out the dataset. To address this issue, we have to carefully select appropriate values for $min\_support$ and $participation$ percentage thresholds by analyzing the results of the experiments presented in Section 5.4.

Another limitation that FPRS may suffer from is the lack of users' and items' characteristics. For future research, we find it very promising to investigate further the application of granular methods in this respect [19, 21]. Here, it would be advisable to incorporate the methods to improve the resilience of the FPRS framework to data discrepancies or loss [23]. The alternative approach could investigate the applicability of dimensionality reduction methods, like PCA, in data modeling [34].

In the future, we plan to investigate more algorithms for association rule and frequent pattern mining, e.g., AprioriTID or Apriori Hybrid. It is also interesting to incorporate more contextual information. We also plan to respond better to changes in users' behavior and preferences, addressing the possible drifts and shifts in data. One viable option is to periodically update frequent itemsets based on recent changes in rating history. It would also be of value to extend the users' and items' data representation by applying a more advanced feature extraction to model the similarities among them more effectively [18, 24, 84].

7. Conclusions

This article presents FPRS, a recommender system, which methodically utilizes the ratings to discover frequent itemsets associated with selected users/items features and then incorporates these frequent itemsets in generating recommendations for new items. Our study evaluates multiple strategies for creating frequent itemsets to produce meaningful and relevant recommendations. The presented pipeline also includes the clustering-based

feature extraction phase, which aims at modeling similarities between investigated entities. This way, we not only extend the data representation but also increase their density, allowing us to alleviate the omnipresent problem of too few interactions in historical data, especially severe for new products or services.

To evaluate FPRS, we conducted experiments on MovieLens (100K and 1M) and LDOS-CoMoDa datasets with the FP-growth algorithm to generate the frequent itemsets. The experimental results show that FPRS has outperformed two state-of-the-art models, designed to address the cold-start problem, in terms of precision, recall, F_1, and accuracy measures.

Acknowledgments. Research co-funded by Polish National Science Centre (NCN) grant no. 2018/31/N/ST6/00610.

References

1. Afoudi, Y., Lazaar, M., Al Achhab, M.: Hybrid recommendation system combined content-based filtering and collaborative prediction using artificial neural network. Simulation Modelling Practice and Theory 113, 102375 (2021)
2. Alamdari, P.M., Navimipour, N.J., Hosseinzadeh, M., Safaei, A.A., Darwesh, A.: A Systematic Study on the Recommender Systems in the E-Commerce. IEEE Access 8, 115694–115716 (2020)
3. Asid, M., Ali, R.: Use of Soft Computing Techniques for Recommender Systems: An Overview, pp. 61–80. Springer Singapore, Singapore (2017)
4. Barria-Pineda, J., Akhuseyinoglu, K., Zelem-Celap, S., Brusilovsky, P., Klasnja-Milicevic, A., Ivanovic, M.: Explainable recommendations in a personalized programming practice system. In: Roll, I., McNamara, D.S., Sosnovsky, S.A., Luckin, R., Dimitrova, V. (eds.) Artificial Intelligence in Education - 22nd International Conference, AIED 2021, Utrecht, The Netherlands, June 14-18, 2021, Proceedings, Part I. Lecture Notes in Computer Science, vol. 12748, pp. 64–76. Springer (2021)
5. Batmaz, Z., Yürekli, A., Bilge, A., Kaleli, C.: A review on deep learning for recommender systems: challenges and remedies. Artif. Intell. Rev. 52(1), 1–37 (2019)
6. Baydogmus, G.K.: Solution for TSP/MTSP with an improved parallel clustering and elitist ACO. Computer Science and Information Systems 20(1), 195—-214 (2023), https://doi.org/10.2298/CSIS220820053B
7. Chen, H.H., Chen, P.: Differentiating Regularization Weights – A Simple Mechanism to Alleviate Cold Start in Recommender Systems. ACM Trans. Knowl. Discov. Data 13(1) (jan 2019), https://doi.org/10.1145/3285954
8. Chen, R., Hua, Q., Chang, Y.S., Wang, B., Zhang, L., Kong, X.: A Survey of Collaborative Filtering-Based Recommender Systems: From Traditional Methods to Hybrid Methods Based on Social Networks. IEEE Access 6, 64301–64320 (2018)
9. Choi, S.M., Jang, K., Lee, T.D., Khreishah, A., Noh, W.: Alleviating Item-Side Cold-Start Problems in Recommender Systems Using Weak Supervision. IEEE Access 8, 167747–167756 (2020)
10. Cui, Z., Xu, X., XUE, F., Cai, X., Cao, Y., Zhang, W., Chen, J.: Personalized Recommendation System Based on Collaborative Filtering for IoT Scenarios. IEEE Transactions on Services Computing 13(4), 685–695 (2020)
11. Feng, J., Xia, Z., Feng, X., Peng, J.: RBPR: A hybrid model for the new user cold start problem in recommender systems. Knowledge-Based Systems 214, 106732 (2021)
12. Feng, W., Zhu, Q., Zhuang, J., Yu, S.: An expert recommendation algorithm based on Pearson correlation coefficient and FP-growth. Clust. Comput. 22(Supplement), 7401–7412 (2019)

13. de Gemmis, M., Lops, P., Musto, C., Narducci, F., Semeraro, G.: Semantics-Aware Content-Based Recommender Systems, pp. 119–159. Springer US, Boston, MA (2015), https://doi.org/10.1007/978-1-4899-7637-6_4
14. Ghazinour, K., Matwin, S., Sokolova, M.: Monitoring and recommending privacy settings in social networks. In: Guerrini, G. (ed.) Joint 2013 EDBT/ICDT Conferences, EDBT/ICDT '13, Genoa, Italy, March 22, 2013, Workshop Proceedings. pp. 164–168. ACM (2013)
15. Goy, S., Coors, V., Finn, D.: Grouping techniques for building stock analysis: A comparative case study. Energy and Buildings 236, 110754 (2021)
16. Grzegorowski, M.: Scaling of complex calculations over big data-sets. In: Slezak, D., Schaefer, G., Vuong, S.T., Kim, Y. (eds.) Active Media Technology - 10th International Conference, AMT 2014, Warsaw, Poland, August 11-14, 2014. Proceedings. Lecture Notes in Computer Science, vol. 8610, pp. 73–84. Springer (2014), https://doi.org/10.1007/978-3-319-09912-5_7
17. Grzegorowski, M.: Governance of the Redundancy in the Feature Selection Based on Rough Sets' Reducts. In: Flores, V., Gomide, F.A.C., Janusz, A., Meneses, C., Miao, D., Peters, G., Ślęzak, D., Wang, G., Weber, R., Yao, Y. (eds.) Rough Sets - International Joint Conference, IJCRS 2016, Santiago de Chile, Chile, October 7-11, 2016, Proceedings. Lecture Notes in Computer Science, vol. 9920, pp. 548–557 (2016), https://doi.org/10.1007/978-3-319-47160-0_50
18. Grzegorowski, M.: Massively Parallel Feature Extraction Framework Application in Predicting Dangerous Seismic Events. In: Ganzha, M., Maciaszek, L.A., Paprzycki, M. (eds.) Proceedings of the 2016 Federated Conference on Computer Science and Information Systems, FedCSIS 2016, Gdańsk, Poland, September 11-14, 2016. Annals of Computer Science and Information Systems, vol. 8, pp. 225–229. IEEE (2016), https://doi.org/10.15439/2016F90
19. Grzegorowski, M.: Selected aspects of interactive feature extraction. Trans. Rough Sets 23, 121–287 (2023), https://doi.org/10.1007/978-3-662-66544-2_8
20. Grzegorowski, M., Janusz, A., Lazewski, S., Swiechowski, M., Jankowska, M.: Prescriptive analytics for optimization of FMCG delivery plans. In: Ciucci, D., Couso, I., Medina, J., Ślęzak, D., Petturiti, D., Bouchon-Meunier, B., Yager, R.R. (eds.) Information Processing and Management of Uncertainty in Knowledge-Based Systems - 19th International Conference, IPMU 2022, Milan, Italy, July 11-15, 2022, Proceedings, Part II. Communications in Computer and Information Science, vol. 1602, pp. 44–53. Springer (2022)
21. Grzegorowski, M., Janusz, A., Ślęzak, D., Szczuka, M.S.: On the role of feature space granulation in feature selection processes. In: Nie, J., Obradovic, Z., Suzumura, T., Ghosh, R., Nambiar, R., Wang, C., Zang, H., Baeza-Yates, R., Hu, X., Kepner, J., Cuzzocrea, A., Tang, J., Toyoda, M. (eds.) 2017 IEEE International Conference on Big Data (IEEE BigData 2017), Boston, MA, USA, December 11-14, 2017. pp. 1806–1815. IEEE Computer Society (2017)
22. Grzegorowski, M., Litwin, J., Wnuk, M., Pabis, M., Marcinowski, L.: Survival-based feature extraction - application in supply management for dispersed vending machines. IEEE Transactions on Industrial Informatics 19(3), 3331–3340 (2023)
23. Grzegorowski, M., Ślęzak, D.: On resilient feature selection: Computational foundations of r-C-reducts. Inf. Sci. 499, 25–44 (2019)
24. Grzegorowski, M., Stawicki, S.: Window-based feature extraction framework for multi-sensor data: A posture recognition case study. In: Ganzha, M., Maciaszek, L.A., Paprzycki, M. (eds.) 2015 Federated Conference on Computer Science and Information Systems, FedCSIS 2015, Lódz, Poland, September 13-16, 2015. Annals of Computer Science and Information Systems, vol. 5, pp. 397–405. IEEE (2015)
25. Guo, G., Qiu, H., Tan, Z., Liu, Y., Ma, J., Wang, X.: Resolving data sparsity by multi-type auxiliary implicit feedback for recommender systems. Knowl. Based Syst. 138, 202–207 (2017)
26. Hamedani, M.R., Ali, I., Hong, J., Kim, S.W.: Trustrec: An effective approach to exploit implicit trust and distrust relationships along with explicitones for accurate recommendations. Comput. Sci. Inf. Syst. 18, 93–114 (2021)

27. Han, J., Kamber, M., Pei, J.: 6 - mining frequent patterns, associations, and correlations: Basic concepts and methods. In: Han, J., Kamber, M., Pei, J. (eds.) Data Mining (Third Edition), pp. 243–278. The Morgan Kaufmann Series in Data Management Systems, Morgan Kaufmann, Boston, third edition edn. (2012), https://www.sciencedirect.com/science/article/pii/B978012381479100006X
28. Heidari, N., Moradi, P., Koochari, A.: An attention-based deep learning method for solving the cold-start and sparsity issues of recommender systems. Knowl. Based Syst. 256, 109835 (2022)
29. Himeur, Y., Alsalemi, A., Al-Kababji, A., Bensaali, F., Amira, A., Sardianos, C., Dimitrakopoulos, G., Varlamis, I.: A survey of recommender systems for energy efficiency in buildings: Principles, challenges and prospects. Information Fusion 72, 1–21 (2021)
30. Jalili, M., Ahmadian, S., Izadi, M., Moradi, P., Salehi, M.: Evaluating Collaborative Filtering Recommender Algorithms: A Survey. IEEE Access 6, 74003–74024 (2018)
31. Janusz, A., Grzegorowski, M., Michalak, M., Wróbel, Ł., Sikora, M., Ślęzak, D.: Predicting Seismic Events in Coal Mines Based on Underground Sensor Measurements. Engineering Applications of Artificial Intelligence 64, 83–94 (2017)
32. Kajan, E., Faci, N., Maamar, Z., Sellami, M., Ugljanin, E., Kheddouci, H., Stojanovic, D., Benslimane, D.: Real-time tracking and mining of users' actions over social media. Comput. Sci. Inf. Syst. 17(2), 403–426 (2020)
33. Kannout, E.: Context clustering-based recommender systems. In: 2020 15th Conference on Computer Science and Information Systems (FedCSIS). pp. 85–91 (2020)
34. Kannout, E., Grodzki, M., Grzegorowski, M.: Considering various aspects of models' quality in the quality pipeline - application in the logistics sector. In: Ganzha, M., Maciaszek, L.A., Paprzycki, M., Slezak, D. (eds.) Proceedings of the 17th Conference on Computer Science and Intelligence Systems, FedCSIS 2022, Sofia, Bulgaria, September 4-7, 2022. Annals of Computer Science and Information Systems, vol. 30, pp. 403–412 (2022)
35. Kannout, E., Grodzki, M., Grzegorowski, M.: Utilizing Frequent Pattern Mining for Solving Cold-Start Problem in Recommender Systems. In: Ganzha, M., Maciaszek, L.A., Paprzycki, M., Ślęzak, D. (eds.) Proceedings of the 17th Conference on Computer Science and Intelligence Systems, FedCSIS 2022, Sofia, Bulgaria, September 4-7, 2022. Annals of Computer Science and Information Systems, vol. 30, pp. 217–226 (2022)
36. Kannout, E., Nguyen, H.S., Grzegorowski, M.: Speeding up recommender systems using association rules. In: Intelligent Information and Database Systems, pp. 167–179. Springer Nature Switzerland (2022), https://doi.org/10.1007/978-3-031-21967-2_14
37. Kannout, E., Nguyen, H.S., Grzegorowski, M.: Efficient Techniques to Recommender System. Springer Cham (2023), revised Selected Papers from the 29th International Workshop on Concurrency, Specification and Programming (CS&P'21), Berlin, Germany
38. Karpus, A., Raczynska, M., Przybylek, A.: Things You Might Not Know about the k-Nearest Neighbors Algorithm. In: Fred, A.L.N., Filipe, J. (eds.) Proceedings of the 11th International Joint Conference on Knowledge Discovery, Knowledge Engineering and Knowledge Management, IC3K 2019, Volume 1: KDIR, Vienna, Austria, September 17-19, 2019. pp. 539–547. ScitePress (2019), https://doi.org/10.5220/0008365005390547
39. Karpus, A., Vagliano, I., Goczyla, K.: Serendipitous recommendations through ontology-based contextual pre-filtering. In: Kozielski, S., Mrozek, D., Kasprowski, P., Malysiak-Mrozek, B., Kostrzewa, D. (eds.) Beyond Databases, Architectures and Structures. Towards Efficient Solutions for Data Analysis and Knowledge Representation - 13th International Conference, BDAS 2017, Ustroń, Poland, May 30 - June 2, 2017, Proceedings. Communications in Computer and Information Science, vol. 716, pp. 246–259 (2017)
40. Karpus, A., Vagliano, I., Goczyla, K., Morisio, M.: An ontology-based contextual pre-filtering technique for recommender systems. In: Ganzha, M., Maciaszek, L.A., Paprzycki, M. (eds.) Proceedings of the 2016 Federated Conference on Computer Science and Information Systems, FedCSIS 2016, Gdańsk, Poland, September 11-14, 2016. Annals of Computer Science and Information Systems, vol. 8, pp. 411–420. IEEE (2016)

41. Kashef, R.: Enhancing the Role of Large-Scale Recommendation Systems in the IoT Context. IEEE Access 8, 178248–178257 (2020)
42. Kawai, M., Sato, H., Shiohama, T.: Topic model-based recommender systems and their applications to cold-start problems. Expert Systems with Applications 202, 117129 (2022)
43. Khan, Z., Hussain, M.I., Iltaf, N., Kim, J., Jeon, M.: Contextual recommender system for e-commerce applications. Applied Soft Computing 109, 107552 (2021)
44. Kolahkaj, M., Harounabadi, A., Nikravanshalmani, A., Chinipardaz, R.: Incorporating multidimensional information into dynamic recommendation process to cope with cold start and data sparsity problems. J. Ambient Intell. Humaniz. Comput. 12(10), 9535–9554 (2021)
45. Kwasnicka, H., Ovedenski, T.: Pix2trips - a system supporting small groups of urban tourists. In: Ganzha, M., Maciaszek, L.A., Paprzycki, M., Ślęzak, D. (eds.) Proceedings of the 16th Conference on Computer Science and Intelligence Systems, Online, September 2-5, 2021. Annals of Computer Science and Information Systems, vol. 25, pp. 141–145 (2021)
46. Kwiecinski, R., Gorecki, T., Filipowska, A.: Learning edge importance in bipartite graph-based recommendations. In: 2022 17th Conference on Computer Science and Intelligence Systems (FedCSIS). pp. 227–233 (2022)
47. Lee, H., Im, J., Jang, S., Cho, H., Chung, S.: MeLU: Meta-Learned User Preference Estimator for Cold-Start Recommendation. In: Proceedings of the 25th ACM SIGKDD International Conference on Knowledge Discovery and Data Mining. p. 1073–1082. KDD '19, Association for Computing Machinery, New York, NY, USA (2019)
48. Lee, S., Kim, S., Park, S., Chae, D.: A tripartite-graph based recommendation framework for price-comparison services. Comput. Sci. Inf. Syst. 16(2), 333–357 (2019)
49. Lika, B., Kolomvatsos, K., Hadjiefthymiades, S.: Facing the cold start problem in recommender systems. Expert Systems with Applications 41(4, Part 2), 2065–2073 (2014)
50. Liu, F., Tang, R., Li, X., Zhang, W., Ye, Y., Chen, H., Guo, H., Zhang, Y.: Deep Reinforcement Learning based Recommendation with Explicit User-Item Interactions Modeling (2018)
51. Lu, Y., Fang, Y., Shi, C.: Meta-learning on heterogeneous information networks for cold-start recommendation. In: Proceedings of the 26th ACM SIGKDD International Conference on Knowledge Discovery &; Data Mining. p. 1563–1573. KDD '20, Association for Computing Machinery, New York, NY, USA (2020), https://doi.org/10.1145/3394486.3403207
52. Luna, J.M., Fournier-Viger, P., Ventura, S.: Frequent itemset mining: A 25 years review. Wiley Interdisciplinary Reviews: Data Mining and Knowledge Discovery 9(6), e1329 (2019)
53. Merabet, F.Z., Benmerzoug, D.: QoS prediction for service selection and recommendation with a deep latent features autoencoder. Comput. Sci. Inf. Syst. 19(2), 709–733 (2022), https://doi.org/10.2298/csis210518054m
54. Najafabadi, M.K., Mohamed, A.H., Mahrin, M.N.: A survey on data mining techniques in recommender systems. Soft Comput. 23(2), 627–654 (2019)
55. Natarajan, S., Vairavasundaram, S., Natarajan, S., Gandomi, A.H.: Resolving data sparsity and cold start problem in collaborative filtering recommender system using linked open data. Expert Systems with Applications 149, 113248 (2020)
56. Nilashi, M., Ibrahim, O., Bagherifard, K.: A recommender system based on collaborative filtering using ontology and dimensionality reduction techniques. Expert Systems with Applications 92, 507–520 (2018)
57. Obeid, C., Lahoud, C., El, K.H., Champin, P.A.: A novel hybrid recommender system approach for student academic advising named COHRS, supported by case-based reasoning and ontology. Computer Science and Information Systems 19(2), 979–1005 (2022), https://doi.org/10.2298/CSIS220215011O
58. Odic, A., Tkalcic, M., Tasic, J.F., Kosir, A.: Predicting and detecting the relevant contextual information in a movie-recommender system. Interact. Comput. 25(1), 74–90 (2013)
59. Papadakis, H., Papagrigoriou, A., Panagiotakis, C., Kosmas, E., Fragopoulou, P.: Collaborative filtering recommender systems taxonomy. Knowl. Inf. Syst. 64(1), 35–74 (2022)

60. Pasricha, R., McAuley, J.: Translation-Based Factorization Machines for Sequential Recommendation. In: Proceedings of the 12th ACM Conference on Recommender Systems. p. 63–71. RecSys'18, Association for Computing Machinery, New York, NY, USA (2018)
61. Pawlicka, A., Pawlicki, M., Kozik, R., Choraś, R.S.: A systematic review of recommender systems and their applications in cybersecurity. Sensors 21(15) (2021), https://www.mdpi.com/1424-8220/21/15/5248
62. Pondel, M., Korczak, J.: Collective clustering of marketing data - recommendation system upsaily. In: Ganzha, M., Maciaszek, L.A., Paprzycki, M. (eds.) Proceedings of the 2018 Federated Conference on Computer Science and Information Systems, FedCSIS 2018, Poznań, Poland, September 9-12, 2018. Annals of Computer Science and Information Systems, vol. 15, pp. 801–810 (2018)
63. Pulis, M., Bajada, J.: Siamese Neural Networks for Content-Based Cold-Start Music Recommendation., p. 719–723. Association for Computing Machinery, New York, NY, USA (2021)
64. Pérez-Almaguer, Y., Yera, R., Alzahrani, A.A., Martínez, L.: Content-based group recommender systems: A general taxonomy and further improvements. Expert Systems with Applications 184, 115444 (2021)
65. Sikora, M., Matyszok, P., Wróbel, L.: SCARI: separate and conquer algorithm for action rules and recommendations induction. Inf. Sci. 607, 849–868 (2022)
66. Silveira, T., Zhang, M., Lin, X., Liu, Y., Ma, S.: How good your recommender system is? A survey on evaluations in recommendation. International Journal of Machine Learning and Cybernetics 10, 813–831 (2019)
67. Singh, M.: Scalability and sparsity issues in recommender datasets: a survey. Knowl. Inf. Syst. 62(1), 1–43 (2020)
68. Sobhanam, H., Mariappan, A.K.: Addressing cold start problem in recommender systems using association rules and clustering technique. In: 2013 International Conference on Computer Communication and Informatics. pp. 1–5 (2013)
69. Sofikitis, E., Makris, C.: Development of recommendation systems using game theoretic techniques. Computer Science and Information Systems 19(00), 1133–1154 (2022)
70. Steck, H.: Collaborative filtering via high-dimensional regression. CoRR abs/1904.13033 (2019)
71. Sulc, Z., Rezanková, H.: Comparison of similarity measures for categorical data in hierarchical clustering. J. Classif. 36(1), 58–72 (2019), https://doi.org/10.1007/s00357-019-09317-5
72. Tilahun, Z., Jun, H., Oad, A.: Solving cold-start problem by combining personality traits and demographic attributes in a user based recommender system. International Journal of Advanced Research in Computer Science and Software Engineering 7(5), 231–239 (may 2017)
73. Tsagkias, M., King, T.H., Kallumadi, S., Murdock, V., de Rijke, M.: Challenges and Research Opportunities in ECommerce Search and Recommendations. SIGIR Forum 54(1) (feb 2021)
74. Valiente, J.A.R., Merino, P.J.M., Díaz, H.J.P., Ruiz, J.S., Kloos, C.D.: Evaluation of a learning analytics application for open edX platform. Comput. Sci. Inf. Syst. 14(1), 51–73 (2017), https://doi.org/10.2298/CSIS160331043R
75. Vančura, V., Alves, R., Kasalický, P., Kordík, P.: Scalable Linear Shallow Autoencoder for Collaborative Filtering. In: Proceedings of the 16th ACM Conference on Recommender Systems. p. 604–609. RecSys '22, Association for Computing Machinery, New York, NY, USA (2022)
76. Viktoratos, I., Tsadiras, A., Bassiliades, N.: Combining community-based knowledge with association rule mining to alleviate the cold start problem in context-aware recommender systems. Expert Systems with Applications 101, 78–90 (2018)
77. Vizine Pereira, A.L., Hruschka, E.R.: Simultaneous co-clustering and learning to address the cold start problem in recommender systems. Knowledge-Based Systems 82, 11–19 (2015)
78. Walek, B., Fojtik, V.: A hybrid recommender system for recommending relevant movies using an expert system. Expert Systems with Applications 158, 113452 (2020)

79. Wei, Y., Wang, X., Li, Q., Nie, L., Li, Y., Li, X., Chua, T.S.: Contrastive Learning for Cold-Start Recommendation. In: Proceedings of the 29th ACM International Conference on Multimedia. p. 5382–5390. MM '21, Association for Computing Machinery, New York, NY, USA (2021), https://doi.org/10.1145/3474085.3475665
80. Wu, H., Zhang, Z., Yue, K., Zhang, B., He, J., Sun, L.: Dual-regularized matrix factorization with deep neural networks for recommender systems. Knowledge-Based Systems 145, 46–58 (2018)
81. Yan, H.C., Wang, Z.R., Niu, J.Y., Xue, T.: Application of covering rough granular computing model in collaborative filtering recommendation algorithm optimization. Advanced Engineering Informatics 51, 101485 (2022)
82. Yeh, J.Y., Tsai, C.J.: A graph-based feature selection method for learning to rank using spectral clustering for redundancy minimization and biased PageRank for relevance analysis. Computer Science and Information Systems 19(1), 141–164 (2022)
83. Yi, B., Shen, X., Liu, H., Zhang, Z., Zhang, W., Liu, S., Xiong, N.: Deep Matrix Factorization With Implicit Feedback Embedding for Recommendation System. IEEE Transactions on Industrial Informatics 15(8), 4591–4601 (2019)
84. Zdravevski, E., Lameski, P., Mingov, R., Kulakov, A., Gjorgjevikj, D.: Robust histogram-based feature engineering of time series data. In: Ganzha, M., Maciaszek, L.A., Paprzycki, M. (eds.) 2015 Federated Conference on Computer Science and Information Systems, FedCSIS 2015, Lódz, Poland, September 13-16, 2015. Annals of Computer Science and Information Systems, vol. 5, pp. 381–388. IEEE (2015), https://doi.org/10.15439/2015F420
85. Zhang, F., Qi, S., Liu, Q., Mao, M., Zeng, A.: Alleviating the data sparsity problem of recommender systems by clustering nodes in bipartite networks. Expert Syst. Appl. 149, 113346 (2020), https://doi.org/10.1016/j.eswa.2020.113346
86. Zhu, Y., Xie, R., Zhuang, F., Ge, K., Sun, Y., Zhang, X., Lin, L., Cao, J.: Learning to Warm Up Cold Item Embeddings for Cold-Start Recommendation with Meta Scaling and Shifting Networks. In: Proceedings of the 44th International ACM SIGIR Conference on Research and Development in Information Retrieval. p. 1167–1176. SIGIR '21, Association for Computing Machinery, New York, NY, USA (2021), https://doi.org/10.1145/3404835.3462843
87. Zhu, Z., Kim, J., Nguyen, T., Fenton, A., Caverlee, J.: Fairness among New Items in Cold Start Recommender Systems, p. 767–776. Association for Computing Machinery, New York, NY, USA (2021)

Eyad Kannout is currently pursuing a Ph.D. in the Institute of Informatics at the University of Warsaw, wherein he is also delivering the labs of Machine Learning course for many years. His research activities are mainly focused on Recommendation Systems and ML/AI. He obtained his Master in Computer Science at Warsaw University of Technology, Poland in 2016, and received his Bachelor in Informatics Engineering from University of Aleppo, Syria in 2012. In addition to his academic career, Eyad Kannout held several software engineering positions in the financial sector.

Michał Grodzki is student at faculty of Mathematics, Informatics and Mechanics at the Warsaw University. He received the Bachelor's degree in 2020 in the field of ordinary differential equations. Currently, he is pursuing his Master and mainly interested in Machine Learning and Recommender Systems research.

Marek Grzegorowski is for many years, associated with the Institute of Informatics at the University of Warsaw, wherein, in 2021, received Ph.D. in computer science. He is an

active and experienced researcher in the fields of science related to data exploration, machine learning, artificial intelligence, and recommender systems. He authored a number of scientific articles. In his career, conducted several research and development projects related to the application of ML/AI in academic and industry collaboration.

Received: April 11, 2022; Accepted: November 16, 2022.

Computer Science and Information Systems 20(4):1367–1387 https://doi.org/10.2298/CSIS221210055K

Sentence Embedding Approach using LSTM Auto-encoder for Discussion Threads Summarization

Abdul Wali Khan[1], Feras Al-Obeidat[2], Afsheen Khalid[1], Adnan Amin[1], and Fernando Moreira[3]

[1] Center for Excellence in Information Technology,Institute of Management Sciences
Peshawar, Pakistan
abdulwalikhanafridi@gmail.com
{adnan.amin, afsheen.khalid}@imsciences.edu.pk
[2] College of Technological Innovation, Zayed University
Abu Dhabi, UAE
Feras.Al-Obeidat@zu.ac.ae
[3] REMIT, IJP, Universidade Portucalense & IEETA, Universidade de Aveiro
Portugal
fmoreira@uportu.pt

Abstract. Online discussion forums are repositories of valuable information where users interact and articulate their ideas and opinions, and share experiences about numerous topics. These online discussion forums are internet-based online communities where users can ask for help and find the solution to a problem. A new user of online discussion forums becomes exhausted from reading the significant number of irrelevant replies in a discussion. An automated discussion thread summarizing system (DTS) is necessary to create a candid view of the entire discussion of a query. Most of the previous approaches for automated DTS use the continuous bag of words (CBOW) model as a sentence embedding tool, which is poor at capturing the overall meaning of the sentence and is unable to grasp word dependency. To overcome these limitations, we introduce the LSTM Auto-encoder as a sentence embedding technique to improve the performance of DTS. The empirical result in the context of the proposed approach's average precision, recall, and F-measure with respect to ROGUE-1 and ROUGE-2 of two standard experimental datasets demonstrates the effectiveness and efficiency of the proposed approach and outperforms the state-of-the-art CBOW model in sentence embedding tasks and boost the performance of the automated DTS model.

Keywords: Sentence embedding, LSTM Auto-encoder, CBOW, Deep learning, Machine learning, NLP.

1. Introduction

Online discussion forums are web services where users can post a query about a specific topic and provide an online environment for individuals to articulate their thoughts. These online discussion forums are online communities where people with similar interests may exchange ideas, points of view, and experiences on a variety of topics. Because of user interaction and conversation, these forums become ideal archives of textual content. Online discussion forums may be used for various purposes, including getting students to discuss

the course subject before class and reflecting on readings or assignments they have completed outside of class. Most of the queries generate huge replies in the discussion, so a new user becomes unable to scan all discussions and find the valuable and relevant text content shared by the users[44]. Some of the latest online discussion forums facilitate the users' finding their problem-relevant user discussions [13].

In our daily lives, we frequently engage in multidimensional conversations with each other through blogs, online discussion forums, and online video meetings which generate an overwhelming amount of data and lead to information overload problems. The overwhelming amount of data generated from online interaction sometimes leads to information overload problems. On online discussion forums, the users hurriedly reply to the query, which may not always be relevant to the question. Extracting the relevant content from this growing raw text is a tough task for new users of the discussion forum [27]. This becomes stress-inducing and discourages the user's perception of online discussion forums. To maintain problem-relevant user replies in an online discussion forum, monitoring and filtering processes should be used. By using this process, new users will be able to easily find relevant content in thread discussions. The authors in the literature use numerous approaches to grasp the relevant and most valuable text content from this massive amount of data. Some of the commonly used methods are user-phrase queries to extract the most relevant text content from textual data [21], and an act-guided approach for tweets summarization based on word-based and symbol-based features [43], [42].

This study proposes an automated DTS model for online discussion forums that can automatically extract query-relevant user replies. The proposed model is based on the LSTM Auto-encoder techniques which is a deep learning architecture for sentence embedding to transform the sentences of the discussion replies into feature space for the extraction of the most relevant and significant text content using different similarity measures between the query and replies of the discussion. By using this automated model, users of online discussion forums can easily grasp the idea of the entire discussion by generating a candid view of the entire discussion.

The proposed technique for sentence embedding is a novel approach for embedding replies to sentences in online discussion forums. In literature, the CBOW model has been a widely used technique for sentence embedding in the field of natural language processing (NLP) for text summarizing tasks that have multiple flows for sentence embedding. This model considers only the surrounding words and ignores the structure and order of the words in the sentence. The CBOW model is also sensitive to the frequency of words, in which case common words have a high impact on sentence embedding. For the vector representation of a sentence, this model uses the average word vector approach, which disregards the word order in the long sequence of words [1]. We used the LSTM Auto-encoder in our model, which has the capability to remember patterns in long sequences of input. The model is fully generic and can be used for the summarizing of thread discussion of any English-based online discussion forum. The rest of the paper is organized as follows.

In Section 2, we review the previous state-of-the-art approaches for text summarization, which include numerous techniques related to text summarization, extractive and abstractive summarization approaches, and applications of discussion thread summarization. section 3 consists of the most important part of this study. The purpose of this section is to describe a novel approach to thread discussion summarization using the LSTM auto-

encoder technique for automated summarization of thread discussion of online discussion forums. Section 4 elaborates on the outcomes, discusses the procedure that was suggested, and compares it with the most effective technique for the task of embedding sentences, section 5 describes the conclusion and future work of the study.

2. Literature Review

As an integral part of Natural Language Processing, text summarization has a wide range of applications, including news summarization, email thread summarization, social media content summarization, and thread discussion summarization of online discussion forums. There are two main approaches to text summarization which are extractive and abstractive summarization. In extractive summarization, the most significant textual chunks are extracted from the source text and merged in an extractive summary to reflect the core concept and flow of the original text. Abstractive summarization is a more complex and critical task that paraphrases the original text in a new version which can reflect the main clue of the original text. Based on the source documents, Text summarization is further divided into two classes which are multi-document and single-document summarization.

The extractive summarization approach for text summarization has various applications. The authors in the literature employ various techniques for the extraction of relevant text chunks. For an extractive summary generation, the text needs to be classified in order to identify and extract the relevant chunks. In the classification technique, similar textual units are classified in the same clusters independent of their significance in textual data [15]. For document categorization in some studies, the textual units are treated as typical sentences [17], in meeting conversations summarization the units are usually utterances [20], [26], and in the case of DTS, the units treat as a reply sentence [32],[31]. In the next step, various ranking methods are used to identify the importance of each textual chunk and assign a salience score to each textual chunk to arrange all in decreasing order based on their score. The textual chunks with a high score are considered to be the most significant. Based on a specific threshold or predefined cutoff, the significant textual chunks are extracted for the final summary. Cue dictionary techniques introduced in which the significance chunks of text are computed based on the presence or absence in the cue dictionary [23], In the title method, the weight of the sentences is computed based on the sum of all the text appearing in the title of the heading of source documents. For the extraction of relevant content from text [37] uses ontology and TF-IDF concept-based clustering approach for extractive summarization, similarly [38] uses numerous text mining techniques to create an extractive summary of the patent record. The TF-IDF and machine learning-based techniques are also used for the extraction [7].

One of the most critical parts of the extractive summarization process is to keep both coherence and consistency of the previously chosen textual units in the newly created version of the original text [6], [24]. Some feature-based summarization methods such as cue phrases and sentence locations are proposed to identify the relevant sentences for a final summary generation [39]. A combined TF-IDF and ontology tree structure techniques introduce for the extraction of keywords which is used for the selection of salient textual units from source text documents. after extraction and selection of keywords, a clustering technique is applied to cluster salient sentences to extract the relevant text chunks from a condensed text [14]. Search engine-based techniques are proposed on an extended query

using the WordNet database to find the relevant web pages and on the bases of relevant keywords, the relevant identified sentences are extracted for final summarization [11].

Recently Graph-based approaches have been proposed for extractive summarization. Graph-based approaches are used as a PageRank (PR) algorithm [28] to rank the different textual units in sentences or passages. In graph-based approaches a sentence is represented as a node in a graph, if this node has a certain relation in a graph then it is more salient for the final summary [3].

Due to the advent of deep learning in the field of NLP, extractive summarization has become an exciting field of research. using deep learning for text-processing jobs, the performance of various machine learning methods improved. Recent research studies proposed many deep learning techniques for extractive summarization such as Query-oriented based extractive summarization proposed using the deep auto-encoder (AE) to compute the feature space from the input of term-frequency (TF) based on two vocabularies [41]. Similarly, [38] uses Tree Augmented NBN (TAN) variance of Bayesian network to generate extractive summarization of patent record. Sequence-to-sequence auto-encoder for extractive summarization is also used for long and noisy social media text content [18], Multi-document extractive text summarization approach is proposed which uses an auto-encoder neural network to compare the scoring and performance of multiple documents [30].

In this study, we use LSTM Auto-encoder for sentence embedding and an extractive approach for DTS, similar to the one suggested by [30], which is based on recurrent neural network architecture. The proposed LSTM Auto-encoder of this study is also a deep learning architecture that is mostly used as embedding techniques for image data but recent research studies prove that it is also a powerful tool for text data [1]. LSTM auto-encoder consists of two parts which are Encoder and Decoder. The input sequence is read by the encoder which encodes the entire input sequence into an internal representation. The second part decoder reads the internal representation of the encoder and generates the output sequence.

2.1. Preliminary study

LSTM Auto-Encoder as a sentence embedding: The sentence embedding vector can be obtained by using the average word vector in a sentence. Similarly, we can obtain the paragraph vector by calculating the average sentence vectors in a paragraph. The average vector technique is inefficient in capturing the semantic information in sentences. To obtain the rich embedding vector of the sentence we used LSTM Auto-encoder to grasp the semantic relation between words in a sequence of input using the recurrent neural network architecture for the DTS model.

Auto Encoder: Previous approaches for automated DTS use different embedding techniques. One of the most common techniques is the Continues Bag of Words (CBOW) model [13]. All these embedding techniques are based on the distributional hypothesis in which the similarity of words is based on their contextual representation in the sentence [1]. With the emergence of deep neural networks in the field of Natural language processing, neural word embedding received a lot of attention [2]. Many research studies prove that the neural word embedding technique is a powerful tool for understanding the

semantic relation between words such as dynamic convolutional neural network (DCNN) for sentence embedding tasks to extract the most active feature from sentences [33]. This model allowed extracting the most active features in the sentences independently of their location. The authors of [36] build a general-purpose sentence encoder for multiple objectives which are classification of text, machine transition, parse tree generation, and skip-thought tasks. The proposed model is trained by several data sources on over 100 million sentences with multiple training objectives. In [5] the authors proposed a recursive auto-encoder (RAE) based on unfolding objectives for the similarity of two sentences. In [8] the authors proposed an auto-encoder model which can denoise the sentence by deleting words and changing the positions of words in a sentence where the decoder is used to reconstruct the original sentence by swapping bi-grams. In [25] the authors introduce a neural topic model to capture the global semantic meaning of the document and integrate that model with an automatic text summarization model. [12] Proposed a hierarchical encoder-decoder model for DTS which is pre-trained on synthetic interleaved text. This approach aims to overcome the limitation of the traditional thread discussion summarization system.

Long Short-Term Memory (LSTM): LSTM is another variant of recurrent neural networks. An LSTM-based neural network is better than traditional neural networks due to its memory. The traditional neural network is not virtuous at memorizing short-term patterns and also suffers from vanishing gradient problems [19]. The LSTM improves the performance of the traditional neural network in these problems. Numerous studies use LSTM in many natural language processing tasks such as a combined model based on word embedding using LSTM for semantic similarity in text classification tasks [40]. LSTM-based sentence encoder that is trained by an annotated training corpus to capture the useful feature from sentences and use these features for text classification tasks [35]. LSTM-CNN proposed by [34] for extractive summarization to construct new sentences by exploring semantic phrases of text. A multilayered attentional peephole convolutional long short-term memory (LSTM) for extractive text summarization task [29]. The model is based on an attentional mechanism that gives weight to the most significant parts of the text. Attention-based bidirectional LSTM is used which is also known as BiLSTM for text generation to enhance the correlation between generated text and the source text [10]. This model is also able to eliminate repeated words and solves out-of-vocabulary word problems. The use of LSTM in Auto-encoder is demonstrated in Fig. 1 improves the performance of automated thread discussion summarization. Text processing tasks are highly dependent on the representation of the text in the feature space. Most of the machine learning or deep learning algorithm performs better using efficient embedding techniques [22].

Text quality features: Text features refer to words or groups of words in a text which help to understand the core idea of the text. In text processing, text features play very important roles. Some of the most common text features are as follows:

Semantic distance between texts: Word Mover's Distance (WMD) is the most commonly used technique for semantic distance calculation between text documents. This technique is used to find the minimum cumulative distance between two text documents in multi-dimensional space.

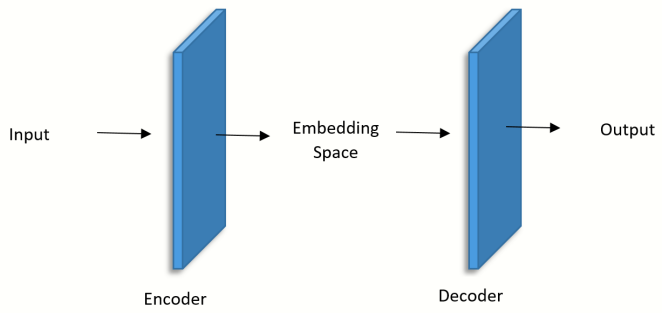

Fig. 1. LSTM Auto-encoder based sentence embedding

$$Sem.Distance = WMD\ (text\ A,\ text\ B) \tag{1}$$

Cosine similarity between texts: Cosine similarity is the process of finding the similarity between the inner product of the vectors of two texts. It calculates the angle between the vectors of the text documents. In Python, cosine similarity can be calculated using the following formula.

$$Cosin.Sim{=}Cosine\_Sim(text\ A,text\ B) \tag{2}$$

Unique word count: Unique words are unrepeated words in the text which are considered text features in text processing. It can be found by counting the unique words minus the repeated words in a sentence or text. In Python, the following formula can be used to count the unique words.

$$Uniqe\_Word{=}Unique\_words(text) \tag{3}$$

Common overlapping words in texts: overlapping words are those words that have a common semantic characteristic. These words can be found by using Jaccard similarity in Python using the following formula which finds the similarity of asymmetric binary vectors of text A and B.

$$Com\_words{=}Jaccard\_Sim\ (text\ A,\ text\ B) \tag{4}$$

Length of texts: text length is another feature of text in which the length of two texts or two sentences is used as a common feature. In python the following formula can be used to find the length of a text.

$$Text\_length = \frac{No.\ of\ words\ in\ a\ text}{Max\ length\ of\ text} \tag{5}$$

Number of Nouns and Verbs in a text: In this technique, the number of nouns and verbs are considered as text features. In python, the following formula is used to find the number of nouns and verbs in texts.

$$Noun\_verb = \frac{No.\ of\ verbs\ and\ nouns}{Text\ length} \tag{6}$$

3. Methodology

In this section, we discuss the proposed methodology to summarize the discussions of online discussion forums using an automated discussion thread summarization model. The order of the steps is shown in the methodology framework Fig. 2 and the description of each step is given below.

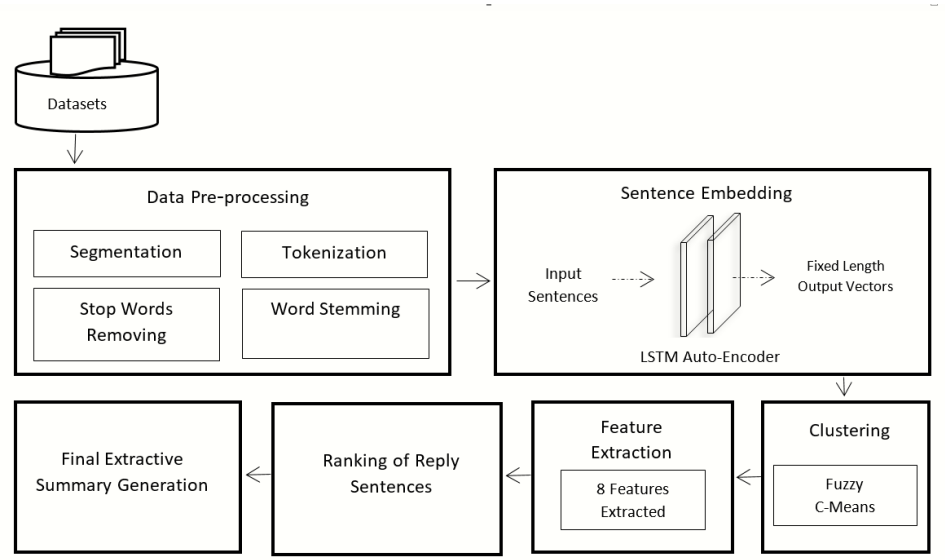

Fig. 2. Methodology Framework

3.1. Datasets

In this study, we used two standard discussion forum datasets: Ubuntu datasets generated by Ubuntu Online discussion forums and *NYC* datasets obtained from the TripAdvisor discussion forum. The Ubuntu dataset contains *756* user conversations. Similarly, the *NYC* dataset has *788* user conversations. for evaluation of the proposed methodology, the query of each thread is referred to as the initial posts and the replies to the query are called the candidate answers.

3.2. Data preprocessing

The preparation of data is the first step for any machine-learning task. To prepare data for our machine learning algorithm, we performed the following four types of text preprocessing tasks.

1. *Sentence segmentation:* This is the process of splitting lengthy text into small chunks or sentences. Sentence boundaries are the points where a text sequence is split into

sentences. We have used signs of interrogation (?), exclamation (!), and full stop (.) as sentence boundaries to segment the text.

2. *Tokenization:* After segmenting the text into sentences, word tokenization is performed. Different techniques have been applied to split the sentence into tokens of words such as the white space technique, we have divided the reply sentences into tokens of words using the widely used tools for text processing which is *(NLTK)* library of Python.
3. *Removing stop words:* Stop words such as "the", "an", "a", "is", "all", etc. are not significant words. These words are used frequently in the text and cannot be identified as having any particular value, hence they are not taken into account in our feature-embedded space. To reduce noise and prepare the text for the machine learning model to be applied, these words need to be removed.
4. *Word stemming:* It is the process in which each word is derived into its base or root word. The word-stemming process aims to help the algorithm to catch the word similarity in embedding. An example of word-stemming is to convert the stem words *'playing', 'played', 'plays'* to its root word which is *'play'*. In this process, we used the Porter stemmer to get the stems of the words.

3.3. Embedding of reply sentences

Word embedding is the building block of sentence embedding that transforms the distinct words into a single vector of 1s and 0s. This type of embedding is known as one-hot encoding and is completely dependent upon the corpus. In the vector of this embedding technique, 1's indicates the presence of a word and 0's represents the absence of a word in the corpus. In this approach, we cannot capture any semantic information in a sentence.

Sentence embedding is the extension of word embedding where the entire variable-length sentence is converted into a fixed numerical vector. One of the simplest ways of converting a variable-length sentence into a fixed-length vector is to encode all the words of the sentence into vectors and then take the average of all these word vectors in a single numerical vector. This average word vector approach is followed by Word2vec models, which is not sufficient for capturing various semantic information, such as word ordering information and other semantic relation between the words. In textual data Transformation tasks, most of the previous approaches used averaging vector concepts [13] or weighted representation of text using TF-IDF [14]. In the literature, the word2vect is used in two versions: the CBOW model and the skip-gram model. The CBOW approach predicts the word using the surrounding context while the skip-gram model is the inverse of CBOW which uses the distributed representation of the input word and predicts the context. to capture the semantic information of a sentence, word2vect model embedding is unsuitable as they provide semantic information only in a limited context.

LSTM Auto-encoder is a recurrent neural network architecture demonstrated in Fig. 3. With the help of using LSTM, Auto-encoder can memorize the previous sequence of words and can capture word order dependency and other semantic information in a long sequence of words and produce a rich embedding vector of a sentence. We used LSTM encoder and decoder models and a combined model for the sentence embedding process. The first encoder model takes the tokenized sequence and embeds it into dense vectors of fixed length. the embedded vectors are then fed into an LSTM encoder layer with 128 units to learn the encoding of the input sequence into a fixed-length vector representation.

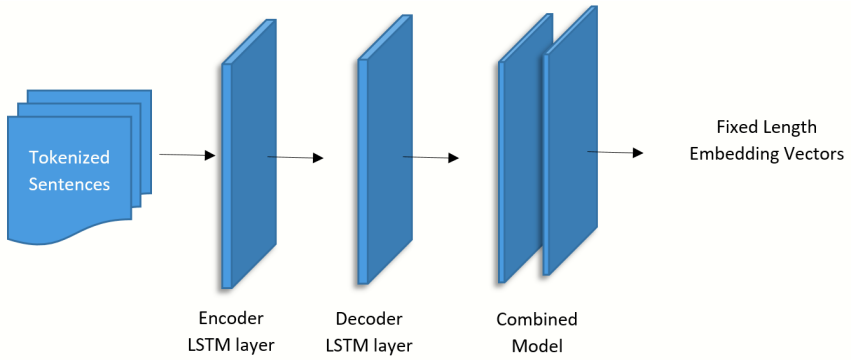

Fig. 3. LSTM Auto-encoder based sentence embedding.

In the second step, the decoder model takes the fixed length vector from the encoder model and generates the output sequence. the decoder model also has an LSTM layer with 128 units, followed by a dense output layer that produces a probability distribution over the output tokens. the last model is the combined model which integrates the encoder and decoder models. The purpose of the combined model is to learn the fixed-length vector representation of the input sequence and minimize the loss. we trained our model for *10* epochs. during training the model learn to generate a fixed-length vector representation of the input sequence.

The proposed study also uses the CBOW model for the assessment of the proposed sentence embedding technique. Both LSTM Auto-encoder and CBOW models are applied on both datasets for sentence embedding tasks. After applying embedding approaches, three clustering techniques are applied respectively on each dataset which is briefly described below.

3.4. Clustering

In thread discussions of online discussion forums, different users participate and share opinions about the topic. The initial question or query received mostly semantic similar replies. For extraction of the most relevant user replies to the initial question, similar replies must be clustered together to extract the most relevant replies from the discussion. In clustering, the most similar text chunks are clustered together is the crucial phase of clustering, from which Nemours scoring procedures are used to retrieve largely pertinent replies. Clustering has two types which are hard clustering and soft clustering. In hard clustering, each data point belongs to only one cluster, and in the soft clustering approach, the data point may belong to many clusters. In soft clustering, a similarity score is used which is also known as the membership score of each data point which designates the significance of the data points towards the cluster centroid which is an average vector of all the clustered sentence vectors.

In the proposed methodology we used three clustering techniques to cluster the reply sentences which are K-means, K-medoid, and FCM. Out of these three techniques, FCM outperforms other clustering techniques with LSTM Auto-encoder-based sentence

embedding vectors. FCM is a soft clustering technique that assigns a likelihood score to each reply sentence [4]. The way FCM works Initially, a sentence may belong to more than one cluster which converges to only one cluster after FCM iterations. The iterations use a step-wise approach to converge a sentence to only one cluster. These steps recalculate the centroid of the cluster and the membership score of the reply sentence [9].

Fuzzy C-means Convergence

1. Selected the number of clusters K = 10
2. Initially random values are assigned to each sentence which shows the probability of a sentence to clusters where pi is the point and k is the cluster (pi, k).

$$\mu_k(n+1) = \frac{\sum_{p_i \in k} P_i * P(\mu_k|P_i)^b}{\sum_{p_i \in k} P(\mu_k|P_i)^b} \tag{7}$$

3. After random initialization, iteratively cluster centroid and membership score are recalculated until the convergence.
4. The iteration will be continued until convergence or until the user-specified limit of iteration.

After the clustering process, we extracted only a single sentence from each cluster based on a certain score assigned to each sentence in the cluster using the quality text features scoring technique which is discussed in the next step.

3.5. Quality text features extraction

In the extractive text summarization process mostly text features are used as a scoring technique. The purpose of text feature extraction is to identify the salient sentence in the user reply sentences based on the assigned text feature score. Based on these quality features each sentence is scored in all clusters. A high score for the sentence indicates that the particular sentence has all the quality features and it is the most relevant one to the query of the discussion. In this work, eight different types of quality text features are extracted. The feature values for each reply sentence are normalized between zero and one which are further described below.

1. *Semantic distance between thread reply and thread centroid:* Semantic distance means the semantic difference between replies and thread centroid. TF-IDF is used to calculate the thread centroid. The thread centroid is the centre point of all replies to thread discussions. After the mapping of the thread centroid vector, word mover distance (WMD) is used to calculate the semantic distance between the reply sentence vector and the thread centroid vector in each thread discussion. In this process, the distance between the thread reply and the thread centroid is calculated. This technique extracts the most important and unique terms/words in a thread which is also known as the features of that thread discussion.
2. *Cosine similarity between reply sentences and thread centroid:* In cosine similarity, the cosine angle is calculated between the reply sentence vector and the thread centroid vector. Cosine similarity is a multi-dimensional space technique used for the

measurement of the similarity between two vectors. The purpose of this step of feature extraction is to capture the cosine similarity between reply sentence vectors and thread centroid vectors as text features.

3. *Unique word count in a reply sentence:* In this step of feature extraction, the unique word in each reply sentence is counted. This unique word played a very important role as a feature of the reply sentence. A reply sentence is considered for a final summary generation if it contains unique words.
4. *Common or overlapping words between thread reply and initial post:* Common or overlapping words are those words that share common semantic characteristics. In this step of feature extraction, the overlapping word between the reply sentence and the initial post is extracted. This task is performed using Jaccard similarity which is used for the similarity of asymmetric binary vectors of thread reply sentences and initial posts or queries.
5. *Semantic Distance between thread reply sentence and thread title:* Semantic similarity is also an important feature of extractive summarization. In this step, the semantic similarity between the reply sentence of a discussion and the thread title is calculated. For this purpose, the word mover distance (WMD) is used to calculate the semantic distance between reply sentences and thread titles.
6. *Semantic Distance between thread reply sentences and initial post:* A reply sentence is considered to be salient for the final summary if it has semantic similarity with the initial post. Word mover distance (WMD) is used for the calculation of semantic distance between thread reply sentences and initial posts.
7. *Length of reply sentence:* Reply sentence length means the number of words in a sentence. In this step, the number of words in each sentence is counted as a feature of a reply sentence to a discussion.
8. *Number of Nouns and Verbs in a reply sentence:* In this step, the number of verbs and nouns in a thread reply sentence is counted. The number of verbs and nouns considered is a feature of thread reply sentences.

3.6. Ranking of Reply Sentences

In this phase, a ranking score is assigned to each reply sentence in each cluster. This score indicates the salient sentences for extraction from thread discussions and helps to eliminate irrelevant replies for the final summary generation. In the previous step, different quality text features were extracted from reply sentences. In the ranking process, the extracted features are used as a scoring technique for each sentence. A sentence that has a high score is considered to be a salient sentence for a final summary of the thread discussion. According to the extracted features, if a sentence has all these features, it will be more analogous to the asked query. Based on eight quality text features, each sentence is represented as an eight-dimensional vector that specifies the significance of a sentence based on a certain distance from centroid vectors of the cluster. To score each sentence, the text features score is calculated for each reply sentence in each cluster. After individual calculation, all features are summed up to score each reply in clusters. The summation function of features is as follows;

$$Score(sentence) = \sum_{k=1}^{8} reply\_sent_{f_i} \tag{8}$$

Where *Score(sentence)* indicates the overall score of reply sentences and *reply_sent* represents the features score of each reply sentence. After the calculation of feature scores, each sentence in each cluster is ranked based on this feature score. As in the previous section of clustering, the number of clusters is 10. In the next step, only a single sentence is extracted based on these features.

3.7. Summary Generation

The most important part of extractive summarization is to take the most relevant sentence from the source text and place it in order to maintain the overall concept and fluency of the paragraph. Numerous techniques are used in the literature for extraction to obtain relevant replies for the final summary which are discussed in the literature review section. To extract the most relevant replies to the initial post, we proposed eight different types of text features in this study. Before extraction of relevant replies from discussions all discussion replies are clustered in 10 clusters using FCM clustering algorithms. The purpose of clustering is to group similar sentences and apply text feature extraction techniques to identify the most relevant replies for extraction. based on these features, only high-ranked sentences are extracted for a final summary generation.

4. Result and Discussion

In this section, we elaborate on the effectiveness of our proposed sentence embedding technique and compare it with the state-of-the-art CBOW embedding model in the context of two standard discussion forums Ubuntu and TripAdvisor datasets. The average recall, precision, and F-measure obtained with ROUGE-N (N = 1, 2) [16] are used to compare the effectiveness of our proposed sentence embedding technique with the alternative CBOW embedding model. The empirical result of ROUGE-1 using two discussion forums datasets shown in Tables 1 and 2 illustrates the performance of the proposed sentence embedding technique in comparison of FCM, K-Medoid and K-means clustering algorithms the FCM outperform other clustering algorithms using the proposed sentence embedding technique.

Table 1. ROUGE-1 of NYC dataset based using both LSTM Auto-encoder and CBOW embedding models

Average Metrics	Algorithms	LSTM Auto-encoder	CBOW model
Precision	Kmediod	24.80	25.70
	FCM	39.43	26.95
	Kmeans	26.78	21.45
Recall	Kmediod	34.27	35.33
	FCM	40.60	24.46
	Kmeans	36.58	26.79
F measure	Kmediod	28.25	29.32
	FCM	39.86	24.39
	Kmeans	30.33	23.14

Table 2. ROUGE-1 of Ubuntu dataset based on both LSTM Auto-encoder and CBOW embedding models

Average Metrics	Algorithms	LSTM Auto-encoder	CBOW model
Precision	Kmediod	34.92	35.86
	FCM	37.11	31.09
	Kmeans	36.20	33.10
Recall	Kmediod	36.79	37.63
	FCM	39.33	29.73
	Kmeans	38.88	35.28
F measure	Kmediod	35.63	36.53
	FCM	38.08	29.79
	Kmeans	37.10	33.94

It is clear from the figures 4 and 5 in the context of average precision, recall, and F-measure of ROUGE-1 using two standard datasets, the proposed sentence embedding technique outperforms the CBOW embedding model in terms of average precision, recall and F-measure.

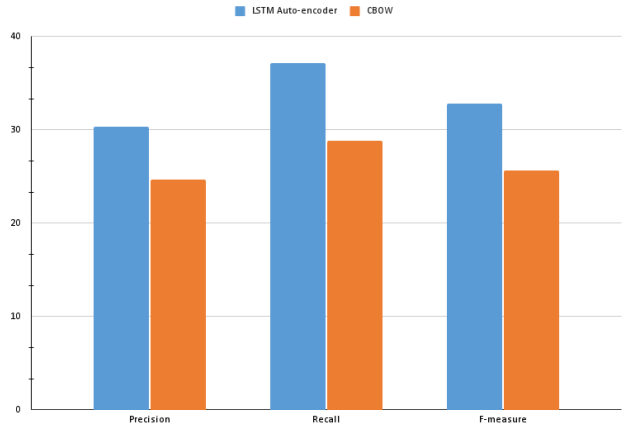

Fig. 4. ROUGE-2 of LSTM Auto-encoder and CBOW model using NYC dataset.

Referring to the ROUGE-2 result presented in Table 3 and 4 The proposed sentence embedding technique performs better than the CBOW embedding model. In comparison to the three clustering algorithms FCM, K-Mediod and K-means, in terms of two standard discussion forums datasets FCM offered better outcomes for summarization using the embedding vectors of the proposed sentence embedding technique.

In the context of average precision, recall and F-measure of ROUGE-2, illustrated in the figure 6 and 7, the proposed sentence embedding technique outperforms the CBOW embedding models in sentence embedding tasks for text summarization. Using the pro-

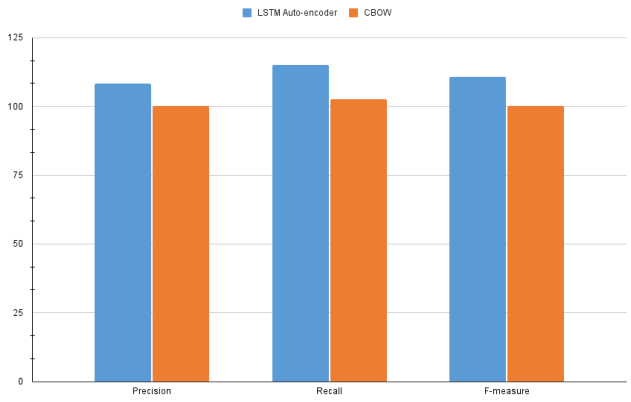

Fig. 5. ROUGE-2 of LSTM Auto-encoder and CBOW model using Ubuntu dataset.

Table 3. ROUGE-2 of NYC dataset based on both LSTM Auto-encoder and CBOW embedding models

Average Metrics	Algorithms	LSTM Auto-encoder	CBOW model
Precision	Kmediod	5.14	6.79
	FCM	16.87	8.31
	Kmeans	7.47	3.68
Recall	Kmediod	7.81	10.04
	FCM	17.59	6.81
	Kmeans	10.73	5.29
F measure	Kmediod	6.05	7.93
	FCM	17.14	7.12
	Kmeans	8.60	4.13

Table 4. ROUGE-2 of Ubuntu dataset based on both LSTM Auto-encoder and CBOW embedding models

Average Metrics	Algorithms	LSTM Auto-encoder	CBOW model
Precision	Kmediod	11.27	13.98
	FCM	15.33	8.50
	Kmeans	14.74	12.41
Recall	Kmediod	11.65	14.49
	FCM	16.63	8.52
	Kmeans	16.38	12.60
F measure	Kmediod	11.44	14.19
	FCM	15.89	8.27
	Kmeans	15.32	12.47

posed sentence embedding technique, the results of the experiment indicate that the auto-

mated summarization model performs better on a dataset taken from Ubuntu discussion forums as well as a dataset taken from NYC discussion forums when assessed.

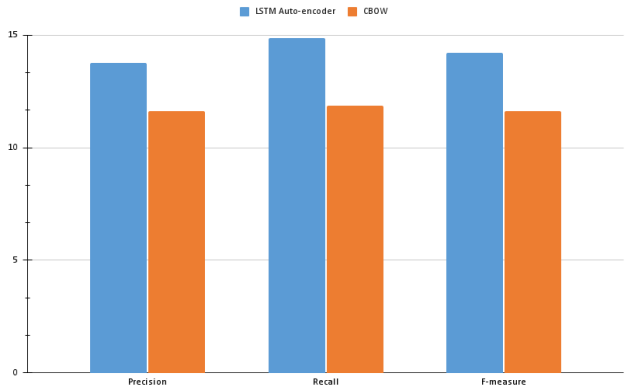

Fig. 6. ROUGE-1 of LSTM Auto-encoder and CBOW model using Ubuntu dataset.

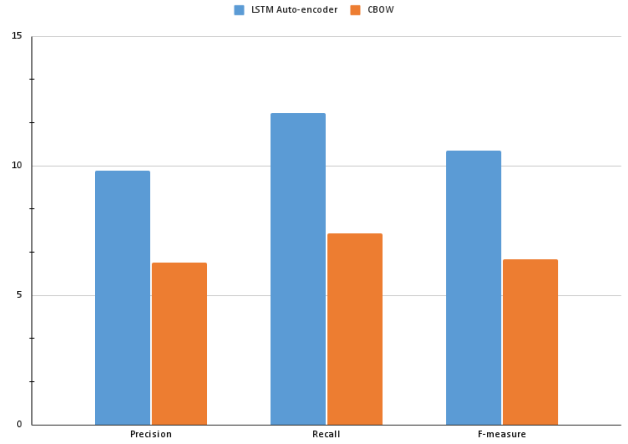

Fig. 7. ROUGE-1 of LSTM Auto-encoder and CBOW model using NYC dataset.

4.1. Comparison

By comparing our proposed technique with the state-of-the-art CBOW model which uses the average word vector technique for sentence embedding. The empirical result given in Table 5 and graphical visualization in Figure 8 proved that our proposed sentence embedding technique performs better than the CBOW approach with FCM clustering.

Table 5. Comparison with state of the art approach [13]

Average Metrics	Algorithms	LSTM Auto-encoder	CBOW model
Precision	Kmediod	24.8	34.68
	FCM	39.43	28.2
Recall	Kmediod	34.27	39.83
	FCM	40.6	28.31
F measure	Kmediod	28.25	36.03
	FCM	39.86	27.46

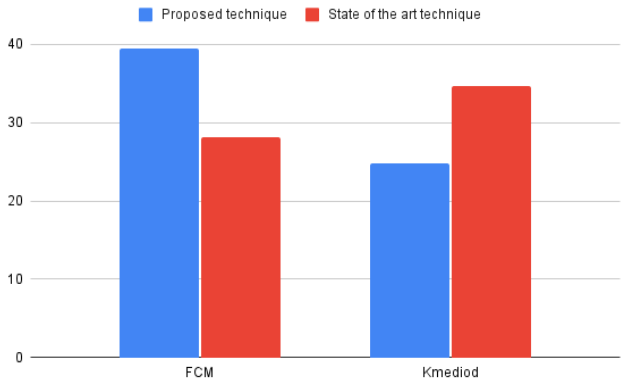

Fig. 8. Comparison with state of the art approach [13]

5. Threat to Validity

Selection bias: The proposed LSTM auto-encoder method was examined on only two standard datasets, which may not be typical of all conceivable datasets.

Generalizability: The study only evaluated the proposed approach on DTS tasks, and it is unclear whether the proposed approach would perform similarly on other NLP tasks or in different domains. Therefore, the generalizability of the proposed approach to other tasks or domains is uncertain.

Evaluation metric bias: The proposed method was evaluated using the ROUGE-1 and ROUGE-2 assessment metrics. Although these measures are commonly employed in text summarization tasks, they may not capture all aspects of summary quality, and alternative metrics may provide a different view of the performance of the proposed method.

6. Conclusion and Future Work

Thread discussion summarization is a challenging task in the field of NLP. The recent trend of deep learning-based natural language processing has proposed new techniques that attract the researchers' attention. This study introduces a deep learning-based sentence embedding approach using a recurrent neural network architecture to boost the performance of automated DTS. The state-of-the-art CBOW model is an inefficient approach for sentence embedding and is unable to capture semantic information of the overall sentence due to its commutative calculation of embedding vectors. To overcome the limitations of the CBOW model in DTS, this study proposed an LSTM Auto-encoder for efficient sentence representation in embedding space. The proposed methodology is evaluated on two standard datasets and compares both the CBOW model and LSTM Auto-encoder in sentence embedding tasks. In the context of precision, recall, and F-measure, the empirical results prove that the LSTM Auto-encoder improves the performance of the DTS model concerning both ROUGE-1 and ROUGE-2 evaluation metrics.

In the future, we plan to modify and apply our proposed methodology to the non-English online discussion forums dataset. Deep learning-based clustering approaches will also be considered to further enhance the performance of the proposed methodology. Furthermore, we plan to extend our proposed approach for the abstractive summarization tasks and also intend to compare our novel sentence embedding technique with other recently introduced neural sentence embedding techniques [2].

Acknowledgments. This work was supported by the FCT – Fundação para a Ciência e a Tecnologia, I.P. [Project UIDB/05105/2020].

References

1. Adi, Y., Kermany, E., Belinkov, Y., Lavi, O., Goldberg, Y.: Fine-grained analysis of sentence embeddings using auxiliary prediction tasks. arXiv preprint arXiv:1608.04207 (2016)
2. Blagec, K., Xu, H., Agibetov, A., Samwald, M.: Neural sentence embedding models for semantic similarity estimation in the biomedical domain. BMC bioinformatics 20(1), 1–10 (2019)
3. Erkan, G., Radev, D.: Lexpagerank: Prestige in multi-document text summarization. In: Proceedings of the 2004 Conference on Empirical Methods in Natural Language Processing. pp. 365–371 (2004)
4. Ghosh, S., Dubey, S.K.: Comparative analysis of k-means and fuzzy c-means algorithms. International Journal of Advanced Computer Science and Applications 4(4) (2013)
5. Grover, J., Mitra, P.: Sentence alignment using unfolding recursive autoencoders. In: Proceedings of the 10th Workshop on Building and Using Comparable Corpora. pp. 16–20 (2017)
6. Gupta, V., Lehal, G.S.: A survey of text summarization extractive techniques. Journal of emerging technologies in web intelligence 2(3), 258–268 (2010)
7. Harabagiu, S.M., Lacatusu, F.: Generating single and multi-document summaries with gistexter. In: Document Understanding Conferences. pp. 11–12. Citeseer (2002)

8. Hill, F., Cho, K., Korhonen, A.: Learning distributed representations of sentences from unlabelled data. arXiv preprint arXiv:1602.03483 (2016)
9. Jain, A.K., Murty, M.N., Flynn, P.J.: Data clustering: a review. ACM computing surveys (CSUR) 31(3), 264–323 (1999)
10. Jiang, J., Zhang, H., Dai, C., Zhao, Q., Feng, H., Ji, Z., Ganchev, I.: Enhancements of attention-based bidirectional lstm for hybrid automatic text summarization. IEEE Access 9, 123660–123671 (2021)
11. Kallimani, J.S., Srinivasa, K., Reddy, B.E.: Summarizing news paper articles: experiments with ontology-based, customized, extractive text summary and word scoring. Cybernetics and Information Technologies 12(2), 34–50 (2012)
12. Karn, S.K., Chen, F., Chen, Y.Y., Waltinger, U., Schütze, H.: Few-shot learning of an interleaved text summarization model by pretraining with synthetic data. arXiv preprint arXiv:2103.05131 (2021)
13. Khan, A., Shah, Q., Uddin, M.I., Ullah, F., Alharbi, A., Alyami, H., Gul, M.A.: Sentence embedding based semantic clustering approach for discussion thread summarization. Complexity 2020 (2020)
14. Khan, R., Qian, Y., Naeem, S.: Extractive based text summarization using k-means and tf-idf. International Journal of Information Engineering & Electronic Business 11(3) (2019)
15. Kupiec, J., Pedersen, J., Chen, F.: A trainable document summarizer. In: Proceedings of the 18th annual international ACM SIGIR conference on Research and development in information retrieval. pp. 68–73 (1995)
16. Lin, C.Y.: Rouge: A package for automatic evaluation of summaries. In: Text summarization branches out. pp. 74–81 (2004)
17. Liu, F., Liu, Y.: Correlation between rouge and human evaluation of extractive meeting summaries. In: Proceedings of ACL-08: HLT, short papers. pp. 201–204 (2008)
18. Ma, S., Sun, X., Lin, J., Wang, H.: Autoencoder as assistant supervisor: Improving text representation for chinese social media text summarization. arXiv preprint arXiv:1805.04869 (2018)
19. Macintyre, J., Iliadis, L., Maglogiannis, I., Jayne, C.: Engineering Applications of Neural Networks: 20th International Conference, EANN 2019, Xersonisos, Crete, Greece, May 24-26, 2019, Proceedings, vol. 1000. Springer (2019)
20. Marge, M., Banerjee, S., Rudnicky, A.: Using the amazon mechanical turk to transcribe and annotate meeting speech for extractive summarization. In: Proceedings of the NAACL HLT 2010 workshop on creating speech and language data with Amazon's Mechanical Turk. pp. 99–107 (2010)
21. Mehdad, Y., Carenini, G., Ng, R.: Abstractive summarization of spoken and written conversations based on phrasal queries. In: Proceedings of the 52nd Annual Meeting of the Association for Computational Linguistics (Volume 1: Long Papers). pp. 1220–1230 (2014)
22. Min, E., Guo, X., Liu, Q., Zhang, G., Cui, J., Long, J.: A survey of clustering with deep learning: From the perspective of network architecture. IEEE Access 6, 39501–39514 (2018)
23. Murray, G., Renals, S., Carletta, J.: Extractive summarization of meeting recordings. (2005)
24. Nallapati, R., Zhai, F., Zhou, B.: Summarunner: A recurrent neural network based sequence model for extractive summarization of documents. In: Thirty-first AAAI conference on artificial intelligence (2017)
25. Nguyen, T., Luu, A.T., Lu, T., Quan, T.: Enriching and controlling global semantics for text summarization. arXiv preprint arXiv:2109.10616 (2021)
26. Oortmerssen, G.v., Raaijmakers, S., Sappelli, M., Boertjes, E., Verberne, S., Walasek, N., Kraaij, W.: Analyzing cancer forum discussions with text mining (2017)
27. Osman, A., Salim, N., Saeed, F.: Quality dimensions features for identifying high-quality user replies in text forum threads using classification methods. PloS one 14(5), e0215516 (2019)
28. Page, L., Brin, S., Motwani, R., Winograd, T.: The pagerank citation ranking: Bringing order to the web. Tech. rep., Stanford InfoLab (1999)

29. Rahman, M.M., Siddiqui, F.H.: Multi-layered attentional peephole convolutional lstm for abstractive text summarization. ETRI Journal 43(2), 288–298 (2021)
30. Rezaei, A., Dami, S., Daneshjoo, P.: Multi-document extractive text summarization via deep learning approach. In: 2019 5th Conference on Knowledge Based Engineering and Innovation (KBEI). pp. 680–685. IEEE (2019)
31. Silla Jr, C.N., Kaestner, C.A., Freitas, A.A.: A non-linear topic detection method for text summarization using wordnet. In: Proceedings of the Workshop of Technology Information Language Human (TIL 2003) (2003)
32. Sipos, R., Shivaswamy, P., Joachims, T.: Large-margin learning of submodular summarization models. In: Proceedings of the 13th Conference of the European Chapter of the Association for Computational Linguistics. pp. 224–233 (2012)
33. Socher, R., Huang, E., Pennin, J., Manning, C.D., Ng, A.: Dynamic pooling and unfolding recursive autoencoders for paraphrase detection. Advances in neural information processing systems 24 (2011)
34. Song, S., Huang, H., Ruan, T.: Abstractive text summarization using lstm-cnn based deep learning. Multimedia Tools and Applications 78(1), 857–875 (2019)
35. Subramanian, S., Trischler, A., Bengio, Y., Pal, C.J.: Learning general purpose distributed sentence representations via large scale multi-task learning. arXiv preprint arXiv:1804.00079 (2018)
36. Tai, K.S., Socher, R., Manning, C.D.: Improved semantic representations from tree-structured long short-term memory networks. arXiv preprint arXiv:1503.00075 (2015)
37. Trappey, A.J., Trappey, C.V., Wu, C.Y.: Automatic patent document summarization for collaborative knowledge systems and services. Journal of Systems Science and Systems Engineering 18(1), 71–94 (2009)
38. Tseng, Y.H., Wang, Y.M., Lin, Y.I., Lin, C.J., Juang, D.W.: Patent surrogate extraction and evaluation in the context of patent mapping. Journal of Information Science 33(6), 718–736 (2007)
39. Vazhenin, D., Ishikawa, S., Klyuev, V.: A user-oriented web retrieval summarization tool. In: 2009 Second International Conference on Advances in Human-Oriented and Personalized Mechanisms, Technologies, and Services. pp. 73–78. IEEE (2009)
40. Wang, J.H., Liu, T.W., Luo, X., Wang, L.: An lstm approach to short text sentiment classification with word embeddings. In: Proceedings of the 30th conference on computational linguistics and speech processing (ROCLING 2018). pp. 214–223 (2018)
41. Yousefi-Azar, M., Hamey, L.: Text summarization using unsupervised deep learning. Expert Systems with Applications 68, 93–105 (2017)
42. Zajic, D.M., Dorr, B.J., Lin, J.: Single-document and multi-document summarization techniques for email threads using sentence compression. Information Processing & Management 44(4), 1600–1610 (2008)
43. Zhang, R., Li, W., Gao, D., Ouyang, Y.: Automatic twitter topic summarization with speech acts. IEEE transactions on audio, speech, and language processing 21(3), 649–658 (2012)
44. Zhou, L., Hovy, E.H.: On the summarization of dynamically introduced information: Online discussions and blogs. In: AAAI Spring symposium: Computational approaches to analyzing weblogs. p. 237 (2006)

Abdul Wali Khan pursued his academic journey with a passion for cutting-edge technologies. After completing his MSc from Peshawar University in 2017, he set his sights on delving deeper into the realm of artificial intelligence. Enrolling at the Institute of Management Sciences Peshawar, he dedicated himself to mastering the intricacies of machine learning, natural language processing, text mining, and big data. With unwavering

determination, he successfully obtained his MS Degree in 2022, solidifying his expertise in this rapidly evolving field. With an eye toward the future, he is now in pursuance of his PhD, driven by his unwavering curiosity and commitment to making groundbreaking advancements in the world of AI.

Feras Al-Obeidat is an Associate Professor at the College of Technological Innovation at Zayed University. Dr. Al-Obeidat also holds an admin position as a Graduate Program Coordinator. He received his Master's and Ph.D. in Computer Science from the University of New Brunswick, Canada. Dr. Al-Obeidat's primary field of research in Artificial Intelligence and Machine Learning. Directly following his Ph.D., Dr. Al-Obeidat contributed to industrial, university, and government teaching and research with premier organizations including IBM Canada, the University of New Brunswick, Salesforce, and the National Research Council of Canada. Dr. Al-Obeidat is honored to join Zayed University and pursue and sustain ties with government and industry research.

Afsheen Khalid received Ph.D. in computational linguistics in 2018 from the Institute of Management Sciences, Peshawar, Pakistan. She completed her M.S. degree in computer engineering from CASE (Center of Advanced Studies in Engineering) in Islamabad, Pakistan in 2008. She is currently an Assistant Professor at the Department of Computer Science, Institute of Management Sciences. Her research interests include text mining, big data, NLP, and machine learning.

Adnan Amin earned his M.Sc. in Computer Science from the University of Peshawar in 2008. He received his MS-CS degree (highest 1st class honors with distinction) and a Ph.D. degree (with Scholastic Honours) in data mining and machine learning from the Institute of Management Sciences (IMSciences) Peshawar, Pakistan, in 2015 and 2023, respectively. In November 2015, he joined IMSciences as a lecturer at the Center for Excellence in Information Technology. He is the lead of IM—DigiSol and the faculty adviser for the Computing and Innovation Society (IMCIS) at IMSciences. Before, he worked as an international consultant for curriculum and academic development at the School of ICT, NIMA Kabul, which was connected to the University of Jyvaskyla in Finland. This was part of a World Bank-funded project for Maxwell Stamp PLC, London (Project Code: P102573). Dr. Adnan's research and innovation interests are industry-driven and cross-disciplinary. He focuses on developing and commercializing digital solutions and data mining/machine learning research innovations for a variety of industries, such as education, telecommunications, and healthcare. He has completed nearly 8 research projects in collaboration with international universities. He has served as the journal editorial board member, track chair, session chair, and a member of the program committees of numerous conferences including. He has (co) authored 30+ publications, including 16+ journal articles, 12+ conferences, and 2 book chapters, and obtained nearly 1076+ citations with an h-index score of 14 and an i-index score of 16.

Fernando Moreira was the head of the Science and Technology Department from May 2018 until February 2022. He graduated in Computer Science (1992), M.Sc. in Electronic Engineering (1997) and PhD in Electronic Engineering (2003), both at the Faculty of Engineering of the University of Porto and Habilitation (2018). He has been a member of the Science and Technology Department at Portucalense University since 1992 as a

Full Professor. He teaches subjects related to undergraduate and post-graduate studies. He supervises several PhD and M.Sc. students. He is a (co-)author of more than 250 scientific publications with peer-review in national and international journals and conferences. He serves as a member of the Editorial Advisory Board for several journals and books. He organized several special issues from JCR journals. He has already regularly served on Programme and Scientific committees of national and international conferences. He was the MSc in Computation coordinator for ten years. He holds editorial experience, and he is a co-editor of several books. He is associated with NSTICC, ACM and IEEE. His principal research areas are mobile computing, ICT in Higher Education, Mobile learning, Social Business and Digital transformation. He was awarded Atlas Elsevier Award in April 2019.

Received: December 10, 2022; Accepted: June 01, 2023.

Computer Science and Information Systems 20(4):1389–1417 https://doi.org/10.2298/CSIS230130043P

PARSAT: Fuzzy logic for adaptive spatial ability training in an augmented reality system

Christos Papakostas, Christos Troussas, Akrivi Krouska, and Cleo Sgouropoulou

Department of Informatics and Computer Engineering,
University of West Attica, Greece
{cpapakostas, ctrouss, akrouska, csgouro}@uniwa.gr

Abstract. Personalized training systems and augmented reality are two of the most promising educational technologies since they could enhance engineering students' spatial ability. Prior research has examined the benefits of the integration of augmented reality in increasing students' motivation and enhancing their spatial skills. However, based on the review of the literature, current training systems do not provide adaptivity to students' individual needs. In view of the above, this paper presents a novel adaptive augmented reality training system, which teaches the knowledge domain of technical drawing. The novelty of the proposed system is that it proposes using fuzzy sets to represent the students' knowledge levels more accurately in the adaptive augmented reality training system. The system determines the amount and the level of difficulty of the learning activities delivered to the students, based on their progress. The main contribution of the system is that it is student-centered, providing the students with an adaptive training experience. The evaluation of the system took place during the 2021-22 and 2022-23 winter semesters, and the results are very promising.

Keywords: Fuzzy logic, augmented reality, spatial ability, adaptive training, personalized system.

1. Introduction

All technologically enhanced realities fall under the broad concept of Extended Reality (XR), which combines the experiences of augmented reality (AR), virtual reality (VR), and mixed reality (MR) [1]. To improve this experience, AR overlays virtual content on top of the already existing real-world environment [2]. Contrarily, VR immerses viewers in an entirely new environment that is often developed and rendered by computers [3]. Finally, MR is a user environment that combines digital content and physical reality in a manner that makes it possible for users to interact with both real-world and virtual objects [4].

A user's perspective of the real world is altered through AR technology [2], [5]. Digital input, such as visual components, are used to create an improved version of the real world, which is delivered through technology. User-friendly AR applications offer a straightforward and enjoyable form of human-computer interaction. AR has been used into a wide range of industries, and it has especially great potential in educational settings, more particularly, in the training of engineers [6].

In order to improve engineering students' design skills, it is essential for engineering education to enhance students' spatial ability [7]–[9]. Numerous studies have investigated how using AR technology might support students become more efficient at technical drawings and develop their spatial skills, both of which are important for their academic work and potential professions [10]–[13]. Even though many researchers have explored the integration of AR in spatial ability training, no study has specifically developed a personalized AR spatial ability training system, which takes the student profile into account [14].

For greater educational outcomes, a training system should, nevertheless, be adaptable to the various students' individual needs. As a teacher would do in an in-person approach in a real classroom, the training system should also be able to periodically change the teaching technique and instructional approach in light of the student's needs. As a result, designing an adaptive learning system that satisfies the demands of the students might be challenging, since each student has unique learning needs and preferences [15].

Fuzzy logic developed by [16] can help with this challenge, as it is able to deal with ambiguity and inaccurate data. Knowledge level, in particular, is a concept that cannot be described as a variable that accepts distinct values, since learning is a complex process. In order to better accurately depict the learner's knowledge level, fuzzy sets and fuzzy logic may be employed. Since fuzzy logic techniques can deal with the uncertainty in data concerning students' cognitive state and behavior, they can be utilized to enhance the effectiveness of training systems.

The primary goal of the research, as stated in this paper, is to propose a spatial ability training system that helps students in learning technical drawing. The system incorporates every knowledge domain found in a conventional course curriculum. Our research is innovative in that it combines adaptive learning strategies with learning theory to offer students individualized learning activities within the context of spatial ability training, utilizing augmented reality.

Fuzzy sets are used each time to represent the knowledge level of the students. The assignments and training flow are then determined by the system. The training system specifically considers the student's progress, each time it has to select which learning activities need to be dynamically supplied to the student.

Particularly, the training system determines the length and complexity of the video tutorials that constitute each chapter, which in turn determines the quantity and difficulty of the learning activities and the evaluation questions. As a result, the student receives more personalized training using fuzzy logic techniques, which select the questions to be delivered to the student in the training's upcoming evaluation questions, based on the test results as input. In addition, the student receives a more individualized training experience due to AR characteristics which are dynamically shown in accordance with the student's progress and requirements.

The paper's contribution is as follows:

- **Contribution to intelligent tutoring systems:** The use of fuzzy logic and the Mamdani inference system allows for the incorporation of imprecise and uncertain information in decision-making, which can lead to more accurate and personalized feedback for the learners. The use of fuzzy weights further allows for the weighting of different factors in the decision-making process, depending on their relative importance. Together, these techniques enable PARSAT to

provide personalized support for learners based on their individual needs and progress.

- **Contribution to domain knowledge model:** The integration of educational taxonomies, augmented reality technology, and intelligent tutoring systems can help to create a more engaging and effective learning environment for students.
- **Contribution to student modeling:** The integration of fuzzy logic and AR technology offers a promising avenue for developing personalized training systems in the domain of spatial skills training.
- **Contribution to electronic assessment:** The study does contribute to the collection of data on student performance during the training session. The proposed system collects information on the number of errors made by students during assessment tasks, which is an important metric for evaluating performance and providing personalized feedback. By tracking this data and using it to adjust the difficulty and amount of learning activities, the system can provide a more tailored and effective training experience for engineering students [17].

The structure of this paper is as follows. The literature review, regarding AR and adaptivity, is examined in Section 2. The description of the training system is presented in Section 3. The enhancement of the domain knowledge using taxonomy is discussed in Section 4. The modeling of students' knowledge through fuzzy logic is presented in Section 5. Experimental results obtained from training and the outcome of the system's evaluation are presented in Section 6. Finally, in Section 7, the work is concluded and continues with restrictions and future work.

The present paper is an extended and revised version of our preliminary conference paper that was presented in [18]. This paper significantly expands the evaluation of the proposed adaptive AR training system.

2. Literature Review

Various studies have been conducted examining the use of AR technology in domains such as education [19], [20], healthcare [21], [22], tourism [23], [24], culture [25], marketing [26], [27], industry [28], [29], all of which highlighted the impact that AR technology had. Their main objective is to keep users motivated and interested in the subject by providing them a pleasant experience. An AR application, called adaptive AR, offers useful and effective real-time information based on the user's specific features, interests, and context [30].

In [31] the authors introduced the concept of plasticity of augmentations and defined it as the ability of human-computer interaction (HCI) interface to fit the context of use defined by the user, the environment and the platform. The study evaluated adaptive AR by taking into consideration the size of augmentations, the illumination level of the scene, and the ambient noise. More specific, the system modifies the scale of the augmented object based on distance, adjusts the scene's luminosity to match ambient lighting, and levels the sound based on background noise.

In [32] the authors recognized adaptive behavior as the main challenge in developing AR systems, especially in the case of systems which provide information to the end users. The authors presented the trend inside the research community to develop techniques for better adaptation of the form and size of information that will be

delivered to the users. Such systems have numerous challenges in identifying the user's behavior, determining in real-time what kind of adaptation to perform, so that it continuously adapts the AR content to the user's interest.

In [33] a user interface (UI) was presented, based on AR with head-mounted display (HMD), for increasing situational awareness during critical operations and improve human efficacy. The interface allowed the user to control a swarm of drones in order to explore the outside world, by presenting information in a virtual environment using 2D and 3D widgets. The research findings indicate that AR has the potential to increase human productivity and the success of mission-critical tasks.

In [34] the authors address how adaptation in AR could enable 3D objects to have their contrast adjusted to the degree of the ambient lighting of the environment. Now that mobile phones have sensors built in, mobile AR can become more adaptive, taking advantage of their built-in sensor modules which can be used to gather information about the user, the surrounding, and the device.

Explicit modalities, according to [35], are techniques that allow the system to receive input from users through gesture, speech, and touch. Information about changes at the environment (such as temperature, noise, and light) and changes at the device (such as orientation) are known as implicit modalities. A user's present location, for instance, can trigger a POI, based on the GPS sensor, while in order to provide a clearer view on the screen in low-light environments, the screen illuminance will be raised. Depending on the mobile device's orientation, the AR display screen can be changed.

In [36] the authors carried out research to enhance the knowledge provided to museum visitors, based on their emotional state at the time of their visit. Sensors are utilized to track visitor engagement and interest levels in order to adapt the experience. Their work has completely changed the way that adaptive AR approaches cultural heritage.

Even while adaptivity is significant and has a good impact on users, there are not many examples of educational systems that employ it. Only a few educational adaptive systems exist, however there is not an adaptive AR application for training students' spatial skills. As a result, an educational AR system that uses a different model to evaluate the student's cognitive state and makes the proper adjustments can be useful. The process of learning is multifaceted, and user's level of knowledge is an intangible concept. Knowledge is not a variable that can take on discrete values, and therefore, it is not accurate to claim if a domain concept is either known, or unknown. Fuzzy logic can be used to solve issues involving non-measurable entities [16].

As a result, fuzzy logic appears to be the best method for describing the students' level of knowledge. Adaptive tutoring systems have employed fuzzy logic, however spatial ability training systems have not. In light of this, we present a personalized AR training system that includes a cutting-edge module that employs fuzzy logic to develop student models, and provide on-the-spot modifications to the learning path's flow.

As a testbed for our research, we developed a personalized mobile application, namely PARSAT, for the training of spatial skills. PARSAT offers adaptivity regarding students' preferences, plus it creates a learning environment providing individualized learning activities that assure the training quality. PARSAT was used by university students and the results were really encouraging. The main difference, between PARSAT and the existing AR applications, is that the educational process is adaptive

[37], [38]. The basic idea of the application is to deliver relevant content, based on student's current level of knowledge [39].

3. Description of the System

The research described in the current paper involves the implementation of the novel approach of a spatial ability training system, incorporating fuzzy logic for the automatic recognition of the students' knowledge level, and augmented reality digital technology for the spatial ability training. Specifically, an innovative mobile environment for spatial skills training, namely PARSAT, has been developed. A set of hardware and software components, along with data that describe the real world and virtual content, form the basis of the augmented reality system. Fig. 1 presents the architecture of PARSAT, which is structured in three layers, as follows: the hardware is in the upper section, the software is in the middle, and the data is in the lower half.

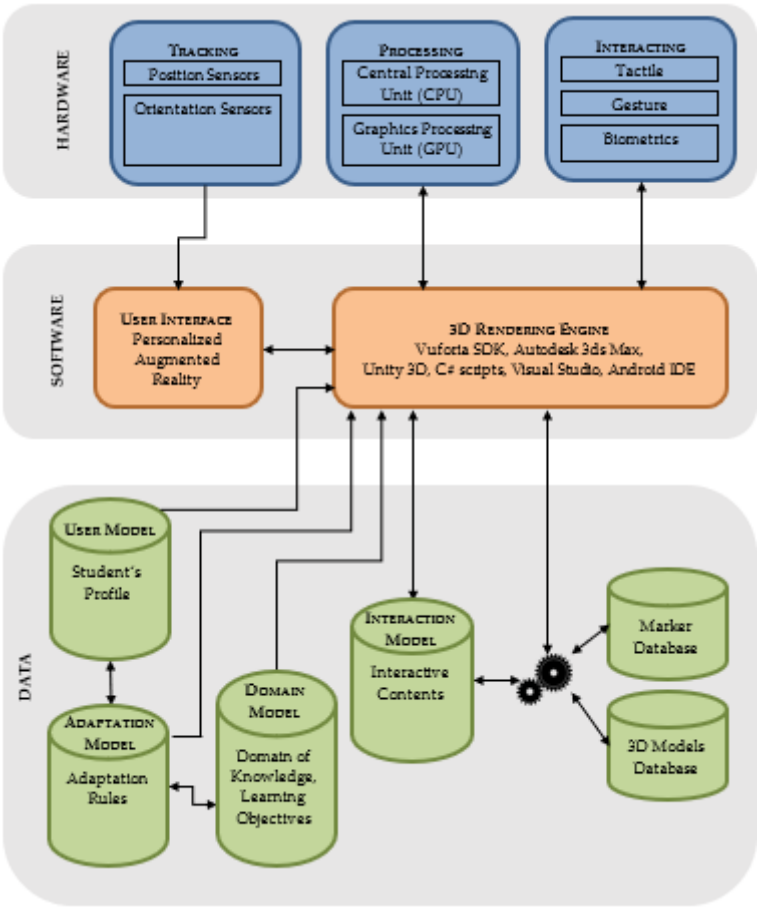

Fig. 1. The architecture of PARSAT

3.1. Hardware Layer

The tracking module consists of a range of sensors, such as accelerometer, gyroscope, magnetometer, and GPS, which determine the position and the orientation of the system, so that the virtual information will be in-line with the physical environment. Almost all mobile devices (smartphones and tablets) incorporate most of the aforementioned sensors.

The processing module consists of the fuzzy inference system, the 3D rendering, and overall, the system's user interface, are computational processes, and as such, they require significant hardware resources. To this purpose, all mobile devices embed powerful processing units. The graphics processing unit of mobile devices is specifically designed to accelerate the image output to a display, while the central processing unit of the mobile devices executes all the tasks and instructions from the user.

The interacting component incorporates a range of sensors, such as tactile surfaces, gesture recognition, and biometrics, which translate the user's interaction with the system. Tactile sensor is integrated in PARSAT, so that the identified information is due to the contact of the student's fingers on the mobile screen. All mobile devices support touch commands, which are identified by key components, such as a tactile sensor.

3.2. Software Layer

A user interface's success is determined by how discretely people may use it, without interruptions from other interface components. In the context of AR applications, this is also accurate. Due to AR's immersive and captivating nature, PARSAT's user interface aims to focus on how students engage with the system. It is achieved by focusing on the five essential User Interface (UI) – User Experience (UX) AR pillars [40]–[42] as listed below:

- Environment: for AR design, the environment in which users will interact with the application, must be considered. Everything is included, from the lighting to the actual area where users are positioned. In the case of PARSAT, students used the application in their university laboratories, which are organized taking into consideration the best user ergonomics and safety.
- Interaction design: this parameter is also crucial, as the interaction design determines how the user interacts with the context of PARSAT. The main gestures that are used to manipulate the application, and make the most of the AR experience, are: a) tapping, which is performed with a light touch of student's finger, and it is used for pressing buttons and selecting, b) double tapping, which is used to zoom in on the 3D models, c) pinching, which needs two fingers close together, or spread apart, to adjust the size of the 3D models, and d) rotating, which is the basic gesture for the understanding the spatial geometry of the 3D models from different perspectives, and revealing their hidden views.
- Colors: the science of color theory applies to AR, just as it does to print, mobile, and the web. PARSAT's colors are acceptable for its educational scope. The text is visible, and fonts are appropriate, so the student find it simple to read. Depending on the situation, San Serif fonts may be simpler to read than Serif fonts. The optimum contrast schemes for reading are selected using light text on a dark background.
- Feedback: it is a critical parameter which is considered, defining how students will be informed of their activities and the results or outcome of those actions. Whether it is the feedback on the assessment score, or feedback encouraging the student to continue the effort on training, it is a parameter which adaptive systems usually integrate.

The 3D rendering engine is a combination of the software integrated in the PARSAT application. More specific, this engine maintains an internal 3D representation of the virtual scene augmenting the real world.

This internal representation is updated in real-time according to several factors such as the user's profile, student's interactions, the 3D objects behavior, the updated knowledge domain, and the fuzzy inference adaptation. Both, hardware components

such as the CPU and the GPU, and data components, are dedicated to the 3D rendering engine for the creation of the user interface screens.

PARSAT is implemented using Unity 3D cross-platform game engine, v. 2020.3.43f1 LTS, Vuforia Software Development Kit (SDK), Autodesk 3ds Max 2020, scripts in C# programming language, Visual Studio 2019, and Android Studio Integrated Development Environment (IDE).

3.3. Data Layer

PARSAT integrates marker-based AR, requiring a trigger image or a QR code to activate the AR experience. The student detects and scans the marker using the mobile device's camera, the image is identified as a marker, and then, the device renders the virtual content on top of the marker. This feature allows the student to move around the marker and observe the perspectives of the 3D content.

Cloud-based or device-localized are the two categories of marker-based AR. In the first category, since the AR assets must be downloaded from the server, a cloud-based AR experience may require a few additional minutes to load. In the second category, since the AR assets have already been pre-downloaded to the student's mobile device via the application, a localized AR experience may be accessed instantly. For greater storage capacity, the choice of the cloud-based AR is preferred, but localized AR is less expensive and not dependent on network availability. PARSAT integrates localized marker-based AR.

The marker-based AR experience is created using a software development kit (SDK), namely Vuforia, one of the best-known AR tool sets, which adds advanced computer vision functionality by creating AR experiences that realistically interact with the 3D geometrical objects displayed at each level, supporting a broad range of devices, not only Android and iOS smartphones and tablets, but also AR headsets, such as Microsoft Hololens and Magic Leap.

The 3D models database is crucial, as the students interact with the virtual models to train their spatial visualization skills. 3D modeling software options are separated into two main categories, the first one is the free and the second category is the license-paid software.

The effective selection of 3D modeling software depends on the objects which are to be designed, the interface of the software, the community behind the software offering tutorials, step-by-step guides, and commonly asked questions, and, in case of a paid license, the actual cost of the product. PARSAT's 3D models database is prepared using Autodesk 3ds Max.

4. Enhancing Domain Knowledge with SOLO Taxonomy

In this section, the training system's domain knowledge is presented, considering the Structure of Observed Learning Outcomes (SOLO) taxonomy. The content of the domain model is a critical component of the application's structure, whereas the

combination of the learning theory with adaptive learning activities enhances the students' motivation and improves their learning outcome.

4.1. Domain Model

The content of the domain knowledge is consisted of three levels, covering the topic of the Technical Drawing (TD) course, and its objectives in detail, as follows:

- Recognize the exploratory potential of technical drawing while acknowledging the universality of objective language in information transmission and comprehension.
- Strengthen the skills necessary for them to represent graphical solutions precisely and objectively.
- Have a basic understanding of technical drawing so that students can utilize it to read and interpret simple designs and artistic creations as well as to develop well-thought-out solutions to mathematical challenges in both the plane and space.
- Recognize normalization as the optimum realist for condensing communication and giving it a more universal tone.
- Include technical drawing tasks in a study area where aesthetic considerations are relevant, such as art, architecture, or industrial design.
- Recognize and depict shapes in accordance with ISO standards.
- Recognize how different approaches enhance the traditional idea of technical drawing.
- Include the information provided by technical drawing in technological, artistic, or scientific research process.
- Encourage method and rationality in sketching, as a way to convey scientific and technological concepts.
- Acquire abilities that enable the expression of graphical solutions with accuracy, clarity, and objectivity.
- Skillfully employ the specialized tools of technical drawing, and pay attention to the drawing's proper execution, as well as the enhancements that various graphical styles can provide to the depiction.
- Master the art of sketching to improve the speed and accuracy while expressing graphically.
- Connect the space to the plane, recognizing the requirement to complete exercises from the activity book.

4.2. Domain Knowledge Alongside SOLO Taxonomy

SOLO taxonomy was created, within a constructivist context, as a tool for teaching students how to use basic rubrics to think more thoroughly about their own understanding. In addition to evaluation, SOLO is used in the developed system to design the curriculum according to the expected level of learning outcomes, which helps in establishing constructive alignment.

PARSAT has used the SOLO taxonomy in the development of the assessment items for the learning objectives in technical drawing. These items had to fit to curriculum's

objectives and levels, and measure both surface and deep cognitive states. Throughout the PARSAT development, experienced faculty members in the field of technical drawing have been involved in designing and reviewing the assessment tasks according to the SOLO taxonomy. Table 1 illustrates the learning goals and the corresponding activities per SOLO level.

Table 1. Learning goals and activities per SOLO level [43], [44]

SOLO level	Learning goal	Learning activities	Description of the activities
Pre-structural (L1)	Students get information on the subject	1. Define concepts 2. List items 3. Match information 4. Name facts	Introduction to Technical Drawing: A history and current importance of drawing are presented Students are asked to illustrate the significance of drawing by presenting applications and reports of both good and negative uses of the skill
Unistructural (L2)	Students define, recognize, name, sketch, reproduce, recite, follow simple instructions, calculate, reproduce, arrange, find	5. Identify content to be memorized, show examples 6. Provide disciplinary context 7. Mnemonics in groups 8. Repetition of procedures 9. Games 10. Repetitive testing and matching 11. Peer testing (one student asks, one answers)	Setting up a model space in CAD software by defining limits, grid, snap, layers, and object snap Video tutorials on standard views, views' alignment, completion of activity sheet, and setting up the model space Border creation with a completed title block to be used for all future drawings, and drawing templates with all the settings necessary saved within it
Multi-structural (L3)	Students describe, list, classify, structure, enumerate, conduct, complete, illustrate, solve	12. Glossaries of key terms with definitions, classifications, examples to build disciplinary vocabulary 13. Simple laboratory exercises 14. Define terms, compare to glossary 15. Games modelled on Trivial Pursuit, Family Feud	Orthographic drawing creation Lines, layers Isometric object drawing Video tutorials on linetype, lineweight and isometric drawing creation of objects in the activity
Relational (L4)	Students relate, analyze, compare, integrate, plan, construct, implement, summarize	16. Case studies, simulations, and complex lab exercises 17. Concept maps 18. Research projects and experiential learning cycles 19. Application of theoretical models 20. Reflective journals 21. Student seminars and debates 22. Syndicate groups (each group is part of whole) 23. Problem-Based Learning and Inquiry Learning	Scaling the border and title block to fit the orthographic drawing Dimensioning an orthographic drawing Video tutorials on basic dimensioning rules and parts of dimensions Filling in a title block, including Name, Date, Title, Drawing No., and the correct scale Snapping and Text commands
Extended abstract (L5)	Students generalize, hypothesize, theorize, predict, judge, evaluate, assess, predict, reason, criticize	24. Self-directed projects involving research, design, application, argumentation, evaluation 25. Case studies involving extensive analysis, debate, reflection, argumentation, evaluation, forecasting 26. Development of a theory or model 27. Experiential learning cycles 28. Problem Based Learning and Inquiry learning	Printing the drawing on 8.5" × 11" paper (letter size) in landscape orientation Video tutorial on cutting plane, half and full sections Printer/plotter settings Export/plot an object that has been drawn in CAD so it can be exported or printed to a variety of other applications CAD software to create objects that are more precise and sometimes easier to draw in CAD than in other software

4.3. Examples of learning activities of each SOLO level

A simple uni-structural assignment is presented in Fig. 2, while the student must observe the object in 3D, place herself/himself on the spot that the black arrow points to, and identify the object's front view in 2D, ignoring the other views, and following simple procedure of the general principles of graphical representation of objects on technical drawings.

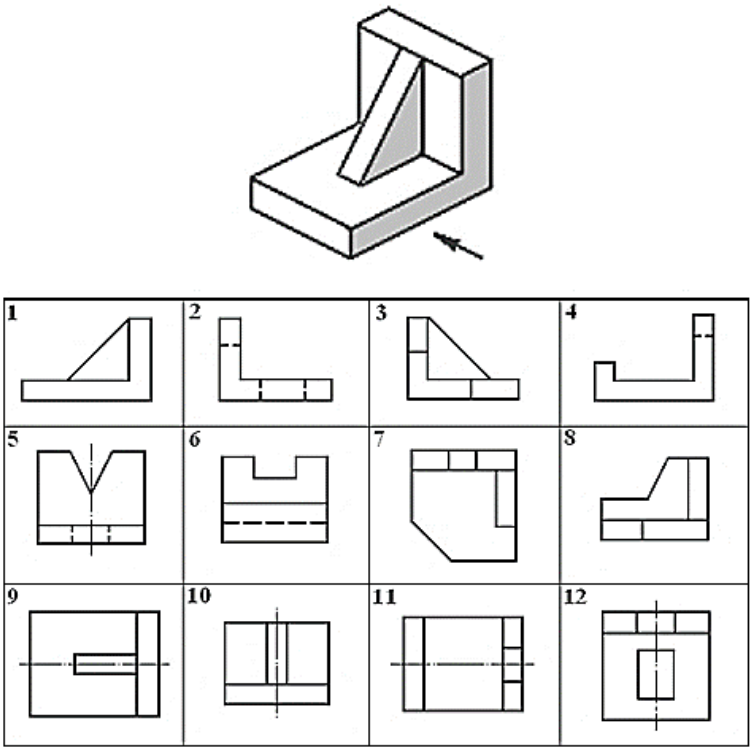

Fig. 2. Sample activity of uni-structural SOLO level

In the assignment of the relational SOLO level of Fig. 3, the students would need to analyze the individual views of the object and consider how they relate to one another. They would need to identify key features and elements in each view and determine how they fit together to create a complete picture of the object's structure and geometry.

Students would also need to think critically about the limitations of each view and consider how they might be used together to overcome these limitations. For example, the front view might provide a clear representation of the object's height and width, while the top view might be better for showing its depth and overall shape.

Overall, this assignment requires students to engage in higher order thinking and consider the relationships between different pieces of information to create a more integrated and holistic understanding of the object.

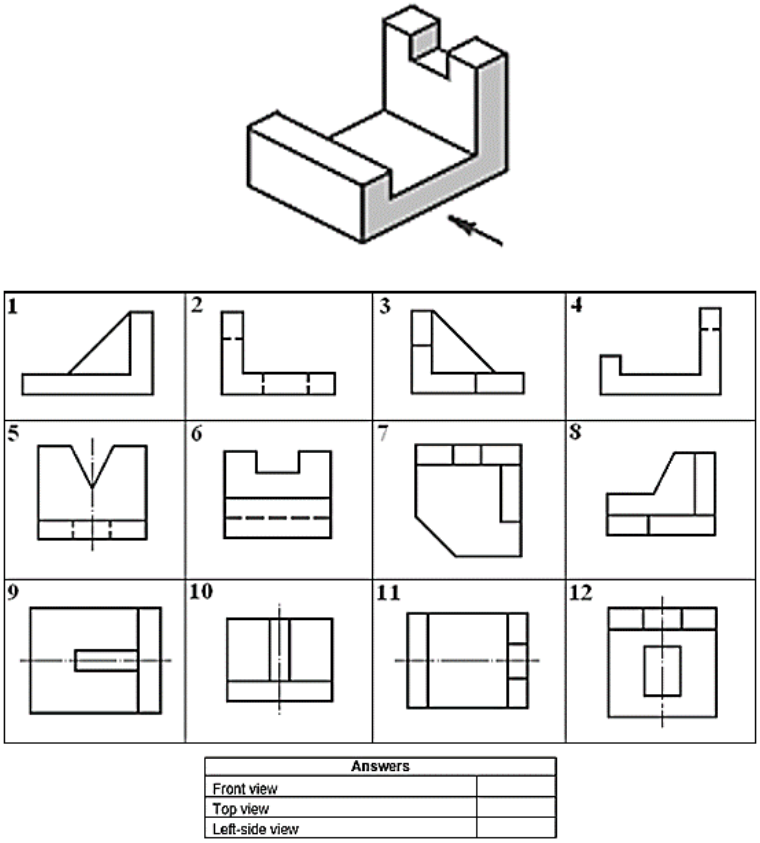

Fig. 3. Relational level question of SOLO taxonomy

5. Modelling the Knowledge of Students with Fuzzy Logic

In this section, the principles of the design of the student model, within the spatial ability training platform, are discussed. The model allows steering of the sequence of the educational material and the deliverable learning activities, through the incorporation of fuzzy logic, quantitative inputs, and fuzzy weights.

5.1. Fuzzy Logic Algorithm

The student model, which may be found in most of the latest adaptive educational software [45], is responsible for defining the student's knowledge level. The purpose of the student model is to represent the students' current level of knowledge [37], and it is essential for the system to provide the necessary level of customization on every

student's learning requirement. Other approaches regarding adaptivity, are those of neural networks, machine learning, fuzzy logic networks etc., which can be utilized to build the student model [46]. The backbone of PARSAT's student model is fuzzy logic, which defines the students' current level of knowledge.

PARSAT's fuzzy system consists of three main parts: a) the part of the linguistic variables, b) the part of the membership functions, and c) the rules. This section describes the general process of designing the fuzzy system.

The process of developing the fuzzy system starts by defining the linguistic variables, which represent, in words, the system's input and output variables. Each linguistic variable is described by a specific number of linguistic values, while in most cases three to seven terms are enough.

The proposed fuzzy model has four inputs, namely prior knowledge (PRK), video-based learning duration (VLD), augmented-reality interaction duration (ARID), and number of errors (NoE). The first input is derived from the student profile, while the remaining three inputs are derived from the interaction model. Furthermore, the output value and its linguistic name is the current knowledge level (CKL). Table 2 presents the input linguistic variables and their ranges.

Table 2. Linguistic input variables and their ranges

Linguistic Variable: Prior Knowledge (PRK)		
Linguistic Value	Notation	Range (normalized)
Poor	PRK_PR	[0, 0.35]
Medium	PRK_MDM	[0.30, 0.75]
Good	PRK_GD	[0.70, 1.00]
Linguistic Variable: Video-based Learning Duration (VLD)		
Linguistic Value	Notation	Range (normalized)
Short	VLD_SRT	[0, 0.35]
Normal	VLD_NRML	[0.30, 0.70]
Long	VLD_LNG	[0.60, 1.00]
Linguistic Variable: Augmented-Reality Interaction Duration (ARID)		
Linguistic Value	Notation	Range (normalized)
Short	ARID_SRT	[0, 0.60]
Normal	ARID_NRML	[0.40, 0.80]
Long	ARID_LNG	[0.70, 1.00]
Linguistic Variable: Number of Errors (NoE)		
Linguistic Value	Notation	Range (normalized)
Small	NoE_SMLL	[0, 0.40]
Medium	NoE_MDM	[0.35, 0.65]
Large	NoE_LRG	[0.60, 1]

5.2. Fuzzy Sets

At the second part, fuzzy sets are determined. All input values are mapped into fuzzy ones using the membership functions. We integrated membership functions, which are formed using straight lines, having the advantage of simplicity, and more specific the trapezoidal membership function. A trapezoidal membership function is assigned to each linguistic variable. A curve with four points (a, b, c, d) representing a lower limit

(a), an upper limit (b), a lower support limit (c), and an upper support limit (d) is known as a trapezoidal membership function. The curve's values range from 0 to 1. Real values between b and c are represented by degree of membership 1. Values between a and b have a higher degree of membership as they move closer to element b, whereas values between c and d have a lower degree of membership as they move closer to element d. The membership degree is zero in all other cases.

The student's video-based learning duration of each topic is recorded in seconds, and the current level's cumulative sum is normalized, resulting in the values of the linguistic variable of this input, namely short (VLD_SRT), normal (VLD_NRML) and long (VLD_LNG) (Fig. 4).

$$\mu_{VLD\_SRT}(x) = \begin{cases} 1\,; & x \leq 0.20 \\ 1 - \dfrac{x - 0.20}{0.15}\,; & 0.20 \leq x \leq 0.35 \\ 0\,; & x \geq 0.35 \end{cases}$$

$$\mu_{VLD\_NRML}(x) = \begin{cases} \dfrac{x - 0.30}{0.10}\,; & 0.30 \leq x \leq 0.40 \\ 1\,; & 0.40 \leq x \leq 0.60 \\ 1 - \dfrac{x - 0.60}{0.10}\,; & 0.60 \leq x \leq 0.70 \\ 0\,; & x \leq 0.30 \; or \; x \geq 0.70 \end{cases}$$

$$\mu_{VLD\_LNG}(x) = \begin{cases} \dfrac{x - 0.60}{0.20}\,; & 0.60 \leq x \leq 0.80 \\ 1\,; & 0.80 \leq x \leq 1.00 \\ 0\,; & x \leq 0.60 \end{cases}$$

Fig. 4. Membership functions describing video-based learning duration

Another example is the variable of the fourth input, namely number of errors, which is defined by the average student's performance in the level's test, rated on a 100-point scale. The values of the linguistic variable are small (NoE_SMLL), medium (NoE_MDM) and large (NoE_LRG) (Fig. 5).

Figures 6 and 7 present the rest two input variables, namely prior knowledge, and augmented-reality interaction duration, which take the linguistic variables poor (PRK_PR), medium (PRK_MDM), good (PRK_GD) and short (ARID_SRT), normal (ARID_NRML), long (ARID_LNG), respectively.

The fuzzy system's output value, and its linguistic term, is the student's current level of knowledge (CLK), taking the values namely Novice (N), Beginner (B), Competent (C), Very Good (VG), Proficient (P), and Expert (E).

$$\mu_{NoE\_SMLL}(x) = \begin{cases} 1\,; & x \le 0.20 \\ 1 - \dfrac{x - 0.20}{0.20}\,; & 0.20 \le x \le 0.40 \\ 0\,; & x \ge 0.40 \end{cases}$$

$$\mu_{NoE\_MDM}(x) = \begin{cases} \dfrac{x - 0.30}{0.10}\,; & 0.30 \le x \le 0.40 \\ 1\,; & 0.40 \le x \le 0.60 \\ 1 - \dfrac{x - 0.60}{0.05}\,; & 0.60 \le x \le 0.65 \\ 0\,; & x \le 0.30 \; or \; x \ge 0.65 \end{cases}$$

$$\mu_{NoE\_LRG}(x) = \begin{cases} \dfrac{x - 0.60}{0.20}\,; & 0.60 \le x \le 0.80 \\ 1\,; & 0.80 \le x \le 1.00 \\ 0\,; & x \le 0.60 \end{cases}$$

Fig. 5. Membership functions describing number of errors

$$\mu_{PRK\_PR}(x) = \begin{cases} 1\,; & x \le 0.20 \\ 1 - \dfrac{x - 0.20}{0.15}\,; & 0.20 \le x \le 0.35 \\ 0\,; & x \ge 0.35 \end{cases}$$

$$\mu_{PRK\_MDM}(x) = \begin{cases} \dfrac{x - 0.30}{0.10}\,; & 0.30 \le x \le 0.40 \\ 1\,; & 0.40 \le x \le 0.60 \\ 1 - \dfrac{x - 0.60}{0.15}\,; & 0.60 \le x \le 0.75 \\ 0\,; & x \le 0.30 \; or \; x \ge 0.75 \end{cases}$$

$$\mu_{PRK\_GD}(x) = \begin{cases} \dfrac{x - 0.70}{0.10}\,; & 0.70 \le x \le 0.80 \\ 1\,; & 0.80 \le x \le 1.00 \\ 0\,; & x \le 0.70 \end{cases}$$

Fig. 6. Membership functions describing student's prior knowledge

$$\mu_{ARID\_SRT}(x) = \begin{cases} 1; & x \leq 0.40 \\ 1 - \dfrac{x - 0.40}{0.20}; & 0.40 \leq x \leq 0.60 \\ 0; & x \geq 0.60 \end{cases}$$

$$\mu_{ARID\_NRML}(x) = \begin{cases} \dfrac{x - 0.40}{0.10}; & 0.40 \leq x \leq 0.50 \\ 1; & 0.50 \leq x \leq 0.70 \\ 1 - \dfrac{x - 0.70}{0.10}; & 0.70 \leq x \leq 0.80 \\ 0; & x \leq 0.40 \; or \; x \geq 0.80 \end{cases}$$

$$\mu_{ARID\_LNG}(x) = \begin{cases} \dfrac{x - 0.70}{0.10}; & 0.70 \leq x \leq 0.80 \\ 1; & 0.80 \leq x \leq 1.00 \\ 0; & x \leq 0.70 \end{cases}$$

Fig. 7. Membership functions describing augmented-reality interaction duration

5.3. Fuzzy Rule Base

A set of linguistic statements, known as a fuzzy rule base, describes how PARSAT's fuzzy inference system makes decisions by classifying input, or controlling output. Fuzzy IF-THEN rules are used to aggregate all the variables, as there are input and output variables.

A set of 81 fuzzy rules were formulated, and they have been incorporated in the proposed system, which were specifically designed to create the logical outcome. The rest part of this subsection presents a representative sample of the aforementioned rules, showing how inputs affect the output.

Example Rule 1:

IF PRK is PRK_PR AND VLD is VLD_LNG AND ARID is ARID_LNG AND NoE is NoE_LRG THEN CLK is N

The aforementioned rule indicates that a student, with poor prior knowledge background, spending long time, both in watching the session's video tutorials (maybe by replaying them all the time, or constantly pausing and rewinding them) and in manipulating the 3D models through the AR environment (maybe finding it difficult to conceptualize their geometry), and finally scoring a large number of errors in the assessment section, then the user is classified as a novice student.

Example Rule 2:

IF PRK is PRK_GD AND VLD is VLD_NRML AND ARID is ARID_NRML AND NoE is NoE_SMLL THEN CLK is E

The above rule highlights a student who is an expert, while the main contributing factor is that the student has a good background in technical drawing, and the assessment's measured errors are small.

Example Rule 3:

IF PRK is PRK_MDM AND VLD is VLD_NRML AND ARID is ARID_NRML AND NoE is NoE_SMLL THEN CLK is P

The 3rd example of rule results in a proficient student, as the starting point is at medium level, but through training and personalized learning activities, managed to achieve excellent assessment score.

The next two rules consider the various inputs that all contribute to the knowledge level rating of the student being beginner.

Example Rule 4:

IF PRK is PRK_PR AND VLD is VLD_NRML AND ARID is ARID_LNG AND NoE is NoE_LRG THEN CLK is B

Example Rule 5:

IF PRK is PRK_PR AND VLD is VLD_LNG AND ARID is ARID_NRML AND NoE is NoE_LRG THEN CLK is B

The next rule indicates that spending normal time watching the educational tutorials and interacting with the virtual models, results in a competent knowledge rating.

Example Rule 6:

IF PRK is PRK_PR AND VLD is VLD_NRML AND ARID is ARID_NRML AND NoE is NoE_LRG THEN CLK is C

Example Rule 7:

IF PRK is PRK_MDM AND VLD is VLD_SRT AND ARID is ARID_NRML AND NoE is NoE_MDM THEN CLK is VG

Example Rule 8:

IF PRK is PRK_GD AND VLD is VLD_NRML AND ARID is ARID_SRT AND NoE is NoE_MDM THEN CLK is VG

Example rules 7 and 8 highlight a very good student, and case it when a student answers the assessment's evaluation test with normal number of errors.

5.4. Fuzzy Inference System

The fuzzy inference system (FIS) evaluates the rules saved the rule base and combines the results of each rule. The proposed system gets four inputs, namely prior knowledge, video-based learning duration, augmented-reality interaction duration and number of errors, fuzzified through the trapezoidal membership functions (Fig. 8).

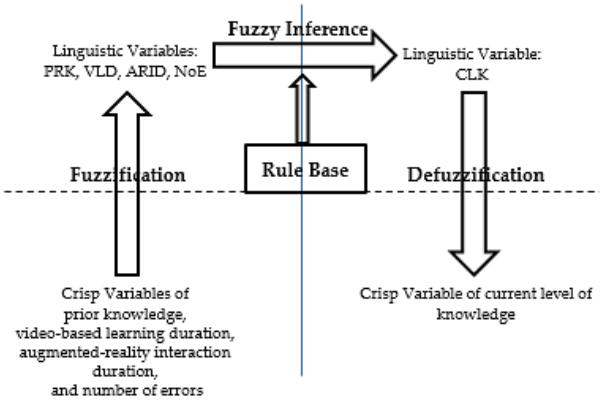

Fig. 8. Architecture of the fuzzy inference system

Then, 81 fuzzy rules were fed to the inference engine, in order to determine output, namely the student's current knowledge level. In this research, the Mamdani FIS [47] is employed, as it is typically used to capture expert knowledge. It enables us to communicate more naturally, while describing the expertise.

The fuzzy inputs must be combined into a single fuzzy output, by using the Mamdani inference engine's fuzzy implication. The fuzzy input variables for each of the rules are then connected using the AND operator. This operator's function is to extract the minimum membership function value from the fuzzy input variables. Using the value obtained from the input component, the fuzzy output variable is truncated. By taking the maximum value of the membership degree, the entire shortened output is therefore aggregated into a single graph and employed in the final stage of the fuzzy logic system.

5.5. Defuzzification

Defuzzifier procedure maps the fuzzy output to a crisp value according to the membership function of output variable. In order to get the crisp value, a diverse method is required. This defuzzification is not part of the "mathematical fuzzy logic" and various methods are possible [48]–[50]. The input for the defuzzification process is the aggregate output fuzzy set, while the output is a single number. The Center of gravity (COG) method is most prevalent and physically appealing of all the defuzzification methods [51], which was taken into consideration in this model, resulting the gravity center procedure to be applied in this study. The basic principle in COG method is a centroid approach, which finds the point where a vertical line slices the aggregate set into two equal masses.

5.6. Adaptation of the Learning Activities Based on Fuzzy Weights

Technical drawing assumes high level training of spatial ability, while it is achieved by using adaptive learning activities considering the student's level of knowledge. This is accomplished by converting student's current knowledge level to fuzzy weights to deliver appropriate learning activities both in quantity and level of difficulty, learning activities.

Six fuzzy weights have been defined in this approach to represent the current knowledge level of students in the domain of technical drawing. The membership functions which are used to calculate the sextet that best defines the student's current level of knowledge are presented in Fig. 9.

$$\mu_N(x) = \begin{cases} 1; & x \le 0.10 \\ 1 - \dfrac{x - 0.10}{0.10}; & 0.10 \le x \le 0.20 \\ 0; & x \ge 0.20 \end{cases}$$

$$\mu_B(x) = \begin{cases} \dfrac{x - 0.10}{0.10}; & 0.10 \le x \le 0.20 \\ 1; & 0.20 \le x \le 0.30 \\ 1 - \dfrac{x - 0.30}{0.10}; & 0.30 \le x \le 0.40 \\ 0; & x \le 0.10 \text{ or } x \ge 0.40 \end{cases}$$

$$\mu_C(x) = \begin{cases} \dfrac{x - 0.30}{0.10}; & 0.30 \le x \le 0.40 \\ 1; & 0.40 \le x \le 0.50 \\ 1 - \dfrac{x - 0.50}{0.10}; & 0.50 \le x \le 0.60 \\ 0; & x \le 0.30 \text{ or } x \ge 0.60 \end{cases}$$

$$\mu_{VG}(x) = \begin{cases} \dfrac{x - 0.50}{0.10}; & 0.50 \le x \le 0.60 \\ 1; & 0.60 \le x \le 0.70 \\ 1 - \dfrac{x - 0.70}{0.10}; & 0.70 \le x \le 0.80 \\ 0; & x \le 0.50 \text{ or } x \ge 0.80 \end{cases}$$

$$\mu_P(x) = \begin{cases} \dfrac{x - 0.70}{0.10}; & 0.70 \le x \le 0.80 \\ 1; & 0.80 \le x \le 0.90 \\ 1 - \dfrac{x - 0.90}{0.10}; & 0.90 \le x \le 1.00 \\ 0; & x \le 0.70 \end{cases}$$

$$\mu_E(x) = \begin{cases} \dfrac{x - 0.90}{0.05}; & 0.90 \le x \le 0.95 \\ 1; & 0.95 \le x \le 1.00 \\ 0; & x \le 0.90 \end{cases}$$

Fig. 9. Membership functions describing student's knowledge level

The output of the aforementioned membership functions is limited to between 0 and 1, and they are used in the fuzzification and defuzzification steps of the fuzzy logic system, as they map the non-fuzzy input values to fuzzy linguistic terms and vice versa. We integrated membership functions which are formed using straight lines, having the advantage of simplicity, and more specific the trapezoidal membership function (Fig. 10).

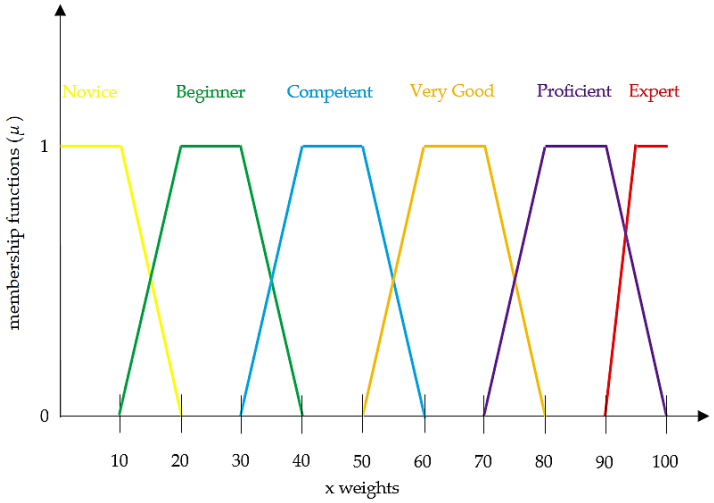

Fig. 10. Fuzzy weights of knowledge level in linguistic terms

Student's knowledge level is described by the sextet (N, B, C, VG, P, and E), and as such, the student may be fully assigned to one, or partially assigned to more fuzzy sets, meaning that student's knowledge level can be described as 'Competent' or partially 'Very Good' and partially 'Proficient', respectively. As an example, a student's sextet of (0, 1, 0, 0, 0, 0), classifies the student as 100% 'Beginner'. Another example of a student's sextet which is (0, 0, 0, 0.70, 0.30, 0), classifies the student to be 70% 'Very Good' and 30% 'Proficient'. But whatever the values of the sextet are, the equation $\mu N(x) + \mu B(x) + \mu C(x) + \mu VG(x) + \mu P(x) + \mu E(x) = 1$ stands.

In this section, the analysis of the rules, in combination with the fuzzy weights, is presented to adapt the teaching strategy to the students' knowledge level [52]–[54]. The number of learning activities of each level's chapter that the student must learn each time, is dynamically defined according to the current level of knowledge [55].

The rules' design plays an important role in determining the number and the difficulty of the learning activities delivered to the students. The rules have been defined by eight professors from the Department of Informatics and Computer Engineering, who utilized the fuzzy rules, and their related thresholds at the membership functions. The faculty members were asked to define, in more detail, the technical drawing knowledge levels that students gain during the course throughout the course of an entire semester. All the faculty members have more than 15 years of experience instructing technical drawing in academic contexts, and they can attest to the accuracy of the depiction of students' knowledge levels. They contributed to the current stage by matching each learning activity with the corresponding SOLO level.

As an example, a beginner student needs to study many topics of low difficulty of the initial levels of SOLO taxonomy, such as pre-structural and unistructural level, whereas an expert student can deal topics of the multi-structural and relational level of SOLO taxonomy of lesser quantity. The set of rules in total is presented in Table 3.

Table 3. Decision rules for adaptive instruction

Current level of knowledge	L1	L2	L3	L4	L5	Sum of LAs
$\mu_N = 1$	9	5	0	0	0	14
$\mu_N < 1$ and $\mu_B < 1$	8	5	0	0	0	13
$\mu_B = 1$	6	6	0	0	0	12
$\mu_B < 1$ and $\mu_C < 1$	5	5	1	0	0	11
$\mu_C = 1$	4	4	2	0	0	10
$\mu_C < 1$ and $\mu_{VG} < 1$	3	3	3	0	0	9
$\mu_{VG} = 1$	1	1	3	2	1	8
$\mu_{VG} < 1$ and $\mu_P < 1$	0	1	2	3	1	7
$\mu_P = 1$	0	0	1	4	1	6
$\mu_P < 1$ and $\mu_E < 1$	0	0	0	3	2	5
$\mu_E = 1$	0	0	0	1	3	4

According to Table 3, a student who was assigned a crisp output value of 76 per cent, has been classified as partially very good and partially proficient, and will be delivered learning activities (LAs), as follows:

- no learning activity of SOLO-L1;
- one learning activity of SOLO-L2;
- two learning activity of SOLO-L3;
- three learning activities of SOLO-L4; and
- one learning activities of SOLO-L5.

6. Evaluation and Discussion

The evaluation of PARSAT took place for the winter academic semester 2022-2023 during the tutoring of the undergraduate course of "Technical Drawing" of a public University of the capital city of the country. In particular, three educators, and 240 undergraduate students, participated in the evaluation process. All the measurements of gender and age were derived from a randomly selected sample and do not have an impact on our research findings. The demographics analysis is shown in Table 4.

The population was equally divided by the instructors in two groups, each of which had equal number of students. The first group, namely experimental group, were asked to operate the PARSAT by themselves, taking advantage of the system's adaptivity. For instance, the modeling of the students' domain knowledge, offered them the opportunity to watch video tutorials of different duration, to rotate 3D objects of different complexity in order to visualize and understand their structures, and overall face different learning activities according to their personalized profile.

The second group, namely control group, used the learning material with the same learning activities, without any adaptivity in students' personal profile. All three instructors were engaged in both groups.

Table 4. Demographics

Measure	Item	Frequency	Percentage (%)
Sample size		240	100.0
Gender	Male	151	62.9
	Female	88	36.7
	Non-binary	1	0.4
Age	15-17	0	0
	18-19	199	82.9
	Over 20	41	17.1
Prior knowledge	None	198	82.5
	High school course	42	17.5

After the completion of the course at the end of the semester, the two groups (experimental and control) were asked to answer a questionnaire, based on a 7-point Likert scale ranging from (1) strongly disagree to (7) strongly agree. The questions are the following [56], [57]:

Question 1 (Q1): The learning activities were in accordance with your knowledge level;

Question 1 (Q2): The number of the learning activities was effective;

Question 3 (Q3): PARSAT successfully identified your learning style.

Analyzing the answers to the aforementioned questions, we present the results in three pie charts (Figures 11-13).

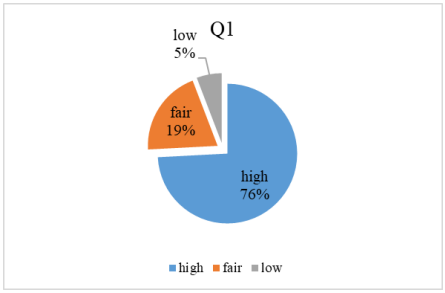

Fig. 11. Question 1 results

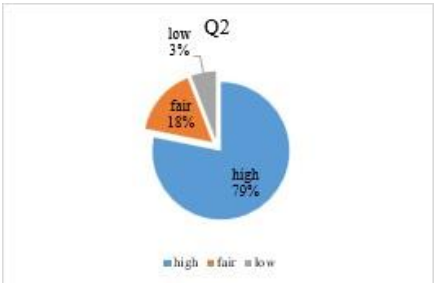

Fig. 12. Question 2 results

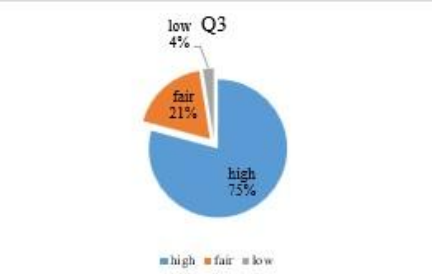

Fig. 13. Question 3 results

According to the evaluation results presented in the paper, a majority of the students found the learning activities to be appropriate for their knowledge level and effective for learning. Specifically, 182 students (76%) found the learning activities to be in accordance with their knowledge level, while 190 students (79%) found the number of learning activities to be appropriate for effective learning. Additionally, most students (180 or 75%) highly evaluated PARSAT as pedagogically useful for supporting their learning process. These positive evaluation results suggest that the proposed system, which utilizes fuzzy logic and AR technology, can provide a personalized and effective training experience for engineering students in the domain of technical drawing.

A statistical hypothesis test was used to assess the system more thoroughly. The 2-tailed *t*-test results indicate that there is a significant difference between the mean values of all three questions, which relate to the appropriateness of the learning activities, the number of learning activities, and the overall pedagogical usefulness of PARSAT. The *t*-Stat values for all three questions are greater than the critical *t* values, indicating that the results are statistically significant. This suggests that the proposed system, which incorporates an adaptive mechanism for learning activities, had a positive effect on student satisfaction and improved learning outcomes. Overall, the statistical analysis provides further evidence of the effectiveness of the PARSAT system for training engineering students in technical drawing.

Table 5. *t*-test results

	Question 1		**Question 2**		**Question 3**	
	Experimental group	Control group	Experimental Group	Control group	Experimental Group	Control group
Mean	6.03	3.71	6.48	3.66	6.01	3.29
Variance	0.74	0.43	0.42	0.49	0.57	0.65
t-Stat	2.72		4.04		3.79	
P two-tail	0.0016		0.00061		0.00035	
t Critical two-tail	2.01		1.89		1.97	

As far as the learning outcome is concerned, the authors compared the pretest-posttest results of an experimental group (120 students) who used the PARSAT system's adaptive learning material distribution using fuzzy logic, to a control group (also consisting of 120 students) who did not have access to this advanced functionality. All

students, both in the experimental and control groups, took the same pretest to establish their prior knowledge of technical drawing. At the end of the semester, both groups took the same posttest, and a paired *t*-test was used to compare the differences in learning outcomes between the two groups. This approach allows the researchers to assess the effectiveness of the PARSAT system in improving learning outcomes in technical drawing.

Table 6 presents the evaluation results of the pretest and posttest scores of both the experimental and control groups. The experimental group had a pretest mean score of 4.19 and a posttest mean score of 6.24, indicating an improvement of 2.05 points. On the other hand, the control group had a pretest mean score of 4.38 and a posttest mean score of 5.01, indicating an improvement of only 0.63 points. While both groups improved their scores, the improvement in the experimental group was significantly greater than that of the control group, indicating that the adaptive system used by the experimental group had a positive impact on their learning outcomes.

Table 6. *t*-test results of the pretest and the posttest scores

	Experimental group	**Control group**
Pretest Mean	4.19	4.38
Posttest Mean	6.24	5.01
Difference	2.05	0.63
t-Stat	4.23	1.64
P-value	0.00033	0.0038

The evaluation results presented in Table 6 show the pretest and posttest mean scores of the experimental and control groups. A pretest is a test administered before the instruction, while a posttest is a test administered after the instruction. By comparing the pretest and posttest scores, the authors determined how much the instruction has improved students' learning outcomes.

In this study, the experimental group used the PARSAT system, which provided adaptive learning material distribution using fuzzy logic, while the control group did not have access to this system. The results show that both groups improved their scores from the pretest to the posttest. However, the experimental group showed a much greater improvement than the control group, indicating that the adaptive system used by the experimental group had a positive impact on their learning outcomes.

7. Conclusion

This paper presents PARSAT, which is a mobile augmented reality application for the training of spatial skills. PARSAT asks the user to insert three inputs, namely age, gender and prior knowledge, and personalizes the educational experience to each student. The adaptivity is accomplished by employing fuzzy weight-based decisions, defining the students' domain knowledge level, and according to the fuzzy logic results, each student receives different learning activities.

The findings of the system's evaluation are quite encouraging, as they show a high level of student satisfaction and improved learning outcomes. Students gave this personalized teaching approach a high feedback grade, indicating the correctness of the learning activities supplied, depending on their knowledge level. Finally, the pretest and posttest evaluations revealed a considerable improvement in students' scores, verifying the pedagogical suitability of the proposed learning approach.

In addition to the findings, there are some limitations related to screen size, hardware variability, and the limited computational resources of mobile devices. This can result in slower performance and limitations in the types of augmented reality experiences that can be created.

The current research focuses on providing students with appropriate learning activities based on their knowledge level as the primary determinant of their adaptability. Incorporation of extra fuzzy weights regarding other students' characteristics, such as emotional state and/or types of mistakes is a future inquiry coming from this work, with the goal of improving system adaptation, and, hence learning outcomes.

Integrating hybrid algorithmic techniques for modelling student knowledge can be a promising future extension. By combining different techniques, such as fuzzy logic, Bayesian networks, and decision trees, it may be possible to create more accurate and reliable student models. This can lead to more personalized and effective learning experiences for individual learners.

References

1. A. Çöltekin et al., "Extended Reality in Spatial Sciences: A Review of Research Challenges and Future Directions," ISPRS International Journal of Geo-Information, vol. 9, no. 7. 2020. doi: 10.3390/ijgi9070439.
2. R. Azuma, Y. Baillot, R. Behringer, S. Feiner, S. Julier, and B. MacIntyre, "Recent advances in augmented reality," IEEE Comput Graph Appl, vol. 21, no. 6, pp. 34–47, 2001, doi: 10.1109/38.963459.
3. E. Zaretsky and V. Bar, "Intelligent virtual reality and its impact on spatial skills and academic achievements," in The 10th International Conference on Information Systems Analysis and Synthesis: ISAS 2004 and International Conference on Cybernetics and Information Technologies, Systems and Applications: CITSA, 2004, pp. 107–113.
4. S. Rokhsaritalemi, A. Sadeghi-Niaraki, and S.-M. Choi, "A Review on Mixed Reality: Current Trends, Challenges and Prospects," Applied Sciences, vol. 10, no. 2. 2020. doi: 10.3390/app10020636.
5. T. Lavric, E. Bricard, M. Preda, and T. Zaharia, "A low-cost AR training system for manual assembly operations," Computer Science and Information Systems, no. 00, p. 13, 2022.
6. K. Takrouri, E. Causton, and B. Simpson, "AR Technologies in Engineering Education: Applications, Potential, and Limitations," Digital, vol. 2, pp. 171–190, May 2022, doi: 10.3390/digital2020011.
7. D. F. Ali, M. Omar, N. H. Ibrahim, J. Surif, M. Ali, and S. Ismail, "Overcoming the problems faced by student's in learning engineering drawing with the implementation of augmented reality learning environment," Man India, vol. 97, no. 17, pp. 147–159, 2017.
8. Z. Kanetaki, C. I. Stergiou, G. Bekas, C. Troussas, and C. Sgouropoulou, "Creating a Metamodel for Predicting Learners' Satisfaction by Utilizing an Educational Information System During COVID-19 Pandemic.," in NiDS, 2021, pp. 127–136.

9. Z. Kanetaki, C. Stergiou, G. Bekas, C. Troussas, and C. Sgouropoulou, “A Hybrid Machine Learning Model for Grade Prediction in Online Engineering Education,” International Journal of Engineering Pedagogy (iJEP), vol. 12, no. 3, pp. 4–24, May 2022, doi: 10.3991/ijep.v12i3.23873.
10. S. Sorby, “Developing 3D spatial skills for engineering students,” Australasian Journal of Engineering Education, vol. 13, pp. 1–11, Jan. 2007, doi: 10.1080/22054952.2007.11463998.
11. A. R. Arslan and S. Dazkir, “Technical Drafting and Mental Visualization in Interior Architecture Education,” International Journal for the Scholarship of Teaching and Learning, vol. 11, no. 2, 2017, doi: 10.20429/ijsotl.2017.110215.
12. H. B. P. Gerson, S. A. Sorby, A. Wysocki, and B. J. Baartmans, “The development and assessment of multimedia software for improving 3-D spatial visualization skills,” Computer Applications in Engineering Education, vol. 9, no. 2, pp. 105–113, 2001.
13. A. Šafhalter, S. Glodež, A. Šorgo, and M. Ploj Virtič, “Development of spatial thinking abilities in engineering 3D modeling course aimed at lower secondary students,” Int J Technol Des Educ, 2020, doi: 10.1007/s10798-020-09597-8.
14. C. Papakostas, C. Troussas, A. Krouska, and C. Sgouropoulou, “Exploration of Augmented Reality in Spatial Abilities Training: A Systematic Literature Review for the Last Decade,” Informatics in Education, vol. 20, no. 1, pp. 107–130, Mar. 2021, doi: 10.15388/infedu.2021.06.
15. J.-J. Lo, Y.-C. Chan, and S.-W. Yeh, “Designing an adaptive web-based learning system based on students’ cognitive styles identified online,” Comput Educ, vol. 58, pp. 209–222, Jan. 2012, doi: 10.1016/j.compedu.2011.08.018.
16. L. A. Zadeh, “Fuzzy logic = computing with words,” IEEE Transactions on Fuzzy Systems, vol. 4, no. 2, pp. 103–111, 1996, doi: 10.1109/91.493904.
17. Z. Kanetaki et al., “Acquiring, Analyzing and Interpreting Knowledge Data for Sustainable Engineering Education: An Experimental Study Using YouTube,” Electronics (Basel), vol. 11, no. 14, p. 2210, 2022.
18. C. Papakostas, C. Troussas, A. Krouska, and C. Sgouropoulou, “Modeling the Knowledge of Users in an Augmented Reality-Based Learning Environment Using Fuzzy Logic,” in Novel & Intelligent Digital Systems: Proceedings of the 2nd International Conference (NiDS 2022), A. Krouska, C. Troussas, and J. Caro, Eds., Cham: Springer International Publishing, 2023, pp. 113–123.
19. C. Papakostas, C. Troussas, A. Krouska, and C. Sgouropoulou, “Measuring User Experience, Usability and Interactivity of a Personalized Mobile Augmented Reality Training System,” Sensors, vol. 21, no. 11, p. 3888, Jun. 2021, doi: 10.3390/s21113888.
20. J. Yu, A. R. Denham, and E. Searight, “A systematic review of augmented reality game-based Learning in STEM education,” Educational technology research and development, 2022, doi: 10.1007/s11423-022-10122-y.
21. C. Rodríguez-Abad, J.-C. Fernández-de-la-Iglesia, A.-E. Martínez-Santos, and R. Rodríguez-González, “A Systematic Review of Augmented Reality in Health Sciences: A Guide to Decision-Making in Higher Education,” Int J Environ Res Public Health, vol. 18, p. 4262, Apr. 2021, doi: 10.3390/ijerph18084262.
22. R. Monterubbianesi et al., “Augmented, Virtual and Mixed Reality in Dentistry: A Narrative Review on the Existing Platforms and Future Challenges,” Applied Sciences, vol. 12, no. 2, 2022, doi: 10.3390/app12020877.
23. P. Kourouthanassis, C. Boletsis, C. Bardaki, and D. Chasanidou, “Tourists responses to mobile augmented reality travel guides: The role of emotions on adoption behavior,” Pervasive Mob Comput, vol. 18, pp. 71–87, 2015, doi: https://doi.org/10.1016/j.pmcj.2014.08.009.

24. D.-I. Han, M. C. tom Dieck, and T. Jung, “User experience model for augmented reality applications in urban heritage tourism,” Journal of Heritage Tourism, vol. 13, no. 1, pp. 46–61, Jan. 2018, doi: 10.1080/1743873X.2016.1251931.
25. H. Kim, T. Matuszka, J.-I. Kim, J. Kim, and W. Woo, “Ontology-based mobile augmented reality in cultural heritage sites: information modeling and user study,” Multimed Tools Appl, vol. 76, no. 24, pp. 26001–26029, 2017, doi: 10.1007/s11042-017-4868-6.
26. T. Bekus, “THE APPLICATION OF AUGMENTED REALITY IN MARKETING,” Zeszyty Naukowe Wyższej Szkoły Humanitas Zarządzanie, vol. 19, pp. 279–296, Oct. 2018, doi: 10.5604/01.3001.0013.0068.
27. K. Mitrovic, N. Novakovic, J. Spajić, and I. Cosic, “Augmented Reality in Marketing – State of Art,” 2021, pp. 566–575. doi: 10.2507/32nd.daaam.proceedings.081.
28. F. de Pace, F. Manuri, and A. Sanna, “Augmented Reality in Industry 4.0,” American Journal of Computer Science and Information Technology, vol. 06, Jan. 2018, doi: 10.21767/2349-3917.100017.
29. S. S. Alam, S. Susmit, C.-Y. Lin, M. Masukujjaman, and Y.-H. Ho, “Factors Affecting Augmented Reality Adoption in the Retail Industry,” Journal of Open Innovation: Technology, Market, and Complexity, vol. 7, no. 2, 2021, doi: 10.3390/joitmc7020142.
30. M. Tenemaza, A. de Antonio, and J. Ram\’\irez, “The User Model, Vocabulary and Logical Architecture for Adaptive Augmented Reality,” in Proceedings of the Latin American Conference on Human Computer Interaction, in CLIHC ’15. New York, NY, USA: Association for Computing Machinery, 2015. doi: 10.1145/2824893.2824901.
31. N. Ghouaiel, J.-M. Cieutat, and J.-P. Jessel, “Adaptive Augmented Reality: Plasticity of Augmentations,” in Proceedings of the 2014 Virtual Reality International Conference, in VRIC ’14. New York, NY, USA: Association for Computing Machinery, 2014. doi: 10.1145/2617841.2620695.
32. N. Stojanovic, A. Damala, T. Schuchert, L. Stojanovic, S. Fairclough, and J. Moores, “Tutorial 1: Adaptive augmented reality (A2R): Where AR meets user’s interest,” in 2012 IEEE International Symposium on Mixed and Augmented Reality - Arts, Media, and Humanities (ISMAR-AMH), 2012, p. 1. doi: 10.1109/ISMAR-AMH.2012.6483973.
33. D. Naser Addin and B. Ozell, Design and Test of an adaptive augmented reality interface to manage systems to assist critical missions. 2021.
34. T. Langlotz, T. Nguyen, D. Schmalstieg, and R. Grasset, “Next-Generation Augmented Reality Browsers: Rich, Seamless, and Adaptive,” Proceedings of the IEEE, vol. 102, pp. 155–169, Feb. 2014, doi: 10.1109/JPROC.2013.2294255.
35. R. Z. Abidin, H. Arshad, and S. A. A. Shukri, “A framework of adaptive multimodal input for location-based augmented reality application,” Journal of Telecommunication, Electronic and Computer Engineering (JTEC), vol. 9, no. 2–11, pp. 97–103, 2017.
36. I. M. Rodríguez-Marco, A. Damala, T. Schuchert, J. Moragues, K. Gilleade, and N. Stojanovic, “Exploring the Affective Museum Visiting Experience: Adaptive Augmented Reality (A2R) and Cultural Heritage,” International Journal of Heritage in the Digital Era, vol. 2, Mar. 2013, doi: 10.1260/2047-4970.2.1.117.
37. C. Papakostas, C. Troussas, A. Krouska, and C. Sgouropoulou, “On the Development of a Personalized Augmented Reality Spatial Ability Training Mobile Application,” in Novelties in Intelligent Digital Systems, IOS Press, 2021, pp. 75–83.
38. C. Troussas, K. Chrysafiadi, and M. Virvou, “An intelligent adaptive fuzzy-based inference system for computer-assisted language learning,” Expert Syst Appl, vol. 127, Mar. 2019, doi: 10.1016/j.eswa.2019.03.003.
39. C. Troussas, A. Krouska, and C. Sgouropoulou, “A novel teaching strategy through adaptive learning activities for computer programming,” IEEE Transactions on Education, vol. 64, no. 2, pp. 103–109, 2020.
40. T. Masood and J. Egger, “Adopting augmented reality in the age of industrial digitalisation,” Comput Ind, vol. 115, p. 103112, 2020, doi: https://doi.org/10.1016/j.compind.2019.07.002.

41. F. Redzuan, A.-N. A. Khairuddin, and N. A. Daud, “Emotional augmented reality-based mobile learning design elements: a kansei engineering approach,” Indones. J. Electr. Eng. Comput. Sci, vol. 14, no. 1, pp. 413–420, 2019.
42. X. Wang, S. K. Ong, and A. Y. C. Nee, “A comprehensive survey of augmented reality assembly research,” Adv Manuf, vol. 4, 2016, doi: 10.1007/s40436-015-0131-4.
43. J. Biggs, “Teaching for Quality Learning at University. Society for Research into Higher Education,” The Higher Education Academy.(2008). Groupwork, Retrieved August, vol. 6, p. 2008, Jan. 2003.
44. J. Biggs and C. Tang, Teaching for Quality Learning at University. in UK Higher Education OUP Humanities & Social Sciences Higher Education OUP. McGraw-Hill Education, 2011. [Online]. Available: https://books.google.gr/books?id=VC1FBgAAQBAJ
45. N. Medina-Medina and L. García-Cabrera, “A taxonomy for user models in adaptive systems: special considerations for learning environments,” Knowl Eng Rev, vol. 31, pp. 124–141, Mar. 2016, doi: 10.1017/S0269888916000035.
46. E. Mousavinasab, N. Zarifsanaiey, S. R. Niakan Kalhori, M. Rakhshan, L. Keikha, and M. Ghazi Saeedi, “Intelligent tutoring systems: a systematic review of characteristics, applications, and evaluation methods,” Interactive Learning Environments, vol. 29, no. 1, pp. 142–163, Jan. 2021, doi: 10.1080/10494820.2018.1558257.
47. E. H. Mamdani and S. Assilian, “An experiment in linguistic synthesis with a fuzzy logic controller,” Int J Man Mach Stud, vol. 7, no. 1, pp. 1–13, 1975, doi: https://doi.org/10.1016/S0020-7373(75)80002-2.
48. A. Chandramohan, M. V. C. Rao, and M. Senthil. Arumugam, “Two New and Useful Defuzzification Methods Based on Root Mean Square Value,” Soft comput, vol. 10, no. 11, pp. 1047–1059, 2006, doi: 10.1007/s00500-005-0042-6.
49. H. Diab, “Defuzzification methods and new techniques for fuzzy controllers,” Iranian Journal of Electrical and Computer Engineering, vol. 3, Jul. 2004.
50. N. Mogharreban and L. Dilalla, Comparison of Defuzzification Techniques for Analysis of Non-interval Data. 2006. doi: 10.1109/NAFIPS.2006.365418.
51. T. Takagi and M. Sugeno, “Fuzzy identification of systems and its applications to modeling and control,” IEEE Trans Syst Man Cybern, vol. SMC-15, no. 1, pp. 116–132, 1985, doi: 10.1109/TSMC.1985.6313399.
52. T. K. F. Chiu and I. Mok, “Learner expertise and mathematics different order thinking skills in multimedia learning,” Comput Educ, vol. 107, pp. 147–164, Apr. 2017, doi: 10.1016/j.compedu.2017.01.008.
53. N. Elghouch, M. Kouissi, and E.-N. el Mokhtar, “Multi-Agent System of an Adaptive Learning Hypermedia Based on Incremental Hybrid Case-Based Reasoning,” 2020, pp. 143–156. doi: 10.1007/978-3-030-37629-1_12.
54. A. Khamparia and B. Pandey, “SVM and PCA Based Learning Feature Classification Approaches for E-Learning System,” International Journal of Web-Based Learning and Teaching Technologies, vol. 13, pp. 32–45, Apr. 2018, doi: 10.4018/IJWLTT.2018040103.
55. C. Papakostas, C. Troussas, A. Krouska, and C. Sgouropoulou, “Personalization of the Learning Path within an Augmented Reality Spatial Ability Training Application Based on Fuzzy Weights,” Sensors, vol. 22, no. 18, 2022, doi: 10.3390/s22187059.
56. A. Krouska et al., “Language Learning Assisted by Group Profiling in Social Networks,” International Journal of Emerging Technologies in Learning (iJET), vol. 8, pp. 1–6, Jun. 2013, doi: 10.1109/IISA.2017.8316430.
57. C. Troussas, A. Krouska, and M. Virvou, “Using a Multi Module Model for Learning Analytics to Predict Learners’ Cognitive States and Provide Tailored Learning Pathways and Assessment BT - Machine Learning Paradigms: Advances in Learning Analytics,” M. Virvou, E. Alepis, G. A. Tsihrintzis, and L. C. Jain, Eds., Cham: Springer International Publishing, 2020, pp. 9–22. doi: 10.1007/978-3-030-13743-4_2.

Christos Papakostas is a Postdoctoral Researcher in the Department of Informatics and Computer Engineering at the University of West Attica. He earned his Ph.D. from the same department at the University of West Attica. Additionally, he holds a B.Eng. and an M.Sc. degree from the Department of Electrical and Computer Engineering at Democritus University of Thrace. His research interests include augmented reality, adaptive tutoring systems, and human-computer interaction.

Christos Troussas is Assistant Professor in the Department of Informatics and Computer Engineering at the University of West Attica. He has received a Ph.D., an M.Sc. and a B.Sc. degree from the Department of Informatics at the University of Piraeus. His current research interests include personalized software technologies and human-computer interaction.

Akrivi Krouska is a Postdoctoral Researcher in the Department of Informatics and Computer Engineering at the University of West Attica. She has received a Ph.D. and a B.Sc. degree from the Department of Informatics at the University of Piraeus and an M.Sc. degree from AUEB. Her research interests include social information systems and data analytics.

Cleo Sgouropoulou is Professor in the Department of Informatics and Computer Engineering at the University of West Attica. She has received a Ph.D. and a B.Eng. degree from the Department of Electrical and Computer Engineering at the National Technical University of Athens. Her research interests include software engineering and artificial intelligence in education.

Received: January 30, 2023; Accepted: June 20, 2023.

Computer Science and Information Systems 20(4):1419–1437 https://doi.org/10.2298/CSIS230310047L

Explaining Deep Residual Networks Predictions with Symplectic Adjoint Method

Xia Lei[1], Jia-Jiang Lin[1], Xiong-Lin Luo[1⋆], and Yongkai Fan[2]

[1] Department of Automation, China University of Petroleum Bejing
102249 Beijing, China
leixia2008530059@163.com
lawliet3@qq.com
luoxl@cup.edu.cn

[2] State Key Laboratory of Media Convergence and Communication
Communication University of China
100024 Beijing, China
fanyongkai@gmail.com

Abstract. Understanding deep residual networks (ResNets) decisions are receiving much attention as a way to ensure their security and reliability. Recent research, however, lacks theoretical analysis to guarantee the faithfulness of explanations and could produce an unreliable explanation. In order to explain ResNets predictions, we suggest a provably faithful explanation for ResNet using a surrogate explainable model, a neural ordinary differential equation network (Neural ODE). First, ResNets are proved to converge to a Neural ODE and the Neural ODE is regarded as a surrogate model to explain the decision-making attribution of the ResNets. And then the decision feature and the explanation map of inputs belonging to the target class for Neural ODE are generated via the symplectic adjoint method. Finally, we prove that the explanations of Neural ODE can be sufficiently approximate to ResNet. Experiments show that the proposed explanation method has higher faithfulness with lower computational cost than other explanation approaches and it is effective for troubleshooting and optimizing a model by the explanation.

Keywords: Deep residual networks, Explanation, Neural ODE, Symplectic adjoint method.

1. Introduction

Deep neural networks, such as deep residual networks (ResNets) [9], have been widely applied due to their superior performance. However, they are usually regarded as black box models driven by data, and it is difficult to explain how the models work and predict their decisions. Therefore, the result of ResNets may be out of control. For instance, the networks are easily tricked into incorrect classification results by adversarial instances, which are produced by artificially created hostile perturbations that are invisible to humans [19], [28],[25]. The uninterpretability of ResNets makes them potentially dangerous for applications in safety-critical tasks such as intelligent medical diagnosis and autonomous driving [12],[18],[10].

⋆ Corresponding author

How to make black box models transparent is a significant and intriguing subject given the requirements for trusted and safe AI. Finding the ResNets' decision-making attribution is a focus of several researchers. By identifying the attribution and creating an explanation why ResNets' predictions are going, gradient-based backpropagation methods such as Guided-BP [27], IntegratedGrad [29] and SmoothGrad [26], and the combined gradient class activation map (CAM) methods such as Grad-CAM [23] and Grad-CAM++ [3] have been proposed. Although these gradient-based methods make it easy to understand the contribution of the input features and can locate meaningful image regions with good semantic visual performance for humans, the gradient vanishing and saturation issues may result in inaccurate explanations. Moreover, they require the gradients layer-by-layer backpropagation, which leads to low computational efficiency. On the other hand, the gradient-free methods such as Score-CAM [31] and Group-CAM [33] use feature maps as masks on the original image to output the forward passing score as the weights instead of gradients. Although the methods outperform current state-of-the-art methods on both visual performance and localization tasks, the weights are obtained entirely based on training, the lack of theoretical analysis cannot demonstrate the faithfulness of the explanation, and retraining greatly reduces the computational efficiency.

Considering the problem of the naive gradient and the lack of theoretical analysis to guarantee the faithfulness of the explanation, this paper proposes a novel explanation method for ResNet with the symplectic adjoint method. An explainable neural ordinary differential equation network (Neural ODE), which is proved to be the convergent model of ResNets, as shown in Fig. 1, is built as a surrogate model to explain the decision features of ResNets. Thus, inspired by [17], the symplectic adjoint method is used to get over the naive gradient problem. Our method takes advantage of gradient-based methods, and it makes up for the lack of theoretical analysis to demonstrate the faithfulness of the explanation. The contributions of this paper are as follows.

1. ResNets are proved to converge to a Neural ODE which is obtained as a surrogate model to explain ResNet predictions. And then the symplectic adjoint method instead of the naive backpropagation algorithm is used to obtain a more accurate calculation of the decision features with less memory and lower computational cost than other explanation approaches.

2. The proposed method has class sensitivity not only in the deep layer but also in the input layer. The gradient decomposition produces an explanation map for the Neural ODE in the input layer that is sufficiently close to the explanation of ResNets under certain conditions, based on a trade-off between faithfulness and intelligibility.

3. The faithfulness of the proposed explanation method is quantitatively evaluated through the evaluation indicators of the deletion and insertion metrics. Experiments results show that the proposed approach has higher faithfulness with lower computational cost than others, and it is effective for troubleshooting and optimizing a model by the explanation.

The remainder of the paper is structured as follows: In Section 2, the related work is presented, while the definitions of ResNet and Neural ODE, and the relationship between ResNet and Neural ODE are introduced in Section 3. Section 4 proposes the symplectic adjoint method. The faithfulness of the explanation between ResNet and the surrogate model - Neural ODE is demonstrated in Section 5. In Section 6, the experimental results

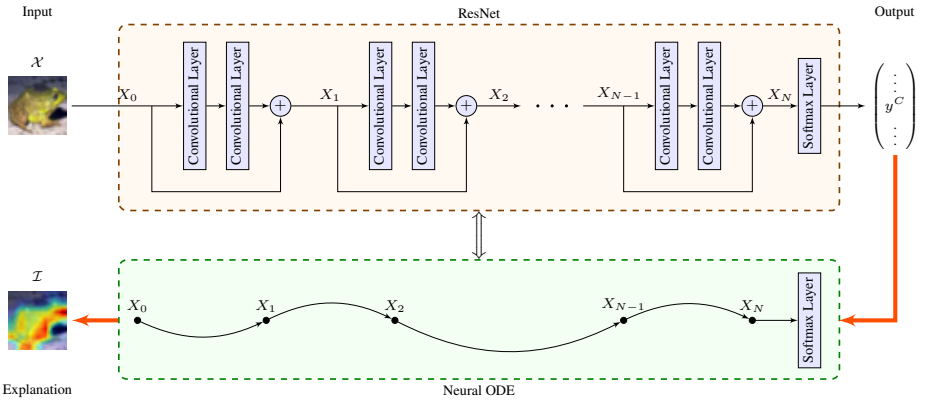

Fig. 1. Overview of our proposed method

are discussed, and finally, the concluding remarks and future directions are depicted in Section 7.

2. Related works

With the widespread application of ResNets, making them interpretable is the impelling priority to be solved to make them trustworthy. Recently, many researches on explicitly explaining the decision attribution of models have emerged. Gradient-based backpropagation methods, CAM-based methods, and Surrogate-based methods are the three major methods.

Gradient-based backpropagation methods. These approaches compute and visualize the gradient of the output concerning the input features for the target class to interpret the contribution of the input features for the prediction result. Simonyan et al. [24] proposed an explanation method to compute the gradient by the backpropagation algorithm to visualize the saliency maps, highlighting the importance of the decision features of the target class. Considering that the saliency maps obtained by the approach are noisy, Guided-BP [27] only backpropagates positive error signals during the process of gradient backpropagation, which is helpful to explain the positive influence of each neuron in the deep network on the input image. Instead of only computing the gradient of the output to the current input, IntegratedGrad [29] calculates the integral of the gradient of the input scaled up from some starting value to the current value. In addition, SmoothGrad [26] adds Gaussian noise to the sample to be interpreted to obtain similar samples, and then the backpropagation algorithm is implemented to generate a saliency map for each input sample. Finally, the average of all the saliency maps of the similarity-generated samples is an explanation of ResNet's decisions with less visual noise. Although the gradient-based explanation methods have theoretical analysis to compute the gradient to make it easy to understand the contribution of the input features, the explanations lack semantic intelligibility and the gradient obtained by the backpropagation algorithm has vanishing and saturation issues, which are the main reason to generate inaccurate explanations.

CAM-based methods. For better visual performance than gradient-based backpropagation methods, CAM-based methods calculate and visualize the linearly weighted combination of the gradient of the target class and feature maps of the last convolutional layer to locate meaningful image regions to explain important decision features. In [34], the fully connected layer is replaced by a global average pooling layer to project the weight of the output for the target class to the weighted combination of the last convolution layer. And the class activation map is obtained to explain the region of the input image that the model mainly depends on when making classification decisions. Without modifying the architecture of the network, Grad-CAM [23] calculates the average gradients of feature maps in the last convolutional layer for the target class as the weight of feature maps to obtain gradient-weighted class activation maps. To obtain more exact explanation results, Grad-CAM++ [3] uses higher-order gradients instead of the average gradient in Grad-CAM as the weight of feature maps. But the gradient vanishing and saturation issue during the backpropagation may also result in a trustless explanation, sometimes image regions with higher weight values contribute less to the target class. To get rid of the gradient, Score-CAM [31] applies feature maps as a mask on the original image as the input image to obtain the forward passing score as the weight of each feature map on the target class instead of the gradients, finally computes the linear combination of the weights and feature maps. Furthermore, for less visual noise, Group-CAM [33], Augmented Score-CAM [11] and FIMF Score-CAM [15] performs meaningful perturbations on initial masks, which are then fed into the network to obtain new weights. However, these weights are obtained entirely based on retraining, which requires high computational costs, and the faithfulness of the explanation cannot be demonstrated due to the lack of theoretical analysis.

Surrogate-based methods. Surrogate-based methods attempt to explain the local or global decision-making basis of the initial network by using a simple interpretable model as a surrogate model. By perturbing the input samples and constructing a local linear model as a model-independent local explanation method LIME to show the image region that is highly sensitive for the target score. While LIME cannot accurately explain neural networks such as Recurrent Neural Networks (RNN), Guo, et al. [5] proposed a high-fidelity explanation method LEMNA suitable for security applications, and a simple regression model is trained to approximate the local decision boundaries of RNN. Then, by introducing the fused lasso regularization to deal with the feature-dependent problem in RNN, LEMNA effectively improves the approaches such as LIME in the fidelity of the explanation. Although LIME and LEMNA are simple to understand, random perturbation and feature selection methods lead to unstable explanations. Bramhall et al. [2] proposed the quadratic approximation framework QLIME redefine the linear representation by LIME as a quadratic relationship, extending the flexibility in non-linear cases and improving the accuracy of explanations. However, there is no theoretical analysis to guarantee the consistency of the explanation between the initial network and the surrogate model.

All these methods visualize the decision features of ResNets and help explain the mechanism of ResNets, but there is no theoretical analysis to guarantee the faithfulness of the explanation. In this paper, the advantages of gradient-based methods and CAM-based methods are integrated, on a trade-off between explanation faithfulness and intelligibility, an explainable Neural ODE, which is proved to be the convergent model of ResNets, is

built as a surrogate model to explain ResNets to improve the faithfulness of the explanation and reduce computational cost.

3. ResNets and Neural ODE

In this section, we first introduce the definitions of ResNets, and a neural ordinary differential equation network, namely Neural ODE, is obtained to be a convergent model of ResNets, i.e. ResNets is sufficiently close to the Neural ODE. Thus, the Neural ODE can be regarded as a surrogate model to explain ResNets predictions.

3.1. Definitions of ResNets

First, we generalize the mathematical definitions of ResNets $\mathcal{R}_N$. Suppose that an input $\boldsymbol{x} \in \mathbb{R}^d$ and its corresponding class label $\boldsymbol{y} \in \mathbb{R}^s$ are given for a ResNet. The input layer of ResNet is usually composed of $\mathcal{C}(\boldsymbol{x}) \triangleq \boldsymbol{X}_0$ which is obtained by the convolution operation $\mathcal{C} : \mathbb{R}^d \to \mathbb{R}^m$, and then it is composed of a series of residual blocks. One residual block is composed of the identity mapping part and the residual part, which can be described as

$$\boldsymbol{X}_{l+1} = \boldsymbol{X}_l + \lambda f\left(\boldsymbol{X}_l, \boldsymbol{\theta}_l^{(N)}\right), l = 0, 1, \ldots, N-1 \tag{1}$$

where $\boldsymbol{\theta}_l^{(N)}$ is the model parameters of the l-th residual block, N represents the number of residual blocks, $\lambda = T/N$, T is a given constant. $\boldsymbol{X}_l = \left(\boldsymbol{X}_l^{(i)}\right)_{m\times 1} \in \mathbb{R}^m$. And the residual part is generally composed of two convolution operations. To simplify the discussion, let

$$f\left(\boldsymbol{X}_l, \boldsymbol{\theta}_l^{(N)}\right) = \sigma\left(\boldsymbol{\omega}_l^{(N)}\boldsymbol{X}_l + \boldsymbol{b}_l^{(N)}\right), l = 0, 1, \ldots, N-1 \tag{2}$$

where $\sigma(\cdot)$ indicates the ReLU activation function, $\boldsymbol{\omega}_l^{(N)} \in \mathbb{R}^{m\times m}$ is the weight matrix and $\boldsymbol{b}_l^{(N)} \in \mathbb{R}^m$ is the bias.

Finally, let $\boldsymbol{\theta}^{(N)} = \left\{\boldsymbol{\theta}_l^{(N)}\right\}_{l=0}^{N-1}$, $\boldsymbol{X}_N$ is the output of the last residual block and it is operated by a fully connected layer and Softmax normalization operation ψ to obtain the classification prediction probability

$$\boldsymbol{y}_N = \boldsymbol{y}_N\left(\boldsymbol{\theta}^{(N)}\right) = \psi\left(\boldsymbol{\omega}\boldsymbol{X}_N + \boldsymbol{b}\right) \tag{3}$$

where $\boldsymbol{\omega} \in \mathbb{R}^{s\times m}$ is the weight matrix and $\boldsymbol{b} \in \mathbb{R}^s$ is the bias.

Consequently, if the input and label pairs $\left\{\boldsymbol{x}^i, \boldsymbol{y}^i\right\}_{i=1}^n$ of n samples are given, the learning process of ResNets $\mathcal{R}_N$ can be described as the following optimization problem

$$\begin{aligned} \min_{\theta^{(N)}} \quad & \varepsilon_N = \frac{1}{n}\sum_{i=1}^{n} L\left(\boldsymbol{y}^i, \boldsymbol{y}_N^i\left(\theta^{(N)}\right)\right) + R\left(\boldsymbol{\theta}^{(N)}\right) \\ \text{s.t. } & \boldsymbol{X}_{l+1}^i = \boldsymbol{X}_l^i + \lambda f\left(\boldsymbol{X}_l^i, \boldsymbol{\theta}_l^{(N)}\right) \\ & \boldsymbol{X}_0^i = C\left(\boldsymbol{x}^i\right) \\ & l = 0, 1, \ldots, N-1, i = 1, \ldots, n \end{aligned} \tag{4}$$

where $L\left(\boldsymbol{y}^i, \boldsymbol{y}_N^i\right)$ is the loss function between $\boldsymbol{y}^i$ and $\boldsymbol{y}_N^i$, R is the regularization term.

3.2. Relationship between ResNet and Neural ODE

As observed in [32,6,16], Eq. (1) is the Euler discretization of the ordinary differential equation

$$\frac{dX(t)}{dt} = f(X(t), \theta(t)), t \in [0, T] \tag{5}$$

when the initial condition $X(0) = \boldsymbol{X}_0$ is satisfied and the time step λ is selected.

Let $t_l = Tl/N$, the network obtained by replacing the residual blocks $\boldsymbol{X}_{l+1} = \boldsymbol{X}_l + \lambda f\left(\boldsymbol{X}_l, \boldsymbol{\theta}_l^{N)}\right)$ in the residual network $\mathcal{R}_N$ with the ordinary differential equation $\dot{X}(t) = f(X(t), \theta(t)), t \in [t_l, t_{l+1}]$ is called the neural ordinary differential equation network (Neural ODE) $\mathcal{D}$. Suppose that the output of the Neural ODE $\mathcal{D}$ is

$$\boldsymbol{y}_T = \boldsymbol{y}_T(\theta) = \psi(\boldsymbol{\omega} X(T) + \boldsymbol{b}) \tag{6}$$

Therefore, the learning process of the Neural ODE $\mathcal{D}$ can be described as the following optimization problem

$$\begin{aligned} \min_{\theta} \quad & \varepsilon = \frac{1}{n} \sum_{i=1}^{n} L\left(y^i, y_T^i(\theta)\right) + R(\theta) \\ \text{s.t. } & \dot{X}^i(t) = f\left(X^i(t), \theta(t)\right), t \in [0, T] \\ & X^i(0) = X_0^i, i = 1, \ldots, n \end{aligned} \tag{7}$$

Remark 1. As observed in [8,30], If the functions ψ and L are continuous, σ is Lipschitz continuous and $\sigma(0) = 0$, then for $N \to \infty$, the optimal solution of Eq. (4) converges to the optimal solution of Eq. (7). Moreover, assume that $f(t, X)$ be continuous, and $|f| \leq p$ satisfy the Lipschitz condition

$$|f(t, \boldsymbol{X}) - f(t, \boldsymbol{Y})| \leq k|\boldsymbol{X} - \boldsymbol{Y}| \tag{8}$$

on $D = \{(t, \boldsymbol{X}) | 0 \leq t \leq T, |\boldsymbol{X} - \boldsymbol{X}_0| \leq \eta\}$. Suppose that $f(t, \boldsymbol{X})$ is differentiable with respect to t and $\boldsymbol{X}$, and $|\partial f/\partial \boldsymbol{X}| \leq k, |\partial f/\partial t| \leq q$, If $T \leq \eta/p$, then it can be easily proved that when $N \to \infty, \boldsymbol{X}_N$ converges to the value at the solution $X(T)$ of Eq. (5) when $t = T$, and the error estimate is

$$|X(T) - \boldsymbol{X}_N| \leq \left(\frac{q}{k} + p\right) \frac{T}{N} \left(e^{kT} - 1\right) \tag{9}$$

In addition, the output $\boldsymbol{y}_N = \psi\left(\omega \boldsymbol{X}_N + b\right)$ of the residual network $\mathcal{R}_N$ and the output $y_T = \psi(\omega X(T) + b)$ of the Neural ODE $\mathcal{D}$ satisfy that

$$\|y_T - y_N\| = o\left(\frac{1}{N}\right) \tag{10}$$

Thus, we call that ResNet $\mathcal{R}_{\mathrm{N}}$ converges to the Neural ODE $\mathcal{D}$, that is, the Neural ODE $\mathcal{D}$ can be sufficiently approximated with ResNet $\mathcal{R}_{\mathrm{N}}$ when N is large enough. Therefore, in the following, the Neural ODE is applied to explain the decision attribution of the ResNet $\mathcal{R}_{\mathrm{N}}$.

4. Symplectic Adjoint Method

Since the Neural ODE can be regarded as a surrogate model to explain the influence of the input features for the ResNets' prediction, this section presents the symplectic adjoint method, which can be used to calculate the gradient that exactly characterizes the contribution of input features for the target class.

First, we discuss the influence of the perturbation for a given input on the prediction of Neural ODE. For the differential system Eq. (5), when the initial value $X(0) = \boldsymbol{X}_0$ is perturbed by τ to be $X'(0) = \boldsymbol{X}_0 + \tau$, the corresponding perturbed solution $X'(t)$ satisfies

$$X'(t) = X(t) + \delta(t) + o(\tau), \tau \to 0 \tag{11}$$

where $\delta(t)$ is the variational variable which solves the variational equation

$$\frac{d\delta(t)}{dt} = \frac{\partial f(X(t), \theta(t))}{\partial X(t)} \delta(t) \tag{12}$$

for $\delta(0) = I$.

Remark 2. As observed in [8], suppose that $f(X(t), \theta(t))$ is continuous and differentiable with respect to X, then there exists $\partial X(t)/\partial \boldsymbol{X}_0$ and $\partial X(t)/\partial \boldsymbol{X}_0 = \delta(t)$, where the variational variable $\delta(t)$ satisfies the variational equation Eq. (12).

According to Remark 2,, the gradient of $X(T)$ with respect to initial values $\boldsymbol{X}_0$ is $\partial X(T)/\partial \boldsymbol{X}_0 = \delta(T)$. Furthermore, we consider the adjoint equation of Eq. (12)

$$\frac{d\alpha(t)}{dt} = -\left(\frac{\partial f(X(t), \theta(t))}{\partial X(t)}\right)^T \alpha(t) \tag{13}$$

Where the adjoint variable $\alpha(t)$ is the gradient of $L(X(T))$ with respect to $X(t)$ and $\alpha(T) = \partial L(X(T))/\partial X(T)$, and the conservation property Eq. (14) for the solutions of variational equation Eq. (12) and adjoint equation Eq. (13) below holds

$$\alpha(T)^{\mathrm{T}} \delta(T) = \alpha(0)^{\mathrm{T}} \delta(0) \tag{14}$$

Aim at computing the gradients of $L(X(T))$ with respect to the initial condition $\boldsymbol{X}_0$ and the parameters $\boldsymbol{\theta}$ for the Neural ODE $\mathcal{D}$, [4] proposed the adjoint method to solve the gradient, but this approach cannot obtain the accurate gradient and requires high computational costs to suppress numerical errors, we present the symplectic adjoint Method, which solves the adjoint equation by the Symplectic Runge-Kutta method to obtain the exact gradient and the final trained network is denoted as the Neural ODE $\mathcal{D}_N$. The symplestic adjoint method consumes much less memory consumption, but performs faster computation and more robust to rounding errors than the naive backpropagation algorithm.

Firstly, the ordinary differential equation Eq. (5) is discretized by the Runge-Kutta method

$$\boldsymbol{X}'_{l+1} = \boldsymbol{X}'_l + \lambda \sum_{i=1}^{s} \boldsymbol{b}_i f_{l,i}, l = 0, 1, \ldots, N-1 \tag{15}$$

Where

$$f_{l,1} = f\left(t_l, \boldsymbol{X}'_l\right), f_{l,i} = f\left(t_l + c_i\lambda, \boldsymbol{X}'_l + \lambda\sum_{j=1}^{i-1} a_{i,j} f_{i,j}\right) \tag{16}$$

$i = 2, \ldots, s$, $a_{i,j}, b_i, c_i$ are summarized as the Butcher tableau [8,7,22], and there is $\left\|X(T) - \boldsymbol{X}'_N\right\| = o(1/N)$ for $N \to \infty$. Suppose that the output of the Neural ODE $\mathcal{D}_N$ is $\boldsymbol{y}'_N = \psi\left(\boldsymbol{\omega}\boldsymbol{X}'_N + \boldsymbol{b}\right)$.

Remark 3. ([7,1]) When the ordinary differential equation Eq. (5) is discretized by the Runge-Kutta method in Eq. (15), the variational equation Eq. (12) is discretized by the same Runge-Kutta method as follows

$$\boldsymbol{\delta}_{i+1} = \boldsymbol{\delta}_i + \lambda\sum_{i=1}^{s} b_i p_{l,i}, l = 0, 1, \ldots, N-1 \tag{17}$$

Where δ_i is the discretization of the variational variable $\delta(t)$ in Eq.(12) and

$$\begin{aligned} p_{l,1} &= \frac{\partial f}{\partial \boldsymbol{X}}\left(t_l, \boldsymbol{X}_l\right) \\ p_{l,i} &= \frac{\partial f}{\partial \boldsymbol{X}}\left(t_l + c_i\lambda_l, \delta_l + \lambda\sum_{j=1}^{i-1} a_{i,j} p_{i,j}\right), i = 2, \ldots, s \end{aligned} \tag{18}$$

Moreover, assume the adjoint variable $\boldsymbol{\alpha}_N = \partial L\left(\boldsymbol{X}'_N\right)/\partial \boldsymbol{X}'_N$, to obtain the exact backpropagation gradient for the Neural ODE $\mathcal{D}_N$ efficiently, the Symplectic Runge-Kutta method solves the adjoint equation by the Symplectic Runge-Kutta method as follows

$$\begin{aligned} \boldsymbol{\alpha}_{l+1} &= \boldsymbol{\alpha}_l + \lambda_l\sum_{i=1}^{s} \tilde{b}_i \phi_{l,i}, l = 0, 1, \ldots, N-1 \\ \phi_{l,i} &= -\left(\frac{\partial f}{\partial \boldsymbol{X}}\left(t_l + c_i\lambda, \boldsymbol{X}'_l + \lambda\sum_{j=1}^{i-1} a_{i,j} f_{l,j}\right)\right)^T \xi_{l,i} \\ \xi_{l,i} &= \begin{cases} \boldsymbol{\alpha}_l + \lambda\sum_{j=1}^{s} \tilde{b}_j\left(1 - \frac{a_{j,i}}{b_i}\right)\phi_{l,j}, & \text{if } i \notin \mathrm{I}_0 \\ -\sum_{j=1}^{s} \tilde{b}_j a_{j,i}\phi_{l,j}, & \text{if } i \in \mathrm{I}_0 \end{cases} \end{aligned} \tag{19}$$

where

$$\tilde{b}_i = \begin{cases} b_i, \text{ if } i \notin \mathrm{I}_0 \\ \lambda, \text{ if } i \in \mathrm{I}_0, \end{cases} \mathrm{I}_0 = \{i \mid i = 1, \ldots, s, b_i = 0\} \tag{20}$$

Finally, the gradient that exactly characterizes the contribution of input features for the output $\boldsymbol{\alpha}_0 = \partial L\left(\boldsymbol{X}'_N\right)/\partial \boldsymbol{X}_0$ can be obtained by the backpropagation iteration.

5. Explaining ResNet Predictions

In this section, we show that our proposed method guarantees the faithfulness of the explanation between ResNet and the surrogate model - Neural ODE. First, the decision feature

and the explanation map of an input to the target class for Neural ODE are generated via the symplectic adjoint method. Then, we prove that the explanations of Neural ODE can be sufficiently approximate to the true behavior of ResNet when N is large enough.

5.1. Understanding Neural ODE Predictions via symplectic adjoint method

Since it is well known that the deep convolution layer has high-level semantics, the previous CAM-based explanation methods focused on the analysis of the feature maps in the last convolution layer, while the feature maps in the shallow layer is noisy and lacks semantic intelligibility. However, in theory, to explain the importance of the input features for the output prediction score of the target class, the gradient of the target class should be back-propagated to the input layer to highlight the image region that has a great influence on the prediction. In this paper only positive influence on the prediction is considered, as observed in [14], the definition of the explanation map based on the gradient decomposition of the input layer is given as follows.

Definition 1. *Assume that any instance $\boldsymbol{x}$ and the trained Neural ODE $\mathcal{D}_N$ is given, the input layer of $\mathcal{D}_N$ is $\boldsymbol{X}_0$ and the output prediction vector is y, the i-th row vector $\partial y_i/\partial \boldsymbol{X}_0$ of $\partial y/\partial \boldsymbol{X}_0$ is called the decision feature about $\boldsymbol{X}_0$ that $\boldsymbol{x}$ belongs to class i. If the derivative of $\boldsymbol{y}$ with respect to the input $\partial y/\partial \boldsymbol{X}_0$ is obtained, then $\mathcal{D}_N$ is called explainable and the explanation map that x belongs to class i for $\mathcal{D}_N$ is*

$$\boldsymbol{I} = \mathrm{ReLU}\left(\frac{\partial y_i}{\partial \boldsymbol{X}_0}\right)^{\mathrm{T}} \circ \boldsymbol{X}_0 \tag{21}$$

where $\circ$ denotes Hadamard product.

Considering the problem of the gradient $\partial y_i/\partial \boldsymbol{X}_0$ computed by previous research, we first introduce a novel gradient solution method to ensure the accuracy of the explanation. The symplectic adjoint method for Neural ODE which consumes less memory than the naive backpropagation algorithm and has faster computational efficiency, is used to compute the gradient to explain the Neural ODE $\mathcal{D}_N$. By section 4, according to the symplectic adjoint Method, the initial $\boldsymbol{\alpha}_0 = \partial L\left(\boldsymbol{X}'_N\right)/\partial \boldsymbol{X}_0$ has been obtained by the iteration of the adjoint variable $\boldsymbol{\alpha}_N = \partial L\left(\boldsymbol{X}'_N\right)/\partial \boldsymbol{X}'_N$ into Eq. (19). On the other hand, as observed in [22], if α_0, δ_N are respectively the solutions for Eq. (19) and Eq. (17), then we have

$$\boldsymbol{\alpha}_{\mathrm{N}}{}^{\mathrm{T}}\boldsymbol{\delta}_{\mathrm{N}} = \boldsymbol{\alpha}_0{}^{\mathrm{T}}\boldsymbol{\delta}_0 \tag{22}$$

where $\delta(0) = \boldsymbol{I}$. Therefore, it is not necessary to spend much more time on iterative calculations in Eq. (12), the variational variable $\delta_N = \partial \boldsymbol{X}'_N/\partial \boldsymbol{X}_0$ can be solved from the Eq. (22) and

$$\frac{\partial \boldsymbol{y}'_N}{\partial \boldsymbol{X}_0} = \frac{\partial \boldsymbol{y}'_N}{\partial \boldsymbol{X}'_N}\boldsymbol{\delta}_N = \psi'\boldsymbol{\omega}\boldsymbol{\delta}_N \tag{23}$$

Thus the i - th row vector $\left(\psi'\boldsymbol{\omega}\boldsymbol{\delta}_N\right)_i$ of $\psi'\boldsymbol{\omega}\boldsymbol{\delta}_N$ is called the decision feature about $\boldsymbol{X}_0$ that $\boldsymbol{x}$ belongs to class i for Neural ODE $\mathcal{D}_N$.

Therefore, by Definition 1, we have that the Neural ODE $\mathcal{D}_N$ is explainable, and the explanation map that $\boldsymbol{x}$ belongs to class i for $\mathcal{D}_N$ is

$$\boldsymbol{I} = \mathrm{ReLU}\left(\left(\psi'\boldsymbol{\omega}\boldsymbol{\delta}_N\right)_i\right)^{\mathrm{T}} \circ \boldsymbol{X}_0 \tag{24}$$

where $\circ$ denotes Hadamard product. Since we are only interested in features that have a positive impact on the target class and are good for visualization, the function is to filter the negative impact. The explanation map I is can explain the image region where the Neural ODE $\mathcal{D}_N$ is for image recognition has a high influence on the prediction result of the input image belonging to class i.

5.2. Relationship between explanations of ResNet and Neural ODE

To show the consistency of the explanation between ResNet and the Neural ODE, the metrics of the approximation of the two models is first introduced as follows [13].

Definition 2. *For a neural network $\mathcal{D}_n$, if there is a neural network $\mathcal{D}'_n$ which is explainable and the explanation map that $\boldsymbol{x}$ belongs to class i for $\mathcal{D}'_n$ is $\boldsymbol{I}$, and for $\forall \varepsilon > 0, \exists K \in \mathbb{N}^+$, when $n > K$, there is*

$$\kappa\left(\mathcal{D}_n, \mathcal{D}'_n\right) = \|\boldsymbol{y} - \boldsymbol{y}'\| < \varepsilon \tag{25}$$

for any instance $\boldsymbol{x}$, where $\boldsymbol{y}$ and $\boldsymbol{y}'$ are the prediction vectors obtained by the model $\mathcal{D}_n$ and $\mathcal{D}'_n$ for the input $\boldsymbol{x}$ respectively, then we define $\mathcal{D}'_n$ as an approximate interpretable model of $\mathcal{D}_n$ when n is large enough.

According to Definition 2, it is obvious that when $\kappa\left(\mathcal{D}_n, \mathcal{D}'_n\right)$ is smaller, the model approximation degree of the two models is higher and $\mathcal{D}'_n$ is considered to be a better explainable model of $\mathcal{D}_n$. In the following, we demonstrate that the Neural ODE $\mathcal{D}_N$ is the approximate explainable model of RessNet $\mathcal{R}_N$.

Theorem 1. *For the ResNet $\mathcal{R}_N$ and the corresponding Neural ODE $\mathcal{D}_N$, If the functions L and ψ are continuous, the function σ is Lipschitz continuous and $\sigma(0) = 0$, $f(X(t), \theta(t))$ is continuous and differentiable with respect to $\boldsymbol{X}$, then for $\forall \varepsilon > 0, \exists K \in \mathbb{N}^+$, when $N > K$, there is $\kappa\left(\mathcal{D}_N, \mathcal{R}_N\right) < \varepsilon$ for any $\boldsymbol{x}$.*

Proof. For any input $\boldsymbol{x}$, it is known that Eq. (1) in ResNet $\mathcal{R}_N$ is the Euler discretization of the ordinary differential equation Eq. (5) when the initial condition $X(0) = X_0$ is satisfied and the time step λ is selected. By Remark 1, if the functions ψ and L are continuous, σ is Lipschitz continuous and $\sigma(0) = 0$, then the numerical solution obtained from Eq. (1) converges to the exact solution of Eq. (5). So X_N converges to the solution $X(T)$ of Eq. (5) when $t = T$, that is, $\lim_{N\to\infty}\left(\boldsymbol{X}_N - X(T)\right) = 0$, then for $\forall \varepsilon' > 0, \exists M_1 \in \mathbb{N}^+$, when $N > M_1$, there is $\|\boldsymbol{X}_N - X(T)\| < \varepsilon'$.

Moreover, let

$$\boldsymbol{\omega}\boldsymbol{X}_N + \boldsymbol{b} = \left[x_N^{(1)}, x_N^{(2)}, \ldots, x_N^{(s)}\right] \in \mathbb{R}^s \tag{26}$$

$$\boldsymbol{\omega}\boldsymbol{X}(T) + \boldsymbol{b} = \left[x^{(1)}, x^{(2)}, \ldots, x^{(s)}\right] \in \mathbb{R}^s \tag{27}$$

then when $N > M_1$, there is $\left|x_N^{(i)} - x^{(i)}\right| < \boldsymbol{\omega}\varepsilon'$. Moreover, the output prediction vectors obtained by ResNet $\mathcal{R}_N$ and Neural ODE $\mathcal{D}$ are

$$y_N = \psi\left(\boldsymbol{\omega}\boldsymbol{X}_N + \boldsymbol{b}\right), y_T = \psi(\boldsymbol{\omega}X(T) + \boldsymbol{b}) \tag{28}$$

Let $\boldsymbol{y}_N = \left[y_N^{(1)}, y_N^{(2)}, \ldots, y_N^{(s)}\right], \boldsymbol{y}_T = \left[y_T^{(1)}, y_T^{(2)}, \ldots, y_T^{(s)}\right] \in \mathbb{R}^s$, then there exists $c_i \in \mathbb{R}$

$$\begin{aligned} \left|y_N^{(i)} - y_T^{(i)}\right| &= \left| \frac{e^{x_N^{(i)}}}{\sum_{j=1}^{s} e^{x_N^{(j)}}} - \frac{e^{x^{(i)}}}{\sum_{j=1}^{s} e^{x^{(j)}}} \right| \\ &\leq \left| e^{x_N^{(i)}} - e^{x^{(i)}} \right| \\ &\leq \omega c_i \varepsilon' \end{aligned} \tag{29}$$

Let $\varepsilon = 2\omega \sum_{i-1}^{s} c_i \varepsilon'$, so we have

$$\kappa\left(\mathcal{R}_N, \mathcal{D}\right) = \|\boldsymbol{y}_N - \boldsymbol{y}_T\| < \omega \sum_{i=1}^{s} c_i \varepsilon' = \varepsilon/2 \tag{30}$$

Therefore, $\forall \varepsilon > 0, \exists M_1 \in \mathbb{N}^+$, when $N > M_1$, there is $\kappa\left(\mathcal{R}_{\mathrm{N}}, \mathcal{D}\right) < \varepsilon/2$ for any $\boldsymbol{x}$.

Similarly, $\forall \varepsilon > 0, \exists M_2 \in \mathbb{N}^+$, when $N > M_2$, there is $\kappa\left(\mathcal{D}, \mathcal{D}_N\right) < \varepsilon$ for any $\boldsymbol{x}$, assume that the output prediction vector obtained by the Neural ODE $\mathcal{D}_N$ is

$$\boldsymbol{y}'_N = \psi\left(\boldsymbol{\omega} \boldsymbol{X}'_N + \boldsymbol{b}\right) = \left[y_N^{(1)}, y_N^{(2)}, \ldots, y_N^{(s)}\right] \in \mathbb{R}^s \tag{31}$$

then let $K = \max\left\{M_1, M_2\right\} \in \mathbb{N}^+$, when $N > K$, we have

$$\kappa\left(\mathcal{R}_{\mathrm{N}}, \mathcal{D}_N\right) \leq \kappa\left(\mathcal{R}_{\mathrm{N}}, \mathcal{D}\right) + \kappa\left(\mathcal{D}, \mathcal{D}_N\right) < \varepsilon \tag{32}$$

Overall, the Neural ODE $\mathcal{D}_N$ is proved to be an explainable model sufficiently close to ResNet $\mathcal{R}_N$ when N is large enough, and the explanation map $\boldsymbol{I} = \mathrm{ReLU}\left(\left(\psi' \omega \delta_N\right)_i\right)^{\mathrm{T}} \circ \boldsymbol{X}_0$ can explain the image region where the ResNet $\mathcal{R}_N$ for image recognition has high influence on the prediction result of the input image belonging to class i. Theorem 1 ensures the faithfulness of the explanation between ResNet and the surrogate model, and since the symplectic adjoint method instead of the naive backpropagation algorithm is used, the proposed explanation method has lower computational cost than other explanation approaches.

6. Experimental Implementation and Evaluation

In this section, we evaluate the effectiveness of the explanation method for ResNet in this paper. First, we visualize the saliency maps obtained by the CAM-based explanation of ResNet with the gradient via the symplectic adjoint method to compare other CAM-based methods with the gradient obtained by the naive backpropagation algorithm. Second, we demonstrate the faithfulness of the proposed explanation method for ResNet by conducting deletion and insertion tests to compare with the ones in Grad-CAM and Group-CAM. Moreover, we present the proposed explanation method, which is more efficient than others and effective for users to find out the reason for the wrong decision on some samples in the prediction. Finally, by modifying the training set and retraining, the effectiveness of the explanation for debugging and optimizing a model can be validated.

In the following experiments, the model architecture we performed is a pre-trained ResNet with six standard residual blocks [4] and the publicly available classification

dataset Cifar10 is used. For the input images, all images are resized to $3 \times 32 \times 32$, and then transformed to tensors and normalized to the range [0, 1]. The performance of the proposed explanation method via the symplectic adjoint method and existing methods is evaluated by PyTorch 1.7.0 [20] and demonstrated by extending the adjoint method implemented in the package torchdiffeq 0.8.1 [34].

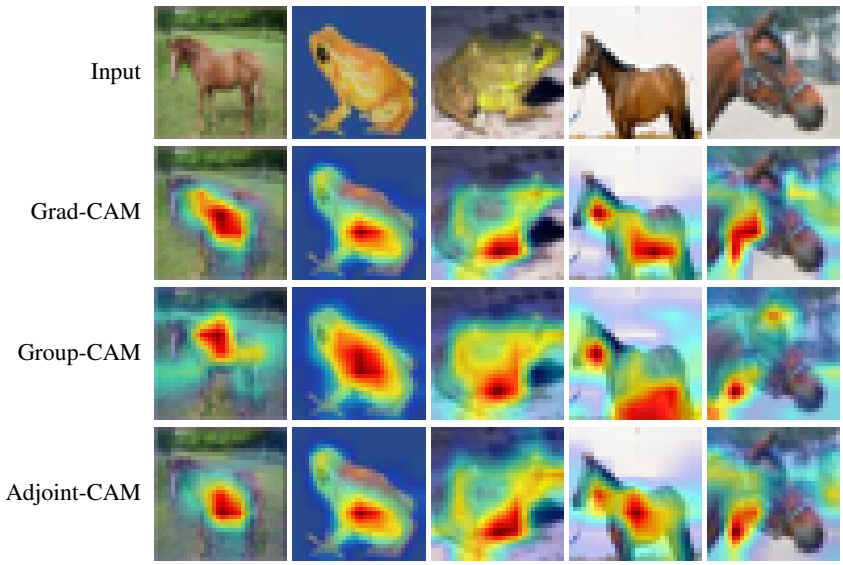

Fig. 2. Visualization results of Grad-CAM, Group-CAM, and Adjoint-CAM. The class activation maps are similar for the various explanation methods in the last convolutional layer, especially for Grad-CAM and Adjoint-CAM

6.1. CAM-based explanation of ResNet via symplectic adjoint method and naive backpropagation Algorithm

Since the CAM-based explanation methods have a good performance on class discriminative visualization and localization ability, they have been widely applied to visualize the task of locating objects in images. For instance, Grad-CAM calculates the average of the naive gradients of feature maps in the last convolutional layer for the target class as the weight of feature maps to obtain gradient-weighted class activation maps to highlight important features. In this section, the method that generates the weighted class activation maps by computing the average of gradients of feature maps in the last convolutional layer for the target class via the symplectic adjoint method as the weight of feature maps is called Adjoint-CAM, and the weighted class activation maps obtained by Adjoint-CAM can be demonstrated to be similar to those generated by Grad-CAM which computes the average of gradients via the naive backpropagation algorithm. Therefore, the proposed method also has a good performance on the visualization of class-conditional localization of objects in the last convolutional layer for the target class.

As shown in Remark 1, the output of the last residual block of ResNet is approximate to the output of the corresponding Neural ODE at $t = T$,which means the feature maps of ResNet and Neural ODE in the last convolutional layer are similar. On the other hand, the output of ResNet and Neural ODE is Eq. (3) and Eq. (6) respectively, then it is obvious that the gradients of feature maps in the last convolutional layer for the target class via the symplectic adjoint method for Neural ODE are the same as the gradients via the naive backpropagation algorithm for ResNet. Therefore, the weighted class activation maps obtained by Adjoint-CAM which computes the weight via the symplectic adjoint method approximate with that generated by Grad-CAM to locate the important region of given images. We visualize the depth-wise saliency maps through Grad-CAM, Group-CAM, and Adjoint-CAM in Fig. 2. As shown in Fig. 2, the class activation maps are similar for the various methods and localize the target object well in the last convolutional layer.

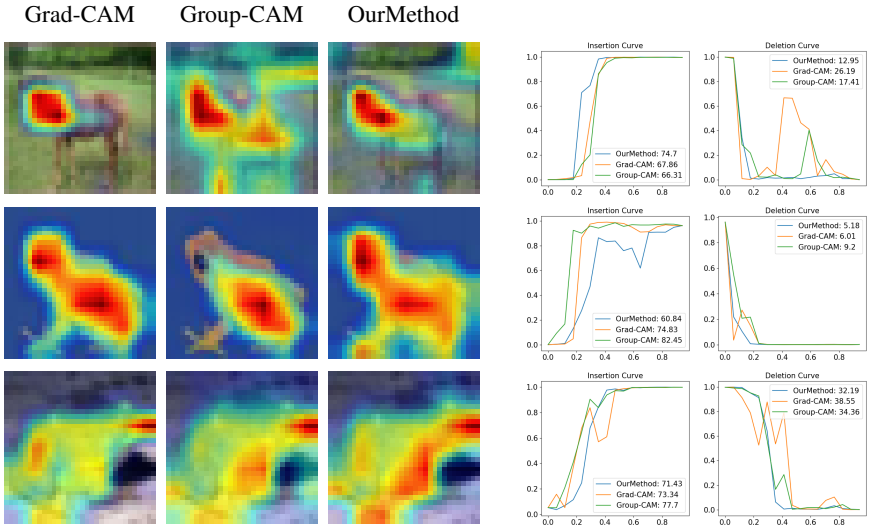

Fig. 3. The explanation maps generated by Grad-CAM, Group-CAM, and OurMethod for representative images with deletion and insertion curves. In the insertion curve, a more faithful explanation should increase faster, the area under the curve is expected to be large. While in the deletion curve, a more faithful explanation should drop faster, the area under the curve is expected to be small

6.2. Evaluating Faithfulness of Explanations

Although the CAM-based explanation methods outperform other methods on visualization performance in the last convolutional layer, the gradient obtained by the naive backpropagation algorithm in the shallow layer may result in an inaccurate explanation for the gradient vanishing and saturation issue. Sometimes, image regions with higher weight values contribute less to the target class. Therefore, we propose a novel explanation method in which the shallow gradient is obtained exactly by the symplectic adjoint method. To

demonstrate the faithfulness of the explanation of our proposed method in this paper is higher than that of other methods, the deletion and insertion metrics that are prepared in [21] are used to qualitatively evaluate the faithfulness of the interpretation methods.

Intuitively, if the pixels obtained from the explanation methods are more important for decisions, the removal of pixels will cause the predicted score for the target class to drop more significantly, which shows that the explanation method is more faithful. Therefore, the deletion metric is a qualitative evaluation metric to measure the decrease in the probability of the predicted class when more and more important pixels obtained by the explanation methods are removed from the original image. A lower area under the probability curve indicates a more faithful explanation. In addition, the insertion metric, which starts with a blurred image, evaluates the increase in the probability of the predicted score for the target class as more and more pixels are introduced, and a higher area under the probability curve means a more faithful explanation.

In detail, for the deletion test, there are several approaches to removing pixels from an image and all of these have different pros and cons. In our experiment, the deletion test gradually replaces 1% of pixels from the original image with a highly blurred one according to the importance of pixels for decisions obtained by the explanation methods until no pixels are left. On the other hand, for the insertion test, we gradually replace 1% pixels of the blurred image with the original version according to the importance of pixels until the image is well recovered. Some examples generated by Grad-CAM, Group-CAM, and our proposed method for the first layer of the ResNet block and the corresponding deletion and insertion curves are illustrated in Fig. 3. Furthermore, for a more general comparison, the average results calculated by area under the probability curve of deletion and insertion tests over 1000 images are demonstrated in Table 1. As shown in Table 1, our proposed method outperforms other CAM methods in terms of deletion AUC compared with gradient-based CAM methods.

Table 1. Comparative evaluation in terms of insertion (higher is better) and deletion (lower is better) scores

	Grad-CAM	Group-CAM	OurMethod
Insertion	0.614	**0.623**	0.616
Deletion	0.161	0.152	**0.132**

6.3. Comparative Evaluation in Terms of Memory and Computation Efficiency

In the experiment, the Neural ODE obtained by replacing residual blocks of ResNet with ODESolve modules is the surrogate explainable model of ResNet and the explanation map is generated by the gradient calculated by the symplectic adjoint method. Table 2 summarizes the test error and number of parameters for ResNet and the Neural ODE on Cifar10, respectively. As shown in Table 2, the Neural ODE has around the same performance as the ResNet with fewer parameters.

Furthermore, the memory consumption and running time for the explanation by Grad-CAM, Grad-CAM++, Group-CAM and the proposed method are shown in Table 3. L

Table 2. Comparative evaluation in terms of the test accuracy and number of parameters for ResNet and neural ode on Cifar10.

	Test Accuracy	Parameters
ResNet	83.89	0.58M
Neural ODE	83.57	0.21M

is the number of layers in the ResNet, and all the feature maps and neuron importance weights are splited into G groups. Grad-CAM and Grad-CAM++ which generate the shallow layer gradients via the naive backpropagation algorithm for the ResNet requires a memory of $O(L)$ for the backpropagation, and compute gradients by the chain rule step by step with roughly computational cost $O(L)$. Group-CAM needs to input the constructed mask back into the network for training to obtain new weights for G rounds, so the computational cost is $O(GL)$. While the symplectic adjoint method has superior performance than the naive backpropagation in terms of the memory consumption and running time. Our proposed method had no more need of storing any intermediate quantities of the backpropagation, only the first and last adjoint variable is required to obtain the explanation map, and then the memory consumption and running time are both $O(1)$. Therefore, as shown in Table 3, the proposed explanation approach outperforms Grad-CAM, Grad-CAM++ and Group-CAM in terms of the memory consumption and computational cost.

Table 3. Comparative evaluation in terms of the memory consumption and running time for Grad-CAM, Grad-CAM++, Group-CAM and our proposed method on cifar10.

	Grad-CAM	Grad-CAM++	Group-CAM	OurMethod
Memory	$O(L)$	$O(L)$	$O(L)$	$O(1)$
Running Time	$O(L)$	$O(L)$	$O(GL)$	$O(1)$

6.4. Effectiveness for Troubleshooting and Optimizing a Model by the Explanation

When we know how the deep learning model thinks, it provides us with the privilege to optimize it. This section illustrates that our proposed approach can explain why ResNet makes a wrong prediction, and then improve the performance of the model pertinently. Intuitively, if the pixels obtained from the explanation methods are more important for prediction, the modification of pixels will cause the probability of the predicted class to decrease more significantly. As shown in Fig.3, the deletion of less than 10% pixels from the original image can generate adversarial images to producing incorrect classification results. Furthermore, Fig.4 shows the explanation maps for two misclassified images with respect to their top-3 predicted classes by the proposed method. As shown in Fig. 4, the first image labeled “horse” is classified as an airplane, the second one labeled “horse” is classified as a frog, and the second column are the explanation maps generated by our method to show the image region has a high influence on the prediction results for the

top-1 predicted classes of airplane and frog. It can be seen that ResNet makes a wrong prediction for the two images, mostly in terms of the background of the images. It seems reasonable that the sky is white and the frog is green in the training dataset, but the reason why the model makes a wrong prediction is that it ignores the shape of images.

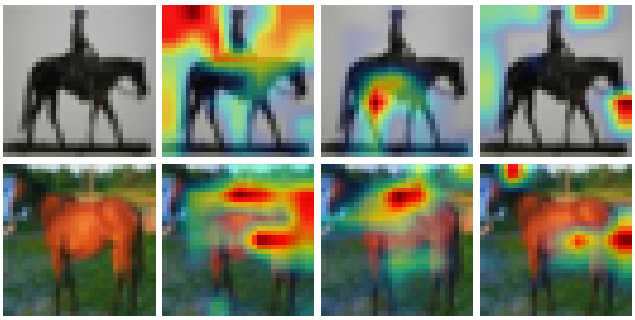

Fig. 4. The explanation maps with respect to top3 predicted class for mis-classified images. The first column is the input images. The prediction score for the first input image with respect to top3 predicted class is 0.6373 (airplane), 0.1715 (horse), 0.1623 (bird), the second is 0.6770 (frog), 0.1336 (automobile), 0.1306 (horse)

Table 4. Comparative evaluation in terms of the test accuracy before and after debugging

	No debugging	After debugging
Test Accuracy	83.89%	87.29%

Therefore, by diagnosing the reason why the model makes a wrong prediction, these mistakes can be avoided with sufficient training. Specifically, for a given misclassified sample, first we identify the corresponding regions in the model that were undertrained. Then some targeted training samples are generated by replacing the values of important pixels with random values to augment the original training data and retrain the model. Due to the addition of new samples, the impact of misleading features is reduced, and target errors are patched without reducing the previous accuracy of the model. We consider the proposed explanation method is practical for optimizing a model by modifying the training set and retraining. After adding 3000 artificially constructed images by the interpretation method to the original training set, ResNet is retrained by the reconstructed training set. As shown in Table 4, the test accuracy of the pre-trained model is 83.89% and the test accuracy of the model is improved to 87.29% after the training of the new training set. Moreover, after retraining, the image labeled ”horse” in Fig.4 can be correctly identified, and the corresponding predicted probabilities are increased to 0.6312 and 0.7065, respectively. Overall, the explanation map obtained by our method is helpful for overall diagnosing and debugging of the model.

7. Conclusion and Future Work

Using the Neural ODE as the surrogate model, we proposed a new way for a more faithful explanation of ResNets predictions. To get over the naive gradient problem and make sure that images regions with higher gradient values contribute more to the target class, the gradients with respect to the input layer are calculated using the symplectic adjoint method. Additionally, the gradient decomposition method yields an explanation map for the Neural ODE at the input layer that can be shown to be sufficiently near to the explanation of ResNets. Quantitative analyses are provided to demonstrate that our method outperforms than other cutting-edge methods in terms of effectiveness and explanation faithfulness, and it is effective for troubleshooting and debugging a model by the explanation. In the future work, we will analyze the stability and generalization ability of ResNet with symplectic adjoint method.

References

1. Bochev, P.B., Scovel, C.: On quadratic invariants and symplectic structure. BIT-Computer Science Numerical Mathematics 34(3), 337–345 (1994)
2. Bramhall, S., Horn, H., Tieu, M., Lohia, N.: Qlime-a quadratic local interpretable model-agnostic explanation approach. SMU Data Science Review 3(1), 4 (2020)
3. Chattopadhay, A., Sarkar, A., Howlader, P., Balasubramanian, V.N.: Grad-cam++: Generalized gradient-based visual explanations for deep convolutional networks. In: 2018 IEEE winter conference on applications of computer vision (WACV). pp. 839–847. IEEE (2018)
4. Chen, R.T., Rubanova, Y., Bettencourt, J., Duvenaud, D.K.: Neural ordinary differential equations. Advances in neural information processing systems 31 (2018)
5. Guo, W., Mu, D., Xu, J., Su, P., Wang, G., Xing, X.: Lemna: Explaining deep learning based security applications. In: proceedings of the 2018 ACM SIGSAC conference on computer and communications security. pp. 364–379 (2018)
6. Haber, E., Ruthotto, L.: Stable architectures for deep neural networks. Inverse problems 34(1), 014004 (2017)
7. Hairer, E., Lubich, C., Wanner, G.: Solving geometric numerical integration: Structure-preserving algorithms (2006)
8. Hairer, E., Nørsett, S.P., Wanner, G.: Solving ordinary differential equations. 1, Nonstiff problems. Springer-Vlg (1993)
9. He, K., Zhang, X., Ren, S., Sun, J.: Deep residual learning for image recognition. In: Proceedings of the IEEE conference on computer vision and pattern recognition. pp. 770–778 (2016)
10. Hengstler, M., Enkel, E., Duelli, S.: Applied artificial intelligence and trust—the case of autonomous vehicles and medical assistance devices. Technological Forecasting and Social Change 105, 105–120 (2016)
11. Ibrahim, R., Shafiq, M.O.: Augmented score-cam: High resolution visual interpretations for deep neural networks. Knowledge-Based Systems 252, 109287 (2022)
12. Kleppe, A., Skrede, O.J., De Raedt, S., Liestøl, K., Kerr, D.J., Danielsen, H.E.: Designing deep learning studies in cancer diagnostics. Nature Reviews Cancer 21(3), 199–211 (2021)
13. Lei, X., Fan, Y., Li, K.C., Castiglione, A., Hu, Q.: High-precision linearized interpretation for fully connected neural network. Applied Soft Computing 109, 107572 (2021)
14. Lei, X., Fan, Y., Luo, X.L.: On fine-grained visual explanation in convolutional neural networks. Digital Communications and Networks (2022)
15. Li, J., Zhang, D., Meng, B., Li, Y., Luo, L.: Fimf score-cam: Fast score-cam based on local multi-feature integration for visual interpretation of cnns. IET Image Processing 17(3), 761–772 (2023)

16. Ma, C., Wu, L., et al.: Machine learning from a continuous viewpoint, i. Science China Mathematics 63(11), 2233–2266 (2020)
17. Matsubara, T., Miyatake, Y., Yaguchi, T.: Symplectic adjoint method for exact gradient of neural ode with minimal memory. Advances in Neural Information Processing Systems 34, 20772–20784 (2021)
18. Muhammad, K., Ullah, A., Lloret, J., Del Ser, J., de Albuquerque, V.H.C.: Deep learning for safe autonomous driving: Current challenges and future directions. IEEE Transactions on Intelligent Transportation Systems 22(7), 4316–4336 (2020)
19. Nguyen, A., Yosinski, J., Clune, J.: Deep neural networks are easily fooled: High confidence predictions for unrecognizable images. In: Proceedings of the IEEE conference on computer vision and pattern recognition. pp. 427–436 (2015)
20. Paszke, A., Gross, S., Chintala, S., Chanan, G., Yang, E., DeVito, Z., Lin, Z., Desmaison, A., Antiga, L., Lerer, A.: Automatic differentiation in pytorch (2017)
21. Petsiuk, V., Das, A., Saenko, K.: Rise: Randomized input sampling for explanation of black-box models. arXiv preprint arXiv:1806.07421 (2018)
22. Sanz-Serna, J.M.: Symplectic runge–kutta schemes for adjoint equations, automatic differentiation, optimal control, and more. SIAM review 58(1), 3–33 (2016)
23. Selvaraju, R.R., Cogswell, M., Das, A., Vedantam, R., Parikh, D., Batra, D.: Grad-cam: Visual explanations from deep networks via gradient-based localization. In: Proceedings of the IEEE international conference on computer vision. pp. 618–626 (2017)
24. Simonyan, K., Vedaldi, A., Zisserman, A.: Deep inside convolutional networks: Visualising image classification models and saliency maps. arXiv preprint arXiv:1312.6034 (2013)
25. Slack, D., Hilgard, S., Jia, E., Singh, S., Lakkaraju, H.: Fooling lime and shap: Adversarial attacks on post hoc explanation methods. In: Proceedings of the AAAI/ACM Conference on AI, Ethics, and Society. pp. 180–186 (2020)
26. Smilkov, D., Thorat, N., Kim, B., Viégas, F., Wattenberg, M.: Smoothgrad: removing noise by adding noise. arXiv preprint arXiv:1706.03825 (2017)
27. Springenberg, J.T., Dosovitskiy, A., Brox, T., Riedmiller, M.: Striving for simplicity: The all convolutional net. arXiv preprint arXiv:1412.6806 (2014)
28. Su, J., Vargas, D.V., Sakurai, K.: One pixel attack for fooling deep neural networks. IEEE Transactions on Evolutionary Computation 23(5), 828–841 (2019)
29. Sundararajan, M., Taly, A., Yan, Q.: Gradients of counterfactuals. arXiv preprint arXiv:1611.02639 (2016)
30. Thorpe, M., van Gennip, Y.: Deep limits of residual neural networks. Research in the Mathematical Sciences 10(1), 6 (2023)
31. Wang, H., Wang, Z., Du, M., Yang, F., Zhang, Z., Ding, S., Mardziel, P., Hu, X.: Score-cam: Score-weighted visual explanations for convolutional neural networks. In: Proceedings of the IEEE/CVF conference on computer vision and pattern recognition workshops. pp. 24–25 (2020)
32. Weinan, E.: A proposal on machine learning via dynamical systems. Communications in Mathematics and Statistics 1(5), 1–11 (2017)
33. Zhang, Q., Rao, L., Yang, Y.: Group-cam: Group score-weighted visual explanations for deep convolutional networks. arXiv preprint arXiv:2103.13859 (2021)
34. Zhou, B., Khosla, A., Lapedriza, A., Oliva, A., Torralba, A.: Learning deep features for discriminative localization. In: Proceedings of the IEEE conference on computer vision and pattern recognition. pp. 2921–2929 (2016)

Xia Lei received the B.S. degree in Mathematics and Applied Mathematics from Jimei University, China, in 2012; the M.S. degree in Basic Mathematics from Fuzhou University, China, in 2015, the Ph.D. degree of Computer Science and Technology in China

University of Petroleum (Beijing), in 2023. Her current research interests include theories of explainable AI.

Jia-Jiang Lin received Bachelor and Ph.D. degrees in automation from China University of Petroleum (Beijing), in 2014 and 2020, respectively. At present, he is an assistant professor at China University of Petroleum (Beijing). His main research direction is the theoretical solution and numerical solution of the hybrid system optimal control problem in the chemical process and machine learning.

Xiong-Lin Luo (Corresponding author: luoxl@cup.edu.cn) received the Ph.D. degree in China University of Petroleum (Beijing) in 1997. He is a professor at China University of Petroleum (Beijing). Main research directions: control theory and process control, chemical system engineering and machine learning.

Yongkai Fan received Bachelor, Master, and Ph.D. degrees from Jilin University, China, in 2001, 2003, and 2006, respectively. From 2006 to 2009, he was an assistant researcher at Tsinghua University, China. Currently, he is an associate professor at the Communication University of China, He was a visiting scholar in the Department of Computer science and Engineering at Lehigh University in the USA (2015) and a visiting scholar in the Department of Computer Science and Engineering at Penn State University in the USA (2016). He has published more than 50 journal/conference papers in journals and his research interests include theories of data security and software security.

Received: March 10, 2023; Accepted: June 25, 2023.

Computer Science and Information Systems 20(4):1439–1457 https://doi.org/10.2298/CSIS230315048T

A Framework for Fake News Detection Based on the Wisdom of Crowds and the Ensemble Learning Model

Hai Bang Truong[1,2] and Van Cuong Tran[3,⋆]

[1] Faculty of Computer Science, University of Technology
[2] National University
700000 Ho Chi Minh City, Vietnam
bangth@uit.edu.vn
[3] Faculty of Engineering and Information Technology, Quang Binh University
47100 Quang Binh, Vietnam
vancuongqbuni@gmail.com

Abstract. Nowadays, the rapid development of social networks has led to the proliferation of social news. However, the spreading of fake news is a critical issue. Fake news is news written to intentionally misinform or deceive readers. News on social networks is short and lacks context. This makes it difficult for detecting fake news based on shared content. In this paper, we propose an ensemble classification model to detect fake news based on exploiting the wisdom of crowds. The social interactions and the user's credibility are mined to automatically detect fake news on Twitter without considering news content. The proposed method extracts the features from a Twitter dataset and then a voting ensemble classifier comprising three classifiers namely, Support Vector Machine (SVM), Naive Bayes, and Softmax is used to classify news into two categories which are fake and real news. The experiments on real datasets achieved the highest F1 score of 78.8% which was better than the baseline by 6.8%. The proposed method significantly improved the accuracy of fake news detection in comparison to other methods.

Keywords: Fake news detection, Social interaction, User's credibility, User's opinion

1. Introduction

Nowadays, social network services have developed rapidly and become a popular information channel for the community. Social networks have an important role in spreading news and people can rate the news easily. In 2021, about half of U.S. adults often or sometimes got news from social media[4]. Social network services have attracted a lot of people who publish and share news and personal opinions every day. Social networks with multiple useful characteristics, like faster transformation and less expensive, have become an important channel of communication and information sharing. However, due to the increasing popularity of social networks and the ease of posting news on those platforms, it becomes an ideal way of communicating and spreading fake news. Fake news has negative effects on society. It could cause political instability [5][14]. In recent years,

⋆ Corresponding author
[4] https://www.pewresearch.org/journalism/2021/09/20/news-consumption-across-social-media-in-2021/

social media and technology companies face criticism for not doing enough to stem the flow of fake news on social network platforms.

Fact-checking is a process that seeks related information to verify factual information and to promote the veracity and correctness of news. In reality, fact-checking action can be conducted before or after the news is posted. Internal fact-checking is such checking done in-house by the publisher or system and the news is analyzed by a third party called external fact-checking. Preventing the spread of misinformation can be done through human intervention by verifying the authenticity of the content. Using the international fact-checking network and manual fact-checking websites such as washingtonpost.com, snopes.com, Politifact.com, etc. are the methods commonly used in practice [10]. The assessment of experts on fact-checking websites can bring forward the reader's realistic viewpoints about related information. Figure 1. is a flowchart of a fact-checking system for the news on social media. Fact-checking websites is an efficient way to verify the authenticity of the information, especially news on social media. However, handling large volumes of data is a great obstacle. It is very difficult for humans to evaluate all up-to-date information on social media. Automatic fact-checking is a promising method to overcome this problem.

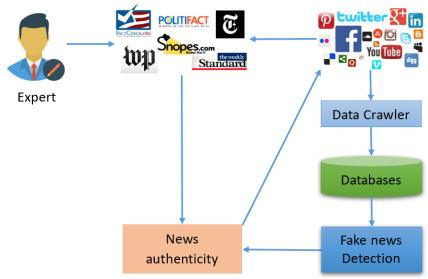

Fig. 1. The flowchart of a fact-checking system

Fake news detection topics have got a lot of attention from researchers. There are different fake news detection approaches have been proposed in the literature. The most common approach is news content analysis [2], [18], [20], [25]. The language features are analyzed to determine the authenticity of the news. Generally, news content analysis is suitable for formal and long news. However, social news is quite different from formal and long news. The short and abbreviation characteristics are the big challenges for the algorithms applying to formal news. Therefore, the approaches combining the content and news context for fake news detection have gotten a lot of attention from researchers [26], [27]. Using the user's profile and news content features to analyze the behavior of the user is an approach receiving much attention currently [21]. Machine learning approaches have been applied quite effectively for detecting fake news [5]. SVM, Random forest, and logistic regression models have been used and achieved high accuracy in the fake news detection experiments [6], [12], [16], [19]. Ensemble methods aim at improving the accuracy of individual models by combining multiple models. Generally, the combined models can increase performance significantly [10]. Social networking service is an online social media platform in which people can share personal viewpoints. The tremendous growth of

social networks has attracted research communities to discover collective intelligence by mining social data [3], [4]. Collective intelligence has been enhanced under the emergence of social networks [8]. Exploiting the wisdom of crowds is another research direction that has received a lot of attention to detect fake news on social networks. In this approach, the authenticity of the news is identified by analyzing the interaction data from users [13], [30]. Combining social interactions can significantly improve the performance of fake news detection problems on social networks. The user's interactions such as comments are an important feature. Figure 2. is an example of tweet content and comments representing the user opinion on Twitter. The misinformation can be detected by exploiting the user's comments.

Fig. 2. News and comments representing the user opinion on Twitter

Limited social-related information is a challenge for fake news detection. First, newly emerged events often have not been stored in existing knowledge-based so it is difficult to be inferred. Second, the features of fake news in the past may not be available in the present, especially due to the constant evolution of misleading writing styles. Finally, limited information may reduce the performance of machine learning models. Analyzing short messages to detect fake news is a difficult task. Some characteristics such as up-to-date information, the lack of context, misspellings, and abbreviations are challenges for machine learning algorithms. The user insight extracted from engagement data is valuable information for fake news detection problems. The user's viewpoints on social networks, especially from high-credibility users, could help to identify fake news effectively. In this study, we present a fake news detection method based on exploiting the wisdom of crowds.

We focus only on analyzing the user's viewpoints to detect fake news without considering news content. The proposed method exploits the user data on Twitter such as the user's profile and interaction data of news. Three features are extracted from the dataset to classify news that are the user's opinion, the user's credibility level, and the exhortation level. The users' viewpoints are useful information to determine the veracity of the news. The users' insights and opinions are presented by actions such as comments, likes, and shares. Exploiting interaction data can reveal the user's viewpoint toward the news. However, the accuracy of opinions from users is different. In our work, we assessed the accuracy of viewpoints based on the user's credibility level. The user's profiles including account information and historical data were analyzed to determine their credibility level. The user's news posted in the history was also matched against the fact-checking database to discover fake news. Fake news in history is important in determining a user's credibility level. The user's trustworthiness level will be reduced if they have previously posted fake news. The historical data provides a better assessment of a user's trustworthiness level and enhance the accuracy of classifying a user's opinion.

Besides, spreading news actions and relationships between users were also exploited to determine the user's credibility level. To overcome the weakness of the single model, we used an ensemble learning model that combines the predictions from three models namely, Support Vector Machine (SVM), Naive Bayes, and Softmax. The proposed method classified news into two categories which are fake and real news. The proposed method experimented on datasets collected from Twitter. The experiments revealed that the proposed method significantly improved the performance of fake news detection problems. The highest F1 score was 78.8% and it was better than the baseline by 6.8%. The experiments demonstrated the effectiveness of using features extracted from social interactions and user profiles.

The major contributions of this paper are as follows:

- We propose to exploit the users' interaction data to detect fake news on social networks. We focus only on analyzing the user's profile and viewpoints to detect fake news without considering shared content.
- We applied the voting ensemble method to the extracted features to classify news on Twitter. The achieved results demonstrated the effectiveness of the proposed method in improving the performance of the fake news detection problems.

The remainder of the paper is structured as follows: Section 2 presents an overview of related works; Section 3 presents the problem statement and the proposed methodology; The experiments are presented in Section 4; Section 5 concludes the paper.

2. Related Works

Social media has developed rapidly and become a popular information channel for everyone. The users create news pies spreading them in the community. Misleading information propagating on social networks is a big challenge that has attracted much more attention from researchers in recent years. Automatic fake news detection is very essential on social media. In this section, we discuss some commonly used perspectives in the literature such as content-based, social context-based, knowledge-based, user's credibility, etc.

2.1. Content and Social Context-based Approach

Style-based concerning how fake news is written. Analyzing the content to detect fake news is a popular approach, especially for long and formal news. The vocabulary and writing style are important features to determine fake information [2], [20]. Pérez-Rosas et al. analyzed text to determine linguistic features that express fake information [18]. Their experiments achieved high accuracy in fake news detection. The linguistic characteristics change when people try to hide their lying writing style [2]. Afroz et al. proposed a method to identify deception in the stylistics of documents. The experiments on the real dataset achieved an F1 score of 96.6%. The linguistic characteristics are suitable for fake news detection in formal news. However, the linguistic characteristics of news on social media are usually different from formal news. The writing style of social news is informal. This is a reason why the methods of analyzing content are inefficient and reduce accuracy when applied to social news. Therefore, exploring auxiliary information has the potential to improve the performance of fake news detection problems.

Combining content and social context analysis is an appropriate method for fake news detection on social networks [24], [27]. Kai Shu proposed a tri-relationship of social context during spreading the news on social media [27]. They exploited the relationship among publishers, news, and users. The authors used a tri-relationship framework to model relations between the publishers and news, and interactions between the user and news to identify fake news. Kai Shu et al. also proposed to exploit the combination of content, social and temporal in the news spread ecosystem on social media [24]. They analyzed the network structure of spreading the news to discover fake news. The experiments demonstrated that the social context analysis methods overcome the disadvantages of traditional text analysis.

2.2. Knowledge-based Approach

Fake news detection based on analyzing content and writing style is a hard problem, especially with social media news. Knowledge-based approaches utilize the fact-checking method to compare news content with external sources to verify veracity. The fact-checking methods can be categorized as manual and automatic fact-checking [11]. The manual fact-checking method uses assessments from experts or crowdsourcing. The expert-based method relies on human experts working in specific domains (e.g, fact-checking websites like Snopes, PolitiFact, GossipCop, etc.). The expert-based method is reliable but it is time-consuming and inappropriate for the huge volume of data on social media. Crowdsourcing uses the wisdom of crowds to check the accuracy of news. The user can provide their discussion on news via a platform. Although crowdsourcing fact-checking is difficult to manage and has low reliability, it is more suitable than expert-based fact-checking [33]. On social networks, users can present their viewpoints about the news by leaving comments. Jin et al. exploited collective intelligence to detect fake news in microblogs by exploiting the user's conflicting viewpoints [13]. A topic model was used to discover the conflicting viewpoints of news and then, a propagation network with supporting or opposing relations was built to infer credibility. Their experiments demonstrated the effectiveness of the proposed method on a real dataset. Wei et al. applied a Bayesian aggregation model to relevant human and machine judgment extracted from news content and crowd judgment [30]. The proposed framework demonstrated the effectiveness of

exploiting crowd intelligence in fake news detection. Using ontologies in fake news detection is a promising research approach. Seddari et al. proposed a hybrid method for fake news detection that combines linguistic and knowledge-based [22]. They used ontologies to model fake news domain knowledge. Ontologies and linguistic features were used to distinguish fake news. Groza et al. also used ontology reasoning to detect deceptive information about COVID-19 [9]. The major challenge of fake news detection based on ontologies is the lack of scientific knowledge related to a specific category of news. Although knowledge-based approaches can achieve good results in fake news detection, they are not suitable for new topics without corresponding entries in any knowledge base. This approach is often combined with others to get better results.

2.3. Credibility-based Approach

The credibility-based approach investigates the credibility of creators, readers, and spreaders. The credibility characteristic can be extracted from the user's profile such as account information, news in the history, community, following users, etc. The user's credibility plays an important role in fake news detection problems. The users can propagate news in the community by posting, sharing, commenting, etc. The user with a low-credibility level has high probability to post or share fake news than others [1]. News posted on an unreliable website and shared by low-credibility users is more likely to be fake news than news posted by authoritative and credible users [32]. Yang et al. treated the authenticity of the news and the user's credibility as latent random variables [31]. The user's interactions on social networks were mined to determine their opinions towards the news. They used a Bayesian network model to capture the conditional dependencies among the authenticity of the news, the user opinions, and the user's credibility. Shao et al. analyzed the news spreading thousands of articles on Twitter during the 2016 U.S. presidential campaign and election [23]. They found evidence that bots played a big role in amplifying low-credibility news. The accounts actively spread content from low-credibility sources that are more likely to be bots.

In our previous study [29], we used the SVM model to classify news based on a set of four features that are the content, the user's credibility, the user opinion, and the exhortation level. The method is still based on analyzing the news content to determine fake news. In this study, we propose an improved method to detect fake news automatically by exploiting multiple features extracted from social interactions and the user's profile. The methodology and experiment results are presented in the next sections.

3. Proposed Methodology

In this section, we describe the problem of fake news detection from the wisdom of crowds and the features used to classify news. The proposed model is presented at the end of this section.

3.1. Problem Statement

In social networks, once a user posts a piece of news that spreads to the group of users following that user. Other users who read that news can present their viewpoints towards the news by emotional action or reposting or leaving comments about their opinions.

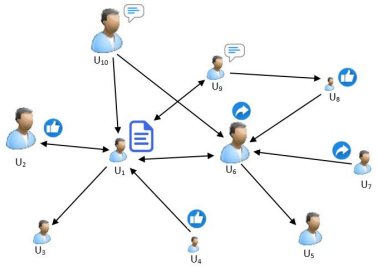

Fig. 3. The illustration of user's relationships on Twitter

Let $U = \{u_1, u_2, ..., u_n\}$ be a set of n users on a social network, $A = \{T_1, T_2, ..., T_m\}$ be a set of news posting by users in U.

For example, Figure 3. describes a simple graph of relationships among users on Twitter. In this graph, user u_1 has five followers $u_2, u_4, u_6, u_9, u_{10}$. Once user u_1 posts news that shows on the timeline of his/her followers. The users can present their viewpoints on that news through comments or emotional actions or retweets. Intuitively, each user has a credibility level to the community/group (e.g., politicians, journalists, and influencers are high credibility; new members and users having few friends are low credibilities). In this example, the high-trust users are drawn to a bigger size and a less size in the opposite case. The credibility level of each user is a parameter to evaluate the validity of their opinion. The comments from high-trust users are more valuable than those of low-trust users.

Given a targeted tweet T posted by user u_j. The news spreads to the community of users following u_j. In general, when followers read the news either they can leave comments expressing their viewpoints or they can present their opinions such as like, retweet, etc. Assuming that each user has a credibility level determined relying on his/her profile. A set of social interactions related to that news is collected to extract the features. Let's determine the authenticity of news if it is fake or real news by analyzing data from the user's social interactions related to the news and the user's profiles.

A tweet is a short text and lacks context to clearly understand its content. Therefore, detecting fake news only relying on its content usually obtains low accuracy. Generally, the reader has to have a wide knowledge of the related subject to be able to understand the inside meaning of the news. A deep understanding helps the reader to leave helpful comments that point out the authenticity of the news. In this study, we exploit the wisdom of crowds which is social interactions related to the news from users to detect fake news on social networks. A framework of the proposed method for fake news detection is described in Figure 4. It contains the following steps:

- First, crawling the interactive data related to the targeted tweet.
- Second, collecting user data on Twitter and measuring the user's credibility level.
- Third, determining the user opinions and exhortation level of the targeted tweet based on comments, likes, and retweets.
- Fourth, building a feature vector.
- Finally, an ensemble model is applied to the features to classify news.

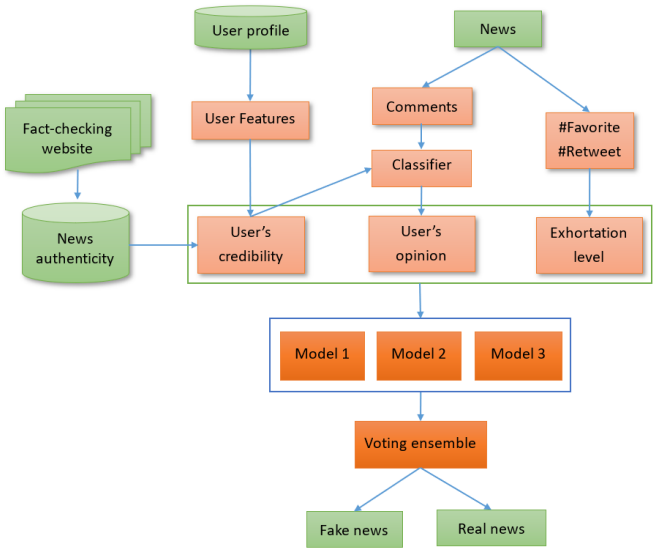

Fig. 4. A framework for detecting fake news based on exploiting the user's interactions

3.2. Feature Extraction

User's Credibility Feature The user's profiles and historical data contain valuable information to determine the user's credibility. Some properties of the user's profile should be considered such as created date, the number of followers, the number of followings, the total of tweets, the total of retweets, etc. These features reflect the seniority of the account, influence level, and the community's level of interest in their posts. Besides, the authenticity of news in history is an important feature to determine the user's reliability. An account that has published fake news is more likely to publish fake news in the future [26]. People who have posted fake news have less credible than people who have not posted fake news yet. The user's news in history needs to be analyzed to determine whether fake news or not and the number of published fake news includes in their profile.

The user's credibility feature is extracted as described in Algorithm 2. To determine the posted fake news in the history of the user, as described in Algorithm 1, the user's historical news is matched with the fact-checking source to find out the fake news. The user's features are a 6-dimensional vector U described as follows:

$$U = \{t, fo, fa, co, re, fn\}, \tag{1}$$

where t is an account age, fo is the ratio of the number of followers to the number of followings, fa is the ratio of the number of likes to the number of tweets, co is the ratio of the number of comments to the number of tweets, re is the ratio of the number of retweets to the number of tweets, fn is the percentage of published fake news to the number of tweets.

User Opinion Feature In social networks, users present viewpoints on news through actions such as emotion, comments, sharing, etc. The user's comments usually express their

Algorithm 1 Fact-checking phase for historical data

Input: Historical data of user, D
Fact-checking source, FS
Output: The percentage of published fake news to the number of news
function CHECK_NEWS_IN_HISTORY(D, FS)
$count \leftarrow 0$;
for $T \in D$ **do**
Pre-processing T;
if T in FS **then** ▷ news exists in the fake news database
$count \leftarrow count + 1$;
end if
end for
return $count/|D|$;
end function

understanding and opinion about news content. On Twitter, users can comment on any tweet even if they are not following the person who posted it. A tweet is a short message and lacks context so the users generally leave comments relying on their understanding of that content. Users have a wide knowledge and can analyze related problems to understand the news content. The comments from users provide useful information for fake news detection. They can leave comments to express their personal opinions. Therefore, these opinions can be a useful source for exploiting the collective intelligence on social networks to detect fake news.

Algorithm 2 Determining user's credibility

Input: User's profile and historical data of user, D
Fact-checking source, FS
Output: A feature vector expressing user's credibility, C
function USER_CREDIBILITY(D)
Determining t, fo, fa, co, re;
$fn \leftarrow Check\_news\_in\_history(D, FS)$; ▷ Algorithm 1
$C \leftarrow t \oplus fo \oplus fa \oplus co \oplus re \oplus fn$; ▷ Integrating features
return C;
end function

To exploit the user opinions, first, the comments related to a targeted tweet are collected. Then, data is cleaned by removing inessential elements such as hyperlinks, hashtags, symbols, mentions, and emoticons. To construct the comment vector, we use the implementation of doc2vec from the gensim package[5]. The comment vector Co is a k-dimensional vector denoted as follows:

$$Co = (w_1, w_2, ..., w_k) \tag{2}$$

A vector of the user opinion OV is constructed by concatenating the vector of the user's comment Co and the user's credibility C.

[5] https://radimrehurek.com/gensim/models/doc2vec.html

$$OV = Co \oplus C \tag{3}$$

Algorithm 3 Classify users' opinions

Input: Users' data interact with a target news, I
Users' profiles, D
Output: users' opinions, O
function USERS_OPINION(D, I)
$O \leftarrow \emptyset$;
for comments $t \in I$ **do**
Pre-processing t;
$Co \leftarrow$ Doc2vec(t);
$C \leftarrow$ User_credibility(D); ▷ Algorithm 2
$OV = Co \oplus C$;
$Op \leftarrow$ multiSVM(OV);
$O \leftarrow O \cup Op$;
end for
return O;
end function

The combination of the user's comment and his/her credibility can increase the efficiency of exploiting the user's opinion. Since the comments from high-credibility users are more valuable than those of low-credibility users. A multiSVM model[6] is utilized to classify the comments into three categories (i.e., $positive$, $neutral$, and $negative$). In which $negative$, $positive$ denote comments that rate the news as fake news, real news, respectively. The comments do not present the veracity of news classified as $neutral$. Since a tweet can receive many comments from different users. Therefore, the users' opinions toward a tweet are determined based on combining the opinions. Pseudocode describes the idea of user opinions extraction described in Algorithm 3. The users' opinions toward a tweet are presented as follows:

$$O = \{pos, neu, neg\}, \tag{4}$$

where pos is the percentage of positive comments, neu is the percentage of neutral comments, and neg is the percentage of negative comments.

Exhortation Feature The comments from users usually present their viewpoints toward news. Analyzing users' comments to know their opinions is helpful for fake news detection problems. Otherwise, the exhortation is another feature to enhance the user opinion feature. In general, users usually encourage the news by like or retweet actions. Once users are interested in the news they will click on the Like button to express their interest. To spread the news, they can also repost the news, called Retweet. Retweet is a way to spread the news to more people. In general, like and retweet actions express the user's agreement with the news. Since fake news is intentionally written to mislead readers to

[6] https://scikit-learn.org/stable/modules/svm.html

believe false information so the readers are easy to believe news content. Fake news has a great ability to attract users. The users usually encourage fake news by like or retweet actions to spread the news to the community. This is one reason that fake news spreads so quickly. Spreading rapidly combined with the user's comments is a good indicator of fake news detection. Since the user's tweet only shows on the timeline of followers. Therefore, in this work, we only consider the ratio of the number of likes to the number of followers ($like$) and the ratio of the number of retweets to the number of followers (ret). The news exhortation E is presented as:

$$E = \{like, ret\}. \tag{5}$$

3.3. Ensemble Model Selection

The ensemble learning approach helps improve machine learning results by combining several models to improve predictive performance compared to a single model. The ensemble learning approach is a widely-used in machine learning. A voting ensemble is an ensemble machine learning model that combines the prediction results from multiple models. The core idea is that the results obtained from a combination of models can be more accurate than any individual machine learning model in the group. In this technique, multiple classifiers are used to make predictions for each data point. The outputs of each classifier are passed into the voting classifier to choose the outputs based on the majority of voting. There are two different types of voting prediction for classification that are hard voting/majority voting and soft voting.

Algorithm 4 Feature vector construction

Input: A target news, T
User's profiles, D
User's data interact with target news, I
Output: A feature vector, F
function FEATURE_VECTOR(T, D, I)
$C \leftarrow$ User_credibility(D); ▷ Algorithm 2
$O \leftarrow$ Users_opinion(T, D, I); ▷ Algorithm 3
$E \leftarrow$ Exhortation_level(T, D, I); ▷ Section 3.2
$F \leftarrow C \oplus O \oplus E$; ▷ Integrating features
return F;
end function

The majority voting approach involves summing the predictions for each class. The majority voting is considered differently when weights associated with the different classifiers are equal or not. The predictions that we get from the majority of the models are used as the final prediction. The prediction of the ensemble classifier can be mathematically represented as the following:

$$\hat{y} = \underset{i}{\operatorname{argmax}} \sum_{j=1}^{m} w_j (C_j(x) = i), \tag{6}$$

where $C_j(x)$ is the predicted label of classifier C_j applied to sample x, x is a sample, w_j represents the weight associated with the prediction of the classifier C_j and $\hat{y}$ is a class label.

Soft voting involves averaging the predicted probabilities for each class. Classifiers can be assigned weights corresponding to the classifier's importance. The class label with the highest averaging of weighted probabilities wins the vote. The prediction of the ensemble classifier can be mathematically represented as the following:

$$\hat{y} = \underset{i}{\operatorname{argmax}} \frac{1}{m_{classifiers}} \sum_{j=1}^{m} w_j (C_j(x) = i), \tag{7}$$

where $C_j(x)$ is the predicted probability of classifier C_j applied to sample x.

Algorithm 5 Ensemble learning model for fake news detection

Input: A target news, T
Output: Veracity of T, V
function FAKE_NEWS_DETECTION(T)
Pre-processing T;
Determining a set of users related to T (i.e., publisher, users have interacted with T);
Collecting user's profile and historical data of users, D;
Collecting social interaction data related to T (i.e., Comments, #Like, #Retweet), I;
$F \leftarrow$ Feature_vector(T, D, I); ▷ Algorithm 4
V = VotingClassifier(αNaiveBayes(F), γSVM(F), βSoftmax(F));
▷ α, γ, β is the weights assigned to classifiers
return V;
end function

In this study, we implement the voting ensemble model for fake news detection by using three supervised algorithms that are Naive Bayes, SVM, and Softmax Regression. We use the implementations of the models from the scikit-learn library[7]. The experiments were conducted with the adjusted parameters to test the extracted features and the proposed method, especially the weight representing the importance of classifiers. Algorithm 5 illustrates the proposed idea of the ensemble learning model. The interaction data and the users' profiles interacting with the news are collected to construct the feature vector as described in Section 3.2. The feature vectors are generated by combining the user's credibility, the user's opinion, and the exhortation feature. The steps of feature vector construction are presented in Algorithm 4. The models are trained individually to produce the classifiers and then applied to the feature vectors to achieve the prediction results.

[7] https://scikit-learn.org

4. Experiments

4.1. Evaluation metrics

In this experiment, we used precision and recall measurements to evaluate the results. Precision (P) and Recall (R) are calculated as follows:

$$P = \frac{|TruePositive|}{|TruePositive| + |FalsePositive|} \tag{8}$$

$$R = \frac{|TruePositive|}{|TruePositive| + |FalseNegative|} \tag{9}$$

where True Positive is the correctly predicted fake news, False Positive is the incorrectly predicted fake news, False Negative is the incorrectly predicted real news. The $F1$ score is the harmonic mean of P and R defined as follows:

$$F1 = 2 \times \frac{P \times R}{P + R} \tag{10}$$

Table 1. Data statistics

	Quantity
#News	515
#Fake news	255
#Real news	260
#Publisher's profiles	357
#Comments	2532
#Negative	847
#Positive	840
#Neutral	845

4.2. Datasets

To carry out experiments with the proposed method, we explored data from two sources. First, the data from fact-checking sites are collected to have an expert-validated dataset. In this study, we got data from a fact-checking website that is www.politifact.com. News on this website rated the accuracy of claims by elected officials and others who speak up in American politics. Fact-checking data is utilized to match the historical news of users to determine the user's credibility. Second, we used the data crawled from Twitter that was used in our previous study [29]. The dataset included interaction data related to news and user profile data from all users interacting with the news. Based on a set of rated news, Twitter's search API was used to crawl related tweets. Finally, the experiments were conducted on a dataset including 255 fake news and 260 real news. These tweets belong to 357 different users. The publisher's data and interaction data are also collected

to construct the feature vectors as described in Section 3.2. There 2532 comments were selected and annotated into three classes. Comments that reflect the news as fake news are labeled as negative, comments that believe news content are labeled as positive and other comments are labeled as neutral. Statistics of the dataset are provided in Table 1. In this study, we used the available tool Twitter4J[8] to collect data. Data were cleaned to eliminate unnecessary elements such as hyperlinks, hashtags, symbols, mentions, and emoticons.

Table 2. Performance comparison among individual classifiers and voting classifiers

Model	Precision	Recall	F1
Baseline	73.5	70.6	72.0
Naive Bayes	73.1	74.5	73.8
SVM	75.5	72.5	74.0
Softmax	76.0	74.5	75.2
Hard voting	78.0	**76.5**	77.2
Soft voting	**81.3**	**76.5**	**78.8**

4.3. Experiment Results

In this work, we conducted the experiments of the proposed method by using the scikit-learn and gensim libraries. The features as described in Section 3.2 were crawled and built into feature vectors. The data were crawled from Politifact and Twitter as presented in Section. The models were applied to feature vectors to train classifiers. The training and testing were implemented with the scikit-learn library in Python. For the multiSVM classifier, the kernel parameter was set to 'rbf'. The multi_class parameter was set to 'multinomial' for the softmax classifier. For the voting classifiers, the weights parameter was set to 'None' in the case of hard voting, and a sequence of weights in order to weight the occurrences of class probabilities before averaging in the case of soft voting. The other parameters were set to default. To evaluate the effectiveness of the proposal, we experimented with a 5-fold cross-validation strategy. At a time, 1-fold was chosen for a test set and 4-fold remaining was the training set. The process was repeated 5 times for each model to cover all tests and training sets. Five models were used to train on 4-fold treated as a training set and evaluated with a 1-fold test set remaining. The results of the 5-fold cross-validation runs were summarized with the mean of all experiments. We conducted the fake news detection experiments with five classifiers which were three individual classifiers (i.e., Naive Bayes, SVM, and Softmax), hard voting, and soft voting classifiers. Each model was analyzed in terms of Precision, Recall, and F1 Score. The results from [29] were treated as the baselines.

The results of the experiments are shown in Table 2. The highest performance was achieved by the soft voting ensemble model and the Naive Bayes model was the lowest. More specifically, the soft voting ensemble classifier achieved an F1 score of 78.8%, the

[8] http://twitter4j.org

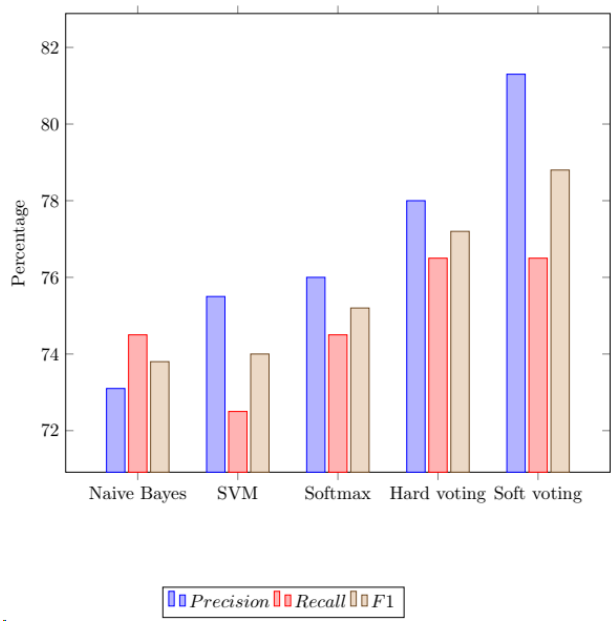

Fig. 5. Comparison of performance in different classification models

best among all the classifiers. The Naive Bayes and the SVM model achieved the same performance. The Softmax classifier and the SVM classifier predicted quite correctly. However, the Softmax classifier surpassed the SVM classifier in the number of predicted samples. Both voting ensemble classifiers outperform the remaining individual classifiers. In terms of precision, the soft voting classifier achieved the best result. It was better than the hard voting, softmax, SVM, and Naive Bayes classifiers by 3.3%, 5.3%, 5.8%, and 8.2%, respectively. The soft voting ensemble classifier only surpassed the hard voting ensemble classifier in precision. However, the predicted results of these two classifiers were the same. As shown in Figure 5, the soft voting ensemble classifier improved the accuracy compared to the hard voting ensemble classifier. The soft voting classifier achieved the F1 score of 78.8%. It was better than the best individual classifier by 3.6% and better than the baseline by 6.8% [29]. In this work, the user's credibility was enhanced based on the fact-checking source. The results demonstrated the effectiveness of the feature set and the proposed method.

The experiments demonstrated the effectiveness of the voting ensemble technique applied to extracted features in the fake news detection problem. The soft voting classifier exceeds the hard voting classifier in detecting fake news. In the above experiments, we set the weights of classifiers to be equal. To evaluate the impact of each classifier, in the soft voting method, we changed the weights associated with classifiers. Table 3 shows the results with different weights of the soft voting technique. In the experiment, one classifier was assigned the weight of 2, remaining classifiers were assigned 1. In Table 3, the first column presents the weights α, γ, and β assigned to the classifiers Naive Bayes, SVM, and Softmax, respectively. Figure 6 is a graphical representation of the performance of

Table 3. The performance of the soft voting classifiers with different weights

Weights assign for classifiers (α, γ, β)	Precision	Recall	F1
2, 1, 1	73.6	76.5	75.0
1, 2, 1	76.5	76.5	76.5
1, 1, 2	**80.0**	**78.4**	**79.2**

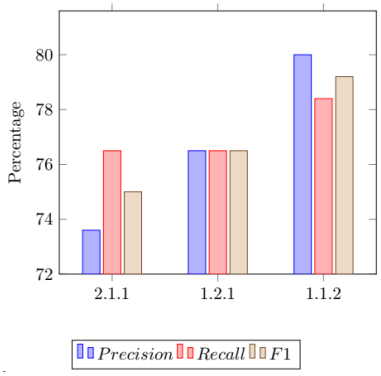

Fig. 6. The performance of the soft voting classifier with different weights

the soft voting classifier with different weights. The experiment with the weight of the softmax classifier of 2 was the most effective. It achieved an F1 score of 79.2%. Meanwhile, the Naive Bayes classifier with a weight of 2 did not perform well, especially the precision was low. In general, the weight associated with the classifiers should be set proportional to the effectiveness of the model. However, the experiments have not revealed the best weight value for each classifier. Obviously, efficient classifiers play an important role in improving the performance of the voting ensemble method.

5. Conclusions

In this paper, we proposed a voting ensemble model to detect fake news on social media based on exploiting the features of the wisdom of crowds. The voting ensemble model comprised three classifiers namely, SVM, Naive Bayes, and Softmax. The feature set was extracted from the user's interaction data and the user's profiles. The method mainly focused on the user's viewpoints to determine the authenticity of the news. We exploited three features that were user's opinions, user's credibility, and exhortation level. The user's credibility was enhanced effectively by matching the user's historical data with fact-checking sources. The individual classifiers and ensemble classifiers were applied to the extracted features to evaluate the effectiveness of the proposed methods. The proposed method experimented on a Twitter dataset. The experimental results showed that the voting ensemble classifiers achieved high performance on all metrics. The soft voting classifier achieved an F1 score of 78.8%. It was better than the best individual classifier

by 3.6% and better than the baseline by 6.8%. The experiments demonstrated the effectiveness of using features extracted from the wisdom of crowds on social networks.

For future works, we are planning to build a multi-agent system model for simulating the process of fake new propagation and to use consensus-based methods for making decisions regarding assigning fake status for news [7], [28]. For determining user opinions, consensus methods will be used to unify different user opinions for determining a common opinion that best represents a given set of user opinions [15], [17].

Acknowledgments. This research is funded by Vietnam National University Ho Chi Minh City (VNU-HCM) under grant number DS2021-26-03.

References

1. Abbasi, M.A., Liu, H.: Measuring user credibility in social media. In: International Conference on Social Computing, Behavioral-Cultural Modeling, and Prediction. pp. 441–448. Springer (2013)
2. Afroz, S., Brennan, M., Greenstadt, R.: Detecting hoaxes, frauds, and deception in writing style online. In: 2012 IEEE Symposium on Security and Privacy. pp. 461–475. IEEE (2012)
3. Awal, G.K., Bharadwaj, K.K.: Team formation in social networks based on collective intelligence–an evolutionary approach. Applied intelligence 41, 627–648 (2014)
4. Böhringer, M., Helmholz, P.: "what are they thinking?"-accessing collective intelligence in twitter (2011)
5. Bondielli, A., Marcelloni, F.: A survey on fake news and rumour detection techniques. Information Sciences 497, 38–55 (2019)
6. Della Vedova, M.L., Tacchini, E., Moret, S., Ballarin, G., DiPierro, M., de Alfaro, L.: Automatic online fake news detection combining content and social signals. In: 2018 22nd Conference of Open Innovations Association (FRUCT). pp. 272–279. IEEE (2018)
7. Duong, T.H., Nguyen, N.T., Jo, G.S.: A hybrid method for integrating multiple ontologies. Cybernetics and Systems: An International Journal 40(2), 123–145 (2009)
8. Gholami, B., Safavi, R.: Harnessing collective intelligence: Wiki and social network from end-user perspective. In: 2010 International Conference on e-Education, e-Business, e-Management and e-Learning. pp. 242–246. IEEE (2010)
9. Groza, A.: Detecting fake news for the new coronavirus by reasoning on the covid-19 ontology. arXiv preprint arXiv:2004.12330 (2020)
10. Hakak, S., Alazab, M., Khan, S., Gadekallu, T.R., Maddikunta, P.K.R., Khan, W.Z.: An ensemble machine learning approach through effective feature extraction to classify fake news. Future Generation Computer Systems 117, 47–58 (2021)
11. Hangloo, S., Arora, B.: Fake news detection tools and methods–a review. arXiv preprint arXiv:2112.11185 (2021)
12. Hardalov, M., Koychev, I., Nakov, P.: In search of credible news. In: International Conference on Artificial Intelligence: Methodology, Systems, and Applications. pp. 172–180. Springer (2016)
13. Jin, Z., Cao, J., Zhang, Y., Luo, J.: News verification by exploiting conflicting social viewpoints in microblogs. In: Proceedings of the AAAI conference on artificial intelligence. vol. 30 (2016)
14. Karnyoto, A.S., Sun, C., Liu, B., Wang, X.: Transfer learning and gru-crf augmentation for covid-19 fake news detection. Computer Science and Information Systems (00), 53–53 (2022)
15. Katarzyniak, R., Nguyen, N.T.: Reconciling inconsistent profiles of agents' knowledge states in distributed multiagent systems using consensus methods. Systems Science 26(4), 93–119 (2000)

16. Kwon, S., Cha, M., Jung, K., Chen, W., Wang, Y.: Prominent features of rumor propagation in online social media. In: 2013 IEEE 13th International Conference on Data Mining. pp. 1103–1108. IEEE (2013)
17. Nguyen, N.T.: Conflicts of ontologies–classification and consensus-based methods for resolving. In: Knowledge-Based Intelligent Information and Engineering Systems: 10th International Conference, KES 2006, Bournemouth, UK, October 9-11, 2006. Proceedings, Part II 10. pp. 267–274. Springer (2006)
18. Pérez-Rosas, V., Kleinberg, B., Lefevre, A., Mihalcea, R.: Automatic detection of fake news. arXiv preprint arXiv:1708.07104 (2017)
19. Qin, Y., Wurzer, D., Lavrenko, V., Tang, C.: Spotting rumors via novelty detection. arXiv preprint arXiv:1611.06322 (2016)
20. Rashkin, H., Choi, E., Jang, J.Y., Volkova, S., Choi, Y.: Truth of varying shades: Analyzing language in fake news and political fact-checking. In: Proceedings of the 2017 Conference on Empirical Methods in Natural Language Processing. pp. 2931–2937 (2017)
21. Sahoo, S.R., Gupta, B.B.: Multiple features based approach for automatic fake news detection on social networks using deep learning. Applied Soft Computing 100, 106983 (2021)
22. Seddari, N., Derhab, A., Belaoued, M., Halboob, W., Al-Muhtadi, J., Bouras, A.: A hybrid linguistic and knowledge-based analysis approach for fake news detection on social media. IEEE Access 10, 62097–62109 (2022)
23. Shao, C., Ciampaglia, G.L., Varol, O., Yang, K.C., Flammini, A., Menczer, F.: The spread of low-credibility content by social bots. Nature communications 9(1), 1–9 (2018)
24. Shu, K., Bernard, H.R., Liu, H.: Studying fake news via network analysis: detection and mitigation. In: Emerging Research Challenges and Opportunities in Computational Social Network Analysis and Mining, pp. 43–65 (2019)
25. Shu, K., Sliva, A., Wang, S., Tang, J., Liu, H.: Fake news detection on social media: A data mining perspective. ACM SIGKDD Explorations Newsletter 19(1), 22–36 (2017)
26. Shu, K., Wang, S., Liu, H.: Understanding user profiles on social media for fake news detection. In: 2018 IEEE Conference on Multimedia Information Processing and Retrieval (MIPR). pp. 430–435. IEEE (2018)
27. Shu, K., Wang, S., Liu, H.: Beyond news contents: The role of social context for fake news detection. In: Proceedings of the Twelfth ACM International Conference on Web Search and Data Mining. pp. 312–320. ACM (2019)
28. Sliwko, L., Nguyen, N.T.: Using multi-agent systems and consensus methods for information retrieval in internet. International Journal of Intelligent Information and Database Systems 1(2), 181–198 (2007)
29. Tran, V.C., Nguyen, V.D., Nguyen, N.T.: Automatic fake news detection by exploiting user's assessments on social networks: A case study of twitter. In: International Conference on Industrial, Engineering and Other Applications of Applied Intelligent Systems. pp. 373–384. Springer (2020)
30. Wei, X., Zhang, Z., Zhang, M., Chen, W., Zeng, D.D.: Combining crowd and machine intelligence to detect false news on social media. Mis Quarterly (2019)
31. Yang, S., Shu, K., Wang, S., Gu, R., Wu, F., Liu, H.: Unsupervised fake news detection on social media: A generative approach. In: Proceedings of the AAAI conference on artificial intelligence. vol. 33, pp. 5644–5651 (2019)
32. Zhou, X., Zafarani, R.: Fake news: A survey of research, detection methods, and opportunities. arXiv preprint arXiv:1812.00315 2 (2018)
33. Zhou, X., Zafarani, R.: A survey of fake news: Fundamental theories, detection methods, and opportunities. ACM Computing Surveys (CSUR) 53(5), 1–40 (2020)

Hai Bang Truong received a Ph.D. degree in computer science from Viet Nam National University Ho Chi Minh City, in 2016. He is currently a professor at the Faculty of Com-

puter Science, University of Technology, Ho Chi Minh City, Vietnam. He has authored 7 journal articles and 14 conference papers. His research interests include collective intelligence, knowledge integration methods, and social network analysis.

Van Cuong Tran received a B.S. degree in computer science from the Hue University of Sciences, Vietnam, in 2012, and a Ph.D. degree in computer engineering from Yeungnam University, South Korea, in 2017. He is currently a professor at Quang Binh University, Vietnam, and the assistant dean of the Faculty of Engineering and Information Technology. He has authored 10 journal articles and 14 conference papers. His research interests include named entity recognition, sentiment analysis, recommendation systems, and social network analysis.

Received: March 02, 2023; Accepted: June 22, 2023.

Computer Science and Information Systems 20(4):1459–1481https://doi.org/10.2298/CSIS230115042T

Deep Learning-based Sentiment Classification in Amharic using Multi-lingual Datasets*

Senait Gebremichael Tesfagergish[1] and Robertas Damaševičius[1] and Jurgita Kapočiūtė-Dzikienė[2]

[1] Department of Software Engineering,
Kaunas University of Technology, Kaunas 51368, Lithuania
sengeb@ktu.lt
robertas.damasevicius@ktu.lt
[2] Department of Applied Informatics,
Vytautas Magnus University, Kaunas 44404, Lithuania
jurgita.kapociute-dzikiene@vdu.lt

Abstract The analysis of emotions expressed in natural language text, also known as sentiment analysis, is a key application of natural language processing (NLP). It involves assigning a positive, negative (sometimes also neutral) value to opinions expressed in various contexts such as social media, news, blogs, etc. Despite its importance, sentiment analysis for under-researched languages like Amharic has not received much attention in NLP yet due to the scarcity of resources required to train such methods. This paper examines various deep learning methods such as CNN, LSTM, FFNN, BiLSTM, and transformers, as well as memory-based methods like cosine similarity, to perform sentiment classification using the word or sentence embedding techniques. This research includes training and comparing mono-lingual or cross-lingual models using social media messages in Amharic on Twitter. The study concludes that the lack of training data in the target language is not a significant issue since the training data 1) can be machine translated from other languages using machine translation as a data augmentation technique [33], or 2) cross-lingual models can capture the semantics of the target language, even when trained on another language (e.g., English). Finally, the FFNN classifier, which combined the sentence transformer and the cosine similarity method, proved to be the best option for both 3-class and 2-class sentiment classification tasks, achieving 62.0% and 82.2% accuracy, respectively.

Keywords: sentiment analysis, monolingual vs. cross-lingual approaches, deep learning, sentence transformers, Amharic.

1. Introduction

The origin of Sentiment Analysis dates back to the 1950s when it was initially applied to written paper documents, becoming a vital topic in the NLP field with the emergence of the Internet and electronic texts (especially non-normative texts). sentiment analysis is a process of analyzing text to detect its author's overall positive, negative, mixed, and neutral sentiment toward the discussed topic. However, opinions are usually subjective expressions, texts are full of hidden meanings and sarcasm. Due to all these factors, the sentiment analysis problem is still complicated even for such widely used and resource-rich languages as English.

* An extended version of the paper presented at the ICT Innovations 2022 conference.

The need for analyzing text and identifying their sentiments relies on the technological era we live in today. Everything is shifting online and online comments and reviews from the end users affect the decision taken by stakeholders in different domains [50]. News with a generally favorable tone has been linked to a significant price increase. Negative news, on the other hand, may be connected to a price drop with longer-term consequences. In marketing, the analysis of news articles can help evaluating online reputation of business companies and brands [52]. In the entertainment industry, customer reviews and comments are used for decision-making for other potential buyers of the products [63]. Similarly, producers use it to improve their service quality and outline a plan for their coming products or services. In politics, it helps authorities to make decisions based on the overall sentiment from the population surveys [16], or manage crisis communication [7]. A dark side of social networks is that they can be used to criticize government officials [17], spread hate speech [3], homophoby [25], racism [32], and conspiracies [23,56,55], aiming to influence events in the real world.

Due to ambiguities in each language and our human understanding, there is no single solution that could work for all languages. Each language is different and difficult in its own way, therefore requires adaptation. The identification and processing of morphological features of a specific language are required for real-life natural language processing (NLP) tasks [13]. Under-researched languages like Amharic [21] could not benefit from the application and tools already developed for the resource-rich languages like English [34]. It is due to its morphological complexity and unavailability of enough data for solving the sentiment analysis [39] task. Innovative artificial intelligence (AI) methods such as ensemble learning [42,29], deep learning models [15] for learning high-dimensional representations (word embeddings) [35], which can be combined with heuristic optimization methods [5], are helping under-resourced languages to pass the hardships of collecting and preprocessing large datasets, instead, they provide a deep insight into the available data features to make the classification more efficient [24]. Recently, multi-lingual approaches that can deal with numerous languages at the same time were proposed to alleviate the problem of scarcity of data for sentiment analysis in low-resourced languages such as Bengali [57], Serbian [19], Tamil [51], Urdu [31] and others [48]. However, multilingual models often encounter issues with highly imbalanced training data across the supported languages. As a consequence, the effectiveness of these multilingual models for different languages also varies: e.g., the well-supported English language demonstrates superiority in performance while resource-scarce languages may suffer from poor or even unacceptable performance.

The aim of this work is to address sentiment analysis for Amharic by benefiting from 1) datasets that are available for other languages; 2) state-of-the-art multilingual and cross-lingual solutions mainly focused on deep learning and transformer models [59]. The paper is an extended version of conference paper [54].

The main novelty and contribution of this study is as follows:

– State-of-the-art sentence transformer embedding model (that projects sentences into semantic space) has rarely been used as a sentence vectorization technique for Amharic sentiment classification (see our previous work [53]).

- We explore multiple approaches: 1) classical machine learning techniques (such as cosine similarity and K-Nearest Neighbor (KNN)) and 2) traditional deep learning approaches (such as Feed Forward Neural Network (FFNN), Convolutional Neural Network (CNN), Long Short-Term Memory (LSTM), Bidirectional LSTM (BiLSTM)) a applied on the top of Word2Vec as word embeddings; 3) hybrid methods connecting the sentence transformer model with cosine similarity and KNN.
- The lack of Amharic data problem was solved with the help of data machine translation when translating from English. English is the resource-rich language that allowed us to choose datasets in the domain of short texts on general topics.
- Monolingual (training and testing on the same language) and cross-lingual (training on one language, testing on another language) solutions compared.
- In the control experiment, we machine-translated the English data into 8 other languages and performed similar experiments to investigate the impact of the machine translation quality on the sentiment analysis task.

This paper is structured as follows. Related works are described in Section 2. The dataset used for this experiment is presented in Section 3. Analysis of vectorization, classification models, and optimization techniques are discussed in Section 4. Section 5 explains the experiment and its results. Section 6 concludes with a discussion and conclusion about the overall objectives and achievements of this research and future works.

2. Related works

Semitic languages like Arabic, Amharic, and Hebrew are widely spoken languages by over 250 million people in the east, north Africa, and the Middle east. Semitic languages exhibit unique morphological processes challenging syntactic construction and various other phenomena that are less prevalent in other natural languages [64]. Amharic, despite being the second biggest language in the Semitic language with 27 million native speakers and the official language of Ethiopia 100 million population), is one of the low-resourced languages and lacks the availability of resources for electronic data and basic tools for Natural language processing applications. We choose Amharic intentionally, as a good example of a rather complex, low-resource language. Hence, our further theoretical research work analysis on sentiment analysis will also consider these factors.

In this overview, we skip all outdated rule- and dictionary-based approaches, focusing on the sentiment analysis problem as a supervised text classification problem by following the current trend in the sentiment analysis community. E.g., the popular Papers with code portal [37] contains 1047 research papers of authors competing to achieve better sentiment analysis accuracy on 42 benchmark datasets. The variety of their tested methods covers a huge range of different approaches: traditional machine learning, traditional deep learning to state-of-the-art transformer models. However, these competitions make clear that the transformer models achieve the highest classification accuracy. Despite the majority of these

papers summarizing the research done on the English language, it demonstrates what to aim for and what might work for other languages.

The SemEval competitions also attract many researchers from all over the world to compete when solving various sentiment analysis problems: i.e, in SemEval-2019 (311 teams tried to detect emotion classes) [12]; in SemEval-2020 (the 3-class sentiment analysis problem with the code-switching for Hinglish and Spanglish was addressed by 61 and 28 teams, respectively) [44]; in SemEval-2022 (structural 3-class sentiment analysis problem was solved by 32 teams for Norwegian, Catalan, Basque, Spanish, and English languages) [10]. If in 2019 traditional machine learning approaches Naive Bayes, Logistic Regression, and SVM were still "on the table", achieving comparative results to traditional deep learning approaches (as, e.g., BiLSTM) [43,30], graph convolutional networks [62], attention networks [22] and 3D-CNN [58], transformer models (e.g., BERT, XLM, Roberta etc.) become popular in 2020 and dominant in 2022 [26]. Consequently, it motivates us to investigate transformer models for our sentiment analysis problems. The success of the pre-trained transformer models (which are later integrated into the classification framework) highly depends on how well they support the target language (i.e., how large and comprehensive the training corpora of the target language were used). Hence, this factor cannot be controlled by us, therefore next to the transformer models, we are planning to overview and test other (more stable) approaches.

Machine learning (ML) approaches such as Support Vector Machine (SVM), Logistic Regression (LR), and Naïve Bayes (NB) were used to solve various NLP tasks for a long time [49]. Amharic sentiment analysis study [45] used NB with unigram, bigram, and hybrid variants as features. The research was conducted on 600 posts labeled to two classes. The authors managed to get their highest result at 44% using the bigram feature. Multi-lingual Twitter sentiment analysis in [6] presented 95% accuracy using the Bag-of-words vector and SVM classifier in English, Telugu, and Hindi. Naïve Bayes achieves the highest precision performance in [8] of the Catalan language 2-class sentiment classification of 50,000 tweets, which is +3% of the Neural network precision. Multi-class sentiment analysis in the Russian and Kazakh languages presented in [38] proposes their best model for this classification are Linear Regression, Decision Tree and Random Forest with 74%, 64%, and 70% accuracy respectively on the Russian texts.

Deep learning is a branch of machine learning which aims to model high-level abstraction in data. This is done using model architectures that have complex structures or those composed of multiple nonlinear transformations [24]. Many studies are conducted using deep learning for Amharic sentiment analysis (see Table 1). Since Arabic shares many similar characteristics with Amharic in terms of morphology a few research using deep learning methods are also described in Table 1. Sentiment analysis in Arabic catches the attention of many researchers as it has a bigger number of speakers with different dialects all over the world and plenty of datasets are available for conducting such research. In [40], a systematic review from year January 2000 until June 2020 was conducted to analyze the status of deep learning for Arabic subjective sentiment analysis tasks. The authors' findings described that 45% of the selected papers conducted their experiment using the CNN and RNN (LSTM) methods.

Table 1. Related works using deep learning techniques

Ref.	Corpus	Language	Classification Algorithm	Embedding and Features	Accuracy
[2]	8,400 tweets (positive, negative, and neutral)	Amharic	Flair	Graphical embedding	60.51%
[3]	1,602 reviews	Amharic	Deep learning	TF-IDF vectorization	90.1%
[17]	6,652 samples (positive and negative)	Amharic	BERT	Fine-tuned BERT	95%
[4]	15,100 (positive and negative)	Arabic	CNN-LSTM, SVM	Fast Text Embedding	90.75%
[5]	2,026, positive (628) and negative (1,398)	Arabic	BILSTM	Not mentioned	92.61%

Summarizing, the sentiment analysis task for Amharic has been conducted using different traditional machine learning approaches (SVM, multinomial NB, Maximum Entropy applied on the top of bag-of-words, Decision Tree) and deep learning methods. As for all languages, the recent research for Amharic is focused on deep learning methods because they outperform the traditional machine learning approaches. However, our goal is to conduct accuracy-oriented comprehensive comparative research, therefore we will test various Deep Learning methods, from traditional to transformer models.

Cross-lingual solutions for the sentiment analysis problems are the salvation for the low-resourced languages [11,1,28,18]. Their aim is to learn a universal classifier which can be applied to languages with limited labeled data [2], which is exactly what we have in sentiment analysis problems [6]. The cross-lingual approaches in sentiment analysis usually vary from the early solutions based on machine translation to cross-lingual embeddings and multi-BERT pre-trained models [41]. English – Arabic cross-lingual sentiment analysis presented in [2] concludes that regardless of the artificial noise added by the machine translation they managed to achieve the best result of 66.05% in the Electronics domain with the BLUE score of 0.209. Another study [1] tested the performance of cross-lingual sentiment analysis without good translation from English to Chinese and Spanish language. Authors explained that in their experiment they observed that sentiment is preserved accurately even if the translation is not accurate, and this inexpensive approach maintains fine-grained sentiment information between languages.

To our best knowledge, the sentiment analysis problem for Amharic has never been solved with cross-lingual approaches [4]. In advance, it is difficult to guess which solution 1) machine-translation-based (not knowing how much the quality of machine translation can affect the classification result), or 2) cross-lingual transformers (not knowing how well they support Amharic and their semantic relations with other languages) can be the best. Besides, the machine translation will help us not only in the cross-lingual settings, but in general when creating the sentiment analysis dataset we lack for Amharic.

3. Datasets

Since we formulate sentiment analysis as the supervised text classification problem, we need the labeled data, but the selection of Amharic as our research object limits our choices. To overcome this obstacle, we have decided to use:

1. The Ethiopic Twitter Dataset for Amharic (ETD-AM) dataset [60] which is probably the only publicly available sentiment analysis dataset for Amharic. It was introduced by Yimam et al. after being collected from Twitter and annotated with the Amharic Sentiment Annotator Bot (ASAB) [61]. ETD-AM stores only tweet ids and their sentiments, therefore for retrieving raw tweets via the Twitter API, the tweepy python library was used. The retrieved original dataset consisted of around 8.6K tweets mapped to 3 (positive/negative/neutral) classes. Some tweets could not be retrieved via API calls, resulting in a very small number of samples for the neutral class, this class was omitted in our experiments. Hence, our sentiment analysis problem became a 2-class classification problem and the distribution of samples between these classes can be found in Figure 1.
2. Tweet_Eval [9] the dataset which was borrowed from English. It is an English dataset containing tweets and adjusted for seven heterogeneous tasks, namely, irony detection, hate speech detection, offensive language identification, stance detection, emoji prediction, emotion recognition, and sentiment analysis. Thus, we used this dataset for our sentiment analysis problem. Its original version consisted of around 60K texts from social media, was noisy (full of spelling mistakes, slang phrases, multi-lingual words, etc.), and needed pre-processing. This step was utilized to eliminate unnecessary content and convert it into useful information for the sentiment analysis task. The original dataset is a non-normative data resource consisting of a non-Geez script; therefore – emojis, web links, non-Latin letters, and non-English words were removed. During the tokenization, the texts were split into tokens with the Tokenizer from the Python Keras library. The final version of this dataset used in our sentiment analysis experiments is presented in Figure 1.

Creating a model for a sentiment classification task depends on many factors. Apart from the parameters of the selected classification model, the quality and quantity of the dataset used for the training phase have a great impact on the performance of the trained model. A larger dataset with good quality data will train a better accurate model. In the case of 2-class sentiment analysis, the dataset available was small and we needed to augment it with more translated data from English. The English dataset from Twitter (Sentiment 140) [27] was translated to Amharic and six other languages, and added to the original dataset. The added data is balanced where the positive and negative class has 15,000 instances each. The example of the tweet and its translations is presented in Table 2.

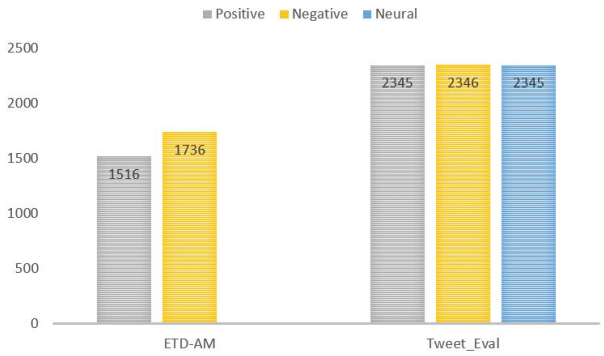

Figure 1. Distribution of sentiments in ETD-AM and Tweet_Eval datasets

Table 2. Example of dataset tweet in seven languages.

Language	Sentence
English	Its to be expected from electing a Fascist Nazi
Amharic	**ፋሽስት ናዚን ከመምረጥ የሚጠበቅ ብቃት**
Tigrinya	**ፋሺሽታዊ ናዚ ብምምራጽ ትጽቢት ክግበረሉ ኣለዎ**
Lithuanian	Jo reikia tikėtis išrinkus fašistinį nacį
Arabic	الفاشية النازية انتخاب من المتوقع من
Czech	Je třeba se očekávat od zvolení fašisty nacisty
German	Es ist zu erwarten, einen faschistischen Nazi zu wählen
French	Il faut attendre de l'élection d'un nazi fasciste

4. Methodology

Our methodology is summarized in Figure 2. It includes the following stages: data cleaning, tokenization, vectorization, and sentiment classification, which are described in more detail in the following subsections.

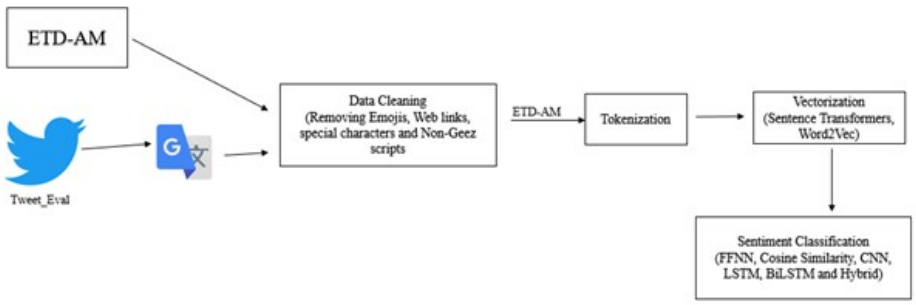

Figure 2. Workflow of methodology and Experiment

4.1. Vectorization

In Section 2, we have discussed which methods are suitable for sentiment analysis; this choice is also influenced by the specificity of the datasets (Section 3). However, the supervised classifiers cannot be trained directly from raw texts. Thus, encoding of texts into low-dimensional and dense numeric vectors plays an important role in making these methods applicable. We tested the following embeddings:

- Word2Vec. These types of word embeddings are usually monolingual models that map each distinct word into its stable fixed-size vector. These embeddings (skip-gram and CBOW) are trained to consider the word and its context in the fixed window. The amount of data used to learn the embeddings have a huge impact on their quality . The larger the amount of training data used, the better mapping of the vector space is determined . However, these types of embeddings suffer from word ambiguity problems: words written in the same form, but having different semantical meanings will always be vectorized alike. Unlike other resource-rich languages, the Amharic pre-trained Word2Vec embeddings are not publicly available. Thus, we trained them using the same Ethiopic Twitter Dataset for Amharic (ETD-AM) with 300 dimensions, a window size equal to 5 and with all other parameters with the default values. For training word embeddings we have used python library.
- Sentence Transformers. These embeddings are state-of-the-art technology that allows mapping whole sentences into fixed-size vectors [36]. The variety of sentence transformers is rather large, we are most interested in being capable to capture the semantics of sentences in relation to similar ones. . Moreover, the most important requirement is that the model would support Amharic and preferably be multi-lingual and able to benefit from other languages. The pre-trained language-agnostic BERT sentence embedding model (LaBSE) [20] seems the perfect solution to all of it, despite Amharic is not highly supported.

4.2. Classification Methods

We have investigated the following text classification methods:

- CNN was originally developed to image processing and classification but successfully adapted to text classification. First, it seeks patterns in the input by sliding through it with a 1D convolution filter. CNN considers patterns of sequential words (in our case: word embeddings) thus making it more like the keyword search-type approach. However, for some problems, CNN demonstrates rather good performance. In our experiments we use the architecture presented in Figure 3.
- LSTM, BiLSTM or hybrid. Recurrent Neural Networks (RNNs), LSTMs, and BiLSTMs are adjusted to work with sequential data (in our case: word embeddings). These models (Figure 4) use the output of the previous hidden state as an input for a current one. However, the RNNs suffer from the vanishing gradient problem (especially having longer word sequences), it is highly recommended to choose LSTMs or BiLSTMs instead as they have input/forget/output gates to control this problem. Besides, BiLSTMs are also

adjusted to learn from two directions at the same time (by processing text from the start to its end and vice versa). Architectures of used LSTM and BiLSTM approaches are presented in Figure 5.
- The hybrid models that blend different architectures of CNN with LSTM/BiLSTM sometimes allow to achieve even better performance. We also tested such architectures (Figure 6): the CNN model is responsible for the extraction of features, and BiLSTM or LSTM is used for generalizing them[14].
- Cosine similarity with KNN. This memory-based approach is used with the LaBSE sentence embeddings. After the LaBSE model projects sentences into the semantical space, the cosine similarity measure can help determine similarities between these sentences. The calculated value can be in the range [-1,1], where 0 means that sentences are not similar; 1 - are the same; -1- opposite. This memory-based method does not have any training phase: it simply stores all vectorized training samples. Each new testing sample has to be compared to all training samples and obtains the class of that training sample to which the cosine similarity value is the largest.
- Feed Forward Neural Network (FFNN) is a simple classifier used when nonlinear mapping is done between inputs and outputs. This method is chosen with our sentence transformers because other deep neural network model cannot be applied (LaBSE sentence vectors do not retain any patterns or sequential characters of the input). The model (Figure 2) is trained to learn the relationship between sentences from the embeddings. When testing, it returns the class of the most similar sentence in the training set.
- Bidirectional Encoder Representations from Transformer (BERT) is a transformer-based technique for NLP pre-training developed by Google. Its generalization capability is such that it can be easily adapted for various downstream NLP tasks such as question answering, relation extraction, or sentiment analysis [46]. Transformers are used to learn the relationship of words in the context. BERT generates a language model using the encoder. The bidirectional encoder reads the sequence in both directions (left-to-right and right-to-left), so the model is trained from the right and left sides of the target word. Because the core architecture is trained on a huge text corpus, the parameters of the architecture's most internal levels remain fixed. The outermost layers, on the other hand, adapt to the job and are where fine-tuning takes place. Sentiment analysis is done by adding a final classification layer on top of the transformer output for the [CLS] token. Currently, the Amharic pre-trained Bert model is not available. Therefore, the English model was adapted.

5. Experiment and Results

The dataset described in Section 3 is vectorized by different embeddings explained in subsection 4.1 and classified using the methods described in subsection 4.2. Tensorflow, Keras, and PyTorch are used for the implementation of the methods. Both used datasets ETD-AM (2 classes) and Tweet_Eval (3 classes) were split for training and testing. Since we formulate our sentiment analysis tasks as the text classification problem, the usual evaluation metrics such as accuracy, precision,

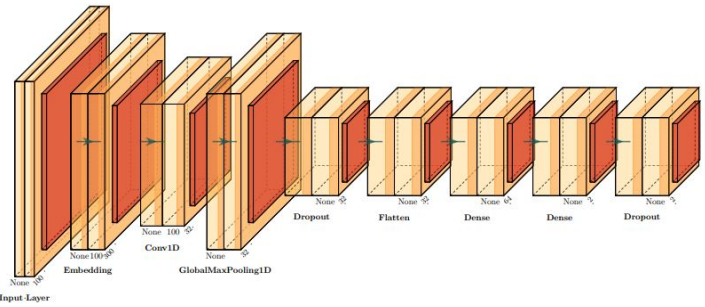

Figure 3. Architecture of CNN model

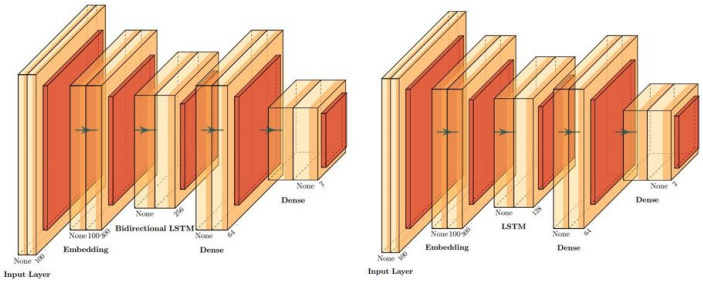

Figure 4. Architecture of BiLSTM (right) and LSTM (left) model

recall, and f-score were applied. We have also calculated the majority baseline to see if the accuracies achieved by methods are acceptable (if the achieved accuracy is above the majority baseline the method is considered appropriate for the solving problem). Approaches (in which initial parameters are generated randomly and later adjusted during training) were trained and evaluated several times to calculate their average result. Table 3 summarizes the results for Amharic with ETD-AM (2 classes) and Tweet_Eval (3 classes) datasets.

Table 3. Accuracies with ETD-AM (2 classes) and Tweet_Eval (3 classes) datasets for Amharic.

Model	ETD-AM (2-Class)	Tweet_Eval (3-Class)
CNN + Word2Vec	0.46	0.43
LSTM + Word2Vec	0.54	0.32
BILSTM + Word2Vec	0.62	0.39
CNN & BILSTM + Word2Vec	0.41	0.48
CNN & LSTM + Word2Vec	0.39	0.44
Cosine Similarity + Sentence Transformer + KNN	0.82	0.57
FFNN + Sentence Transformer	0.80	0.62

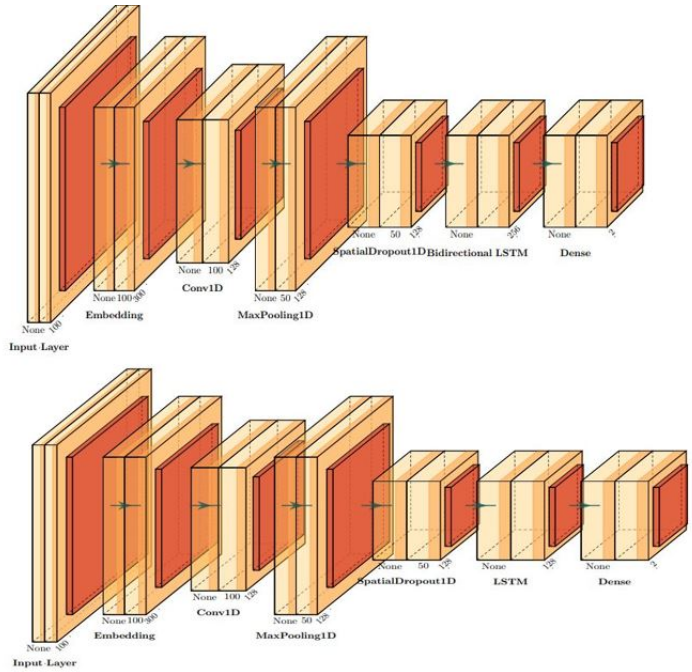

Figure 5. Architecture of hybrid (CNN-BiLSTM & CNN-LSTM) models

Results of different classifiers for binary classification using original and augmented datasets are given in Table 4. Addition of more data translated from English improves the result of Word2Vec vectorization and deep learning methods (CNN, BILSTM, CNN-LSTM, CNN-BILSTM), while the best model with the highest accuracy of 82% that uses the sentence transformer is downgraded by 5%. A possible reason can be the domain of the texts as sentence transformers use the semantics of the sentence for embedding.

Table 4. Accuracy of Original data and Accuracy with added translated data

Model	Accuracy (Original dataset)	Accuracy (Augmented dataset)
CNN + Word2Vec	0.46	0.64
LSTM + Word2Vec	0.54	0.49
BILSTM + Word2Vec	0.62	0.68
CNN & BILSTM +Word2Vec	0.41	0.69
CNN & LSTM + Word2Vec	0.39	0.70
Cosine Similarity + Sentence Transformer +KNN	0.82	0.77
FFNN + Sentence Transformer	0.80	0.76

The determined best classification model for the 2-class is the Cosine Similarity with the sentence transformer embedding. To improve the accuracy of this model, we made a cluster of training sets that have more similarity with the testing instance then voted for the training instance classes label in that cluster and assign that class to the testing instance. In other words, we used the KNN classifier on top of the Cosine Similarity, and in search of the best hyperparameter, we performed the ablation study and presented the result in Table 5. The best accuracy was achieved with 157 nearest neighbors.

Table 5. Accuracy of Cosine Similarity with the K-nearest neighborhoods

Hyperparameter value (number of nearest neighbors (NN))	Accuracy of Sentence Transformer + Cosine Similarity + KNN model
1-NN	0.72
3-NN	0.78
31-NN	0.80
59-NN	0.81
157-NN	0.82

Finally, the Precision, Recall, F1-Score, and Accuracy of all the tested classifiers are summarized in Table 6. The best result was achieved by the hybrid Cosine Similarity + KNN model and Feed Forward Neural Network for the 2-Class and 3-Class respectively with the state-of-the-art Sentence Transformers embeddings. The confusion matrix of the best models is also presented in Figure 8.

Table 6. Performance of all tested classification models

Model	Classification	Precision	Recall	F1-Score	Accuracy
CNN + Word2Vec	2-class	0.65	0.57	0.60	0.64
CNN + Word2Vec	3-class	0.44	0.43	0.42	0.43
LSTM + Word2Vec	2-class	0.27	0.50	0.35	0.54
LSTM + Word2Vec	3-class	0.11	0.32	0.16	0.32
BILSTM + Word2Vec	2-class	0.66	0.60	0.62	0.68
BILSTM + Word2Vec	3-class	0.39	0.39	0.38	0.39
CNN & BILSTM + Word2Vec	2-class	0.72	0.62	0.67	0.69
CNN & BILSTM	3-class	0.48	0.48	0.46	0.48
CNN & LSTM + Word2Vec	2-class	0.69	0.73	0.71	0.70
CNN & LSTM	3-class	0.45	0.44	0.43	0.44
Cos. Similarity + Sentence Transformer + KNN	2-class	0.822	0.821	0.821	0.821
Cos. Similarity + Sentence Transformer + KNN	3-class	0.52	0.53	0.52	0.53
FFNN + Sentence Transformer	2-class	0.806	0.799	0.801	0.804
FFNN + Sentence Transformer	3-class	0.61	0.60	0.61	0.62

For the 3-class experiment we used the translated data from English Tweets. To compare the machine translation quality, we also translated the same data into six other languages. The result is presented in Figure 6 and in Figure 7.

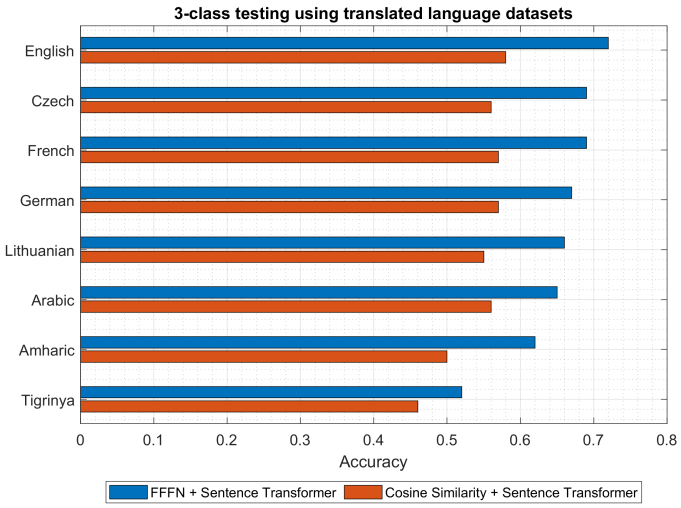

Figure 6. Different language accuracy for FFNN and Cosine Similarity with Sentence Transformer embedding

For comparison, we performed an experiment with 3 different training sets and the same Amharic testing sets. The training sets are:

1. English-language (gold-standard data) training set.
2. Machine-translated Amharic-only training set
3. Machine translated 7 languages + English in no.1 (Tigrinya, Amharic, Arabic, Czech, German, French, Lithuanian) The result of this monolingual, Cross-lingual, and all translated training sets are presented in Figure 7. The confusion matrix for the same sets is also presented in Table 7.

In order to investigate if the translation of the dataset has an impact to change the meaning of the sentence and degrade the quality of the dataset in Amharic we annotated 100 translated Amharic sentences manually (see Table 8) and tested using our first and second best methods with the two sets (1. The original sentiment from the English dataset and translated Amharic Sentences 2. The manually annotated sentiment and translated Amharic Sentences). The comparison of some examples of some English tweets and their translation to Amharic is presented in 9. Note the difference of sentiments between the English and Amharic languages.

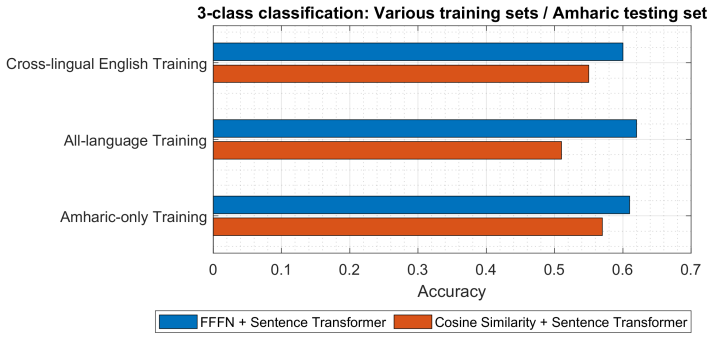

Figure 7. Accuracy of different training set and Amharic Testing sets for 3-class

Table 7. Confusion matrices of Cosine similarity Vs FFNN for cross-lingual, mono-lingual and multi-lingual training.

Training-testing mode	COS + ST + KNN	FFNN + ST
Cross-Lingual (English-Amharic)	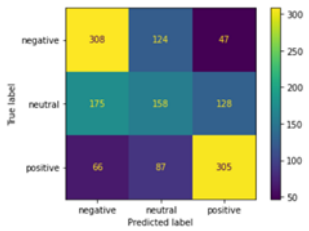	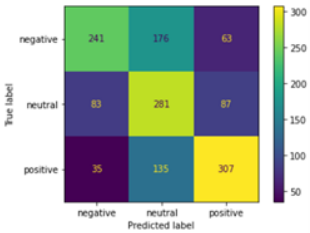
Cross-Lingual (All languages–Amharic)	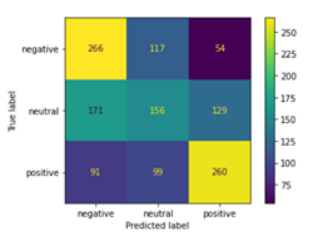	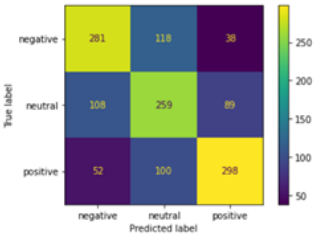
Mono-lingual (Amharic-Amharic)	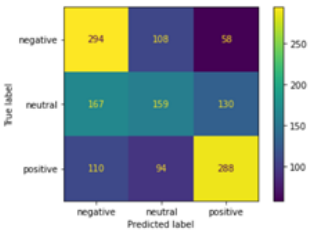	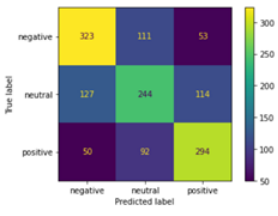

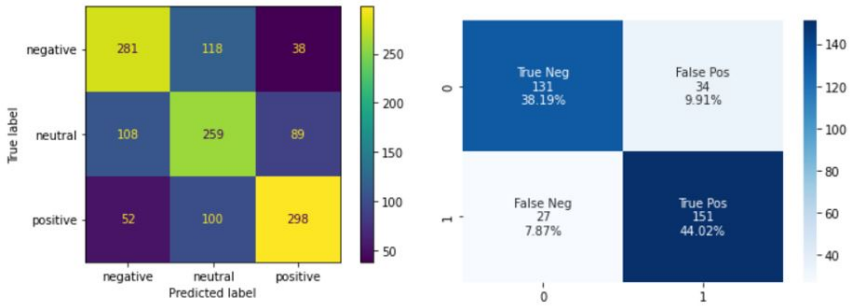

Figure 8. Confusion matrix of best models using Cosine Similarity and FFNN with Sentence Transformer for 2-class and 3-class respectively

Table 8. Accuracy with original and human annotated datasets for Amharic.

Model	Original Sentiment (From Original English Dataset)	Amharic Sentiment (Human annotated when data is translated)
FFNN	0.57	0.55
COS + Sentence Transformer + KNN	0.86	0.63

6. Discussion

We have solved 2-class (positive/negative) and 3-class (positive/negative/neutral) sentiment classification problems for Amharic. We have investigated a wide range of classification approaches: traditional Deep Learning (LSTM, BiLSTM, CNN-LSTM, CNN-BiLSTM applied on top of word vectors); sentence transformer models with FFNN as the classifier or memory-based learning (Cosine + KNN) Due to the scarcity of dataset in Amharic, we added English translated dataset to the original ETD-AM Amharic dataset for the 2-class classification while we used only the translated English dataset for the 3-class. The experimental investigation of different vectorization and classification techniques revealed that the most accurate approach is the sentence transformers with Cosine Similarity + KNN or FFNN for the 2-class or 3-class sentiment analysis problems respectively. The used LaBSE sentence transformer model vectorizes sentences as a whole (without focusing on separate words or their order) compared to Word2Vec word embeddings. There are several reasons why the chosen sentence vectorizer outperforms the word-level vectorizer. Firstly, Amharic has relatively free word order in sentences, therefore sequences of concatenated word embeddings bring more variety to the training data due to which the classifiers cannot make robust generalizations. Secondly, the LaBSE model is the cross-lingual transformer itself as fine-tuned on the parallel corpora of similar sentences for various languages. Despite Amharic is not very highly supported in the LaBSE model (because of less training data for Amharic), the cross-linguality mechanisms within LaBSE can compensate for it.

The use of sentence transformers (that accumulate the entire sentence by mapping it into the fixed-size vector) limits the options for the classifier. From the

Table 9. Difference between sentiment annotations when sentences are translated to Amharic. 0 - positive, 1 - negative, and 2 - neutral.

English (Original Dataset)	Amharic (Translated Dataset)	English Sentiment (Original Dataset)	Amharic Sentiment (Translated Dataset)
Wow first Hugo Chavez and now Fidel Castro Danny Glover Michael Moore Oliver Stone and Sean Penn are running out of heroes	የዎፕስት ሂዩጎ ቻቬዝ እና አሁን ፊደል ካስትሮ ዳኒ ግሎቨር ሚካኤል ሙር ጽላት ኦቨር ኦቨር ሲግናን ፔን ከጀግኖች እየራቁ ነው	0	1
The left has really gone Full retard haven't they	እነርሱም ዘንድ ተውራት እያለች በውስጢ ዘውታሪዎች ሲኾኑ የግራ ጓዶች ናቸው ፡ ፡	0	2
The fact that mike pence think there's a cure for being gay is absolutely the most ridiculous statement I have ever heard in my life	ማይክ ፖምፒዮ ፣ ግብረ ሰዶማዊ መሆን ፈውስ ያስገኛል ብለው የሚያስቡ ሰዎች መኖራቸው በሕይወቴ ውስጥ ከሰማሁት ሁሉ እጅግ የሚያስደስት ነው	0	2
it's free with insurance because of Obamacare which Trump wants to repeal	በኦባማካሬ ምክንያት የመድን ዋስትና በማግኘቱ መለከት ሊደግምለት ይፈልጋል	0	2
Thousands flee Raqqa as Turkish Kurdish tensions threaten antiIS campaign ISIS	በሺዎች የሚቆጠሩ ሰዎች ራቃን ሸሽተው የቱርክ እንቅስቅሴዎች ፀረ አይሲስን ዘመቻ አስጊ ሁኔታ ላይ ሲጥሉ ነበር	1	0
You're also young.	እርስዎም ወጣት ነዎት	2	1
I find myself humming the notes of This Is Us sang a few episodes ago Missing her angelic voice Love the show	የዚህ መጽሐፍ ማስታወሻዎችን እያዋዛሁ ሳለ ከጥቂት ክፍለ ጊዜ በፊት አንድ መላእክታዊ ድምፅዋን ከፍ አድርጋ ትመለከተዋለች	2	1
hi love the tweet got stuff on social security tweet	ሰላም ትዊቱ በማኅበራዊ ደህንነት ትዊተር ላይ ብዙ ነገር ተወጥቷል	2	1

possible options, we have tested the two most promising, but we could not determine the best one as the COS + KNN approach was better with ETD-AM, whereas FFNN with the Tweet_Eval. However, the result is not surprising. The ETD-AM dataset is the gold dataset that is originally prepared in Amharic; whereas Tweet_Eval is only machine translated. The translated dataset contains ambiguities and noise due to inaccurate translations of slang, abbreviations, etc., whereas the original Amharic dataset is clean. However, the COS + KNN method is very sensitive to noise: since for the testing instance, it can select the label of the most similar training instance which is not a good representative of the class or even

misleading. On the contrary, FFNN is a less risky option: instances of each class are generalized therefore some amount of noise makes little impact.

There is a risk that the machine-translated version of the dataset is not suitable for the solving sentiment analysis problem. To investigate the impact of the machine translation (both training and testing split) we ran the control experiment on the original Tweet_Eval English dataset and the same dataset machine-translated into 7 different languages (see Figure 7). The top line, i.e., the accuracy achieved with the original English dataset is 72%. The machine translation quality and the less support in the LaBSE model are the factors that degrade the performance (with a 3% of accuracy drop for Czech and French; 10% for Amharic, and even 20% for Tigrinya). The results are not surprising, it perfectly correlates with how well these languages are supported. For the less supported languages, the results are expected to be lower, but the sentiment analysis task is still solvable.

In additional experiments we eliminated the machine translation step from the training data preparations by training the model on the original English dataset and testing on Amharic. Thus, in these cross-lingual experiments, we relied on the robustness of the LaBSE model and its inner mechanisms to capture the semantics between languages. It better worked with the FFNN classifier, but the accuracy of 60% was still 1% lower compared to the monolingual model (trained and tested only on Amharic). In the second experiment, we used the training data of all 8 languages (including Amharic); the trained model was again tested on Amharic. This time it achieved 62% which is only 1% higher compared to the monolingual setting. These results allow us to conclude that there is no big difference in which approach to choose, but it opens more options. The machine translation of the training dataset is not necessary: similar results can be achieved with the cross-lingual models. However, if the usage of the machine translation tool is still considered, it is worth translating the training dataset into better-supported languages (into which translating we can expect better quality and better support in the sentence transformer models).

7. Conclusion

Sentiment analysis is a widely recognized NLP task that assigns sentiment labels, including positive, negative, and neutral (sometimes mixed) to texts. Its successful implementation can make significant contributions to resolving several societal issues [47]. However, even for resource-rich languages like English, which possess extensive data resources and accurate vectorization models, sentiment analysis remains a relevant and challenging task due to issues such as sarcasm, hidden meaning, and domain-specific language. In contrast, our study focuses on the sentiment analysis problem for a resource-scarce language, using Amharic as a main example.

We formulated the sentiment analysis problem as the supervised 2-class (positive/negative) and 3-class (positive/negative/neutral) classification problem, therefore it requires the training data. We experimented with ETD-AM and Tweet_Eval datasets originally in Amharic and English, respectively.

During our experimentation, we tested a wide range of techniques, including the latest advances such as sentence transformer models, enabling us to attain higher levels of accuracy. The best accuracy of 82.2% on the ETD-AM dataset was achieved using the sentence transformer model in combination with the COS + KNN classifier, which significantly surpassed the baseline. The sentiment analysis problem with the ETD-AM dataset was also solved in [60], but due to different experimental conditions, our results are not directly comparable.

We conducted experiments on the Tweet_Eval dataset under monolingual, cross-lingual, and multi-lingual settings. For the monolingual experiments, both the training and testing splits were machine-translated into Amharic. In cross-lingual experiments, we used English texts for model training and machine-translated Amharic texts for model testing. In the multi-lingual experiments, we used a mix of machine-translated texts in eight languages (including Amharic) for the model training, but only Amharic for the model testing. Across all the monolingual, cross-lingual, and multi-lingual settings, the FFNN classifier applied on top of sentence transformers performed the best, achieving the accuracy of 61%, 60%, and 62%, respectively. However, neither of these settings was significantly superior to the others. Through the control experiments that involved the machine-translated Tweet_Eval dataset texts (8 different languages), we observed the correlation between the language support (machine translation quality, coverage level in the sentence transformer model) and the sentiment analysis accuracy.

Despite achieving lower accuracy for Amharic compared to English, our results are still significant and state-of-the-art for Amharic sentiment analysis. Besides, our research is interesting as it addresses the sentiment analysis problem for a resource-scarce language and determines the most effective solutions. These findings can also be applied to other low-resource languages facing similar challenges. We consider this to be an important research direction and we intend to continue working on this topic in future research.

References

[1] Abdalla, M., Hirst, G.: Cross-lingual sentiment analysis without (good) translation. In: Eighth International Joint Conference on Natural Language Processing (Volume 1). pp. 506–515 (2017)

[2] Al-Shabi, A., Adel, A., Omar, N., Al-Moslmi, T.: Cross-lingual sentiment classification from english to arabic using machine translation. International Journal of Advanced Computer Science and Applications 8(12) (2017)

[3] Aldjanabi, W., Dahou, A., Al-Qaness, M.A.A., Elaziz, M.A., Helmi, A.M., Damaševičius, R.: Arabic offensive and hate speech detection using a cross-corpora multi-task learning model. Informatics 8(4) (2021)

[4] Alemu, Y.: Deep learning approach for amharic sentiment analysis (2018)

[5] Alhaj, Y.A., Dahou, A., Al-Qaness, M.A.A., Abualigah, L., Abbasi, A.A., Almaweri, N.A.O., Elaziz, M.A., Damaševičius, R.: A novel text classification technique using improved particle swarm optimization: A case study of arabic language. Future Internet 14(7) (2022)

[6] Arun, K., Srinagesh, A.: Multilingual twitter sentiment analysis using machine learning. International Journal of Electrical and Computer Engineering (IJECE) 10(6), 5992 (Dec 2020)
[7] Babić, K., Petrović, M., Beliga, S., Martinčić-Ipšić, S., Matešić, M., Meštrović, A.: Characterisation of covid-19-related tweets in the croatian language: Framework based on the cro-cov-csebert model. Applied Sciences 11(21) (2021)
[8] Balaguer, P., Teixidó, I., Vilaplana, J., Mateo, J., Rius, J., Solsona, F.: CatSent: a catalan sentiment analysis website. Multimedia Tools and Applications 78(19), 28137–28155 (Jul 2019)
[9] Barbieri, F., Camacho-Collados, J., Espinosa Anke, L., Neves, L.: TweetEval: Unified benchmark and comparative evaluation for tweet classification. In: Findings of the Association for Computational Linguistics: EMNLP 2020. pp. 1644–1650. Association for Computational Linguistics, Online (Nov 2020)
[10] Barnes, J., Oberlaender, L., Troiano, E., Kutuzov, A., Buchmann, J., Agerri, R., Øvrelid, L., Velldal, E.: SemEval 2022 task 10: Structured sentiment analysis. In: 16th International Workshop on Semantic Evaluation (SemEval-2022). pp. 1280–1295. Association for Computational Linguistics (Jul 2022)
[11] Bel, N., Koster, C.H.A., Villegas, M.: Cross-lingual text categorization. In: Koch, T., Sølvberg, I.T. (eds.) Research and Advanced Technology for Digital Libraries. pp. 126–139. Springer Berlin Heidelberg, Berlin, Heidelberg (2003)
[12] Chatterjee, A., Narahari, K.N., Joshi, M., Agrawal, P.: SemEval-2019 task 3: EmoContext contextual emotion detection in text. In: 13th International Workshop on Semantic Evaluation. pp. 39–48 (2019)
[13] Choi, M., Shin, J., Kim, H.: Robust feature extraction method for automatic sentiment classification of erroneous online customer reviews. International Information Institute (Tokyo). Information 16(10), 7637 (2013)
[14] Dang, C.N., Moreno-García, M.N., la Prieta, F.D.: Hybrid deep learning models for sentiment analysis. Complexity 2021, 1–16 (Aug 2021)
[15] Deng, L., Yu, D.: Deep learning: Methods and applications. Found. Trends Signal Process. 7(3–4), 197–387 (jun 2014)
[16] Dhiman, A., Toshniwal, D.: Ai-based twitter framework for assessing the involvement of government schemes in electoral campaigns. Expert Systems with Applications 203 (2022)
[17] Dimova, G.: Who criticizes the government in the media? the symbolic power model. Observatorio (OBS*) 6(1) (Mar 2012)
[18] Dong, X., de Melo, G.: A robust self-learning framework for cross-lingual text classification. In: 2019 Conference on Empirical Methods in Natural Language Processing and the 9th International Joint Conference on Natural Language Processing (EMNLP-IJCNLP). pp. 6306–6310. Association for Computational Linguistics (2019)
[19] Draskovic, D., Zecevic, D., Nikolic, B.: Development of a multilingual model for machine sentiment analysis in the serbian language. Mathematics 10(18) (2022)
[20] Feng, F., Yang, Y., Cer, D., Arivazhagan, N., Wang, W.: Language-agnostic BERT sentence embedding. In: 60th Annual Meeting of the Association for Computational Linguistics (Volume 1). pp. 878–891. Association for Computational Linguistics (2022)

[21] Gereme, F., Zhu, W., Ayall, T., Alemu, D.: Combating fake news in "low-resource" languages: Amharic fake news detection accompanied by resource crafting. Information 12(1), 20 (2021)
[22] Gunasekar, M., Thilagamani, S.: Improved feature representation using collaborative network for cross-domain sentiment analysis. Information Technology and Control 52(1), 100–110 (2023)
[23] Kant, G., Wiebelt, L., Weisser, C., Kis-Katos, K., Luber, M., Säfken, B.: An iterative topic model filtering framework for short and noisy user-generated data: analyzing conspiracy theories on twitter. International Journal of Data Science and Analytics (2022)
[24] Kapočiūtė-Dzikienė, J., Damaševičius, R., Woźniak, M.: Sentiment analysis of lithuanian texts using traditional and deep learning approaches. Computers 8(1) (2019)
[25] Karayiğit, H., Akdagli, A., Aci, . .: Homophobic and hate speech detection using multilingual-bert model on turkish social media. Information Technology and Control 51(2), 356–375 (2022)
[26] Karayiğit, H., Akdagli, A., Acı, . .: Bert-based transfer learning model for covid-19 sentiment analysis on turkish instagram comments. Information Technology and Control 51(3), 409–428 (2022)
[27] KazAnova, . .: Sentiment140 dataset with 1.6 million tweets (Sep 2017), https://www.kaggle.com/kazanova/sentiment140
[28] Keung, P., Lu, Y., Bhardwaj, V.: Adversarial learning with contextual embeddings for zero-resource cross-lingual classification and NER. In: 2019 Conference on Empirical Methods in Natural Language Processing and the 9th International Joint Conference on Natural Language Processing (EMNLP-IJCNLP). pp. 1355–1360. Association for Computational Linguistics (Nov 2019)
[29] Khalid, M., Ashraf, I., Mehmood, A., Ullah, S., Ahmad, M., Choi, G.S.: Gbsvm: Sentiment classification from unstructured reviews using ensemble classifier. Applied Sciences 10(8) (2020)
[30] Khan, L., Amjad, A., Ashraf, N., Chang, H..: Multi-class sentiment analysis of urdu text using multilingual bert. Scientific Reports 12(1) (2022)
[31] Khan, L., Amjad, A., Afaq, K.M., Chang, H.T.: Deep sentiment analysis using CNN-LSTM architecture of english and roman urdu text shared in social media. Applied Sciences 12(5), 2694 (Mar 2022)
[32] Lee, E., Rustam, F., Washington, P.B., Barakaz, F.E., Aljedaani, W., Ashraf, I.: Racism detection by analyzing differential opinions through sentiment analysis of tweets using stacked ensemble gcr-nn model. IEEE Access 10, 9717–9728 (2022)
[33] Liu, X., He, J., Liu, M., Yin, Z., Yin, L., Zheng, W.: A scenario-generic neural machine translation data augmentation method. Electronics 12(10), 2320 (2023)
[34] Liu, X., Shi, T., Zhou, G., Liu, M., Yin, Z., Yin, L., Zheng, W.: Emotion classification for short texts: an improved multi-label method. Humanities and Social Sciences Communications 10(1) (2023)
[35] Ljajić, A., Marovac, U.: Improving sentiment analysis for twitter data by handling negation rules in the serbian language. Computer Science and Information Systems 16(1), 289–311 (2019)

[36] Maas, A.L., Daly, R.E., Pham, P.T., Huang, D., Ng, A.Y., Potts, C.: Learning word vectors for sentiment analysis. In: 49th Annual Meeting of the Association for Computational Linguistics: Human Language Technologies. pp. 142–150. Association for Computational Linguistics (Jun 2011)

[37] Meta AI Research: Sentiment analysis, `https://paperswithcode.com/task/sentiment-analysis`

[38] Mutanov, G., Karyukin, V., Mamykova, Z.: Multi-class sentiment analysis of social media data with machine learning algorithms. Computers, Materials and Continua 69(1), 913–930 (2021)

[39] Nandwani, P., Verma, R.: A review on sentiment analysis and emotion detection from text. Social Network Analysis and Mining 11(1) (Aug 2021)

[40] Nassif, A.B., Elnagar, A., Shahin, I., Henno, S.: Deep learning for arabic subjective sentiment analysis: Challenges and research opportunities. Applied Soft Computing 98, 106836 (Jan 2021)

[41] Neshir, G., Atnafu, S., Rauber, A.: Bert fine-tuning for amharic sentiment classification. In: Workshop RESOURCEFUL Co-Located with the Eighth Swedish Language Technology Conference (SLTC), University of Gothenburg, Gothenburg, Sweden. vol. 25 (2020)

[42] Neshir, G., Rauber, A., Atnafu, S.: Meta-learner for amharic sentiment classification. Applied Sciences 11(18) (2021)

[43] Ombabi, A.H., Ouarda, W., Alimi, A.M.: Deep learning CNN–LSTM framework for arabic sentiment analysis using textual information shared in social networks. Social Network Analysis and Mining 10(1) (Jul 2020)

[44] Patwa, P., Aguilar, G., Kar, S., Pandey, S., PYKL, S., Gambäck, B., Chakraborty, T., Solorio, T., Das, A.: SemEval-2020 task 9: Overview of sentiment analysis of code-mixed tweets. In: Fourteenth Workshop on Semantic Evaluation. pp. 774–790. International Committee for Computational Linguistics, Barcelona (online) (Dec 2020)

[45] Philemon, W., Mulugeta, W.: A machine learning approach to multi-scale sentiment analysis of amharic online posts. HiLCoE Journal of Computer Science and Technology 2(2), 8 (2014)

[46] Reimers, N., Gurevych, I.: Sentence-BERT: Sentence embeddings using Siamese BERT-networks. In: 2019 Conference on Empirical Methods in Natural Language Processing and the 9th International Joint Conference on Natural Language Processing (EMNLP-IJCNLP). pp. 3982–3992. Association for Computational Linguistics (Nov 2019)

[47] Roth, S.: The great reset. restratification for lives, livelihoods, and the planet. Technological Forecasting and Social Change 166, 120636 (May 2021)

[48] Sagnika, S., , Pattanaik, A., Mishra, B.S.P., Meher, S.K.: A review on multilingual sentiment analysis by machine learning methods. Journal of Engineering Science and Technology Review 13(2), 154–166 (Apr 2020)

[49] Sarker, I.H.: Machine learning: Algorithms, real-world applications and research directions. SN Computer Science 2(3) (Mar 2021)

[50] Shambour, Q.Y., Abu-Shareha, A.A., Abualhaj, M.M.: A hotel recommender system based on multi-criteria collaborative filtering. Information Technology and Control 51(2), 390–402 (2022)

[51] Shanmugavadivel, K., Sathishkumar, V.E., Raja, S., Lingaiah, T.B., Neelakandan, S., Subramanian, M.: Deep learning based sentiment analysis and offensive language identification on multilingual code-mixed data. Scientific Reports 12(1) (2022)

[52] Syllaidopoulos, I., Skraparlis, A., Ntalianis, K.: Evaluating corporate online reputation through sentiment analysis of news articles: Threats, maliciousness and real opinions. International Journal of Cultural Heritage 7, 8–22 (2022)

[53] Tesfagergish, S.G., Kapočiūtė-Dzikienė, J., Damaševičius, R.: Zero-shot emotion detection for semi-supervised sentiment analysis using sentence transformers and ensemble learning. Applied Sciences 12(17) (2022)

[54] Tesfagergish, S., Robertas Damaševičius, R., Kapočiūtė-Dzikienė, J.: Deep learning-based sentiment classification of social network texts in amharic language. In: ICT Innovations 2022. Reshaping the Future Towards a New Normal. Springer International Publishing (2023)

[55] Tuters, M., Willaert, T.: Deep state phobia: Narrative convergence in coronavirus conspiracism on instagram. Convergence: The International Journal of Research into New Media Technologies 28(4), 1214–1238 (Aug 2022)

[56] Vergani, M., Martinez Arranz, A., Scrivens, R., Orellana, L.: Hate speech in a telegram conspiracy channel during the first year of the covid-19 pandemic. Social Media and Society 8(4) (2022)

[57] Wadud, M.A.H., Mridha, M.F., Shin, J., Nur, K., Saha, A.K.: Deep-bert: Transfer learning for classifying multilingual offensive texts on social media. Computer Systems Science and Engineering 44(2), 1775–1791 (2023)

[58] Xu, X., Zhu, G., Wu, H., Zhang, S., Li, K..: See-3d: Sentiment-driven emotion-cause pair extraction based on 3d-cnn. Computer Science and Information Systems 29(1), 77–93 (2023)

[59] Xu, Y., Cao, H., Du, W., Wang, W.: A survey of cross-lingual sentiment analysis: Methodologies, models and evaluations. Data Science and Engineering 7(3), 279–299 (Jun 2022)

[60] Yimam, S.M., Alemayehu, H.M., Ayele, A., Biemann, C.: Exploring Amharic sentiment analysis from social media texts: Building annotation tools and classification models. In: 28th International Conference on Computational Linguistics. pp. 1048–1060. International Committee on Computational Linguistics, Barcelona, Spain (Online) (Dec 2020)

[61] Yimam, S.M., Ayele, A.A., Biemann, C.: Analysis of the ethiopic twitter dataset for abusive speech in amharic (2019)

[62] Zhang, S., Zhao, T., Wu, H., Zhu, G., Li, K.: Ts-gcn: Aspect-level sentiment classification model for consumer reviews. Computer Science and Information Systems 29(1), 117–136 (2023)

[63] Zinko, R., Patrick, A., Furner, C.P., Gaines, S., Kim, M.D., Negri, M., Orellana, E., Torres, S., Villarreal, C.: Responding to negative electronic word of mouth to improve purchase intention. Journal of Theoretical and Applied Electronic Commerce Research 16(6), 1945–1959 (2021)

[64] Zitouni, I.: Natural Language Processing of Semitic Languages. Springer (2014)

Senait Gebremichael Tesfagergish has received hre MSc from Vytautas Magnus University, Kaunas, Lithuania. Currently she is Ph.D. Student at Kaunas University of Technology, Kaunas, Lithuania. Her topics of interest are Natural language processing, Deep Learning and Artificial intelligence solutions. She is an author of 7 research papers.

Robertas Damaševičius received the Ph.D. degree in informatics engineering from the Kaunas University of Technology, Lithuania, in 2005. He is currently a Professor with the Department of Applied Informatics, Vytautas Magnus University, Lithuania, and Department of Software Engineering, Kaunas University of Technology. He is the author of more than 500 articles and a monograph published by Springer. His research interests include sustainable software engineering, human–computer interfaces, assisted living, and AI explainability. He is also the Editor-in-Chief of the Information Technology and Control journal.

Jurgita Kapočiūtė-Dzikienė is a full professor at Vytautas Magnus University and a language technology specialist at JSC Tilde IT. She has been working in the field of AI since 2005 and her main research focuses on language technologies. Despite her hobby being methodologies/solutions for her native Lithuanian language, she also enjoys working with other languages, especially if it is related to multilingualism/cross-linguality problem-solving. Jurgita has worked on 20 projects. She is an editorial board/program committee member of several international journals/conferences and a co-author of 60 scientific publications.

Received: January 15, 2023; Accepted: June 25, 2023.

Computer Science and Information Systems 20(4):1483–1501 https://doi.org/10.2298/CSIS230418059H

Heart Sounds Classification using Adaptive Wavelet Threshold and 1D LDCNN

Jianqiang Hu[1,3,⋆], Qingli Hu[2], and Mingfeng Liang[1,3]

[1] School of Computer and Information Engineering, Xiamen University of Technology, 361024 Xiamen, P. R. China
hujianqiang@tsinghua.org.cn
[2] iFlytek Research, iFlytek Co. Ltd., 230088 Hefei, P.R. China
huqingli2014@outlook.com
[3] Key Laboratory of Internet-of-Things Applications of Fujian Province, Xiamen University of Technology, 361024 Xiamen, P.R. China
lmfanny115@hotmail.com

Abstract. Heart sounds classification plays an important role in cardiovascular disease detection. Currently, deep learning methods for heart sound classification with heavy parameters consumption cannot be deployed in environments with limited memory and computational budgets. Besides, de-noising of heart sound signals (HSSs) can affect accuracy of heart sound classification, because erroneous removal of meaningful components may lead to heart sound distortion. In this paper, an automated heart sound classification method using adaptive wavelet threshold and 1D LDCNN (One-dimensional Lightweight Deep Convolutional Neural Network) is proposed. In this method, we exploit WT (Wavelet Transform) with an adaptive threshold to de-noise heart sound signals (HSSs). Furthermore, we utilize 1D LDCNN to realize automatic feature extraction and classification for de-noised heart sounds. Experiments on PhysioNet/CinC 2016 show that our proposed method achieves the superior classification results and excels in consumption of parameter comparing to state-of-the-art methods.

Keywords: heart sounds classification, adaptive wavelet threshold, lightweight deep convolutional neural network.

1. Introduction

Population aging is the trend of population development in the world. According to China Cardiovascular Health Index (2019), the mortality rate of residents from cardiovascular diseases (CVD) accounts for all disease mortality more than 85% of the total, and the trend is increasing [28]. Most seriously, heart disease is one of the biggest challenges of cardiovascular disease in China, and there currently are 11 million coronary heart diseases, 5 million pulmonary heart diseases, 4.5 million heart failures, 2.5 million rheumatic heart diseases, and 2 million congenital heart diseases. Heart sounds contain a large number of biomedical signals of cardiac activity. Heart sound classification is one of the most economical and effective non-invasive diagnostic methods for various cardiac abnormalities,

⋆ Corresponding Author

and is also of great significance for primary screening and early treatment of cardiovascular diseases.

Heart sounds classification based on manual auscultation has greater uncertainty and delay in diagnosis, and it is difficult to meet the increasing patients. Since hospitals, community hospitals, nursing centers and other places are crowded with people, manual auscultation is easily affected by many factors such as the surrounding environment, the quality of the stethoscope, and the doctor's experience. Currently, digital stethoscopes based on IoT (Internet of Things) are developing rapidly. Three products of digital stethoscopes are currently available in the market: Eko Core [8], Thinklabs[35] and Hefei Huake Electronic HKY-06C [15] . Digital stethoscopes are rapidly entering family healthcare monitoring. However, automatic heart sounds classification is insufficient in terms of objectivity and effectiveness, which restricts the popularization of digital stethoscopes. Currently, automatic heart sounds classification is developing in the direction of high accuracy, lightweight deployment, and real-time response, so as to effectively support family health monitoring and clinical applications, which is becoming a research hot issue.

In general, signal preprocessing, feature extraction and classification are the mainly steps of heart sound signals (HSSs) diagnosis.

(i) In the first step, signal pre-processing includes noise removal and signal segmentation. Empirical Mode Decomposition (EMD) [1], STFT (short-time Fourier Transform)[40], Hidden Markov Model [19] and Hibernate transform, wavelet threshold de-noising method [3] were usually used to measure cardiac cycle durations and de-noise the signals. The above methods are mainly unsupervised heart sound de-noising algorithms, which needs to manually set thresholding parameters and decomposition levels. Signal segmentation plays a crucial role for feature extraction and classification. Heart sound signals is segmented into series of fundamental heart sounds (FHSs), and each FHS includes a number of the first (S1), the second (S2), systolic and diastolic hear sounds. For example, an event detection approach with deep recurrent neural networks (DRNNs) [24] was proposed for heart sound segmentation, i.e. the detection of the state-sequence first heart sound (S1)-systole-second heart sound (S2)-diastole. In order to accurately segment PCG signals, most of PCG segmentation algorithms need synchronous ECG (Electrocardiograph) as reference signals. However, it is not convenient to collect heart sounds and their reference ECG signals at the same time and ensure their synchronization in practice.

(ii) In the second step, extracted features can be divided into three major types: time-domain, frequency-domain and time-frequency domain-based features. Generally, it is relatively easy to extract the time-domain features or frequency-domain domain, but it is difficult to calculate the features in the time-frequency domain, because these features are difficult to represent discriminative features. Extracted features can also be divided into handcrafted features and deep features. Hand-crafted feature refers to extracting the discriminative features from HHSs, such as MFCC (Mel Frequency Cepstrum Coefficient), LPC (Linear Prediction Coefficient), and LPCC (Linear Prediction Cepstrum Coefficient) features. For example, STFT (Short-time Fourier Transform), Wavelet transform and S-transform method can be adopted to transform and represent signals in different time-frequency-domain. Extraction of handcrafted features still is a challenging task because of the non-stationary and diversity of heart sound signals. Besides, it is easy to be subjectively affected and produces actual deviations. Deep feature refers to extract features from HSSs through specific model which is obtained by learning and training. Owing to

the strong feature representation power of deep learning technologies, deep learning has recently been used for exploratory applications in heart sounds, such as Depth Recurrent Neural network (DRNN), ShuffleNet [41], and 1D CNN (Convolutional Neural Network) [39].

(iii) In the last step, the classifier is trained over the extracted features in order to the prediction results of each heart sound signal. Various classifiers, such as Artificial Neural Network (ANN)[7], twin Support Vector Machine(tSVM)[20], and improved duration-dependent HMM, have been used to classify heart sounds. Feature extraction and classification are inseparable in deep learning-based heart sound classification. Heart sounds classification based deep convolution neural network (DCNN), such as 1D CNN , 1D DCNN [32], DS-CNN [13] , require a large scale of annotated data. Furthermore, DCNN model with heavily parameters consumption relies on high-performance GPU and parallel processing technology.

To sum up, the main challenges of heart sounds classification under are as follows: (i) The quality of heart sound is affected by the complex noise of internal physiological changes and external environmental changes. Besides, de-noising algorithms for HSSs can erroneously remove meaningful heart sound components due to manual setting of parameters, and even lead to heart sound distortion. (ii) Most of heart sound segmentation algorithms ideally assume that heart sounds are collected under strictly constrained environment. In practice, it is difficult to capture the state sequence S1-systole-S2-diastole, resulting in insufficient segmentation accuracy. (iii) The size of deep neural networks is not suitable for deployment on digital stethoscopes with strict constraints on memory and computational budget.

In this paper, we develop an automated heart sound classification method using adaptive wavelet threshold and 1D LDCNN (one-dimensional Lightweight Deep Convolutional Neural Network) with low parameters and high accuracy. In this method, wavelet transform with an adaptive threshold is used to de-noise heart sound signals. The denoised heart sound is segmented by a 3s sliding window and then fed into 1D LDCNN for automatic feature extraction and classification. Compared with several related work in heart sound classification methods, the proposed 1D LDCNN obtains the better classification performances with an accuracy of 97.92%, a sensitivity of 98.20%, an F1-score of 0.9859 and the lowest parameters consumption of 0.02M.

The key contributions of our work are as follows:

(i) We propose a wavelet transform with an adaptive threshold which de-noises the heart sound signal and avoids filtering out the approximate components of heart sound in the process of wavelet transform decompose.

(ii) We build a new 1D LDCNN which includes tem blocks, dense blocks and transition blocks. Among them, a point-wise convolution and a depth-wise separable convolution are used to effectively reduce the amount of parameters in dense blocks. The channel attention mechanism is introduced to recalibrate feature maps and further increase representation power in transition blocks.

(iii) Experiments demonstrate the superiorities of the proposed architecture with other state-of-the art CNN-based methods in terms of classification performance and parameters consumption. Besides, a heart sound acquisition system is implemented, which includes acquisition module of heart sounds and a mobile application. It deploys the proposed architecture to achieve automated heart sounds classification.

This paper is framed in different sections. Section 2 introduces related works of automatic heart sound classification. Section 3 proposes the framework of automatic heart sound classification and discusses the architecture of 1D LDCNN. Section 4 explains experimental results and deploys 1D LDCNN on mobile system. In Section 5, we draw the conclusions and discuss the future work.

2. Related Works

HSSs have periodicity, randomness and non-stationarity, and many of their features are recessive. Due to strong feature representation ability, deep learning is suitable for HSSs. Most of research works use deep neural networks and end-to-end architecture to learn and classify heart sound signals. Related works are discussed as follows:

(i) Deep neural networks are only used for heart sound segmentation. In response to the problem of insufficient utilization of cardiac cycle duration information, a Duration Long-short Term Memory network [5] was exploited to address heart sound segmentation by incorporating the duration features. Ma et al. [23] proposed a diagnosis method for congenital heart disease-related pulmonary arterial hypertension. This method first utilized a double-threshold adaptive method to segment heart sound. And then, deep learning features and time-frequency domain features were combined to form the fusion feature. Finally, XGBoost was used to classify heart sounds. Chen et al.[3] proposed a method for heart sounds classification that combined an improved frequency slice wavelet transform with CNN. This method converted 1D cardiac signal into a 2D time-frequency picture, and selected appropriate classifiers by SampEn (sample entropy) threshold to determine whether the heart sound recordings is normal. Besides, Humayun et al.[16] proposed a classification framework, consisting of a CNN with 1D CNN time-convolutional layers. In addition, representation learning was utilized to generate features. Finally, SVM and LDA (linear discriminant analysis) classifiers were exploited to classify heart sounds. Similarly, Li et al.[21] utilized convolution module to extract frequency-domain features and recurrent module to extract the time-domain features, and finally implemented heart sounds classification based on the fusion features.

(ii) Deep neural networks are only used for heart sound classification. In[26] Markov switching autoregressive model (MSAR) was exploited to segment heart sound and further a continuous-density HMM with Gaussian mixtures was utilized to classify heart sounds. Oh et al. [27] exploited deep WaveNet model to classify heart sounds, which includes fives Heart valve diseases (HVD) as follows: mitral valve prolapse (MVP), mitral stenosis (MS), mitral regurgitation (MR) and aortic stenosis (AS), normal (N). In addition, Ismail et al. [17] introduced a hybrid network-based heart sounds classification using transfer learning.

(iii) Deep neural networks are used for feature extraction and classification with end-to-end architecture. Xiao et al. [39] proposed an automatic heart sound classification method using deep learning, which includes pre-processing, heart sound classification of patches using CNN with attention mechanism, and majority voting for heart sounds classification. Raza et al.[29] depended on band filter removed the noise from HSSs, and further exploited RNN that is based on LSTM, Dropout, Dense and Softmax layer to classify heart sound recordings. Due to the low SNR, 497 features were extracted and then fed these features into the CNN, performing heart sounds classification. Ghosh et al. [12]

proposed a time-frequency-domain (TFD) deep neural network approach for automated FHSA detection using PCG signals. Xiang el al.[37] proposed a heart sound classification using two-dimensional features, which transferred heart sound classification into image classification. An end-to-end Le-LWTNe, which embedded the trainable CNN into the lifting wavelet transform (LWT), is proposed for automatic abnormality detection of heart sounds [11]. Wang et al. [36] proposed an automatic approach for heart failure typing based on heart sounds and one-dimensional CNN (1D CNN). Guo et al. [13] developed a dual-stream convolutional Neural Networks (DS-CNN) to detect abnormal from heart sound recordings.

(iv) Deep neural networks are used for feature extraction and classification (not end-to-end architecture). Shukla et al. [33] proposed an efficient method for automatic segmentation detection. Furthermore, a supervised ANN model is exploited to detect S1-S2 and non-S1-S2 segments of the cardiac cycle. Finally, a CNN model is used to automatically diagnose the heart diseases based on heart sounds. Rubin et al.[32] captures the time-frequency distribution of signal energy and classifies normal and abnormal heat maps using DCNN. A combination of WT and WPT energy-based features followed by a deep recurrent neural network (RNN) model was proposed for recognizing heart sounds [18]. Ren et al. [30] proposed deep attention-based neural networks for heart sounds classification, which exploited attention mechanisms to a CNN and an RNN to capture feature and context information.

Compared to the above methods, we can highlight the contributions of our proposed method. (i) The use of wavelet transform with an adaptive threshold is more benefit to remove noise and enhance the quality of HSSs than the other methods. In practice, it is not sufficient to only use the frequency domain filtering method, such as elliptic filter [6] and band filter, and wavelet threshold to remove the noise from HSSs. This is because that the main frequency of heart sound signal overlaps with the main frequency of the noise signal[4]. Besides, the parameters of wavelet transform in this paper are adaptive thresholds for their superior effect in the de-noising of HSSs. (ii) Deep learning methods for heart sounds classification, such as [21] [20], etc., are getting deeper and wider which bring a mass of trainable parameters and need to consume a lot of memory and computing resources. 1D LDCNN is a kind of lightweight models, which is more conducive to large-scale application of heart sounds classification.

3. Proposed Framework

In this section, we will give a detailed description about our proposed method as follows: HSSs pre-processing phase, de-noising the heart sound signal based on wavelet transform with an adaptive threshold; HSSs classification phase recognizing normal and abnormal heart sounds based on 1D LDCNN which constitutes stem block, three simplified dense blocks and transition blocks, and Softmax layer. A GAP (Global Average Pool) layer is followed by FC (Fully Connected Layer) and a Softmax. FC is usually used before the classification layer is replaced with a GAP to obtain global information about the feature map and avoid overfitting. The method increases the types of distinguishable heart sounds and improves the performance without affecting the accuracy while reducing its computational complexity.

3.1. Pre-processing of HSSs

Heart sounds have the following characteristics: (i) HSSs have periodicity, randomness and non-stationarity; (ii) HSS has obvious common characteristics and weak individual characteristics; (iii) The important information of heart sound is concentrated in the frequency of 25Hz-400Hz; (iv) The primary murmurs of heart sound span between 30Hz and 700Hz. Heart sound signals often contain noise such as lung sound and internal body noise. Therefore, effective filtration is of critical important to enhance the heart sounds signal by reducing the influence of background noise and removing spike noise. In this paper, first, the Butterworth bandpass filter is used to filter out frequencies above 400Hz and frequencies below 25Hz of heart sound signal. Butterworth bandpass filter can eliminate most of the noise signal, and reduce the calculations of subsequence wavelet transform. Then, because the main frequency of heart sound overlaps with the main frequency of the noise signal, wavelet transform is used for secondary noise eliminated. When wavelet transform decomposes HSSs, only the low-frequency part is further decomposed, and the high-frequency part, that is, the detailed part of the signal, is no longer decomposed [34]. Wavelet coefficients with relatively small amplitude values are mostly noise, while the wavelet coefficients are relatively large for the effective signal of heart sounds [42]. The threshold is set on the basis of this property. The wavelet coefficients below the selected threshold are zeroed or smoothed by threshold quantization processing to suppress the influence of high-frequency noise, while the coefficients not below the selected threshold are retained.

In general, the hard and soft threshold function method was proposed as follows: Mini-max threshold, Sqtwlolg threshold, and Rigrsure threshold[25]. Mini-max threshold is directly related to the length of HSSs. Sqtwlolg threshold is a hard threshold which the reconstructed signal after de-noising processing is very rough. When the heart sound signals are too long, the Mini-max threshold is too larger to filter out the most of the wavelet coefficients and reconstructed signal will be easily lose useful signal. Rigrsure threshold relies on Stein's unbiased risk estimate to obtain adaptive threshold of wavelet coefficients of decomposed layers. Rigrsure threshold is continuous, we first calculate the square value of each element in the signal S, and then sort from the largest to the smallest as a new sequence $M = \{M_1, M_2, \cdots, M_L\}$,and finally calculate the risk estimate for each element in M according to formula (1). Let M_k be square root of the smallest element k_0 in the risk estimate, and λ is used as the threshold.

$$R_k = \frac{L - 2k + \sum_{i=1}^{k} M_k + (L-k)\, M_{L-k}}{L} \qquad k = 1, 2, ..., L \tag{1}$$

$$\lambda = \sqrt{\sigma M_{k_0}} \tag{2}$$

Where L is the length of the signal, and k represents the index in corresponding to the element currently calculated.

Stein's unbiased risk estimate mainly calculates the threshold based on the variance of the high-frequency coefficients decomposed in the first layer, and then uses the threshold to process the wavelet coefficients of other layers. It does not take into account the problem of high-frequency component reduction and results in removing useful heart sound components. Wavelet decomposition is performed in accordance with the high and low

frequency coefficients. For this reason, this paper introduces adaptive factor of the number of decomposition layers, and its formula is as follows:

$$\lambda_j = \frac{\lambda}{\alpha_j} \tag{3}$$

$$\alpha_j = \ln\left(j + \frac{j}{J}\right) \tag{4}$$

where j is the threshold of the $j-th$ layer, J is the number of decomposition layers, α_j denotes the adaptive factor, and λ_j is related to the number of layers of wavelet decomposition. The threshold increases and decreases with the number of layers. When we calculate the high-frequency coefficient, a larger threshold can be obtained. When we calculate the low-frequency coefficient, a slight smaller threshold can be obtained. The detailed algorithm of de-noising is shown as Algorithm 1.

Algorithm 1: Heart sound signals de-noising based on wavelet transform with an adaptive threshold

Input: Heart sound signals
Output: The reconstructed heart sound signal

1. Using the Butterworth bandpass filter to filter out frequencies above 400Hz and frequencies below 25Hz of heart sound signal.
2. Using wavelet transform to further eliminate noise.
3. Selecting the appropriate wavelet function to suppress the influence of high frequency noise.
4. Calculating the Stein's unbiased risk estimate for each element in sequence according to formula (1).
5. Introducing the layer number adaptive factor on the original basis, according to fomula (4).
6. The processed wavelet coefficients are inversely transformed to obtain the final de-noised heart sound signal.
7. Return the reconstructing of heart sound signal.

Heart sound signals de-noising based on wavelet transform with an adaptive threshold has some advantages as follows:

(i) The effect of wavelet transform with hard threshold remains rough because it neglects to processes wavelet coefficients larger than hard threshold and results in de-noising distortion. Wavelet transform with an adaptive threshold compensates for the deficiency of hard threshold by taking into account high-frequency and low-frequency coefficients.

(ii) The effect of wavelet transform with rigrsure threshold improves smooth because it performs continuous compression on wavelet coefficients and results in filtering out the approximate components of heart sound signals. Wavelet transform with an adaptive threshold in this paper retains a large coefficient and avoids de-noising distortion in the process of wavelet decomposition.

3.2. An Architecture of 1D LDCNN

In order to reduce extra computing of raw input signals, we employ the sliding windows to split the Heart sound recordings into a series of patches with fixed length, i.e., 3s length and 1s stride (from empirically selected). On one hand, segmenting heart sound recordings into FHSs accurately is very difficult. On the other hand, sliding windows can extends the scale of training set. This method does not need to extract features in advance, so as to avoid the loss of features due to improper design and affect the classification effect. We construct a 1D LDCNN to automatically learn the discriminative features of heart sounds. The network first uses the stem block to enhance the characterization ability of features, and then uses simplified dense blocks and transition blocks to extract deep features, and finally uses softmax as the heart sound classifier. In particular, deep separable convolution in dense blocks can reduce the amount of network parameters. Furthermore, channel attention in transition blocks highlights the channel features with high contribution. The detail architecture of 1D LDCNN is as follows:

(i) Stem Block

We design stem block which can be effectively increase representation power while increasing a small amount of computational cost. At the beginning, the first convolutional layer uses a 1×3 kernel size, stride 2, followed by batch normalization (BN) and Rectified Linear Unit (ReLU), the output feature map can be obtained. In order to enhance the richness of features, we use a 2-way convolutional layer to get different scales of receptive fields. One way of the layer uses a Cov 1×1 , stride 1 and Cov 1×3 , stride 2, followed by BN and ReLU, respectively. The other way of the layers uses max-pooling 1×2, stride 2. The output feature map G_2 and G_3 can be obtained respectively. Finally, in order to finally connect in the channel dimension, we use convolution to compress the amount of channels to 24, and the output feature map G_4 can be obtained. In order to reduce the computational complexity, the maximum pooling compression feature dimension with a step size of 2 is used to obtain the final output feature map. The calculation of the entire stem block is as follows

$$G_1 = F\left[\sum_{i=1}^{24}\left(W_{1\times3_i}\times X_{1\times w}\right)\right] \tag{5}$$

$$G_2 = F\left\{\sum_{j=1}^{24}\left[W_{1\times3_j}\times F\left[\sum_{i=1}^{12}\left(W_{1\times1_i}\times G_1\right)\right]\right]\right\} \tag{6}$$

$$G_3 = M\mathrm{axPool}(G_1)_{1\times2} \tag{7}$$

$$G_4 = F\left\{\sum_{i=1}^{24}\left[W_{1\times1_i}\times \mathrm{Cat}\left(G_2, G_3\right)\right]\right\} \tag{8}$$

$$G_{out} = M\mathrm{axPool}[G_4]_{1\times3} \tag{9}$$

$$F = \mathrm{Re}LU\left[BN\left(\cdot\right)\right] \tag{10}$$

where $X_{1\times w}$ indicates the input of stem block; w is the dimension of input data; $W_{1\times3}$, $W_{1\times1}$ are the 1×3 convolutional kernel and 1×1 convolutional kernel, respectively;

$Cat()$ denotes concatenation operation; $MaxPool()$ denotes the max-pooling neural network operation.

(ii) Simplified dense block

Dense concatenation is an important feature reuse in DenseNet. Since DenseNet allows all previous feature maps are used to as input to the subsequent layer of the network. This method can make the network simple, but it also causes the memory access cost to increase quadratically with network depth and in turn leads to computation cost. In order to reduce the amount of original dense connections, each layer of the network is directly connected to all previous layers with only retaining the reuse of low-level features, thereby reducing redundant connections. In the simplified dense network, the output of each block is divided into two parts: one part is used for the input of the next block to extract higher-level features; the other part is used for the final concatenation operation, so that low-level features can be obtained so as to improve feature expression ability. The formula of a simplified dense block is as follows

$$G_{dense} = cat\left(H_1, H_2, \cdots, H_k\right) \tag{11}$$

where G_{dense} denotes output of a simplified dense block, $H_k(k > 1)$ is a composite function which includes a series of operations, i.e., BN, H_SWISH, Dropout and convolutional layers.

In order to further lower the parameter consumption of simplified dense block, a separable convolution is utilized to extract features. DWconv can effectively reduce the amount of parameters and computation cost by separating spatial features and channel features. Besides, the H-Swish activation function is used instead of the ReLU activation function to further reduce the computation cost. The formula of H_k is as follows

$$H_k = \begin{cases} J\left\{S\left[J\left[\sum_{i=1}^{C}\left(W_{1\times 1_i} \times G_{k-1}\right)\right]\right]\right\}, stride = 1, \\ cat\left(J\left[S\left(G_{k-1}\right)\right], J\left\{S\left[J\left[\sum_{i=1}^{C}\left(W_{1\times 1_i} \times G_{k-1}\right)\right]\right]\right\}\right), stride = 2. \end{cases} \tag{12}$$

$$J = H\_SWISH\left[BN\left(\cdot\right)\right] \tag{13}$$

where G_{k-1} denotes the output of dense block, $G_{k-1} = G_{out}(k = 1)$; i denotes $i - th$ convolution kernel; C denotes the current number of convolution kernels; S denotes the depth-wise separable convolution.

(iii) Transition block

The output G_{dense} of simplified dense block can be seen that the amount of output channels is very high and cannot be directly used as the input of the next dense module. Transition block is used to squeeze the dimensionality of the output map of simplified dense block. In order to improve representation power, attention mechanism module is introduced into transition blocks. The transition blocks with pooling layers are introduced to divide the networks into two blocks processing feature maps at different resolutions. Using a convolution 1×1 instead of fully connected layer, the number of output channels is a half of the original dense block. In the attention mechanism module, it exploits global maximum pooling and global average pooling (GAP) to simultaneously generate average-pooled features and max-pooled features respectively. And then, both features are forward to a shared two-layer convolution, where the amount of output channels of the

first convolution is a half of that of the second convolution. The two output features are added and the corresponding weights are obtained through Sigmoid. In short, the channel attention is computed as

$$G_{att} = \sigma \left\{ Conv \left[AvgPool \left(G'_{dense} \right) \right] + Conv \left[MaxPool \left(G'_{dense} \right) \right] \right\} \tag{14}$$

where σ denotes the sigmoid activation function; G'_{dense} represents the two-layer convolutions; $AvgPool(G'_{dense})$ and $MaxPool(G'_{dense})$ represent the global average pooling calculation and global maximum pooling calculation, respectively.

3.3. Heart sound classification

Heart sounds classification is the last step of the model. Heart sounds are mainly divided into two categories: Normal and Abnormal, with 0 for Normal and 1 for Abnormal. The GAP layer averages the features extracted by the network and maps the features to 2 channel dimensions through the FC (fully connected) layer, and finally uses softmax layer to calculate the probabilities of the 2 channels, and takes the corresponding index of the maximum probability as the final output of the network. Softmax is an effective way that handles multi-class classification problems in which output represents in categorical ways. The activation function of softmax is defined as

$$S(y) = \frac{e^{y_i}}{\sum_{k=1}^{K} e^{y_k}} \tag{15}$$

where y, S are the input and the output, respectively. The Softmax function is used in the last layer of the neural network to obtain the probabilities of the category class of each input.

4. Experimental Setup and Analysis

4.1. Experimental Setting

We conduct the experiments on publicly available heart sound dataset which provided by PhysioNet/CinC Heart Sound Classification Challenge held in 2016. The heart sound records of PhysioNet/CinC 2016 data set [22] are collected from different clinical and non-clinical real environments, including clean and noisy heart sound records. The targets of its collection are both healthy subjects and pathological patients, including children and adults. The database includes six sub-data sets a-b-c-d-f, which are integrated from data sets provided by different research organizations such as MIT, AAD, AUTH, TUT, UHA, etc., and are strictly labeled to divide the data into normal and abnormal. There are two types of normal heart sound records from healthy subjects, and abnormal records from pathological patients who have been diagnosed with heart disease. There are a total of 3240 heart sound records from 764 subjects. The shortest record is only 5s and the longest lasts over 120s. This experiment exploits python and PyTorch (Deep Learning Framework) to build the proposed network. The training environment of the networks as follows: CPU (Intel i5-10400F), GPU (Nvidia RTX 2070Super), and 8GB video memory. The operating system is Ubuntu 18.04.

4.2. Evaluation Metrics

In order to compare with state-of-the art heart sound classification method, we choose Accuracy (Acc), Sensitivity (Se), Specificity (SP), Precision (Pr), F_1 score and $MAcc$ as several evaluation metrics, which are defined as follows

$$Acc : \frac{TP + TN}{TP + FP + TN + FN} \tag{16}$$

$$Se : \frac{TP}{FP + TN} \tag{17}$$

$$Sp : \frac{TN}{FP + TN} \tag{18}$$

$$Pr : \frac{TP}{TP + FP} \tag{19}$$

$$F_1 : 2 \times \frac{Se \times \mathrm{Pr}}{Se + \mathrm{Pr}} \tag{20}$$

$$MAcc : \frac{Se + Sp}{2} \tag{21}$$

where TP, TN, FP, FN denotes true-positive, true-negative, false-positive and false-negative.

4.3. Pre-Processing of HSSs

The a0074 record is de-noised by a 5-layer db6 wavelet decomposition. The choice of threshold rules will have a certain effect on the noise reduction effect. Fig. 1 shows the noise reduction effect of wavelet transform with Rigrsure threshold of a0074 record. Although the noise is basically eliminated, some meaningful components of heart sound signal heart are also excessively eliminated. Fig. 2 shows the noise reduction effect of wavelet transform with an adaptive threshold. Compared to Fig. 1, more meaningful components are retained in Fig. 2.

4.4. Classification Effect of 1D LDCNN

In order to fully learn the potential features of the provided dataset, we need train the proposed architecture of 1D LDCNN as much as possible. Therefore, we can divide the provided dataset (PhysioNet/CinC 2016) into three parts, a training set/a validation set/a test set with a percentage of 8:1:1 respectively. The training set is used to train the model, the validation set to optimize the model and the test set to evaluate and check the performance of the model. Our proposed model is trained with a batch size of 64. The WCE (Weighted cross-entropy) with rate 1 to 0.25 (Abnormal to Normal) is chosen as loss function. Adam optimizer function uses momentum and adaptive learning rates to converge faster.

Table 1 summarizes the experimental results. Our proposed method is mainly compared with five state-of-art methods. It can be seen that the proposed method outperforms other methods except Sp. In terms of Acc, Se and Pr, our proposed method obtains an

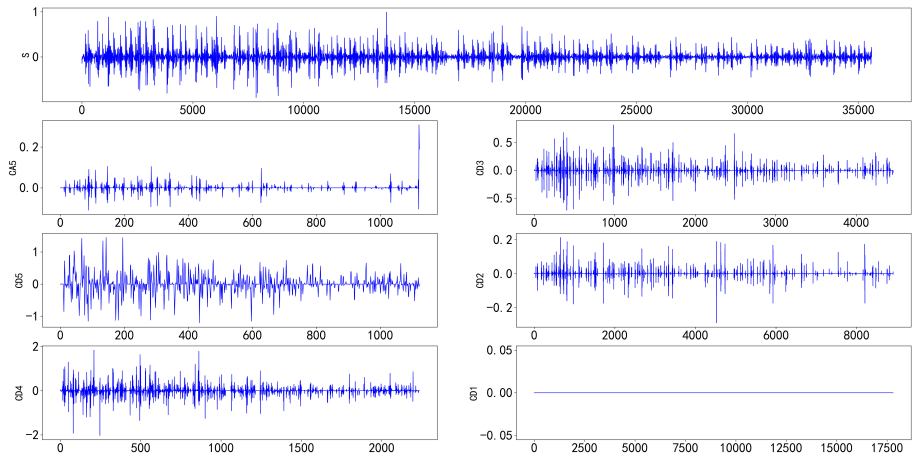

Fig. 1. The de-noising effect of 5-layer db6 wavelet decomposition with Rigrsure threshold

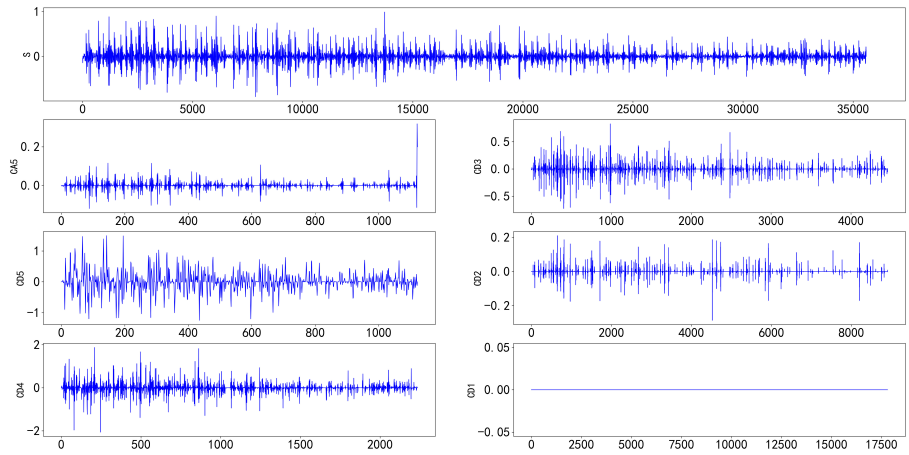

Fig. 2. The de-noising effect of 5-layer db6 wavelet decomposition with an adaptive threshold

accuracy of 97.92%, a sensitivity of 98.20% and a precision of 98.98%. It obtains the first place. The effect of MFCC-CNN [31] method is obtained with an accuracy of 93.31%, a specificity of 95.16%, and a sensitivity of 82.66%, which uses MFCC-based features to transform 1D to 2D time-frequency heat map, and exploits MFCC heart maps using CNN to classify heart sounds recordings. In addition, a modified AlexNet model [10] achieves an accuracy of 97.05%, a specificity of 93.20% and a sensitivity of 95.12%. A cross-wavelet assisted AlexNet model [9] obtains an accuracy of 97.89%, a specificity of 97.12% and an F_1 score of 0.9421, which exploits thresholding-based wavelet transform to remove noise, and convolution neural network (Alex Net architecture) recognizes abnormal/normal PCG signals. Notably, 1D Clique [39], 1D Dense [38] and 1D LDCNN, all the three focus on feature reuse and parameter efficiency to automatic heart sounds classification. Compared with 1D Clique and 1D Dense, 1D LDCNN provides the best sensitivity (98.20% vs. 86.21% vs. 85.29%), which indicates that the positive feature of 1D LDCNN is to avoid missed diagnosis as much as possible. Besides, 1D LDCNN provides the lowest specificity (92.22% vs. 95.16% vs. 95.73%), which demonstrates that 1D Clique and 1D Dense overemphasize to avoid misdiagnosis at the expense of missed diagnosis. Table 3 also shows that only our proposed method and cross-wavelet assisted AlexNet employ WT-HSEGAN and wavelet transform for de-noising, respectively.

In addition, 1D LDCNN, 1D Clique and 1D Dense all put raw heart sound data into the network to automatically extract features and perform classification. Among them, the model sizes, namely the trainable parameters (Params) are 0.02M, 0.19M, and 0.11M, respectively. And interestingly, model size of 1D LDCNN without deep separable convolution is 0.023M, i.e., deep separable convolution can further reduce parameters by 0.003M, which is more conducive to use in resource-constrained terminals.

Table 1. Evaluation results for the proposed method in comparisons with state-of-art methods

Methods	$Acc(\%)$	$Se(\%)$	$Pr(\%)$	$Sp(\%)$	F_1	$Parms$(M)
MFCC-CNN	93.31	82.66	95.38	95.16	0.8857	-
Modified AlexNet	97.05	95.12	-	93.20	-	-
1D Dense	93.56	85.29	96.09	95.73	0.9037	0.11
1D Clique	93.28	86.21	96.27	95.16	0.9096	0.19
Cross-wavelet assisted AlexNet	97.89	97.12	-	-	0.9421	-
1D LDCNN	97.92	98.20	98.98	92.22	0.9859	0.02

In order to verify the effect of different modules on the improvement performance of proposed model, this paper constructs a basic DCNN model in which the stem module and separable convolution are replaced by conventional convolution operations with convolution kernel sizes of 7 and 3, respectively. The attention mechanism is removed from the transition module. Then, stem module, channel attention mechanism, and separable convolutions are added to the basic DCNN model, and the network structure used by each model remains the same. Finally, under the same data set conditions, the network is trained and tested, and the final results are shown in Table 2. It can be observed that adding each module in sequence has a relatively obvious improvement effect on the model, and can obtain a high F_1 score. The deep neural network model

$(DCNN + stem\_block + attention + DWconv)$ uses the stem structure to enhance the model's initial feature presentation ability for original heart sound data, and reuses low-level features in subsequent dense modules to further improve the network. The feature presentation ability of the transition module introduces the channel attention mechanism to highlight the channel features with large contributions, which makes the extracted features more distinguishable, and is more conducive to the classification and recognition of heart sounds.

Table 2. Performance comparison of different modules on the performance of the model

Methods	Acc(%)	Se(%)	Pr(%)	Sp(%)	F_1	MAcc
DCNN	89.13	95.27	91.26	66.77	0.9322	0.8102
DCNN+stem_block	91.76	94.54	94.93	81.60	0.9473	0.8807
DCNN+stem_block+attention	94.89	96.74	96.74	88.13	0.9674	0.9244
DCNN+stem_block+attention+DWconv	97.70	98.20	98.98	92.22	0.9859	0.9521

4.5. A Real-Time Heart Sound Detection System

The real-time heart sound detection system is developed by our group, which includes acquisition module of heart sounds and a mobile application. In Fig. 3, acquisition module of heart sounds consists of a transducer (acquisition probe), microcontroller, analog signal processing, audio AD module, power amplifier, and communication module. The sensitivity of a transducer is $-36db \pm 3d$. The acoustic vibration generated during the cardiac activity is output through the transducer, amplifier circuit, detection circuit and serial port in the form of vibration wave.

The following points should be noted:

(i) During the heart sound acquisition, the patient should keep the probe relatively still, and try to avoid holding the acquisition probe with hands.

(ii) The patient collects heart sounds as far as possible in a temperature-friendly and quiet environment, keeping relaxed and breathing evenly. The mobile application is used to display real-time HSSs, preprocess and classify HSSs transmitted from via serial port.

We deploy 1D LDCNN on a resource constrained device with CUP (Qualcomm Snapdragon 865), GUP (Adreno 650), Memory (12GB) and 256GB storage capacity[14]. The deployment process of 1D LDCNN is as follows:

(i) Convert 1D LDCNN to an ONNX model, and further convert an ONNX model to a NCNN model.

(ii) Build an Android application package (APK) using a NCNN model.

(iii) Migrate the APK to mobile phone for installation and operation. The deployed mobile application is relatively simple, mainly including three buttons of preprocessing, de-noising and classification.

Fig. 4 shows two screenshots of heart sounds classification in a mobile phone. In Fig. 4(a), the normal heart sound has an SNR of 20.358465dB and a positive predictive value (PPV) of 31.8356%. Correspondingly, the abnormal heart sound has an SNR of 19.945709dB and a PPV of 99.96306% in Fig. 4(b). The results verify the feasibility of deployment.

Fig. 3. Acquisition module of heart sounds

5. Conclusions

In this paper, a novel heart sound classification method using adaptive wavelet threshold and 1D LDCNN is proposed. Taking advantages of wavelet transform with an adaptive threshold, the noise of HSSs can be effectively removed. More importantly, it can avoid filtering out meaningful component in the process of wavelet transform decomposition. Furthermore, 1D LDCNN is exploited to realize the automatic feature extraction and final classification, which uses simplified dense blocks and attention mechanism to reduce parameters. Experiment results on PhysioNet/CinC 2016 Challenge database show that our proposed method achieves better performances in terms of classification performance and parameters consumption. To a certain extent, easy lightweight deployment of the proposed method also promotes the application of digital stethoscopes in unconstrained environment.

In our future works, we will explore more efficient de-noising method for heart murmurs and environments noises. We will take into consider to build more efficient architecture suitable for deployment in resource-constrained terminals. Additionally, 1D LDCNN effectively captures hidden patterns of HSSs in Euclidean space, but we hope to achieve better prediction results using graph neural network (GNN) [2][43], provided that sufficient training data is available.

Acknowledgments. This work was supported by National Natural Science Foundation of China under Grant No. 62173285; Natural Science Foundation of Fujian Province under Grant No.2023J011426; The New Generation Information Technology Innovation Project of China University Industry-University-Research Innovation Fund under Grant No. 2020ITA03015; Research Climbing Program of Xiamen University of Technology under Grant No. 2020044.

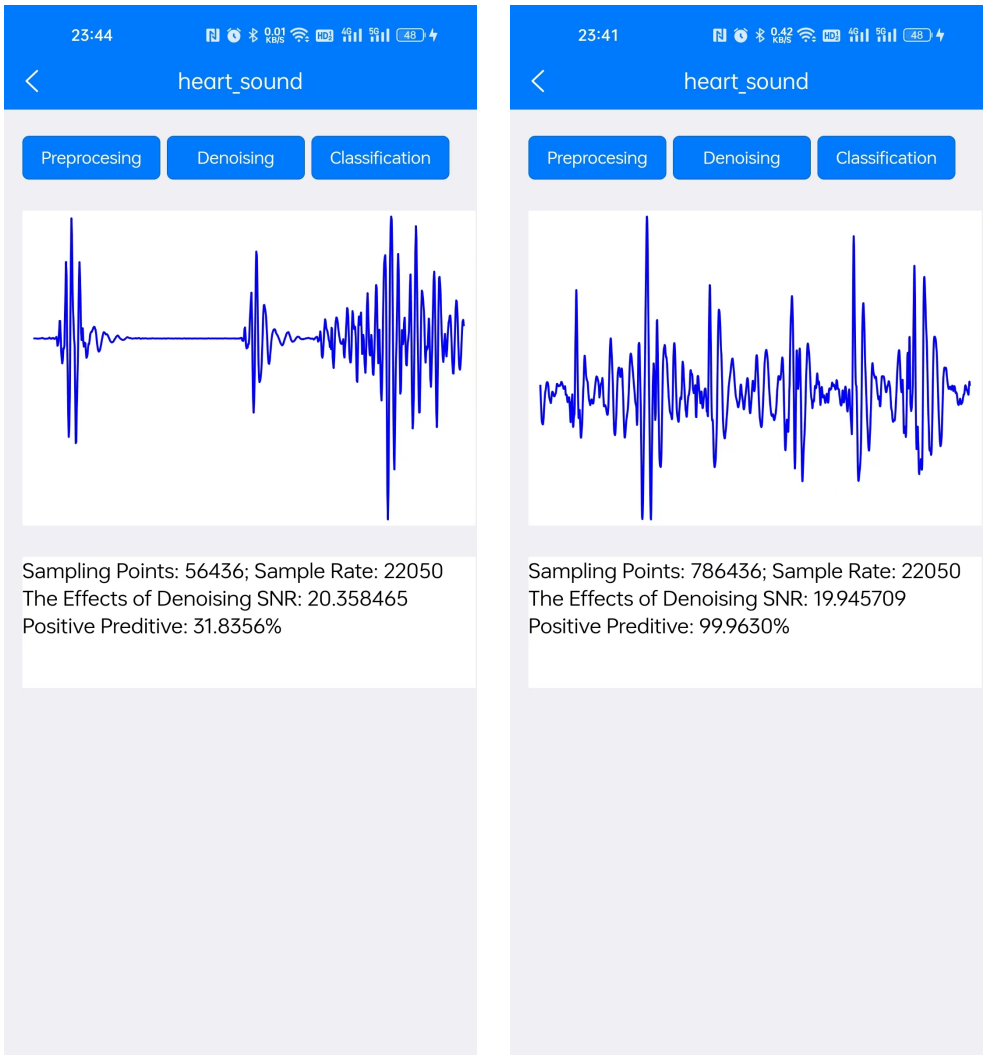

(a) Normal (b) Abnormal

Fig. 4. Screenshot of heart sounds classification in a mobile phone.

References

1. Altuve, M., Suárez, L., Ardila, J.: Fundamental heart sounds analysis using improved complete ensemble emd with adaptive noise. Biocybernetics and Biomedical Engineering 40(1), 426–439 (2020)
2. Cen, Y., Hou, Z., Wang, Y., Chen, Q., Luo, Y., Yao, X., Zeng, A., Guo, S., Yang, Y., Zhang, P., et al.: Cogdl: toolkit for deep learning on graphs. arXiv preprint arXiv:2103.00959 (2021)
3. Chen, P., Zhang, Q.: Classification of heart sounds using discrete time-frequency energy feature based on s transform and the wavelet threshold denoising. Biomedical Signal Processing and Control 57, 101684 (2020)
4. Chen, P., Zhang, Q.: Classification of heart sounds using discrete time-frequency energy feature based on s transform and the wavelet threshold denoising. Biomed. Signal Process. Control. 57 (2020)
5. Chen, Y., Lv, J., Sun, Y., Jia, B.: Heart sound segmentation via duration long–short term memory neural network. Applied Soft Computing 95, 106540 (2020)
6. Coskun, H., Deperlıoğlu, Ö., Yığıt, T.: Classification of extrasystole heart sounds with mfcc features by using artificial neural network. In: 2017 25th Signal Processing and Communications Applications Conference (SIU). pp. 1–4. IEEE (2017)
7. Das, S., Pal, S., Mitra, M.: Supervised model for cochleagram feature based fundamental heart sound identification. Biomedical Signal Processing and Control 52, 32–40 (2019)
8. Devices, E.: Eko core digital stethoscope, [Online]. Available: https://ekodevices.com/(current June 2023)
9. Dhar, P., Dutta, S., Mukherjee, V.: Cross-wavelet assisted convolution neural network (alexnet) approach for phonocardiogram signals classification. Biomedical Signal Processing and Control 63, 102142 (2021)
10. Dominguez-Morales, J.P., Jimenez-Fernandez, A.F., Dominguez-Morales, M.J., Jimenez-Moreno, G.: Deep neural networks for the recognition and classification of heart murmurs using neuromorphic auditory sensors. IEEE transactions on biomedical circuits and systems 12(1), 24–34 (2017)
11. Fan, J., Tang, S., Duan, H., Bi, X., Xiao, B., Li, W., Gao, X.: Le-lwtnet: A learnable lifting wavelet convolutional neural network for heart sound abnormality detection. IEEE Transactions on Instrumentation and Measurement (2023)
12. Ghosh, S.K., Ponnalagu, R., Tripathy, R.K., Panda, G., Pachori, R.B.: Automated heart sound activity detection from pcg signal using time–frequency-domain deep neural network. IEEE Transactions on Instrumentation and Measurement 71, 1–10 (2022)
13. Guo, Z., Chen, J., He, T., Wang, W., Abbas, H., Lv, Z.: Ds-cnn: Dual-stream convolutional neural networks based heart sound classification for wearable devices. IEEE Transactions on Consumer Electronics (2023)
14. Hu, J., Wu, K., Liang, W.: An ipv6-based framework for fog-assisted healthcare monitoring. Advances in Mechanical Engineering 11(1), 1687814018819515 (2019)
15. Huake, H.: Hky-06c heart sound sensor, [Online]. Available: http://www.hfhuake.com/(current June 2023)
16. Humayun, A.I., Khan, M., Ghaffarzadegan, S., Feng, Z., Hasan, T., et al.: An ensemble of transfer, semi-supervised and supervised learning methods for pathological heart sound classification. arXiv preprint arXiv:1806.06506 (2018)
17. Ismail, S., Ismail, B., Siddiqi, I., Akram, U.: Pcg classification through spectrogram using transfer learning. Biomedical Signal Processing and Control 79, 104075 (2023)
18. Karhade, J., Dash, S., Ghosh, S.K., Dash, D.K., Tripathy, R.K.: Time–frequency-domain deep learning framework for the automated detection of heart valve disorders using pcg signals. IEEE Transactions on Instrumentation and Measurement 71, 1–11 (2022)

19. Kui, H., Pan, J., Zong, R., Yang, H., Wang, W.: Heart sound classification based on log mel-frequency spectral coefficients features and convolutional neural networks. Biomedical Signal Processing and Control 69, 102893 (2021)
20. Li, J., Ke, L., Du, Q.: Classification of heart sounds based on the wavelet fractal and twin support vector machine. Entropy 21(5), 472 (2019)
21. Li, S., Li, F., Tang, S., Luo, F.: Heart sounds classification based on feature fusion using lightweight neural networks. IEEE Transactions on Instrumentation and Measurement 70, 1–9 (2021)
22. Liu, C., Springer, D., Li, Q., Moody, B., Juan, R.A., Chorro, F.J., Castells, F., Roig, J.M., Silva, I., Johnson, A.E., et al.: An open access database for the evaluation of heart sound algorithms. Physiological measurement 37(12), 2181 (2016)
23. Ma, P., Ge, B., Yang, H., Guo, T., Pan, J., Wang, W.: Application of time-frequency domain and deep learning fusion feature in non-invasive diagnosis of congenital heart disease-related pulmonary arterial hypertension. MethodsX p. 102032 (2023)
24. Messner, E., Zöhrer, M., Pernkopf, F.: Heart sound segmentation-an event detection approach using deep recurrent neural networks. IEEE transactions on biomedical engineering 65(9), 1964–1974 (2018)
25. Naing, H., Hidayat, R., Hartanto, R., Miyanaga, Y.: Discrete wavelet denoising into mfcc for noise suppressive in automatic speech recognition system. International Journal of Intelligent Engineering and Systems 13(2), 74–82 (2020)
26. Noman, F., Salleh, S.H., Ting, C.M., Samdin, S.B., Ombao, H., Hussain, H.: A markov-switching model approach to heart sound segmentation and classification. IEEE Journal of Biomedical and Health Informatics 24(3), 705–716 (2019)
27. Oh, S.L., Jahmunah, V., Ooi, C.P., Tan, R.S., Ciaccio, E.J., Yamakawa, T., Tanabe, M., Kobayashi, M., Acharya, U.R.: Classification of heart sound signals using a novel deep wavenet model. Computer Methods and Programs in Biomedicine 196, 105604 (2020)
28. Organization, W.H., et al.: World health statistics overview 2019: monitoring health for the sdgs, sustainable development goals. Tech. rep., World Health Organization (2019)
29. Raza, A., Mehmood, A., Ullah, S., Ahmad, M., Choi, G.S., On, B.W.: Heartbeat sound signal classification using deep learning. Sensors 19(21), 4819 (2019)
30. Ren, Z., Qian, K., Dong, F., Dai, Z., Nejdl, W., Yamamoto, Y., Schuller, B.W.: Deep attention-based neural networks for explainable heart sound classification. Machine Learning with Applications 9, 100322 (2022)
31. Rubin, J., Abreu, R., Ganguli, A., Nelaturi, S., Matei, I., Sricharan, K.: Classifying heart sound recordings using deep convolutional neural networks and mel-frequency cepstral coefficients. In: 2016 Computing in cardiology conference (CinC). pp. 813–816. IEEE (2016)
32. Rubin, J., Abreu, R., Ganguli, A., Nelaturi, S., Matei, I., Sricharan, K.: Recognizing abnormal heart sounds using deep learning. arXiv preprint arXiv:1707.04642 (2017)
33. Shukla, S., Singh, S.K., Mitra, D.: An efficient heart sound segmentation approach using kurtosis and zero frequency filter features. Biomedical Signal Processing and Control 57, 101762 (2020)
34. Taranenko, Y.K.: Efficiency of using wavelet transforms for filtering noise in the signals of measuring transducers. Measurement Techniques 64(2), 94–99 (2021)
35. Thompson, J.: Thinklabs digital stethoscopes, electronic stethoscope systems (2013)
36. Wang, H., Guo, X., Zheng, Y., Yang, Y.: An automatic approach for heart failure typing based on heart sounds and convolutional recurrent neural networks. Physical and Engineering Sciences in Medicine 45(2), 475–485 (2022)
37. Xiang, M., Zang, J., Wang, J., Wang, H., Zhou, C., Bi, R., Zhang, Z., Xue, C.: Research of heart sound classification using two-dimensional features. Biomedical Signal Processing and Control 79, 104190 (2023)

38. Xiao, B., Xu, Y., Bi, X., Li, W., Ma, Z., Zhang, J., Ma, X.: Follow the sound of children's heart: a deep-learning-based computer-aided pediatric chds diagnosis system. IEEE Internet of Things Journal 7(3), 1994–2004 (2019)
39. Xiao, B., Xu, Y., Bi, X., Zhang, J., Ma, X.: Heart sounds classification using a novel 1-d convolutional neural network with extremely low parameter consumption. Neurocomputing 392, 153–159 (2020)
40. Yang, Y., Guo, X.M., Wang, H., Zheng, Y.N.: Deep learning-based heart sound analysis for left ventricular diastolic dysfunction diagnosis. Diagnostics 11(12), 2349 (2021)
41. Zhang, X., Zhou, X., Lin, M., Sun, J.: Shufflenet: An extremely efficient convolutional neural network for mobile devices. In: Proceedings of the IEEE conference on computer vision and pattern recognition. pp. 6848–6856 (2018)
42. Zhang, Y., Ding, W., Pan, Z., Qin, J.: Improved wavelet threshold for image de-noising. Frontiers in neuroscience 13, 39 (2019)
43. Zhao, J., Dong, Y., Ding, M., Kharlamov, E., Tang, J.: Adaptive diffusion in graph neural networks. Advances in Neural Information Processing Systems 34, 23321–23333 (2021)

Jianqiang Hu is an associate professor in school of computer and information engineering, Xiamen University of Technology, China. He once worked as a postdoctoral researcher at Tsinghua University. He received his Ph.D. degree in computer science and engineering from National University of Defense Technology, China, in 2005. He is the author of more than 60 articles, and more than 8 inventions. His current research interests include Edge Computing, Biomedical Signal Processing, and Big Data Analytics.

Qingli Hu is a senior researcher at iFlytek Research, iFlytek Co. Ltd.. He received B.S. and M.S. degrees from Anhui Jianzhu University and Xiamen University of Technology, China, in 2017 and 2021, respectively. His current research interests include Speech Enhancement and Big Data Analytics.

Mingfeng Liang is a master student at school of computer and information engineering, Xiamen University of Technology, China. She received her B.S. degree from Shenzhen University in 2019. Her interest include Biomedical Signal Processing and Big Data Analytics.

Received: April 18, 2023; Accepted: July 15, 2023.

Computer Science and Information Systems 20(4):1503–1517 https://doi.org/10.2298/CSIS230223056A

Ensemble of Top3 Prediction with Image Pixel Interval Method Using Deep Learning ⋆

Abdulaziz Anorboev[1], Javokhir Musaev[1], Sarvinoz Anorboeva[1], Jeongkyu Hong[2⋆⋆], Yeong-Seok Seo[1], Ngoc Thanh Nguyen[3,4], and Dosam Hwang[1]

[1] Department of Computer Engineering, Yeungnam University
38541 Gyeongsan, South Korea
{abdulaziz.anorboyev, javokhirmuso, sarvinozanorboeva, dosamhwang}@gmail.com
[2] School of Electrical and Computer Engineering, University of Seoul,
Seoul, 02504, South Korea
jhong0301@uos.ac.kr
[3] Faculty of Information and Communication Technology, Wroclaw University of Science and Technology
50-370 Wroclaw, Poland
ngoc-thanh.nguyen@pwr.edu.pl
[4] Faculty of Information Technology, Nguyen Tat Thanh University
Ho Chi Minh 70000, Vietnam

Abstract. Computer vision (CV) has been successfully used in picture categorization applications in various fields, including medicine, production quality control, and transportation systems. CV models use an excessive number of photos to train potential models. Considering that image acquisition is typically expensive and time-consuming, in this study, we provide a multistep strategy to improve image categorization accuracy with less data. In the first stage, we constructed numerous datasets from a single dataset. Given that an image has pixels with values ranging from 0 to 255, the images were separated into pixel intervals based on the type of dataset. The pixel interval was split into two portions when the dataset was grayscale and five portions when it was composed of RGB images. Next, we trained the model using both the original and newly constructed datasets. Each image in the training process showed a non-identical prediction space, and we suggested using the top-three prediction probability ensemble technique. The top three predictions for the newly created images were combined with the corresponding probability for the original image. The results showed that learning patterns from each interval of pixels and ensembling the top three predictions significantly improve the performance and accuracy, and this strategy can be used with any model.

Keywords: Classification probability, model optimization, ensemble learning.

1. Introduction

With the advent of neural networks (NNs) and the advancements in deep learning (DL), computer vision (CV) is no longer limited to science-based fundamental experiments and is now increasingly being applied to practical applications. The automotive sector, IoT,

⋆ This is an extended version of our INISTA 2022 conference paper [26]

⋆⋆ Corresponding author

healthcare, and finance are only a few among the industries that are increasingly using CV products as their main source of supply. In addition, there is a sharp increase in the demand for high- accuracy models. To satisfy this requirement, numerous studies have been conducted on DL and CV. Future advancements in this sector will be affected by a slight improvement in model accuracy. The evolution of DL has led to the development of numerous models and methods for each DL subfield to address various issues. To address the issues and close the gaps in literature, numerous algorithms and tools have been proposed. The first is ensemble learning, which enables DL models to exchange knowledge using ensemble approaches.

Numerous researchers [1] - [7] have demonstrated the advantages of DL ensembles. The models, data, and methods that enable the leveraging of the knowledge of ensemble units have been approached in various ways. The outcomes of the ensemble models have been presented in [8] - [20], among other domains, including medical, financial risk analysis, and oil price prediction . Improvements in the DL models can aid their evolution in the future.

To resolve DL classification issues, we present an image pixel interval power (IPIP) ensemble technique. We propose two sub-methods (IPDR and IPMR), described by IPIP, to create new datasets from the original dataset utilized for DL classification tasks. We replicated the original dataset using the IPDR and replaced any pixel having value 127 or less with zero. Consequently, we obtained a second dataset for training. We duplicated the initial dataset to create the third dataset; however, this time, all pixel values higher than 127 were changed to zero. In the second stage, we trained three datasets using three models and their ensemble prediction outcomes. The outcomes of this strategy were favorable. The accuracy of the model improved from 98.84% to 99.11%. Similar to IPDR, IPMR uses more than two intervals to extract datasets from the original dataset and applies them to training.

This paper is an extended version of our conference paper [26]. The new methods consist of the following elements: the Sole-Top3 ensemble and Sum-Top3 ensemble are two unique ensemble methods for enhancing the precision of image classification models. This approach benefits from the fact that many image-classification methods can generate precise predictions for the top three classes of images. Each submodel that we trained was tailored to a certain subset of the classes. The top three prediction probabilities from each submodel were then combined to create one prediction for the main model. We tested our method on a number of image classification datasets and verified that it consistently outperformed the competing ensemble methods. The proposed method makes two key contributions to the literature. First, it can effectively combine the predictions of multiple models even when the models are trained on different datasets. Second, it can improve the accuracy of the image classification models without significantly increasing the training time or computational cost.

An improvement in the accuracy to nearly 100% is an important factor to highlight. It can be challenging to improve the results of various DL ensemble models once the accuracy has reached close to 100%. The prediction scope of an ensemble typically overlaps with that of the main model and does not permit improved accuracy. Using our approach, we partially resolve this issue and improve the outcomes of our models. This model is not able to interfere with the primary model's training ¬because it was developed independently and incorporates nearly all its knowledge, which is another appealing aspect.

This section provided background information on ensemble learning and an overview of the subject matter. The remainder of this paper is organized as follows. Information on relevant studies and issues related to ensemble learning is provided in Section 2. The challenges described in Section 2 are addressed in Section 3, which offers extensive justification for the proposed methodology. Detailed information about the dataset, base method, training configuration, evaluation metrics, experimental findings, and discussions is included in Section 4, along with the experiments and findings of the study. Section 5 concludes the paper with a few observations of the research as a whole, and suggests areas for further investigation.

2. Literature Review

Deep neural networks include multiple nonlinear hidden layers, leading to expressive models that learn complex relationships between inputs and outputs. With limited training data, many complex relationships involve noise, resulting in overfitting. The transfer learning of image pixel values and prediction probability-based methods have shown advantages in numerous research areas, such as image classification [21], natural language processing [22], speech recognition, and remote sensing. In recent years, several machine-learning [23], [24] and deep-learning models [29], including convolutional neural networks [25] and recurrent neural networks, have been evaluated for image classification tasks.

To address the limitations of conventional classification approaches, [26] we pro¬pose a novel ensemble learning paradigm with imbalanced data, which comprises three phases: data preprocessing , base classifier training, and an output ensemble. CNNs and deep residual networks are used as individual classifiers and random subspaces, respectively. To diversify the ensemble system in a simple and effective manner to further improve classification accuracy, ensemble and transfer learning were evaluated, as specified in [28], to transfer the learned weights from one individual classifier to another (i.e., CNNs). The generalization of the existing semi-supervised ensembles can be strongly affected by incorrect label esti¬mates produced by ensemble algorithms to train supervised base learners. [27] proposed cluster-based boosting, which is a multiclass classification algorithm with cluster regularization. In contrast to existing algorithms, cluster-based boosters and their base learners jointly perform cluster-based semi-supervised optimization.

Clustering ensembles and their applications in different disciplines have been the focus of numerous studies [30,31,32,33]. The clustering ensemble investigates the joint success of clustering models; however, it generates a large number of clustering partitions and combines them to obtain a better consensus function. Soares et al. [34] investigated the labeling of data in dense locations with overlapping classes and suggested a cluster-based boosting technique with cluster regularization for multiclass classification. Numerous studies have been conducted on semi-supervised clustering methods. One of them is [35], which uses the random subspace technique and constraint propagation approach for incremental semi-supervised clustering for high-dimensional data clustering. Furthermore, this method selects incremental ensemble members using newly proposed local and global cost functions.

The advantage of using the DL ensemble employing faster RCNN, TOOD, YOLOX , and cascade with Swin-Transformers in detecting intestinal parasite illnesses was pre-

sented by [36] and achieved better performance than each technique when used separately. Another recent study [37] integrated convolutional and bidirectional LSTM in a customized deep learning ensemble model for the time-series forecasting of COVID-19. The results obtained for several measures were remarkable. [38] improved COVID detection using CT scan images by combining the retrieved features from the CNN and ML algorithms. [39] used a DL ensemble comprising robustly optimized bidirectional encoder representations from transformers approach (RoBERTa), long short-term memory (LSTM), bidirectional long short-term memory (BiLSTM), and a gated recurrent unit (GRU) in sentiment analysis. The model outperformed state-of-the-art models in terms of performance.

During image preprocessing, visual data is captured as pixel arrays. Convolutions, which is the de facto deep learning operator for computer vision, are then used to process these pixel arrays. Convolutions attempt to relate to spatially distant concepts by explicitly modeling all concepts across all images, regardless of content, and taking into account all image pixels equally, regardless of relevance. The majority of the research under review left missing the ensemble of the top three prediction outcomes and knowledge of the image pixel interval variance, which could be useful for improving the classification accuracy of CNN models. To close this gap, we conduct this study to examine the outcomes of the aforementioned approach.

3. Proposed Methodology

3.1. Image Pixel Interval

In data pre-processing, we applied a method comprising two sub-methods that studies image pixel variance. The main contribution of our method is the use of datasets copied from the original dataset, except certain interval pixel values . The difference in the number of intervals enabled us to create an initial double representation of the main dataset and multiple representations of the main dataset. The IPDR is a simple double representation of the main dataset. For IPDR, we created two zero arrays of the same size as the main dataset. We used the MNIST and CIFAR-10 dataset in our experiments. For the MNIST dataset, we created two arrays of size 60000 x $32 \times 32 \times 1$, all filled with zeros. For the first subdataset, we selected pixel values from the main dataset that belonged only to the [0:127] interval, copied and pasted them at the same position in the image, and all other image pixels in the dataset were changed to zero. The second subdataset was built using the same method as the first subdataset, except that the pixel value interval for the second subdataset was [128:255]. All values higher than 127 were copied and pasted at appropriate positions in the image, and all other image pixels in the dataset were changed to zero (figure 1).

For the IPMR, we applied the same method as previously described; however, instead of two intervals, we used multiple intervals of 50 (i.e., [0:50], [51:100], [101:150], [151:200], and [201:255]) for the CIFAR-10 dataset, as shown in figure 2. Number of intervals depends on the type of dataset. During our experiments, we observed that to achieve high accuracy in training, the RGB channel images should be divided into five parts.

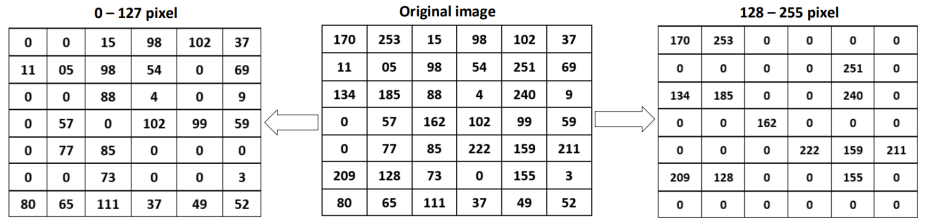

Fig. 1. Image pixel interval process for MNIST dataset

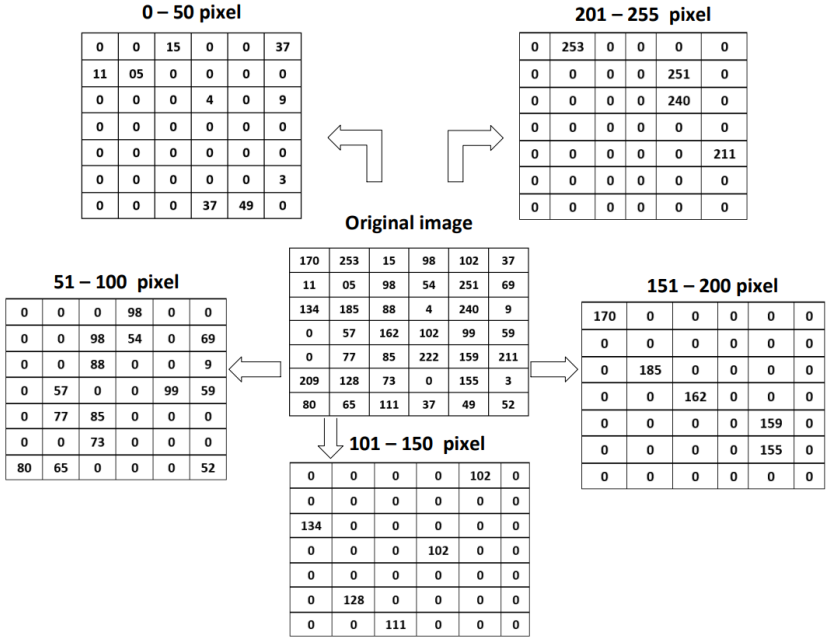

Fig. 2. Image pixel interval process for Cifar 10 dataset

3.2. Transfer Learning

Two model architectures with different numbers of parameters were used during the training process. The first model included 259,658 trainable parameters, as shown in Figure 3. The other proposed model had 165,514 trainable parameters.

We selected a model with a small number of parameters to avoid the overuse of time and power during IPIP implementation. However, the important aspect of our study was that we could achieve the same outcomes using a decreased-size model. The architecture for the regular model comprised three convolutional layers with 32, 64, and 128 filters

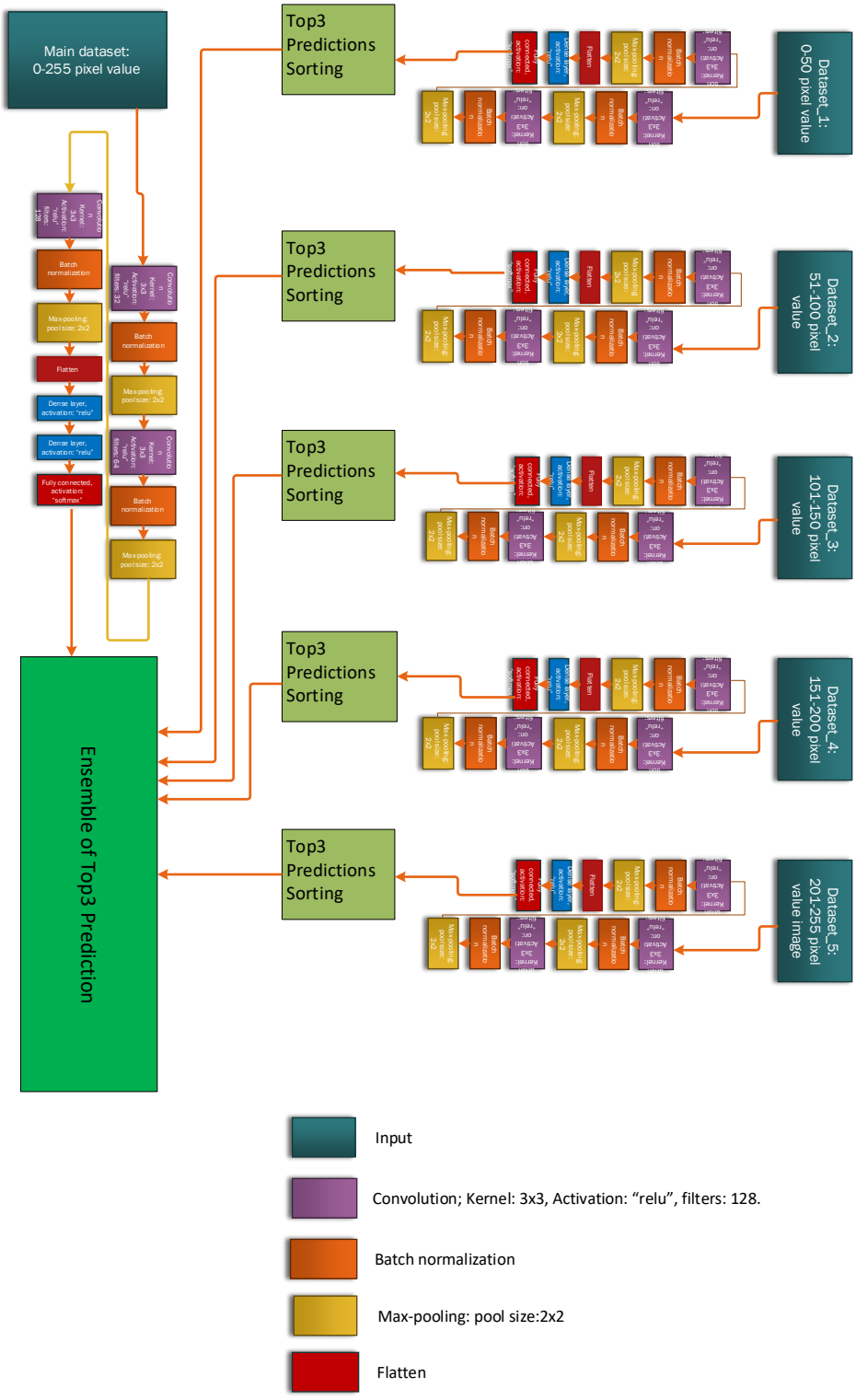

Fig. 3. Proposed model

and four dense layers with 256, 256, 128, and the number of class nodes for each dataset. In addition, we used max pooling with a 2 × 2 filter and batch normalization layers in both model architectures. The filter of size 3 × 3 was used for the convolutional layers in both the models. The architecture of the proposed model, as presented in Figure 3, comprises three convolutional layers with 32, 64, and 128 filters, and one fully connected layer in Part 1. The entire model in Part 1 was replicated by excluding the output layer from the new sequential model. We then iterated each layer in a new sequential model and set it as nontrainable. This froze the weights and other trainable parameters in each layer so that they would not be trained or updated. We added new fully connected layers and an output layer with a softmax activation function. The model was identical to the original model except that the number of trainable parameters decreased.

3.3. Prediction Probability Ensemble

In this section, we propose the top-three prediction probability ensemble. Each training dataset in our instance—three datasets each for the MNIST and Fashion MNIST datasets and six datasets for the CIFAR-10 dataset—represents a different prediction space. To create the main models that correspond to the prediction 5 probabilities, we ensembled the top three prediction probabilities of each image trained in the sub-model. The Sole-Top3 ensemble and Sum-Top3 ensemble were both used to test the ensemble method. The top three prediction probabilities from each submodel were combined with the corresponding prediction probabilities from the main model in the Sole-Top3 ensemble procedure. The top three prediction probabilities from each submodel were combined into the corresponding prediction probabilities for the main model in the Sum-Top3 ensemble. Equation 1 shows method of sorting prediction probabilities for each trained model. Here, k is the number of ensemble model indices, and k=1–5. Equation 2 shows the ensemble of each prediction probability from the submodels to the main model. Here, i is the number of the image in the datasets, that is, i= 0,1,2...m and j is the top three maximum probability indices, where j= 0,1,2.

$$b_k = np.argsort(A_k, axis = 0).sort(reverse = True). \tag{1}$$

$$A[b_k[:, i][j], i] += A_k[b_k[:, i][j], i]. \tag{2}$$

4. Experiments and Results

4.1. Datasets

We used two widely used grayscale and RGB color datasets in our proposed method: CIFAR-10, Fashion MNIST, and MNIST shown in Fig. 4, 5(a), and 5(b), respectively. The MNIST database of handwritten digits contains a training set of 60000 examples and a test set of 10000 examples. It is a subset of a larger set available from NIST . The digits were size normalized and centered on a fixed-size image.

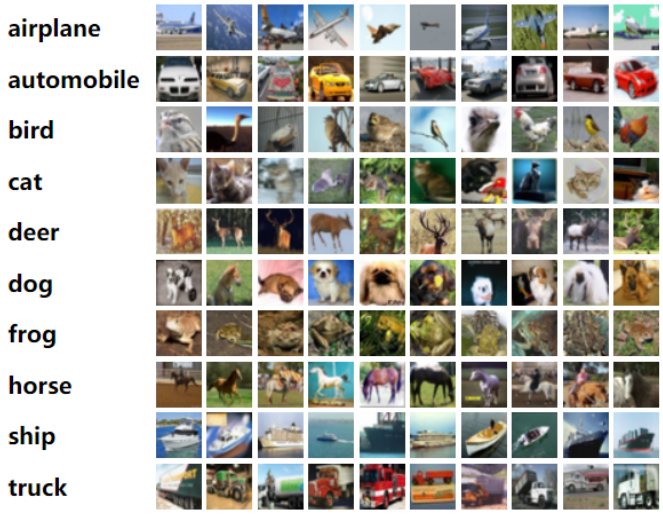

Fig. 4. Cifar 10 dataset

This is a database for people who want to test learning techniques and pattern 2recognition methods on real-world data while spending minimal effort on preprocessing and 3formatting. It contains 60000 training sets and 10000 test sets. The MNIST dataset was originally selected and tested by Chris Burges and Corinna Cortes. They used bounding box 5 normalization and centering. Yann LeCun's version used center of mass6 to center within a larger window. This is an extremely light-task DL model used to train the dataset. The 7CIFAR-10 dataset consists of 60000 color images of size 32 x 32 in 10 classes, with 6000 images8 per class. It includes 50000 training images and 10000 test images. The dataset was 9 divided into five training batches and one test batch, each containing 10000 images. The 10test batch contained exactly 1000 randomly selected images from each class. The training 11batches contained more images from one class than from another. The 12training batches contained exactly 5000 images from each class.

4.2. Experimental Setup

Python 3.6.12 and TensorFlow 2.1.0 were used to build the model architecture for the proposed method. For the experiments, we used a 12 GB Nvidia GeForce RTX 3080 Ti 16 with CUDA 10.2, on a computer with an AMD Ryzen 7 3700X and 64 GB of RAM. For training, the weight of the model was randomly initialized and trained for certain epochs. To train the model, we used the Adam optimizer with a default learning rate of 0.001 and 19 sparse categorical loss function. Each model was trained for 15 epochs. Results 20 from the 15th epoch were used to build a new ensemble and were evaluated using metrics addressed in this study.

4.3. Evaluation Metrics

For this study, we selected two metrics that meaningfully explained the method's achievements in different datasets. The accuracy is the ratio of true predictions to the total number

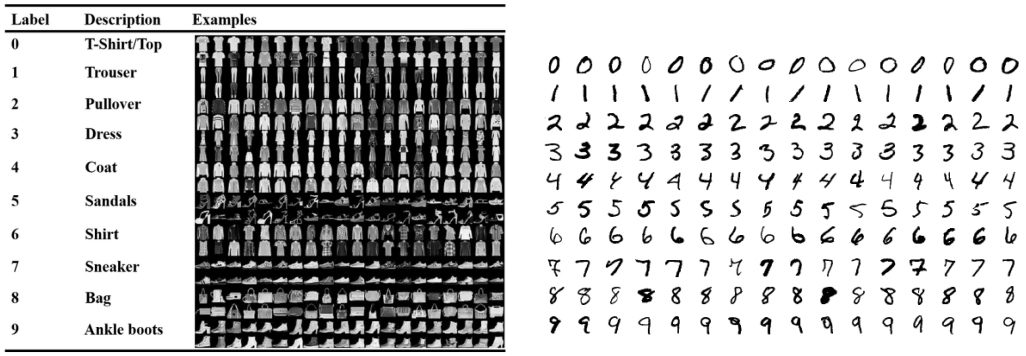

(a) **(b)**

Fig. 5. Fashion MNIST (a) and MNIST (b) datasets

of cases used to evaluate the model. Equation 3 shows the accuracy of the calculations. The next evaluation metric was the UTP , which is the percentage of unique predictions for each model with respect to another model. In Equation 4, UTP(X, Y) determines the unique true predictions of Model X with respect to those of Model Y. These metrics explain why the proposed model achieved better results than the main model, for which only the main dataset was trained. The indices of the true predicted images were different for each model but had the same accuracy. This enabled the ensemble to achieve better results.

$$Accuracy = \frac{TP + TN}{TP + TN + FP + FN}. \tag{3}$$

$$UTP(X, Y) = X - X \cap Y \tag{4}$$

4.4. Experimental Results and Discussions

The main motivation for this study was to utilize knowledge from pixel-level variance by changing the data representation and achieve better accuracy metrics for the classification task. After changing the data representation, we proposed an ensemble of the outcomes of each subdataset from the top three predictions to the corresponding three predictions of the main model, as shown in fig. 6. Classic training was used as the baseline method for the experimental evaluation. Classic training was selected because of the difficulty in finding alternative methods that could be used to compare the results. Most DL ensemble models focus on model architectures and data representations by image-level preprocessing rather than on researching pixel-level variances. The main objective of this method is to apply it simultaneously to various combinations with many other DL ensembles. The training dataset was prepared by dividing it into different parts depending on the image. CIFAR-10 was divided into six types. The first copy of the dataset included all pixel values in the images from 0 to 255. The second dataset had pixel values between 0 and 50, and all other pixel values were set to zero. In all the other datasets, a certain interval

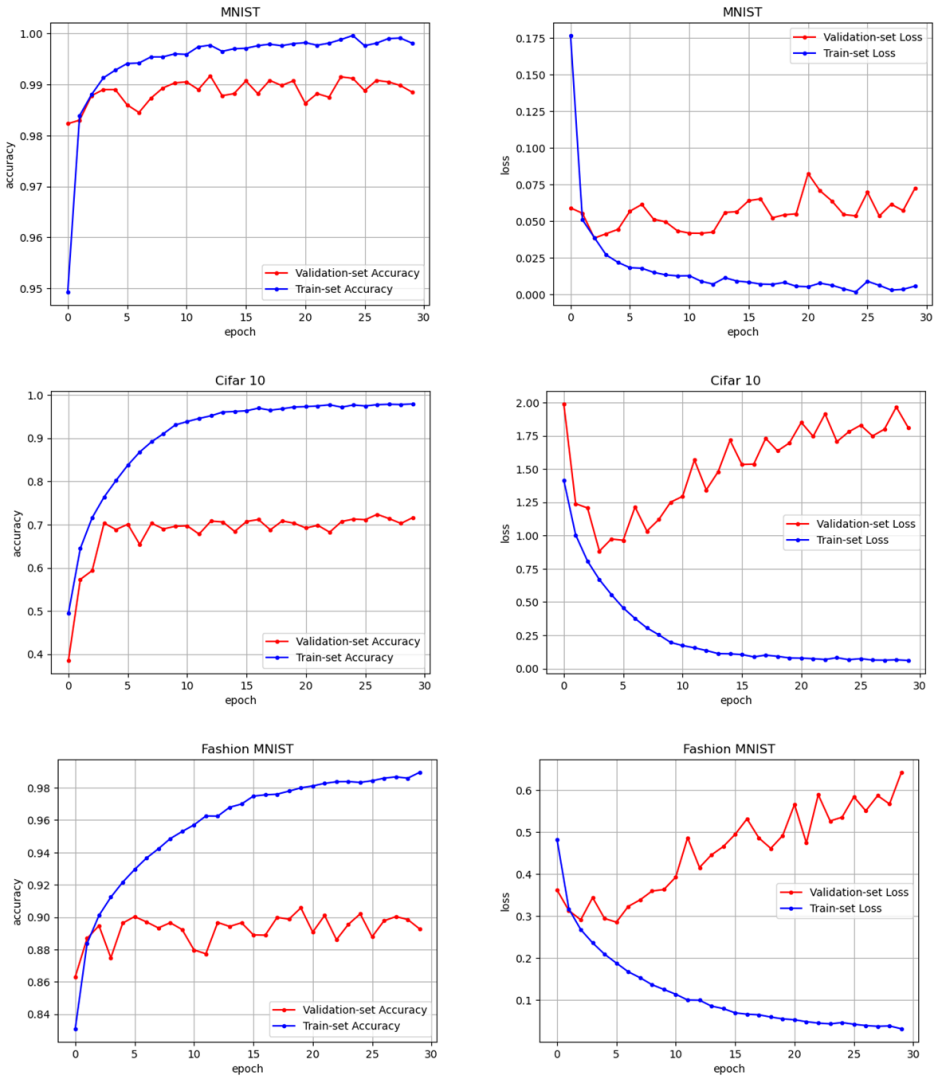

Fig. 6. Experimental results of accuracy and loss metrics using proposed model on the validation set and training set of the datasets: MNIST, Cifar10 and Fashion MNIST

of pixel values was maintained by ignoring the other values at intervals of 50, [51:100], [101:150], [151:200], and [201:255]. The primary purpose of the pixel interval method is to study and classify image pixels individually. After splitting the images, each dataset was individually trained using the specified CNN models described in Section 3. The experiments were conducted using the same method as for the MNIST dataset, although the data preprocessing was different. Because the MNIST dataset is grayscale, the image interval splitting of dataset consisted of two equal parts. The first part included pixel values from 0 to 127 and excluded all other values by equaling them to zero. The second part had pixel values between 128 and 255. All datasets were trained using the proposed fine-tuned model with 165,514 trainable parameters, whereas the original model used 259,658 trainable parameters. There was a reduction of approximately 100,000 parameters that saved computational power and memory and also helped to increase the training speed. The numbers were more visible when the model epochs were set to 100: 16,551,400 and (1) 25,965,800. By applying the proposed model, we achieved output results of 73.58% and 99.07% of the original model, for the CIFAR-10 and MNIST datasets, respectively (Table 1).

Table 1. Test set accuracy for MNIST, Fashion MNIST and CIFAR-10 datasets and proposed methods

Dataset	Method	Accuracy Score
MNIST	IPIP	98.90
	Sole-Top3	99.01
	Sum-Top3	99.07
Cifar 10	IPIP	73.38
	Sole-Top3	73.45
	Sum-Top3	73.58
Fashion MNIST	IPIP	89.46

5. Conclusion

In this study, we proposed an enhanced version of the layer dropout technique and transfer learning to regularize deep neural networks. By applying transfer learning, we extracted features from the images before feeding them into the model. A fine-tuned convolutional neural network was applied by placing dropout operations before each convolutional layer. In addition to image classification, we tested the proposed method on a pixel-interval dataset. The proposed method could generalize deep neural networks with lower gradient descent and faster convergence during training and achieved promising results on classification tasks. Deactivation of the basic components of the neural network models discussed in this study are based on randomly setting a particular component to zero. The main disadvantage of this technique is the risk of losing useful information in the image. In future research, we will focus on further improving the pixel-interval image pre-processing method and we plan to combine with the analysis of user opinions in social media to improve the accuracy. We will use consensus methods for integrating the user

opinions yielding a common opinion which can be taken into account for determining the prediction. Consensus methods have been proved to be very useful in many integration tasks and should be also useful in integrating user opinions [40, 41, 42].

Acknowledgments. This work was supported by the National Research Foundation of Korea (NRF) grant funded by the Korea government (MSIT) (No. 2022R1F1A1074641).

References

1. S. Vega-Pons and J. Ruiz-Shulcloper, "A survey of clustering ensemble algorithms," International Journal of Pattern Recognition and Artificial Intelligence, vol. 25, no. 3, pp. 337–372, May 2011.
2. Zhou, ZH. (2009). Ensemble Learning. In: Li, S.Z., Jain, A. (eds) Encyclopedia of Biometrics. Springer, Boston, MA.
3. Lappalainen, H., Miskin, J.W. (2000). Ensemble Learning. In: Girolami, M. (eds) Advances in Independent Component Analysis. Perspectives in Neural Computing. Springer, London.
4. T. Alqurashi and W. Wang, "Clustering ensemble method," International Journal of Machine Learning and Cybernetics, vol. 10, no. 6, pp. 1227–1246, Jun. 2019.
5. A. Krogh, "Neural Network Ensembles, Cross Validation, and Active Learning."
6. O. Sagi and L. Rokach, "Ensemble learning: A survey," Wiley Interdisciplinary Re¬views: Data Mining and Knowledge Discovery, vol. 8, no. 4. Wiley-Blackwell, Jul. 01, 2018.
7. X. Dong, Z. Yu, W. Cao, Y. Shi, and Q. Ma, "A survey on ensemble learning," Frontiers of Computer Science, vol. 14, no. 2. Higher Education Press, pp. 241–258, Apr. 01, 2020.
8. G. I. Webb and Z. Zheng, "Multistrategy ensemble learning: reducing error by combining ensemble learning techniques," in IEEE Transactions on Knowledge and Data Engineering, vol. 16, no. 8, pp. 980-991, Aug. 2004.
9. K. Faceli, A. de Carvalho, M. Carlos, and P. de Souto, "Multi-objective clustering ensemble. Classical Weightless Neural Systems View project Feature Extraction and Se-lection Analysis in Biological Sequences View project SEE PROFILE," 2007. [Online]. Available: https://www.researchgate.net/publication/220515994
10. H. M. Gomes, J. P. Barddal, A. F. Enembreck, and A. Bifet, "A survey on ensemble learning for data stream classification," ACM Computing Surveys, vol. 50, no. 2. Asso-ciation for Computing Machinery, Mar. 01, 2017.
11. S. Qummar et al., "A Deep Learning Ensemble Approach for Diabetic Retinopathy De-tection," IEEE Access, vol. 7, pp. 150530–150539, 2019.
12. D. P. Gaikwad and R. C. Thool, "Intrusion detection system using bagging ensemble method of machine learning," in Proceedings - 1st International Conference on Com-puting, Communication, Control and Automation, ICCUBEA 2015, Jul. 2015, pp. 291–295.
13. S. Hamori, M. Kawai, T. Kume, Y. Murakami, and C. Watanabe, "Ensemble Learning or Deep Learning? Application to Default Risk Analysis," Journal of Risk and Financial Management, vol. 11, no. 1, p. 12, Mar. 2018.
14. Y. Zhao, J. Li, and L. Yu, "A deep learning ensemble approach for crude oil price fore-casting," Energy Economics, vol. 66, pp. 9–16, Aug. 2017.
15. Z. Yu et al., "Incremental Semi-Supervised Clustering Ensemble for High Dimensional Data Clustering," IEEE Transactions on Knowledge and Data Engineering, vol. 28, no. 3, pp. 701–714, Mar. 2016.
16. H. Sarmadi, A. Entezami, B. Saeedi Razavi, and K. V. Yuen, "Ensemble learning-based structural health monitoring by Mahalanobis distance metrics," Structural Control and Health Monitoring, vol. 28, no. 2, Feb. 2021.

17. L. Yu, S. Wang, and K. K. Lai, "Credit risk assessment with a multistage neural network ensemble learning approach," Expert Systems with Applications, vol. 34, no. 2, pp. 1434–1444, Feb. 2008.
18. Y. Xiao, J. Wu, Z. Lin, and X. Zhao, "A deep learning-based multi-model ensemble method for cancer prediction," Computer Methods and Programs in Biomedicine, vol. 153, pp. 1–9, Jan. 2018.
19. T. Zhou, H. Lu, Z. Yang, S. Qiu, B. Huo, and Y. Dong, "The ensemble deep learning model for novel COVID-19 on CT images," Applied Soft Computing, vol. 98, Jan. 2021.
20. A. Galicia, R. Talavera-Llames, A. Troncoso, I. Koprinska, and F. Martínez-Álvarez, "Multi-step forecasting for big data time series based on ensemble learning," Knowledge-Based Systems, vol. 163, pp. 830–841, Jan. 2019.
21. D. Müller, I. Soto-Rey, and F. Kramer, "An Analysis on Ensemble Learning optimized Medical Image Classification with Deep Convolutional Neural Networks."
22. B. T. Pham et al., "Ensemble modeling of landslide susceptibility using random subspace learner and different decision tree classifiers," Geocarto International, 2020.
23. D. P. Gaikwad and R. C. Thool, "Intrusion detection system using bagging ensemble method of machine learning," in Proceedings - 1st International Conference on Computing, Communication, Control and Automation, ICCUBEA 2015, Jul. 2015, pp. 291–295.
24. I. Tolstikhin et al., "MLP-Mixer: An all-MLP Architecture for Vision," May 2021.
25. A. Krogh, "Neural Network Ensembles, Cross Validation, and Active Learning."
26. A. Anorboev, M. Javokhir, J. Hong, N. T. Nguyen and D. Hwang, "Input Image Pixel Interval method for Classification Using Transfer Learning," 2022 International Conference on INnovations in Intelligent SysTems and Applications (INISTA), Biarritz, France, 2022.
27. R. G. F. Soares, H. Chen, and X. Yao, "A Cluster-Based Semisupervised Ensemble for Multiclass Classification," IEEE Transactions on Emerging Topics in Computational Intelligence, vol. 1, no. 6, pp. 408–420, Dec. 2017.
28. Y. Chen, Y. Wang, Y. Gu, X. He, P. Ghamisi, and X. Jia, "Deep Learning Ensemble for Hyperspectral Image Classification," IEEE Journal of Selected Topics in Applied Earth Observations and Remote Sensing, vol. 12, no. 6, pp. 1882–1897, Jun. 2019.
29. F. Chollet, "Xception: Deep Learning with Depthwise Separable Convolutions," Oct. 2016.
30. K. Faceli, A. de Carvalho, M. Carlos, and P. de Souto, "Multi-objective clustering ensemble. Classical Weightless Neural Systems View project Feature Extraction and Selection Analysis in Biological Sequences View project SEE PROFILE," 2007. [Online]. Available: https://www.researchgate.net/publication/220515994
31. T. Alqurashi and W. Wang, "Clustering ensemble method," *International Journal of Machine Learning and Cybernetics*, vol. 10, no. 6, pp. 1227–1246, Jun. 2019, doi: 10.1007/s13042-017-0756-7.
32. S. olah Abbasi, S. Nejatian, H. Parvin, V. Rezaie, and K. Bagherifard, "Clustering ensemble selection considering quality and diversity," *Artificial Intelligence Review*, vol. 52, no. 2, pp. 1311–1340, Aug. 2019, doi: 10.1007/s10462-018-9642-2.
33. S. Vega-Pons and J. Ruiz-Shulcloper, "A survey of clustering ensemble algorithms," *International Journal of Pattern Recognition and Artificial Intelligence*, vol. 25, no. 3, pp. 337–372, May 2011, doi: 10.1142/S0218001411008683.
34. R. G. F. Soares, H. Chen, and X. Yao, "A Cluster-Based Semisupervised Ensemble for Multiclass Classification," *IEEE Transactions on Emerging Topics in Computational Intelligence*, vol. 1, no. 6, pp. 408–420, Dec. 2017, doi: 10.1109/TETCI.2017.2743219.
35. Z. Yu *et al*., "Incremental Semi-Supervised Clustering Ensemble for High Dimensional Data Clustering," *IEEE Transactions on Knowledge and Data Engineering, vol. 28, no. 3, pp. 701–714, Mar. 2016, doi: 10.1109/TKDE.2015.2499200*.
36. J. Ruiz-Santaquiteria, A. Pedraza, N. Vallez, and A. Velasco, "Parasitic Egg Detection with a Deep Learning Ensemble," IEEE Xplore, Oct. 01, 2022. https://ieeexplore.ieee.org/stamp/stamp.jsp?arnumber=9897858 (accessed Dec. 21, 2022).

37. S. Shastri, K. Singh, M. Deswal, S. Kumar, and V. Mansotra, "CoBiD-net: a tailored deep learning ensemble model for time series forecasting of covid-19," Spatial Information Research, Jun. 2021, doi: 10.1007/s41324-021-00408-3.
38. Md. R. Islam and Md. Nahiduzzaman, "Complex features extraction with deep learning model for the detection of COVID19 from CT scan images using ensemble based machine learning approach," Expert Systems with Applications, vol. 195, p. 116554, Jun. 2022, doi: 10.1016/j.eswa.2022.116554.
39. K. L. Tan, C. P. Lee, K. M. Lim, and K. S. M. Anbananthen, "Sentiment Analysis With Ensemble Hybrid Deep Learning Model," IEEE Access, vol. 10, pp. 103694–103704, 2022, doi: 10.1109/access.2022.3210182.
40. Nguyen N.T. (2006): Conflicts of Ontologies – Classification and Consensus-based Methods for Resolving. In: Proceedings of KES 2006, Lecture Notes in Artificial Intelligence 4252, 267-274
41. Nguyen N.T., Sobecki J. (2003): Using Consensus Methods to Construct Adaptive Interfaces in Multimodal Web-based Systems. Journal of Universal Access in the Information Society 2(4), 342-358
42. Katarzyniak R., Nguyen N.T. (2000): Reconciling inconsistent profiles of agents' knowledge states in distributed multi-agent systems using consensus methods. System Science 26(4), 93-119

Abdulaziz Anorboev is currently pursuing the Ph.D. degree with the Department of Computer Engineering, Yeungnam University, South Korea. His research interests includes deep learning, computer vision and pattern recognition.

Javokhir Musaev is currently pursuing the Ph.D. degree with the Department of Computer Engineering, Yeungnam University, South Korea. He has authored two conference papers and one patent. His research interests include computer vision and pattern recognition using deep learning techniques.

Sarvinoz Anorboeva is currently pursuing the M.S. degree with the Department of Computer Engineering, Yeungnam University, South Korea. Her research interests includes artificial intelligence, machine learning and computer vision.

Dosam Hwang received the Ph.D. degree in Kyoto University, Kyoto, Japan. He is a full professor of the Department of Computer Engineering at Yeungnam University in the Republic of Korea, whose research interests mainly include Natural Language Processing, Ontology, Knowledge Engineering, Information Retrieval, and Machine translation.

Yeong-Seok Seo was an Assistant Professor (Tenure Track) with the Department of Computer Engineering, Yeungnam University, Gyeongsan, Gyeongbuk, Republic of Korea from September 2016 to August 2022, he. Since September 2022, he has been an Associate Professor (Tenure Track) with the same university. His research interests include software engineering, artificial intelligence, Internet of Things, and big data analysis.

Ngoc Thanh Nguyen (Senior Member, IEEE) is currently a Full Professor with the Wroclaw University of Science and Technology, and the Head of Information Systems Department, Faculty of Computer Science and Management. He is the author or coauthor

of five monographs and more than 350 journal and conference papers. He has given 22 plenary and keynote speeches for international conferences, and more than 40 invited lectures in many countries. His research interests include collective intelligence, knowledge integration methods, inconsistent knowledge processing, and multi-agent systems.

Jeongkyu Hong received his PhD in computer science from the Korea Advanced Institute of Science and Technology (KAIST), Korea, in 2017. From 2018 to 2023, he served as an Associate Professor in the Department of Computer Engineering at Yeungnam University, South Korea. Since 2023, he has been an Associate Professor at the School of Electrical and Computer Engineering, University of Seoul. His current research interests lie in the design of reliable and low-power embedded systems and software.

Received: February 23, 2023; Accepted: July 20, 2023.

Computer Science and Information Systems 20(4):1519–1540 https://doi.org/10.2298/CSIS230418058W

Intrusion Detection Model of Internet of Things Based on Deep Learning ⋆

Yan Wang, Dezhi Han, and Mingming Cui

College of Information Engineering
Shanghai Maritime University , China
202130310093@stu.shmtu.edu.cn
dzhan@shmtu.edu.cn
mmcui@stu.shmtu.edu.cn

Abstract. The proliferation of Internet of Things (IoTs) technology is being seriously impeded by insecure networks and data. An effective intrusion detection model is essential for safeguarding the network and data security of IoTs. In this paper, a hybrid parallel intrusion detection model based on deep learning (DL) called HPIDM features a three-layer parallel neural network structure. Combining stacked Long short-term memory (LSTM) neural networks with convolutional neural network (CNN) and SK Net self-attentive mechanism in the model allows HPIDM to learn temporal and spatial features of traffic data effectively. HPIDM fuses the acquired temporal and spatial feature data and then feeds it into the CosMargin classifier for classification detection to reduce the impact of data imbalance on the performance of the Intrusion Detection System (IDS). Finally, HPIDM was experimentally compared with classical intrusion detection models and the two comparative models designed in this paper, and the experimental results show that HPIDM achieves 99.87% accuracy on the ISCX-IDS 2012 dataset and 99.94% accuracy on the CICIDS 2017 dataset. In addition, it outperforms other comparable models in terms of recall, precision, false alarm rate (FAR), and F1_score, showing its feasibility and superiority.

Keywords: intrusion detection, deep learning (DL), Long short-term memory (LSTM), convolutional neural network (CNN), SK Net self-attentive mechanism.

1. Introduction

With the rapid development of wireless sensor networks (WSN), 5G communication technology, big data processing technology, and artificial intelligence technology, the IoTs have been widely used and opened a new era of the Internet of Everythings [27]. According to a white paper released by Cisco, global mobile data traffic has surged by 17 times over the last five years, with nearly 650 million new mobile devices added.

In the era of the IoTs, everything is interoperable, which also means that cyber-attacks can easily invade the real world. Data shows that in the past 10 years, cyber attacks have evolved from individual hackers to organized cyber armies, and the areas of attack are becoming larger and larger, from Internet computers and information networks to military

⋆ The Top-notch Innovative Talent Training Program for Graduate students of Shanghai Maritime University under Grant 2021YBR008

and civilian critical information infrastructures. The use of standards and specifications for the IoTs has become a crucial factor in the development of the industry, the premise of which is to ensure the security of the network and data. An IDS is software or hardware that detects malicious activity on a specific computer or network [37], [14]. IDS reacts to detected intrusions in real-time and alerts administrators and is used to secure the network.

As network attacks become more sophisticated and efficient, traditional intrusion detection methods based on machine learning (ML) are insufficient in detecting and preventing such attacks. As a result, new network attack defense methods must be explored. Intrusion detection technology based on DL has garnered significant attention from both academic and business communities, providing a novel idea for the network security research of the IoTs [46]. DL-based IDS identifies suspicious network activity, prevents hackers from gaining access, and notifies users. They usually have well-known labels and common attack formats. This helps protect against risks such as data breaches. By analyzing traffic more accurately, reducing the number of false alarms, and assisting security teams in distinguishing malicious from legitimate network activity, DL, CNN, and recurrent neural networks (RNNs) can be used to develop smarter IDS [25]. The primary contributions of our paper are as follows.

(1) A DL-based hybrid parallel intrusion detection model (HPIDM) is proposed. The three-layer parallel neural network structure of HPIDM is composed of stacked LSTM and CNN as well as the SK Net attention mechanism, which enables HPIDM to learn the Spatial and temporal features of traffic data effectively. Not only can HPIDM automatically and fully learn the spatial and temporal features of traffic data, but it can also effectively address the issue of data imbalance through multiple-feature fusion.

(2) Based on the HPIDM, two comparison versions are proposed. Comparison model 1 is to change the Fully Convolutional Network(FCN) module of the first layer to a conventional CNN model on HPIDM to verify the effectiveness of the FCN module, and comparison model 2 is to change the combination of the CNN and the stacked LSTM module of the second layer to a conventional CNN module to verify the effectiveness of the stacked LSTM.

(3) The results of the ablation experiments showed that the experimental accuracy of the HPIDM on the ISCX 2012 dataset was 99.87%, which was 0.06%, 0.05%, 0.11%, 0.13%, and 0.12% higher than the TPCNN, TPCNN-C, CROSS_CNN, CROSS_CNN_LSTM, and HPM models respectively, and 0.13% and 0.12% higher than the comparison models model1 and model2 by 0.13% and 0.02% respectively. The experimental accuracy on the CIC-IDS 2017 dataset was 99.94%, which was 0.03%, 0.02%, 0.02%, 0.03%, and 0.04% higher than the TPCNN, TPCNN-C, CROSS_CNN, CROSS_CNN_LSTM, and HPM models, respectively. Moreover, the HPIDM outperforms its counterparts in terms of accuracy, recall, precision, FAR, F1 score, and other related metrics. This validates its feasibility and superiority, as well as the effectiveness of the FCN module and the stacked LSTM module in the HPIDM.

Based on the abbreviations in this document, important symbols are explained in this section using Table 1. The remainder of this paper is structured as follows. In Second 2, the DL-based approach, intrusion detection models, and Back Propagation (BP) neural networks are briefly introduced. Section 3 provides a detailed description of the dataset, data preprocessing algorithms, and the proposed intrusion detection model. The experimental environment and parameters are first presented, and then ablation experiments on

both the ISCX-IDS2012 and CICIDS2017 datasets are conducted in Section 4. Finally, the full paper is summarized, and future work prospects are in Section 5.

Table 1. Explanation of abbreviations.

Abbreviations	Explanation
IoTs	Internet of Things
DL	deep learning
LSTM	Long short-term memory
CNN	convolutional neural network
SK Net	Selective Kernel Networks
IDS	Intrusion Detection System
FAR	false alarm rate
WSN	wireless sensor networks
ML	machine learning
RNNs	recurrent neural networks
FCN	Fully Convolutional Network
RFF	radio frequency fingerprinting
FPN	Feature pyramid network

2. Related Work

Early IDS used a single-layer architecture that could only detect misuse or anomaly attacks. To accurately identify misuse and anomaly attacks, Zhang et al. [43] propose an adaptive serial hierarchical attack identification system (SHIDS) that can automatically train a new classifier and adaptively modify its structure after the new classifier is trained. However, the adaptive learning capability is limited and is not able to learn the features of malicious traffic autonomously. Hall et al. [24] propose a new approach to integrate radio frequency fingerprinting (RFF) technology into a wireless IDS. This approach can effectively control the unauthorized use of network resources by media but is superior to the aging of transceivers and other reasons, which can affect the classification success rate and is relatively homogeneous in terms of scalability.

With the development of machine learning techniques, intrusion detection is gradually shifting towards machine learning-based methods. These methods automatically identify new attacks by learning patterns of attack behavior from large amounts of network data and are thus better able to respond to unknown attack methods [2], [22]. Dina et al. [6] propose a comprehensive summary of machine learning-based intrusion detection methods proposed in the literature over the past decade: artificial neural networks, association rules, fuzzy association rules, Bayesian networks, clustering, decision trees, integrated learning, evolutionary computation, hidden Markov models, inductive learning, etc. Sarnovsky et al. [30] propose a hierarchical IDS based on a primitive symmetric combination of machine learning methods and knowledge-based methods to support the detection of the severity of existing types and novel network attacks.

But with the rise of emerging technologies such as cloud computing and the IoTs, intrusion detection is also facing new challenges. For example, virtualization technologies

in cloud computing environments may result in traditional intrusion detection methods being unable to accurately distinguish traffic between virtual machines; and the large number of devices in the IoTs may pose a large data volume and complexity challenges for intrusion detection [4], [28]. Conventional machine learning methods can no longer meet cybersecurity needs, and DL networks with end-to-end features can solve new types of malicious traffic feature extraction problems. Researchers are therefore applying DL to the field of intrusion detection to improve the accuracy and real-time performance of intrusion detection, as well as to better adapt to the changing network environment. Tao et al. [33] propose a deep reinforcement learning approach to detect malicious attacks in aerial computing networks of UAVs. Fatani et al. [7] propose an advanced feature extraction and selection method for an IoTs IDS based on DL and Aquila optimizer. Cai et al. [3] propose a hybrid parallel DL model for efficient intrusion detection based on metric learning, which improves the detection accuracy of malicious traffic.

Although DL-based intrusion detection techniques are currently the main techniques for network traffic intrusion, a major drawback is that they are highly dependent on feature design and have a high FAR, which does not perform well in real-world applications [35], [17]. Researchers have made several efforts to improve the detection and classification performance of malicious traffic, however, they have neglected the accuracy of malicious sample classification. To this end, this paper abstracts the CNN underlying intrusion traffic data into high-level features, extracts sample features autonomously, interweaves stacked LSTM and multi-scale convolutional operations into the neural network, automatically learns the spatial and temporal features of the traffic data adequately through multiple feature fusions, and optimizes the network parameters to converge the model through a stochastic gradient descent algorithm, and finally performs a sample test to detect the network's intrusion behavior. Simulation results show that the method proposed in this paper has high detection accuracy and true positive rate, as well as a low FAR.

3. Models and Methods

This section introduces the design of a hybrid parallel neural network model, HPIDM, which leverages DL techniques to improve the performance of IoTs anomaly traffic detection.

3.1. Data Pre-processing

In this study, the ICSX 2012 and CIC-IDS 2017 datasets are utilized that include both header and payload information and are considered more novel than the KDD99 dataset [34], [13]. Before conducting experiments, data preprocessing is performed to reduce the interference of noise, missing values, and inconsistent data. The preprocessing steps in this study comprise traffic segmentation, traffic cleaning, image generation, and IDX conversion [36], [20].

(1) Flow cut-off

First, the continuous pcap traffic is divided into discrete traffic units based on quintuple information to extract information from each data file. The discrete traffic data file is created by considering every 5th packet in the data stream as a whole traffic cell. If the number of packets is less than 5, the forward padding method is used. Since packet

lengths are variable, the first 96 bytes of each packet are used to represent it. All malicious traffic is then stored in a CSV file by iterating over the packets [38], [26].

(2) Flow cleaning

The traffic cleaning process involves the replacement of MAC addresses at the data link layer and IP addresses at the IP layer with new randomly generated addresses [5]. This strategy is employed to eliminate the influence of these addresses on the identification results. Specifically, the IP and MAC addresses of each flow are replaced with random numbers, ensuring that the addresses are consistent within each flow after the replacement. Once this process is completed, file cleaning is performed.

(3) Image generation

The preprocessed files are normalized to a fixed length in bytes. If the file is longer than the designated number of bytes, it is truncated, and if it is shorter, it is padded with 0x00 at the end. The normalized file is then converted into a binary grayscale image, where each byte represents a grayscale pixel value. Specifically, the value 0x00 corresponds to black, and 0xff corresponds to white. This conversion allows for visual analysis of the data in an easily interpretable format. The resulting image is saved in PNG format.

(4) IDX conversion

To train the CNN and LSTM networks in the experiments, the collected data must be transformed into the appropriate format. For the CNN, the images must be converted into IDX format files. And for the LSTM network, the input format is flexible, but the maximum input length is limited to prevent excessively long inference times [45].

3.2. Model Design

As shown in Fig. 1, HPIDM consists mainly of a three-layer parallel convolutional neural network, which is used to extract temporal and spatial features of the data by interspersing stacked LSTM and SK Net self-attentive mechanism structures in the convolutional neural network, and achieve accurate classification of small sample datasets through feature fusion, and good experimental results were obtained on the test set. Furthermore, the HPIDM leverages feature fusion technology to enhance the learning performance of traffic data features and effectively address data imbalance issues. The model achieves good detection rates on the CIC-IDS 2017 and ISCX 2012 datasets.

The HPIDM utilizes a three-layered neural network. The first layer implements the Fully Convolutional Network (FCN) to capture more detailed traffic features. To avoid losing the temporal features of traffic data, a combined network structure of CNN and LSTM is used in the second layer to learn the temporal features and improve the accuracy of the predicted values. Lastly, the third layer integrates the convolutional layer and pooling layer (Max pool) with the SK attention mechanism to enhance the model's performance.

(1) Top branch

In HPIDM, the upper branch employs a FCN to extract more precise traffic features. The FCN pioneers the use of convolutional neural networks for semantic segmentation, enabling it to process input images of any size. Unlike traditional CNN, the FCN incorporates a fully convolutional layer, which grants it the flexibility to handle images of varying dimensions. By utilizing a deconvolutional layer for upsampling, the FCN can generate segmentation results that match the input image's size. Furthermore, it dispenses

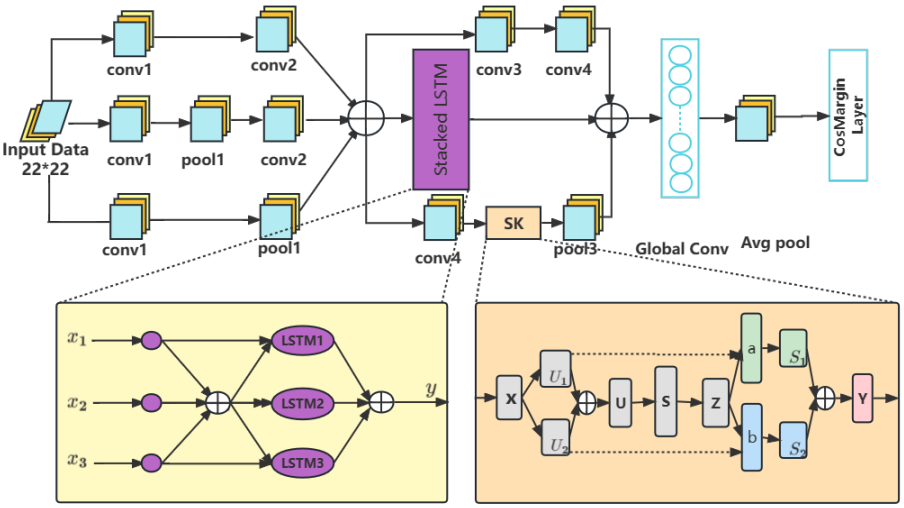

Fig. 1. Local details of the HPIDM

with pooling layers, thereby reducing the model's parameters and computational requirements. As a result, the efficiency of the model is significantly improved.

The input data is convolved four times. The kernel size is 3, the padding is 1, and the stride size is 1 in the first and third convolutions. While the second and fourth convolutional layers have a kernel size of 3, padding of 1, and stride size of 2.

From Eq. (1), it can be seen that $n_{out} = n_{in}$in convolution layers 1 and 3, i.e., the output size is equal. And $n_{out} = \frac{n_{in}}{2}$in convolution layers 2 and 4, i.e., the output is 1/2 of the input.

$$n_{out} = \frac{n_{in} - kernel + 2padding}{stride} + 1 \tag{1}$$

Where $kernel$ is the number of convolution kernels, padding is the filling value, stride is the sliding step size.

(2) Intermediate layer branching

The convolutional layer of the CNN model enables local perception within each feature of the data, followed by higher-level synthesis operations to obtain global information. The pooling layer serves to reduce feature dimensions, compress data and parameters, decrease overfitting, and enhance the fault tolerance rate of the model, thereby ensuring adequate feature learning [29] [12]. Consequently, the lower branch utilizes a combination of convolution and pooling to eliminate redundant information, expand the perception field, and reduce dimensionality and parameter numbers. Considering that the temporal features of the traffic data would be lost if only the traffic features learned using the convolutional network were used, an LSTM structure was added to this layer to learn the temporal features of the traffic.

The HPIDM utilizes the heap LSTM network to capture time sequence features of traffic data. The core idea of LSTM is gated logic. LSTM is made up of memory blocks

rather than neurons. Through a storage unit and three control gates, it can allow the model to selectively process data and develop memories of pertinent historical information over extended time intervals.

The LSTM model comprises three gates, the forgetting gate, the input gate, and the output gate. The forgetting gate utilizes the sigmoid function to regulate the extent of memory retention from the previous time, as shown in Eq. (2), where f_t is between 0 and 1.

$$f_t = \sigma(U_f \times X_t + W_f \times h_{t-1} + b_f), \tag{2}$$

Where σ represents the sigmoid function, U and W are the weights of variables, X_t is the input variables, h is the input variables, and b is the intercept term.

The input gate first employs activation and excitation functions to filter and store input variables, then produces new vectors, and finally updates cell states based on the old cell states and the new variables, as depicted in Eqs. (3) to (5).

$$i_t = \sigma(U_i \times X_t + W_i \times h_{t-1} + b_i) \tag{3}$$

$$\tilde{c_t} = tanh(U_c \times X_t + W_c \times h_{t-1} + b_c)) \tag{4}$$

$$c_t = f_t c_{t-1} + i_t \tilde{c_t} \tag{5}$$

where i_t takes the value of 0 or 1, $\tilde{c_t}$ is the saved input variable, $tanh$ is the tangent excitation function, c_{t-1} is the old cell state value, c_t is the new cell state value, and f_t is the degree of forgetting.

The output gate determines the output variables according to the activation function and processes the data using the excitation function, as shown in Eqs. (6) to (7).

$$o_t = \sigma(U_o \times X_t + W_o \times h_{t-1} + b_o) \tag{6}$$

$$h_t = o_t \times tanh(c_t) \tag{7}$$

where o_t is the input gate activation function and h is the output variable.

CNN is used to extract spatial features, which are subsequently forwarded to the LSTM module for time series feature learning. The resulting time series features are combined with the spatial features learned in the first and third layers for feature fusion. The fused features are fed to each layer to facilitate further learning.

(3) Bottom branch

The bottom branch utilizes traditional CNN in conjunction with the SK Net self-attentive mechanism. While extracting data features alone, CNN may fail to fully reflect the influence of high-frequency features. In recent years, multi-scale geometric analysis theory has introduced a novel approach to image edge detection. Non-subsampling Shearlet multi-scale decomposition is the feature of multi-scale, multi-directionality, translation invariance, and anisotropy, and has high operational efficiency and unrestricted decomposition methods [15], [9]. To enable different images to learn convolution kernels of varying importance, the SK attention mechanism is incorporated into the local path, allowing it

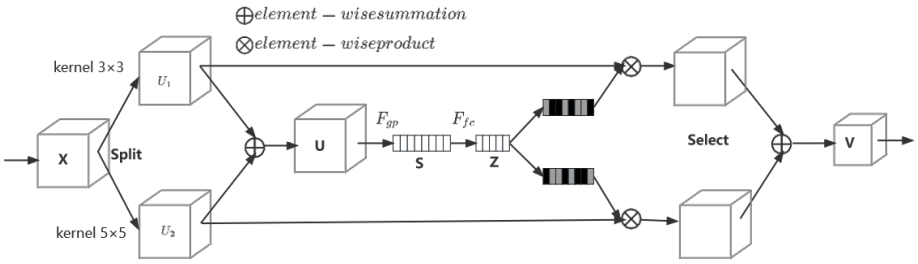

Fig. 2. SK Net model diagram

to select convolution kernels of different sizes depending on the target scale and produce differing effects [31], [41]. The specific model diagram is presented in Fig. 2.

SK Net can be divided into three phases, splitting, fusion, and selection. In the splitting stage, the original feature map is passed through two parallel convolution kernels of size 3×3 and 5×5 filters for parallel convolution operations, and the convolution results of different scales U_1 and U_2 are fused with features. In the fusion stage, the part of each convolutional kernel weight is calculated and the feature maps of the two parts are summed by the element, as shown in Eq. (8).

$$U = U_1 + U_2 \tag{8}$$

The generated U is globally averaged pooled, S is obtained by the F_{gp} function, and the feature map dimension changes from [C×H×W] to [1×1×C], as shown in Eq. (9).

$$S = F_{gp}(U) = \frac{1}{H \times W} \sum_{i=1}^{H} \sum_{j=1}^{W} U(i,j) \tag{9}$$

Full concatenation is used to generate compact features z. δ is the RELU activation function, $\mathcal{B}$ denotes batch normalization (BN), the dimension of z is the number of convolution kernels, the dimension of W_s is $d \times C$, d represents the feature dimension after full concatenation, L has a value of 32 in the text, and r is the compression factor, as shown in Eqs. (10) and (11).

$$z = F_{fc}(S) = \delta(\mathcal{B}(W_s)) \tag{10}$$

$$d = max(C/r, L) \tag{11}$$

After the first two stages, the weight information of different scale spaces is obtained. $Select$ is the process of the new feature map obtained after the calculation of the convolution kernel with different weights. If it is two convolution kernels, then $a_c + b_c = 1$, the dimension of Z will be $d * 1$, the dimension of A will be $C * d$, B will be $C * d$, then the dimension of $a = A * Z$ will be $1 * C$. A_c and B_c are the cth row data of A and B, and a_c is the b_c element of a. This gives the weights of each convolution kernel, respectively, as shown in Eq. (12).

$$a_c = \frac{e^{A_c z}}{e^{A_c z} + e^{B_c z}}, b_c = \frac{e^{B_c z}}{e^{A_c z} + e^{B_c z}} \tag{12}$$

Applying the weights to the feature map, where $V = [V_1, V_2, ..., V_c]$, the dimension of V_c is H*W and the final feature map V is obtained by the attention weights on each kernel. The final output is presented in Eq. (13).

$$V_c = a_c \times U_{1c} + b_c \times U_{2c}, a_c + b_c = 1 \tag{13}$$

Due to the limited perceptual field of convolutional operations, feature extraction of images using a single convolutional kernel of fixed scale size has certain limitations On the contrary, multi-scale feature extraction can get more comprehensive features.

(4) Feature cross-fertilization

The feature fusion method can make comprehensive use of multiple image features to achieve the complementary advantages of multiple features and obtain the robustness and accuracy of recognition results [23]. Feature pyramid network (FPN) is mainly proposed for the multi-scale features of targets in images. It is used to extract features of different scales for classification in the field of target recognition [8], [42]. Based on the high resolution of low-level features and the semantic information of high-level features, the prediction effect is achieved by fusing these features of different layers [21]. FPN upsamples the deep layer information and sums the shallow layer information element by element, thus constructing a feature pyramid structure.[10]

The main methods of feature fusion are early fusion, late fusion, feature non-fusion, etc. In this experiment, concat and add in the early fusion method is used. add is the increase of information under the features describing the image, but the dimension of the image itself does not increase, only the amount of information under each dimension increases [44]. And concat is the merging of the number of channels, which means that the number of features (the number of channels) describing the image itself increases, while the amount of information under each feature does not increase [11].

In this paper, the multi-scale feature fusion of FPN is applied to the HPIDM. The output features of different layers are cascaded several times to obtain the fused feature matrix, which enables the model to fully learn the spatial and temporal features of the traffic data.

First, after the first down sampling of the three-layer neural network, the output feature maps are fused using channel cascading, which does not change the size of the feature maps, but only the multiplicity of channels [32].

Since the convolution kernel of each output channel is independent, only the output of a single channel is concerned. Suppose the two input channels are $X_1, X_2, ..., X_c$ and $Y_1, Y_2, ..., Y_c$.

Then the single output channel of concat is presented in Eq.(14), where * denotes convolution.

$$Z_{concat} = \sum_{i=1}^{c} X_i * K_i + \sum_{i=1}^{c} Y_i * K_{i+c} \tag{14}$$

The fused feature maps are fed simultaneously into a three-layer neural network, with the first layer first passing through a 3*3 sliding convolution window and then downsampling to reduce the size of the feature maps. The second layer is passed through a

stacked LSTM module. The third layer is downsampled after passing through a sliding convolution window and an SK attention mechanism.

The three output feature mappings are subjected to an add fusion operation and then outputted after a global convolution operation and a global average pooling layer [40].

The single output channel of add is Eq.(15).

$$Z_{add} = \sum_{i=1}^{c}(X_i + Y_i) * K_i = \sum_{i=1}^{c} X_i * K_i + \sum_{i=1}^{c} Y_i * K_i \tag{15}$$

The output data is fed into a fully connected layer and a CosMargin layer to classify multiclass imbalanced malicious traffic. A batch processing normalization layer is shelved after each convolutional layer to speed up the convergence of the network model.

4. Experiment and Result Analysis

This section presents the experimental environment and parameter settings. The systematic evaluation of the experiment employs primarily five evaluation metrics. The validity of the model is verified on the ISCX-IDS 2012 ID and CICIDS2017 datasets. The control group comprises classical models such as TPCNN, TPCNN_C, CROSS_CNN, CROSS_CNN_LSTM, and HPM.

4.1. Experimental Environment and Parameter Settings

Table 2. Experiment environment.

Equipment	Example
OS	Windows 10 Professional Edition
CPU	Intel(R)Core(TM)i7-8700CPU@3.20GHz3.19GHz
GPU	RTX 2060
RAM	8G
Compiler environment	Python 3.8

The experimental environment is shown in Table 2. The proposed model is verified using three features, namely data header, payload, and data header with payload. 256-dimensional features are extracted from each data stream and then scaled to 16*16 grayscale images for network training. In the experiments, Adam is employed as an accelerated convergence method, and the optimizer is set to 0.0005 to prevent overfitting, with a fixed momentum factor of 0.9. The learning rate is set to 0.001 for the first eight phases for better speed. In the next three phases, the learning rate is reduced to 0.0001, and the learning rate is set to 0.00001 with a batch size of 256 in the last two phases. No additional data enhancement is used during the testing and training phases to effectively validate the proposed model.

4.2. Selection of Datasets

Compared to other datasets, the CIC-IDS 2017 and ISCX 2012 datasets use the original traffic and contain various types of attacks. Furthermore, they are relatively new and have good robustness and stability.

The CIC-IDS2017 dataset is generated in a simulated environment and spans over five days, incorporating both benign and common attacks to emulate real-world data. The dataset is fully labeled for various types of traffic and consists of source data (PCAP) and network traffic analysis results (CSV files) based on timestamps, source and target IP addresses, source and target ports, protocols, and attack flow. The CIC-IDS2017 dataset divides the acquired network traffic data into a total of 12 categories, there is an unbalanced number of different attacks, which are distributed among the pcap network traffic. Table 3 shows the collection date of the dataset and its corresponding data volume.[39][16]

Table 3. Category distribution of the CIC-IDS2017 dataset.

Data	Description	Data volume size
Monday, July 3, 2017	Normal flow	11G
Tuesday, July 4, 2017	Normal traffic + malicious traffic	11G
Wednesday, July 5, 2017	Normal traffic + malicious traffic	13G
Thursday, July 6, 2017	Normal traffic + malicious traffic	7.8G
Friday, July 7, 2017	Normal traffic + malicious traffic	8.3G

Unlike the KDD99 dataset, the content of the ISCX2012 dataset is newer and its data sample size is larger. The dataset is created using a dynamic approach that encompasses both malicious and non-malicious network behaviors.

The anomaly distribution in the CIC-IDS 2017 and the ISCX 2012 datasets are shown in Figs. 3 and 4, respectively.

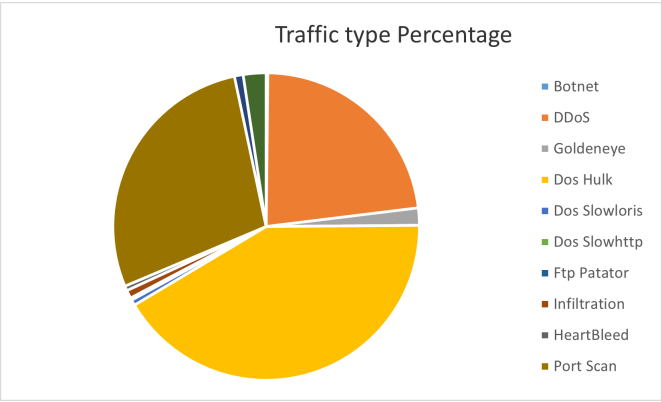

Fig. 3. Anomaly distribution in the CIC-IDS 2017 dataset

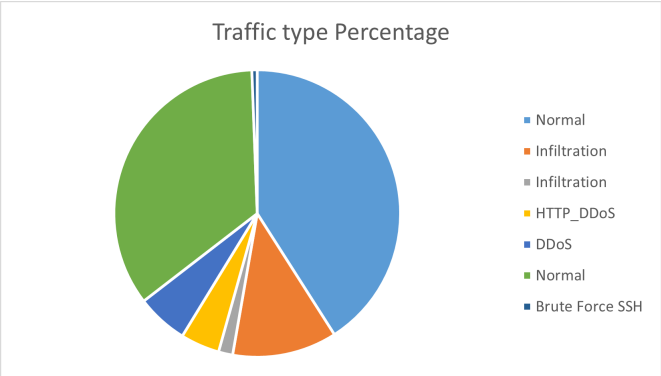

Fig. 4. Anomaly distribution in the ISCX 2012 dataset

The CICIDS2017 dataset is divided into experiments, of which 80% is used as the training set and the remaining 20% as the test set. To distribute each category equally between the training and test sets, it is necessary to divide each type in a ratio of 4:1.

4.3. Five Indicators for experimental evaluation

This paper focuses on the evaluation of intrusion detection from five metrics, accuracy, recall, precision, FAR, and F1_score. The classification of indicators is shown in Table 4.

Table 4. Classification of indicators.

	Relevant	**Not Relevant**
Retrieved	True Positives (TP)	False Positives (FP)
Not Retrieved	False Negatives (FN)	True Negatives (TN)

TP refers to the number of accurately identified positive samples, TN refers to the number of accurately identified negative samples, FP represents the number of falsely identified positive samples, and FN represents the number of falsely identified negative samples.

(1) Accuracy

a metric that measures the ratio of correctly classified samples by the classifier to the total number of samples in a given test data set. It indicates the system's ability to accurately identify intrusions from various behaviors. A detection system with a low accuracy may mistake legitimate activities for intrusions and produce false alarms, which is called false alarm phenomena.[19]It is defined as in Eq. (16).

$$Accuracy = \frac{TP + TN}{TP + TN + FP + FN} \tag{16}$$

(2) Recall

It is the ratio of the number of positive samples that are correctly identified to the total number of all positive samples that should be retrieved, and it is defined as Eq. (17).

$$Recall = \frac{TP}{TP + FN} \tag{17}$$

(3) Precision

It is also called accuracy rate which is the ratio of the number of positive samples correctly retrieved to the number of positive samples retrieved, which is defined in Eq. (18).

$$Precision = \frac{TP}{TP + FP} \tag{18}$$

(4) FAR

It is also known as the false positive rate which is defined as the ratio of incorrectly predicted attack samples to all normal samples and is defined in Eq. (19).

$$FAR = \frac{FP}{FP + TN} \tag{19}$$

(5) F1_score

an evaluation metric that reflects both precision and recall. It is defined as the harmonic mean of precision and recall, as shown in Eq. (20). The F1 score can provide a balanced evaluation of the model's performance by considering both the true and false positives.

$$F1\_score = 2 * (\frac{Precision * Recall}{Precision + Recall}) \tag{20}$$

In the experiments, the positive categories are considered to be the accurately detected categories, while the negatively detected categories are considered negative. The quality of the model is assessed using the five evaluation metrics mentioned earlier. A higher value of accuracy, precision, recall, and F1_score indicates better model performance, while a lower value of the FAR indicates better performance.[18][1]Accuracy is a general measure of a model's classification effectiveness, while Precision, Recall, and F1_score are more focused on assessing the model's effectiveness in detecting different categories.

4.4. Ablation Experiment and Result

To further verify the performance of abnormal network traffic detection, the HPIDM is compared with the conventional network models like TPCNN, TPCN_C, CROSS_CNN, CROSS_CNN_LSTM, and HPM using the datasets ISCX-IDS 2012 and CICIDS2017. Fig. 5 shows the results of the comparison of the recognition accuracy of the models on the ISCX-IDS 2012 dataset. Fig. 6 presents the comparison between the HPIDM and other models in terms of precision, recall rate, F1%score, and FAR. As seen in Fig. 5, the HPIDM has the highest overall detection accuracy on the ISCX-IDS 2012 dataset, outperforming the classical model by 0.06%, 0.05%, 0.11%, 0.13%, 0.12%, respectively, outperforming the two comparison models by 0.13%, 0.02%. From Fig. 6 (A), it can be seen that the detection accuracy of the HPIDM is higher and smoother, which indicates that the proposed method in this paper effectively improves the problem of low detection

rate due to data imbalance. As shown in Fig. 6 (B), the recall rate of the HPIDM is higher than that of other comparable models, indicating that it has a stronger positive sample identification ability. As shown in Fig. 6 (C), compared with other models, the F1_score of the HPIDM is higher, which means that the HPIDM is more robust. It can be seen from Fig.6 (D) that the FAR of the HPIDM is lower and smoother. The experimental results show that the HPIDM is significantly better than other classical network traffic anomaly detection models.

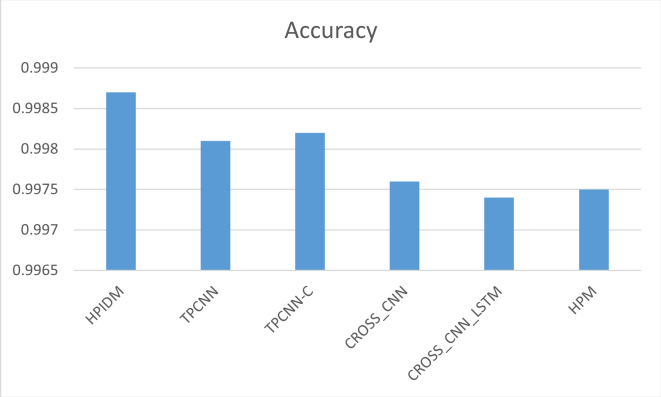

Fig. 5. Comparison of the recognition accuracy of each model on the ISCX-IDS 2012 dataset

Moreover, a comparison of the HPIDM with other classical models in terms of time consumption is shown in Figs. 7and 8. It is evident that although the HPIDM is not the fastest in training time, its testing time is much less than the TPCNN and TPCNN_C models. Additionally, while the training and testing time of the CROSS_CNN and CROSS_CNN_LSTM models are shorter than the HPIDM, they exhibit inferior performance regarding precision, recall, and other relevant aspects. In summary, the HPIDM has high training accuracy and feasibility despite its relatively longer training time.

Additional experiments are conducted in the CICIDS2017 dataset to further validate the efficacy of the HPIDM. The experimental results are presented in Tables 5 to 9. As shown in Table 9, all classifiers exhibit a classification accuracy of over 99%. Notably, the HPIDM displays the highest classification accuracy compared to all other models. Moreover, Table 5 to9 indicate that the HPIDM surpasses other models in terms of accuracy, recall, and F1_score on the CICIDS2017 dataset, thus reinforcing its effectiveness.

Furthermore, the training duration of distinct classifiers is also evaluated on the CICIDS2017 dataset, as depicted in Fig. 9. Tables 5 to 8 and Fig. 9 reveal that the HPIDM outperforms other models in terms of accuracy and training time. The experimental outcomes obtained from the CICIDS2017 dataset provide evidence of the HPIDM's feasibility.

Additionally, two upgraded versions of the HPIDM are introduced and the FCN structure of the first layer and the stacked LSTM module of the second layer are taken as variables for comparative experiments to validate the fusion of feature information. The

Fig. 6. Comparison of precision, recall, F1 score, and FAR for each model on the ISCX-IDS 2012 dataset

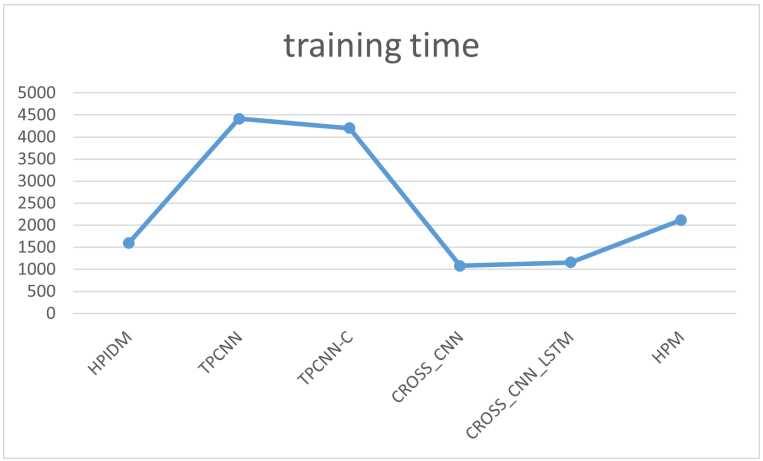

Fig. 7. Comparison of training time for each model on ISCX-IDS 2012 data

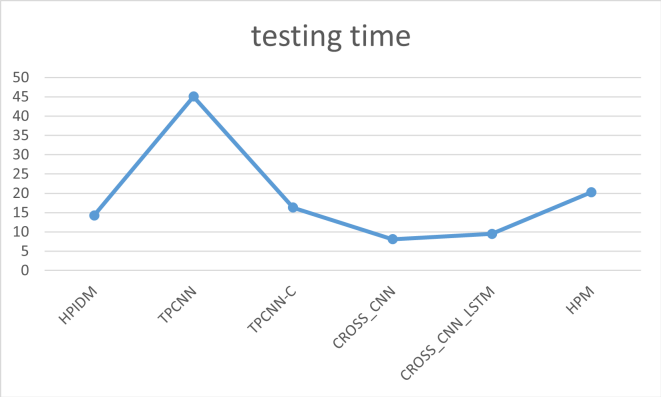

Fig. 8. Comparison of test times for each model on ISCX-IDS 2012 data

Table 5. Precision comparison

Label	0	1	2	3	4	5	6	7	8	9	10	11
HPIDM	1.0000	1.0000	0.9928	0.9987	0.9911	0.9919	1.0000	1.0000	1.0000	0.9999	1.0000	0.9991
TPCNN	1.0000	1.0000	0.9848	0.9992	0.9800	0.9967	0.9997	1.0000	1.0000	1.0000	0.9998	0.9967
TPCNN_C	1.0000	1.0000	0.9955	0.9990	0.9817	0.9938	1.0000	1.0000	1.0000	0.9999	1.0000	0.9972
CROSS_CNN	1.0000	1.0000	0.9956	0.9992	0.9860	0.9924	0.9997	1.0000	1.0000	1.0000	0.9997	0.9976
CROSS_CNN_LSTM	1.0000	1.0000	0.9906	0.9987	0.9889	0.9910	0.9998	1.0000	1.0000	1.0000	1.0000	0.9986
HPM	1.0000	1.0000	0.9913	0.9986	0.9889	0.9910	1.0000	1.0000	1.0000	0.9999	0.9998	0.9967

Table 6. Recall comparison

Label	0	1	2	3	4	5	6	7	8	9	10	11
HPIDM	1.0000	1.0000	0.9706	0.9998	0.9801	0.9934	0.9997	1.0000	1.0000	1.0000	0.9998	0.9995
TPCNN	1.0000	1.0000	0.9796	0.9996	0.9750	0.9891	0.9995	1.0000	1.0000	1.0000	0.9998	1.0000
TPCNN_C	1.0000	1.0000	0.9754	0.9999	0.9867	0.9862	0.9999	1.0000	1.0000	0.9999	0.9998	0.9995
CROSS_CNN	1.0000	1.0000	0.9803	0.9998	0.9860	0.9929	0.9994	1.0000	1.0000	1.0000	0.9998	0.9991
CROSS_CNN_LSTM	1.0000	1.0000	0.9698	0.9997	0.9838	0.9929	0.9995	1.0000	1.0000	1.0000	0.9998	0.9991
HPM	1.0000	1.0000	0.9681	0.9997	0.9809	0.9924	0.9995	0.9995	1.0000	1.0000	0.9996	0.9986

Table 7. F1_score comparison

Label	0	1	2	3	4	5	6	7	8	9	10	11
HPIDM	1.0000	1.0000	0.9815	0.9993	0.9856	0.9927	0.9999	1.0000	1.0000	0.9999	0.9999	0.9991
TPCNN	1.0000	1.0000	0.9822	0.9994	0.9775	0.9929	0.9996	1.0000	1.0000	1.0000	0.9998	0.9983
TPCNN_C	1.0000	1.0000	0.9854	0.9994	0.9842	0.9900	0.9997	1.0000	1.0000	0.9999	0.9999	0.9983
CROSS_CNN	1.0000	1.0000	0.9879	0.9995	0.9860	0.9926	0.9996	1.0000	1.0000	0.9998	0.9998	0.9991
CROSS_CNN_LSTM	1.0000	1.0000	0.9801	0.9992	0.9863	0.9919	0.9997	1.0000	1.0000	1.0000	0.9999	0.9988
HPM	1.0000	1.0000	0.9796	0.9992	0.9848	0.9917	0.9997	0.9997	1.0000	0.9999	0.9997	0.9976

Table 8. FAR comparison

Label	0	1	2	3	4	5	6	7	8	9	10	11
HPIDM	0.0	0.0	0.0001	0.0009	0.0001	0.0	0.0	0.0	0.0	0.0	0.0	0.0
TPCNN	0.0	0.0	0.0003	0.0006	0.0001	0.0001	0.0	0.0	0.0	0.0	0.0	0.0
TPCNN_C	0.0	0.0	0.0001	0.0007	0.0001	0.0001	0.0	0.0	0.0	0.0	0.0	0.0
CROSS_CNN	0.0	0.0	0.0001	0.0006	0.0001	0.0001	0.0	0.0	0.0	0.0	0.0	0.0
CROSS_CNN_LSTM	0.0	0.0	0.0002	0.0009	0.0001	0.0001	0.0	0.0	0.0	0.0	0.0	0.0
HPM	0.0	0.0	0.0002	0.0009	0.0001	0.0001	0.0	0.0	0.0	0.0	0.0	0.0

Table 9. Comparison of the recognition accuracy of each model on the CICIDS2017 dataset

Label	HPIDM	TPCNN	TPCNN_C	CROSS_CNN	CROSS_CNN_LSTM	HPM
Accuracy	0.9994	0.9991	0.9992	0.9992	0.9991	0.99900

Fig. 9. Comparison of training time for each model on the CICIDS2017 dataset

network model structures for comparison tests 1 and 2 are illustrated in Figs. 10and 11. The experiments remain consistent except for the FCN structure of the first layer and the stacked LSTM module of the second layer.

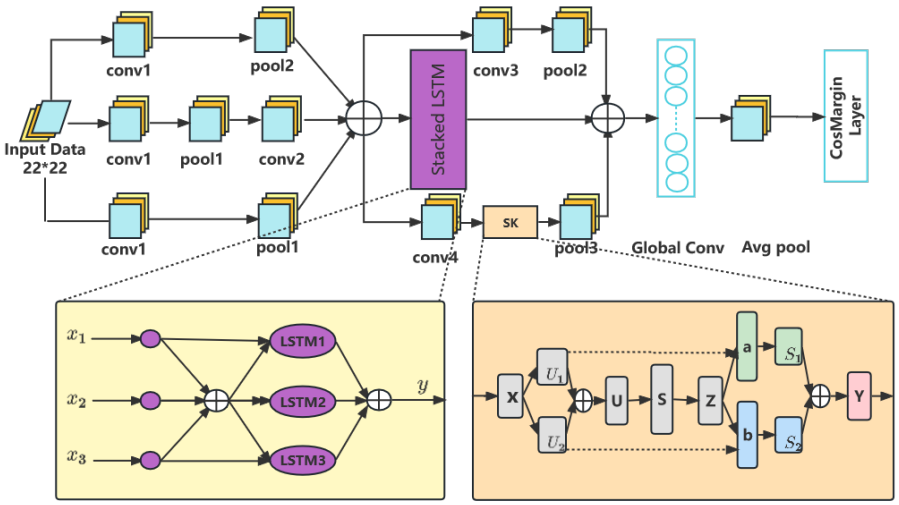

Fig. 10. Model-1 structure

Table 10 shows the accuracy, recall, precision, FAR, F1_score of HPIDM, model-1, and model-2 on the ISCX 2012 dataset. The detection accuracy of the HPIDM on the ISCX 2012 dataset remains the highest, 0.13% higher than that of the comparison model 1 and 0.02% higher than that of the comparison model 2, and F1_score and Recall are optimal, thus demonstrating the effectiveness of the FCN structure and stacked LSTM module in the HPIDM, which indicates that the structure can better learn the features of the traffic data and is more effective in detecting abnormal network traffic.

Table 10. Comparison of experimental results between the HPIDM and the improved model on the ISCX-IDS 2012 dataset

Classifier	Accuracy	Precision	Recall	F1_score	FAR	Training time
HPIDM	0.9987	0.9988	0.9988	0.9987	0.0004	1593.5
Model-1	0.9974	0.9984	0.9979	0.9981	0.0006	1901.8
Model-2	0.9986	0.9987	0.9984	0.9985	0.0005	1104.08

5. Conclusion

This paper introduces a novel hybrid parallel intrusion detection model (HPIDM) based on deep learning. Ablation experiments conducted demonstrate the superior performance

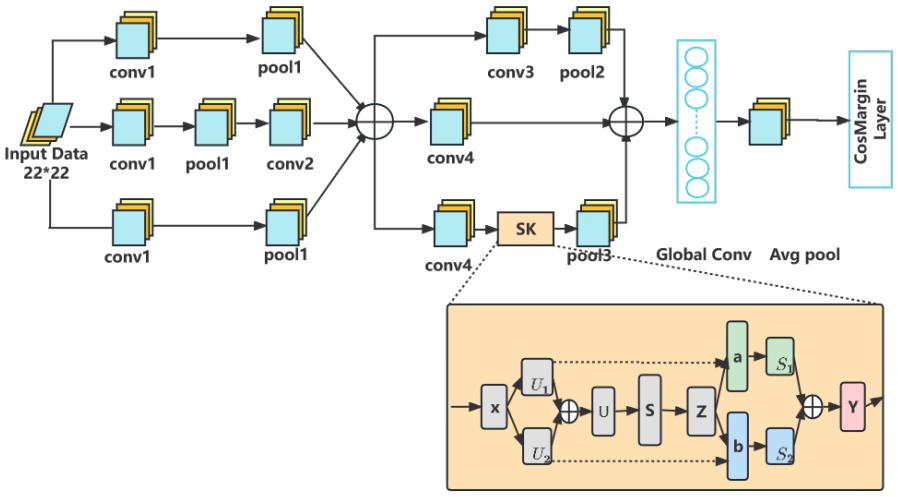

Fig. 11. model-2 structure

of HPIDM compared to other models. On the ISCX-IDS 2012 and CICIDS 2017 datasets, HPIDM achieves remarkable accuracy rates of 99.87% and 99.94%, respectively, surpassing the comparison models. Furthermore, HPIDM exhibits superior recall, accuracy, FAR, and F1_score compared to existing classical models. The success of HPIDM can be attributed to its three-layer parallel neural network structure, which combines a stacked long and short-term memory (LSTM) neural network with a convolutional neural network (CNN), along with the SK Net self-attentive mechanism. This unique combination enables HPIDM to efficiently learn both the temporal and spatial features of traffic data. The experiments comparing the improved models Model1 and Model2 with the HPIDM model also show the soundness of the design of our model in the FCN module and the stacked LSTM module. HPIDM fuses the acquired temporal and spatial feature data several times and then feeds it into the CosMargin classifier for classification detection to reduce the impact of data imbalance on Intrusion Detection System (IDS) performance, resulting in a model with strong robustness and positive sample recognition rate.

HPIDM shows better results in terms of detection accuracy and other evaluation criteria. This model effectively identifies malicious activities and network attacks on specific computers or networks, providing timely alerts to administrators for network security. Its versatility extends to various applications, such as smart homes where it detects unauthorized access to home networks, safeguarding residents' privacy. In industrial control systems, the model detects cyber attacks on critical infrastructure, preventing potential damage. Additionally, it contributes to healthcare systems by detecting and preventing unauthorized access to sensitive patient data.

However, it is important to note that the dataset used in this study comprises a large number of labeled samples, covering various anomalous network traffic classes. In real-world network environments, a substantial amount of data remains unlabeled, and the anomalous traffic classes are unknown. Given the impracticality of labeling all data, fu-

ture research will focus on exploring semi-supervised intrusion detection methods. The aim is to design effective models and methods that can be trained using limited labeled data and abundant unlabeled data. One potential approach involves leveraging Generative Adversarial Networks (GANs) to learn the underlying distribution of network traffic, enabling anomaly detection by comparing real and generated data. This research direction aims to further enhance the accuracy of anomalous network traffic detection, thereby ensuring the network and data security of IoT systems.

References

1. Akshay Kumaar, M., Samiayya, D., Vincent, P.M.D.R., Srinivasan, K., Chang, C.Y., Ganesh, H.: A Hybrid Framework for Intrusion Detection in Healthcare Systems Using Deep Learning. Frontiers in Public Health 9 (2022)
2. Cai, S., Han, D., Li, D.: A Feedback Semi-Supervised Learning With Meta-Gradient for Intrusion Detection. IEEE Systems Journal (2022)
3. Cai, S., Han, D., Yin, X., Li, D., Chang, C.C.: A Hybrid parallel deep learning model for efficient intrusion detection based on metric learning (2022)
4. Chen, P., Han, D.: Effective wind speed estimation study of the wind turbine based on deep learning. Energy 247 (2022)
5. Cui, Z., Chen, W., Chen, Y.: Multi-Scale Convolutional Neural Networks for Time Series Classification (2016)
6. Dina, A.S., Manivannan, D.: Intrusion detection based on Machine Learning techniques in computer networks (2021)
7. Fatani, A., Dahou, A., Al-qaness, M.A.A., Lu, S., Abd Elaziz, M.A.: Advanced Feature Extraction and Selection Approach Using Deep Learning and Aquila Optimizer for IoT Intrusion Detection System (2021)
8. Fu, Y., Cao, L., Guo, G., Huang, T.S.: Multiple Feature Fusion by Subspace Learning
9. Gao, N., Han, D., Weng, T.H., Xia, B., Li, D., Castiglione, A., Li, K.C.: Modeling and analysis of port supply chain system based on Fabric blockchain. Computers & Industrial Engineering 172 (2022)
10. Golz, M., Sommer, D., Chen, M., Trutschel, U., Mandic, D.: Feature Fusion for the Detection of Microsleep Events. The Journal of VLSI Signal Processing Systems for Signal, Image, and Video Technology 49(2) (2007)
11. Golz, M., Sommer, D., Chen, M., Trutschel, U., Mandic, D.: Feature Fusion for the Detection of Microsleep Events. The Journal of VLSI Signal Processing Systems for Signal, Image, and Video Technology 49(2) (2007)
12. Guo, Z., Han, D.: Sparse co-attention visual question answering networks based on thresholds. Applied Intelligence 53(1) (2023)
13. Han, D., Zhu, Y., Li, D., Liang, W., Souri, A., Li, K.C.: A Blockchain-Based Auditable Access Control System for Private Data in Service-Centric IoT Environments. IEEE Transactions on Industrial Informatics 18(5) (2022)
14. Hassan, M.M., Gumaei, A., Alsanad, A., Alrubaian, M., Fortino, G.: A hybrid deep learning model for efficient intrusion detection in big data environment. Information Sciences 513 (2020)
15. Hu, H., Pang, L., Shi, Z.: Image matting in the perception granular deep learning. Knowledge-Based Systems 102 (2016)
16. Jiang, K., Wang, W., Wang, A., Wu, H.: Network Intrusion Detection Combined Hybrid Sampling With Deep Hierarchical Network. IEEE Access 8 (2020)
17. Lakshminarayana, D.H., Philips, J., Tabrizi, N.: A Survey of Intrusion Detection Techniques. In: 2019 18th IEEE International Conference On Machine Learning And Applications (ICMLA). IEEE, Boca Raton, FL, USA (2019)

18. Li, D., Han, D., Weng, T.H., Zheng, Z., Li, H., Liu, H., Castiglione, A., Li, K.C.: Blockchain for federated learning toward secure distributed machine learning systems: a systemic survey. Soft Computing 26(9) (2022)
19. Li, D., Han, D., Xia, B., Weng, T.H., Castiglione, A., Li, K.C.: Fabric-GC: A Blockchain-based Gantt chart system for cross-organizational project management. Computer Science and Information Systems 19(3) (2022)
20. Li, H., Han, D., Tang, M.: A Privacy-Preserving Storage Scheme for Logistics Data With Assistance of Blockchain. IEEE Internet of Things Journal 9(6) (2022)
21. Li, J., Han, D., Wu, Z., Wang, J., Li, K.C., Castiglione, A.: A novel system for medical equipment supply chain traceability based on alliance chain and attribute and role access control. Future Generation Computer Systems 142 (2023)
22. Li, M., Han, D., Yin, X., Liu, H., Li, D.: Design and Implementation of an Anomaly Network Traffic Detection Model Integrating Temporal and Spatial Features. Security and Communication Networks 2021 (2021)
23. Li, Z., Zhou, F.: FSSD: Feature Fusion Single Shot Multibox Detector (2018)
24. Liang, C., Shanmugam, B., Azam, S., Karim, A., Islam, A., Zamani, M., Kavianpour, S., Idris, N.B.: Intrusion Detection System for the Internet of Things Based on Blockchain and Multi-Agent Systems. Electronics 9(7) (2020)
25. Liu, H., Han, D., Cui, M., Li, K.C., Souri, A., Shojafar, M.: IdenMultiSig: Identity-Based Decentralized Multi-Signature in Internet of Things. IEEE Transactions on Computational Social Systems (2023)
26. Ma, W., Zhang, Y., Guo, J., Yu, Q.: Few-Shot Abnormal Network Traffic Detection Based on Multi-scale Deep-CapsNet and Adversarial Reconstruction. International Journal of Computational Intelligence Systems 14(1) (2021)
27. Maheswari, M., A. Karthika, R.: A Novel Hybrid Deep Learning Framework for Intrusion Detection Systems in WSN-IoT Networks. Intelligent Automation & Soft Computing 33(1) (2022)
28. Marir, N., Wang, H., Feng, G., Li, B., Jia, M.: Distributed Abnormal Behavior Detection Approach Based on Deep Belief Network and Ensemble SVM Using Spark. IEEE Access 6 (2018)
29. Meliboev, A., Alikhanov, J., Kim, W.: Performance Evaluation of Deep Learning Based Network Intrusion Detection System across Multiple Balanced and Imbalanced Datasets. Electronics 11(4), 515 (2022)
30. Sarnovsky, M., Paralic, J.: Hierarchical Intrusion Detection Using Machine Learning and Knowledge Model (2020)
31. Shen, X., Han, D., Guo, Z., Chen, C., Hua, J., Luo, G.: Local self-attention in transformer for visual question answering. Applied Intelligence (2022)
32. Sun, Q.S., Zeng, S.G., Liu, Y., Heng, P.A., Xia, D.S.: A new method of feature fusion and its application in image recognition. Pattern Recognition 38(12) (2005)
33. Tao, J., Han, T., Li, R.: Deep-Reinforcement-Learning-Based Intrusion Detection in Aerial Computing Networks (2021)
34. Tian, Q., Han, D., Li, K.C., Liu, X., Duan, L., Castiglione, A.: An intrusion detection approach based on improved deep belief network. Applied Intelligence 50(10) (2020)
35. Wang, Z., Han, D., Li, M., Liu, H., Cui, M.: The abnormal traffic detection scheme based on PCA and SSH. Connection Science 34(1) (2022)
36. Wei, G., Wang, Z.: Adoption and realization of deep learning in network traffic anomaly detection device design. Soft Computing 25(2) (2021)
37. Xia, B., Han, D., Yin, X., Na, G.: RICNN: A ResNet&Inception convolutional neural network for intrusion detection of abnormal traffic. Computer Science and Information Systems 19(1) (2022)
38. Xiao, Y., Xing, C., Zhang, T., Zhao, Z.: An Intrusion Detection Model Based on Feature Reduction and Convolutional Neural Networks. IEEE Access 7 (2019)

39. Yang, H., Wang, F.: Wireless Network Intrusion Detection Based on Improved Convolutional Neural Network. IEEE Access 7 (2019)
40. Yang, J., Yang, J.y., Zhang, D., Lu, J.f.: Feature fusion: parallel strategy vs. serial strategy. Pattern Recognition 36(6) (2003)
41. Yang, Y., Xia, X., Lo, D., Grundy, J.: A Survey on Deep Learning for Software Engineering (2020)
42. Zhang, C., Costa-Perez, X., Patras, P.: Adversarial Attacks Against Deep Learning-Based Network Intrusion Detection Systems and Defense Mechanisms. IEEE/ACM Transactions on Networking 30(3) (2022)
43. Zhang, C., Jiang, J., Kamel, M.: Intrusion detection using hierarchical neural networks (2005)
44. Zhang, Z., Zhang, X., Peng, C., Xue, X., Sun, J.: ExFuse: Enhancing Feature Fusion for Semantic Segmentation. In: Computer Vision – ECCV 2018, vol. 11214. Springer International Publishing, Cham (2018)
45. Zhou, X., Hu, Y., Liang, W., Ma, J., Jin, Q.: Variational LSTM Enhanced Anomaly Detection for Industrial Big Data. IEEE Transactions on Industrial Informatics 17(5) (2021)
46. Zong, B., Song, Q., Min, M.R., Cheng, W., Lumezanu, C., Cho, D., Chen, H.: DEEP AUTOENCODING GAUSSIAN MIXTURE MODEL FOR UNSUPERVISED ANOMALY DETECTION (2018)

Yan Wang is a second-year graduate student majoring in Computer Science and Technology at Shanghai Maritime University, China. Her research interests include deep learning, cyber security, and the Internet of Things.

Dezhi Han is a professor at the School of Information Engineering, Shanghai Maritime University, a senior member of the Chinese Computer Society, a member of the Special Committee on Computer Information Storage, an expert in communication review for several authoritative journals, and an expert in communication review for the National Natural Science Foundation of China. His research interests include cloud computing and cloud storage security technology, IOT network security technology, intelligent image processing and pattern recognition, blockchain theory and application technology, massive network data information storage, retrieval and analysis technology, machine learning, and intelligent information processing.

Mingming Cui received a B.S. degree in Computer Science and Technology from the Anhui University of Finance and Economics, China. She is currently pursuing a Ph.D. degree from Shanghai Maritime University, China, and is a Visiting Ph.D. student at the Nanyang Technological University, Singapore. Her research interests include cryptology, blockchain, data privacy protection, network security, VANETS security, and the Internet of Things.

Received: April 18, 2023; Accepted: July 25, 2023.

Computer Science and Information Systems 20(4):1541–1568 https://doi.org/10.2298/CSIS230401063G

BI-FERH: Blockchain-IoT Based Framework for Securing Smart Hotel

Quanlong Guan[1,2,4], Jiawei Lei[1,3], Chaonan Wang[3], Guanggang Geng[3], Yuansheng Zhong[4], Liangda Fang[1,2,3], Xiujie Huang[1,2,⋆], and WeiQi Luo[1,2,3]

[1] Guangdong Institute of Smart Education,
Jinan University, Guangzhou 510632, China
[2] College of Information Science and Technology,
Jinan University, Guangzhou 510632, China
[3] College of Cyber Security, Jinan University,
Guangzhou 510632, China
[4] Key Laboratory of Safety of Intelligent Robots for
State Market Regulation, Guangdong Testing Institute of Product
Quality Supervision, Guangzhou 510670, People's Republic of China

Abstract. IoT devices and applications are growing rapidly as a result of the advancement of IoT technology. In the case of smart hotels with many IoT devices, the majority of the data generated by those devices contains the private information of users, which is susceptible to being changed and leaked during transmission and storage. To overcome it, this paper proposes a blockchain-IoT based Framework for securing smart hotels(BI-FERH) to enhance the security of hotel information systems. The high performance BI-FERH architecture takes advantage of real-time data transmission capabilities offered by IoT devices. Sensitive data generated by IoT devices is protected in BI-FERH, enhancing tamper-proof capabilities. The results of the experiment demonstrate that BI-FERH can increase the security of smart hotel systems while preserving operational efficacy. An innovative and safe solution for the information management system of smart hotels is offered by the BI-FERH framework.

Keywords: Blockchain, Smart Hotel, IoT, Privacy Protection, Hyperledger Fabric, Data Security.

1. Introduction

IoT devices and blockchain technology are increasingly mature, enhancing people's quality of life. Smart hotels leverage modern technologies like IoT, cloud computing, smart devices, and big data to enhance guest experiences [1]. Over time, IoT devices have elevated the hotel industry's service levels with innovations like Smart Speakers, Social Robots [2], and Hotel intelligent guidance [3]. However, the use of IoT devices in hotels introduces security risks, as they handle sensitive personal information. Protecting this data effectively is challenging, as it faces threats like data leakage and manipulation during service enhancement [4]. Unfortunately, scant literature exists on hotel information security despite its significance, as hotels harbor private data that, if misused, could

⋆ Corresponding author.

lead to cybercrimes. The term ”cybercrime” denotes illegal activities employing computer technology to compromise systems or data. Cybercrime has surged globally, resulting in substantial financial losses, with data breaches causing losses to rise from 3.8 million in 2021 to 4 million in 2022 [5]. Notably, small businesses, including hospitality, face cyberattacks that compromise customer data [6]. Such businesses often lack the means to safeguard data, which, if misused, can facilitate crimes like fraud. Enhancing information systems' security is imperative to protect user data, which entails improving the information management system of smart hotels to utilize guest data effectively and withstand cyberattacks.

Presently, hotel information management systems typically adopt a centralized data storage strategy, which poses challenges in ensuring data integrity due to potential tampering and lack of traceability. Furthermore, central databases become vulnerable to hacking attacks, compromising data availability. Data reliability issues are inherent in this model, with limited security improvement options such as key replacement and enhanced management. The proliferation of data in smart hotels amplifies data protection complexities, necessitating an effective and secure information management system to safeguard guest data. Unfortunately, comprehensive security solutions for hotel information systems against various attackers are lacking.

This paper introduces the Blockchain-IoT-based Framework for sEcuring smaRt Hotel (BI-FERH), aiming to provide a secure and reliable data management solution for the hospitality sector. This framework addresses data integrity compromise and enhances information systems' resilience against malicious attackers. Combining real-time data transmission of IoT devices with blockchain's tamper-evident and traceable characteristics, the BI-FERH framework promises efficient and secure information systems. By leveraging blockchain, the framework elevates data security and trustworthiness in hotels, contributing to enhanced smart hotel data security.

The paper's main contributions are as follows:

(1) Introducing the novel BI-FERH framework, combining blockchain and IoT to secure hotel data while enhancing customer service.

(2) Employing edge computing and edge servers to establish blockchain network nodes at the IoT device layer, enhancing data redundancy and decentralizing resources in the hotel industry.

(3) Designing and implementing the BI-FERH framework, coupled with an Autoencoder + TCN machine learning model to create an Intrusion Detection System (IDS). The IDS identifies 8 types of attack traffic with 97% accuracy, benefiting from the distributed structure's tamper-evident and traceable data attributes.

(4) Conducting experimental tests on the BI-FERH framework, revealing 30% greater efficiency compared to similar blockchain applications, with 10% lower memory consumption and 7% lower CPU consumption. The study delves into usability, performance, and security aspects of the experimental results.

The paper is organized as follows: Section II presents related work, Section III details the BI-FERH solution, Section IV discusses experimental tests, Section V analyzes experimental results, and Section VI concludes the paper. Some parts of this article were first presented in Guan et al. [7].

2. Related Work

The blockchain, introduced by Satoshi Nakamoto [8], presents a peer-to-peer payment and electronic cash system. As Bitcoin's underlying technology, it has immense potential for applications and development, impacting services reliant on trusted third parties. Blockchain finds utility in data structures, verification methods, communication protocols, and information storage [9]. Its hashing algorithm converts variable-length input data to fixed-length digests irreversibly [10]. Public key cryptography, an asymmetric encryption algorithm, verifies identities within blockchain networks [11], enhancing security for data transmission [12]. Consensus mechanisms foster trust among blockchain nodes and ensure transaction consistency [13], spawning diverse algorithms like Proof of Work (POW), Proof of Stake (POS), and Practical Byzantine Fault Tolerance (PBFT).

The Internet of Things (IoT) has seen widespread adoption, necessitating secure, accessible, and reliable infrastructure to process and store data. Blockchain addresses challenges in traditional IoT security protocols [14], especially as a centralized model for IoT data communications introduces privacy and security issues [15].

Studies like Donet, Pérez-Solà, and Herrera-Joancomartí's [16] analyze bitcoin network attributes, while the Bitcoin system prioritizes user privacy and anonymity through public key concealment [17]. Smart contracts elevate blockchain interactivity [18], with Ethereum showcasing blockchain and smart contract synergy, albeit hindered by proof-of-work's inefficiency [19]. Hyperledger Fabric, a Linux Foundation-backed project, employs the Practical Byzantine Fault Tolerance (PBFT) mechanism, enabling transaction validation [20]. Hao et al. [21] determined PBFT's superiority over proof-of-work (PoW) regarding latency and throughput. Fabric's chaincode enables application interaction [22], granting high throughput (>20,000 tps) without proof-of-work [23]. Comparative evaluations of Ether and Hyperledger Fabric address aspects such as throughput, latency, security, and scalability [24] [25].

Table 1 summarizes differences between these blockchain platforms.

Table 1. Platform comparison

Name	Type	Consensus	Smart contract language	Cost	Security
Bitcoin	Public	PoW	Stack based script	Extremely high	Extremely high
Ethereum	Public	PoW/PoS	Solidity	High	High
Hyperledger Fabric	Consortium	Solo/Kafka/PBFT	Go/Java	low	Higher

IoT devices have navigated various challenges, as highlighted by Da Xu, He, and Li in 2014 [26], who outlined the IoT industry's development and dilemmas at that time. Edge computing meets low-latency requirements for compute or data-intensive tasks [27], aligning well with efficient IoT operation. Combining edge architectures with blockchain is viable [28]. Expanding edge computing, Du et al. explored a blockchain-enhanced EC market, where data service operators rent edge nodes, leasing them to user terminals for computation offloading [29]. The advent of blockchain facilitated IoT and blockchain integration [30]. Kshetri [31] proposed blockchain's use in supply chains to mitigate cost

and risk. Blockchain elevates IoT interactivity, data security, reliability, and scalability [30]. Khan and Salah [32] surveyed IoT security issues, suggesting blockchain solutions. Blockchain's impact extends beyond finance to non-monetary domains like smart factories [33], traceable supply chains [34], fake news detection [35], smart homes [36], medical records [37], smart hospitals [38], secure transportation [39], decentralized voting [40], and more. The IoT-blockchain combination streamlines data transactions [41]. Evaluating merged systems challenges researchers, with Lao et al. using throughput and consensus security to assess IoT ecosystems and blockchain platforms [42]. Alshudukhi et al. introduced a blockchain-microservices security framework for IoT federated cloud systems [43].

Inspired by Daidone et al. [44] who used blockchain to protect IoT privacy, this paper addresses IoT devices' role in enhancing hotel service quality. Privacy concerns persist due to the sensitive data inherent in the hotel industry. Sahu and Gutub [5] highlighted personal information leakage risks in hotels and proposed grayscale steganography for protection. Presently, hotel data is centralized, risking tampering and leakage. A blockchain-based privacy scheme for IoT is feasible [45]. To elevate hotel services and data security, this paper proposes a blockchain-integrated smart hotel framework. Martinez-Rendon et al. [46] merged blockchain with edge IoT architecture for heightened security. Edge computing efficiently transfers IoT data, while blockchain safeguards guest data in hotels.

3. Blockchain-IoT based Framework for securing smart Hotel(BI-FERH)

To improve the quality of hotel services and data security, Blockchain-IoT based Framework for securing smart Hotel(BI-FERH) is proposed and shown by Figure 1 with three parts. The first part is made up of IoT devices and artificial intelligence for quality service. The second part consists of blockchain for data reliability and security. And the last part is connected by the Internet between users, devices, and databases. Hotel guests and staff request different services from the server through their respective Internet API interfaces. For example, the booking of various hotel services, the setting of IoT devices, and the viewing of hotel guests' private data, etc. The privacy data generated by the IoT devices is stored in the Hyperledger Fabric blockchain network. The confidentiality, integrity, and availability of the system data are improved by using blockchain data security and tamper-evident features. Through the use of channels in Fabric, data interoperability of multiple hotels can be achieved, while hotels outside the channels can achieve data confidentiality.

3.1. System Framework

As shown in Figure 2, the BI-FERH framework consists of five independent modules, which are the application layer, edge IoT layer, IDS layer, edge server layer, and blockchain layer. The functions of each layer in the framework are described below.

- Application Layer: Hotel guests and staff access specific services through this layer, like check-in, information management, and remote control of smart devices. It serves as the interface for interacting with the hotel system. It links to the next layer through human-machine interaction and network connections.

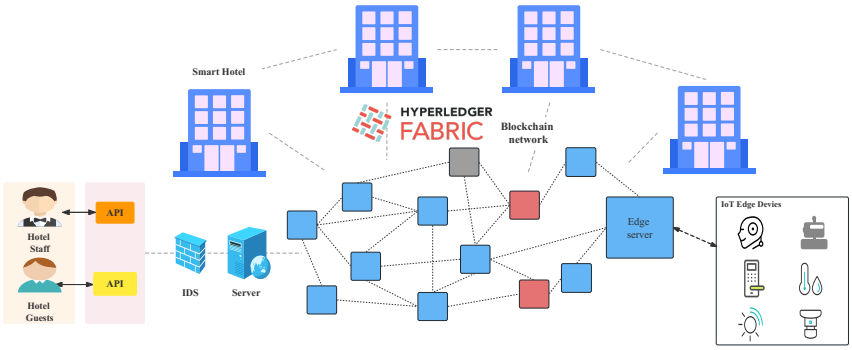

Fig. 1. BI-FERH architecture

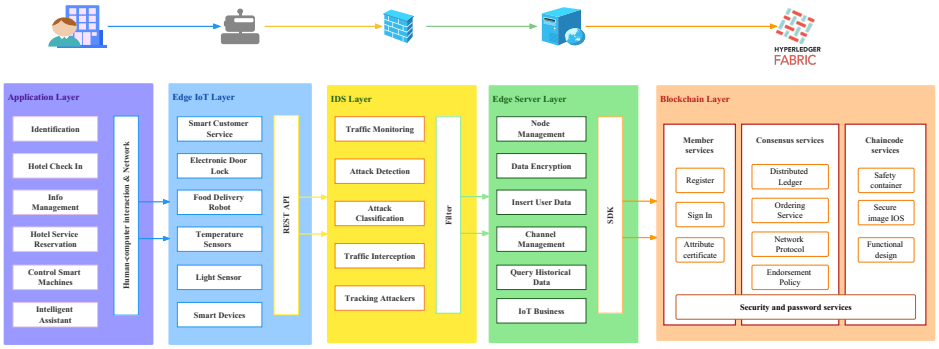

Fig. 2. System framework

- Edge IoT Layer: This layer provides hardware support for smart hotels. Given the limited computing power of IoT devices, edge computing architecture is adopted to efficiently process operations. Complex tasks are sent to edge servers for processing.
- IDS Layer: This layer aims to prevent malicious attacks on the information system. It collects network data via traffic monitoring for attack identification and classification. Malicious traffic is intercepted, and attacker information is traced.
- Edge Server Layer: This layer has two primary functions: processing edge device data and interacting with the blockchain layer. Edge devices send data for processing and receive processed data. It manages the blockchain network using the SDK, storing necessary data in the blockchain.
- Blockchain Layer: Hyperledger Fabric is chosen as the platform. It includes three key modules: the member service module, consensus service module, and chaincode module. Secure communication among these modules relies on security and cryptographic services, protected by public-private key pairs and TLS protocols. The member service module handles member vetting, registration, and authentication.

The Consensus Service module ensures secure ledger booking and data agreement among nodes. The chaincode service module automates business logic calculations.

3.2. Edge IoT Architecture

In the BI-FERH framework, IoT devices employ an edge IoT architecture. Edge computing is utilized to reduce latency and bandwidth by processing data closer to its source. This architecture comprises edge servers and edge devices. Edge devices collect data and send it to the edge server. The edge server processes data, provides computational resources, and returns results to edge devices. Figure 3 illustrates the fusion of blockchain and edge IoT architecture. Edge devices deliver intelligent services and data processing occurs on the edge server. The edge server, doubling as a blockchain network node, broadcasts and stores data. This harnesses blockchain features to enhance data reliability and security.

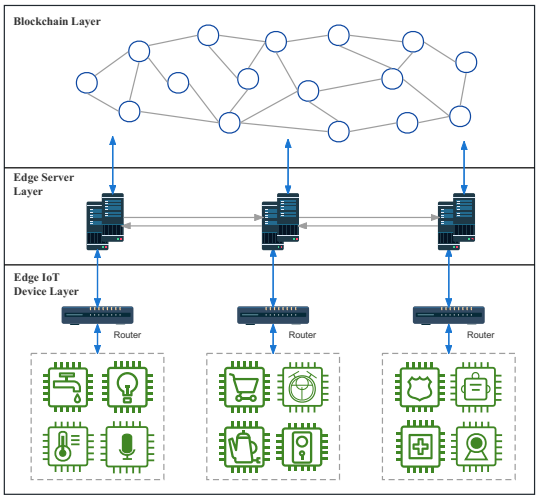

Fig. 3. Edge IoT Architecture

3.3. Intrusion Detection System

Traditional security tools are inadequate against sophisticated network attacks. Machine learning, especially in intrusion detection, is on the rise. In the BI-FERH framework (Figure 4), an autoencoder + TCN hybrid model is used for identifying and classifying attack traffic in network data.Network traffic's feature values enter the autoencoder (AE). Unlike manual feature engineering, AE automatically transforms input into suitable training data. Encoded data then goes into a temporal convolutional network (TCN), excelling in processing time-series data.After TCN's convolutional operation, data is flattened and sent to a fully connected layer for attack classification training. This hybrid approach strengthens BI-FERH's ability to detect and classify network attacks.

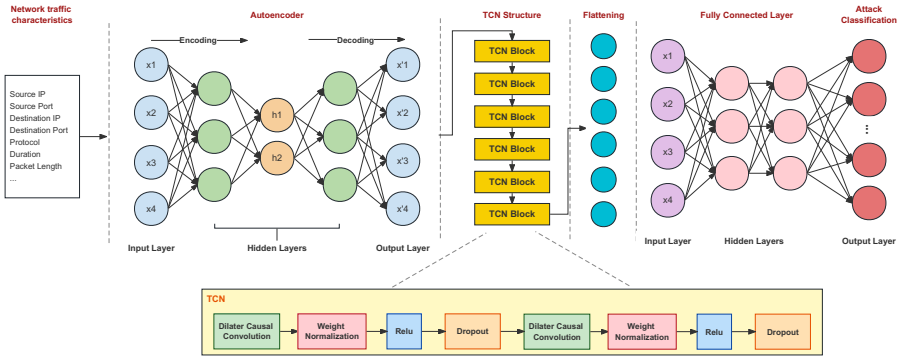

Fig. 4. Autoencoder + TCN Architecture

3.4. Workflow

As shown in Figure 5, the workflow of the BI-FERH solution consists of five main parts. The details of the steps in the workflow will be described in this section. The symbols used are explained in Table 2.

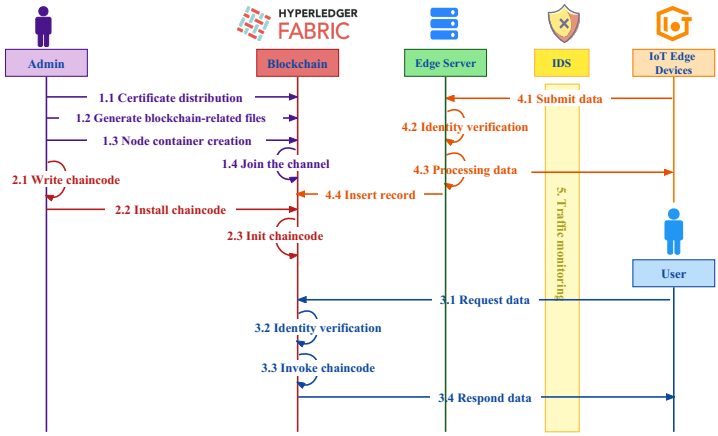

Fig. 5. Workflow of BI-FERH

Part 1 The main purpose of this part is the construction of the Hyperledger Fabric blockchain, which requires the admin to design and configure the network structure and finally build the basic network architecture. The first part mainly includes 4 steps.

Step 1 In order to secure communication and identity, certificates need to be issued for all members such as peers, orderers, channels, users, and devices. The certificate is generated and issued by the CA authority.

$$CA \rightarrow \{Cert_{user}, Cert_{orderer}, Cert_{peer}, Cert_{channel}, Cert_{device}\} \quad (1)$$

Table 2. Symbol descriptions

Symbol	Meaning
CA	Certificate Authority
$Cert$	Certificates and digital signature files
$user$	Hotel guests and staff
$device$	IoT devices
$channel$	Hyperledger Fabric channel
$conf_{net}$	Blockchain network configuration file
$conf_{node}$	Blockchain node docker configuration file
$File_{channel}$	Channel files for blockchain networks
$File_{Anchor}$	Anchor node files for building blockchain networks
$File_{Genesis}$	The first block data of the blockchain
$Image$	Docker Image
$Container$	Docker Container
$Ledger$	A ledger for recording information in the Hyperledger Fabric
CC	Chaincode in Hyperledger Fabric
$Code(business)$	Code corresponding chaincode for business logic requirements
SDK_{Go}	SDK written in golang in Hyperledger Fabric
$TxId$	Transaction id in blockchain
IDS	Intrusion Detection System
$Traffic$	Network traffic of users and IoT
$Invoke(CC_{Init})$	Invoke chaincode to initialize node information
$CC_{Identify}(Request)$	Chaincode for identity authentication of HTTP request packets
$Response$	Response package processed by chaincode
$Install(CC)$	Install chaincode for blockchain
$Traffic_{attatck}$	Attack traffic in the network
$Request$	HTTP business request package
$Response$	Response information for data processing.

Step 2 The admin designs the network structure to generate the configuration file $conf_{net}$. According to the configuration file, the relevant files needed for the blockchain network are generated, including the channel, anchor node and creation block files.

$$Generate\,(conf_{net}) \rightarrow \{File_{channel}, File_{Anchor}, File_{Genesis}\} \tag{2}$$

Step 3 According to the node configuration file $conf_{node}$ written by the admin, build docker images for peer and orderer nodes, and then store them in the docker container to run. The respective certificates also need to be packed into the image.

$$Build\,(conf_{node}, Cert) \rightarrow Image \xrightarrow{run} Container \tag{3}$$

Step 4 After the container is started, the container, ledger, and related files are added to the channel together to build out a complete blockchain environment.

$$\{Container, File_{channel,Anchor,Genesis}, Ledger\} \xrightarrow{join} Channel \tag{4}$$

Part 2 After the blockchain base environment is constructed, the admin needs to design the corresponding chaincode for the actual application and deploy it to the blockchain. This part is completed in three steps.

Step 1 The admin writes the chaincode for the blockchain application according to different business logic.

$$Code(business) \rightarrow CC \tag{5}$$

Step 2 Install the chaincode into all peer nodes via the SDK_{Go}.

$$Install(CC) \xrightarrow{SDK_{Go}} Peer \tag{6}$$

Step 3 Initialize the chaincode of the peer node by invoking the initialization function of chaincode through SDK_{Go}.

$$Invoke(CC_{Init}) \xrightarrow{SDK_{Go}} Peer \tag{7}$$

Part 3 This section focuses on the process of hotel guests and staff interacting with the system as users. The interaction between the user and the system can be divided into three steps.

Step 1 The user generates a request package Request with userId, certificate, target url and data packaged together.

$$\{userId, data, Cert_{user}, url\} \rightarrow Request \tag{8}$$

Step 2 After receiving the user request, the server determines whether the request has permission based on the user's identity and the requested data. If the user has permission, the request is accepted, and if not, the request is rejected.

$$CC_{Identify}\,(Request) \rightarrow \begin{cases} 1 & Accept \\ 0 & Reject \end{cases} \tag{9}$$

Step 3 After accepting the request, the SDK_{Go} invokes the chaincode according to the url and data to complete the corresponding operations, and finally returns the response to the user.

$$CC(url, data) \xrightarrow{SDK_{Go}} Response \tag{10}$$

Part 4 The fourth part is the process of IoT devices interacting with the blockchain network. It is mainly for the data processing of IoT devices. This part can be divided into three steps.

Step 1 Send the deviceId, certificate, target url and data of the IoT device packaged as $Request$ to the blockchain.

$$\{deviceId, data, Cert_{device}, url\} \rightarrow Request \tag{11}$$

Step 2 Authenticate the IoT device, based on the deviceId and certificate of the device. If the authentication is passed, the access request is accepted, otherwise it is rejected.

$$CC_{Identify}\,(Request) \rightarrow \begin{cases} 1 & Accept \\ 0 & Reject \end{cases} \tag{12}$$

Step 3 After receiving the request from the device, it can be divided into two types depending on the url of the request. One is to store the device data, first encrypt the privacy data, then call the chaincode through the SDK_{Go} to store it in the blockchain, and finally get the new ledger data and transaction id. The other is to execute the request from the device and return the corresponding result.

$$Request \rightarrow \begin{cases} CC_{Insert}(Encrypt(data), deciveId, url) \xrightarrow{SDK_{Go}} \{Ledger, TxId\} \\ CC(url, data) \xrightarrow{SDK_{Go}} Response \end{cases} \tag{13}$$

Part 5 The last part is the IDS used to resist malicious attackers by monitoring the access traffic of users and IoT devices, identifying malicious access data and blocking it.

Step 1 All network traffic entering the edge server must be inspected by the IDS, and packets that are judged to be malicious traffic will be discarded, and only legitimate traffic can pass through.

$$IDS(Traffic) \rightarrow \begin{cases} Attack \rightarrow Reject \\ Legal \rightarrow Accpet \end{cases} \tag{14}$$

Step 2 When illegal traffic is denied, the type of attack is identified and the attack event is written to the security log.

$$IDS(Traffic_{Attack}) \rightarrow Log(IP_{src}, Port_{src}, IP_{dst}, Port_{dst}, Type_{Attack}) \tag{15}$$

3.5. Chaincode Design

The most important parts of BI-FERH are identity verification, data insertion and querying of data. The pseudo-code of the identity chaincode is verified by algorithm 1, and its time complexity is *O(n)*. The certificate(*cert*) and *Id* value of the user or IoT device are as input parameters. The output value *Pass* of the algorithm is a Boolean value, True means the authentication is passed and belongs to a legitimate account in the blockchain, and False means the verification fails. The function **CheckCA**(*Cert*) returns the CA of the user's certificate as *MyCA* variable. Then this *MyCA* would be checked whether it belongs to the trusted root CA(*RootCAlist*) or intermediate CA(*IntermediateCAlist*). After that, **CheckId**(*Cert*) function is used to check if the user is the MSP licensed user(*MSPlist*) and to determine if the *Id* value is the same as the one entered. Finally, the certificate is checked within the validity period by **TimeOut**(*Cert*) function. if all judgments have been passed, it means the authentication is passed.

Algorithm 2 pseudocode inserts data into the blockchain, with a time complexity of *O(n)*. Inputs include IoT device certificate (*Cert*), device ID (*deviceId*), and access data (*AccessData*). Output is transaction ID (*TxId*) or error message (*error*).

Verify device identity using **CC.Identify**(*Cert,deviceId*). If authentication fails, return -1. Check device permission with **CheckPermission**(*deviceId*). If not permitted, return -1. Parse incoming *AccessData* into *Day*, *Room*, *Time*, and *Operator* using **Split**(*AccessData*). Encrypt *Time* for user privacy using AES encryption and Base64 encoding. Package information and invoke **stub.PutState**(*Day,data*) to store data in blockchain. Returns transaction ID or error message. Output *error* if message not empty, else return *TxId*.

Storage key is *Day*, used as primary key. Using room number as key leads to inefficiencies during retrieval due to data volume growth over time.

Algorithm 1 CC.Identify(*Cert*, *Id*): Verify the legitimacy of identity

Input: *Cert*, *Id(userId or deviceId)*
Output: *Pass (bool)*

Pass ← *True*
MyCA ← **CheckCA**(*Cert*)
if *MyCA* ∉ *RootCAlist* and *MyCA* ∉ *IntermediateCAlist* **then**
    Pass ← *False*
end if
if CheckId(*Cert*) ∉ *MSPlist* **then**
    Pass ← *False*
end if
if CheckId(*Cert*)! = *userId* **then**
    Pass ← *False*
end if
if TimeOut(*Cert*) ← *True* **then**
    Pass ← *False*
end if

return *Pass*

Algorithm 2 CC.Insert(*Cert*, *deviceId*, *AccessData*): Insert data into the blockchain

Input: *Cert*, *deviceId*, *AccessData*
Output: *TxId or error*

TxId ← -1
Legal ← **CC.Identify**(*Cert*, *deviceId*)
if *Legal* == *False* **then**
    return *TxId*
end if
if CheckPermission(*deviceId*) == *False* **then**
    return *TxId*
end if
Day,Room,Time,Operator ← **Split**(*AccessData*)
encryptedT ← **AESEncrypt**(*Time*)
encodedT ← **Base64Encode**(*aes-encrypted*)
data ← {*Day, Room, encodedT, Operator*}
Txid,err ← **stub.PutState**(*Day, data*)
if *error* ! = *null* **then**
    return *error*
end if

return *Txid*

Algorithm 3 pseudocode queries blockchain data with time complexity *O(n)*. Inputs: user's credentials (*Cert*), *userId*, and *Request*. Output: hotel room access record (*Room-Record*) or error message (*error*).

Call **Identify**(*Cert,userId*) to verify identity, return *null* if successful. If verified, match *userId* to admin (*AdminList*), staff (*StaffList*), or guest (*GuestList*). Admins can view all data, staff can view staff data within chosen time range, guests can view own room data from check-in to present. Use **CheckInTime**(*roomNum*) to query target room's latest check-in time. Use **NowTime()** for current time. Call **GetHistoryForKey**(*day*) to query modification records (*raw*) for key. Extract required data by *roomNum*. Decode and decrypt time info for data restoration. If data extraction produces error, return *error*; else return *RoomRecord* based on user's identity.

Algorithm 3 CC.Query(*Cert*, *userId*, *Request*)
Query the history of blocks in the blockchain

Input: *Cert*, *userId*, *Request*
Output: *RoomRecord or error*

```
1: Legal ← CC.Identify(Cert, userId)
2: tmpList ← []
3: if Legal == False then
4:     return null
5: end if
6: if userId ∈ AdminList then
7:     StartTime, EndTime, roomNum ← Request
8:     for day in range(StartTime, EndTime) do
9:         raw, error ← GetHistoryForKey(day)
10:        if error ! = null then
11:            return error
12:        end if
13:        for d in raw do
14:            if d[room] == roomNum then
15:                tempList.append(d)
16:            end if
17:        end for
18:    end for
19: else if userId ∈ StaffList then
20:    StartTime, EndTime,roomNum ← Request
21:    for day in range(StartTime, EndTime) do
22:        raw, error ← GetHistoryForKey(day)
23:        if error ! = null then
24:            return error
25:        end if
26:        for d in raw do
27:            if d[room] == roomNum and
               d[operator] == Staff then
28:                tempList.append(d)
29:            end if
30:        end for
31:    end for
32: else if userId ∈ GuestList then
33:    roomNum ← Request
34:    StartTime ← CheckInTime(roomNum)
35:    EndTime ← NowTime()
36:    for day in range(StartTime, EndTime) do
37:        raw, err ← GetHistoryForKey(day)
38:        if error ! = null then
39:            return null
40:        end if
41:        for d in raw do
42:            if d[room] == roomNum then
43:                tempList.append(d)
44:            end if
45:        end for
46:    end for
47: end if
48: for t in tempList do
49:    tmp ← AESDecrypt(Base64Decode(t[time]))
50:    t[time] ← tmp
51: end for
52: RoomRecord ← tempList
53: return RoomRecord
```

4. Experiment

The system integrates IoT electronic door locks with blockchain, as shown in Figure 6. When the electronic door lock in the smart hotel activates, it wirelessly transmits details like room number, operator, and timestamp to the server. Network traffic undergoes attack identification via IDS, eliminating malicious traffic. The server encrypts and stores

data in the blockchain using Hyperledger Fabric. The experimental part adopts the same configuration and experimental test method as the paper[7].

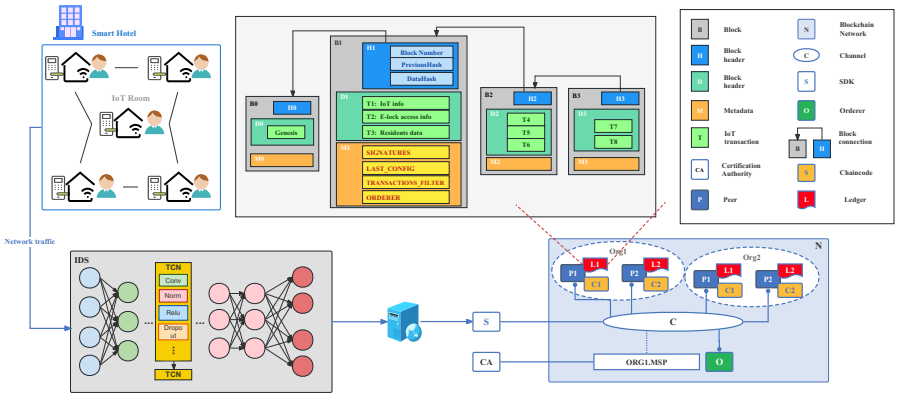

Fig. 6. Framework of this experimental system

4.1. Environment Configuration

The configuration information of the experimental environment is consistent with our previous work on the paper[7]. Refer to Table 3 for a detailed test environment overview.

4.2. System performance

The Fabric network is initialized using the SDK, involving steps such as channel creation, node addition, chaincode packaging, installation, approval, submission, and initialization. Table 4 presents time consumption for each phase in the BI-FERH system. Notably, the endorsement strategies of organizations contribute to the time-consuming approval, submission, and initialization phases. Despite this, blockchain network setup takes under 8 seconds on average, which is remarkably swift compared to manual network creation. SDK construction time is also rapid, and next, the performance of SDKs built with different programming languages will be compared.

The SDK can be developed in Go, Node.js, or Java. This paper opts for Go due to its lightweight, efficient, and parallel nature, as analyzed in [47]. The experiment compares data update and query operations times across different SDKs.In Figure 7, time spent by various SDKs for ledger update operations is depicted. Go (blue curve) stands out, offering optimal performance even with a slight increase in time as node count grows. For instance, with few nodes, Go is around 100 ms faster compared to other languages. This performance advantage amplifies with more nodes; at 16 nodes, Go is approximately 0.5s quicker than other languages.

Figure 8 illustrates query operation times across different SDKs. Queries involve only Fabric's consensus algorithm and a single-node ledger inquiry. Thus, the overall time is minimal. Notably, Java's query time increases with node count, unlike other SDKs. Go and Node.js lead with the best results, both achieving around 20ms. Java, comparatively,

Table 3. Development environment information

Hardware	
CPU	AMD R7 5800H
Hard Disk	516G
Memory	16G
Software	
OS	Windows 10 Unbutu 20.04
Docker	v20.10.7
Docker-compose	v1.29.2
Golang	v1.15.5
Platform	Hyperledger Fabric

Table 4. Time cost for initialization operations

Phase	Time(ms)
SDK generation	26
Create channel	48
Join Channel	320
Packing chaincode	670
Install chaincode	274
Organization approval	2617
Commit chaincode	2547
Initialize chaincode	2625

takes approximately 45ms. In data updates and query efficiency, the Go SDK outperforms other languages.

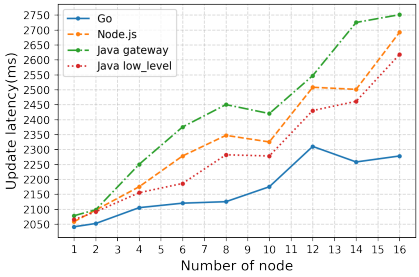

Fig. 7. Update speed of different SDK

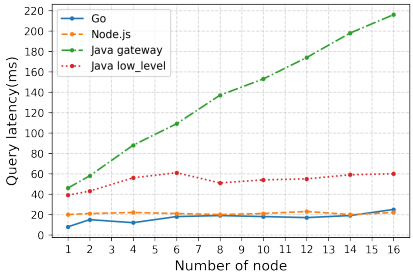

Fig. 8. Query speed of different SDK

Table 5 displays resource usage during data insertion for different nodes in the experiment. It includes node names, maximum/average CPU usage, memory consumption, and block input/output. CPU and memory consumption are highest for peer and CouchDB nodes, essential for data processing. Peers and CouchDB have average CPU usage of 13% and 20%, and memory usage around 194.5MB and 80.4MB respectively. The Orderer node, vital for consensus, consumes less CPU (7.74%) and memory (96.66MB). Chaincode and CA nodes show lower resource demands.

This system ensures efficient data processing with minimal resource utilization despite significant block input/output. Future experiments will further compare its superiority against other blockchain applications.

4.3. Comparison with traditional structure

In order to compare with the traditional database, a MySQL-IoT traditional database system with exactly the same functions as the BI-FERH system is constructed in this exper-

Table 5. Resource consumption

NAME	CPU (Max)	CPU (Avg)	MEM USAGE	BLOCK I/O
Chaincode-Peer0	1.93%	1.87%	12.05MB	9.58MB/0B
Chaincode-Peer1	2.07%	1.76%	14.18MB	9.29MB/0B
Peer0	22.76%	15.58%	171MB	16.6MB/8MB
Peer1	23.77%	10.69%	218.1MB	17.3MB/7MB
Orderer	9.87%	7.74%	94.66MB	5.8MB/8MB
Ca.Org1	0.36%	0.10%	16.56MB	20.1MB/311KB
CouchDB0	24.87%	20.01%	85.77MB	20.5MB/19.4MB
CouchDB1	25.88%	19.74%	75.14MB	5.88/20.3MB

iment. Both of them have completed the same functions, such as data encryption, permission control, login management, etc., except for the different data storage structures. The experiment compares the concurrent performance and data processing efficiency of the two systems by sending requests for queries and inserting data in multiple threads. Figure 9 is the content of the inserted data, which contains the packet number, date, operator number, specific time, and room number. The experiment uses 100 threads to send packets continuously for 10 minutes to two servers, containing data queries, insertions, and updates. The total number of packets received by a single system was 289192, and the packet loss rate was 0% for both systems. By recording the data processing time of the two systems, the final test results were obtained as shown in Figure 10.

```
{
    "id": 1283,                          //Packet ID
    "Day": "2022-07-15",                 //Date
    "Operator": "Staff-cleaner-18",      //Operator number
    "Time": "1657864954",                //Specific time stamp
    "Username": 701,                     //Room number

}
```

Fig. 9. Experimental sample data

Regarding query times (Figure 10(a)), the distributed database exhibits an average query time of 135 ms (ranging from 123 to 142 ms). In comparison, the MySQL database has an average query time of 23 ms (ranging from 22 to 25 ms). Despite the disparity, this difference in response speed is minor and unlikely to significantly impact user experience, as users can obtain desired history in a single query. In terms of data insertion operations (Figure 10(b)), inserting data into the distributed database takes an average of 1815 ms (ranging from 1550 to 2113 ms), whereas the MySQL database averages 45 ms (ranging from 39 to 51 ms). The noticeable gap in data insertion time is expected, considering the inherent complexity of blockchain data insertion steps. However, according to research from the Encyclopedia of Software Testing Technology, most users accept response times under 4 seconds. Thus, the 2-second insertion time remains well within acceptable limits. Moreover, data insertion doesn't involve active user interaction; it's simply the IoT device submitting data to the server for processing. Overall, the system's feasibility is promising.

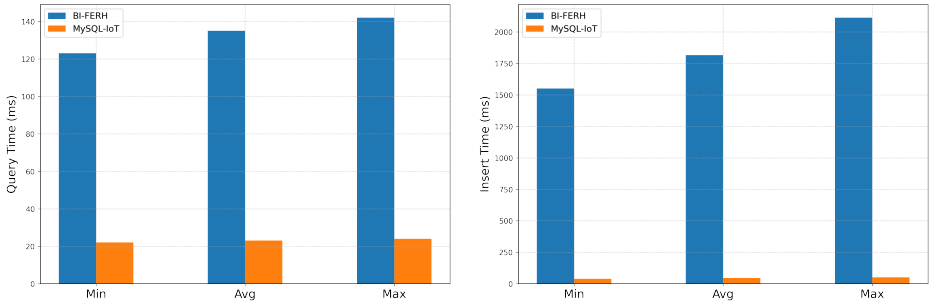

(a) Query time comparison (b) Insert time comparsion

Fig. 10. Comparison with MySQL-IoT

Hyperledger Fabric offers quicker consensus compared to traditional blockchain systems using proof-of-work. This experiment contrasts Fabric's speed with proof-of-work difficulties of 15 and 20 [48]. In Figure 11, Fabric's consensus outperforms proof-of-work by around 20 ms at low difficulties. As nodes increase, Fabric maintains efficiency. However, with proof-of-work's difficulty at 20, consensus time escalates significantly as nodes grow. At 100 nodes, Fabric takes about 0.2 s while proof-of-work (difficulty 20) takes 6.3 s. Fabric's consensus efficiency is thus prominent.

Table 6 provides a visual comparison between the two frameworks. MySQL-IoT boasts efficient data processing, especially in updates. Yet, its security is compromised. In contrast, BI-FERH sacrifices some efficiency for vastly improved data security. Its distributed storage structure resists DDoS attacks, while blockchain storage ensures traceability and tamper resistance. Hyperledger Fabric's chaincode enhances blockchain scalability. TLS secures data transmission. BI-FERH strengthens data security without harming business efficiency, offering a secure IoT storage solution.

Table 6. BI-FERH vs. MySQL-IoT

	BI-FERH	MySQL-IoT
Storage System	Hyperledger Fabric v2.2	MySQL v5.7.26
Storage Structure	Distributed	Centralized
DDoS Defense Capability	Strong(IDS 99.9% recognition rate)	Weak
Traceability	Strong(TxId)	Weak
Data Redundancy	Strong(Distributed Storage)	Weak(Centering)
Untamperability	Strong(Hash Chain)	Weak
Scalability	Chaincode	None
Data Packet Loss Rate	0%	0%
Data Transmission Protocol	TLS	TCP
Data Query (average time)	135ms	23ms
Data Update (average time)	1815ms	45ms

4.4. Comparison with blockchain applications

Comparing the BI-FERH system's performance with similar blockchain applications is essential. To validate its advantages over other blockchain solutions, the proposed approach is evaluated against systems from four papers: [34], [37], [38], and [39], all previously discussed in the related work section.

The experiment involved sending data insertion requests to different blockchain systems at varying rates: 50, 100, 150, 200, and 250 transactions per second. Each phase had 1000 transaction requests over five rounds, totaling 5000 transactions. This assessed concurrency performance and transaction processing speed. Resource consumption, including CPU, memory, and block I/O, was recorded for system evaluation.

Table 7 displays specific data for the five systems across phases, including rates, throughput, and processing times. Initially ranking 3rd in the first phase, the BI-FERH approach gains ground with higher sending speeds. It secures 2nd place at 100/s. In later phases, it consistently leads. At 250/s, BI-FERH achieves 125 tps throughput and 8 ms processing time. This is 28.33 tps higher and 2.79 ms faster than the 2nd place, and 77.66 tps higher with 13.12 ms saved compared to the 5th place.

Table 7. Detailed experimental data with other blockchain applications

Phrase	Transactions No.1 to 1000			Transactions No.1001 to 2000			Transactions No.2001 to 3000			Transactions No.3001 to 4000			Transactions No.4001 to 5000		
Indicators / Reference	Sending Rate	Throughput (TPS)	Average Time(ms)	Sending Rate	Throughput (TPS)	Average Time(ms)	Sending Rate	Throughput (TPS)	Average Time(ms)	Sending Rate	Throughput (TPS)	Average Time(ms)	Sending Rate	Throughput (TPS)	Average Time(ms)
BI-FERH	50/s	25.0	40	100/s	50.0	20	150/s	75.24	13.29	200/s	100.0	10.0	250/s	125.0	8.0
[34]	50/s	48.07	20.8	100/s	50.76	19.7	150/s	34.21	29.23	200/s	37.89	26.39	250/s	47.34	21.12
[37]	50/s	23.25	43	100/s	40.0	25	150/s	41.2	25	200/s	37.04	27	250/s	50.0	20
[38]	50/s	19.08	52.4	100/s	37.87	26.4	150/s	56.49	17.7	200/s	74.62	13.4	250/s	92.67	10.79
[39]	50/s	25.25	39.6	100/s	42.21	23.69	150/s	54.67	18.29	200/s	63.49	15.75	250/s	70.82	14.12

Figure 12 displays a line graph illustrating the time required by the five systems to process 5000 data points. The x-axis represents phases with increasing data sending speeds. The blue curve, representing the BI-FERH method, completes the task in the shortest time. Observing the graph, the blue curve initially takes the second longest time, then reverses this trend after 3000 transactions, outperforming other methods. Changes in slope reflect concurrency and data processing capabilities. BI-FERH excels in handling large data volumes and maintaining good concurrency, avoiding transaction blockages and ensuring efficient data processing.

Figure 13 presents a bar chart depicting resource usage and block data volume for the five blockchain systems during transaction processing. The chart illustrates CPU and memory consumption for peer and orderer nodes. Figure 13(a) and (b) reveal CPU and memory consumption across the five systems. The BI-FERH system (blue) exhibits lower resource consumption than the other applications, with slightly more memory usage in peer nodes compared to the application represented by purple. Notably, BI-FERH consumes minimal CPU resources across all nodes. Efficient resource usage is crucial for maintaining overall computer performance. Although blockchain systems inherently demand additional computational resources due to distributed data storage and security-enhancing operations, a good system should minimize resource usage while ensuring efficient performance. In this context, the BI-FERH system excels by consuming fewer resources than other applications.

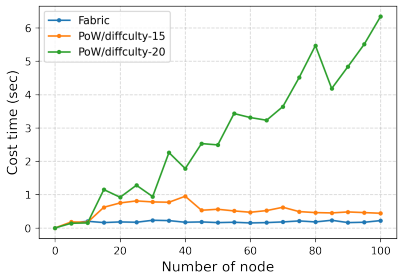

Fig. 11. Consensus consumption for Fabric and PoW

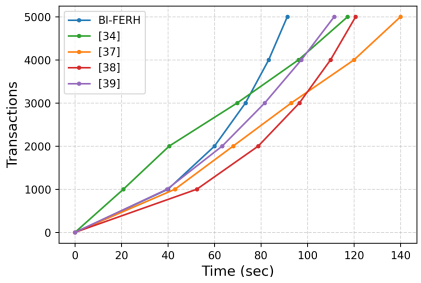

Fig. 12. Transaction speed comparison

Figure 13(c) and (d) display block data volume in the five blockchain networks. Larger volumes signify more content and efficient data transmission. BI-FERH (blue) consistently shows higher data volume than other apps, except in orderer node's block output. Overall, BI-FERH excels in block data volume, implying its network handles data efficiently.

The experiment compares BI-FERH across various dimensions, emphasizing its transaction speed, resource usage, and block data volume advantages.

4.5. Attack traffic identification

The experiment employs the CICIDS2017 dataset [49], encompassing diverse network attacks like DDoS, DoS, brute force, and web attacks. This dataset comprises 14 attack types and normal access traffic, as outlined in Table 8. The data is divided into 70% training and 30% testing sets. The BI-FERH framework utilizes an Autoencoder + TCN model. For comparison with other contemporary studies, experiments are also performed on the CICIDS2017 dataset using Autoencoder + LSTM and Autoencoder + BRNN models.

To measure the accuracy of different models, the following four common machine learning evaluation metrics are used for the experiments.

Accuracy: Accuracy is the ratio of correctly predicted traffic to all traffic.

$$Accuracy = \frac{TP + TN}{TP + FP + FN + TN} \tag{16}$$

Precision (PR): the ratio of the number of correctly classified positive samples to the number of samples determined to be positive by the classifier.

$$Precision = \frac{TP}{TP + FP} \tag{17}$$

Recall (RE): The ratio of the number of correctly classified positive samples to the number of true positive samples.

$$Recall = \frac{TP}{TP + FN} \tag{18}$$

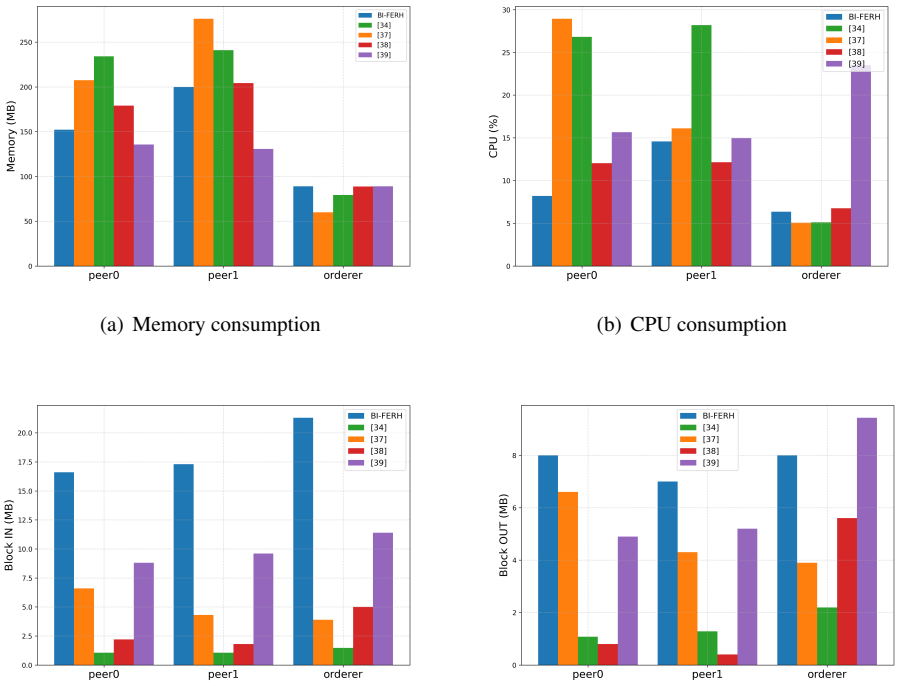

(a) Memory consumption

(b) CPU consumption

(c) Block Input

(d) Block Output

Fig. 13. Resource consumption and performance

Table 8. Composition of CICIDS2017 dataset

Type	Total	Percent	Training Set	Percent	Test Set	Percent
DoS Hulk	230124	8.14%	161087	5.70%	69037	2.44%
DDoS	128025	4.53%	89618	3.17%	38408	1.36%
DoS GoldenEye	10293	0.36%	7205	0.26%	3088	0.11%
DoS slowloris	5796	0.21%	4057	0.14%	1739	0.06%
DoS Slowhttptest	5499	0.19%	3849	0.14%	1650	0.06%
PortScan	158804	5.62%	111163	3.93%	47641	1.69%
FTP-Patator	7935	0.28%	5555	0.20%	2381	0.08%
SSH-Patator	5897	0.21%	4128	0.15%	1769	0.06%
Bot	1956	0.07%	1369	0.05%	587	0.02%
Web Attack Brute Force	1507	0.05%	1055	0.04%	452	0.02%
Web Attack XSS	652	0.02%	456	0.02%	196	0.01%
Infiltration	36	0.00%	25	0.00%	11	0.00%
Web Attack Sql Injection	21	0.00%	15	0.00%	6	0.00%
Heartbleed	11	0.00%	8	0.00%	3	0.00%
BENIGN	2271320	80.32%	1589923	56.22%	681395	24.10%
Total	2827874	100%	1979512	70%	848362	30%

F1 Score: F1 Score is the balanced average of recall and precision.

$$F1 = \frac{2 * (Recall * Precision)}{Recall + Precision} \tag{19}$$

Table 9 shows the training and the final accuracy of the three models. From the table, it can be analyzed that the training time spent by the Autoencoder +TCN model is shorter, but there is not much difference between the accuracy rates of the three models. The overall results are all relatively good.

Table 9. Training situation

	Train Parameters	epoch	Batch Size	Training Time	Accuracy
Autoencoder + TCN	140320	10	512	25min	99.90%
Autoencoder + LSTM	3204688	5	512	42min	99.40%
Autoencoder + BRNN	2517822	5	512	183min	99.20%

Table 10 displays attack identification results using Precision, Recall, and F1 scores across the three models. Figure 14 visualizes F1 scores for 15 classification cases. The Autoencoder + TCN model achieves F1 scores of 0.97 or higher in 9 cases, showing its superior performance. All models accurately identify normal network traffic. In scenarios with limited data like Bot and web attacks, F1 values, while not reaching 0.97, still surpass those of other models. Increasing training data could enhance recognition capability in these scenarios.

Table 10. Attack scenario identification

CICIDS2017	**Autoencoder + TCN**			**Autoencoder + LSTM**			**Autoencoder + BRNN**		
	PR	**RE**	**F1**	**PR**	**RE**	**F1**	**PR**	**RE**	**F1**
DoS Hulk	0.999	1.0	0.998	0.991	0.996	0.993	0.972	0.998	0.986
DDoS	1.0	0.998	0.999	0.995	0.987	0.991	0.997	0.991	0.993
DoS GoldenEye	0.985	0.991	0.988	0.965	0.736	0.835	0.804	0.867	0.834
DoS slowloris	0.971	0.971	0.971	0.772	0.347	0.479	0.816	0.656	0.727
DoS Slowhttptest	0.965	0.982	0.974	0.507	0.572	0.537	0.766	0.632	0.691
PortScan	0.994	0.998	0.996	0.992	0.997	0.994	0.992	0.995	0.994
FTP-Patator	0.998	0.993	0.996	0.937	0.995	0.965	0.876	0.958	0.915
SSH-Patator	0.975	0.988	0.981	0.665	0.988	0.795	0.912	0.474	0.624
Bot	0.979	0.726	0.834	0	0	0	0	0	0
Web Attack Brute Force	0.669	0.858	0.752	0	0	0	0	0	0
Web Attack XSS	0.500	0.015	0.30	0	0	0	0	0	0
Infiltration	0.308	0.727	0.432	0	0	0	0	0	0
Web Attack Sql Injection	0.332	0.500	0.400	0	0	0	0	0	0
Heartbleed	0	0	0	0	0	0	0	0	0
Benigh	1.0	1.0	1.0	0.996	0.998	0.997	0.997	0.998	0.998

5. Results and discussions

Table 11 offers a comparison between BI-FERH and other blockchain applications across five categories: blockchain type, platform, IoT device, consensus algorithm, and data algo-

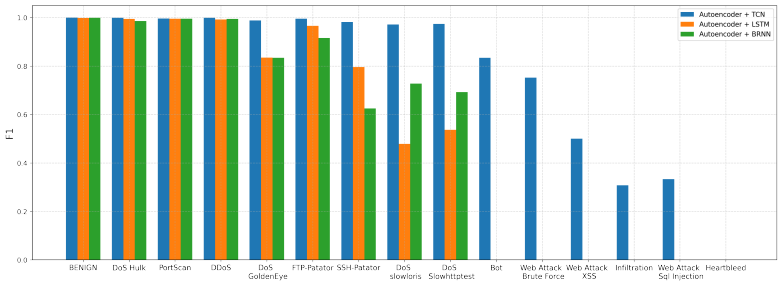

Fig. 14. F1 values for different models of attack identification

rithm. BI-FERH's choice of consortium and private blockchains aligns with non-currency applications. Hyperledger Fabric as the platform provides scalability and performance advantages over other platforms like Indy and Composer. Kafka consensus suits the hotel application's cluster environment, enhancing efficiency. PBFT's node trust issues don't apply here. BI-FERH enhances data protection via AES encryption and Base64 encoding, contrasting with other applications that lack data processing, except for watermarking in one case.

Table 11. Comparison of related applications

Reference	Description	Blockchain type	Platform	IoT	Consensus	Data algorithms
BI-FERH	Smart hotel info management system	Consortium blockchains	Hyperledger Fabric	√	Kafka	AES128, Base64
[11]	Mobility data transactions	Consortium blockchains	Hyperledger Indy	×	PBFT	×
[34]	Transparent supply chain for coffee	Consortium blockchains	Hyperledger Fabric	√	RAFT	×
[35]	Tracking sources of fake news	Private blockchain	BloXroute	×	PBFT	ARX Digital Watermark
[36]	Security system for smart home	Private blockchains	Hyperledger Composer	√	PoW	×
[37]	Electronic healthcare record system	Consortium blockchains	Hyperledger Composer	×	PBFT	×
[38]	Smart Hospital patient data detection	Consortium blockchains	Hyperledger Composer	√	Solo	×
[39]	Smart city safety transportation System	Consortium blockchains	Hyperledger Fabric	√	Solo	×
[40]	IoT decentralized voting system	Public blockchains	Solidity	√	PoW	×

5.1. Availability

The experiments, focusing on system performance and comparison with traditional storage structures, highlight BI-FERH's usability. The Fabric SDK plays a key role in node operation and data processing. Network initialization and construction took just 9,127ms. Comparison of SDKs in different languages favored Go for data updates and queries, affirming its suitability. Assessing traditional centralized storage versus BI-FERH's blockchain

approach aimed to gauge efficiency trade-offs. Results indicate that the efficiency sacrificed for decentralized storage through blockchain remains acceptable for user functionality.

5.2. Performance

The experiment's third segment compares the consensus algorithms' pivotal role in achieving data consensus among nodes, contrasting Fabric and PoW. In the fourth part, BIFERH's performance is gauged against other blockchain systems across five dimensions: transaction speed, memory consumption, CPU usage, and block input/output data volume. Results indicate this system outperforms others with 1.3x faster transaction speed, 10% lower memory consumption, 7% lower CPU usage, and increased block data input/output by 14MB and 3.8MB respectively. Overall, the system exhibits heightened transaction speed, improved concurrency, reduced memory and CPU consumption, and enhanced data transfer efficiency.

5.3. Security

Data Integrity Arthur Gervais et al.'s research on blockchain security [50] examines the potential for data tampering. If an attacker aims to alter a block before the latest one (h-th block), they must modify the prior block's hash and recalculate subsequent hashes to create a new longest chain. Assuming honest node hash computation speed as p times/s and the attacker's speed as q times/s, the hash's difficulty requires the first g binary digits to be 0. When no new node joins, an honest node's probability of acquiring a block is $p/2^g$, and the attacker's is $q/2^g$. Initially, differing nodes between the honest node and attacker are $z_0 = h$. Subsequently, z_{i+1} possibilities are: z_i+1, z_i-1, z_i with probabilities P_1, P_2, P_3, corresponding to events X_1, X_2, X_3.

$$z_{i+1} = \begin{cases} z_i + 1, & P_1 = \frac{p}{2^g}(1 - \frac{q}{2^g}) \\ z_i - 1, & P_2 = \frac{q}{2^g}(1 - \frac{p}{2^g}) \\ z_i, & P_3 = 1 - P_1 - P_2 \end{cases} \tag{20}$$

When $z_i+1 = -1$, it means that the attacker successfully tampered with the blockchain data. Within t seconds, there will be t times of changes in the number of nodes apart. Let n be the number of occurrences of X_1; when tampering is successful, X_2 will occur at least $(n + h + 1)$ times, Let j be the difference between the actual number of occurrences of event X_2 and the minimum number of occurrences, then the actual number of occurrences of X_2 is $(n+h+1+j)$, and the number of occurrences of event X_3 is $(t-2n-h-1-j)$, where $n \in [0, (t-1-h)/2], j \in [0, t-2n-h-1]$. Within t seconds, the probability of an attacker successfully tampering with blockchain data is

$$P_t(h) = \sum_0^{n_{max}} \sum_0^{j_{max}} \left(\frac{2!}{n!(h+n+1+j)!(t-2n-h-1-j)!} \cdot P_1^n P_2^{h+n+1+j} P_3^{t-2n-h-1-j}\right) \tag{21}$$

The final analysis shows that the success probability of the attacker decreases as the depth h of the tampered block increases and the probability of successful tampering increases as the attacker increases. If an attacker wants to tamper with the data of a specific

ledger on a local node, it requires the attacker to have the ability to forge signatures and modify the hash values of blocks on all nodes. So blockchain can prevent data tampering and makes data integrity guaranteed.

Signature forgery The external attacker's attempt to forge a trader's signature in the block involves brute force cracking to guess the private key, excluding key theft. The ECDSA elliptic curve digital signature algorithm's private key lengths of 160, 224, and 256 bits result in cracking times of 10^{12}, 10^{24}, and 10^{28} seconds, respectively, using a computer with one million instructions per second. The private key utilized in this system is 256 bits, requiring significant time and computational resources for cracking. Even with a high-cost professional machine, it takes a month to calculate the discrete logarithm of an elliptic curve with a prime order of 2^{120}. Consequently, elliptic curve algorithms with large prime orders substantially reduce the feasibility of brute force attacks, rendering signature forgery infeasible for attackers.

DDOS Defense Distributed Denial of Service (DDOS) attacks involve multiple attackers targeting multiple targets simultaneously, overloading servers to induce network paralysis and disrupt regular services. Traditionally, hotel industry information systems relied on centralized servers for data computation, storage, and business access. Any server attack would lead to widespread operational halts. In contrast, the BI-FERH framework leverages a distributed blockchain network, decentralizing computing and data resources. This decentralized structure poses challenges for DDOS attacks, and the framework employs an Intrusion Detection System (IDS) layer to pre-filter malicious access before processing. Experimental findings indicate the classification model accurately detects DDOS attack scenarios with a 99.9% accuracy rate. The IDS successfully identifies 8 distinct attack types with over 97% probability. This enhances the resilience of hotel information systems against external attacks.

6. Conclusion

This paper introduces the BI-FERH security framework for smart hotels, leveraging blockchain, IoT, and machine learning to establish a robust data management system. The framework's composition and technologies are explained, showcasing its potential to enhance security in the hotel industry. Through experiments, an IoT-based information management system for hotel door locks is developed, demonstrating its performance, efficiency, and security. The machine learning-driven IDS accurately identifies various attack scenarios in the CICIDS2017 dataset. In conclusion, this work provides a pioneering solution to address security challenges in the hotel industry's information systems.

Acknowledgments. This work is supported by the Science and Technology Planning Project of Guangdong (2021B0101420003, 2020B0909030005, 2020B1212030003, 2023ZZ03, 2020ZDZX3013), the Science and Technology Planning Project of Guangzhou(202206030007), Key Laboratory of Smart Education of Guangdong Higher Education Institutes, Jinan University(2022LSYS003), Guangdong Key Laboratory of Data Securit and Privacy Preserving (2017B030301004), the Opening Project of Key Laboratory of Safety of Intelligent Robots for State Market Regulation (GQI-

KFKT202205) and the High-Performance Public Computing Service Platform of Jinan University, NSF of Guangdong Province (No. 2021A1515011906).

References

1. Yang, H., Song, H., Cheung, C., Guan, J.: How to enhance hotel guests' acceptance and experience of smart hotel technology: An examination of visiting intentions. International journal of hospitality management 97, 103000 (2021)
2. Nakanishi, J., Baba, J., Kuramoto, I., Ogawa, K., Yoshikawa, Y., Ishiguro, H.: Smart speaker vs. social robot in a case of hotel room. In: 2020 IEEE/RSJ International Conference on Intelligent Robots and Systems (IROS). pp. 11391–11396 (2020)
3. Shen, X., Shao, W., Zhang, Z., Xu, P.: Hotel intelligent guidance system based on zigbee technology. Microprocessors and Microsystems 77, 103160 (2020)
4. Hassija, V., Chamola, V., Saxena, V., Jain, D., Goyal, P., Sikdar, B.: A survey on iot security: application areas, security threats, and solution architectures. IEEE Access 7, 82721–82743 (2019)
5. Sahu, A.K., Gutub, A.: Improving grayscale steganography to protect personal information disclosure within hotel services. Multimedia Tools and Applications pp. 1–21 (2022)
6. Seamans, E.: The unique challenges of data security in the hospitality industry (2018), https://hospitalitylawyer.com/the-unique-challenges-of-data-security-in-the-hospitality-industry
7. Guan, Q., Lei, J., Wang, C., Geng, G., Zhong, Y., Fang, L., Huang, X., Luo, W.: A practical framework of blockchain in iot information management. In: 2023 IEEE International Conference on Systems, Man, and Cybernetics (SMC) (2023)
8. Nakamoto, S.: Bitcoin: A peer-to-peer electronic cash system. Decentralized Business Review p. 21260 (2008)
9. Wang, Y., Singgih, M., Wang, J., Rit, M.: Making sense of blockchain technology: How will it transform supply chains? International Journal of Production Economics 211, 221–236 (2019)
10. Maesa, D.D.F., Mori, P.: Blockchain 3.0 applications survey. Journal of Parallel and Distributed Computing 138, 99–114 (2020)
11. Lopez, D., Farooq, B.: A multi-layered blockchain framework for smart mobility data-markets. Transportation Research Part C: Emerging Technologies 111, 588–615 (2020)
12. Ali, J., Ali, T., Alsaawy, Y., Khalid, A.S., Musa, S.: Blockchain-based smart-iot trust zone measurement architecture. In: Proceedings of the International Conference on Omni-Layer Intelligent Systems. pp. 152–157 (2019)
13. Feng, J., Zhao, X., Chen, K., Zhao, F., Zhang, G.: Towards random-honest miners selection and multi-blocks creation: Proof-of-negotiation consensus mechanism in blockchain networks. Future Generation Computer Systems 105, 248–258 (2020)
14. Kamalov, F., Gheisari, M., Liu, Y., Feylizadeh, M.R., Moussa, S.: Critical controlling for the network security and privacy based on blockchain technology: A fuzzy dematel approach. Sustainability 15(13), 10068 (2023)
15. Albulayhi, A.S., Alsukayti, I.S.: A blockchain-centric iot architecture for effective smart contract-based management of iot data communications. Electronics 12(12), 2564 (2023)
16. Donet Donet, J.A., Pérez-Solà, C., Herrera-Joancomartí, J.: The bitcoin p2p network. In: Böhme, R., Brenner, M., Moore, T., Smith, M. (eds.) Financial Cryptography and Data Security. pp. 87–102 (2014)
17. Biryukov, A., Khovratovich, D., Pustogarov, I.: Deanonymisation of clients in bitcoin p2p network. In: Proceedings of the 2014 ACM SIGSAC Conference on Computer and Communications Security. p. 15–29. CCS '14 (2014)

18. Zou, W., Lo, D., Kochhar, P.S., Le, X.B.D., Xia, X., Feng, Y., Chen, Z., Xu, B.: Smart contract development: Challenges and opportunities. IEEE Transactions on Software Engineering 47(10), 2084–2106 (2021)
19. Wohrer, M., Zdun, U.: Smart contracts: security patterns in the ethereum ecosystem and solidity. In: 2018 International Workshop on Blockchain Oriented Software Engineering (IWBOSE). pp. 2–8 (2018)
20. Sousa, J., Bessani, A., Vukolic, M.: A byzantine fault-tolerant ordering service for the hyperledger fabric blockchain platform. In: 2018 48th Annual IEEE/IFIP International Conference on Dependable Systems and Networks (DSN). pp. 51–58 (2018)
21. Hao, Y., Li, Y., Dong, X., Fang, L., Chen, P.: Performance analysis of consensus algorithm in private blockchain. In: 2018 IEEE Intelligent Vehicles Symposium (IV). pp. 280–285 (2018)
22. Lee, J.W., Park, S.: A study on performance improvement of hyperledger fabric through batched chaincode message. In: 2020 21st Asia-Pacific Network Operations and Management Symposium (APNOMS). pp. 259–262 (2020)
23. Javaid, H., Yang, J., Santoso, N., Upadhyay, M., Mohan, S., Hu, C., Brebner, G.: Blockchain machine: A network-attached hardware accelerator for hyperledger fabric. In: 2022 IEEE 42nd International Conference on Distributed Computing Systems (ICDCS). pp. 258–268 (2022)
24. Dinh, T.T.A., Wang, J., Chen, G., Liu, R., Ooi, B.C., Tan, K.L.: Blockbench: A framework for analyzing private blockchains. In: Proceedings of the 2017 ACM international conference on management of data. pp. 1085–1100 (2017)
25. Pongnumkul, S., Siripanpornchana, C., Thajchayapong, S.: Performance analysis of private blockchain platforms in varying workloads. In: 2017 26th International Conference on Computer Communication and Networks (ICCCN). pp. 1–6 (2017)
26. Da Xu, L., He, W., Li, S.: Internet of things in industries: A survey. IEEE Transactions on industrial informatics 10(4), 2233–2243 (2014)
27. Liu, B., Jiang, X., He, X., Qi, L., Xu, X., Wang, X., Dou, W.: A deep learning-based edge caching optimization method for cost-driven planning process over iiot. Journal of Parallel and Distributed Computing 168, 80–89 (2022)
28. Pavithran, D., Al-Karaki, J.N., Shaalan, K.: Edge-based blockchain architecture for event-driven iot using hierarchical identity based encryption. Information Processing & Management 58(3), 102528 (2021)
29. Du, Y., Wang, Z., Li, J., Shi, L., Jayakody, D.N.K., Chen, Q., Chen, W., Han, Z.: Blockchain-aided edge computing market: Smart contract and consensus mechanisms. IEEE Transactions on Mobile Computing (2022)
30. Reyna, A., Martín, C., Chen, J., Soler, E., Díaz, M.: On blockchain and its integration with iot. challenges and opportunities. Future generation computer systems 88, 173–190 (2018)
31. Kshetri, N.: 1 blockchain's roles in meeting key supply chain management objectives. International Journal of information management 39, 80–89 (2018)
32. Khan, M.A., Salah, K.: Iot security: Review, blockchain solutions, and open challenges. Future generation computer systems 82, 395–411 (2018)
33. Wan, J., Li, J., Imran, M., Li, D., et al.: A blockchain-based solution for enhancing security and privacy in smart factory. IEEE Transactions on Industrial Informatics 15(6), 3652–3660 (2019)
34. Ravi, D., Ramachandran, S., Vignesh, R., Falmari, V.R., Brindha, M.: Privacy preserving transparent supply chain management through hyperledger fabric. Blockchain: Research and Applications 3(2), 100072 (2022)
35. Dwivedi, A.D., Singh, R., Dhall, S., Srivastava, G., Pal, S.K.: Tracing the source of fake news using a scalable blockchain distributed network. In: 2020 IEEE 17th International Conference on Mobile Ad Hoc and Sensor Systems (MASS). pp. 38–43 (2020)
36. Ammi, M., Alarabi, S., Benkhelifa, E.: Customized blockchain-based architecture for secure smart home for lightweight iot. Information Processing & Management 58(3), 102482 (2021)

37. Tanwar, S., Parekh, K., Evans, R.: Blockchain-based electronic healthcare record system for healthcare 4.0 applications. Journal of Information Security and Applications 50, 102407 (2020)
38. Jamil, F., Ahmad, S., Iqbal, N., Kim, D.H.: Towards a remote monitoring of patient vital signs based on iot-based blockchain integrity management platforms in smart hospitals. Sensors 20(8), 2195 (2020)
39. Abbas, K., Tawalbeh, L.A., Rafiq, A., Muthanna, A., Elgendy, I.A., El-Latif, A., Ahmed, A.: Convergence of blockchain and iot for secure transportation systems in smart cities. Security and Communication Networks 2021 (2021)
40. Li, Y., Susilo, W., Yang, G., Yu, Y., Liu, D., Du, X., Guizani, M.: A blockchain-based self-tallying voting protocol in decentralized iot. IEEE Transactions on Dependable and Secure Computing 19(1), 119–130 (2022)
41. Chen, F., Wang, J., Jiang, C., Xiang, T., Yang, Y.: Blockchain based non-repudiable iot data trading: Simpler, faster, and cheaper. In: IEEE INFOCOM 2022 - IEEE Conference on Computer Communications. pp. 1958–1967 (2022)
42. Lao, L., Li, Z., Hou, S., Xiao, B., Guo, S., Yang, Y.: A survey of iot applications in blockchain systems: Architecture, consensus, and traffic modeling. ACM Computing Surveys 53(1), 1–32 (2020)
43. Alshudukhi, K.S., Khemakhem, M.A., Eassa, F.E., Jambi, K.M.: An interoperable blockchain security frameworks based on microservices and smart contract in iot environment. Electronics 12(3), 776 (2023)
44. Daidone, F., Carminati, B., Ferrari, E.: Blockchain-based privacy enforcement in the iot domain. IEEE Transactions on Dependable and Secure Computing 19(6), 3887–3898 (2022)
45. Zhao, Q., Chen, S., Liu, Z., Baker, T., Zhang, Y.: Blockchain-based privacy-preserving remote data integrity checking scheme for iot information systems. Information Processing & Management 57(6), 102355 (2020)
46. Martinez-Rendon, C., González-Compeán, J., Sánchez-Gallegos, D.D., Carretero, J.: Cd/cv: Blockchain-based schemes for continuous verifiability and traceability of iot data for edge–fog–cloud. Information Processing & Management 60(1), 103155 (2023)
47. Foschini, L., Gavagna, A., Martuscelli, G., Montanari, R.: Hyperledger fabric blockchain: Chaincode performance analysis. In: ICC 2020 - 2020 IEEE International Conference on Communications (ICC). pp. 1–6 (2020)
48. Liu, H., Han, D., Li, D.: Fabric-iot: A blockchain-based access control system in iot. IEEE Access 8, 18207–18218 (2020)
49. Sharafaldin, I., Lashkari, A.H., Ghorbani, A.A.: Toward generating a new intrusion detection dataset and intrusion traffic characterization. Proceedings of the 4th International Conference on Information Systems Security and Privacy pp. 108–116 (2018)
50. Gervais, A., Karame, G.O., Wüst, K., Glykantzis, V., Ritzdorf, H., Capkun, S.: On the security and performance of proof of work blockchains. In: Proceedings of the 2016 ACM SIGSAC conference on computer and communications security. pp. 3–16 (2016)

Quanlong Guan received the M.S. and Ph.D. degrees from Jinan University, China, in 2006 and 2014, respectively, where he is currently a Professor of engineering. He is directing the Guangdong Research and Development Institute for the big data of service and application on education. His research has been funded by the National Natural Science Foundation of China and the Guangdong Key Technologies Research and Development Program of China. His research interests include network security, big data protection and processing, information system, big data application, and mobile security.

Jiawei lei received the B.S. degree in information security from Guangzhou University, Guangzhou, China in 2020. He is currently a graduate student with the College of Cyber Security, Jinan University, Guangzhou, China. His research interests include information system, data security, and blockchain.

Chaonan Wang is currently a full professor in the College of Cyber Security of Jinan University in China. She has been working in the area of system reliability engineering since she joined the graduate program in 2010 at the University of Massachusetts (UMass) Dartmouth, where she received her PhD degree in 2014. During 2014 to 2016, she continued her research as a Postdoctoral Research Associate at UMass Dartmouth. Her research focuses on reliability analysis, information system and performance evaluation of complex systems and networks. She is the recipient of "Shanghai Eastern Scholar" reward (2015). She has served as committee member for ORSC Reliability Society and Youth Academic Committee of Guangdong Computer Society.

Guanggang Geng received the Ph.D. degree from the Institute of Automation, Chinese Academy of Sciences, Beijing, China, in 2008. He is currently a Professor with the College of Cyber Security or College of Information Science and Technology, Jinan University, Guangzhou, China. His current research interests include machine learning, information system, computer networking, anti-fraud, and web search.

Yuansheng Zhong is currently the deputy director of Electronics and Electromagnetic Compatibility Testing Lab of Guangdong Testing Institute of Product Quality Supervision. He is a senior engineer and a member of the C branch of the National Technical Committee for Electromagnetic Compatibility Standardization. He is engaged in the inspection and testing, certification, standard preparation and revision and scientific research in the fields of electronic products, intelligent robots, electromagnetic compatibility, information system, etc.

Liangda Fang received the B.Sc. degree from Guangzhou University, Guangzhou, China, the M.Sc. degree from the Guangdong University of Technology, Guangzhou, and the Ph.D. degree from Sun Yat-sen University, Guangzhou, all in computer science, in 2007, 2010, and 2015, respectively, He is currently an Assistant Professor with the Department of Computer Science, Jinan University, Guangzhou. His current research interests include artificial intelligence, information system and algorithmic learning theory.

Xiujie Huang received the M.Sc. degree in applied mathematics and the Ph.D. degree in communication and information system from Sun Yat-sen University, Guangzhou, China, in 2006 and 2012, respectively. She was a Post-Doctoral Fellow with the Department of Electrical Engineering, University of Hawaii at Manoa, Honolulu, HI, USA, from July 2012 to October 2013. Since November 2013, she has been with Jinan University, Guangzhou. Her research interests include information theory, information security and their applications in digital communications, IoT, IoV and storage systems.

Weiqi Luo received the B.S. and M.S. degrees from Jinan University, Guangzhou, China, in 1982 and 1985, respectively, and the Ph.D. degree from South China University of

Technology, Guangzhou, in 1999. He is currently a Professor with the School of Information Science and Technology, Jinan Univer- sity. He has published more than 100 high-quality papers in international journals and conferences. His research interests include network security, big data, information system and artificial intelligence.

Received: April 01, 2023; Accepted: August 20, 2023.

Computer Science and Information Systems 20(4):1569–1589 https://doi.org/10.2298/CSIS230110060S

Digital Remote Work Influencing Public Administration Employees Satisfaction in Public Health Complex Contexts

Maria Sousa[1], Ana Mendes[2], Dora Almeida[3], and Álvaro Rocha[4]

[1] Instituto Universitário de Lisboa,
Lisboa, Portugal
maria.jose.sousa@iscte-iul.pt
[2] ISEG, Universidade de Lisboa,
Lisboa, Portugal
cristina.mendes@sapo.pt
[3] Universidade Europeia,
Lisboa, Portugal
dora.serra.almeida@gmail.com
[4]ISEG, Universidade de Lisboa,
Lisboa, Portugal
amrrocha@gmail.com

Abstract. The purpose of this study is to describe and analyze whether digital remote work in times of Covid-19 is influencing the satisfaction of Public Administration employees. Based on the objective of this study, an online survey was conducted in the Portuguese Public Administration, for a sample of 70 individuals, working at home due to the situation of Public Health caused by the Coronavirus. Digital remote work is being applied massively worldwide and is a specific form of work organization supported by information and knowledge. Digital remote workers carry out their activities at home and using digital technologies, depending on the nature of the tasks and work situations. To understand the satisfaction of Public Administration employees, an empirical study was carried out, supported by data collection through an online survey. The main conclusions were that despite the constraints (resistance of top management, organizational culture, autonomy, and flexibility of workers, among others) that existed before the health and socioeconomic crisis caused by the Coronavirus pandemic, digital remote work is a given in the life of organizations, public or private, and of workers with reflection at various levels in society and particularly in the professional fulfillment and satisfaction of employees. According to the analysis carried out on the data collected to support the conclusions of this study, the degree of satisfaction of Public Administration employees is influenced in different ways by the influencing factors studied: autonomy at work, conditions at work, and income. However, regarding the factor of quality of life at work, this link has not been established. Thus, it was possible to conclude that satisfaction increases positively and strongly with autonomy at work. Technological specialization and productivity still have a positive influence, but with low intensity contribute to the satisfaction of AP employees. Working conditions also negatively influence satisfaction, although at an average intensity. However, the average degree of job satisfaction varies according to the different age groups, with employees aged 35 or more having a higher satisfaction average than employees whose ages vary between 34 and the beginning of their working lives.

Keywords: Health Contexts; Digital remote work; Digital technologies; Covid-19; Social Isolation; Public Administration

1. Introduction

The change in Public Health in just a few months with Coronavirus making all the persons all over the world going online a working remotely is only possible because of the radical changes in technology, the development of organizations, the change in relations between employees and employers, and mainly government intervention enforcing digital remote work.

Currently, the main objective is to maintain the Public Services working to help the countries to overcome this critical situation. Digital technologies are now the solution to keep the economies working, in a context of social isolation worldwide.

The concept of digital remote working, created by Jack Nilles in 1973, is considered by the European Union as "the work carried out by a digital remote worker, mainly or much of the time, in a place other than the traditional place of work, for an employer or a client, involving the use of advanced computer technologies as a central and essential element of the work". In the current context, digital technologies provide the necessary basis for the development of digital remote work. In Portugal the introduction of digital remote work has been slow, because, on the one hand, the bureaucratic business culture was still an obstacle, conditioning the workers' autonomy and flexibility. On the other hand, social factors such as equal rights and social protection may, in a first analysis, be pointed out as primary factors of resistance to digital remote work by workers.

However, at the business level, other factors may assume high importance in conditioning the implementation of digital remote work during the past years, such as the characteristics of the managers, the attitude of the managers towards the change in work relations, the organizational culture itself. Managers have always taken a skeptical position regarding the benefits of digital remote working, when these are compared with certain constraints, such as the difficulty in controlling and supervising digital remote workers and the possible decrease in their loyalty to the company. However, now the government had a decisive influence on the speed with which digital remote working spread within Portuguese public organizations, placing all PA workers, whose functions allowed them to work in digital remote situations, as a preventive measure for the dissemination of Covid-19. Thus, and after 3 weeks of isolation of PA workers, to follow the orders of social distance, this study aims to analyze the degree of satisfaction of these workers, based on the variable’s autonomy in digital remote work, routine in digital remote work, and quality of life in digital remote work. The study addresses the perspective of the worker and privileges the subordinate digital remote work of the workers of the Portuguese PA.

The structure of this article is divided into the sections that are described below: first section review of the literature on the current organizational context (derived from the public health situation experienced in 2020), and on the constructs digital remote work and job satisfaction remote; the second section presents the methodology used, followed by the section with data analysis and presentation of results; finally, the main conclusions, limitations and future perspectives for research on the topic of digital remote work are identified and discussed.

2. Literature Review

2.1. Digital Remote Work Conceptualization

Digital remote working is seen as the work that results from digital remote services and digital remote activities, consequently covering the various sectors, using the digital remote transmission of data, images, texts (in short, knowledge).

The concept of digital remote work does not necessarily imply the execution of tasks done exclusively from home (however this idea was reinforced only in the context of the pandemic), but essentially its execution in any place other than the formal place of the employer, during a period at least 4 days a week or full time [1].

The definition of digital remote work and other expressions also used, such as telework or telecommuting, is based on the definition given by the European Framework Agreement on Digital remote work 2002, according to which Telework is a form of organization and/or work, using in-formation technologies, within the scope of a contract/employment relationship, in which the work, which can also be carried out on the employer's premises, is carried out outside these premises. installations regularly ". [2].

However, the origin of the digital remote working concept arose from the need to solve the problem of the displacement of workers from home to their offices, resulting in loss of hours, energy, and other precious resources. In addition to the waste of these resources, there was also the problem of the endless traffic queues that this displacement caused mainly during rush hours. However, this need did not arise suddenly and with the same intensity in the various industries, commerce, and services existing in the market, but it came about when Jack Nilles, in the ’70s, designer of space vehicles and communication systems for the United States Air Force and NASA, began to think about how tele-communications could enable employees to perform their duties close to or even from their home [3].

At the beginning of the concept, this way of working, seen with great suspicion on the part of managers, was implemented in a very slow way by some companies and not always in the best way. The mentality of management and of managers in changing the way companies operate were obstacles of great importance for the expansion of digital remote working or working from home. As Nilles commented [3] the problem is not in management supervision where workers must be controlled by the company in their workplace, but in the effective management of people.

The appropriate level of management, whether telecommuting or working in the office, has to do with the agreement and commitment signed between management and workers in delivering quality work and with previously defined objectives. For this to happen, people need not only to have the professional skills required for the performance of their tasks, but also the tools, conditions, and necessary and adequate training to deliver the final work, with the established quality criteria, within the agreed time.

Whether in the office or at home, responsibility for job delivery is shared between managers and employees. Managers must offer all the necessary conditions for workers to perform their part in delivering the requested work.

Nowadays, office work is often supported by Internet connections and can be done from anywhere at any time. [4].

On the one hand, companies need to guarantee computer support, which was already part of their duties in the traditional office, as well as computer security, but in this case for work done outside the headquarters, with the addition of providing digital remote access to the information system. With the relocation of companies to an increasingly competitive and globalized market, the need for workers' mobility has long been an important point for these tasks to be assured.

The Covid-19 pandemic brought the imperative need to stay at home and at the same time the need to carry out the tasks that could be carried out in that context. Companies, even those that did not yet have digital remote work systems in place, had to address these issues to overcome this phase and adapt to the digital transformation of their business models and their employees.

On the other hand, workers also need to have physical conditions, habitability in their homes or the chosen location to be able to carry out the assigned tasks.

Despite the emergence of new mobile technologies that make digital remote work much easier, such as smartphones and tablets, there are still many managers who prefer their employees to work in offices, such as Yahoo CEO Marissa Mayer, who in the summer of 2013 said that on principle she preferred to have his workers in the offices, despite having a digital remote work policy in place [4].

Also, digital remote work is a means of excellence for attracting talent outside of large cities and who would otherwise never have access to belonging to important companies. It is a strategy used to overcome the challenges of talent acquisition and regional development, contributing to lower unemployment levels outside the main cities [1].

This new way of working supported by technology and carried out regardless of location is part of the revolution that digital transformation operates in the relationship between paid work and personal life [4].

Keeping employees connected and working productively became critical during the COVID-19 pandemic, because digital remote work is not an option, but an imposition on non-essential jobs that can be done from home. Social distance has eliminated face-to-face meetings, with the need for new digital tools to help collaboration between teams [5].

Thus, companies must have a mentality of openness to this type of work, because, in addition to the challenges that arise, there are mutual benefits. A compromise must be made between management and workers. Both parties need to solve the problems that arise in the implementation of digital remote work.

The future of labor relations will no longer be the same after the end of the Covid-19 pandemic. The digital transformation that was taking place before the health crisis triggered by the pandemic has accelerated the way work is viewed. Many companies like Facebook (who do not expect to have more than half of employees in offices in the next decade), Ford Motor Co. (which told employees a year after the pandemic began that they could continue to work from home indefinitely). , allowing them to only use the offices when they need it) or companies like Deutsche Bank AG (which is creating a hybrid system, partly in the office, partly at home) are examples of how companies see the future of industrial relations [6].

On the workers' side, several factors can impact the performance of digital remote work starting with the limits of private life with office work. The people in the companies are leveled in the working conditions and these same people performing the same type of tasks in digital remote work will have home environments with different factors (family size, marital status, electricity, Wi-Fi, dedicated laptop with the

necessary software, noise, other distractions, etc.) that will contribute to different performances, especially when the main needs are not met. [7].

2.2. External and Internal Context of Public Organizations – Implications of COVID-19

Currently, competing on an equal footing and overcoming competition are goals that companies seek to achieve, which they will hardly achieve if they remain attached to habits inherent to Taylorist models (scientific work organization), characterized by the division of tasks, a rigid hierarchical chain, and a flow vertical information.

Technical development at the level of ICT has created new types of jobs and companies specializing in these technologies. Major transformations have already started, and the heads of organizations are now responsible for their continuity, in a policy of making organizational systems more flexible. The diffusion of workgroups, in the company and abroad, outsourcing strategies, the emergence of flexible structures, and the expansion of digital remote working are facts that must be considered by managers.

Digital remote working reinforces and accelerates changes in the world of work and the information society, in which the quality and speed of information are key factors for competitiveness. We are therefore living in a period of great change and ways must be found to manage the risks and maximize the benefits.

Authorities must assume the responsibilities of establishing protection and social cohesion, workers must take a long-term view, which implies a cohesive approach with other actors in the labor market (companies, digital remote workers, social partners, governments, digital remote work organizations). The option is clear: to work together, politically, economically, and socially.

Thus, this chapter aims to present an overview of the conditions that underlie the emergence of digital remote work. The changes that have been generated in the business world, leading to the birth of new forms of organizations, the evolution in the level of information and communication technologies, and the economic changes that have taken place in the last decades of the millennium that is now ending, lead the creation of new concepts inherent to work.

The implementation of new forms of work organization always implies profound cultural changes and management styles and methods, which require a long time to be adopted and incorporated. They change the way of working, the relationship between workers and, in some cases, the function of each one.

We are currently moving towards a networked society, based on telecommunications and information technologies, where people participate in projects with a certain level of independence, initiative, and creativity. All aspects of business life are being affected by technological and social developments: the working methods used, where and when the work is organized, carried out and what is its content.

It is necessary to develop a business reality in which the work is carried out in such a way that the individual needs, as well as the needs of the company, are met (time for family life, exploration of individual knowledge and skills, opportunities that arise in the market and time of companies).

In this context, the concept of telecommuting is increasingly discussed and, although it does not have a specific technical definition, it is usual to frame it as a set of new ways of working, using ICT as tools (tasks and communication) and the digital remote

worker as an individual who spends at least part of the time outside the traditional environment of the company.

At the European level, digital remote working is beginning to be a way to open up new opportunities to increase competitiveness, promote employment, and improve the quality of work. According to the European Commission document "European Digital remote work - Digital remote work 97", digital remote working will grow rapidly over the next five years due to the following set of factors.

External and Internal Context of Public Organizations – Implications of COVID-19

Macroeconomics: globalization in terms of trade and investment, privatizations that open the way to international competition in previously inaccessible sectors of activity. Globalization leads to the need to improve services and support for clients, the flexible networks that digital remote work can provide.

Microeconomics: the local economy is very important, as a company's location no longer depends only on road access or distance, but on the level and quality of its services and available infra-structure. Above all, business success depends on the entrepreneurial and creative spirit of its workers and is closely linked to the competitiveness of the local economy, to which digital remote work can make a significant contribution [8].

Work Organization: companies seek to adapt to the demands of current markets, reducing their costs, through means such as downsizing, outsourcing, de-layering, and "reengineering". Organizational structures have become more horizontal, management has become more entrepreneurial and goal-oriented, challenging concerning the rules and norms traditionally usual in the organization of work. ICT facilitates the creation of work teams, reduces hierarchical rigidity, and stimulates the emergence of so-called "virtual organizations". Such vectors allow digital remote work to flourish.

Public Services and Government: the liberalization of public monopolies and the search for new (and lower cost) public services. In this context, digital remote working can increase the quality and efficiency of existing services, as well as facilitate the emergence of new services.

Work Content: in all sectors of the economy, information, and know-how, as well as individual skills, have become factors that lead to success. Information and know-how can be shared across networks by digital remote workers. Individual skills and involvement can be optimized by empowerment. Digital remote working provides a framework for the emergence and exploitation of new opportunities.

Worker: the desire for greater control over their work reflects a more prosperous society, with higher levels of education and more qualified workers. For those who use the current technology to communicate, there are no constraints for the adoption of digital remote working situations. This allows them to choose their lifestyle, instead of adapting their lifestyle to the obligations imposed by traditionally developed work.

Labor Relations: in the last 10 years, the labor market has undergone several and important trans-formations, which have led to job insecurity, at all levels. This led employers, together with workers (or their union representatives) to look for new ways to combine the benefits of flexibility for the organization, ensuring individual security. Telecommuting allows opportunities to emerge to achieve these goals.

National and European policies: job creation is a major concern and digital remote working can help create more jobs (including across borders).

Thus, the dissemination of digital remote work is the result of the evolution of the markets and the policies implemented, and the effects resulting from its application also contribute to the transformations in the environment of the organizations and the policies developed. Given these organizational changes in the implementation of digital remote working, favorable and unfavorable conditions may arise, as identified below [8].

2.3. Work Satisfaction theories

Thus, the dissemination of digital remote work is the result of the evolution of the markets and the policies implemented, and the effects resulting from its application also contribute to the transformations in the environment of the organizations and the policies developed. Given these organizational changes in the implementation of digital remote working, favorable and unfavorable conditions may arise, as identified below [8].

The global framework assumptions underlying the statistical measures used are:

- H1: Satisfaction in digital remote work varies with income;
- H2: Satisfaction in digital remote work varies with autonomy at work;
- H3: Satisfaction in digital remote work varies with WORK-COND at work;
- H4: Satisfaction in digital remote work is related to productivity, specialization, and quality at work.

Work Organization

The overall productivity and quality of a business process depend on the effectiveness of coordinating and managing formal and informal tasks in an integrated and coherent manner while prioritizing and organizing work according to effective time management is crucial to achieving the defined objectives.

In the work organization process, the manager is faced with tasks such as: - definition of objectives and elaboration of action plans; - organization, supported by the identification of resources, defining standards, and structuring the entire work process; - evaluation of the objectives achieved and respective feedback; - promoting the development of people, building strong work teams, and stimulating interest; - time management and ensuring compliance with deadlines.

A study done by Xerox in the United Kingdom identified six factors of work organization necessary for the successful implementation of digital remote work. These were: - need to be adaptable instead of rigid; - the tendency to decrease overhead costs; - the need to highlight individual contributions; - the need to enhance creativity; - the need to be organic and to involve people; - the need to motivate production and the quality of work.

Thus, to optimize the organization of work, in digital remote working situations, the numerous variables that involve the definition of workflows must be considered, including the available resources, the necessary knowledge, the time needed to perform the tasks, the location of the digital remote workers, customers, and equipment, among others. The establishment of an agreement between managers and digital remote workers about the expectations expected for the project, considering factors such as quality, quantity, and deadlines is essential.

Supervision and Control Systems for Digital Remote Worker Activity

Contrary to what was expected, digital remote working has not spread rapidly, possibly because it does not fit into the predominant organizational structures, which are very hierarchical, with strict control over the performance of workers.

Digital remote working calls into question the style of classical management. It implies achieving objectives without having direct control of the procedures and the time of presence of individuals, thus assuming a climate of trust that managers have difficulty adapting to.

This form of work organization is seen as a decrease in control and even as a loss of managers' power over their subordinates. The control function is seen by many organizations as the first duty of managers, and rewards and incentives are often based on factors related to it. Some companies that have already adopted digital remote working situations use work quality control and objective analysis systems.

ICT has a predominant role at this level, as it can increase control, remotely monitoring the use of equipment, the working hours of the machines, and the deadlines to be met. However, the electronic surveillance process can cause problems in terms of confidentiality and information security.

Traditionally, certain quantitative control techniques have been applied, the main objectives of which are: to elaborate work programs; determine costs to serve as a basis for budgets; determine the performance of people and machines.

Although these techniques have so far proved to be a fundamental tool for the decision-making process, with the adoption of new forms of work organization, management control must necessarily be replaced by work coordination.

The role of managers must be to lead workers and to be facilitating elements in the work development process. However, the culture that exists in most organizations is not open enough to allow such procedures on the part of management bodies and management by objectives instead of direct performance supervision is a strategic option that many companies have not yet taken.

Supervision and Control Systems for Digital Remote Worker Activity

Leadership is the ability to lead groups and individuals to cooperate, which involves sharing information and objectives and resolving conflicts. However, a problem arises concerning the coordination of objectives, tasks, and behaviors so that team members are in tune with the rules and ideas about the organization.

About digital remote workers, the situation becomes more complex, since as they are isolated, there is a tendency to create their own rules and to take a different approach to work. So that digital remote workers do not deviate from the objectives, procedures such as the creation of periodic reports with information about the projects being developed, the action plans, and the new company policies, for example, must be developed.

Digital remote working thus requires the transition from spontaneous coordination in the workplace to more planned coordination, where ICT plays an important role. Godehard, in a study he carried out in 1994, concluded that “most companies do not seem to need new forms of coordination. On the contrary, they feel obliged to apply the existing coordination regulations, in terms of planning and control, but more carefully”.

The manager in his role of leader must be the mentor and the inspiration both at the individual level and at the level of teams. However, it is not very easy to exercise these

influences in an organization with a network structure and where workers are not physically present. Methods such as “on the job training” will have to be replaced by others, such as - feedback to reinforce positive behaviors; - advice via communication tools; - contact the digital remote worker regularly to communicate promptly how the development of his work is going and the necessary changes; - establish a career plan, regularly reviewed with the worker to measure their progress.

Traditional management uses external motivating mechanisms to get workers to perform their duties efficiently and effectively. However, the digital remote worker finds himself alone, without the direct support of these mechanisms. To address this problem, training sessions should be held to teach the digital remote worker how to set goals, devise a plan to meet those goals, and solve the most common problems that may arise.

It is also essential that, in the selection process of the digital remote worker, self-motivation is considered a prerequisite since he will have to resort to internal mechanisms of motivation to perform his tasks with the necessary quality and within the defined deadlines.

The company's participation in motivating the digital remote worker must include providing information about his work and the objectives achieved by the company itself, in the form of graphics and communications. According to [9], the motivating factors that are important in a company with digital remote working situations are - mission (giving people something they believe in); - autonomy in the performance of work (feedback); - values (financial data, awards, public recognition); - learning (development of new knowledge); - reputation (opportunities to highlight each other's achievements).

The manager as the leader of the work teams is therefore responsible for integrating people with different backgrounds and providing networking, using empowerment instead of command and control from the hierarchy.

3. Methods

This investigation will be carried out based on quantitative analysis methodologies, based on the elaboration, and applied a survey to Portuguese PA workers, with the data subsequently analyzed using statistical techniques using IBM SPSS 24 software.

It is intended to verify whether the satisfaction of PA workers to perform work is correlated with the variable’s autonomy at work, WORK-COND at work, quality of life at work, and income. Job satisfaction is presented as a dependent variable and the remaining variables are independent or explanatory.

Thus, an online survey was applied to a sample of PA workers, to collect data that allow analyzing what are the variables that influence workers' satisfaction.

4. Data Analysis and Results

Analyzing and describing data using appropriate statistical procedures increases the credibility of scientific research and its empirical usefulness.

The global framework assumptions underlying the statistical measures used are:

- H1: Satisfaction in digital remote work varies with income.
- H2: Satisfaction in digital remote work varies with autonomy at work.

- H3: Satisfaction in digital remote work varies with conditions at work.
- H4: Satisfaction in digital remote work is related to productivity, technological specialization, and quality of life in digital remote work.

4.1. Sample Characterization

From the data taken from the questionnaire, a characterization of the sample of PA workers was carried out, which is summarized in the tables below.

Table 1 shows the characteristics of the sample in terms of age and number of years in the organization:

Table 1. Characterization of the sample of PA workers

	Age	**Number of Years in the Organization**
Mean	41.56	19.48
Standard Deviation	0.864	0.743
Median	41.00	20.00
Mode	35	17
Minimum	22	1
Maximum	65	37

4.1.1 Antique

Seniority averages 19.48 years, the oldest employee has been with the company for 37 years and the most recent 1 year.

Age

Age has an average of 41.5 years, a minimum age of 22 years, and a maximum age of 65 years.

- Most employees are under the age of 45 (61.4%).
- The age difference between the highest and lowest value of the variable is 43 years.
- The most frequent age is 35 years old.
- And 50% of employees are 39 years old at the most.

Employees Income

The average yield is 1,082 monetary units (u.m.), with a maximum yield of 2,830 (u.m.) and a minimum yield of 680 (u.m.), having been considered as omitted cases, the yields below zero.

Most employees have an income between 680 (u.m.) and 2,830 (u.m.), exclusive.

Sample Characterization

Seniority averages 19.48 years, the oldest employee has been with the company for 37 years and the most recent 1 year (Table 2).

Table 2. Income (Monthly Salary)

	Frequency	Percentage
>= 2000	68	51.1
0-699	6	4.5
1000 – 1999	47	35.3
700-900	12	9.0
Total	133	100.0

Technological Specialization

The majority of workers identified a relatively high level of technological specialization, with the majority being in the "Very High Specialized" category (75%) (Table 3).

Table 3. Level of Technological Specialization

	Frequency	Percentage
High Specialized	20	15.0
Very High Specialized	100	75.2
Not Specialized	9	6.8
Low Specialized	4	3.0
Total	133	100.0

Productivity/Goal Orientation

Most workers identified their productivity/results orientation as being high, as 49.6% have "High" and "Very High" productivity (Table 4).

Table 4. Productivity/Orientation to Results

	Frequency	Percentage
High	49	36.8
Low	21	15.8
Average	45	33.8
Very High	17	12.8
Very Low	1	0.8
Total	133	100.0

Quality of Life in Digital Remote Work

Quality of life at work was classified as "High" in most cases (47%) (Table 5).

Table 5. Quality of Life in Digital remote Work

	Frequency	Percentage
High	62	46.6
Low	16	12.0
Average	29	21.8
Very High	22	16.5
Very Low	4	3.0
Total	133	100.0

Gender

The number of women is higher than the number of men, respectively 91 and 42 elements (Table 6).

Table 6. Gender

	Frequency	Percentage
Female	91	68.4
Male	42	31.6
Total	133	100.0

Online meetings

Many workers participate in online meetings (78.6%), which can be explained by the need to keep in touch with their bosses for guidance and monitoring of work, the remaining workers (21.4% report not having the necessary conditions to participate in the online meetings, namely, computers with video cameras and the bandwidth are also one of the justifications indicated).

4.2. Statistical Analysis

Satisfaction is the Same in Different Age Groups

To verify whether satisfaction is the same in the different age groups, a simple parametric analysis of variance (OneWay ANOVA) was performed, based on the age variable, grouped into classes and the autonomy variable, as explanatory variables.

Grouping by classes allows better visualization of the distribution of workers, although there may be some loss of information. In this case, the necessary conditions for performing the One Way Anova was fulfilled: a) the distribution of the quantitative variable (DV) must be normal, in each group defined by the nominal variable; b) the variances, in the different groups, must be the same, verifying the assumption of homoscedasticity; c) the samples are independent.

Moreover, the dependent variable is Satisfaction, and the independent variables are the Age Groups, driving to the following hypothesis:

H0: In average terms, satisfaction is the same in different age groups.

Ha: In at least one of the age groups, the average satisfaction is different.

To begin the analysis was crucial t perform the test for normality - the Kolmogorov-Smirnov adherence test.

The probabilities associated with the test value for each age group, is greater than 0.05, so the hypothesis of the sample coming from a population with normal distribution is not rejected p1 = 0.3889 p2 = 0.5280 p3 = 0.8963 p4 = 0.5032.

The was performed a Levene test and the value of the test is 1.7703 with an associated significance of 0.161. The null hypothesis (H0) is not rejected, as the assumption of homoscedasticity is verified, that is, in average terms, satisfaction is the same in different age groups.

The decision based on a probability associated with the test value of p = 0.0031 (p <0.05), determines that H0 is rejected, and for this level of significance, it is accepted that the average degree of job satisfaction is at least different in an age group.

Also, it was performed a Scheffé test (table 7) which allows the identification of groups whose means differ significantly, and the results are a) the group 4 average differs significantly from groups 1 and 2, and the mean of group 3 differs significantly from groups 1 and 2.

Table 7. Age Group/ Mean Satisfaction

Age Group	Mean Satisfaction
< 25	2.1250
25 – 34	2.3478
35 – 44	3.1042
>= 45	2.9444

Correlations between Satisfaction and Autonomy, WORK-COND, Technological Specialization, Productivity, and Quality of life

Analyzing the correlations between Satisfaction and Autonomy, WORK-COND, Technological Specialization, Productivity, and Quality of life at work to measure the strength and direction of the association between the variables.

The goal was to use correlation coefficients to describe the reliability and validity of the data, as these are reliable or valid if the coefficients are statistically significant: -1 Perfect negative correlation; 1 Perfect positive correlation. The hypothesis being tested in table 8 is H0: There is no correlation between variables (table 8):

Table 8. Pearson's Correlation Coefficients

	Autonomy	Work Conditions	Technological Specialization	Productivity	Quality of Life
Work Satisfaction	0.7316	-0.5617	0.4594	0.3894	0.2317
	P=0.000	P=0.000	P=0.000	P=0.001	P=0.054

Except for the variable Quality at work, all others correlate with Job Satisfaction. (P <= 0.005, so the null hypothesis is rejected): a) Autonomy increases, Satisfaction increases - Strong correlation; b) WORK-COND increases, Satisfaction decreases -

Average correlation; c) correlations between Technological Specialization and Productivity with the Satisfaction variable are positive but weak; d) Quality of Life at Work is not correlated with Satisfaction ($p = 0.054 > 0.05$).

5. Discussion

Observing the last decade, it is verified that hardly a science, technique, or area evolved as quickly as the Information and Communication Technologies, managing to keep its real application, not only for the technician or specialist but also for the private user, in your home and workplace, which presents information as one of the most precious assets for companies at the end of this millennium.

For this reason, technical progress in information and communication technologies does not leave anyone indifferent. The repercussions caused at an economic level, even those that most people today consider natural, such as withdrawing money at an ATM, solving a business through a mobile phone, or managing your investments through a telephone bank available 24 hours a day were, just a decade ago, very difficult situations to materialize.

Socially, a very strong technological dependence is created, sustained either by the work activity of individuals or by their needs and habits. This situation is, at the same time, driving new technical progress, at a time when accelerated technological change has become a constant in our lives.

On the other hand, the labor market is becoming increasingly diversified and decentralized (use of labor from countries where wages are lower or where the talents needed for business aspirations exist), conducive to the adoption of new ones. forms of work organization, which is progressively developed further away from the bureaucratic enterprise. A new concept of work arises, digital remote working, where people contribute with their values, being part of teams based on partnership, supported by group work, by greater autonomy and accountability of individual.

6. Implications for Policy

Companies should be encouraged to embark on digital remote working situations, through the adoption of measures that must be precisely targeted in terms of regions or sectors of activity.

The problem related to digital remote working is being studied by the European Commission, through the scope of its general directorates and in connection with the Union Centers and Employers' Confederations of the respective Member States. The primary objective is the issuance of directives on digital remote work, considering aspects such as those presented below:

- a legal and social framework to accelerate the development of digital remote work.
- promoting initiatives that raise awareness about the opportunities it provides.
- establish a framework for achieving broad social consensus, in Europe and a wider international context, on how to implement cross-border digital remote work.

- encourage the Member States to clarify the legal and fiscal situation of the different forms of digital remote work.

- encourage the Member States to promote digital remote working experiences.

In Portugal, a way to reduce regional asymmetries may be to resort to the implementation of digital remote work centers in rural regions, leading to compensation for isolation and the periphery of these regions. In the framework of the EU, peripheral regions can fit into regional development projects.

The role to be played by the EU will be to coordinate Member States' legislative experiences to avoid discrimination against foreign and third-country workers, as well as legislative obstacles to cross-border digital remote working.

On the other hand, for the Portuguese state to facilitate the development of digital remote work, it must adopt some policies that promote initiatives to raise awareness about the opportunities that digital remote work offers and encourage the promotion of experiences.

Although the difficulty of defining policies on digital remote working is understandable, as the concept itself is still not clarified at many levels, the Governments are defining measures to regulate digital remote work.

However, it is necessary to study all potential digital remote work situations, so that they do not lead to increased job insecurity and reduced quality of life, but development, especially at the regional level. To this end, the governments must define strategies that consider the changes that will occur in societies.

Analyzing the entire context surrounding digital remote work has the potential to open paths to employability and is a way of enhancing the fight against unemployment.

7. Implications for Organizations

The implementation of digital remote work in the current situation of Public Health is the best solution, but it is important to consider some critical success factors:

- Worker's Personality - Digital remote work is not appropriate for everyone. For example, poorly motivated people need the discipline of fixed working hours and face-to-face supervision. Also, for people entering the business world for the first time, a conventional work environment is beneficial. For other people, “going to work” is an important part of their lives and the workplace is where they establish their social relationships.

- Workplace - Many homes are not prepared to be used as a workplace. For example, in cases where the digital remote worker needs concentration to develop his work.

- Company Characteristics - some companies have management systems and cultures that do not adapt to the flexibility that digital remote work requires. Many managers do not feel confident in their ability to develop management/supervision activities at a distance, others do not believe in the performance of their subordinates and think that productivity decreases.

- Tasks - not all tasks can be performed in digital remote work situations. Some require a constant interaction of various resources (human or material) or benefit from synergies of joint supervision. In some cases, the team spirit and internal

motivation developed by the leaders who participate in person in the teams is an advantage.

- Digital remote Supervision - workers lose some benefits of telecommuting when subjected to electronic digital remote supervision systems.
- Isolation - digital remote workers suffer from the isolation caused by their situation, if the managers, due to these circumstances, do not provide them with opportunities to attend training courses and participate in company meetings. These factors will have a direct connection with the quality of work and, ultimately, with career development.
- Hygiene and Safety at Work - working conditions, especially unfavorable ergonomic conditions, will impair the performance of the worker in the short term.
- Information Security - in digital remote work situations, not only security issues arise (in terms of reliability and integrity) but also intellectual copyright.
- Real Estate and Consumption Market - lower demand for real estate to settle companies and decrease consumption in small commercial units in the company's surroundings.
- Conflicts in the Company - conflicts due to the lack of information regarding the selection of digital remote workers and due to the decrease in personal contact between physically distant colleagues.
- Insufficient Technical Support - lack of equipment, poor maintenance of equipment, lack of technical support for the user.

However, none of these aspects are barriers to digital remote work. They only illustrate the possibility of difficulties arising in its implementation process if a corrective action plan is not created, supported by appropriate business management attitudes.

Specifically, the are some dimensions that should be considered for future maintenance of digital remote work situation:

7.1. At Organizational Level

- Cost Reduction - overhead and space costs (work can be developed where the skills are, minimizing costs). Recruitment costs can also be reduced, as well as costs related to high turnover rates and costs related to the relocation of workers can be eliminated.
- Increased Productivity - productivity increases between 10% and 40% (according to studies by Jala, Inc.) mainly due to greater time optimization (less time wasted on trips, fewer interruptions due to the company's confusing environment).
- Increases Motivation - digital remote workers respond to the trust they are given, adopting a more independent work style and greater motivation.
- Competence Retention - attracting and retaining the best, with more talent and training, who might otherwise not be available (for example, when the family

needs to move to another region in the same country, workers who want to take a break) in their career can continue to work on a part-time basis).

- Organizational Flexibility - in a process of restructuring the company, digital remote workers do not need to move from their homes and change family life. Also, at the level of work teams, these can be made up of the most competent and experienced elements concerning a given project, regardless of their geographical location or the difference in time zones and spending a minimum of travel costs.
- Flexible Workers - In seasonal activities, digital remote workers can work a required number of hours without having to waste time on trips. Extension of working hours according to the needs of customers.
- Greater Immunity to External Disorders - companies with effective digital remote working programs have greater immunity to external disturbances, such as transport strikes, bad weather conditions or natural disasters.

7.2. At Individual Level

- Reduced Travel Time and Costs - it is the most obvious benefit and, for many digital remote workers, the first motivating factor.
- Better Employment Opportunities - these are not limited by distance.
- Increased Level of Independence - workers gain confidence in themselves as a result of their ability to solve problems.
- Minor Disorders in Family Life - reduced need to move to other regions in search of better career opportunities.
- Better Management between Work and Family Life - you can spend more time with the family and participate more in family life activities. About work, you can concentrate more easily, developing higher quality work.
- Participation in Local Community Activities - time recovered from travel can be used to perform functions at the community level, such as running a club or participating in an association.
- Time Flexibility - a flexible approach to digital remote working can mean individual freedom to start and finish work according to your pace (some people are more productive at night and others are not).

7.3. At Social and Economic Level

- Reduction of Urban Traffic Flows - reduction of traffic in urban centers and “rush hours” in accesses, as well as the need for less space for car parks in cities.
- Reduction of Pollution Levels - with the reduction of traffic in cities, pollution levels will necessarily go down.

- Broader Employment Market - Digital remote working will allow people living in areas with high unemployment rates to have access to employment opportunities regardless of their location.
- Access to Work for People with Specific Difficulties - disabled people with mobility problems, single parents whose mother or father needs to be at home with their child, people with responsibilities for the elderly, or with sick family members.
- Regeneration of the Economy - digital remote working as an element to be considered in economic policies at the regional and national level.

Like any technology or technique, digital remote working only benefits when framed by certain business actions and circumstances of the environment. Thus, it is necessary to consider some determining factors for the success of a digital remote working situation.

8. Conclusions

Despite the constraints (resistance of top management, organizational culture, autonomy, and flexibility of workers, among others) that existed before the health and socioeconomic crisis caused by the Coronavirus pandemic, digital remote work is a given in the life of public organizations or private, and workers with reflections at various levels in society and particularly in professional fulfillment and employee satisfaction.

The development of information and communication technologies in recent decades has contributed exponentially to the radical change in habits and ways of acting, both in companies and their employees and in the social life of everyone, with implications at different levels for all stakeholders active in these changes: organizations, their employees, and managers, as well as for official institutions and their policies.

In this way, governments and official institutions must educate and sensitize companies to the benefits and potential of digital remote work. Encourage, through appropriate and guiding legislation, the use of digital remote work in different sectors of activities and in the regions where companies are located. These are already a concern of the European community where Portugal is inserted and where digital remote working opportunities are presented as a way of reducing regional asymmetries and promoting the development of regions that were left behind when workers had to move to meet the needs of professional achievement.

Among other aspects, the appropriate legislation should study and regulate the different aspects of digital remote working to avoid precarious work and a reduction in the quality of life of workers. It should also promote the empowerment of citizens who can contribute their work to society and who do not have the appropriate training to face these challenges. Digital remote working has the potential to pave the way for employability and is a way of enhancing the fight against unemployment.

Despite these benefits, the implementation of digital remote working poses challenges not only for governments but also for organizations at another level.

Organizations, where management systems allow such implementation, must be prepared for the difficulties that may arise and must consider in the implementation of digital remote working some critical success factors, namely the personality of each worker, the conditions for workers in their homes, which the tasks that suit this type of

work, among others. Consideration should also be given to the possibilities of social interaction that work can provide, such as training actions and company meetings, to promote the quality of the overall work carried out and the satisfaction of its workers. Good communication and good technical support are essential factors for the support of digital remote working and the fulfillment of associated objectives.

Organizations can also have benefits in terms of cost savings associated with physical space for offices and overheads, on the one hand. On the other hand, digital remote working increases the motivation and productivity of workers due to the organizational flexibility that this type of work provides, making the adaptation of family life more balanced and the time spent on travel practically non-existent. It also provides the possibility of carrying out seasonal projects, with the adaptation of workers to these projects, and is more protected from external disturbances than centralized office work.

Digital remote working also brings social and economic benefits as the imposition of workers to take off to their company offices, normally located in city centers, greatly decreases, providing an effective reduction in pollution levels as it also reduces the traffic generated previously for those displacements. This form of work also offers the possibility of combating unemployment by providing access for people with specific difficulties and access for people from areas with few jobs offered to other areas where they may be needed without having to move.

For individuals, the advantages are many, starting with the reduction of travel costs and times, as the first motivating factor for adherence to this type of work, as well as the opportunity to access better jobs. Digital remote working increases workers' confidence by the level of independence in problem-solving. It improves family life as long as the physical and temporal spaces of each situation are respected, allowing the availability of schedules for other activities, given the flexibility of hours to meet the proposed objectives.

However, like any technology or technique, digital remote working only benefits when framed when business actions and surrounding circumstances are respected and implemented. It is crucial to establish the determining factors for the success of a digital remote working situation and for the satisfaction of the people who make up the organizations.

Thus, and according to the analysis carried out on the data collected to support the conclusions of this study, the degree of satisfaction of Public Administration employees is influenced in different ways by the influencing factors studied: autonomy at work, conditions at work, and income. However, regarding the factor of quality of life at work, this link has not been established.

However, the average degree of job satisfaction varies according to the different age groups, with employees aged or more having an average higher satisfaction than employees whose ages vary between and the beginning of their working life.

Thus, it was possible to conclude that satisfaction increases positively and strongly with autonomy at work. Technological specialization and productivity still with a positive influence, but with low intensity contribute to the satisfaction of Public Administration employees.

Working conditions also negatively influence satisfaction, although at an average intensity.

This reflection opens a door for the development of the study of the different factors and circumstances that can influence the satisfaction and performance of workers in digital remote working situations.

Some of the limitations of our study are the low sample as it conditionate generalization. The findings may be dependent on the context of the respondents, creating difficulties to be considered as a reference in other contexts influenced by culture, technological development, and management practices.

The projection of implications in the medium and long term will involve the different stakeholders, in a joint effort to continue the adequate and sustainable development of digital remote work, for all stakeholders – Organizations, Workers, State and Society.

Digital remote work is a fact that is present in the day-to-day lives of organizations, public or private, and workers, which is reflected in the various levels of society, particularly in the fulfillment and professional satisfaction of employees and in the balance and achievement of business objectives. with this new working method, which is only possible due to the development of information and communication technologies.

Most organizations no longer have available only the procedures and work structures established before the imposition of digital remote work, due to the Covid-19 pandemic. Organizational processes have been modified and an attractive factor for recruiting/retaining people is the hypothesis that the digital remote work model is available in organizations. This is a short- and medium-term implication, as workers want a better balance between their private and work lives and do not want to be dependent on physical offices, with rigid schedules and little flexibility for the necessary changes, which do not contribute to their professional and personal fulfillment and satisfaction. However, they need to have the minimum conditions to carry out their duties outside these traditional offices.

For both the short and medium term, governments need to improve existing regulations and adequately legislate these new ways of working. Whether for its citizens or for those who choose their territories to come to work, as in the case of digital nomads, for example.

In the medium term, companies whose operational processes can be supported by digital remote work should incorporate a sustainable hybrid system of remote work and occasional and scheduled trips to their employees' physical offices.

It is necessary to have a culture and mentality of delivering quality work, meeting objectives previously signed in the agreement and joint commitment between managers and workers. With computer security, with adequate tools, minimum conditions, and training.

Despite the difficulties that have arisen, digital remote work brings mutual benefits, and it is possible, in the long term, to work from anywhere, deliver quality work and achieve goals, as long as the necessary and appropriate conditions are met. Whether in an office in the middle of the city, at home, traveling or outside urban centers, working on this new concept of networking. With this new way of delivering work, it is possible to improve, in the long run, the costs of operations, services and the environment.

References

1. Soroui ST. Understanding the drivers and implications of digital remote work from the local perspective: An exploratory study into the disreembedding dynamics. Technology in Society. 2021 Feb 1; 64:101328.
2. Melo PC, e Silva JD. Home telework and household commuting patterns in Great Britain. Transportation Research Part A: Policy and Practice. 2017 Sep 1; 103:1-24.

3. Mears, J. Net worker products, services, and strategies for tying digital remote workers to the enterprise. 2007 May 28;1-27. Available online: www.networkwopld.com (accessed on 31 January 2021).
4. Messenger JC, Gschwind L. Three generations of Telework: New ICT s and the (R) evolution from Home Office to Virtual Office. New Technology, Work and Employment. 2016 Nov;31(3):195-208.
5. Finnegan, M. Rethinking collaboration: 6 vendors offer new paths to digital remote work. 2020. Available online: www.computerworld.com (accessed on 31 January 2021).
6. Buhayar, N. How 'Work from Home' Became 'Work from Anywhere. Available online: https://www.bloomberg.com/news/storythreads/2021-02-04/how-work-from-home-became-work-from-anywhere .com (accessed on 31 January 2021).
7. Bhattacharya S, Mittal P. The Impact of Individual Needs on Employee Performance while Teleworking. Australasian Accounting, Business and Finance Journal. 2020; 14(5):65-85.
8. Huws U, Robinson WB, Robinson S. Telework towards the elusive office. John Wiley & Sons, Inc.; 1990 Jan 26.
9. Kanter RM. Work and family in the United States: A critical review and agenda for research and policy. Family Business Review. 1989 Mar;2(1):77-114.
10. Winter C. Digital remote work. Bloomberg Businessweek. 2013; p. 44.
11. Nilles J. The telecommunications-transport tradeoff. options for tomorrow and today. California: Jala Inter-national. 1973.

Maria José Sousa (PhD in Management with Habilitation in Management and Public Management) is a professor and a research fellow at ISCTE/Instituto Universitário de Lisboa

Ana Cristina Mendes holds a master in accounting, Taxation and Corporate Finance, ISEG - Lisbon School of Economics & Management, Bachelor in Management and Marketing, Universiade Europeia.

Dora Almeida holds a Master in Entrepreneurship and Innovation, Universidade Europeia.

Álvaro Rocha holds the title of Honorary Professor, and holds a D.Sc. in Information Science, Ph.D. in Information Systems and Technologies, M.Sc. in Information Management, and BCs in Computer Science. He is a Professor of Information Systems at the University of Lisbon.

Received: January 10, 2023; Accepted: August 25, 2023.

Computer Science and Information Systems 20(4):1591–1638 https://doi.org/10.2298/CSIS230331062B

DG_Summ: A Schema-Driven Approach for personalized Summarizing Heterogeneous Data Graphs

Amal Beldi[1,2], Salma Sassi[2], Richard Chbeir[2] and Abderrazek Jemai[1,3]

[1] Tunis El Manar University, Faculty of Mathematical Physical and Natural Sciences of Tunis, SERCOM Laboratory, 1068 Tunis, Tunisia
amal.beldi@univ-pau.fr
[2] University Pau & Pays Adour, LIUPPA, Anglet, 64600, France
salma.tissaoui@univ-pau.fr
richard.chbeir@univ-pau.fr
[3] Carthage University, Polytechnic School of Tunisia, SERCOM Laboratory, INSAT, 1080, Tunis, Tunisia
abderrazekjemai@yahoo.co.uk

Abstract. Advances in computing resources have enabled the processing of vast amounts of data. However, identifying trends in such data remains challenging for humans, especially in fields like medicine and social networks. These challenges make it difficult to process, analyze, and visualize the data. In this context, graph summarization has emerged as an effective framework aiming to facilitate the identification of structure and meaning in data. The problem of graph summarization has been studied in the literature and many approaches for static contexts are proposed to summarize the graph. These approaches provide a compressed version of the graph that removes many details while retaining its essential structure. However, they are computationally prohibitive and do not scale to large graphs in terms of both structure and content. Additionally, there is no framework providing summarization of mixed sources with the goal of creating a dynamic, syntactic, and semantic data summary. In this paper, our key contribution is focused on modeling data graphs, summarizing data from multiple sources using a schema-driven approach, and visualizing the graph summary version according to the needs of each user. We demonstrate this approach through a case study on the use of the E-health domain.

Keywords: Heterogenous data, labeled graph, Graph summarization,operation, structure, content, versioning

1. Introduction

Graph datasets, such as those found in social networks, astronomy, and bioinformatics, are a common type of big data application. They consist of large−scale interconnected nodes and edges, which provide a more natural representation of the data. By querying and analyzing the relationships between these entities, it is possible to uncover valuable insights into a wide range of phenomena. This type of analysis can lead to profound discoveries and deep understandings of complex systems. However, due to sheer volume, complexity, and temporal characteristics, building a concise representation (i.e., summary) helps to understand these datasets as well as to formulate queries in a meaningful way. Graph

summarization has emerged as a popular research topic to data in recent years. Its goal is to simplify the task of identifying the structure and significance of data represented in a graph format. A summary of a graph is a brief representation of the original graph that can be utilized for a variety of purposes. For example, it can reduce the number of bits required to encode the original graph, or enable more complex database-style operations to summarize graphs with scalable resolution that can be adjusted interactively[69]. Graph summarization is a useful technique that offers several advantages and has a wide range of applications, including interactive and exploratory analysis[24], approximate query processing [25], visualization [28], data-driven Visual graph query interface construction [35] and distributed Graph Systems among others. However, current approaches for summarizing graphs in static contexts, such as modularity-based community detection[32], spectral clustering[62], graph−cut algorithms [21] exist to summarize the graph in terms of its communities, but lack explicit ordering and only provide groupings without characterizing the subgraphs or offering a clear understanding of the outputs[6]. While these approaches are effective in summarizing the structure of graphs, they do not offer comprehensive characterization of the outputs. The increasing prevalence of dynamic graphs and streams has created a need to analyze their evolving properties over time, leading to a renewed interest in developing graph synopsis construction methods that can accurately summarize their characteristics [67]. However, existing approaches often lack explicit ordering in groupings, leaving users with limited time and no clear starting point for understanding their data. Moreover, these approaches are typically designed for static contexts and lack direct dynamic counterparts. Although some algorithms, such as the one presented in [62], can operate in dynamic settings, they only focus on identifying static patterns that persist over multiple time steps. Thus, there is currently no framework available that can provide a comprehensive summary of mixed-source information while also creating a syntactic and semantic summary of the data. This paper addresses the challenges associated with generating a comprehensive summary that captures both the structure and content of mixed-source data, as well as the relationships and interactions with past data. In particular, the paper focuses on addressing the following challenges:

- **Challenge 1**: How can we generate a summary that integrates data from multiple sources in various formats, such as text, video, and images?
- **Challenge 2**: What methods can be developed to generate user-oriented, semantic-based summaries that are tailored to specific information needs and retrieval challenges?
- **Challenge 3**: How can we ensure that a summary can effectively analyze and capture the changing nature of real data over time, while still providing a concise and informative representation of the underlying data?

The remainder of this paper is structured as follows. In Section 2, a scenario in the healthcare domain is presented along with the limitations and requirements for effective summarization. Section 3 provides an overview of models for data representation and summarization techniques. Section 4 describes and discusses related works on graph summarization approaches, with a particular focus on electronic health record summarization approaches to validate the limitations of our proposed scenario. Section 5 outlines the architecture of our approach, followed by a formalism of the Data Graph in Section 6 and a detailed description of the summary process in Section 7. Section 8 provides explana-

tioncof the experiments and Section 9 describes evaluates our approach both qualitatively and quantitatively. Section 10 conclude with perspectives for future work.

2. Motivating scenario

The healthcare scenario involves a pregnant woman who may develop gestational diabetes, which is more likely if she is over 25, overweight, has a family history of diabetes, had gestational diabetes in a past pregnancy, is prediabetic, has high blood pressure, or had COVID-19. To control his gestational diabetes and understand the patient's history, she needs to communicate regularly with her General Practitioner (GP) and share data such as glucose level, temperature, blood pressure, and location. A Type 2 Diabetes Monitoring System called T2DM system shown in Figure 1, is installed to control and monitor the patient's gestational diabetes and is based on patient data including patient history, Electronic Health Records (EHR), clinical documents, and data from Medical Devices (MD).

It enables the GP to summarize patient data and receive automatic alarms that provide feedback on the patient's health status. The system is capable of monitoring gestational diabetes-related parameters using MDs. However these MDs are heterogeneous in terms of deployment, computing capabilities, and communication protocols. This generates a massive volume of heterogeneous and ambiguous data, which makes it challenging to analyze patient data efficiently and understand the patient's medical history, current situation, treatment status, and dynamic contact network.

To better analyze and monitor the patient's gestational diabetes, there is a need for improvements in integrating these systems for better interoperability and data standardization. Additionally, better data management and analysis tools are required to handle the large volume of heterogeneous and ambiguous data generated by MDs. To enhance patient care, there is a requirement for an integrated approach that amalgamates data from various sources, including electronic health records, clinical documents, and medical devices. However, the current systems are inadequate, and there is still room for improvement as they are unable to meet certain requirements. We imagine that a GP requests the system to answer certain queries, and we present below some queries that T2DM, as well as existing solutions, remain unable to handle:

- **Query 1**: Providing a concise and comprehensive summary of the patient's medical history, with a focus on their Type 2 Diabetes, the GP would need to utilize existing medical systems and technologies to present the patient's demographic data, medical and surgical histories, family history, and current medication list simultaneously in a synthesized manner [61], [1], [48]. However, currently, it is not feasible to condense the most recent blood work results (or older results if there have been significant changes) or biological test results into a summarized format.
- **Query 2**: Generating a graphical representation that summarizes the changes in blood sugar levels over the past two months. In order to measure blood sugar levels, the T2DM uses some existing works [26], which presents the results in either a text or a table format. The numbers within the brackets refer to specific blood sugar level measurements, which are taken at different times of the day. However, currently, there is no way to create a graphical or textual summary of the changes in blood sugar levels

over the past two months. This means that it is not possible to visualize how blood sugar levels have fluctuated during this period.

- **Query 3**: Displaying a real-time summary of data from all MDs. This means that the system would need to collect and process data continuously as it is generated by each MD. However, at present, there is no way to generate a real-time synthesis of data, which means that it is not possible to display a constantly updated overview of the data collected from multiple MDs.
- **Query 4**: Displaying a periodic summary of blood sugar and temperature evolution, with an indication of the visited area for each day. This would involve collecting data on blood sugar and temperature levels for each day and presenting it in a graphical format, with an added feature of indicating the geographical location of each data point. For example, a map could be used to show where the data was collected from. However, currently, there is no system in place to create this type of periodic synthesis of data, so it would need to be developed.

Table 1. Queries and Requirements for Handling Clinician Cases in our proposed scenario

Query	Summarization Objective	Data Source	Summary format	Limitations	Requirments
Query 1	Demographic data, medical and surgical histories, family history, and current medication list	EHR data and Biological tests, Blood test	Multiple summarization	Unable to summarize recent blood work results or biological test results	Aggregating the blood work or biological test results over a certain period of time
Query 2	Changes in blood sugar levels over the past two months	Blood sugar level measurements	Graphical or textual summary	Unable to generate graphical or textual summary	Applying arithmetic operators and generating Graphical or tabular summary
Query 3	Real time synthetis of data	Medical Devices	Constantly Updated Graphic	Unable to generate a real time synthesis of data	Summarizing data in real-time Interpreting and displaying it in graphical or tabular form
Query 4	Evolution of Blood sugar and temperature within geographic location information	Daily blood sugar and temperature measurements	Graphical representation with geographic markers	Unable to create periodic synthesis of data	Creating a periodic summary as well as the location and the time of each data points.

The existing Type 2 Diabetes Monitoring System (T2DM) is capable of monitoring various parameters using Medical Devices (MDs), but the heterogeneous nature of these

MDs generates a large volume of ambiguous and heterogeneous data, making it challenging to analyze and understand patient data efficiently. To enhance patient care, there is a need for an integrated approach that combines data from various sources, including electronic health records, clinical documents, and medical devices. However, current systems are inadequate, and there is still room for improvement in terms of data standardization, interoperability, and data management and analysis tools. In this scenario, as shown in table1, several queries remain unanswered by T2DM and existing solutions. For instance, there is a need for a concise and comprehensive summary of the patient's medical history, including recent blood work and biological test results in a synthesized format. Additionally, graphical representations that summarize the changes in blood sugar levels over time and display a periodic summary of blood sugar and temperature evolution, with an indication of the visited area for each day, are not currently available. To address these needs, the system should be able to aggregate data over a certain period of time, apply arithmetic operators to numerical values to generate charts or summary tables depicting the evolution of certain numerical measures. It should be able to collect and process data in real−time, combine and synthesize it to generate a real-time summary, and interpret data to present it in the form of charts, tables, or other visualizations. Also, the system should be capable of creating a graphical output that displays the location of each data point, which can help in understanding the patient's health status and treatment progress. In summary, this healthcare scenario highlights the need for an integrated approach to patient care that combines data from various sources and utilizes better data management and analysis tools. The development of such a system would enhance patient care and facilitate efficient communication between healthcare providers and patients, leading to better treatment outcomes. Thus, towards building such approach, the following challenges emerge:

- **Challenge 1**: How can we generate a summary that integrates data from multiple sources in various formats, such as text, video, and images?
- **Challenge 2**: What methods can be developed to generate user-oriented, semantic-based summaries that are tailored to specific information needs and retrieval challenges?
- **Challenge 3**: How can we ensure that a summary can effectively analyze and capture the changing nature of real data over time, while still providing a concise and informative representation of the underlying data?

3. Background

In this section, we initially provide a concise explanation of various models used for data representation to justify the utilization of graph−based models in the paper. Afterward, we offer a comprehensive overview of diverse techniques for graph summarization.

3.1. Models for data representation

There are various models for representing data including network [17]relational databases [29],RDF and ontology[16] and graph models [7]. Each of these models has its own strengths and weaknesses, and the choice of model depends on the specific requirements and characteristics of the data being analyzed. Network models [17] are commonly used

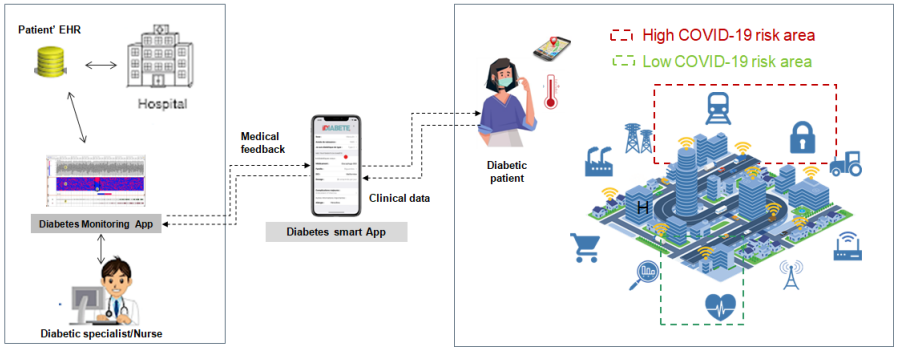

Fig. 1. Type 2 Diabetes Monitoring system (T2DM system)

to represent complex relationships between entities, such as social networks, biological networks, and transportation networks. These models are useful for analyzing the structure and connectivity of the network, as well as identifying patterns and communities within the network.Relational databases [29] are used to represent data in a structured format, with well-defined relationships between tables and fields. These models are useful for querying and analyzing large datasets, and for enforcing data consistency and integrity. RDF and ontology models [16] are used to represent knowledge and metadata in a structured format, with a focus on semantics and relationships between concepts. These models are useful for representing complex and heterogeneous data, and for enabling interoperability and data sharing across different domains. Graph models [7], on the other hand, are a general-purpose model for representing data as a set of nodes and edges. This model is particularly useful for representing and analyzing data that is highly heterogeneous and contains complex relationships between entities. Graph models can handle both structured and unstructured data, and can be easily extended to incorporate additional information or attributes. In the context of data summarization, graph models are often the preferred choice for representing and analyzing large and complex datasets that contain both structured and unstructured data. This is because graph models can capture complex relationships between entities and provide a flexible and scalable framework for data analysis. Additionally, graph models can be used to represent data from different sources and domains, making them well-suited for analyzing data from heterogeneous databases. Therefore, graph models are a suitable choice for summarizing structured and unstructured data from highly heterogeneous databases. In this paper, we have chosen to use the graph-based model for data summarization because it can effectively represent and analyze large and complex datasets that contain both structured and unstructured data. The graph model's ability to capture complex relationships between entities and provide a scalable framework for data analysis also makes it a suitable choice for analyzing data from heterogeneous databases. Moreover, using a graph database can offer significant advantages when dealing with connected data. Graph databases have superior query performance compared to relational databases and other NoSQL alternatives, which is essential for efficiently processing large amounts of data during summarization tasks. Graph databases also offer greater flexibility for adapting to changing needs, as they allow for the addition of relationships, node types, and properties without modify-

ing existing queries. Additionally, their schema-less nature can reduce ambiguity in the domain model and enable more accurate and precise modeling during summarization. Finally, using a graph database can speed up the design-to-delivery process, as developers can create a data model on a whiteboard without having to worry about translating it to a set of tables, ultimately leading to faster delivery of summarization results.

3.2. Summarization Methods

We provide here a background of knowledge about the existing methods related to Data summarization. Many domains have extensively studied summarization, including text analysis, network traffic monitoring, the financial domain, the health sector, and many others. The summarization problem arises in a variety of data analysis tasks and application domains. A variety of summarization techniques for structured versus unstructured data, such as machine learning, statistical, and natural language processing, have been developed to assist with these tasks:

- **Statistical methods** are commonly used in data summarization to identify patterns and summarize large datasets in a meaningful way[69]. These methods involve using statistical techniques to extract important information from the data, such as central tendency, dispersion, and correlation. One of the most common statistical methods used in data summarization is descriptive statistics, which involves calculating measures such as mean, median, mode, standard deviation, and range to describe the characteristics of the dataset. These measures can help provide insights into the distribution and variation of the data, and are useful for identifying outliers and trends. Another statistical method used in data summarization is regression analysis[23], which involves modeling the relationship between two or more variables and using this model to make predictions. This method is often used in finance and economics to forecast future trends and make investment decisions. Cluster analysis[57] is another statistical method used in data summarization, which involves grouping similar data points together based on their characteristics. This method can help identify patterns and similarities within the data, and is often used in marketing and customer segmentation. Overall, statistical methods are very effective in data summarization as they can help identify patterns and summarize large amounts of data in a meaningful and interpretable way. However, they may require more technical expertise and understanding than linguistic methods, and may not always capture the full complexity of the data.
- **Linguistic methods** Linguistic methods[11] are often used in data summarization to help improve human understanding of the summarized data. These methods involve translating the data into natural language statements or summaries, which can be more easily comprehended by humans. One common linguistic method used in data summarization is fuzzy linguistic summarization [77] This method involves converting data into linguistic terms that are easy to understand, such as "high," "medium," and "low," rather than numerical values. In order to address issues with network traffic flow record summarization tools, Pouzols et al [54] proposed a solution that utilizes fuzzy linguistic summaries based on network traffic. The purpose of this approach is to improve human understanding of the network traffic summaries. The summaries produced by this method are often more readable and informative than traditional

numerical summaries. Another linguistic method used in data summarization is text summarization, which involves summarizing large amounts of text data into shorter, more concise summaries. This method uses natural language processing techniques to extract the most important information from a large body of text, and then presents it in a condensed form. Overall, linguistic methods can be very effective in data summarization as they make the information more accessible and easier to understand, especially for non-experts who may not be familiar with the technical jargon or specific domain terminology.

- **Iterative Compression** Iterative Compression[4] is a data summarization technique that involves compressing a large dataset by reducing the number of rows through grouping similar rows and representing them with a single representative row. The goal is to minimize the size of the dataset while preserving its essential characteristics. IT Compression was proposed by Jagadish et al. [34] for relational databases. The approach tries to compress a relation R by reducing the number of rows by grouping similar rows and representing them by a Representative Row (RR). The IT compression algorithm works by iteratively grouping similar rows until the desired compression level is achieved. During each iteration, the algorithm selects a set of similar rows and replaces them with a single representative row, which is a weighted average of the selected rows. The weights are based on the frequency of occurrence of each attribute value in the selected rows. The IT compression algorithm is particularly useful for summarizing relational databases, as it can be used to compress large tables without losing important information. By reducing the size of the dataset, it can also speed up data processing and analysis. One limitation of IT compression is that it requires some prior knowledge of the data and its structure. Additionally, the compression level may not always be optimal, and some information may be lost in the compression process. Nevertheless, IT compression is a powerful data summarization technique that can be used to efficiently summarize large datasets while preserving their essential characteristics
- **Clustering** Clustering is a data summarization technique that involves grouping similar data points together based on their characteristics. The goal is to identify patterns and similarities within the data, and summarize it in a meaningful and interpretable way [5]. There are various clustering algorithms that can be used for data summarization, such as k-means [52], hierarchical clustering[51] , and density-based clustering [36]These algorithms work by assigning each data point to a cluster based on its similarity to other data points in the same cluster. Clustering is particularly useful for summarizing large datasets, as it can help identify patterns and similarities that may be difficult to discern from the raw data. It can also help identify outliers and anomalies within the data, which can be useful for quality control and anomaly detection. One limitation of clustering is that it may not always capture the full complexity of the data, and may not be suitable for datasets with high levels of noise or overlapping clusters. Nevertheless, clustering is a powerful data summarization technique that can be used to efficiently summarize large datasets and identify meaningful patterns and similarities within the data
- **Stream Clustering** Stream clustering is a data summarization technique that involves grouping data points into clusters in real-time as they arrive in a data stream. The goal is to efficiently summarize the data stream and identify meaningful patterns and trends as they unfold over time. Stream clustering algorithms work by continuously process-

ing incoming data points and updating the clustering model to reflect the changing distribution of the data. Some popular stream clustering algorithms include CluStream [73] ,STREAM [67], and Den Stream[14] One key challenge in stream clustering is the need to balance accuracy with computational efficiency. As data streams can contain large volumes of data and may arrive at high velocities, stream clustering algorithms must be able to process data quickly and efficiently, while still maintaining accurate and meaningful cluster representations. To address this challenge, stream clustering algorithms typically use techniques such as windowing, sampling, and approximation to reduce the computational overhead of processing large data streams. For example, some algorithms may use sliding windows to limit the amount of data that needs to be processed at any given time, while others may use random sampling to reduce the size of the dataset without sacrificing accuracy.

– **Graph summarization** Graph summarization is a data summarization technique [4] that involves representing large graphs in a more compact and interpretable form. Graphs are often used to model complex relationships between entities, such as social networks, biological networks, or transportation networks. However, large graphs can be difficult to visualize and analyze, and may contain redundant or irrelevant information. Graph summarization algorithms work by extracting key features or subgraphs from the original graph that preserve the most important information about the underlying structure and relationships. There are various graph summarization algorithms, such as graph sampling, graph clustering, and graph compression. Graph sampling[31] involves selecting a subset of nodes or edges from the original graph that are representative of the overall structure and relationships. This can be useful for visualizing large graphs or analyzing graph properties that are computationally expensive to compute on the entire graph. Graph clustering[3] involves grouping nodes in the original graph into clusters based on their similarity or connectivity. This can be useful for identifying communities or functional modules within the graph, and for detecting anomalies or outliers. Graph compression involves compressing the original graph by identifying and removing redundant or irrelevant information. This can be useful for storing or transmitting large graphs efficiently, or for summarizing the graph in a more interpretable form. Graph summarization is particularly useful for analyzing large and complex graphs, as it can help identify meaningful patterns and relationships that may be difficult to discern from the raw graph data. By summarizing the graph in a more compact form, graph summarization algorithms can also help reduce computational overhead and storage requirements. In this paper, we will be using graph summarization as a technique for analyzing large and complex graphs. Graphs are often used to model complex relationships between entities, and graph summarization can help us identify meaningful patterns and relationships that may be difficult to discern from the raw graph data. Additionally, by summarizing the graph in a more compact and interpretable form, we can reduce computational overhead and storage requirements. We have chosen this technique because it is particularly useful for our data analysis task and can help us gain insights into the underlying structure and relationships of our graph data.

4. Related Work

In this section, describes and discusses related works on graph summarization approaches, with a particular focus on electronic health record summarization approaches

4.1. Graph summarization approaches

In this section, we will provide an overview of the three main categories of graph summarization: static plain, static labeled, and dynamic graphs.

1. **Static plain graph approach** Most research in static graph summarization focuses on the graph structure without considering side information or labels. In general, the problem of summarization, aggregation, or coarsening of static graphs can be described as simplification-based summarization methods that streamline the original graph by removing less "important" nodes or edges, resulting in a sparsified graph [43]. One example of node simplification-based summarization techniques is OntoVis [64], which is a visual analytical tool that relies on node filtering to understand large, heterogeneous social networks with nodes and links. Toivonen et al. [70] focused on compressing graphs with edge weights and proposed to merge nodes with similar relationships to other entities, which are called structurally equivalent nodes. SPINE, an alternative to CSI [76], sparsifies social networks to keep only the edges that "explain" the information propagation, those that maximize the likelihood of the observed data. In the visualization domain, Dunne and Shneiderman [22] introduced motif simplification to enhance network visualization. They suggested simplifying a graph by extracting its repetitive patterns or motifs and replacing them with higher-level motifs. The simplified graph becomes more interpretable, and the high−level motifs reveal the underlying structure of the graph. In summary, these methods focus on simplifying the graph structure while maintaining its essential properties. By removing redundant or less important nodes and edges, the resulting summary graph is more manageable and easier to analyze while preserving the essential features of the original graph.
2. **Static labeled graph approach** Graph summarization methods that focus on labeled graphs aim to leverage both structural connections and node attributes to produce more informative summaries. These methods face challenges such as the efficient combination of these two different types of data, as well as the selection of meaningful subgraphs or nodes for the summary. One of the most well-known approaches in this category is the frequent-subgraph-based summarization scheme, SUBDUE [19]. It employs a greedy beam search to iteratively replace the most frequent subgraph in a labeled graph. The S−Node representation [59] is another lossless graph compression scheme that optimizes specifically for web graphs. Other approaches, such as SNAP and k-SNAP [69], rely on attribute and relationship-compatibility to group nodes with similar attributes and connections into homogeneous groups. Some recent works have also proposed lossy graph summarization frameworks, such as the collection of d-summaries introduced by Song et al. [38], which group similar entities into supergraphs. Overall, while there have been many advances in labeled graph summarization, it remains an active area of research with many challenges and opportunities for further development.

3. **Dynamic graph approach** Analyzing large and complex data is a challenging task, which becomes even more difficult and time-consuming when dealing with time-evolving networks. The temporal graph mining literature has extensively studied laws and patterns of graph evolution. However, summarization techniques for time-evolving networks have not been studied to the same extent as those for static networks, possibly due to the new challenges introduced by the time dimension. Time granularity, which is often arbitrarily chosen, is a sensitive parameter that can be set to minutes, hours, days, weeks, months, years, or some other unit that makes sense in a given context. TimeCrunch[78] are two methods that succinctly describe a large dynamic graph with a set of important temporal structures. Qu et al.[56] represents a stream of time-ordered interactions, represented as undirected edges between labeled nodes. NetCondense[2] is a node-grouping approach that maintains specific properties of the original time-varying graph, like diffusive properties important in marketing and influence dynamics, governed by its maximum eigenvalue.

4.2. Discussion on graph summarization approaches

To better understand and compare graph summarization approaches, it's important to recognize that the notion of a graph summary is not well−defined. The specific goals and applications of a summary can vary widely, and may include preserving structural patterns, focusing on specific network entities, maintaining query answers, or preserving graph property distributions. Graph summarization approaches can be broadly categorized into three main types: static plain, static labeled, and dynamic graphs. To address the challenges inherent in graph summarization, we propose nine criteria that can be used to describe and compare existing approaches. By considering these criteria in the development and evaluation of graph summarization techniques, we can better understand and overcome the challenges of this important field. We have established nine criteria used to describe and evaluate existing approaches. These criteria are designed to address the specific challenges and goals of graph summarization, and provide a framework for understanding and comparing different approaches.

Challenge 1: How can we generate a summary that integrates data from multiple sources in various formats, such as text, video, and images?

- **Type of input Data (C1)**: this criterion pertains to the input data used in graph summarization approaches. The input data can take on different forms, including (i) structured data such as predefined knowledge models that include existing ontologies and database schema/graphs. (ii)Semi-structured data involves a mix of structured data and free text, such as web pages, Wikipedia sources, dictionaries, and XML documents. (iii) Unstructured data refers to any plain text content, videos, signals, and so on. It's important to consider the nature of the input data when designing and evaluating graph summarization techniques, as the data format can impact the effectiveness and accuracy of the summary.
- **Data type (C2)**: this criterion describe the type of data incorporate (text, xml, numeric, video, image). It's important to consider the type of data being summarized, as this can impact the methods and techniques used in the summarization process. Different data types may require different approaches to summarization in order to effectively capture and convey important information.

– **Representation standard (C3)**: this criterion describes if the approach incorporates standard((i.e. information based standard, document based standard or Hybrid standard) (e.g., Yes or No). The use of a standard can facilitate the comparison and integration of graph summaries from different sources. It's important to consider whether a standard is used in the summarization approach, as this can impact the interoperability and compatibility of the summary with other systems and applications.

Challenge 2: What methods can be developed to generate user-oriented, semantic-based summaries that are tailored to specific information needs and retrieval challenges?

– **Summarization approach (C4)**: this criterion pertains to whether the summarizing approach targets the structure or the content of the graph. Some approaches may prioritize preserving the structural relationships between nodes, while others may focus more on the content and attributes of the nodes (i.e. based structure, dbased content).
– **objective (C5)**: this criterion refers to the specific target or goal of the summarization approach. This could include improving query efficiency, reducing the size of the graph, or identifying influential nodes or relationships. By defining the objective of the summarization approach, it becomes easier to evaluate the effectiveness and relevance of the approach in achieving its intended purpose.
– **Summarization technique (C6)**: this criterion refers to the techniques deployed to summarize data which could be: grouping, compression, analysis, pattern- mining, classification, visualization. The choice of technique used can impact the quality and effectiveness of the resulting summary. By considering the summarization technique employed, we can better understand the strengths and limitations of a particular approach.

Challenge 3: How can we ensure that a summary can effectively analyze and capture the changing nature of real data over time, while still providing a concise and informative representation of the underlying data?

– **Output type (C7):**this criterion concerns type of data displayed in the summary output. which is a combination of: numerical data, textual data, document, graph. By considering the output type, we can better understand the format and presentation of the summary information, which can impact its usefulness and accessibility to end users
– **Context-aware criterion (C8):** this criterion refers to the degree to which a summarization approach takes into account the contextual information surrounding the data being summarized. This can be divided into two types of context-awareness: partial and total. (i)Partial context-awareness refers to the use of concepts related to the dynamic context of the data, such as time, location, and trajectory. (ii) Total context-awareness, on the other hand, refers to the use of both the dynamic context of the data and other contextual information related to the static data. By considering the level of context-awareness, we can better understand the extent to which the summarization approach takes into account the broader context of the data being summarized.
– **User oriented summarization (C9):** pertains to the extent to which a summarization approach is designed with the user in mind. This criterion asks whether the approach

is user-oriented, meaning that it is designed to meet the needs and preferences of the user. By considering the user's needs, the summarization approach can be tailored to present information in a way that is meaningful and useful to the user. This can improve the overall effectiveness and usability of the approach (e.g., yes or No).

Our analysis indicates that the field of graph summarization still faces many challenges. Many existing studies, such as Shen et al. [64], Toivonen et al. [70], Xu et al. [76], do not consider real-world data in their analysis. These studies rely solely on synthetic or simulated data to test their summarization approaches, which may not accurately reflect the complexities of real-world scenarios. Furthermore, most existing systems do not consider the context in which the data is being summarized. They rely solely on time-based properties and do not take into account other important contextual factors that could affect the summary. Consequently, existing systems like Tang et al. [67], and Adhikari et al. [2] are still unable to interpret and reason on the transferred knowledge among real data, which hinders their ability to provide accurate desired results. It is worth noting that existing graph summarization approaches have limited functionality and can only satisfy certain aspects of users' needs. For example, Shi et al. [65] propose a framework for summarizing graphs based on visual representations, while Fan et al. [24] propose a method for summarizing graphs based on user queries. However, none of these approaches provide a comprehensive framework that integrates various functionalities to meet users' diverse needs. Finally, the output type of summarized data is another important consideration. Most existing studies do not propose dedicated tools that make the summary accessible to the user, nor do they provide appropriate perceptions of their needs. Users are increasingly concerned about the security, confidentiality, and accuracy of their data, and existing systems do not adequately address these concerns.

4.3. EHR Summarization Approaches

In the following, we present related works on summarization approaches that are relevant to our domain of application, i.e., Electronic Health Records (EHRs). Discussing the related works on EHR summarization approaches is crucial to validate the motivating scenario presented in Section 2 and further highlight the challenges in this domain. By examining the existing approaches, we can identify the strengths and weaknesses of each and gain a better understanding of the current state-of-the-art in EHR summarization. This knowledge can then be used to guide the development of more effective and efficient approaches.

The EHR concept has appeared since the 1960s [46] and we note that there is no common definition of an EHR until today. The EHR−based application has to be accessible, secure and highly usable. In [27], Gunter and Terry define EHR as a set of clinical and electronic data about a given patient and a population.The World Health Organization (WHO) [10] defines EHR as medical records provided in an EHR-based system aiming at collecting data , storing and manipulating, and providing safe access.

The process of EHR summarization involves creating a summary that contains the most relevant information from the original content. Previous research in this area has focused on text summarization, with the aim of providing useful information for healthcare professionals by automatically compressing a given text [47]. The type of summary required may vary depending on the clinician's needs, but in general, it should cover

as much of the medical content as possible, while preserving the overall topical organization of the original text. This review specifically focuses on approaches based on multi-document extractive summarization, which involve producing a summary of multiple documents about the same patient. These summarization approaches are typically focused on extracting clinical variables and visualizing structured and unstructured data [53], in order to provide an overview of the patient's entire medical record. We will discuss and analyze 38 research papers on EHR summarization, which are categorized into four types of EHR text summarization:

1. **Extractive Summaries** EHR summarization typically involves selecting a subset of information from the original content, with text summarization being the primary focus of existing studies [47]. The aim is to provide a compressed version of the text that is relevant to the needs of clinicians. Generic summaries covering the medical content in multiple documents must maintain the general topical organization of the original text. This method synthesizes patient records by displaying the summary in user-friendly interfaces. Studies have explored supervised approaches to extractive summarization, such as [45], which trained a transformer-based neural model using International Classification of Diseases (ICD) codes for specific diagnoses. Radiologists evaluated the approach and found that supervised models generate better summaries than unsupervised approaches. The model aims to include accurate components of EHR data, such as structured data, sentence-level clinical aspects, and structures of clinical records. Authors provide a clinical data processing pipeline based on NLP and the use of concept recognition and relation detection. Other studies have explored the use of NLP to customize user views, such as [41], which uses MedLEE NLP engine to handle modifiers. Some studies have also explored generating meaningful topic summaries from structured clinical data, such as [26], which learns the correspondences between structured data and clinical note topics using existing summaries written by clinicians. Approaches have also been proposed for synthesizing clinical data, such as the SIM card-based system in [1], which displays synthesized clinical data on mobile phones using custom-developed software. [68] proposed a summarization approach to classify patients with and without diabetes, evaluating the approach using traditional classification methods and machine-learning techniques. Another study [66] focused on metastases information extraction from pathology reports of metastatic lung cancer. In [48], authors propose a Bayesian summarization method for summarizing biomedical text documents, involving mapping the input text to the Unified Medical Language System (UMLS) terminology and selecting relevant ones to use as classification features. Finally, [53] proposes UPhenome, an approach based on graphical models and large scale probabilistic phenotyping to model diseases and patient characteristics and generate summarized clinical data. [30] proposes a real-time summarization approach by aggregating clinical data from heterogeneous health care systems using HL7 messages and a distributed architecture.
2. **Abstractive summaries** Abstractive summarization techniques are a type of text summarization approach that goes beyond simply extracting relevant phrases or sentences from the original text. Instead, they generate new text by synthesizing the most important information from the source material. This can provide additional context and insight beyond what is available in the original text[55]. In the medical domain, researchers have explored a variety of abstractive summarization techniques.

For example, [13] and [9] proposed a method called Timeline, which involves clinicians in coding rules to generate abstractive summaries. Another approach, called AdaptEHR, was developed by [13] to infer rules and relationships automatically from ontologies and graphical models. In [63], a hybrid abstractive-extractive summarization approach was proposed. This method aims to perform semantic, temporal, and contextual abstraction using a domain-specific ontology to generate abstractions. Additionally, [33] and [72] explored a graphical approach to summarizing clinical data by generating new text. Overall, these studies demonstrate the potential for abstractive summarization techniques to provide more comprehensive summaries of medical records.

3. **Indicative Summaries** Indicative summarization is an approach that extracts significant terms from the original text and highlights the main parts. This technique is used in conjunction with EHR to indirectly integrate the extractive summarization process. However, there are limited studies in the literature concerning indicative summarization. Rogers and colleagues proposed a new approach to summarize and graphically visualize the EHR, including indicative summaries. Their approach involved creating task-based evaluation summarizers, which extracted the most relevant information for specific clinical tasks. In another study, Clayton and colleagues evaluated how and when clinicians in an ambulatory setting would enter data directly into an EHR. They found that physicians entered more information when the patient's problem was acute, complex, or unfamiliar [18]. This study did not directly focus on indicative summarization, but it provided insight into how physicians interact with EHR and how information is entered into the system. [61] proposed a new approach to summurize and graphically visualize the EHR. [61] proposed a task-based evaluation summarizer. In [18] authors evaluated how and when clinicians in an ambulatory setting will enter data directly into an EHR.
4. **Informative Summaries** The informative summarization approach is distinct from the other approaches in that it aims to replace the original set of raw data rather than simply provide an abstract of it. This approach is designed to create summaries that can be used independently of the EHR. Several studies have proposed methods for informative summarization. For example, Matheny et al. [44] developed a new model for summarizing structured clinical data, such as administrative, computerized provider order entry, and laboratory test data. Their model was used to detect risks by predicting two severity levels of in-hospital Acute Kidney Injury (AKI). Visualization-based summarization approaches have also been proposed in the literature, such as those by Bade et al. [8], Wang et al. [74], and Borland et al. [12]. These methods aim to create summaries by visualizing the data in a more understandable and concise manner. RDF-based summarization approaches have also been proposed, such as Carenini et al. [15]. These methods use RDF (Resource Description Framework) to represent and summarize text data. Many research groups, such as the NUCRSS [61], have proposed clinical data summarization systems based on text input data. These systems aim to reduce the volume of data and make it more manageable for clinicians. Various frameworks have also been proposed for text summarization, such as those by Liu et al. [40], Wright et al. [75], and Radev et al. [58]. In addition, methods for generating new stories and scientific articles to summarize unstructured texts have been proposed, such as those by Nenkova et al. [50], Lukasik et al. [42], Liu et al. [40], and Reeve et al. [60].

4.4. Discussion on EHR summarization approaches

To address the challenges related to EHR summarization and to facilitate a comparison of existing studies on clinical data summarization, the criteria outlined in the previous section were utilized to characterize and compare different methods of clinical data summarization in accordance with the challenges identified in the introduction and we mentionned also other criterion in the same context such as Representation standard (C3), this criterion indicates if the approach incorporates standard((i.e. information based standard, document based standard or Hybrid standard) (e.g., Yes or No). This approach enabled a comprehensive evaluation of various techniques used for EHR summarization, including the extent to which they address the challenges associated with this task. By employing these criteria, researchers can gain insights into the strengths and limitations of different summarization approaches and can make informed decisions about which method is best suited to their specific use case. Additionally, this approach facilitates a comparative analysis of different studies on EHR summarization, providing a better understanding of the current state of the field and identifying areas for future research.

According to the analysis presented in Table 3, the existing approaches for clinical data summarization can be categorized into two groups: those that rely on structured data and those that use unstructured data. The studies [49] fall under the category of approaches that are based on structured data. On the other hand, the studies [15] belong to the group of approaches that rely on unstructured data. It is important to note that none of the approaches analyzed in this study utilize both structured and unstructured data to construct the summary. Another important aspect of the analyzed studies is the type of output provided by the clinical data summarization systems. The studies reviewed in this paper propose either document-based systems [26] or graph-based systems [12]. However, none of these studies offer dedicated tools that facilitate user access to the summary or provide them with appropriate perceptions of their needs. Users are increasingly concerned about the security, confidentiality, understanding, accuracy, and completeness of their data. Therefore, it is essential to ensure that clinical data summarization systems provide users with the necessary means to ensure these aspects. An intuitive and user-friendly graphical user interface (GUI) would significantly benefit clinical data summarization systems. Also, we highlight that none of the studies surveyed are user-oriented and able to satisfy the diverse needs of users. Our analysis, presented in Table 2, reveals that the evolution of data summarization is still an ongoing challenge. Most of the existing studies fail to consider the contextual information of the data in their analysis and do not take into account the context when creating the summary. Instead, they rely solely on the time property, except for a few studies that consider time in their analysis . As a result, current systems are still unable to contextually interpret and reason on the transferred knowledge among real data, and thus cannot synthesize data to provide accurate desired results. It is noteworthy that all existing systems focus on only one objective, while none of them provide multiple functionalities within the same framework, despite their importance in supporting users' preferences to find data according to various needs. Therefore, it is necessary that all objectives should be integrated into a summarization-based system. In addition, our analysis shows that most of the studied approaches are extractive-based, including [45],[39],[40], and [26]. However, three of the studies, namely [13], and [9], are abstractive-based. Furthermore, five studies, including [13], adopt both extractive and abstractive−based approaches. In summary, existing systems tend to focus on only

one objective and adopt extractive-based approaches. Nonetheless, it is important to consider multiple functionalities within the same framework and integrate both extractive and abstractive−based approaches in the summarization-based system. Based on our comparative study, we have identified four main limitations in clinical data summarization:

- **Lack of access to and collection of data from Medical Devices:** Due to the heterogeneity of applications, it is critical to synthesize health data in order to provide a relevant, comprehensive, and understandable view of the patient's history to effectively help clinical diagnostics [37].
- **Lack of semantic interoperability:** Applications generate a huge amount of heterogeneous data, which makes it difficult to synthesize knowledge and communicate between clinical applications to provide efficient results [71].
- **Lack of linking Data and medical devices to their contexts:** It is important to describe the data and device context in order to identify its capacity and reliability to ensure the consistency of the gathered data and to easily repair it when necessary [20].
- **Lack of user-centered summary design:** Existing systems are unable to generate adaptive summaries that adjust based on clinician preferences and needs, leading to increased cognitive workload for clinicians [79] It is nearly impossible to provide interactive and personalized summaries, which can result in reduced efficiency and effectiveness in clinical decision−making.

Table 2. Qualitative Comparative study of static, static labeled dynamic plain Graph summary

()2-10	**Challenge 1**			**Challenge 2**				**Challenge 3**	
Existing study/Criterion	**C1**	**C2**	**C3**	**C4**	**C5**	**C6**	**C7**	**C8**	**C9**
Category 1: Dynamic graph									
Adhikariet al. 2017	Structured	Weighted,Directed	Yes	Structure	Influence	Grouping	Supergraph	Time	Yes
Tan et al. 2016	Structured	Weighted,Directed,	Yes	Structure	Query	Grouping	Supergraph	Time	Yes
Qu et al. 2014	Structured	Unweighted, Undirected	yes	Structure	Influence	Influence	Subgraph	Time	Yes
Category 2: Static graph									
Zhu et al.2016	Structured	Weighted, Undirected	No	Structure	Visualization	Grouping	Supergraph	No	No
Riondato et al. 2014	Structured	Weighted, Undirected	No	Structure	Query	Grouping	Supergraph	No	No
Koutra et al. 2014	Structured	Unweighted, Directed	No	Structure	Visualization	Compression	Graph	No	No
Dunne et al. 2013	Structured	Unweighted, Directed	No	Structure	Visualization	Grouping	Supergraph	No	No
Mathioudakis et al. 2011	Structured	Weighted, Directed	No	Structure	Influence	Influence	Sparsified graph	No	No
Category 3: Static labeled graph									
Song et al. 2016	Structured	Unweighted	No	Structure	Query	Grouping	Supergraph	No	No
Shi et al. 2015	Structured	Weighted, Directed	No	Structure	Influence	Influence	Supergraph	No	No
khan et al. 2014	Structured	Unweighted Directed	No	Structure	Compression	Compression	Supergraph	No	No
Hassnlou et al 2013	Structured	Weighted directed	No	Structure	Grouping	Compression	Supergraph	No	No
Fan et al. 2012	Structured	unweighted, Directed	No	Structure	Query	Grouping	Supergraph	No	No
Zhang et al. 2010	Structured	Unweighted, Undirected	No	Structure	Patterns	Grouping	Supergraph	No	No
Proposed approach	Structured, Unstructured	Labeled, Directed	Yes	Structure, Content	Summarization	Grouping, Aggregation, Mathematical operations, Compression	Supergraph, Subgraph, Graph	Yes	Yes

Table 3. Summary of retrieved studies on electronic health record and medical data summarization

	Challenge 1			**Challenge 2**			**Challenge 3**		
Existing study/Criterion	**C1**	**C2**	**C3**	**C4**	**C5**	**C6**	**C7**	**C8**	**C9**
Denis Jered et al. 2020	Document	Unstructured	No	Structure	Classification	Extractive	text	No	No
Liang et al. 2019	Text	Unstructured	No	Structure	Classification	Extractive	Text	No	No
PDurga et al.2018	Text	Unstructured	No	Structure	Classification	Extractive	Text	No	No
Jen et al. 2018	Document	Unstructured	No	Structure	Classification Filtering	Extractive	Text	Time	No
Soysal et al. 2017	Text	Unstructured	No	Structure	Visualization	Extractive	Text	No	No
Razavian et al.2015	Text	Unstructured	No	Structure	Analysis	Extractive	Text	No	No
Borland. 2014	Text	Unstructured	No	Structure	Visualization	Extractive	Text	No	No
Fei et al. 2013	Numerical	Unstructured	No	Structure	visualization	Extractive	Numerical	No	No
Klann et al. 2013	Document	Unstructured	No	Structure	Classification	Extractive	Text	No	No
Roque et al. 2010	Document	Unstructured	No	Structure	Visualization	Extractive	Text	No	No
Barakat et al. 2010	Text	Unstructured	No	Structure	Analysis	Abstractive	Text	No	No
Savova et al. 2010	Text	Unstructured	No	Structure	Analysis	Extractive	Text	No	No
Krummenacher et al. 2009	XML	Structured	No	Structure	visualization	Extractive	Tuple	No	No
Kumar and al. 2008	Text	Unstructured	No	Structure	Extraction	Extractive	Text	No	No
Huang et al. 2007	Text	Unstructured	No	Structure	Extraction	Extractive	Text	No	No

5. Contribution

The main contribution relies developing a schema-driven approach for handling heterogeneous data sources by modeling and summarizing them within labeled data graphs. The resulting graph summaries are then visualized to meet the specific needs of each user. In essence, the approach relies on using data graphs and a schema to drive the data modeling and summarization process. Our approach aims to provide a comprehensive and personalized model capable of summarizing both the structure and content of data from databases, devices, sensors.etc. We took into consideration the user needs. In order to achieve our goal, our framework architecture includes four main modules, as illustrated in figure 2. First, the Data Collection module is responsible for collecting data from various sources. Second, the Schema Generation module is used to generate a schema based on the collected data, which enables us to create a labeled data graph. Third, the Summarization module summarizes the data graph based on user-submitted questions, and fourth, the Visualization module provides a personalized visualization model to represent the summarized data graph for each user need. Our approach addresses the limitations identified in the comparative study by providing a user-centered, schema-driven approach that can effectively model and summarize data from heterogeneous sources. By providing a personalized visualization model, our approach aims to reduce cognitive barriers related to the complexity of information and its interpretation, ultimately supporting clinical decision-making.

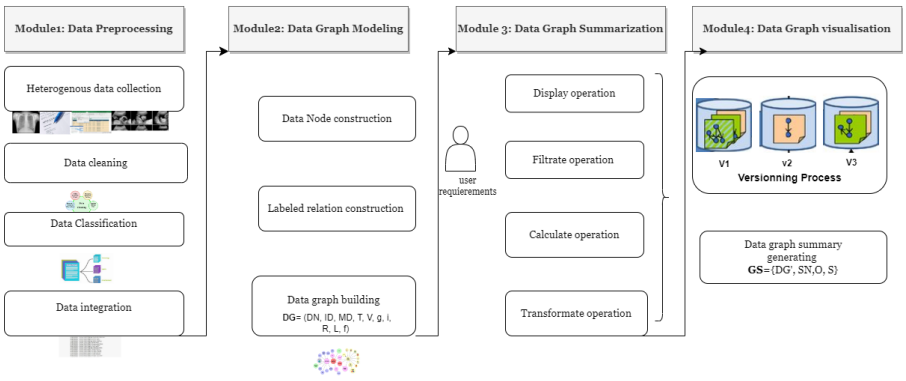

Fig. 2. Architecture of our proposed system

A) **Data Pre-Processing service**: consists of processing and indexing data in order to summarize them. Every incoming data is processed and transformed according to two-steps: data cleaning and data integration. This module is composed of:

1) Data collection: this module is responsible for collecting data in various formats such as pdf documents, images, videos, and numeric data.
2) Data Cleaning: this module involves transforming raw data into an understandable format by extracting data from multiple and heterogeneous sources.

3) Data classification: this module classifies the different data into associated types. To classify documents from a heterogeneous corpus, this module involves text analysis, keyword extraction, and natural language processing.
4) Data Integration: this module integrates different normalized data into a generic framework that supports the direct generation of data in a common format. The objective is to create a unified and consistent data structure that can be used for analysis and modeling purposes.

B) **Data Graph Modeling**: This module is responsible for defining the data graph proposed by our system. The data graph is composed of data nodes and relations between them. The purpose of this graph is to represent the heterogeneous data in a common format, making it easier to process and analyze. By representing data in a structured graph, we can identify patterns, relationships, and dependencies between data nodes, which can be used to generate insights and support decision-making processes. The data graph will be defined in the next section, and it will serve as the backbone of our system for data processing and analysis.
C) **Data Graph summarization**: this module defines the data processing steps that are involved in generating a data summarization model-based graph, which is the core module of our framework. The purpose of this module is to transform input data into a summarized output. It aims at summarizing data using a driven schema approach based on both structure and content. This involves analyzing the data graph schema and extracting relevant information based on user requirements, which are represented using different functions. To achieve this, the module has multiple microservices that operate based on the user needs and requirements. The data summarization model-based graph will be further detailed in section 7
D) **Data Graph visualization**: this module is responsible for the visual representation of data. Its main objective is to provide visual and interactive visualization of the summarized data to help users rapidly find insights in data. It includes interactive techniques to graphically represent the summary, such as charts, graphs, tables, and dashboards. These visual representations provide an intuitive and easy-to-understand view of the summarized data, allowing users to explore and analyze it in a more efficient way. This module generates a graph summary which is a visual representation of the summarized data using the data graph schema.

6. Data Graph Modeling

In this section, we focus on the data graph modeling module, which is responsible for creating a graph-based data model of the input data. The module performs an aggregation process on the transformed input data and generates an aggregated value.

The data graph model is built iteratively, starting from a root node that represents the whole data set. Each aggregated item in the graph consists of one or more children, which can be either original data items (leaves) or aggregated items (nodes). This hierarchy of nodes and leaves allows for a structured representation of the data, which makes it easier to analyze and summarize. To achieve this, we introduce a new Data Graph Model (DGM), which serves as a common synthesis of a large amount of data. The primary goal of the DGM is to facilitate and perform the summarization process by providing a structured representation of the input data.

6.1. Data Graph Definition

The data graph (DG) is a graph-based representation of the input data. It consists of Data Nodes (DN), also known as data entities, which model heterogeneous data such as text, images, videos, and numerical data. These DNs are the building blocks of the graph and serve as the vertices in the graph. In addition to the DNs, the DG also contains relations between them. These relations are the edges in the graph, which connect the DNs to each other. Each relation has a label that defines the nature of the connection between the DNs.

6.2. Data Graph Formalism

Definition 1: Data Node (DN) A Data Node (DN) is a fundamental component of the Data Graph, representing the information contained within a data structure. Each DN holds a value of structured or unstructured data and is associated with a single parent node. The DN is defined by its identification, name, and metadata, which describe its type, value, and acquisition time. It also has a set of attributes, each with a corresponding value and data type. These attributes define the specific properties of the DN and provide additional information about its contents.

Definition 2: Data Graph (DG) A Data Graph (DG) is a representation of important structured and unstructured data within a domain. The purpose of defining the DG is to create an efficient representation of domain data and the relationships between them. Formally, the DG is represented as:

$$\text{DG= (DN, ID, MD, T, V, g, i, R, L, f)}$$

where

- DN: is a set of Data Nodes
- ID : is a set of identifier of Data Node
- MD: is set of attributes (e.g DocName, Date...)
- T: is a set of types $\{String, number, Boolean\} \cup$\{Array,image, son, video\}
- V: is a set of values
- g: DN $\rightarrow$ (MD, T, V)
- i: DN $\rightarrow$ ID
- R: set of relationships: R $\subseteq$DN $*$ DN
- L: set of terms
- f: R$\rightarrow$ L

Algorithm 1: Data Graph Generation

```
   Input  : Heterogenous Data
   Output: DG
 1 Initialize an empty graph DG
 2 for i from 1 to n (n is the total number of data nodes in DN) do
 3 |   Add a node to graph G with identifier i(DN[i])
 4 end
 5 for i from 1 to n do
 6 |   for j From 1 to n do
 7 |   |   if there exists a relationship r in R such that DN[i] is either the source or the destination of r then
 8 |   |   |   Add an edge to graph DG between nodes i(DN[i]) and j(DN[j])
 9 |   |   |   If
10 |   |   end
11 |   end
12 end
13 for i from 1 to n do
14 |   Add a set of attributes to node i(DN[i]) based on the values in MD[i]
15 end
16 for i from 1 to n do
17 |   Add a set of values to the node i(DN[i]) based on the values in V[i]
18 end
19 for i from 1 to n do
20 |   Add a set of types to node i(DN[i]) based on the values in T[i]
21 end
22
23 for  i from 1 to n do
24 |   Add a tuple (MD[i], T[i], V[i]) to the mapping g for node i(DN[i])
25 end
26 for each relationship r in R do
27 |   Add a term l to the set L based on the function f
28 end
29 Return the DG
30
```

This pseudo code describes an algorithm 1 that generates a data graph. The algorithm first initializes an empty graph DG. Then, for each index i from 1 to n (number of data nodes), it adds a node to graph DG with identifier i(DN[i]). Next, for each pair of indices i and j from 1 to n, it checks if there exists a relationship r in R such that DN[i] is either the source or the destination of r. If there is such a relationship, it adds an edge to graph G between nodes i(DN[i]) and j(DN[j]). After that, for each index i from 1 to n, it adds a set of attributes to node i(DN[i]) based on the values in MD[i], a set of values based on V[i], and a set of types based on T[i]. Then, for each index i from 1 to n, it adds a tuple (MD[i], T[i], V[i]) based on the function g for node i(DN[i]). Finally, for each relationship r in R, it adds a term l to the set L based on the function f. The algorithm returns the graph DG as the data graph.

This data includes various resources that provide information about the patient's personal details, medical history, and current health status. Specifically, the data sources consist of medical tests, prescriptions, scans, and radiographs that are associated with the patient. The DG generated is a graphical representation of this data, where nodes represent the different data sources and edges represent the relationships or connections between them.

7. Data Graph summarization

Graph summarization is the process of creating a Graph Summary (GS) from a given DG. The GS captures the essential features of the DG, while reducing its complexity and size. The process of graph summarization involves selecting a subset of the vertices and edges

from the DG to be included in the GS, while still maintaining the overall structure and connectivity of the original graph.

7.1. Data Graph summary Definition

The Graph Summary (GS) contains Summary Nodes (SN) and Operational Relationships, which are represented as functions called Operation (O). These O correspond to various user needs, such as display, filtering, transformation, and calculation. The SN in the GS represent a subset of the nodes in the original DG that capture the most relevant information. The Operations, define how the SN can be generated to satisfy user needs. By using the GS and its associated operations, users can interact with the data in a more efficient and effective way. The GS reduces the complexity of the original DG while still preserving the important information, and the functions provide a flexible and customized way to perform various operations on the summary nodes.

7.2. Data Graph summary formalism

Definition 3: Summary Node (SN) A Summary Node (SN) is a representation of a subset of nodes in the DG that captures the most relevant information. The SN is a node in the GS that summarizes a group of nodes in the original DG and can be generated using various operations to satisfy user needs. The SN is defined identically to DN.

Definition 4: Graph Summary (GS) A Graph Summary (GS) is a condensed representation of a larger Data Graph (DG) that contains Summary Nodes (SN) and Operational (O) in the form of functions. The SNs represent a subset of the nodes in the original DG that capture the most relevant information, while the (O) define how the SNs can be generated to satisfy user needs, such as display, filtering, transformation, and calculation. Formally a GS is defined as follow:

$$SG \doteq (DG', SN, O, S)$$

Where

- DG: $DG' \subseteq DG' * DG$ (DG' is a part of DG)
- SN: is a set of summary nodes, SN is defined identically to DN
- O: is a set of synthesis operations (max, min, avg, display, filtrate, transformate, calculate)
- S: $O \rightarrow DN * SN \cup DN$

The formalism for the Graph Summary (GS) involves defining the SG as a tuple containing a subset of nodes in the original Data Graph (DG'), Summary Nodes (SN), Operational Relationships (O), and a mapping function (S) that defines how the SNs can be generated to satisfy user needs. The subset of nodes in the original DG, denoted as DG', is a part of the original DG and serves as the basis for the summary. The SNs in the GS represent a subset of the nodes in the original DG that capture the most relevant information. These SNs can be generated using various functions represented by the operational relationships (O), such as display, filtering, transformation, and calculation. The mapping function (S) maps these operational relationships to the set of nodes in the original DG

and the set of SNs in the GS. In summary, the Graph Summary formalism defines a condensed representation of a larger Data Graph that captures the most relevant information using a subset of data nodes and operational relationships. The mapping function allows for flexible and customized ways to generate Summary Nodes to satisfy user needs.

Definition 5: Operation (O) An Operation (O) is a function in the GS defining how SN can be generated to satisfy user needs, such as displaying, filtering, transforming, and calculating. The O $\rightarrow$ DN*SN mapping function links the operational relationships to the set of DN in the original DG and the set of SNs in the GS.

Definition 6: Display Operation The Display Operation, denoted by Display(nodetype), is used in constructing the GS based on the projection operator. Its main objective is to remove a specific DN from a common relation in the data graph. The nodetype parameter specifies the type of node to be projected or displayed in the summary. In other words, the display operation is used to generate a SN that captures only the relevant information from a larger set of data nodes.

Algorithm 2: Display Operation (Same NodeType)

Input : DG
Output: GS
Create an empty set of Summary Nodes SN and an empty set of Operations O
Identify important nodes in DG that have a large number of connections or are in the center of the graph
Group the identified nodes into a node grouping DG'(DN): $\text{dn}_1, dn_2, \ldots, dn_m$
foreach *DG'i in DG'* **do**
    Create a Summary Node SN(GSj) and assign it an unique identifier j
end
foreach *DNj in DN(DGi)* **do**
    assign it to SN(GSj) r
end
foreach *dni, dnj in DG* **do**
    if *i=j and sni, snj belong to both DG'i and SGj* **then**
        |
    end
    Then connect them with an edge in GS
end
Return Gs= (DG', SN, O, S)

The following pseudocode outlines the steps for creating a graph summary GS from an input DG. Firstly, an empty set of Summary Nodes SN and Operations O is created. Then, significant nodes in the input DG are identified based on their number of connections or centrality and grouped into a node grouping DG'(DN).For each DG'i in DG', a Summary Node SN(GSj) is created and assigned a unique identifier j. Each DNj in DN(DGi) is then assigned to SN(GSj). For each dni, dnj in DG, if i=j and sni, snj belong to both DG'i and SGj, they are connected with an edge in GS.

Finally, the algorithm defines Operations O that can be used to generate the Summary Nodes SN to satisfy user needs, such as display, filtering, transformation, and calculation.

This algorithm 3 takes as input a graph DG and outputs a graph GS. It first defines the join operation as and then iterates over each DNj in DN(DGi) to select data nodes and metadata based on certain conditions. For each selected data node dn1, it selects metadata md1 such that MD is either in the data nodes DN= dn1, dn2, ..., dnm or MD is the metadata of dn1 or MD is in nodetype and equals acquisition time md1, md2, ..., mdn in DG. The algorithm then selects the relation r1 such that r1 is in DR or r1 is in R(r2$\in$ o

Algorithm 3: Display Operation (Multiple Node Type)

Input : DG
Output: GS
foreach *DNj in DN(DGi)* **do**
  Define the join operation as ⋈:
  DG x DG x cond → G's(dn1, dn2, condj) → dn1, dn2, condj
  Select data nodes based on the condition Let dn1 be the selected data node where $dn_1 \in$ data nodes DN and $dn_1, dn_2, dn_3, .., dn_n (dn_2 \in$ DN $dn_1, dn_2, \ldots, dn_m)$
  Select meta data based on the condition:
  Let md1 be the selected meta data where:
  MD ∈ data nodes
  DN= dn1,dn2,dn3,...,dnn ∨ (md1 ∈ DN= dn1,dn2,...,dnm)
  Let MD be the data node where MD is the meta data of dn1
  or ($md_2 \in$ nodetype | MD = acquisition time md1, $md_2, \ldots, md_n \in$ DG)
  Let r1 be the selected relation where r ∈ DR ∨ (n2 ∈ O r1 ∈ $R(r2 \in$ o | r = r1,r2,...,rn∈ $DG) \wedge$, o, G's
end
Return GS=(DG', SN, O,S)

| r = r1,r2,...,rn∈ DG), and o and G's are determined.
Finally, the algorithm returns GS= (DG', SN, O, S) where DG' contains tuples (dn1, dn2, condj, md1, r1), SN contains tuples (dn1, dn2, condj), O contains tuples (r1, o), and S contains tuples (md1, GS').

Definition 7: Filtering Operation The filtering operation is an operator that selects a subset of nodes from a DG based on a selection predicate or criterion, which produces a GS. The filtering operation uses a selection predicate to determine which nodes in the DG should be included in the GS. The predicate, or selection criterion, can take on various forms, including a combination of node type, attribute, and relation. In other words, the valid selection criteria can be represented as a condition that specifies the node types, attributes, and relations that should be included in the GS.

The Filtering Operation algorithm takes as input a data graph (DG) and outputs a graph summary (GS) by selecting relevant attributes for each data node. The algorithm starts by initializing an empty set of selected attributes, MD Set. For each data node DN in DG, if DN is in the set of multiple data nodes (MD), then the algorithm selects metadata nodes (mdi) that satisfy the set of valid selection criteria (cond) and adds them to the set of selected MD Set. If G's is a supernode, the algorithm selects metadata nodes from the set of selected attributes (MD Set) and adds them to the summary graph GS.

Definition 8: Transformate Operation A Transformation Function consists of transforming numerical data into graphical or tabular format. This type of transformation function involve a variety of mathematical or statistical operations allowing to manipulate and analyze numerical data in meaningful ways.

Algorithm 5 represents the transformation operation. The input to this algorithm is a data node, and the output is a supernode, which can be in the form of a numerical node, a graphical representation, or a table. The local variable 'Operator(o)' is either 'calculmax', 'calculmin', 'calculavg', or a statistical operator. If the numerical node is one of the numeric nodes dn1, dn2, dn3, ..., dnn in the data graph DG, and the operator is 'calculmax', the algorithm calculates the maximum value of the nodes and creates a new supernode containing the numerical node and the maximum value. The algorithm then returns the supernode. If the numerical node is one of the numeric nodes dn1, dn2, dn3, ..., dnn in the data graph DG, and the operator is 'calculmin', the algorithm calculates the minimum value of the nodes and creates a new supernode containing the numerical

Algorithm 4: Filtering Operation (For Same or Multiple Data Node)

Input : DG
Output: GS
Initialize an empty set of selected attributes, MD_set. **foreach** *Data Node DN ∈ DG* **do**
  if *($DN \in MDN$)* **then**
    foreach *mdi* $\in MD(dn)$ **do**
      if *((mdi) ∈ the set of valid selection criteria cond)* **then**
        Add mdi to the set of selected MD_set
    end
  end
  if *(G's is a supernode)* **then**
    foreach *metadata node md ∈ G's* **do**
    end
    if *(mdi ∈ MD(DN))* **then**
      Add mdi to the set of selected attributes, MD_set
    foreach *dN in DG* **do**
      foreach *mdi ∈ MD(DN) such that MDi is MDi-compatible* **do**
        // MDi-compatible refers to a grouping ϕ that satisfies the condition that for every data node dni in DN, if ϕ(dni) = ϕ(dnj,G's)
        if *($MDi \in thesetofselectedattributes$)* **then**
        Add the corresponding metadata node mdi(G's) to the summary graph GS.
      end
    end
  foreach *mdi∈a in MD(dN) such that mdi ∈ set of selected MD* **do**
    Add the corresponding metadata node mdi(G's) to the GS
  end

Algorithm 5: Transformation operation

Input : DN=numerical node
Output: SN=(numerical node, graphical, or table),GS
Local Variables: $Operator(o) = calculmax, calculmin, orcalculavg$
if *(DN ∈ numeric nodes dn1, dn2, dn3, ..., dnn in DG o≐ calculmax)* **then**
  Calculate the maximum value of the nodes: maxVal ≐ max(dn1, dn2, dn3, ..., dnn)
  Create a new supernode sn ⊆
  SN(Gs) ≐ DN(numericnode; dn1, dn2, dn3, ..., dnn) ⊆ DG
  o ≐ maxVal
Return Gs
if *(DN ∈ of numeric nodes dn1, dn2, dn3, ..., dnn ⊆ DG and o ≐ calculmin)* **then**
Calculate the minimum value of the nodes: minval≐ min(dn1, dn2, dn3, ..., dnn)
Create a new supernode Sn ∈ Gs
SN(Gs) ≐ DN(numericnode; dn1, dn2, dn3, ..., dnn) DG
o≐ minVal
Return G's
if *(DN of numeric nodes dn1, dn2, dn3,..., dnn in DG and o is calculavg)* **then**
  Calculate the average value of the nodes: avgVal ≐ average(dn1, dn2, dn3, ..., dnn) Create a new supernode sn ∈ Gs, SN(Gs) ≐ DN(dn1, dn2, dn3, ..., dnn) of DG and the average value avgVal
Return Gs **if** *(DN ⊆ set of numeric nodes dn1, dn2, dn3, ..., dnn ∈ DG and o is a statistic operator)* **then**
  Calculate the statistical data of the nodes (e.g. standard deviation, variance
  Create a new supernode sn ∈ SN(G's) ≐ table(G's) of DG and the calculated statistical data
Return Gs

node and the minimum value. The algorithm then returns the supernode. If the numerical node is one of the numeric nodes dn1, dn2, dn3, ..., dnn in the data graph DG, and the operator is 'calculavg', the algorithm calculates the average value of the nodes and creates a new supernode containing the numerical node and the average value. The algorithm then returns the supernode. If the numerical node is a set of numeric nodes dn1, dn2, dn3, ..., dnn in the data graph DG, and the operator is a statistical operator, the algorithm calculates the statistical data of the nodes (e.g., standard deviation, variance) and creates a new supernode containing the table of the data graph and the calculated statistical data. The algorithm then returns the supernode. If the numerical node is a single numerical node, and the operator is a statistical operator, the algorithm calculates the statistical data of the node (e.g., standard deviation, variance) and creates a new supernode containing the graphical representation of the data graph and the calculated statistical data. The algorithm then returns the supernode.

Definition 9: Calculation operation The Calculation operation is intended to perform mathematical computations on one or multiple DN. It involves various mathematical operations like addition, subtraction, multiplication, division, exponent, and remainder. Two inputs are needed for each operation, and the requirements of inputs vary depending on the type of mathematical operation being performed. For instance, Add, Subtract, Multiply, Divide, and Remainder nodes can accept numeric values or certain time-based values as inputs, while Exponent operations only accept numeric values. Only one output is produced by each operation, representing the outcome of the mathematical calculation performed on the input data node. It is important to note that these calculations can only be carried out on numerical data nodes

Algorithm 6: Calculation Operation (Numerical Node)

Input : DN
Output: SN
Local Variables: $o, FirstVal, SecondVal$
1 SN $= \varnothing$
2 **if** *(DN.FirstVal* $\in \mathbb{R}$ *and DN.SecondVal* $\in \mathbb{R}$*)* **then**
3 **if** *(*$O == +$*)* **then**
4 $SN =$ DN.FirstVal $+$ DN.SecondVal
5 **else if** *(*$O == -$*)* **then**
6 $SN =$ DN.FirstVal $-$ DN.SecondVal
7 **else if** *(*$O == *$*)* **then**
8 $SN =$ DN.FirstVal $*$ DN.SecondVal
9 **else if** *(*$O == /$*)* **then**
10 $SN =$ DN.FirstVal/DN.SecondVal
11 **else if** *(*$O == \%$*)* **then**
12 $SN =$ DN.FirstVal%DN.SecondVal
13 **else if** *(*$O ==$*)* **then**
14 $SN =$ DN.FirstVal$^{\text{DN.SecondVal}}$
 `// If the operator is not any of the above, return an error message indicating that the operator is not supported.`
15 Return SN

Algorithm 6 describes the Calculation Operation algorithm for numerical nodes. It takes a numerical DN as input and produces a supernode SN as output. The algorithm is based on various mathematical operations such as addition, subtraction, multiplication, division, exponent, and remainder. These operations can only be performed on numerical data nodes. The algorithm begins by initializing the supernode SN to an empty set. It then checks if both FirstVal and SecondVal of the input DN are real numbers. If so, the algorithm proceeds to check the operator O. If the operator is addition (+), then the algorithm

calculates the sum of the FirstVal and SecondVal and stores it in SN. Similarly, if the operator is subtraction, multiplication, division, exponentiation, or remainder, the algorithm performs the corresponding mathematical operation on the FirstVal and SecondVal and stores the result in SN. If the operator is not any of the above, the algorithm returns an error message indicating that the operator is not supported. Finally, the algorithm returns the supernode SN as output.

8. Summary Versioning Process

Definition 9: Summary Versioning Summary Versioning is a process of creating and maintaining different versions or snapshots of a graph Summary at different points in time, allowing users to track and analyze changes to the DG over time. This process can help to identify trends, patterns, and inconsistencies in the data, as well as to undo any mistakes made during the editing process. Formally, a history H is a sequence of one or more quadruplets representing versions of the graph summary, defined as:

V_Gs= (DG, O, V, tn)

where :

- DG: is the original Data Graph input
- O: is the Operator used for the summarization process
- V: is the sequence of graph summary versions
- tn: is the history of the last version of the graph summary at time t, where t is any point in the sequence of time intervals of the history. This means that for each new version of the GS, a new timestamp is added to the history. The history provides a record of all the changes made to the GS over time, allowing for a better understanding of its evolution. The VGs component captures the differences between the different versions of the GS. The versioning process in our approach involves keeping track of all the changes made to the graph summary over time, and representing each version as a sequence of changes captured in the VGs component. By maintaining a history of graph summary versions, users can easily access and compare previous versions, as well as track changes and monitor the evolution of the data over time.

This algorithm initializes an empty list H to store the history of graph summary versions and an empty list V to store the sequence of graph summary versions. It then creates the initial version of the graph summary GS using the Operator O and the original Data Graph DG, adds the initial version to V, and creates a quadruplet V_Gs representing the current version of the graph summary. This quadruplet is added to H. The algorithm then makes changes to the original Data Graph DG, creates a new version of the graph summary GS using the Operator O and the updated Data Graph DG, and adds the new version to V. It also updates the current timestamp and creates a new quadruplet V_Gs representing the current version of the graph summary, which is added to H. Finally, the algorithm returns the final V_Gs with the history of graph summary versions.

Algorithm 7: Summary Versioning Process

Input : DG:original Data Graph
Output: $v_$GS: $GraphSummaryversionwithhistory$
Local Variables: $Operator(o), t : Currenttimestamp, H$

Initialize an empty list H to store the history of graph summary versions
Initialize an empty list V to store the sequence of graph summary versions
Create the initial version of the graph summary GS using the Operator O and the original Data Graph DG
Add the initial version to V
Create a quadruplet $V\_Gs = (DG, O, V, t)$ representing the current version of the graph summary
Add V_Gs to H
`// Repeat the following steps as needed`
Make changes to the original Data Graph DG.
Create a new version of the graph summary GS using the Operator O and the updated Data Graph DG
Add the new version to V
Update the current timestamp
Create a new quadruplet$V_Gs = (DG, O, V, t)$ representing the current version of the graph summary
Add V_Gs to H.
Return the final V_Gs with the history of graph summary versions.

9. Experimentation

9.1. Implemented Scenario description

To validate our proposed approach, we tested it on Type 2 Diabetes Monitoring system (T2DM system) Monitoring scenario presented in Section 2 to show how our approach intends to overcome scenario limits mentioned in this study. For our implementation, we developed an Angular-Python Framework called DGsum that implements the services described in this paper. The motivating scenario presented in section 2 was used as a prototype for our implementation, and we utilized a diverse dataset that focused on pregnant women with diabetes. The experimental protocol aims to tackle the difficulty of managing diverse and heterogeneous data from various sources, including medical devices, by providing GP with effective tools to interpret the data according to their specific requirements. To achieve this goal, the protocol entails integrating heterogenous data and medical devices to improve interoperability and enforce data standardization. Furthermore, it involves developing advanced data management and real time analysis tools that can handle the massive amount of ambiguous data. Our evaluation design was based on the implemented scenario in a Service Oriented Architecture (SOA) 3 as an evolution of the Component Based Architecture, Interface Based Design (Object Oriented), and Distributed Systems. SOA provides a simple and scalable paradigm for organizing large networks of systems that require interoperability to realize the value inherent in the individual components. By minimizing trust assumptions that are often implicitly made in smaller scale systems, SOA is scalable and manageable. As architects using SOA principles, we are better equipped to develop systems that are scalable and manageable.

9.2. Experimental Protocol

Experimental Objectives

– **Objective 1: Qualitative Evaluation** To evaluate the usability and user experience of the DGsum system and its impact on data analysis for healthcare professionals. This protocol involved GP with experience in data analysis and diabetes management, who

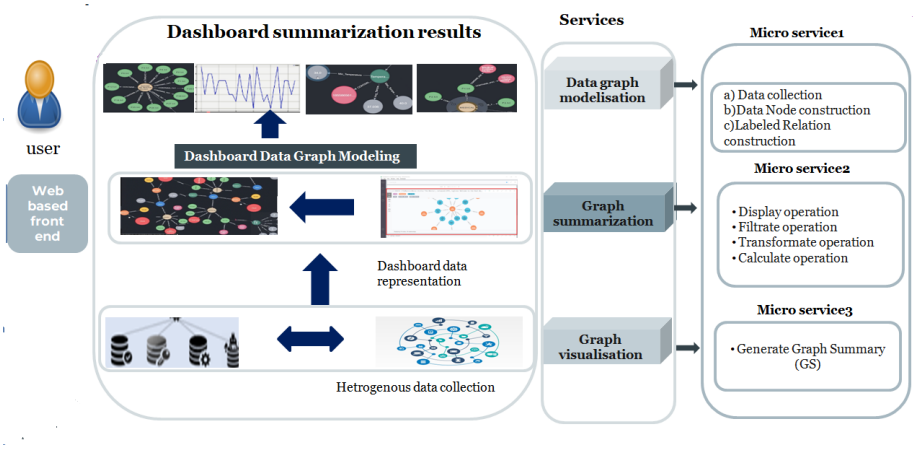

Fig. 3. Proposed technical Architecture oriented services of our system

was asked to perform specific tasks using the DGsum system, such as creating and visualizing a data graph or summarizing data based on a specific query. Participants was asked to provide feedback on the ease of use of the system, the usefulness of the tools provided, and their overall satisfaction with the system. The data collected from this protocol helped to identify any usability issues and inform future improvements to our system.

– **Objective 2: Quantitative Evaluation** To evaluate the effectiveness of the DGsum system in improving patient outcomes in pregnant women with diabetes, we evaluated the performance of our algorithms in terms of runtime, coverage, and loss of information of answers to queries on data graphs and graph summaries. We also conducted user studies to evaluate the effectiveness of the system in supporting the task of analyzing patient health records.

Dataset The dataset for pregnant women with diabetes contains various types of health data, including demographic information such as age, gender, and race, as well as medical history, surgical history, family history, and medication lists. The dataset also includes numerical data such as blood sugar levels, temperature, blood pressure, and BMI, which provide important information about the patient's diabetic condition. In addition to these simple numerical data, the dataset also contains complex data in the form of an ECG recording, Xray image, ultrasound image, MRI scan, blood test results, urine test results, and a symptoms diary. These data provide more detailed and specific information about the patient's health status and can be used to track their progress over time. Overall, the dataset provides a comprehensive view of the patient's health, which can be used by healthcare providers to inform their care and treatment plan. The combination of simple numerical data and complex data allows for a more complete understanding of the patient's health, enabling healthcare providers to make informed decisions about their care.

Participants The experiment are conducted with a group of healthcare professionals, including general practitioners and medical specialists. The participants should have basic knowledge and experience in interpreting medical data.

Procedure

- Participants were given a brief introduction to the DGsum system and the scenario presented in section 2 of the paper.
- Participants were provided access to the system and dataset, and they were asked to create a data graph that summarizes the health data of a pregnant woman with diabetes.
- Participants were asked to visualize the data graph and perform various operations, such as filtering, sorting, and grouping.
- Participants were asked to interpret the data and identify any potential health risks or concerns
- The participants were timed during the experiment, and their progress was recorded.
- After the experiment, participants were asked to provide feedback on the usability and effectiveness of the system, as well as any suggestions for improvement.

Data Analysis

- The time taken by the participants to create the data graph and perform the required operations was recorded and analyzed
- The accuracy and completeness of the data graph created by the participants was assessed.
- The feedback provided by the participants was analyzed and used to improve the system.

Expected outcomes

- The experimental protocol aimed to evaluate the effectiveness of the DGsum system in managing diverse and heterogeneous data from various sources
- The results of the experiment were analyzed to gain insights into the usability and effectiveness of the system and its potential to enhance patient care
- The feedback provided by the participants was analyzed and used to improve the system and make it more user-friendly and effective

Graphs generation

- **Data Graph Generation** To conduct an experimentation with the scenario presented in section 2, we have generated the DG of the pregnant women with diabetes. The generated DG includes:

  - **Data Nodes (DN):**
    - *Demographics Data:* represents demographic data about the patient, such as her age, gender, race, and other relevant information.

- *Medical History:* represents previous medical conditions, surgeries, and procedures they she undergone, as well as allergies, history may include details about the patient's lifestyle habits, such as smoking or alcohol consumption, which could impact her overall health.
- *Surgical History:* represents information about the surgical procedures that the patient has undergone in the past, including the date of the procedure, the name of the procedure, the surgeon who performed it, and any relevant details about the procedure, such as complications or outcomes. It also includes information about anesthesia and post-operative care.
- *Family History:* represents the patient's family medical history, including any relevant genetic or hereditary conditions.
- *Medication Lists:* represents a list of medications the patient is currently taking, including dosages and frequencies.
- *Blood Sugar Levels:* represents the patient's blood sugar levels, which are a key indicator of his diabetic condition.
- *Temperature:* represents the patient's body temperature
- *Blood Pressure:* represents simple numerical data about the patient's blood pressure.
- *BMI:* represents simple numerical data about the patient's body mass index.
- *Electrocardiogram (ECG):* represents complex data in the form of an ECG recording.
- *Xray:* represents complex data in the form of an Xray image.
- *Ultrasound:* represents complex data in the form of an ultrasound image.
- *Magnetic Resonance Imaging (MRI):* represents complex data in the form of an MRI scan.
- *Blood Test Results:* represents complex data in the form of blood test results, including various numerical and textual data points.
- *Urine Test Results:* represents complex data in the form of urine test results, including various numerical and textual data points.
- *Symptoms Diary:* represents complex data in the form of a diary of the patient's symptoms and his severity over time.

- **Relations (R):**
  Here are all relationships with corresponding labels between the different DN:
  - *"hasRecentBloodSugarLevel":* Demographics Data→Blood Sugar Levels
  - *"has RecentBodyTemperature":* Demographics Data→ Temperature
  - *"hasRecentBloodPressure":* Demographics Data→Blood Pressure
  - *"hasRecentBMI":* Demographics Data→hasRecentBMI
  - *"hasSurgicalHistory":* Medical History → Surgical Histories
  - *"has PastMedicationList":* Medical History →Medication Lists
  - *"hasPastbloodTestResult":* Medical History→ Blood Test Results
  - *"hasPastUrineTestResult":* Medical History → Urine Test Results
  - *"hasSymptomsDiary":* Medical History → Symptoms Diary
  - *"has ECG":* Medical History → Electrocardiogram
  - *"has Xray":* Medical History → Ultrasound
  - *"has MRI":* Medical History → Magnetic Resonance Imaging
  - *"hasSurgicalMedicationList":* Surgical Histories → Medication Lists

- *"has SurgicalBloodTestResult":* Surgical Histories →Blood Test Results
- *"haSurgicalUrineTestResult":* Surgical Histories → Urine Test Results
- *"hasMedicationBloodTestResult":* Medication Lists→Blood Test Results
- *"hasMedicationUrineTestResult":* Medication Lists→Urine Test Results
- *"hasBloodUrineTest": :* Blood Test Results → Urine Test Results

We generated in figure 4 the Data Graph (DG) for the pregnant woman with diabetes as described in the motivating scenario in section 2. The DG includes both simple and complex DN that provide information about her health condition. Simple DNs, such as demographic data, blood pressure, and body mass index, represent numerical or basic information. Meanwhile, complex DNs, such as ECG recordings, X_ray and ultrasound images, and MRI scans, contain more intricate data that require specialized interpretation. To depict the relationships between the different DNs, relations (R) were established for example, "hasRecentBloodSugarLevel" connects Demographics Data to Blood Sugar Levels DN. Other relationships connect simple DNs, such as blood sugar levels and temperature, to the Demographics DN. Other relationships link medical history to surgical history, medication lists, blood and urine test results, and symptoms diary. These connections between DNs help to provide a comprehensive view of the patient's health data and enable the identification of potential health risks or concerns.

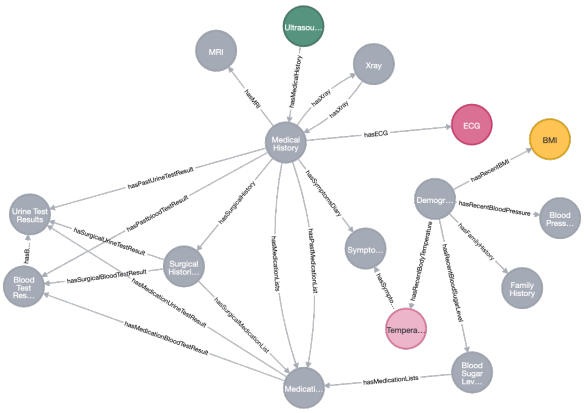

Fig. 4. The DG related to the pregnant women

Graph Summary Generation Table 4 presents the different types of queries that we will be using to extract and analyze the patient's medical data. These queries include transformation queries, which extract specific data points and present them in a certain way, calculation queries, which perform calculations on the extracted data, filtering queries, which narrow down the data based on certain criteria, and display queries, which present the data in an easy−to−understand format. By using these queries, we aim to generate comprehensive summaries of the patient's medical history and progress, which will inform their treatment plan.

Table 4. Querie types for graph summary generation

Operation	***Query***	***Description***
(1)Transformation	Query for blood sugar levels over time (Q1.1)	This query aims to extract the blood sugar levels and create a line chart to show how the levels have changed over time
	Query for blood and urine test results (Q1.2)	This query aims to extract the numerical and textual data points and create a table to show results for each test.
	Query for symptoms diary (Q1.3)	This query aims to extract the medication names and create a chart to show haw the symptoms have changed over time.
	Query for medication usage (Q1.4)	This query aims to extract the symptom description and severities and create a line chart to show how the symptoms have been prescribed.
	Query for surgical history (Q1.5)	This query aims to extract the surgical procedures and their dates and create a timeline to show when each procedure was performed
	Query for family history (Q1.6)	This query aims to extract the relevant data and create a table to show which conditions are present in the patient's family history
(2)Calculation	Calculate the correlation coefficient between blood sugar and BM (Q2.1)	This query aims to extract the blood sugar levels and BMI values and calculate the correlation coefficient between the two varaiables
	Calculate the percentage change in blood pressure (Q2.2)	This query aims to extract the blood pressure values from the Blood Pressure DN and calculate the percentage change from the previous reading.
	Calculate the average frequency of symptoms (Q2.3)	This query aims to extract the symptom data from the Symptoms Diary DN and calculate the average frequency of each symptom over a specified time period

(3) Filtering	Filter The MRI scans by body part and data range(Q3.1)	This query aims to extract the relevant MRI scan data and filter them to display only those for a specific body part and taken within a specified date range
	Filter the blood sugar levels by time of day (Q3.2)	This query aims to extract the blood sugar levels based on the time of day.
	Filter the medical records by data range (Q3.3)	This query aims to retrieve relevant medical information within a designated date interval.
	Filter the symptoms diary by severity (Q3.4)	This query aims to extract the relevant MRI scan data and filter them to display only those for a specific blood part and taken within a specified date rang
(4) Display	Display the Patient' s information (Q4.1)	This query would display the patient's demographics data, blood sugar levels, and symptoms diary
	Display the medical list (Q4.2)	This query aims to display all the medication lists.
	Display the blood test result (Q4.3)	This query aims to display the blood test result for the pregnant women with diabetes
	Display the ultrasound images (Q4.4)	This query aims to display the ultrasound images for the pregnant women with diabetes that were taken during the second trimester.
	Dispaly the surgical History (Q4.5)	This query aims to display the patient's surgical history, including the name of the surgery, the date it was performed, and the name of the surgeon.

We have provided some examples of queries that utilize the graph summary (GS) results to visualize the output. As shown in Figure 6, a doctor may request to visualize a patient's information, which falls under the category of display queries. On the other hand, Figure5 depicts a graph that displays various data nodes filtered based on their connection to surgical histories. This graph is likely generated as a result of a query requested by a GP and falls under the category of filtering queries. Figure 6 depicts a user requesting the summarization and visualization of numerical data nodes related to temperature measurements. The doctor would be able to interpret the curve represented by the variation in temperature. On the other hand, Figure 5 shows a query that involves extracting numerical data nodes related to temperature measures, and calculating the maximum, minimum, and average values of this measure. This query would enable the doctor to analyze and un-

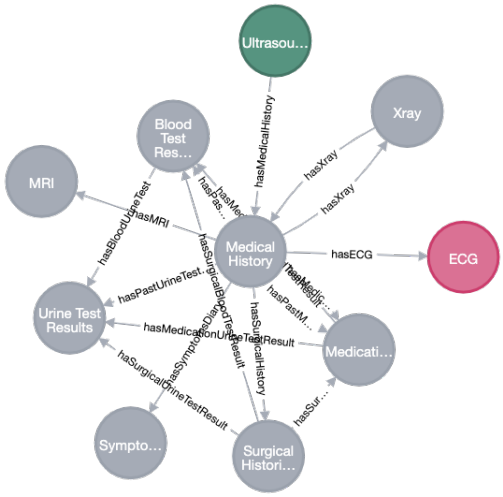

Fig. 5. Generating Summary Graph for query (Q3.3)

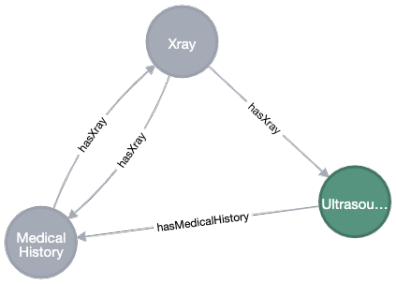

Fig. 6. Generating Summary Graph for query (Q2.3)

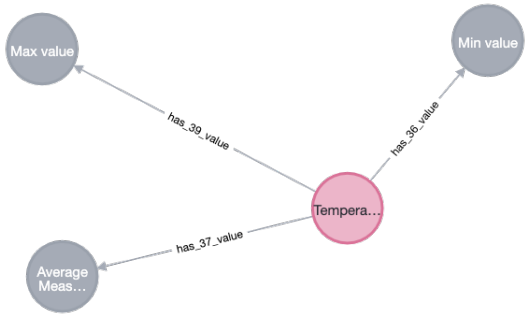

Fig. 7. Generating Summary Graph for query (Q1.3))

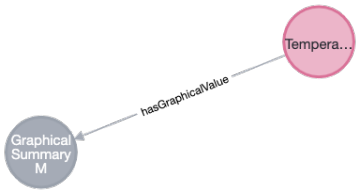

Fig. 8. Generating Summary Graph for query (Q4.3)

derstand the patient's health condition in relation to the given measure. These results fall under the category of calculation operation queries. 8 illustrate the query that synthesis a specific type of date like an image during a specific periode.

10. Evaluation

10.1. Qualitative Evaluation

Evaluation Scenario Ten participants were instructed to complete several tasks using the our system, including creating and customizing data graphs, summarizing data based on specific queries, and exporting data graphs in various formats. Following this, we conducted individual interviews with participants to obtain qualitative feedback on their experience using the system. Additionally, we administered a survey to gather feedback on participant satisfaction, ease of use, and suggestions for improvement. During the interviews, we utilized open-ended questions such as "How satisfied were you with your experience using the DGsumm system?" and "Did you find the data summarization feature useful? Why or why not?" to encourage participants to provide detailed feedback and express their thoughts and opinions. These were just a few examples of the questions asked, but the goal was to allow participants to share their experiences freely. The interview and survey data were analyzed to identify common themes and areas for improvement. Participants' behavior during the tasks was also observed, and any usability issues or roadblocks encountered were noted. The data analysis results were compiled into a comprehensive evaluation report, which included recommendations for improving the DGsmm system based on participant feedback and observations. Finally, based on the evaluation report, recommended improvements were implemented to enhance the DGsum system's usability and user experience.

Evaluation Report After analyzing the data, we identified the following common themes:

- *Overall Satisfaction:* All participants reported a high level of satisfaction with the system. They appreciated the ease of use of the tools provided and found the system to be intuitive and user-friendly.
- *Ease of Use:* Participants praised the system's easy-to-use interface, which allowed them to create and visualize data graphs quickly. They also found the summarization tool to be helpful in summarizing large data sets.
- *Suggestions for Improvement:* Participants suggested several areas for improvement, including the need for more customization options for visualizations, the ability to

export data graphs in various formats, and the addition of more advanced analysis tools.

Based on this feedback, we identified several areas for improvement, such as expanding customization options and adding more advanced analysis tools. We also plan to implement the ability to export data graphs in various formats to address a common suggestion for improvement.

10.2. Quantitative Evaluation

Evaluation metrics and results In the field of graph summarization, the evaluation metrics remain a challenge, and multiple metrics can be employed to assess the quality of graph summarization, depending on the specific objectives of each task. Evaluating the quality of a graph summary may require using multiple metrics to evaluate both the structure and content.In our work we used three metrics, include:

- **Calculation time**: Measures the speed at which the graph summary method can produce a result for a given input data graph.
- **Loss of information**: Measures the number of nodes and relation in original graph that are preserved in the summary result.

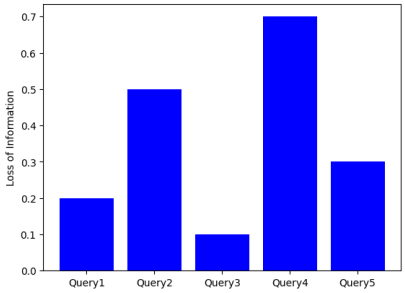

Fig. 9. Loss information behavior during Display operation

Discussion The objective of the initial evaluation was to confirm the extent of information loss that occurred during the summarization process. The tests indicated that the degree of information loss in the graph summary was minimal when compared to the original data graph and was dependent on the query objective

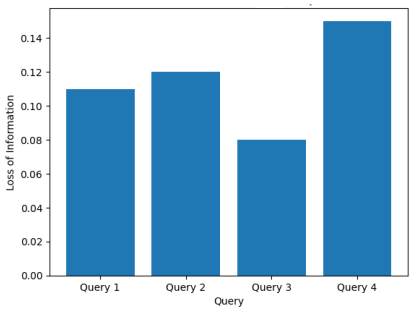

Fig. 10. Loss information behavior during filtering operation

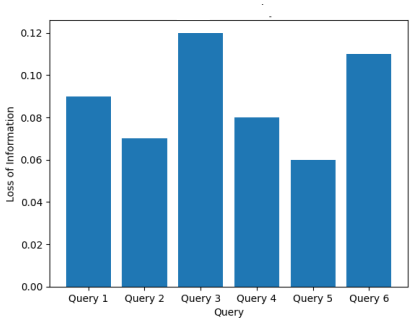

Fig. 11. Loss information behavior duringTransformation operation

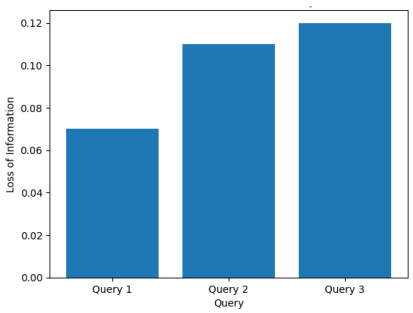

Fig. 12. Loss information behavior during Calculation operation

Table 5. Table of query input and output

Operation	Query	DN source	Output
(1) Transformation	Q1.1	Blood sugar level	Image (line chart)
	Q1.2	Blood test result and Urine result	Table
	Q1.3	Symptoms Diary	Image
	Q1.4	Medication list	Image
	Q1.5	Surgical history	Image (timeline)
	Q1.6	Family history	Table
(2) Calculation	Q2.1	Blood sugar Level and BMI	Numeric (correlation value)
	Q2.2	Blood presure	Numeric (percentage value)
	Q2.3	Symptom Diary	Numeric (average value)
(3) Filtering	Q3.1	Blood sugar level	Numeric
	Q3.2	Medical Data	Text
	Q3.3	Symptom Diary	Text
	Q3.4	MRI	Image
(4) Dispaly	Q4.1	EHR	Text
	Q4.2	EHR	Numeric
	Q4.3	EHR	Image
	Q4.4	EHR	Text
	Q4.5	EHR	Graphical

The information loss resulting from the transformation operation is shown in Figure 11. The results indicate that Query (Q1.3) experiences the highest degree of information loss with 0.12, followed by Query 6 with a loss of 0.11 percent. Query(Q1.1) and Query Q1.4) both exhibit moderate information loss with 0.085 and 0.07, respectively. The query with the lowest information loss is Query(Q1.2), with a value of 0.063. Regarding the second category Display operation shown in Figure 9, it is worth noting that query (Q4.4) had the highest information loss. This is because the objective of this query was to analyze three concepts: demographics data, blood sugar levels, and symptoms diary, and to display only the relevant information in the summary. Moving on to the third category Filtering operation shown in Figure 10, we observed that queries(Q3.2) and (Q3.4) had the highest information loss. This can be attributed to the fact that the filtering operation based on a specified date range may not capture important context or details that are relevant to the medical records, and therefore more data might be lost.

Finally, in the last category, i.e., Calculating operation shown in Figure 12, we found that queries(Q2.2) and (Q2.3) had more information loss than query(Q2.1). While synthesizing the percentage or the average may be relevant for visualizing and interpreting the results, there is no guarantee that information loss will not occur.

In the second metric, we analyzed the run time of various queries for different types of operations performed on the graph summary. We categorized the operations into four categories: filtering, calculation, transformation, and display.
In the filtering category, as shown in Figure 13, query (Q3.4) took the most time (28ms) to generate the result, while queries (Q3.1) and (Q3.3) took approximately the same amount of time. This order is because filtering by body part and date range and filtering med-

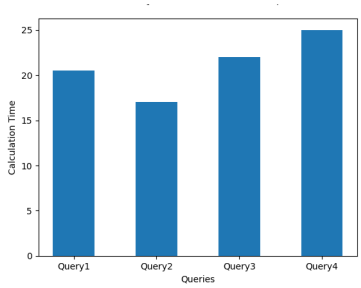

Fig. 13. Run Time behavior during Filtering operation

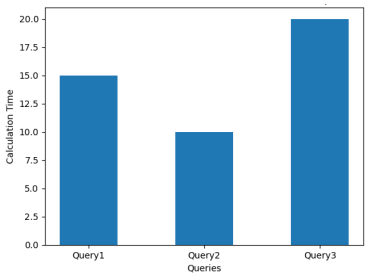

Fig. 14. Run Time behavior during Calculation operation

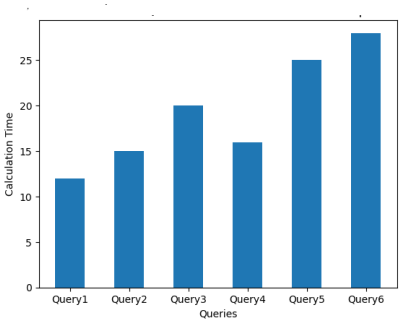

Fig. 15. Run Time behavior during Transformation operation)

ical records by date range involve a large amount of data and require complex queries involving multiple data sources.

In the calculation category, as shown in Figure 14, query(Q2.3) took the most time (21ms) because calculating the correlation coefficient involves a more complex statistical calculation than the other two queries. Calculating the average frequency of symptoms also involves some complexity, as it requires aggregating and analyzing a large amount of symptom data, which took 15ms. Query (Q2.2) is the least complex of the three queries, taking only 10ms.

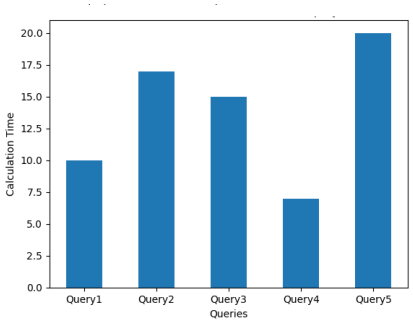

Fig. 16. Run Time behavior during Display operation

In the display category, as shown in Figure 16, we analyzed five queries. Query (Q4.1) took the most time, as it involves extracting and joining data from multiple DNs, such as demographics data, blood sugar levels, and symptoms diary, which could take more time to execute. Query(Q4.2) involves retrieving and displaying large files of ultrasound images, which could take more time to load and display compared to other types of data. Query (Q4.3) focuses on filtering based on multiple criteria, which could also take significant time to execute. Query (Q4.4) involves simply displaying data from the Medication Lists DN, which is likely to be relatively quick to execute compared to the other queries.

In the transformation category, as shown in Figure 15, we found that query (Q1.6) took the most time (28ms). The result of this query is creating a table that shows which conditions are present in the patient. This would likely be the most time-consuming query, as it involves sorting through potentially large amounts of data and compiling it into a table. Query (Q1.1) aims to extract blood sugar levels from the Blood Sugar Levels DN and create a line chart that shows how the levels have changed over time. While this query may still take some time to summarize due to the need to process and plot the data, it may be quicker than the other queries due to the relatively narrow focus of the data extraction.

Overall, the run time of the queries varied depending on the type of operation performed and the complexity of the query.

11. Conclusion

In this paper, we extensively studied utility-driven data graph modeling and graph summarization and made several innovative contributions. Using user queries, we introduced two new lossless graph summaries: a structured one and a content-based one. Furthermore, we illustrated our approach by integrating the proposed data graph formalism into heterogeneous input data. We proposed several primary operations for the summarization process and conducted experiments to design a lossy summarization algorithm based on two metrics: running time and information loss. The aim was to validate our proposed scenario for the medical domain.

The perspectives of this work are promising. The DGsumm system has shown to be effective in summarizing heterogeneous data graphs while maintaining a low degree of information loss. The qualitative evaluation feedback has provided valuable insights into

the user experience and suggestions for improvements that could be implemented in future iterations of the system. The quantitative evaluation metrics have demonstrated the system's capacity to handle user queries and generate graph summaries in a timely manner.

The DGsumm system has the potential to be applied in various domains, including finance, healthcare, and social media, where large and complex data graphs are prevalent. Future work could involve expanding the system's capabilities to handle more complex queries and provide more advanced analysis tools. Additionally, integrating machine learning algorithms could improve the system's ability to personalize summarization based on individual user preferences. Overall, the DGsumm system has shown to be a promising approach for personalized summarization of heterogeneous data graphs with potential for further development and applications.

References

1. Abu-Faraj, Z.O., Barakat, S.S., Chaleby, M.H., Zaklit, J.D.: A sim card-based ubiquitous medical record bracelet/pendant system—a pilot study. In: 2011 4th International Conference on Biomedical Engineering and Informatics (BMEI). vol. 4, pp. 1914–1918. IEEE (2011)
2. Adhikari, B., Zhang, Y., Amiri, S.E., Bharadwaj, A., Prakash, B.A.: Propagation-based temporal network summarization. IEEE Transactions on Knowledge and Data Engineering 30(4), 729–742 (2017)
3. Aggarwal, C.C., Wang, H.: A survey of clustering algorithms for graph data. Managing and mining graph data pp. 275–301 (2010)
4. Ahmed, M.: Data summarization: a survey. Knowledge and Information Systems 58(2), 249–273 (2019)
5. Ahmed, M., Mahmood, A.N., Islam, M.R.: A survey of anomaly detection techniques in financial domain. Future Generation Computer Systems 55, 278–288 (2016)
6. Akoglu, L., Tong, H., Koutra, D.: Graph based anomaly detection and description: a survey. Data mining and knowledge discovery 29, 626–688 (2015)
7. Angles, R., Gutierrez, C.: Survey of graph database models. ACM Computing Surveys (CSUR) 40(1), 1–39 (2008)
8. Bade, R., Schlechtweg, S., Miksch, S.: Connecting time-oriented data and information to a coherent interactive visualization. In: Proceedings of the SIGCHI conference on Human factors in computing systems. pp. 105–112 (2004)
9. Bashyam, V., Hsu, W., Watt, E., Bui, A.A., Kangarloo, H., Taira, R.K.: Problem-centric organization and visualization of patient imaging and clinical data. Radiographics 29(2), 331–343 (2009)
10. Bates, D.W., Ebell, M., Gotlieb, E., Zapp, J., Mullins, H.: A proposal for electronic medical records in us primary care. Journal of the American Medical Informatics Association 10(1), 1–10 (2003)
11. Boran, F.E., Akay, D., Yager, R.R.: An overview of methods for linguistic summarization with fuzzy sets. Expert Systems with Applications 61, 356–377 (2016)
12. Borland, D., West, V.L., Hammond, W.E.: Multivariate visualization of system-wide national health service data using radial coordinates. In: Proc. Workshop on Visual Analytics in Healthcare (2014)
13. Bui, A.A., Aberle, D.R., Kangarloo, H.: Timeline: visualizing integrated patient records. IEEE Transactions on Information Technology in Biomedicine 11(4), 462–473 (2007)
14. Cao, F., Estert, M., Qian, W., Zhou, A.: Density-based clustering over an evolving data stream with noise. In: Proceedings of the 2006 SIAM international conference on data mining. pp. 328–339. SIAM (2006)

15. Carenini, A., Cerri, D., Krummenacher, R., Simperl, E.: Enabling interoperability of patient summaries across europe with triplespaces. In: Interoperability in Healthcare Information Systems: Standards, Management, and Technology, pp. 232–249. IGI Global (2013)
16. Čebirić, Š., Goasdoué, F., Kondylakis, H., Kotzinos, D., Manolescu, I., Troullinou, G., Zneika, M.: Summarizing semantic graphs: a survey. The VLDB journal 28, 295–327 (2019)
17. Chiarandini, L.: Human-centered exploration and discovery of content in large information spaces (2011)
18. Clayton, P.D., Narus, S.P., Bowes III, W.A., Madsen, T.S., Wilcox, A.B., Orsmond, G., Rocha, B., Thornton, S.N., Jones, S., Jacobsen, C.A., et al.: Physician use of electronic medical records: issues and successes with direct data entry and physician productivity. In: AMIA annual symposium proceedings. vol. 2005, p. 141. American Medical Informatics Association (2005)
19. Cook, D.J., Holder, L.B.: Graph-based data mining. IEEE Intelligent Systems and Their Applications 15(2), 32–41 (2000)
20. Crawford, P., Brown, B., Baker, C., Tischler, V., Abrams, B., Crawford, P., Brown, B., Baker, C., Tischler, V., Abrams, B.: Health humanities. Springer (2015)
21. Delong, A., Boykov, Y.: A scalable graph-cut algorithm for nd grids. In: 2008 IEEE Conference on Computer Vision and Pattern Recognition. pp. 1–8. IEEE (2008)
22. Dunne, C., Shneiderman, B.: Motif simplification: improving network visualization readability with fan, connector, and clique glyphs. In: Proceedings of the SIGCHI Conference on Human Factors in Computing Systems. pp. 3247–3256 (2013)
23. Fan, W., McCloskey, J., Yu, P.S.: A general framework for accurate and fast regression by data summarization in random decision trees. In: Proceedings of the 12th ACM SIGKDD international conference on Knowledge discovery and data mining. pp. 136–146 (2006)
24. Fan, W., Li, J., Wang, X., Wu, Y.: Query preserving graph compression. In: Proceedings of the 2012 ACM SIGMOD international conference on management of data. pp. 157–168 (2012)
25. Feigenbaum, J., Kannan, S., McGregor, A., Suri, S., Zhang, J.: Graph distances in the data-stream model. SIAM Journal on Computing 38(5), 1709–1727 (2009)
26. Gong, J.J., Guttag, J.V.: Learning to summarize electronic health records using cross-modality correspondences. In: Machine learning for healthcare conference. pp. 551–570. PMLR (2018)
27. Gunter, T.D., Terry, N.P.: The emergence of national electronic health record architectures in the united states and australia: models, costs, and questions. Journal of medical Internet research 7(1), e383 (2005)
28. Han, W., Miao, Y., Li, K., Wu, M., Yang, F., Zhou, L., Prabhakaran, V., Chen, W., Chen, E.: Chronos: a graph engine for temporal graph analysis. In: Proceedings of the Ninth European Conference on Computer Systems. pp. 1–14 (2014)
29. Harrington, J.L.: Relational database design and implementation. Morgan Kaufmann (2016)
30. Hirsch, J.S., Tanenbaum, J.S., Lipsky Gorman, S., Liu, C., Schmitz, E., Hashorva, D., Ervits, A., Vawdrey, D., Sturm, M., Elhadad, N.: Harvest, a longitudinal patient record summarizer. Journal of the American Medical Informatics Association 22(2), 263–274 (2015)
31. Hu, P., Lau, W.C.: A survey and taxonomy of graph sampling. arXiv preprint arXiv:1308.5865 (2013)
32. Huang, J., Abadi, D.J., Ren, K.: Scalable sparql querying of large rdf graphs. Proceedings of the VLDB Endowment 4(11), 1123–1134 (2011)
33. Hunter, J., Freer, Y., Gatt, A., Logie, R., McIntosh, N., Van Der Meulen, M., Portet, F., Reiter, E., Sripada, S., Sykes, C.: Summarising complex icu data in natural language. In: Amia annual symposium proceedings. vol. 2008, p. 323. American Medical Informatics Association (2008)
34. Jagadish, H., Ng, R.T., Ooi, B.C., Tung, A.K.: Itcompress: An iterative semantic compression algorithm. In: Proceedings. 20th International Conference on Data Engineering. pp. 646–657. IEEE (2004)
35. Kang, U., Faloutsos, C.: Beyond'caveman communities': Hubs and spokes for graph compression and mining. In: 2011 IEEE 11th international conference on data mining. pp. 300–309. IEEE (2011)

36. Kriegel, H.P., Kröger, P., Sander, J., Zimek, A.: Density-based clustering. Wiley interdisciplinary reviews: data mining and knowledge discovery 1(3), 231–240 (2011)
37. Lan, J., Song, Z., Miao, X., Li, H., Li, Y., Dong, L., Yang, J., An, X., Zhang, Y., Yang, L., et al.: Skin damage among health care workers managing coronavirus disease-2019. Journal of the American Academy of Dermatology 82(5), 1215–1216 (2020)
38. Lebanoff, L., Song, K., Liu, F.: Adapting the neural encoder-decoder framework from single to multi-document summarization. arXiv preprint arXiv:1808.06218 (2018)
39. Liang, J., Tsou, C.H., Poddar, A.: A novel system for extractive clinical note summarization using ehr data. In: Proceedings of the 2nd clinical natural language processing workshop. pp. 46–54 (2019)
40. Liu, H., Friedman, C.: Cliniviewer: a tool for viewing electronic medical records based on natural language processing and xml. In: MEDINFO 2004. pp. 639–643. IOS Press (2004)
41. Liu, J., Cao, Y., Lin, C.Y., Huang, Y., Zhou, M.: Low-quality product review detection in opinion summarization. In: Proceedings of the 2007 joint conference on empirical methods in natural language processing and computational natural language learning (EMNLP-CoNLL). pp. 334–342 (2007)
42. Lukas, P.S., Krummenacher, R., Biasiutti, F.D., Begré, S., Znoj, H., von Känel, R.: Association of fatigue and psychological distress with quality of life in patients with a previous venous thromboembolic event. Thrombosis and haemostasis 102(12), 1219–1226 (2009)
43. Maccioni, A., Abadi, D.J.: Scalable pattern matching over compressed graphs via dedensification. In: Proceedings of the 22nd ACM SIGKDD International Conference on Knowledge Discovery and Data Mining. pp. 1755–1764 (2016)
44. Matheny, M.E., Miller, R.A., Ikizler, T.A., Waitman, L.R., Denny, J.C., Schildcrout, J.S., Dittus, R.S., Peterson, J.F.: Development of inpatient risk stratification models of acute kidney injury for use in electronic health records. Medical Decision Making 30(6), 639–650 (2010)
45. McInerney, D.J., Dabiri, B., Touret, A.S., Young, G., Meent, J.W., Wallace, B.C.: Query-focused ehr summarization to aid imaging diagnosis. In: Machine Learning for Healthcare Conference. pp. 632–659. PMLR (2020)
46. Miotto, R., Li, L., Dudley, J.T.: Deep learning to predict patient future diseases from the electronic health records. In: European conference on information retrieval. pp. 768–774. Springer (2016)
47. Moher, D., Liberati, A., Tetzlaff, J., Altman, D.G., Group*, P.: Preferred reporting items for systematic reviews and meta-analyses: the prisma statement. Annals of internal medicine 151(4), 264–269 (2009)
48. Moradi, M., Ghadiri, N.: Different approaches for identifying important concepts in probabilistic biomedical text summarization. Artificial intelligence in medicine 84, 101–116 (2018)
49. Nallaperuma, D., De Silva, D., et al.: A participatory model for multi-document health information summarisation. Australasian Journal of Information Systems 21 (2017)
50. Nenkova, A., McKeown, K.: A survey of text summarization techniques. In: Mining text data, pp. 43–76. Springer (2012)
51. Nielsen, F., Nielsen, F.: Hierarchical clustering. Introduction to HPC with MPI for Data Science pp. 195–211 (2016)
52. Pham, D.T., Dimov, S.S., Nguyen, C.D.: Selection of k in k-means clustering. Proceedings of the Institution of Mechanical Engineers, Part C: Journal of Mechanical Engineering Science 219(1), 103–119 (2005)
53. Pivovarov, R., Perotte, A.J., Grave, E., Angiolillo, J., Wiggins, C.H., Elhadad, N.: Learning probabilistic phenotypes from heterogeneous ehr data. Journal of biomedical informatics 58, 156–165 (2015)
54. Pouzols, F.M., Lopez, D.R., Barros, A.B.: Mining and Control of Network Traffic by Computational Intelligence, vol. 342. Springer (2011)
55. Powsner, S.M., Tufte, E.R.: Summarizing clinical psychiatric data. Psychiatric Services 48(11), 1458–1460 (1997)

56. Qu, Q., Liu, S., Jensen, C.S., Zhu, F., Faloutsos, C.: Interestingness-driven diffusion process summarization in dynamic networks. In: Machine Learning and Knowledge Discovery in Databases: European Conference, ECML PKDD 2014, Nancy, France, September 15-19, 2014. Proceedings, Part II 14. pp. 597–613. Springer (2014)
57. Rabbouch, H., Saâdaoui, F., Mraihi, R.: Unsupervised video summarization using cluster analysis for automatic vehicles counting and recognizing. Neurocomputing 260, 157–173 (2017)
58. Radev, D., Hovy, E., McKeown, K.: Introduction to the special issue on summarization. Computational linguistics 28(4), 399–408 (2002)
59. Raghavan, S., Garcia-Molina, H.: Representing web graphs. In: Proceedings 19th International Conference on Data Engineering (Cat. No. 03CH37405). pp. 405–416. IEEE (2003)
60. Reeve, L.H., Han, H., Brooks, A.D.: The use of domain-specific concepts in biomedical text summarization. Information Processing & Management 43(6), 1765–1776 (2007)
61. Rogers, J.L., Haring, O.M., Watson, R.A.: Automating the medical record: emerging issues. In: Proceedings of the Annual Symposium on Computer Application in Medical Care. p. 255. American Medical Informatics Association (1979)
62. Shah, N., Koutra, D., Zou, T., Gallagher, B., Faloutsos, C.: Timecrunch: Interpretable dynamic graph summarization. In: Proceedings of the 21th ACM SIGKDD international conference on knowledge discovery and data mining. pp. 1055–1064 (2015)
63. Shahar, Y., Goren-Bar, D., Boaz, D., Tahan, G.: Distributed, intelligent, interactive visualization and exploration of time-oriented clinical data and their abstractions. Artificial intelligence in medicine 38(2), 115–135 (2006)
64. Shen, Z., Ma, K.L., Eliassi-Rad, T.: Visual analysis of large heterogeneous social networks by semantic and structural abstraction. IEEE transactions on visualization and computer graphics 12(6), 1427–1439 (2006)
65. Shi, L., Tong, H., Tang, J., Lin, C.: Vegas: Visual influence graph summarization on citation networks. IEEE Transactions on Knowledge and Data Engineering 27(12), 3417–3431 (2015)
66. Soysal, E., Warner, J.L., Denny, J.C., Xu, H.: Identifying metastases-related information from pathology reports of lung cancer patients. AMIA Summits on Translational Science Proceedings 2017, 268 (2017)
67. Tang, N., Chen, Q., Mitra, P.: Graph stream summarization: From big bang to big crunch. In: Proceedings of the 2016 International Conference on Management of Data. pp. 1481–1496 (2016)
68. Tapak, L., Mahjub, H., Hamidi, O., Poorolajal, J.: Real-data comparison of data mining methods in prediction of diabetes in iran. Healthcare informatics research 19(3), 177–185 (2013)
69. Tian, Y., Patel, J.M.: Tale: A tool for approximate large graph matching. In: 2008 IEEE 24th International Conference on Data Engineering. pp. 963–972. IEEE (2008)
70. Toivonen, H., Zhou, F., Hartikainen, A., Hinkka, A.: Compression of weighted graphs. In: Proceedings of the 17th ACM SIGKDD international conference on Knowledge discovery and data mining. pp. 965–973 (2011)
71. Traverso, A., Van Soest, J., Wee, L., Dekker, A.: The radiation oncology ontology (roo): Publishing linked data in radiation oncology using semantic web and ontology techniques. Medical physics 45(10), e854–e862 (2018)
72. Vandenbroucke, J.P., Von Elm, E., Altman, D.G., Gøtzsche, P.C., Mulrow, C.D., Pocock, S.J., Poole, C., Schlesselman, J.J., Egger, M., Initiative, S.: Strengthening the reporting of observational studies in epidemiology (strobe): explanation and elaboration. PLoS medicine 4(10), e297 (2007)
73. Wang, Q., Laramee, R.S., Lacey, A., Pickrell, W.O.: Lettervis: a letter-space view of clinic letters. The Visual Computer 37(9), 2643–2656 (2021)
74. Wang, T.D., Plaisant, C., Shneiderman, B., Spring, N., Roseman, D., Marchand, G., Mukherjee, V., Smith, M.: Temporal summaries: Supporting temporal categorical searching, aggregation and comparison. IEEE transactions on visualization and computer graphics 15(6), 1049–1056 (2009)

75. Wright, A., Pang, J., Feblowitz, J.C., Maloney, F.L., Wilcox, A.R., Ramelson, H.Z., Schneider, L.I., Bates, D.W.: A method and knowledge base for automated inference of patient problems from structured data in an electronic medical record. Journal of the American Medical Informatics Association 18(6), 859–867 (2011)
76. Xu, W., Lu, Z., Wu, W., Chen, Z.: A novel approach to online social influence maximization. Social Network Analysis and Mining 4, 1–13 (2014)
77. Yager, R.R., Ford, K.M., Cañas, A.J.: An approach to the linguistic summarization of data. In: Uncertainty in Knowledge Bases: 3rd International Conference on Information Processing and Management of Uncertainty in Knowledge-Based Systems, IPMU'90 Paris, France, July 2–6, 1990 Proceedings 3. pp. 456–468. Springer (1991)
78. Zhang, N., Tian, Y., Patel, J.M.: Discovery-driven graph summarization. In: 2010 IEEE 26th international conference on data engineering (ICDE 2010). pp. 880–891. IEEE (2010)
79. Zhang, Z., Balay, J., Bertoldi, K., MaCoy, P.: Assessment of water capacity and availability from unregulated stream flows based on ecological limits of hydrologic alteration (eloha) environmental flow standards. River Research and Applications 32(7), 1469–1480 (2016)

Beldi Amal is a dedicated Ph.D. student, currently pursuing her doctoral studies through a cotutelle program between the University of El Manar in Tunisia and the University of Pau et des Pays de l'Adour. Her research focus lies in the realm of data graph modeling and summarization,visualization, topics modeling, and knowledge extraction. As a passionate scholar, she is actively involved as a member of the OpenCEMS chair. Alongside her academic pursuits, Amal also serves as an ATER (Attaché Temporaire d'Enseignement et de Recherche) at the University of Pau, further enriching her academic journey and contributing to the academic community.

Salma Sassi is an assistant professor of computer science with University of Jendouba, and member of DoCSYS research team at VNPC research and LIUPPA laboratory. She received her PhD in computer science from INSA Of Lyon, France and Manouba University, Tunisia in 2009. Her research interests include Representation and visualization of knowledges, indexing and semantic annotation, Healthcare Information Systems and Big Data.

Richard Chbeir is a professor of computer science at the University of Pau and the Adour Region in France, where he leads the computer science laboratory called LIUPPA. He is the director of the Semantics Privacy in Digital Ecosystems Research group (SPiDER).He is currently working on information and knowledge extraction. Chbeir is the head of the OpenCEMS industrial chair, He received his Ph.D. in computer science from the Institut national des sciences appliquées de Lyon in 2001 and got his Habilitation degree in 2010 from the University of Burgundy.

Abderrazak JEMAI Professor at National Institute of Applied Science and Technology (INSAT), University of Carthage, Tunis, Tunisia and former General Director of CNI (National Center of Informatics in Tunisia) dealing with government' applications and related access services, data storage and security (eGov, Intranet, etc.).His last interest is focused on the design (codesign of smart embedded systems) and the deployment of Smart-IoT (Smart Internet of Things) devices in the context of Smart City, Cloud Computing, Smart-Industry (Industry 4.0) and Big Data.

Received: March 31, 2023; Accepted: June 01, 2023.

Computer Science and Information Systems 20(4):1639–1659 https://doi.org/10.2298/CSIS230328049L

A Faceted Discovery Model Architecture for Cyber-Physical Systems in the Web of Things

Juan Alberto Llopis, Manel Mena, Javier Criado, Luis Iribarne, and Antonio Corral

Applied Computing Group (TIC-211), *University of Almería* Almería, Spain
{jalbertollopis, manel.mena, javi.criado, luis.iribarne, acorral}@ual.es

Abstract. A Cyber-Physical System is a set of heterogeneous devices that integrates computational and digital capabilities with their physical system. As technology evolves to facilitate human tasks, more complex Cyber-Physical Systems are being developed, even integrating them with web technologies (Web of Things), e.g., in the context of the Web of Things, supporting smart city scenarios with thousands of devices available to be discovered online. In these complex solutions, some capabilities related to locating, registering, and consulting devices must be provided to adapt to the continuous changes in Cyber-Physical Systems. Suitable capabilities could be using natural language queries, automatically describing and discovering new devices, or locating devices in different subsystems. This paper[1] proposes a discovery model architecture for Cyber-Physical Systems based on the Web of Things, including proactive discovery, recommendation, federation, and query expansion. In an example scenario, the proposed architecture has been implemented with different topologies using Edge Computing facilities to interact and manage Cyber-Physical Systems. The results show that the capabilities of the discovery model architecture facilitate the discovery of CPSs in different smart environments.

Keywords: Discovery Model, Web of Things, Cyber-Physical Systems, WoT Lab.

1. Introduction

Cyber-Physical Systems (CPSs) are characterized by integrating physical devices with computational and digital capabilities, working as a bridge between the physical and digital world [36, 39]. As the Internet of Things (IoT) is focused on communication between devices, CPSs include the interconnection and collaboration of IoT devices for improving the communication between CPSs [17, 30]. Therefore, CPSs consist of heterogeneous devices that make up an ecosystem to solve problems in smart environments, e.g., appliances, smart watches, or sensors working with different technologies and protocols. The Web of Things (WoT) initiative [23] attempts to bring all those different devices of the CPSs together in a reference framework supported by the World Wide Web Consortium (W3C). The WoT aims to establish an abstraction layer based on web technologies for managing Internet of Things (IoT) devices, thus approaching the interconnection problem between heterogeneous devices in smart environments.

Smart environments are scenarios supported by CPSs, such as Smart Cities, Smart Homes, or Smart Healthcare, equipped with computing power and coordinated by intelligent systems to give the environment intelligence for supporting and reducing human

[1] This is an extended version of The 14th International Conference on Management of Digital EcoSystems conference paper "Towards a Discovery Model for the Web of Things".

interaction [22]. Smart environments are evolving into more challenging ecosystems that use a higher number of devices with complex functionality. For instance, a smart garbage collection in a Smart City, where trucks, containers, traffic, and traffic lights are monitored to find time-optimal dynamic routes [4]. In this sense, discovering and managing devices of this kind of smart scenarios and CPSs can be difficult.

A CPS ecosystem may integrate devices from different locations or subsystems, e.g., devices in different buildings; it may require the processing of complex or abstract queries, e.g., natural language queries in a Smart Home or commercial building; or it may need to discover automatically devices, e.g., a laboratory changing continuously. Current Discovery Services in smart scenarios focus on managing many CPSs, but in terms of query efficiency. Devices register themselves into the Discovery Service, and users search for them using syntactic and semantic queries. However, with the evolution of CPSs and smart environments, discovery should include more capabilities to follow the continuous changes of the CPSs. These capabilities must adapt to the requirements when managing and searching for CPSs, and the discovery should be prepared to adopt new faceted capabilities progressively for future needs. A faceted perspective of the proposal facilitates further flexible, scalable, and open features of the architecture of the discovery model.

By capabilities of a Discovery Service, we mean features that are complex enough to be developed alone and support the main task of discovering CPSs. Normally, these features are not included in the Discovery Service system, the Discovery Service is developed as simply as possible in terms of functionality, and the capabilities are developed as individual systems unrelated to the Discovery Service. Nevertheless, with the evolution of CPSs, Discovery Services need additional capabilities as part of the main system to support the search and discovery. For instance, integrating Artificial Intelligence (AI) and federation capabilities with the Discovery Service to process natural language queries and search for devices in large-scale scenarios, where users interact with the system by voice commands. The Discovery Service must return devices located in different subsystems.

In this paper, we present a discovery model architecture for CPSs based on the Web of Things (WoT) that includes different capabilities in a faceted way: (1) discover proactively in a pull configuration, (2) recommending devices and services such as other Discovery Services using AI, (3) federated searches through a federation of Discovery Services, and (4) query expansion. Furthermore, as the discovery model architecture is based on the WoT, it can be used with other implementations and environments as long as the services are described following the Thing Description (TD) structure. The discovery model architecture with two of four capabilities (i.e., proactive discovery and recommendation) has been implemented in a real example scenario of a smart room with different topologies using Edge Computing facilities. The following research questions are addressed to identify the objectives as well as to approach the aforementioned facts:

- ***RQ1:*** *Would it be feasible to extend traditional Discovery Services for discovering cyber-physical devices?*
- ***RQ2:*** *Does implementing additional capabilities improve the discovery of CPSs?*

This paper extends one from *The 14th International Conference on Management of Digital EcoSystems* [27]. In [27], we proposed a discovery model for the WoT. In this paper, we extend that contribution with an architecture supported by four capabilities that complement the discovery model: recommendation system, proactive discovery, query

expansion, and federation (RQ2). Furthermore, we implement and validate the model in a smart room scenario using different topologies to experiment with the architecture in a real scenario with limitations, such as public access to CPS's information in a local network and communication between subsystems through secure connections (RQ1).

This article is structured as follows. Section 2 offers an overview of related projects about Discovery Services in CPSs and WoT, and describes the background information and the fundamentals required to understand the proposed discovery model architecture. Section 3 describes the architecture and the four capabilities complementing the discovery model. Section 4 shows the experimental scenario of a smart room to validate the proposed discovery model, while Section 5 discusses some advantages and limitations of the proposal. Finally, Section 6 presents the conclusions and outlines future work lines.

2. Literature Review

This section offers an overview of existing approaches related to the discovery model. Furthermore, a background is summarized to describe some of the main terms related to our approach.

2.1. Related Work

Related to discovery, there are different topics about discovering systems, e.g., discovery service, process discovery, or component discovery, among others [11]. In all of these topics exists techniques to discover the most relevant information. For instance, in [37], the authors apply process discovery algorithms on some of the event logs instead of applying them on the whole logs, thus increasing the performance in the discovery process. For component discovery, in [21], the authors propose a discovery, called trader, based on the Open Distributed Processing (ODP) trading model, for discovering and integrating COTS (Commercial Off-The-Shelf) components through a federation approach. Other techniques applied are the federation of directories to increase the range of solutions returned to the user [16] or the implementation of security mechanisms when searching for information [5]. In this paper, we focus on discovering CPSs by proposing the addition of capabilities to the Discovery Service to support the search process and to adapt the Discovery Service to the evolution of CPSs.

The proposed discovery model architecture is based on the W3C Discovery Service, which started with DiscoWoT, a Discovery Service for smart things [31]. Additionally, IoT Discovery Services are also relevant to this research work. One of the relevant contributions to discovering IoT devices is IoTCrawler [20]. In IoTCrawler, devices are discovered using the Context Information Management API (NGSI-LD) standard. Using the NGSI-LD standard, users can subscribe directly to the device data. Furthermore, NGSI-LD brokers can be interconnected, creating a federation where every broker can access the information of the other brokers. A feature of IoTCrawler similar to our approach is the layer structure used for the discovery. The discovery is deployed independently from the search, thus speeding up the search and discovery process. In our proposal, each capability is an independent system that supports the discovery system. This approach follows a modular structure, where more systems can be integrated; Furthermore, as they are independent systems, the performance and maintenance benefit from decoupling.

A more industrial approach for discovering IoT devices is the proposal of GS1 [12]. GS1 is an international organization that improves supply chain efficiency by creating standards such as the barcode and the EPC (Electronic Product Code) Tag Data. GS1 developed a Discovery Service for discovering RFID (Radio-frequency identification) items. The Discovery Service performs a broadcast to identify all RFID items deployed in a subnet. Furthermore, GS1 is developing a Discovery Service for choreographing repositories from different businesses that work in the same chain but are unrelated. For instance, connecting the information of a business that produces tomatoes with that of a business that uses tomatoes to create sauces. The solution of GS1 for discovering RFID items is similar to the proactive discovery capability. In both approaches, the Discovery Service scans the subnetwork to locate the items deployed. However, in our proposal, the discovery is focused on CPSs, where multiple communication protocols are involved.

Another approach is QoDisco [15], a semantic-based discovery service that stores the information of the devices following an ontology-based information model. The ontology extends the Semantic Sensor Network, the Semantic Actuator Network, part of the Standard Ontology for Ubiquitous and Pervasive Applications, and the Web Ontology Language for Services. QoDisco focuses on discovering IoT devices registered in repositories. The user selects the query from the repositories more relevant to the query, and QoDisco returns the address and topic of the broker with the desired information. QoDisco focuses on how to store and retrieve the information of IoT devices. Our approach focuses on facilitating the discovery of CPSs, thus proposing capabilities that improve the discovery in different scenarios. Nevertheless, the ideas of QoDisco about using the domain and searching for devices in the repositories could help us research the federation capability.

Regarding the discovery of WoT devices, WoTStore [38] is a framework based on the recommendation of the W3C for managing and deploying *Things* and applications related to the *Things*. WoTStore is microservice-oriented and consists of a Thing Manager for discovering devices, an Application Manager for storing and returning applications related to the *Things*, and a Data Manager for managing complex queries. The Discovery Service of WoTStore allows the subscription to the device's Thing Description (TD) and notifies the user when the TD is modified. Furthermore, the Thing Manager dynamically creates a Graphical User Interface (GUI) for the TD, thus easing the usage of the devices. In contrast to our approach, WoTStore creates a solution focused on creating a platform for using devices. Our approach aims to facilitate the discovery of CPSs, regarding their technology, by implementing a set of features or capabilities that support the discovery process. However, in our proposal, the modification of the Thing Descriptions is notified in the proactive discovery process. Consequently, users cannot subscribe to the devices registered in the directory, while in WoTStore, users can subscribe and be notified when a Thing Description changes.

DomOS [24] is an approach that implements a Discovery Service based on the recommendation of the W3C. DomOS is an ontology for managing and discovering WoT devices, and authors implement the Discovery Service recommendation of the W3C to evaluate it. Our proposal extends and improves the Discovery Service used to implement DomOS with additional capabilities. Furthermore, the discovery model presented in this paper includes a capability for supporting non-WoT devices.

Other implementations based on the Discovery Service specification of the W3C are WoTHive from the Universidad Politécnica de Madrid, LinkSmart Thing Directory from

Fraunhofer, and LogiLab TDD from Siemens[2]. LinkSmart [40] implements the Discovery Service focused on the Thing Directory. LinkSmart implements a RESTful API for CRUD (Create, Read, Update, Delete), notification, validation, and search operations. Furthermore, the Thing Directory of LinkSmart has authorization and authentication features. Although LinkSmart focuses on implementing a Thing Directory, LinkSmart proposes a service catalogue to discover other web services using HTTP and MQTT.

On the other hand, LogiLab TDD is an emerging implementation developed before the W3C started the recommendation of the Discovery Service for the WoT. Later, Siemens developed SparTDD [14], an evolution of LogiLab that uses the Thing Description architecture proposed by the W3C. SparTDD implements the WoT discovery recommendation that introduces the semantic search using a SPARQL endpoint for searching for TDs.

Finally, WoTHive [9] is the most advanced implementation of the three WoT discovery recommendations. WoTHive research is focused on the discovery feature of the recommendation and implements the Discovery Service recommendation from the W3C using SPARQL and a triple store to register the WoT devices. The discovery is implemented using syntactic and semantic operations. Furthermore, WoTHive compares the performance of syntactic and semantic queries when discovering different amounts of devices. The results show that the semantic search resolves faster than the syntactic search and, in some scenarios, better than the syntactic search. In addition, they propose as future work to research the federation of Discovery Services.

The three implementations of the W3C recommendation of the Discovery Service are based on the published specification [10]. WoTHive is the most developed, introducing the semantic search and proposing the federation of Discovery Services. In contrast to our approach, WoTHive and the LogiLab implementation propose a semantic search of WoT devices using SPARQL. In our approach, the API allows syntactic operations to search for CPSs. Nevertheless, we propose using a recommender system to search using natural language sentences. Our Discovery Service searches for CPSs using syntactic and semantic operations and extends the W3C recommendation by introducing capabilities supporting the discovery process. These capabilities facilitate the discovery of CPSs in different smart environments, thus improving the W3C Discovery Service.

2.2. Background

The discovery model architecture aims to facilitate looking for CPSs in smart environments using web technologies, thus making access to public devices available on the web. The discovery model follows the WoT architecture and uses the TD to store and access CPSs information. In addition, techniques such as pull and push discovery federation systems and artificial intelligence are used to develop the capabilities of the discovery model. Finally, Edge Computing is applied in the topology of the scenario to allow the secure access of external users to CPSs deployed inside a network of different subsystems.

Web of Things. The Web of Things is a framework created in 2010 by Guinard *et al.* [19] to build an ecosystem of the IoT in a flexible, scalable, and open way using web technologies. Lately, the WoT proposal was included as a recommendation of the W3C to define IoT devices that use the Web as the underlying technology [8].

[2] W3C Discovery Services: `https://github.com/w3c/wot-discovery/tree/main/implementations`

For storing the information describing a device in the discovery model, we use the W3C WoT Thing Description, a JSON-LD template document that describes the basic information of WoT devices. The TD provides a model for defining, in a common way, WoT devices to integrate devices and applications, allowing them to interoperate.

The Thing Description defines a set of features called `InteractionAffordances`, which can be properties, actions, or events, and describes how the device interacts and how to interact with it [7]. Properties describe the attributes of the device (e.g., the temperature, actions), actions describe the operations that the device can perform (e.g., turning on a light bulb), and events describe asynchronous notifications that a device may send (e.g., turning on the alarm when the movement sensor detects someone). In our discovery model, `InteractionAffordances` are used by the API for syntactic search and by the recommender system capability for extracting the basic information of each device to train the AI model and recommending devices or services that the user may look for. For instance, searching for temperature sensors or asking for a command to turn on a light.

Pull and push discovery. Apart from adapting the Internet of Things devices into the Web of Things technology [25], the Web of Things requires finding and allowing the secure usage of devices deployed worldwide. Discovery Services solve this problem by facilitating the search for suitable services that meet certain users' requests to solve the problem of the increase in the number of services. Services were increasing, and techniques were needed to perform more efficient queries in the search process [35]. As CPSs are also increasing, there is a need for techniques to facilitate searching for devices. Therefore, Discovery Services can help in the search process for finding devices.

Discovery Services are developed to facilitate searching for services; they can register, unregister and search for services in a directory. Services are inserted into the directory after being registered into the Discovery Service [32]. For registering services, traditional Discovery Services use a push model. The push model follows a reactive behavior, i.e., services or external users register the service; for instance, a user registers a new light bulb in the directory. However, services can also be registered proactively using a pull model, following a more intrusive behavior. This paper proposes a discovery model architecture capable of registering CPSs reactively (push) and proactively (pull). Using a pull model, the Discovery Service looks for deployed services to register them into the directory. To identify available services, the Discovery service, using special bots, crawls the net for services and registers them in the directory. In this sense, the Discovery Service can scan the network or do a DNS-SD search to register all the devices that match specific criteria.

Recommender systems. Recommender systems aim to recommend the products or services that best suit the user's requirements. They are developed to reduce information overload, limiting the information the user gets, thus facilitating the product or service selection. For this reason, recommender systems try to return the most relevant information for the user as the first solution [28].

The recommendation process involves techniques influencing how the recommender system works [29]. Some of the techniques most used for the recommendation process are: (a) Content-based recommendation: Based on products or services similar to those previously selected by the user; (b) Collaborative recommendation: Based on products or

services related to those previously selected by users with similar preferences; (c) Computational intelligence-based recommendation: Focused on building the recommender system using Artificial Intelligence, Bayesian techniques, fuzzy systems, etc.

One of the capabilities of the discovery model architecture is a recommender system based on AI for supporting the search process of CPSs. The reason for using a recommender system is to aid in smart decision-making in large-scale IoT environments, where multiple devices can be the solution, the system may not differentiate between two similar devices, or the user may need help selecting the CPS that best suits the request.

3. Discovery Model Architecture

This paper extends the discovery model proposed in *The 14th International Conference on Management of Digital EcoSystems* [27] by adding a set of capabilities to support the discovery process. As explained in Section 2.1, the proposed discovery model is based on the W3C recommendation of Discovery Service [10] but extended with new features for adapting the Discovery Service to the continuous changes of CPSs.

Figure 1 shows the architecture of the discovery model. The discovery model has four layers for interacting, recommending, processing and storing CPSs. The first layer is the interaction layer, used for interacting with the different layers of the discovery model. The **interaction layer** has a RESTful API deployed using Express.js. The API manages the connections between the discovery model and external agents, working as a security layer. The API has a set of endpoints for communication with the directory to facilitate information retrieval. The new endpoints added to the API implementation are: (a) `#/search`, (b) `#/td/:affordance/:name`, (c) `#created-last-week`, (d) `#updated-last-day`, (e) `#updated-last-week`, and (f) `#user-interface`. In addition, the API has endpoints for interacting with the other three layers. For instance, the API can interact with the processing layer with an endpoint for triggering the proactive discovery capability. Finally, the interaction layer has been extended by including a GraphQL system to help create queries for searching CPS devices. GraphQL allows users to build their queries, increasing the range of queries the API can perform, thus facilitating the search process [34].

The second layer is the **recommender layer**, used for supporting the discovery of CPSs by integrating AI techniques with the discovery model to process natural language queries. This layer is deployed offline using the Transformer algorithm [41] as the base

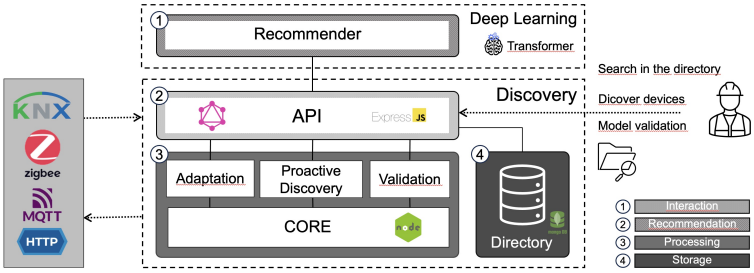

Fig. 1. Discovery model architecture

of the recommender model. In the architecture, this layer is outside the main part of the discovery model architecture to extend it with new features. For instance, a future feature of the recommender layer will be a recommender of Discovery Services to support the federation capability when looking for other Discovery Services in the search process. More in depth-details of the recommender system are explained in Section 3.1.

The third layer is the **processing layer**, which manages the functionality of the architecture. The processing layer uses Node.js and performs all the operations of the discovery model. For instance, creating a paginated list of requested CPSs. These operations are located in the Core of the architecture and are supported by a set of subsystems that extends it; *adaptation*, *proactive discovery*, and *validation*. The adaptation and the proactive discovery subsystems aim to discover WoT devices using a pull model. Furthermore, the adaptation subsystem can also discover CPSs compatible with the TD. In-depth details of these subsystems are described in Section 3.2. Finally, the validation subsystem validates the TD of the CPSs. This subsystem is used to validate the TDs before inserting them into the directory and for validating the dataset used by the recommender system. The TD is validated using the JSON template provided by the W3C.

The fourth layer is the **storage layer**, which stores the CPS information in a MongoDB database following a JSON schema proposed by the W3C. CPSs are stored using the TD and accessed using the identifier of the TD, an immutable field. The stored information is validated by the validation subsystem before inserting them into the directory, thus ensuring that all devices are defined following the same structure. The storage layer can be located outside the main part of the discovery model architecture. Locating the directory outside the main part led to an Edge Computing approach. In an Edge Computing approach, the processing layer is separated from the processing layer, thus adapting the discovery service architecture to federation approaches where directories are located in different subsystems and to topologies in which, for security or network reasons, users cannot access directly the subsystem where devices and the directory are located.

The four layers include a set of capabilities for extending and supporting the discovery model in the discovery process of CPSs. The four proposed capabilities are: (1) a recommender system for matching user queries in natural language with CPSs, (2) proactive discovery for automatically locating CPSs deployed in the same network, (3) a federation for connecting Discovery Services located in different subsystems, and (4) query expansion for improving user queries with additional information which can help in the search process. These four capabilities are described below.

3.1. Recommender system

Discovery Services focus on searching for services using queries. Since natural language is not used in the context of service search, Discovery Services use syntactic and semantic search. However, in the context of CPSs and IoT, natural language may need to be included. For instance, in a smart home scenario, the user may be using both hands, thus needing to interact with CPSs using voice commands. Furthermore, the natural language includes syntactic and semantic, thus allowing more complex searches.

The recommender system capability was presented in a previous paper [26], and it uses natural language for matching user queries in the form of natural language sentences with CPSs. This capability was added to the discovery model to adapt it to the new scenarios of CPSs that were not contemplated in the context of the services. As CPSs can be

deployed in scenarios where users without computer engineering knowledge can interact with them, the system must be adapted to be used by that kind of user. Furthermore, using natural language allows interaction by text or voice, facilitating the use of the system for users with disabilities that may need to interact with the system. In addition, as natural language includes syntactic and semantic techniques, queries for searching devices can be sent to the Discovery Service or the recommender, thus having two ways of searching for devices in the Discovery Service.

The recommender system is proposed as a support system because it needs to be trained when new CPSs are added to the scenario. Therefore, it cannot be used for searching for new CPSs. While the recommender learns from the new CPSs, the Discovery Service API is used together with GraphQL as the search system. The recommender system is built using deep learning through a Transformer approach, a novel sequence transduction model based on multi-head self-attention [41] that presents good results in natural language problems. A user sends a natural language sentence, and the recommender returns the four devices that best suit the user's request. The returned list is sorted by the recommender's confidence about each device being the solution to the user's request.

This capability is being improved to recommend CPSs services, e.g., return the command needed to turn on the light bulb in the kitchen. In addition, this capability will be extended to support recommendations in a Discovery Service federation for CPSs.

3.2. Proactive discovery

Discovering services includes searching for them in a directory and registering the available services in the directory. For registering, services must be inserted manually into the directory, either by the services registering themselves or by an external user registering them. Therefore, services must be adapted to know the presence of the Discovery Service, or an external user has to spend time registering the services.

In the context of CPSs, one of the features of IoT devices is their ability to be dynamic regarding the location where they are deployed. A car, a scooter, or a bike can be CPSs with mobile capabilities that change their location continuously. Regarding less complex scenarios, a laboratory where devices are added and removed every day can also be an example of the non-static feature of CPSs. Therefore, Discovery Services have to be adapted to discover dynamic cyber-physical devices.

The proactive discovery subsystem was initially presented in [27], and extended in this paper. To adapt to the non-static feature of CPSs, the proactive discovery subsystem allows the discovery of CPSs by following a pull model. The Discovery Service scans the subnet, searching for WoT devices. As WoT devices that use the HTTP communication protocol deploy their Thing Description document in port `80`, the subsystem searches for systems with port 80 opened and a TD deployed in the root path. After devices are located, TDs are registered in the directory.

The proposed proactive discovery subsystem facilitated the discovery of WoT devices using the HTTP protocol and deployed them in the same subnetwork as the discovery. However, this solution cannot discover IoT or WoT devices that use other communication protocols, such as MQTT, Zigbee, or KNX. In [25], the discovery model was extended with a new subsystem for adapting IoT devices to the WoT technology, thus proactive discovering IoT and WoT devices. As adapting IoT devices to WoT technology can be difficult, the adapt feature was developed to work with a more structural communication

protocol than HTTP, the MQTT protocol. Therefore, the adaptation subsystem can only adapt IoT devices using the MQTT communication protocol to the WoT technology. Further information about the adaptation process is described in [25]. Finally, the proactive discovery subsystem was extended to discover WoT devices using MQTT. The proactive discovery subsystem can discover WoT devices using HTTP or MQTT and IoT devices using MQTT. For discovering devices using MQTT, the subsystem looks for devices deployed in the same network with the ports `1883`, and `8883` opened.

The adaptation subsystem is linked with the proactive discovery subsystem, i.e., the only way to execute the adaptation operation is by triggering the proactive discovery. The proactive discovery can be executed manually or automatically. The automatic approach executes the proactive discovery operation, triggering the network scan when an event happens. For instance, a timed event triggers the network scan each hour.

The manual approach executes the proactive discovery when an external user triggers the operation. The API has an endpoint for interacting with the proactive subsystem, thus allowing external users to trigger it. When a user executes the proactive discovery, the new CPSs detected are not registered in the directory. The CPSs discovered are returned to the user using three subsets, one subset for the new CPSs, one subset for the CPSs already registered in the directory, and one subset for CPSs that have changed since they were discovered. Therefore, users can decide what to do which each subset. For instance, users can be interested only in CPSs that have changed since the last time they were discovered.

This capability is currently being investigated to support more communication protocols. In addition, because the subnetwork scanning works in a broadcast form, it will be improved to avoid overloading the network, thus being less intrusive, and to solve security problems found when deploying the experimental scenario. Finally, the proactive discovery will be improved to adapt IoT devices using other communication protocols and solve the problem when searching for sleeping devices, i.e., devices that deactivate features that, after some time without being used, reduce energy consumption and limit incoming connections.

3.3. Federation

In the context of Cyber-Physical Systems, users must interact with devices in different subsystems. For instance, using devices located on different floors inside the same building. In some situations, Discovery Services can be deployed to discover all these devices. However, the connection range and security may not allow a single Discovery Service to discover all the available CPSs. Therefore, a set of Discovery Services must work together to discover CPSs deployed in different subsystems.

The federation capability is proposed to connect CPSs in different subsystems, making it easier to discover them. Discovery Services know other Discovery Services, thus looking for CPS devices in other directories when not located locally.

Discovery Services have maximum hops in a federated discovery process to limit the search and reduce the waiting time. For instance, Figure 2 shows a federated Discovery Service; If the hop limit is set to one for the Discovery Service #1, it will only search in those Discovery Services located in Level 1, i.e., #2 and #3.

Another feature of the federation capability is the confidence level of each Discovery Service. Discovery Services have a list of other Discovery Services to delegate queries to them when the CPS is not in their directory. To sort that list, the Discovery Service

gives a confidence value to each Discovery Service based on features such as the number of times the Discovery Service returns the correct device, the security, or reliance, among others. The delegation of queries inside a federation is a feature that could become another capability if it is developed enough to be used as a separate system.

Finally, the recommendation capability works with the federation capability to allow the recommendation of CPS inside each Discovery Service and to extend this feature with the recommendation of Discovery Services in the federation. The recommender works with the confidence value given to each Discovery Service to recommend a Discovery Service over others. For instance, in Figure 2, the recommendation system may recommend to the Discovery Service #1 the query delegation to Discovery Services #2 and #5.

The federation capability is currently an ongoing research. One of the difficulties in finishing this proposal is to propose a discovery model federation that can delegate queries while minimizing the waiting times. For instance, if a query is delegated by sending it one by one to each Discovery Service, the waiting time is the sum of all waiting times. However, if the query is delegated by sending it to all the Discovery Services simultaneously, the waiting time will be the waiting time of the slowest Discovery Service.

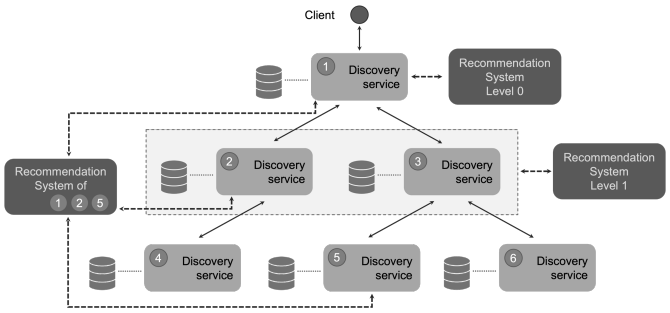

Fig. 2. Federation of Discovery Services

3.4. Query expansion

Searching for CPSs may differ from searching services in the way of the kind of users that interact with the system and how they interact with it. In the research process of the recommender system, we detected that users might not know how to ask for what they need or not include all the required information in the query. For instance, a user wants to turn on the light bulb in the living room and sends a query in the form of a natural language sentence that says: *Turn on the light*. Therefore, the system cannot know which light bulb has to be turned on.

The last proposed capability for the discovery model is **query expansion**, a technique for extending user queries with additional information or reformulating the query to enhance the information retrieval effectiveness [2], [6]. This capability is proposed to support the recommender system by improving the user queries to include information that can help the recommendation process. As natural language sentences can be abstract,

the query expansion system extracts information such as the user's location to extend the query. With abstract sentences, we mean sentences that are not built correctly or sentences that do not specify the user's desired device. For instance, *Turn on the light* can mean illuminating a whole room, but the system does not know the location of the lights, and the room may have more than one light. This sentence can be modified into *Turn on the lights in the living room*, thus improving the recommendations of the recommender system.

Finally, the query expansion capability may be useful for searching devices by reformulating users' queries. After a query is resolved without results, the query is reformulated to get any device in the search result that may suit the user's request. The query expansion capability is being developed. As it may interact with the recommender and the Discovery Service search process and it has to extract information from the user, it will be located in the main Discovery Model as a subsystem. The challenges for this capability are about what information to extract, how to do it, and how to reformulate queries to improve the result without returning devices that the user may not need.

4. Experimental Scenario

In IoT, no public scenarios exist to experiment and interact with CPS. The existing scenarios, such as FIT IoT Lab [1], are limited or with restricted access. Regarding the WoT, there are three available scenarios, Remote Lab from the Technical University of Munich [33], a public scenario from the book *Building Web of Things* [18], and IoTLab [3]. This WoT scenario does not follow the W3C recommendation. However, these laboratories require access rights or are very limited. For instance, IoTLab only uses CoAP devices and does not use the TD, and [18] has only two devices available.

For the experimental scenario, a Discovery Service implementation of the discovery model is deployed in a public laboratory. The laboratory has three rooms connected to a local network inside one of the subnetworks of the institution. This scenario helps researchers experiment with WoT devices of different smart environments and providers. Furthermore, other scenarios can link to our laboratory, thus helping create a federation of Discovery Services.

In this section, first, the public laboratory, the WoT Lab[3], is described. After describing the WoT Lab, a scenario of experimentation and how users interact with the scenario using the Discovery Service is explained.

4.1. WoT Lab

WoT Lab is a public environment where users can experiment with CPSs in different smart scenarios. Users can interact with devices using the user interface or by asking directly to the Discovery Service. Each device has a Thing Description and the endpoints required for interacting with them. For instance, a smart suitcase simulates devices from a Smart Home; the website publishes the Thing Description of the suitcase, and the endpoints for interacting with each device from the suitcase are available on the Thing Description.

Figure 3 shows the architecture of the WoT Lab. Devices are deployed in three different rooms connected to the same local network. Some devices use different communication protocols, including KNX, HTTP, MQTT, and Zigbee. Furthermore, devices are

[3] WoT Lab website: `https://acg.ual.es/projects/cosmart/wot-lab/`

from different brands to experiment with interoperability. For instance, there are motion sensors from Bosch, KNX, and Philips; and light bulbs from Philips and Ikea.

The website, the Discovery Service, and the directory of the Discovery Service are deployed inside a docker container to facilitate their management and deployment of a federation of Discovery Services. Discovery Services can be deployed in containers in different networks and connected to allow the discovery of CPSs in different subsystems.

The Discovery Service and the website must access the deployed devices' network to interact with the devices. As external users have to access the website without access to the internal network and the website must have access to the internal network, it could cause security problems described in the next subsection. Users ask the website for CPSs; the website asks the Discovery Service for the CPSs, and the Discovery Service looks for them in the internal network and the directory.

4.2. Scenario

The experimental scenario describes the interaction of the Discovery Service and its capabilities with the IoT ecosystem. In addition, it shows how users can access and interact with the CPSs through the Discovery Service.

The experimental scenario is based on the WoT Lab approach and has devices in three rooms connected to a local network deployed in one of the rooms (Figure 4). In the local network (LN1), devices can communicate between them, and the Discovery Service can use the proactive capability to search for them by scanning the network. The available devices are (a) a smart suitcase that simulates a Smart Home, (b) three light bulbs, (c) three motion sensors, (d) four contact sensors deployed in two windows and two doors, (e) a video camera, (f) three temperature and humidity sensors, (g) three CO_2 and temperature sensors, and (h) two servos for interacting with the system. All these devices are registered in the Discovery Service directory and are available in the WoT Lab.

To access the Discovery Service, thus interacting with devices, users must connect to the subnetwork N1 of the rooms' building. As N1 can access to LN1, and the Discovery Service must be in LN1 to discover the devices, the Discovery Service is deployed in LN1. The Discovery Service scans the local network once each hour by triggering the proactive discovery capability and registers the new devices deployed. Figure 5 shows a sequence diagram of the interaction of the Discovery Service when making a proactive discovery of two new devices, a smart mailbox that uses MQTT and a smart blind that uses HTTP under the WoT technology. First, the Discovery Service scans the network looking for

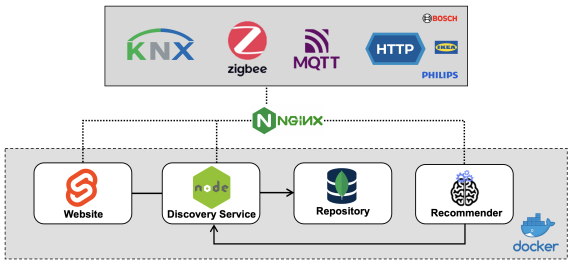

Fig. 3. WoT Lab architecture

HTTP devices; it can discover devices already registered, devices registered whose TD has been modified, and new devices. In this scenario, a new device, the smart blind, is discovered. After detecting HTTP devices, the Discovery Service scans the network for MQTT devices. In this example, one IoT device, the mailbox, is detected. Before registering both devices into the directory, the Discovery Service calls the adaptation subsystem to generate a TD for the mailbox. Finally, the Discovery Service calls the validation subsystem to validate the TD of the smart blind and registers both devices into the directory. In the case of an error when validating the smart blind's TD, the blind is not registered.

The average time of the proactive discovery to scan and register devices in the network of the experimental scenario is 138 seconds. In contrast, the average time for resolving the queries for discovering and registering the devices of the example is 207 milliseconds. The proactive discovery time is higher than it would take to register a device manually. However, proactive discovery does not require human intervention. Therefore, it is lower than the time required to adapt IoT devices to WoT technology or to the time required to register a large number of IoT devices. Furthermore, suppose the network cannot handle a continuous broadcast. In that case, the proactive discovery subsystem can be disconnected and only triggered by querying an endpoint available in the API of the Discovery Service, e.g., calling the endpoint when more than ten new devices have been deployed. This capability can help in scenarios where the user does not know how the devices work or the number of features of the device. For instance, the CO_2 sensors in the three rooms have additional features that were not documented. Using the proactive discovery and adaptation subsystem to discover and register these devices helped to identify their features.

The Discovery Service must be connected to the directory to search for devices. In this scenario, the directory and the Discovery Service are deployed on LN1, thus having bidirectional communication. Users can search for devices using the website, which calls some of the endpoints of the API, or they can directly send the queries to the Discovery Service. For instance, users can see the current online devices on the website and main page. For showing the online devices, the website queries the Discovery Service to list all the devices with the status online in the Thing Description. In addition, users can build their queries using the GraphQL server deployed in the Discovery Service[4]. GraphQL uses the JSON schema file of the Thing Description for structuring the information and helping users in the building process of the queries. However, these search techniques

[4] GraphQL subsystem: `https://acg.ual.es/projects/cosmart/wot-lab/ds/graphql/`

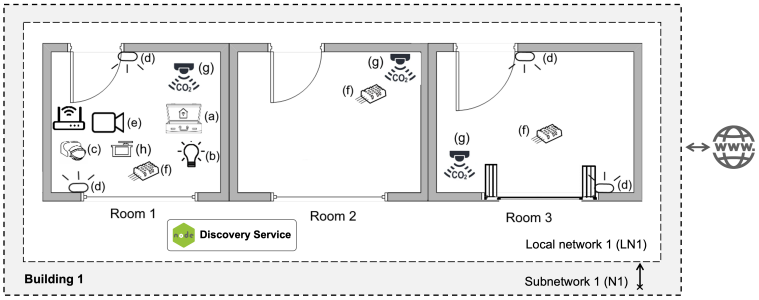

Fig. 4. Experimental scenario

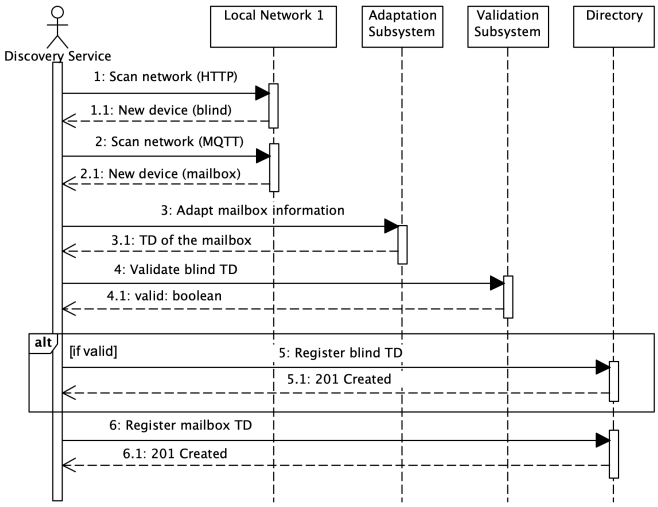

Fig. 5. Sequence diagram of the proactive discovery

cannot process natural language sentences and cannot sort the result of the search query by a value that can help the user make decisions. A user may not know which device wants when searching for it. For instance, in our scenario, a user may want to increase the illumination in the room, but the user may not know that one of the light bulbs is broken and that by opening the blind, the illumination can be increased. Therefore, a recommendation in the query result may help the user decide by returning the blind at the top and the broken light bulb at the bottom of the list.

As the recommender system is a capability that supports the search process of CPSs, it must be connected to the Discovery Service, thus being deployed in LN1. The recommender is deployed in a docker container with the Discovery Service and the website. The dataset used to train the recommender to recommend the deployed CPSs is the dataset from [26]. The dataset was adapted to return the name of each device instead of the generic names of the dataset. For instance, when searching for light bulbs, the available light bulbs are *WoTColorLight1*, *WoTColorLight3*, and *WoTColorLight4*. Since the dataset is limited in the data used for training it, the recommender cannot differentiate between devices of the same type, thus returning all the lights of each room when searching for them. For instance, if the user searches for a specific light bulb in *room1*, the recommender system will return the three light bulbs deployed in *room1*. For the training process, the recommender system accesses the Discovery Service validation subsystem to validate the dataset used for training the model. However, the recommender system can not re-train itself with the information collected when using the recommender system or with the queries sent to the Discovery Service. After training, the recommender system is deployed in LN1, thus allowing external access to the service[5].

As explained, users may not know the device they want. Furthermore, users may not include all the information required to find their desired CPS. The query expansion ca-

[5] RS: `https://acg.ual.es/projects/cosmart/wot-lab/transformer/predict/Turnonthelight`

pability supports the search and recommendation process by completing the queries with additional information and reformulating them. Query expansion is under research, but some experiments were carried out in this scenario as a supporter of the recommender system. In the adaptation process of the dataset, some of the sentences were modified, and new sentences were included. The reformulation of these sentences followed a structure to include the required information for helping the recommender system in the recommendation process (1) (2). As this is the first approach of the query expansion capability, the structure followed for building the sentences is not complex. In the proposed structure, a sentence is built by adding information about the type of device wanted (D), the location of the device (L), and the action desired (A) (3). The action of the device is included because of future Artificial Intelligence models where the recommender system returns a CPS's service instead of a specific device. For instance, the user wants to turn on a light bulb, and the recommender system returns the endpoint used for turning the light bulb on.

$$A = \{a_1, a_2, ..., a_n\}; D = \{d_1, d_2, ..., d_n\}; L = \{l_1, l_2, ..., l_n\} \tag{1}$$

$$a_1 \cup d_1 \cup l_1 \tag{2}$$

Turn on light bulb room 1. (3)

More complex sentences that can be built using the proposed structure involve more than one action, device, or location (1). A simple structure is used because the recommender system cannot process these kinds of sentences.

To access the experimental scenario in LN1, external users must connect to N1. However, the connection between N1 and external networks was restricted for security reasons. Users can now only access N2, a network isolated from all the networks. Therefore, after this change, users could not access the experimental scenario. In the new topology, N1 can still connect to LN1 and N2. However, external users cannot access N1. Furthermore, external users can connect to N2, but N2 cannot connect to N1. To solve the problem in the connection between external users and the experimental scenario, the Discovery Service was deployed following a first approach of a federation of Discovery Services.

The Discovery Service deployed in LN1 continues to work in LN1 to discover the devices deployed in the network. The topology modification focuses on the communication between N1 and N2, allowing external access to the experimental scenario. The topology modification follows a federation approach, where an additional Discovery Service is deployed in N2. External users can access the Discovery Service to access devices in LN1. As N1 can access N2, the Discovery Service in N1 is connected with the Discovery Service in N2, updating the information stored in the directory of N2 with the information of the devices in LN1. Furthermore, as there are no devices in N2, the proactive discovery of the Discovery Service in N2 is disabled to avoid overloading.

The proposed discovery model works as a federation of Discovery Services, where more Discovery Services can be deployed in other networks and connected to the Discovery Service deployed in N2. This scenario is the first approach to the capability of the federation. However, it is still under research, in this experimental scenario, the failure of the Discovery Service of N2 would make all the Discovery Services to disconnect from the external network.

5. Discussion and Threats to validity

A discovery model is proposed and deployed in a scenario presented in [27] and extended with more devices in three rooms. The discovery model consists of multiple capabilities to adapt Discovery Services to the evolution of CPSs. For instance, in a Smart Home scenario, the Discovery Service can facilitate the discovery of new devices deployed by automatically discovering them, thus helping people without technical experience to manage the CPSs of the Smart Home. The recommender system and query expansion capabilities help process natural language sentences sent by the user when using the CPSs. Finally, the federation capability helps in the search process of CPSs deployed in different subnetworks of the Smart Home scenario.

In other scenarios, such as Smart City, the most relevant capability is the federation. As a city is too large for a single Discovery Service, multiple Discovery Services must be deployed in the areas of the city to manage all the CPSs. The Discovery Services are connected to the federation to create a way of searching efficiently for devices in the city.

As shown in the scenarios, the proposed capabilities support the discovery model, adapting it to different smart environments. However, the discovery model proposal is still under research and suffers from limitations and threats to validity. Therefore, to validate our proposal, we answer the four main validity threads discussed in the literature [13]: Conclusion, Internal, Construct, and External validity. This ensures detection of the objectives are fulfilled and the study's limitations.

Conclusion validity. Did the introduced treatment/change have a statistically significant effect on the outcome we measure? Yes, the results obtained using the proposed discovery model differ from those obtained using other Discovery Service approaches. The federation, recommender system, and query expansion capabilities modify the returned list of CPSs. The federation returns devices from the current Discovery Service and other Discovery Services linked to it. The recommender system modifies the output by returning the four devices that best suit the user's request. Finally, the query expansion reformulates the query to improve the search result.

These three capabilities make the output of our proposal differ from the output of other Discovery Services that search in the same scenario. However, there is a lack of comparison between our proposal and other Discovery Services in the literature. For instance, comparing our discovery model with the Discovery Services implementations of the W3C recommendation explained in the Related Work of Section 2.1.

A useful comparison between our approach and other proposals is the precision and recall of the output when searching for devices. This can help measure the output's improvement using the proposed capabilities. Furthermore, the capabilities may slow the response time of the Discovery Service. Therefore, comparing the performance between our Discovery Service and other approaches may be useful.

Internal validity. Did the introduced treatment/change cause an effect on the outcome? Can other factors also have had an effect? The outcome is altered as we use the capabilities to support the discovery process. The discovery result from not using the capabilities differs from the result from using them. In addition, the proactive discovery may alter the devices available in the directory, thus altering the outcome. However, the proactive discovery and recommender capabilities may slow the query time.

In the experimental scenario, we compared the average time of proactive discovery and manually discovering and registering the devices. However, this comparison is not enough to evaluate the capability. Furthermore, the response time between the recommender and the API is not compared. Therefore, the response time of the proactive discovery and the recommender should be studied in-depth. For instance, the proactive discovery must be compared with the manual approach using a different amount of devices.

Construct validity. Does the treatment correspond to the actual cause we are interested in? Does the outcome correspond to the effect we are interested in? The research aims to: (a) propose a discovery model for the WoT that improves and complements the Discovery Service proposed in the W3C recommendation; (b) propose a discovery model that facilitates the discovery of CPSs; and (c) create a public laboratory for the WoT.

Objectives (a) and (b) are fulfilled in Section 3, compared with other approaches in Section 2.1, and studied in Section 4; and objective (c) is fulfilled in Section 4. For objective (a), the questions related to the proposal of a discovery model that complements the recommended by the W3C have been answered affirmatively. However, other questions related to improving the Discovery Service recommended by the W3C were not answered affirmatively. The proposed discovery model has more features than the Discovery Service proposed by the W3C. However, to assert that our approach improves the W3C recommendation, they must be compared using metrics from the literature to evaluate the difference between both approaches.

External validity. Is the cause-and-effect relationship we have shown valid in other situations? Can we generalize our results? Do the results apply in other contexts? The discovery model is deployed in implementing a Discovery Service in the proposed scenario, the WoT Lab. WoT Lab consists of a set of devices from different smart environments to help research the use of CPSs in these devices. Although the number of devices has been increased from the paper, which it extends for, the number of devices is too small for generalizing the usage of the discovery model in all the smart environments. Therefore, the number of devices used in the WoT Lab must be increased. The discovery model must be validated in another scenario to compare both experiments and show that the proposal is valid in other situations.

6. Conclusions

This paper proposes a discovery model architecture for Cyber-Physical systems based on the Web of Things. In particular, the proposed mechanism is intended to store, search and facilitate access to devices represented and controlled under the W3C Web of Things paradigm (commonly referred to as WoT). Furthermore, the presented approach extends previous work by including different capabilities, such as proactive discovery, recommendation, and federation, to facilitate the discovery of CPSs.

A public laboratory, the WoT Lab, was deployed to analyze the discovery model. The WoT Lab is a laboratory presented before and extended in this paper by increasing the number of devices. In addition. a Discovery Service was implemented in the laboratory following the discovery model architecture. As proposed in the previous work, the experimental scenario was modified to improve the security of the approach, using Edge

Computing facilities to interact and manage CPSs. Finally, each capability was validated in the scenario to show how they can facilitate the discovery of CPSs, thus affirmatively answering the second research question.

Regarding the first research question, other implementations of Discovery Services in IoT and WoT were studied in Section 2.1. Furthermore, in Section 3 and 4, the relevance of extending the Discovery Service to adapt to the CPSs was explained and validated, thus answering the first research question affirmatively.

Future work could improve the validation by comparing our proposal with others, such as WoTHive and LinkSmart Thing Directory. Furthermore, the capabilities could be compared to an approach that not uses them to evaluate the performance of a more complex Discovery Service against more traditional ones. Finally, we intend to increase the number of devices in the experimental scenario and include another scenario in the validation to compare the proposal's performance in both and generalize our solution.

Acknowledgments. Grant PID2021-124124OB-I00 funded by MCIN/AEI/10.13039/501100011033 and by the "ERDF A way of making Europe". Grant PY20_00809 funded by the Andalusian Government and the "European Union". Grant FPU19/00727 funded by MIU and the Spanish Government.

References

1. Adjih, C., Baccelli, E., et al.: FIT IoT-LAB: A large scale open experimental IoT testbed. In Proc. of IEEE WFIoT'2015, 459–464. (2015)
2. Azad, H. K., Deepak, A.: Query expansion techniques for information retrieval: A survey. Information Processing & Management, Vol. 56, No. 5, 1698-1735. (2019)
3. Belli, L., Cirani, S., et al.: Design and Deployment of an IoT Application-Oriented Testbed. Computer, Vol. 48, No. 9, 32-40. (2015)
4. Borozdukhin, A., Dolinina, O., Pechenkin, V.: Approach to the garbage collection in the "Smart Clean City" project. In Proc. of IEEE CiSt'2016, 918-922. (2016)
5. Campioni, L., Fontana, N., et al.: A Federated Platform to Support IoT Discovery in Smart Cities and HADR Scenarios. In Proc. of FedCSIS'2020, 511–519. (2020)
6. Carpineto, C., Romano, G.: A Survey of Automatic Query Expansion in Information Retrieval. ACM Comput. Surv., Vol. 44, No. 1, 1-50. (2012)
7. Charpenay, V., Käbisch, S.: On Modeling the Physical World as a Collection of Things: The W3C Thing Description Ontology. In Proc. of ESWC'2020, 599–615. (2020)
8. Charpenay, V., Käbisch, S., Kosch, H.: Introducing Thing Descriptions and Interactions: An Ontology for the Web of Things. In Proc. of IoT'2016, 55–66. (2016)
9. Cimmino, A., García-Castro, R.: WoTHive: Enabling Syntactic and Semantic Discovery in the Web of Things. Open Journal of Internet Of Things, Vol. 8, No. 1, 54–65. (2022)
10. Cimmino, A., McCool, M., Tavakolizadeh, F., Toumura, K.: Web of Things (WoT) Discovery, W3C Candidate Recommendation Snapshot 19 January 2023. (2023)
11. Criado, J., Iribarne, L.: Reusability and discovery models in software systems: a systematic literature review. Journal of Object Technology, Vol. 21, No. 4, 1–17. (2022)
12. EPCglobal.: GS1, Discovery Configuration and Initialization (DCI). (2023) [Online]. Available: https://www.gs1.org/standards/epc-rfid/dci/1
13. Feldt, R., & Magazinius, A.: Validity Threats in Empirical Software Engineering Research - An Initial Survey. In Proc. of SEKE'2010, 374-379. (2010)
14. Glomb, C., Thiéblin, É., Amarger, F.: SparTDD-a SPARQL based Thing Description Directory. In Proc. of ESWC'2022, 1-6 (2022)

15. Gomes, P., Cavalcante, E., et al.: A semantic-based discovery service for the Internet of Things. Journal of Internet Services and Applications, Vol. 10, No. 10., 1–14 (2019)
16. Gomes, P., Cavalcante, E., et al.: A Federated Discovery Service for the Internet of Things. In Proc. of M4IoT'2015, 25-30. (2015)
17. Greer, C., Burns, M., Wollman, D., Griffor, E.: Cyber-physical systems and internet of things. NIST Special Publication 1900–202. (2019)
18. Guinard, D., Trifa, V.: Building the Web of Things. Manning Publications. (2016)
19. Guinard, D., Trifa, V., Wilde, E.: A resource oriented architecture for the web of things. In Proc. of IoT'2010, 1–8. (2010)
20. Iggena, T., Bin Ilyas, E., et al.: IoTCrawler: Challenges and Solutions for Searching the Internet of Things. Sensors, Vol. 21, No. 5, 1559. (2021)
21. Iribarne, L., Troya, J. M., Vallecillo, A.: A Trading Service for COTS Components. The Computer Journal, 47(3), 342–357. (2004)
22. Kabalci, Y., Kabalci, E., et al.: Internet of Things Applications as Energy Internet in Smart Grids and Smart Environments. Electronics, 8(9). (2019)
23. Kovatsch, M., Matsukura, R., et al.: Web of Things (WoT) Architecture, W3C Recommendation. (2023) https://www.w3.org/TR/2020/REC-wot-architecture-20200409/
24. Laadhar, A., Thomsen, C., Pedersen, T. B.: domOS Common Ontology: Web of Things Discovery in Smart Buildings. The Semantic Web: ESWC 2022 Satellite Events, 95–100.
25. Llopis, J. A., Criado, J., Iribarne, L., Padilla, N.: A Discovery Pull Model for Devices in IoT and WoT Environments. In Proc. of IoT'2021, 228–233. (2021)
26. Llopis, J. A., Fernández-García, A. J., Criado, J., Iribarne, L.: Matching user queries in natural language with Cyber-Physical Systems using deep learning through a Transformer approach. In Proc. of INISTA'2022, 1–6. (2022)
27. Llopis, J. A., Mena, M., Criado, J., Iribarne, L., Corral, A.: Towards a Discovery Model for the Web of Things. In Proc. MEDES'2022, 96–103. (2022)
28. Lu, J., Wu, D., Mao, M., Wang, W., Zhang, G.: Recommender system application developments: A survey. Decision Support Systems, 74, 12–32. (2015)
29. Lü, L., Medo, M., Yeung, et al.: Recommender systems. Physics Reports, 519(1), 1–49. (2012)
30. Marwedel, P.: Embedded system design: embedded systems foundations of cyber-physical systems, and the internet of things. Springer Nature. (2021)
31. Mayer, S., Guinard, D.: An extensible discovery service for smart things. Proceedings of the Second International Workshop on Web of Things, 1–6. (2011)
32. Memon, S., Jens, J., Willem, et al.: Towards Federated Service Discovery and Identity Management in Collaborative Data and Compute Cloud Infrastructures. Journal of Grid Computing, 16(4), 663–681. (2018)
33. Remote Lab. Tech. Univ. of Munich, Germany. (2023) https://esiremotelab.esi.ei.tum.de
34. Porcello, E., Banks, A.: Learning GraphQL: declarative data fetching for modern web apps. O'Reilly Media, Inc. (2018)
35. Pourghebleh, B., Hayyolalam, V., Aghaei, A.: Service discovery in the Internet of Things: review of current trends and research challenges. Wireless Networks, 26(7), 5371–5391. (2020)
36. Rajkumar, R., Lee, I., Sha, L., Stankovic, J.: Cyber-physical systems: The next computing revolution. Design Automation Conference, 731–736. (2010)
37. Sani, M. F., et al.: Improving the performance of process discovery algorithms by instance selection. Computer Science and Information Systems, 17(3), 927–958. (2020)
38. Sciullo, L., Gigli, L., Trotta, A., Di Felice, M.: WoT Store: Managing resources and applications on the web of things. Internet of Things, 9. (2020)
39. Shi, J., Wan, J., Yan, H., Suo, H.: A survey of Cyber-Physical Systems. In Proc. of WCSP'2011, 1–6. (2011)
40. Tavakolizadeh, F., Devasya, S.: Thing Directory: Simple and lightweight registry of IoT device metadata. Journal of Open Source Software, 6(60), 3075. (2021)

41. Vaswani, A., Shazeer, N., Parmar, N., et al.: Attention Is All You Need. In Proc. of NIPS'2017, 6000–6010. (2017)

Juan Alberto Llopis is a Phd Student researching, under the national project TIN2017-83964-R, about Federation service discovery in the Web of Things after receiving a FPU grant (ref. FPU19/00727). His research focuses on: Internet of Things, the Web of Things and Smart Environments. His email address is jalbertollopis@ual.es.

Manel Mena is a PhD in CS at the University of Almeria. Currently he is working in researching IoT Systems, Software Architectures and the Web of Things. From 2018 to 2022, he was supported by an FPU grant (ref. FPU17/02010). His interests include Data Engineering, Software Engineering, Cloud Computing, Microservice Architectures, Component-Based Software Engineering, Machine Learning, the Web of Things and Model-Driven Engineering. His email address is manel.mena@ual.es.

Javier Criado is an Associate Professor at the Department of Informatics and the Applied Computing Group (ACG), University of Almería (Spain). His main research areas are model-driven engineering, component-based software engineering, user interfaces, interoperability, service-oriented architectures, microservices and web of things. You can contact the author at javi.criado@ual.es.

Luis Iribarne is a Full Professor at the Department of Informatics, University of Almeria (Spain), and Head of Applied Computing Group. He has served as the Principal Investigator for nine R&D projects founded by the Spanish Ministry of Science and Technology. His main research interests include simulation, component-based software development, model-driven engineering, and software engineering. His email address is luis.iribarne@ual.es.

Antonio Corral is an Associate Professor at the Department of Informatics, University of Almeria (Spain. He has participated actively in several research projects in Spain and Greece. His main research interests include access methods, algorithms, query processing, spatial databases and distributed query processing. His email address is acorral@ual.es.

Received: March 28, 2023; Accepted: July 01, 2023.

Computer Science and Information Systems 20(4):1661–1685 https://doi.org/10.2298/CSIS230401057V

Systematic Exploitation of Parallel Task Execution in Business Processes*

Konstantinos Varvoutas, Georgia Kougka, and Anastasios Gounaris

Department Of Informatics, Aristotle University of Thessaloniki
Thessaloniki, Greece
{kmvarvou,georkoug,gounaria}@csd.auth.gr

Abstract. Business process re-engineering (or optimization) has been attracting a lot of interest, and it is considered as a core element of business process management (BPM). One of its most effective mechanisms is task re-sequencing with a view to decreasing process duration and costs, whereas duration (aka cycle time) can be reduced using task parallelism as well. In this work, we propose a novel combination of these two mechanisms, which is resource allocation-aware. Starting from a solution where a given resource allocation in business processes can drive optimizations in an underlying BPMN diagram, our proposal considers resource allocation and model modifications in a combined manner, where an initially suboptimal resource allocation can lead to better overall process executions. More specifically, the main contribution is twofold: (i) to present a proposal that leverages a variant of representation of processes as Refined Process Structure Trees (RPSTs) with a view to enabling novel resource allocation-driven task re-ordering and parallelisation in a principled manner, and (ii) to introduce a resource allocation paradigm that assigns tasks to resources taking into account the re-sequencing opportunities that can arise. The results show that we can yield improvements in a very high proportion of our experimental cases, while these improvements can reach a 45% decrease in cycle time.

Keywords: business process optimization, process models, resequencing, parallelism, resource allocation

1. Introduction

Business Processes (BPs) have nowadays become quite complex as the business requirements are increasing, e.g. to accommodate multiple and evolving customer needs. This situation renders the significance of Business Process Management (BPM) even higher. BP optimization, also covered by terms such as BP reengineering and redesign, has persisted as a key aspect in BPM since the emergence of BPM as a scientific area.

In general, automated solutions for BP optimization have not been explored as deeply as process modelling, as discussed in several places, e.g., [19],[27],[4]. In such a context, this work is motivated by the more specific observation that, up to date, there is no automated optimization technique for BPs that can benefit from the overlapping task execution in order to improve latency (a.k.a. cycle time or duration) and is generally applicable. Moreover, concurrent task execution is typically addressed separately from task

* An early version of this work has appeared in [26].

resequencing, whereas the latter tends to focus solely on cases where there are tasks that may lead to immediate process termination [11],[4]. In addition, task allocation is also considered independently of task parallelisation and re-sequencing, both of which modify the structure of the business model whereas task allocation does not impact the model structure.

We aim to address the afore-mentioned limitations and more specifically, we target scenarios where a BP is modelled with the help of a procedural approach, such as BPMN[1], and the optimizations on which we focus fall under the BP behavior heuristics according to the taxonomy in [4]. This category of heuristics includes activity resequencing and parallelism, and the impact of their application is reflected on the model diagram. In other words, the optimized model's structure is different than the initial one. The latter is modified so that certain objectives, such as cycle time or total cost, are improved and our main novelty is that we apply these heuristics, not only in a resource-aware manner, but through leveraging resource allocation so that opportunities to enhance the model structure arise. To date, resequencing has been explored in a manner that it is tightly coupled with the existence of knock-out activities either directly or indirectly [1],[11],[25]; knock-out activities are the activities that can lead to immediate process termination, such as automatically rejecting an application if it does not meet certain criteria. Here, we depart from such a narrow consideration of resequencing. In addition, principled parallelism, where different activities overlap in the time domain and are executed concurrently, is an overlooked area in BP in the sense that although it is a well-recognized heuristic, to date, no algorithmic technique has been proposed to leverage it.

In our previous work[26], we have introduced a novel combination of re-sequencing and parallelism enforcement, with the aim of reducing the cycle time of the process in question. To this end, we leverage the task-based variant [6] of representation of processes as Refined Process Structure Trees (RPST) [24]. This representation allows us to check valid resequencing actions systematically, while it is more amenable to cycle time computations. A key aspect in our solution is that we annotate the tree vertices with the resource allocated, i.e., we take into account both the control flow and the resource perspective of the process. This part of our solution has appeared in [26].

The main novelty in this more complete proposal is that we extend the initial conference version in [26] by combining the cost-based task resequencing and parallelism with a reorderability-aware resource allocation mechanism that may take suboptimal task assignments decisions in order to create room for resequencing. Our rationale is not tightly coupled with a specific resource allocation technique, provided that such a technique assigns a suitability score for each resource-task pair. In our proof-of-concept implementation, the Realistic, Investigative, Artistic, Social, Enterprising and Conventional (RIASEC) dimensions are specified to quantify the suitability of the resources to execute specific tasks in line with the proposal [14].

Reorderability potential has already been discussed in [22]. In this work, we depart from simply assessing the reorderability based on model complexity measures and we do perform process redesign. However, another major difference between our work and the work in [22] is that we take into account resource allocation rather than model features in order to reason about the applicability of reordering tasks and putting branches in parallel.

[1] https://www.bpmn.org/

The results of this work are particularly encouraging. We show that we can improve a very high proportion of cases with the maximum improvements in cycle time being 45%. Moreover, we explain that our proposals can be combined so that the best performing flavor in each case can be selected.

The remainder of this work is structured as follows. Next, we present an exemplary use case. In Section 3, we provide the background regarding RPST and its task-based variant along with cost modeling. In Section 4, present a cost-based task-ordering algorithm that is extended in Section 5 by the proposal of an innovative resource allocation algorithm that is reorderability-aware. We continue with the experimental evaluation results of the discussed techniques that shows their benefits in Section 6. Finally, in Sections 7 and 8 the related work and conclusions are discussed, respectively.

2. Our Case Study

Our case study is shown in Figure 1 and refers to a common real-world BP regarding an employee expense reimbursement request[2]. Briefly, the BP consists of 8 activities that are required to analyse, approve and pay an expense statement submitted by an employee of a business, while accounting for essential steps, such as money transfer, notifications and validation that an account exists. Despite its simplicity, this process is amenable to optimizations, where the relative order of some parts can change, e.g., the initial check regarding the account existence can be performed in parallel with other activities. Furthermore, the activities are performed by different actors (automated services, ordinary employees and supervisors), which may result in configurable execution ordering and therefore, lower waiting times at the expense of higher human effort cost. As such, this type of business process forms an excellent candidate to benefit from the advances in automated cost-based flow optimization that we aim to introduce.

More specifically, we handle the example case study as follows. In our approach, we start with the modelling quality and we consider only well-structured models. It is out of our scope to advocate specific automated transformations, but there exist several proposals in the literature, e.g. [17]. Therefore, the model we process is transformed to the well-structured form as shown in Figure 2.

Next, a closer examination of the activities reveals that the review and approval of claims above $200 can be seen as a knock-out activity because one of its outcome can lead to immediate process termination under an additional assumption that the task of advising employees of the rejection has zero cost and can be replaced by a message. Therefore, it makes sense to move the knock-out activity as early as possible using a rank formula that considers both activity cycle time and cost. This is already covered by previous works, e.g., [1],[11]. Our approach can encapsulate these proposals, but, to better show the novelty of this work, in our case study, we treat every activity, including this specific one, as *not* being a knock-out one, i.e., as if all claims are approved. So, the question that arises is: *"If there are no knock-out activities, what type of resequencing is beneficial?"*.

Our answer to this question is to move the block with the review and approval of claims above $200, which is performed by the supervisor, in parallel with the early blocks

[2] `https://www.businessprocessincubator.com/`

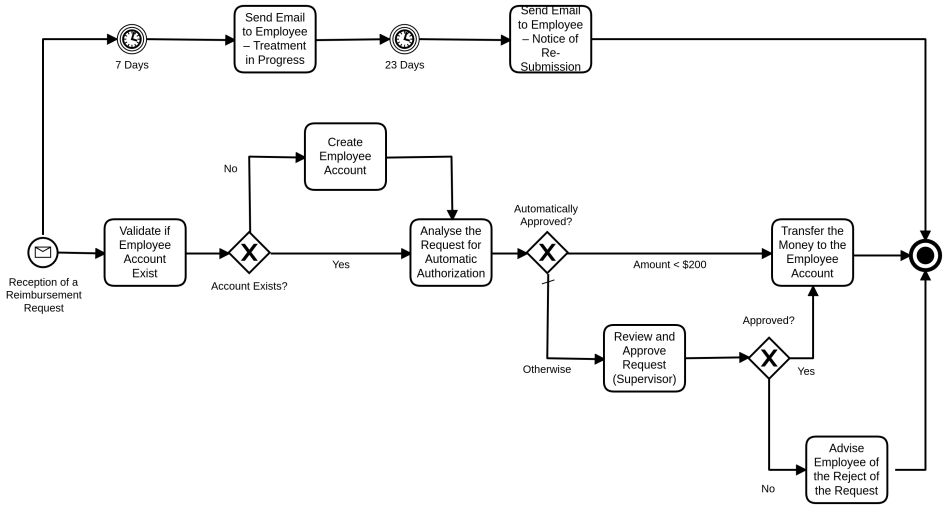

Fig. 1. The process model of an Employee Expense Reimbursement Request

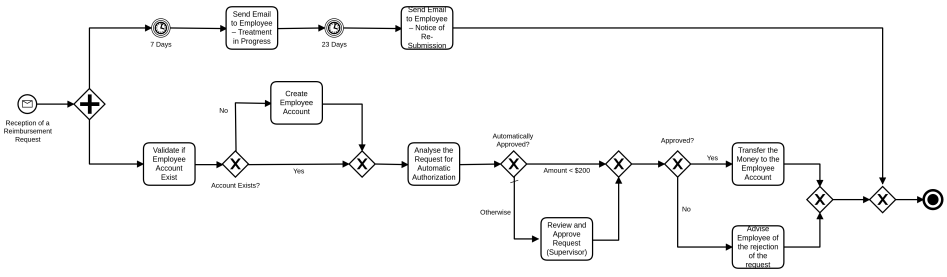

Fig. 2. The well-structured process model of an Employee Expense Reimbursement Request

Table 1. Case Study Activity Cycle Times and Costs

ID	Path	Activity Name	Cost	Time
1	1	Send Email to Employee - Treatment in Progress	1	1 Minute
2	1	Send Email to Employee - Notice of Re-Submission	1	1 Minute
3	2	Validate if Employee Account Exists	2	1 Day
4	2	Create Employee Account	4	1 Day
5	2	Analyze the Request for Automatic Authorization	3	1 Hour
6	2	Review and Approve Request (Supervisor)	8	1 Day
7	2	Transfer the Money to the Employee Account	2	2 Days
8	2	Advise Employee of the rejection of the request	0.1	1 Hour

Table 2. Case Study Path Probabilities

Name of Gate	Path	Probability
XOR_block1	*Path_Account*	0.8
XOR_block1	*Path_No_Account*	0.2
XOR_block2	*Path_Amount*	0.8
XOR_block2	*Path_Otherwise*	0.2
XOR_block3	*Path_Transfer*	0.6
XOR_block3	*Path_Advise*	0.4

of account existence validation and possible creation of an employee account. This allows two distinct types of resources, namely both the supervisor and the supervisee employee, to operate in parallel, so that their cycle times are overlapped. However, it is valid to claim that such resequencing modifications cannot happen because the activity performed by the supervisor should follow the activity for the analysis of the request for the automatic authorization. Therefore, the latter task needs to be moved earlier as well. In our solution, we deal with these issues and in a nutshell, we propose a principled technique that puts blocks of activities in parallel. This movement of activities in the diagram leads to lower cycle times, and entails the incorporation of AND gateways in the model, while ensuring that precedence constraints are met through also moving the necessary activities upstream. I.e., the validity of the optimized model is always guaranteed.

2.1. Statistical Metadata

The solution that we propose is principled in two senses: (i) we follow a cost-based approach, according to which the alternative models are quantitatively annotated in terms of their cycle time and cost; and (ii) we cast our solution as an algorithm that can be easily followed (and re-implemented) by third parties in arbitrary scenarios.

To support the first point above, it is necessary to obtain statistical metadata for the activities that are present in the model. If we are interested in cycle time and cost, there are at least three types of statistical metadata required, namely (a) the activity cycle times; (b) the activity costs and (c) the probability to follow a specific path after (X)OR gateways. These are adequate to compute the process cycle time, as is recorded in several textbooks, e.g., [4]. Tables 1 and 2 present such example metadata for our case study.

3. Process Model Decomposition

We employ a convenient representation of a process, where convenience means that the representation should naturally lend itself to resequencing operations, and process total cycle time and cost can be easily computed. The cost (resp. cycle time) of the entire process is calculated by combining the costs (resp. cycle times) of the individual fragments using appropriate cost functions, e.g., sums, minimum, maximum and so on. We advocate the usage of the Refined Process Structure Tree (RPST) [24] and more specifically a specific variant of RPST, called Task Based Process Structure Tree (TPST) [6]. Both can be deemed as decomposition techniques separating a business process into its individual fragments exactly as we desire.

3.1. Task Based Process Structure Tree (TPST)

The construction of TPST entails a decomposition approach that is based on RPST [6], where a business process model is separated into blocks, which are organised in a hierarchical way. The main differences between TPST and RPST are the following:

- The leaf nodes of a TPST represent a node (i.e., a BPMN activity) of its corresponding process model instead of an edge. This allows us to compute total times and costs based on the activity times and costs, respectively, and also to reorder (blocks of) activities.
- There are multiple types of process fragments into which a process may be separated instead of one generic type. These types include $Sequence$, $Loop$, XOR and AND. These are the same types that are typically employed in flow analysis-based cost computation.
- The leaf nodes of a TPST are ordered, thus making the TPST a semi-ordered tree.
- The internal (i.e., non-leaf) nodes of a TPST represent the control flow.

A subtle point regarding the model in Figure 2 is that, although it is well-structured, an AND split gateway is paired with an XOR merge gateway. Normally, such a situation may lead to erroneous lack of synchronization, but in our case, only a single token is guaranteed to arrive at the merge XOR gateway, as required in valid BPMN models. However, we need to employ a specific *AND/XOR* fragment type to cover this case. In the appendix in [26], we present an alternative modelling of the same process, which employs boundary events in a sub-process in order to show that our approach is not specific model-dependent as long as the model to be optimized is in a well-structured form.

3.2. Decomposition of Our Scenario

The TPST of the model in Figure 2 is depicted in Figure 3. All the leaf nodes of the TPST correspond to BP activities and the waiting events. The root of the TPST represents the complete BP of Figure 2 and it is a *Sequence*. The children of this sequence are (i) a starting event, (ii) an *AND/XOR* gateway node and (iii) an end event. At the next level, there are two other sequences that are children of the *AND/XOR* gateway node. The left sequence represents the top path of the BPMN model, while the right sequence represents

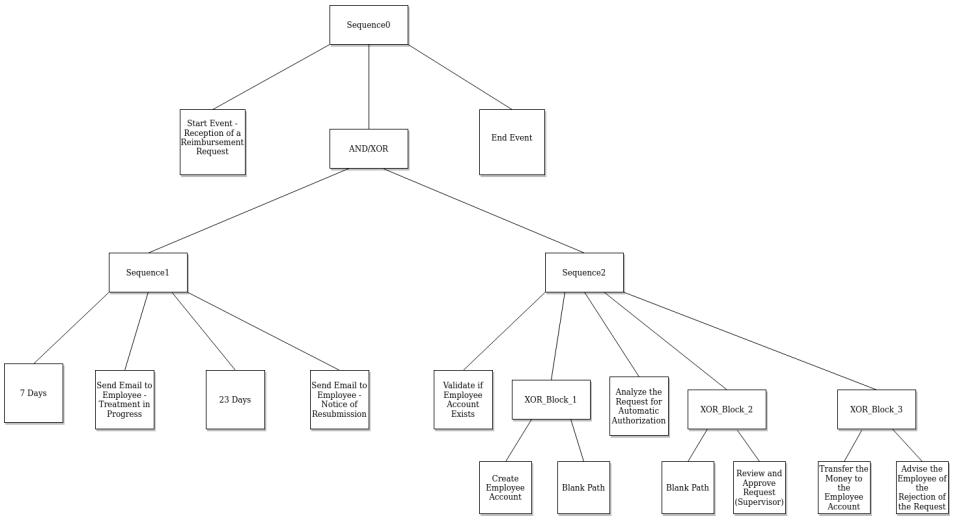

Fig. 3. The TPST of our case study BP model.

the bottom path. Similarly, each of these sequences is connected with its children activities and/or *XOR* blocks comprising activities.

After the decomposition of the BP model to its fragments using the TPST approach, the total cost and cycle time of the process can be calculated in a straightforward manner. When a token arrives at the *AND/XOR* gateway, both upper and bottom paths are initiated. In the upper path, due to the timer activities, the token proceeds when each timer runs out. The two parallel paths are executed independently and the cycle time of the *AND/XOR* subprocess block is the *minimum* of the two paths, while the cost is the cost of the path with the minimum cycle time plus the costs of all TPST nodes that have completed in the other path.

Based on the metadata in Tables 1 and 2, assuming that a day is equal to 8 hours, we can easily compute that the cycle time of the first sequence in Figure 3 is 30 days and 2 minutes, while, for the second sequence it is 2 days and 6.2 hours. The total cycle time is the minimum of these two values. Details are provided in [26]. Using classical formulas in textbooks, such as [4], can help as to compute the cycle time and cost directly from the BPMN diagram, but the TPST representation renders this computation trivial.

However, this cost model is limited to reflect the cost of the execution paths without considering the available resources and the advantage of executing in parallel independent paths. For example, in our case study, if there were more reimbursement requests than request handlers, there would be resource contention that leads to increases in the cycle time. Under such conditions, some instances and their corresponding tasks are put on hold until the required resources become available. Also, the statistics in Table 1 reflect expected times, which lead to a situation that the cycle time computations for all instances will always consider that *Sequence2* is the fastest one for *all* instances. Obviously, it would be more realistic to consider time variations; however these improvements in the cost modelling do not affect our solution.

Table 3. Behavioral constraints considered

Activity constraints	Description
precedence(a_1, a_2)	Whenever activity a_2 is executed, the execution of a_1 must precede
not co-existence(a_1, a_2)	Either activity a_1 or a_2 can be executed, but not both
chain succession(a_1, a_2)	Activity a_2 directly follows a_1

Essentially, our resequencing technique is independent of any model to compute the process cycle time and cost. During resequencing, several alternative models are implicitly generated and checked as to whether they lead to cycle time improvements. Instead of using the technique described above for cycle time computation, advanced simulators, e.g., BIMP[3] or digital twins [3], can be also employed.

4. TPST-based Task Re-ordering with Fixed Resource Allocation

Our methodology accepts as input the TPST representation of the BPMN model and aims to produce an optimized model. To this end, it takes into account (i) the metadata of the input model's tasks, (ii) any behavioral constraints that may apply; and (iii) the given resource allocation. The former item has already been introduced (see also Tables 1 and 2), thus, in this section we focus on the constraints and the resource allocation.

4.1. Notation and Cycle Time Computation Considerations

The main notation required to explain our optimization approach is summarized below.

- $A = \{a_1, \ldots, a_n\}$ defines a set of n activities that appear in the BPMN business process model. The cycle time (resp. cost) of each activity $a_i,\ i = 1n$ is denoted as $ct(a_i)$ (resp. $cost(a_i)$)
- $R = \{r_1, \ldots, r_m\}$ denotes a set of m resources, where the set of activities A are allocated to.
- $A \rightarrow R$ defines the mapping of activities to resources; a_i^j denotes that a_i is mapped to r_j, where $i \in 1 \ldots n$ and $j \in 1 \ldots m$.

In addition, we consider a subset of the constraints defined by DECLARE [15], as depicted in Table 3. Without loss of generality, we assume that the *precedence* constraint subsumes the *chain succession* one, and their existence prohibits the existence of the *not co-existence* constraint. These constraints are used in many works, e.g., [2], and can be accompanied by additional ones, such as existence of alternating ordering, which, however, add no further knowledge in our case and thus are not required by our technique.

The main implication of the resource allocation regarding the computation of the process cycle time is when considering AND blocks: instead of returning the maximum of all branches always, we do so only if the resources are different. Activities belonging to

[3] `https://bimp.cs.ut.ee/simulator/`

Algorithm 1 TPST-based re-ordering

```
1: Annotate TPST with resource allocation info
2: Perform BFS on TPST
3: if node.type is "Sequence" then
4:     for each node_pair in the sequence do
5:         check pair validity for parallel execution
6:         assess impact on cycle time
7:         resolve additional constraint violations
8:     end for
9: end if
```

different branches but executed by the same resource are treated as executing sequentially in terms of their cycle time. Note that the resource-oriented notation is kept as simple as possible at this stage and in the next section, we will include extensions and provide full details.

4.2. Cost-based Task-reordering Algorithm

We annotate each leaf node of the TPST with the resource allocated. Each parent node with all its children annotated with the same resource is annotated accordingly as well; if there are multiple different resource annotations among the node children, the resource annotation of the parent is the union of all children resources. The resequencing algorithm is applied to such a resource-annotated TPST representation of the input model. The next step of the algorithm is to traverse the TPST through performing Breadth-First-Search (BFS). For each *Sequence* node encountered, every possible node pair in the specific sequence is considered as a candidate for parallel execution through the following procedure (see also Algorithm 1).

1. First, it is checked whether any precedence constraints are violated. I.e., for any two activities a_1 and a_2 that are considered to be placed in a parallel (AND) block, behavioral constraints must not include both *Precedence(*a_1, a_2*)* and *Precedence(*a_2, a_1*)*. If a node is not an activity one but a complete fragment, e.g., a XOR block, then this check is performed for all activities in the block. In essence, the absence of these two constraints suggests the existence of the relation of potential parallelism [4].
2. The impact on the cycle time and execution cost is examined when moving the downstream node in parallel with the upstream one in the sequence. If the downstream node has already been moved in parallel with another node in an earlier pair consideration, it is checked whether the upstream node in the initial sequence should be added to the branch of the AND block that does not contain the downstream node. Basically, the cycle time is improved if the nodes considered for parallel execution are assigned to different resources, i.e., the intersection of their resource annotations is null. The total cost remains unaffected unless a knock-out activity is executed in parallel instead of as early as possible. If there is no improvement, this pair is not further considered.
3. A final check whether creating an AND block leads to violation of precedence constraints involving one activity other than a_1 or a_2 is performed. If this the case, we need to consider if the violation can be resolved by reordering the other activity just

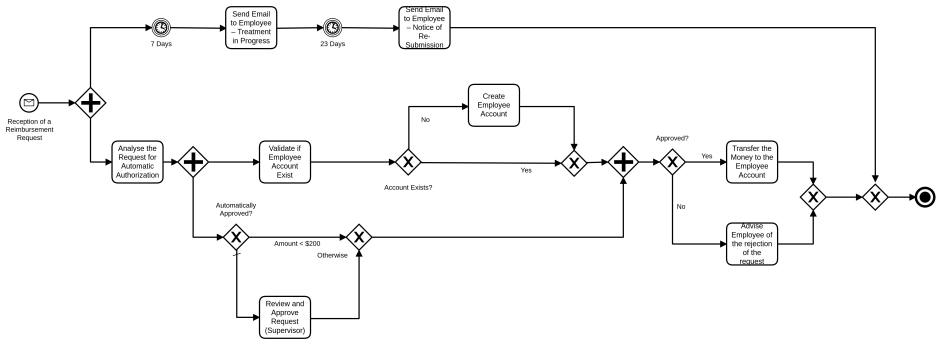

Fig. 4. The result of applying our proposed methodology to the case study BPMN.

before the AND block. If such a reordering is not feasible due to the constraints of the model, then the changes under consideration are rejected and we continue with the next pair.

Complexity Analysis: The complexity of the above solution in $O(n^3)$, where n is the total number of activities. The maximum number of pairs is $O(n^2)$ while each node can participate in $O(n)$ behavioral constraints. Actually, the complexity is lower, since it is cubic in the length of the longest sequence. Apart from the polynomial complexity, it is important to stress that even in large processes, n does not typically grow very large. Finally, due to the same reasoning as in [10],[9], we can characterize the problem in question as NP-hard, thus the polynomial algorithm presented does not aim to find the optimal solution but just to improve the BPMN diagram considered.

4.3. Application in Our Example Case Study

As a proof of concept, we present the application of our proposed methodology to the example case study that was presented in Section 2[4]. The algorithm accepts as input the TPST representation of the input model as shown in Figure 3. The resource annotation (not shown) is based on the activity names: all activities but one are executed by a single resource, while the remaining activity is executed by a different resource named *supervisor*. The constraints are presented in Table 4. The first sequence *Sequence1* has no valid candidate node pairs due to the behavioral constraints in place. However, when applying the algorithm on *Sequence2*, the result is that activity *Validate if Employee Account Exists* and block *XOR_Block_2* are reordered for parallel execution, and then *XOR_Block_1* is placed in the same branch as the former activity[5]. The resulting BPMN is presented in Figure 4.

[4] The prototype implementation can be found at `https://github.com/kmvarvou/bpmn_tpst_optimization`

[5] According to the example metadata, actually this last movement does not lead to improvements (the cycle time remains the same) but we include it for completeness, since it may yields lower times if the cycle time of the supervisor task was longer.

Table 4. Case Study Behavioral Constraints

Constraint	Activity1	Activity2
Precedence	*7 Days*	*Send Email to Employee - Treatment In Progress*
Precedence	*7 Days*	*23 Days*
Precedence	*7 Days*	*Send Email to Employee - Notice of Resubmission*
Precedence	*Send Email to Employee - Treatment In Progress*	*23 Days*
Precedence	*Send Email to Employee - Treatment In Progress*	*Send Email to Employee - Notice of Resubmission*
Precedence	*23 Days*	*Send Email to Employee - Notice of Resubmission*
Precedence	*Review and Approve Request (Supervisor)*	*Transfer the Money to the Employee Account*
Precedence	*Review and Approve Request (Supervisor)*	*Advise the Employee of the Rejection of the Request*
Precedence	*Validate if Employee Account Exists*	*Create Employee Account*
Precedence	*Create Employee Account*	*Transfer the Money to the Employee Account*
Precedence	*Create Employee Account*	*Advise the Employee of the Rejection of the Request*
Precedence	*Validate if Employee Account Exists*	*Transfer the Money to the Employee Account*
Precedence	*Validate if Employee Account Exists*	*Advise Employee of the rejection of the request*
Precedence	*Analyze the Request for Automatic Authorization*	*Review and Approve Request (Supervisor)*

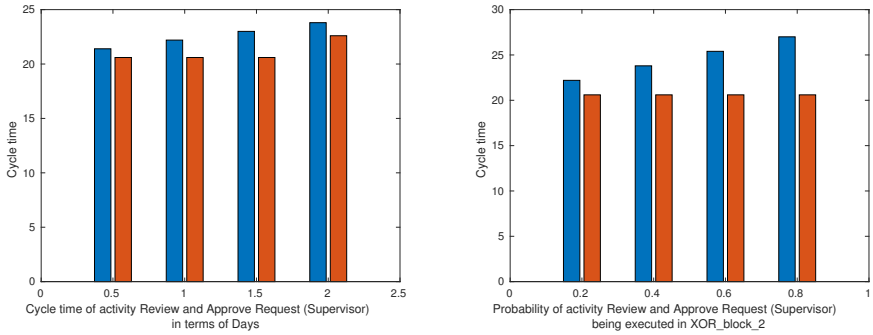

Fig. 5. Process cycle times for different values in terms of cycle time of the *Review and Approve Request (Supervisor)* activity (left) and the probability of the activity being executed in *XOR_block_2* (right). The blue bars refer to the original model and the orange bars to the optimized one.

In the optimized model, the average total cycle time becomes 2 days and 4.6 hours. In other words, the introduction of parallelism leads to a decrease of 7.3 % in terms of cycle time. In Figure 5, we present the results of applying our methodology for a variety of values in terms of cycle time (of the activity *Review and Approve Request (Supervisor)*) and XOR branch probability; all the other values remain the same as the example ones already provided in Section 2. In the two plots in the figure, the improvements are up to 13.5% and 23.8%, respectively.

5. Blending Resource Allocation with Reordering

In the previous section, our approach to task reordering relied on the existence of a resource allocation for a business process model. In this section, we extend our approach to conduct also resource allocation. The components of task reordering and resource alloca-

tion are loosely coupled and the exact resource allocation proposal can be substituted by more sophisticated ones, since the reorderability-aware resource allocation rationale that we propose is easy to be incorporated to additional resource allocation techniques.

5.1. Rationale and Further Notation

We begin with extending the resource modeling specifications, presented in Section 4.1, upon which we build our work. A lot of work has focused on the importance of capturing the differentiated performance of distinct resources when trying to build an accurate process simulation [13],[12]. In this context, we assume a scenario where, to drive the final mapping, there is also a quantified suitability measure when assigning an activity to a resource. More specifically, activities and resources both feature a psychological profile that aims to classify the resource performance per task according to a set of personality traits [14]. These attributes correspond to the *Realistic, Investigative, Artistic, Social, Enterprising and Conventional (RIASEC)* dimensions of resources and tasks. The psychological profile of an activity a_i is defined as a sextuple, one attribute for each RIASEC dimension, denoted as:

$$P_{a_i} =< P_{a_i.1}, P_{a_i.2}, \ldots, P_{a_i.6} >$$

A similar profile characterizes the suitability of each resource as well. Therefore, while a set of resources may be eligible for the execution of a specific activity, each one of them may demonstrate different levels of suitability, depending on its profile, denoted as:

$$P_{r_j} =< P_{r_j.1}, P_{r_j.2}, \ldots, P_{r_j.6} >$$

Furthermore, the cost and duration of the activity execution are differentiated, depending on the allocated resource. In other words, instead of a *single cycle time* for each activity for all resources, $ct(a_i)$, the *cycle time* is dependent on the resource r_j executing a_i, and is denoted as $ct(a_i^j)$. Similarly, for each activity, we assume the existence, apart of the average duration (cycle time), of the cost of execution, $cost(a_i)$, which may be provided by domain experts or through past execution logs. Both these resource allocation-agnostic metrics, namely $ct(a_i)$ and $cost(a_i)$, are indicative of the performance of each activity, without taking into account the resource allocated. When allocating a specific resource for the execution of an activity, these metrics are differentiated according to how suitable this resource is. To this end, the suitability of a resource for a specific activity is quantified using the term *performance coefficient*, denoted as pc.

More specifically, for each activity $a_i \in A$ and for each resource $r_j \in R$ that feature performance psychological profiles P_{a_i} and P_{r_j} respectively, and assuming r_j being a resource that is eligible to be selected for the execution of activity a_i, we calculate the performance coefficient pc_i^j using the following equation:

$$pc_i^j = 1 + \sum_{k=1}^{6} |P_{a_i.k} - P_{r_j.k}|$$

Then, we can derive the resource-aware cycle time and cost metadata as follows: $ct(a_i^j) = ct(a_i) \times pc_{i_j}$, while $cost(a_i^j) = cost(a_i) \times pc_{i_j}$

Additionally, as implied above, we take into account the *eligibility e* of the available resources to execute the corresponding activities. The eligibility is defined as follows:

$$e : A \times R \rightarrow \{0, 1\}$$

As such, the eligibility of each resource r_j with regards to activity a_i is denoted as e_i^j and is a binary variable.

Another factor that affects the resource allocation decisions is the *availability*, denoted as $av(r_j)$. This metric reflects the capacity constraint in the terms of defining the number of activities that can be allocated to a single resource $r_j \in R$.

Finally, a key metric for computing total cycle time closer to reality is the *overhead of intercommunicating* between two different resources in terms of transition cost when activities executed by different resources are connected in the BPMN diagram (ric, standing for resource intercommunication cost):

$$ric(r_i, r_j) : R \times R \rightarrow \mathbb{R}_{\geq 0}$$

5.2. Baseline Allocation

In summary, the allocation approach that is introduced in the following requires as input:

- a TPST structure that consists of a set of activities (A) along with their profiles ($P_{a_i},\ \forall a_i \in A$),
- a set of resources (R) along with their profiles ($P_{r_j},\ \forall r_j \in R$),
- an eligibility mapping of activities to resources (e),
- the baseline cycle time $ct(a_i)$ and cost $cost(a_i)$ of the activity a_i execution, based on which the $ct(a_i^j)$ and $cost(a_i^j)$ metadata can be derived, and
- the capacity of each resource r_j

Based on the key metadata input defined above, the baseline allocation technique is briefly presented as follows.

The first step of this optimization approach is to identify and rank all the activity nodes of the TPST input in terms of their average duration of execution $ct(a_i)$. Then, according to their ranking, each activity is allocated to the most suitable available resource. More specifically, the resource selection depends on the lowest performance coefficient and the resource availability based on the existing resource's capacity constraint. In the case that there is an activity, for which no allocation can be found, this activity is re-ranked and pushed to the top of the ranking. This process is repeated until a valid allocation is found for all activities.

The steps of the technique are presented in Algorithm 2. Basically, after ranking the activities, we choose for an activity a_i the resource r_j with the minimum pc_i^j value, provided that $e(a_i^j) = 1$ and $av(r_j) \geq 1$. After each allocation, the $av(r_j)$ metric is decreased by one. In practice, the re-ranking allows activities that can be executed only by scarce resources to be considered earlier, so that such resources have not reached their capacity.

Algorithm 2 Baseline Resource Allocation Approach

```
1: Rank activity nodes based on average duration of execution
2: for each activity node a_i do
3:    for each resource r_j that is eligible and available for its execution do
4:       calculate performance coefficient pc_i^j
5:       allocate resource with lowest performance coefficient
6:       if there are is no possible allocation for this activity a_i then then
7:          push a_i to the top of the ranking
8:          go to line 2
9:       end if
10:   end for
11: end for
```

5.3. Reorderability-aware Resource Allocation

In this section, we propose a resource allocation approach, which aims to produce an allocation that promotes/enables the parallelization of activities. To this end, our approach entails a pre-processing step where activities, which may be executed parallel, are identified. This is achieved, by taking into account the resource mapping and the behavioral constraints of the input process model.

More specifically, our approach takes as input a process model represented in TPST form, along with the set of execution-related metadata that was outlined in Section 5.1. The input TPST is traversed using DFS in order to identify sequence nodes/blocks. Then, for each sequence block identified, every node pairing is checked on whether it is eligible for parallel execution.

The check entails the following step. The behavioral constraints that apply to the input model are checked, to identify which nodes may be executed in parallel. As already mentioned in Section 4, for each pair of activities a_1 and a_2, the behavioral constraints must not include both *precedence(*a_1, a_2*)* and *precedence(*a_2, a_1*)*. The absence of these two constraints suggests the existence of the relation of potential parallelism [4]. A subsequent step is to ensure that there is at least one possible assignment of resources to tasks so that the two activities are executed by different resources. We also note that in the generic case, a node in the tree is not a leaf, thus it covers a set of activities.

Through these steps, activity pairings which may be placed in parallel are identified and are referred to as *prioritized* activities. Then these node pairings are pushed to the top of the ranking, so that an allocation for them is prioritized. Our approach aims to provide a resource allocation which, by taking into account the prioritized pairings, performs such a resource allocation that enables the parallelization of the aforementioend nodes, even though the initial allocation may be deemed as a suboptimal one.

Our approach comes in two different flavors, with regard to how the allocation is produced for these nodes. In the first flavor, the node pairings are directly assigned to resources, in a way that ensures that nodes of a single pairing are executed by different resources. In the second flavor, the allocation of different resources to each pairing is produced indirectly.

More specifically, in the first flavor, the *prioritized* activities are assigned resources in a direct manner in a way that allows for their placement in parallel. For each activity pair included in the *prioritized* set, their resource mappings are scanned to identify all possi-

ble allocations. The first allocation that satisfies the condition for parallel placement of the two activities, i.e. the intersection of the allocations of the two is null, is chosen. The remaining, non-*prioritized* activities are allocated using the baseline approach presented in Section 5.1. This flavor is termed as *Advanced_Enforced*, since it enforces parallelization.

In the second flavor, termed as *Advanced_Promoted*, the allocation of resources facilitates the placement of $eligible$ activities in parallel in an indirect and configurable manner. For each activity pair $a1, a2$ included in the *prioritized* set, each resource that is present in the resource mapping of only one of the pair's activities has its performance coefficient (for that respective activity) reduced by a factor of p. Then, activities are allocated to resources using the approach presented in Section 5.1. [6]

5.4. Discussion

As implied by the description of the advanced flavors above, their coupling with the baseline resource allocation techniques is a loose one. In other words, the baseline technique, which is a list scheduling one, is replaceable and the reorderability-aware rationale is more generically applicable. The prerequisite is that any base resource allocation technique to be capable of assigning suitability values for each (eligible) resource-activity pair. Overall, the technique is loosely coupled with both the cost model and the base resource allocation technique employed.

Also, this work aims to pave the way for a new line of research work that revisits cost-based activity reordering and the parallelism redesign heuristic in BPMN diagrams. Apart from the aspects discussed above, we focus also on two additional one.

Firstly, the proposed technique, similarly to any cost-based technique, relies on accurate quantitative and qualitative metadata. We expect that the base activity cycle times, possibly allowing for uncertainty, can be provided by process mining techniques applied on previous logs or domain experts or both. This also applies to constraint derivation, which is a topic already considered in depth in process mining. In addition, our claim is that we do not neglect but extend task resequencing techniques considering knock-out activities, as these are discussed in [11]. More specifically, in the algorithm provided, before examining each pair in the sequencing, we can apply node reordering and then to proceed to parallelism investigation. Moving knock out activities upstream is guaranteed to yield lower cycle times and execution costs. Whereas, our parallilized resequencing reduces the cycle times at the expense of an increase in the cost in the generic case. This increase is due to the deliberate suboptimal resource assignment. As shown in the experiments in the next section though, the increase is insignificant compared to the benefits in terms of cycle time.

6. Evaluation

We begin this section by outlining the experimental setting that was used to evaluate our proposal. Then, we proceed to the results' presentation and discussion.

[6] The prototype implementation can be found at `https://github.com/kmvarvou/bpmn_tpst_allocation_optimization`

Table 5. Experimental settings parameters regarding TPSTs

Setting	Nodes	Tree Depth	Tree Breadth
1	18	9	3
2	17	4	8
3	20	5	4

6.1. Experimental Setting

Our software prototype generates process models in the form of TPST trees, and also generates the required metadata. To allow for a comprehensive and wide-scope evaluation, we explore numerous random metadata values. These values cover psychological profiles, behavioral constraints, eligibility and performance metadata, i.e. base cost and duration of execution for each process activity. For each activity, the cost and duration of execution attributes was assigned (integer) values in the [1,10] range. This allows for differences on the order of a magnitude. Additionally, the psychological profiles were assigned random values for each of their RIASEC dimension in the [0,1] range.

Regarding resource eligibility, each activity may be executed by a subset of the full set of resources. We cover two scenarios regarding the eligibility of resources: in the first scenario there are 4 resources: *Clerk, Supervisor, Administrator, Intern*, while in the second scenario there are 8, which are : *Clerk, Supervisor, Administrator, Intern, Automated, Manager, Consultant, Temp*. In the first scenario, all resources have a capacity of 6, while in the second one, they feature a capacity of 3. In other words, both scenarios feature the same amount of distinct resource allocation slots, but in the second scenario, parallelization is inherently easier to achieve due to the larger number of distinct types available. The probability that a node pair features a precedence constraint is 50%. An exception is made for node pairings in the form of *start,a* or *a,end* where *start* is the starting event of the process and *end* is the ending event of the process, where a constraint must always be featured. Lastly, regarding the *ric* values, we again experiment with two scenarios. In the first scenario there is no *ric* overhead. In the second one, *ric* is set to 1 when two consecutive activities are allocated to different resources.

Regarding the process model types, we conducted our experiments by focusing on three distinct TPST cases, with each model featuring different characteristics in terms of depth and breadth. As a reference point, the TPST of the second setting is presented in Figure 6 while the others are in the appendix. The parameters of the experimental evaluation are presented in Table 5 and they cover cases where the tree is (i) narrow and deep, thus leaving little room for reordering improvements; (ii) wide and shallow; and (iii) balanced, with moderate width and depth.

For each of the three TPST designs, we generated 1000 random cases, each one entailing different quantitative and qualitative metadata as described above. We applied all three allocation approaches for each TPST case. Then, our cost-based resequencing approach was applied to each TPST for each of the three allocation approaches. For each approach, we present the number of cases where parallelization was achieved, and also the average and maximum improvement achieved in terms of percentage. The improvements are over the baseline approach without any resequencing.

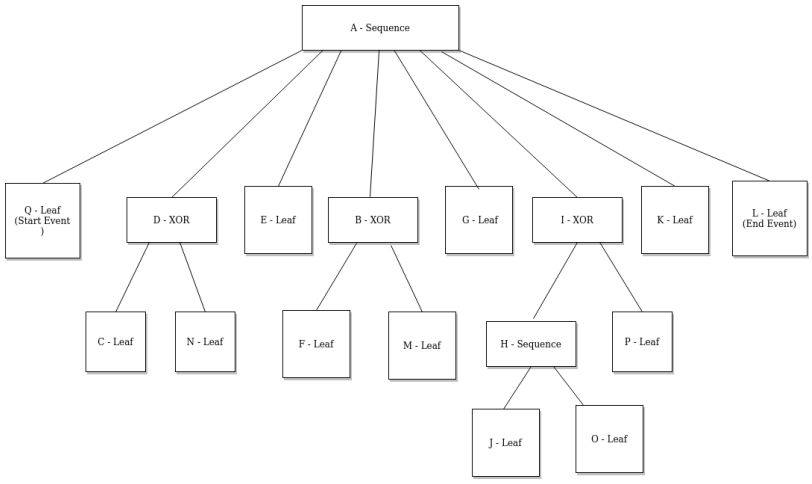

Fig. 6. The TPST of the second experimental setting

Table 6. Results for the 3 experimental settings in terms of the number of cases improved (out of 1000), and the average and maximum improvement in these cases (no *ric*, 4 resources, capacity equal to 6 each)

Setting	Resequencing only			*Advanced_Enforced*			*Advanced_Promoted* (p = 1.0)			*Advanced_Promoted* (p= 0.5)		
	Cases	Average	Maximum	Cases	Average	Maximum	Cases	Average	Maximum	Cases	Average	Maximum
1	248	4.2%	19.9%	502	4.1%	17.35%	556	4.1%	22.76%	510	4.0%	18.3%
2	514	10.7%	29.0%	722	8.7%	35.38%	756	8.5%	36.42%	770	8.4%	31.6%
3	438	12.7%	37%	631	8.8%	44.8%	691	8.2%	39.8%	648	8.4%	36.02%

6.2. Results

We start from the scenario with fewer resources and no *ric* overhead. The results are summarized in Table 6. For each of the three settings (aka TPST types) summarized in Table 5, there is a different row. We compare the effect of resequencing on top of the baseline, the *Advanced_Enforced* proposal and the *Advanced_Promoted* one. For the latter, we investigate two flavors, one with $p = 1$ and another one with $p = 0.5$. For each solution, we mention the number of cases that they lead to improvements in each random set of 1000 instances and the average and maximum improvements in cycle time compared against the cycle time of the baseline resource allocation solution without any resequencing. Note that in terms of total cost, there might be some degradation, but is negligible, i.e., less than 2% at most.

At first glance, the three allocation approaches appear to have complementary benefits with no solution dominating each other in all dimensions. More specifically, in all three settings, applying resequencing on top of the baseline allocation yields higher improvements on average albeit in fewer cases. *Advanced_Enforced* manages to improve more cases than resequencing only, but *Advanced_Promoted* improves even more. Also, there is a trend the more the improvements the less the average improvement.

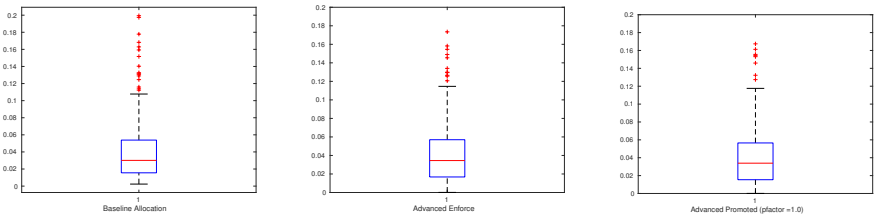

Fig. 7. Results for the first setting

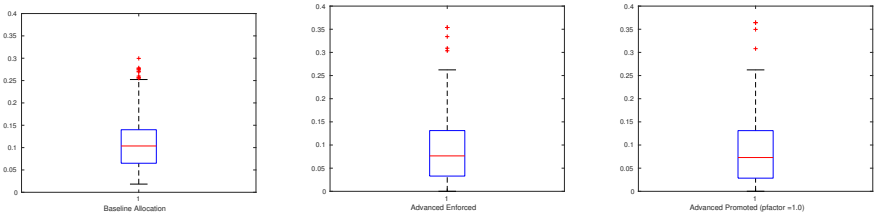

Fig. 8. Results for the second setting

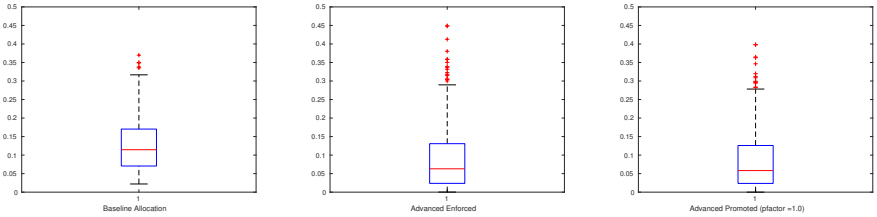

Fig. 9. Results for the third setting

Also, on average the third setting, which corresponds to moderately wide and deep trees, benefits from our solutions the most. This is important, because such trees are encountered more frequently in practice. Another remark is that *Advanced_Promoted* approach is capable of consistently outperforming the other two approaches in all three TPST settings in terms of the cases improved. Compared to the resequencing approach, it was able to yield improvements in 40% more cases (and over 120% in the case of narrow and deep TPSTs). Overall, we can improve more than 75% of the cases for the wide TPSTs and 69.1% of the moderately wide and deep trees, for which the maximum improvements can reach 44.8%.

Based on the observations above, in case we have an efficient simulator at our disposal, we can employ in practice a hybrid solution that first checks the estimates (predictions) if we perform just resequencing over the baseline allocation. Then, if there are no or not satisfactory improvements, to check *Advanced_Enforced*, and finally, to check *Advanced_Promoted*. If we follow this approach, we can combine the highest improvements with the highest number of cases improved.

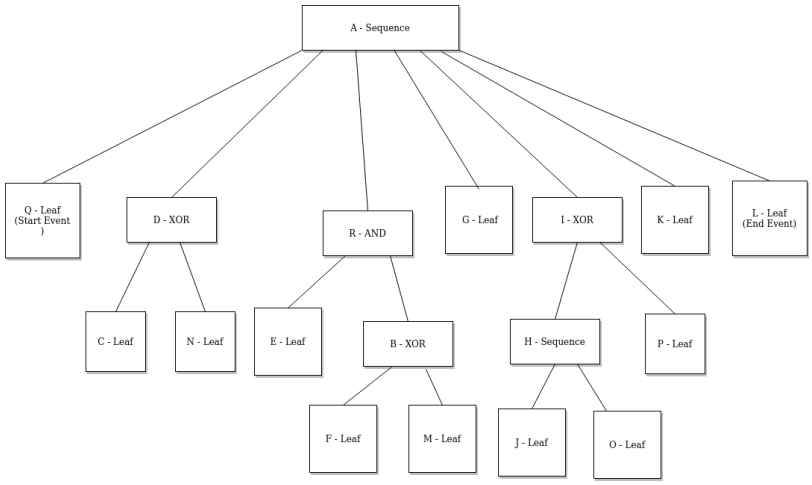

Fig. 10. The result of applying our re-sequencing approach to the TPST of the third experimental setting.

In Table 6, we have presented coarser-grained statistics. In Figures 7,8 and 9, we present the boxplots of improvements for each setting, respectively. We can see that a significant portion of the cases are improved significantly more than the average improvement.

To demonstrate in greater detail the benefits of our proposed approach, we focus in a particular case of the TPST presented in Figure 6. In this specific scenario, nodes E and B do not feature any precedence constraints, meaning that they may be placed in parallel. Additionally, node E has a resource mapping of $\{Clerk, Supervisor\}$. For node B, the resource mapping of its two children nodes, F and M is: $\{Supervisor\}$ and $\{Clerk, Intern, Administrator\}$, respectively. Based on these parameters, the allocations produced by the *Baseline Allocation* approach and *Advanced_Enforced* approach are:

1. $Baseline : E \Rightarrow Supervisor, F \Rightarrow Supervisor, M \Rightarrow Clerk$
2. $Advanced\_Enforced : E \Rightarrow, Clerk, F \Rightarrow Supervisor, M \Rightarrow Intern.$

The allocation produced by the *Advanced_Enforced* approach, enables the placement of nodes E and B in parallel, after applying our resequencing approach, the result of which is presented in Figure 10, leading to a reduction of duration of execution of about 10%. On the contrary, the allocation produced by the baseline allocation approach prevents the placement of the two nodes in parallel.

6.3. Sensitivity Analysis

Next, we aim to discuss the impact that each of the different parameters of the experimental setting has on the performance of the presented allocation approaches. To this end, we continue our experiments testing with *ric* enabled (see Table 7). Then, we repeat both experiments when we increase the resources to 8 (see Tables 8 and 9, respectively). We also assess the impact of the volume of precedence constraints.

Table 7. Results with *ric*, 4 resources, capacity equal to 6 each)

Setting	Resequencing only			*Advanced_Enforced*			*Advanced_Promoted* (p = 1.0)			*Advanced_Promoted* (p= 0.5)		
	Cases	Average	Maximum	Cases	Average	Maximum	Cases	Average	Maximum	Cases	Average	Maximum
1	279	4.4%	23.95%	504	4.4%	25.89%	558	4.36%	26.76%	518	4.31%	25.84%
2	525	10.6%	32.2%	725	8.35%	29.3%	742	8.45%	35.3%	746	8.45%	31.6%
3	431	12.5%	35.8%	665	9.2%	43.4%	680	8.9%	40.8%	662	8.6%	39.8%

Table 8. Results with no *ric*, 8 resources, capacity equal to 3 each)

Setting	Resequencing only			*Advanced_Enforced*			*Advanced_Promoted* (p = 1.0)			*Advanced_Promoted* (p= 0.5)		
	Cases	Average	Maximum	Cases	Average	Maximum	Cases	Average	Maximum	Cases	Average	Maximum
1	347	4.8%	34.8%	494	5.0%	31.7%	580	4.27%	25.8%	532	4.18%	21.2%
2	682	11.58%	31.7%	800	9.73%	32.16%	791	10.22%	36.59%	817	9.78%	32.37%
3	515	13.16%	44.4%	687	9.78%	41.19%	720	9.44%	38.57%	685	9.79%	43.17%

Table 9. Results with *ric*, 8 resources, capacity equal to 3 each)

Setting	Resequencing only			*Advanced_Enforced*			*Advanced_Promoted* (p = 1.0)			*Advanced_Promoted* (p= 0.5)		
	Cases	Average	Maximum	Cases	Average	Maximum	Cases	Average	Maximum	Cases	Average	Maximum
1	337	4.7%	23.1%	482	4.66%	30.0%	585	4.66%	28.4%	531	4.5%	29.5%
2	663	12.24%	35.4%	791	9.87%	41.60%	827	10.24%	35.54%	828	10.39%	36.33%
3	525	13.20%	40.4%	705	10.5%	42.2%	728	9.9%	45.7%	708	10.17%	38.58%

Impact of resource pool size. We begin our discussion with the impact of the size of the resource pool, i.e., the amount of distinct types of resources. Comparing the results of Tables 6 and 7 with the results of Tables 8 and 9, we can observe an increase in the number of cases where parallelization was achieved in all allocation approaches. More specifically, the resequencing approach on top of the baseline allocation exhibited an increase of 34.5% in the number of cases, while the advanced approaches exhibit an average increase of 5.6%, 6.3% and 6.4%, respectively. It should be noted that despite this increase in performance, the simple resequencing approach still trails all advanced approaches by more than 29%. As shown, the advanced allocation approaches exhibit resilient performance, while the resequencing approach with baseline allocation was heavily impacted by the less favorable for parallelization parameters in the first scenario with fewer resources. Overall, the improvements are similar with the highest improvement exceeding 45%, but for wide TPSTs more than 80% of the cases can now be improved; for the 3rd setting, the proportion of improved cases was increased to over 72%.

Impact of resource intercommunication overhead. Here, we focus again on the four same tables but in different combinations. Tables 6 and 8 are compared against Tables 7 and 9, respectively. As we can see, in both settings the incorporation of resource intercommunication overhead did not seem to impact performance in a significant way, with all approaches remaining unaffected in all three dimensions.

Table 10. Results for the TPST of the first experimental setting for three different probabilities of constraint existence with *ric*, 4 resources, capacity equal to 6 each

Probability	Resequencing only			*Advanced_Enforced*			*Advanced_Promoted* (p = 1.0)			*Advanced_Promoted* (p= 0.5)		
	Cases	Average	Maximum	Cases	Average	Maximum	Cases	Average	Maximum	Cases	Average	Maximum
40	349	4.5%	25.4%	513	5.0%	27.1%	586	4.59%	28.5%	564	4.67%	23.9%
50	272	4.2%	23.9%	485	4.15%	28.3%	564	4.3%	24.3%	529	4.4%	19.6%
60	202	3.7%	15%	461	3.8%	22.3%	544	3.83%	17.7%	486	3.9%	21.16%

Impact of precedence constraints. Finally, we would like to examine the impact of different values of probability of a node pair featuring a precedence constraint on performance. In theory, the higher the amount of constraints there are in a model (i.e. higher probability) then the lower the possibility that some of its activities may be parallelized. For this experiment, we focused on the narrow and deep TPST, using probability values of 40%. 50% and 60%. The results are presented in Table 10. As we can see, the resequencing on top of the baseline allocation approach exhibits a 26 % decrease in the number of cases identified when the probability increases from 50% to 60%. On the other hand, it exhibits a 28 & increase in the number of cases identified, when the probability decreases to 40 %. Again, this approach displays a high sensitivity, being affected by the setting's parameters. On the contrary, both advanced allocation approaches displayed higher resiliency in terms of the number of cases they managed to improve. Finally, the average improvements in the cycle time decrease as there are more constraints.

6.4. Summary of observations

Here, we provide a summary of the key observations.

- There is no clear winner between our proposals. We see that we can achieve highest improvements with approaches that manage to improve fewer cases in general.
- The observation above is not actually a limitation. The solutions need not be considered as competitors and can be combined to form a hybrid ensemble solutions, where all are tested at the beginning and the best performing one can be chosen.
- We also note the high insensitivity of the proposed methods in terms of resource pool size, intercommunication overhead and extent of precedence constraints.

7. Related Work

The main cost-based techniques that perform activity reordering in BPMN diagrams leverage the existence of knock-out activities, as explained in [1], or utilize one of the redesign patterns outlined in [18]. The work in [18] presents a set of redesign heuristics, including parallelization, which is partially aligned with the focus of our work, in an attempt to identify the best practices in the field of Business Process Redesign (BPR). In a similar context, a subset of these heuristics have been implemented in [7] as part of an assisted BPR approach. However, contrary to our work, this approach focuses mainly on the control-flow aspect of the process. These techniques are extended with recent advances in

dataflow and query processing optimization [10], as explained in [11]. Similar techniques based on heuristics have been also proposed for declarative models, such as PDM (e.g., [23]). As already stated, we differ in that we perform cost-based resequencing without relying on the existence of knock-outs.

Additionally, there are proposals considering issues of automatic Business Process Redesign. The work in [5] presents an approach that aims to redesign processes in an automatic way by utilizing insights provided by process mining. However, this approach does not take into account the resource perspective and also does not include any evaluation. Furthermore, the work in[20] focuses on configurable process models. Their approach aims to simulate automatically generated variants of the input model and identify the best-performing ones, including previously undiscovered variants.

Up to date, a plethora of objective functions and cost models have already been proposed and applied both for dataflows and business processes, but there are have not been examined in parallel and distributed environments sufficiently. Therefore, there is a need to adopt a cost model that will take into account the parallel execution of the BP activities. The BP execution requires to take into consideration the probability distributions of the input data tokens, the waiting times or the cost of the occupied resources in a realistic manner; these challenges are aligned to the effort to construct digital twins for BPs [3] and are orthogonal to our proposal; the optimization we propose relies on a good and realistic cost model but is not tightly coupled with any specific one. Similarly, the authors of [21] propose building predictive and prescriptive models. The former model estimates the undesired case outcome probability. The latter one refers to a causal model that estimates the impact of a given intervention. Our resequencing proposal can benefit from advances in cost models for BPs to better assess the impact of resequencing.

A significant portion of recent research has highlighted the importance of resource allocation in the context of BPR and BP optimization. The work in [14] presents an allocation approach that aims to represent more accurately the unique characteristics of workers (i.e. resources) by utilizing a personality assessment framework. The framework used is *Holland's person–job fit theory (HPJFT)* upon which we also build our work. In a similar context, the work in [12] proposes an allocation approach that focuses on maximizing cooperation between resources. We differ in that we leverage a resource allocation approach to raise more reorderability opportunities without being tightly coupled with a specific resource allocation proposal.

Overall, our work also relates to resource allocation optimization proposals but differs in that it leverages an existing, potentially optimized resource allocation for activity resequencing rather than targeting on resource allocation as its final goal. Examples of resource allocation appear in [13], where the trade-off between cycle time and resource cost is examined. Additionally, the proposal in [8] discusses an allocation technique to minimize the cloud infrastructure costs in the terms of resource (CPU, RAM, Database size) consumption when executing real-world BPs with different number of simulated users. Other examples of resource allocation techniques achieving resource balancing can be found in [16],[28]. All these proposals are orthogonal to our work as well.

8. Conclusions

In this work, we deal with the problem of proposing a systematic approach to reordering BPMN activities and putting them in parallel. We start with advocating to leverage a given resource allocation with regards to a BPMN model in order to reorder activities so that they can be executed in parallel. Then, we move to proposing techniques that modify the resource allocation so that more reorderability opportunities arise. Our solutions modify the BPMN diagram through inserting AND blocks and moving (blocks of) activities to other places. The intermediate representation that we employ are TPSTs, while we respect all relevant behavioral constraints. We show that we can yield improvement in a very high number of cases examined (in some settings, exceeding 80%), while both the average and the maximum decreases in cycle time are important. For example, the maximum observed improvement exceeded 45%. In the future, we aim to extend our work to optimize several process instances together rather than treating each process instance in isolation.

Acknowledgments. The research work was supported by the Hellenic Foundation for Research and Innovation (H.F.R.I.) under the "First Call for H.F.R.I. Research Projects to support Faculty members and Researchers and the procurement of high-cost research equipment grant" (Project Number:1052, Project Name: DataflowOpt) and by the European Commission under the Horizon 2020 Programme, through funding of the Trineflex project (Grant 101058174). We would also like to acknowledge the support of Dr. Christos Bellas during the implementation.

References

1. van der Aalst, W.M.P.: Re-engineering knock-out processes. Decis. Support Syst. 30(4), 451–468 (2001)
2. De Smedt, J., Deeva, G., De Weerdt, J.: Mining behavioral sequence constraints for classification. IEEE Transactions on Knowledge and Data Engineering 32(6), 1130–1142 (2020)
3. Dumas, M.: Constructing digital twins for accurate and reliable what-if business process analysis. In: Proceedings of the International Workshop on BPM Problems to Solve Before We Die (PROBLEMS 2021). CEUR Workshop Proceedings, vol. 2938, pp. 23–27 (2021)
4. Dumas, M., Rosa, M.L., Mendling, J., Reijers, H.A.: Fundamentals of Business Process Management, Second Edition. Springer (2018)
5. Essam, M., Mansar, S.L.: Towards a software framework for automatic business process redesign (2011)
6. Fan, J., Wang, J., An, W., Cao, B., Dong, T.: Detecting difference between process models based on the refined process structure tree. Mob. Inf. Syst. 2017, 6389567:1–6389567:17 (2017)
7. Fehrer, T., Fischer, D.A., Leemans, S.J., Röglinger, M., Wynn, M.T.: An assisted approach to business process redesign. Decision Support Systems p. 113749 (2022)
8. Ferme, V., Ivanchikj, A., Pautasso, C.: Estimating the cost for executing business processes in the cloud. In: La Rosa, M., Loos, P., Pastor, O. (eds.) Business Process Management Forum. pp. 72–88 (2016)
9. Kougka, G., Gounaris, A.: Optimization of data flow execution in a parallel environment. Distributed Parallel Databases 37(3), 385–410 (2019)
10. Kougka, G., Gounaris, A., Simitsis, A.: The many faces of data-centric workflow optimization: a survey. Int. J. Data Sci. Anal. 6(2), 81–107 (2018)

11. Kougka, G., Varvoutas, K., Gounaris, A., Tsakalidis, G., Vergidis, K.: On knowledge transfer from cost-based optimization of data-centric workflows to business process redesign. Trans. Large Scale Data Knowl. Centered Syst. 43, 62–85 (2020)
12. Kumar, A., Dijkman, R., Song, M.: Optimal resource assignment in workflows for maximizing cooperation. pp. 235–250 (08 2013)
13. López-Pintado, O., Dumas, M., Yerokhin, M., Maggi, F.M.: Silhouetting the cost-time front: Multi-objective resource optimization in business processes. In: Business Process Management Forum. pp. 92–108 (2021)
14. Pereira, J.L., Varajão, J., Uahi, R.: A new approach for improving work distribution in business processes supported by bpms. Business Process Management Journal ahead-of-print (03 2020)
15. Pesic, M., Schonenberg, H., van der Aalst, W.M.P.: DECLARE: full support for loosely-structured processes. In: 11th IEEE International Enterprise Distributed Object Computing Conference (EDOC 2007), 15-19 October 2007, Annapolis, Maryland, USA. pp. 287–300 (2007)
16. Peters, S.P.F., Dijkman, R.M., Grefen, P.W.P.J.: Resource optimization in business processes. In: 2021 IEEE 25th International Enterprise Distributed Object Computing Conference (EDOC). pp. 104–113 (2021)
17. Polyvyanyy, A., García-Bañuelos, L., Dumas, M.: Structuring acyclic process models. Inf. Syst. 37(6), 518–538 (2012)
18. Reijers, H., Mansar, S.: Best practices in business process redesign: An overview and qualitative evaluation of successful redesign heuristics. Omega 33, 283–306 (08 2005)
19. Reijers, H.A., Vanderfeesten, I.T.P., Plomp, M.G.A., Gorp, P.V., Fahland, D., van der Crommert, W.L.M., Garcia, H.D.D.: Evaluating data-centric process approaches: Does the human factor factor in? Software and Systems Modeling 16(3), 649–662 (2017)
20. Schunselaar, D.D., Verbeek, H.E., van der Aalst, W.M., Reijers, H.A.: Petra : Process model based extensible toolset for redesign and analysis (2014)
21. Shoush, M., Dumas, M.: Prescriptive process monitoring under resource constraints: A causal inference approach. CoRR abs/2109.02894 (2021)
22. Tsakalidis, G., Vergidis, K., Kougka, G., Gounaris, A.: Eligibility of bpmn models for business process redesign. Information 10(7) (2019)
23. Vanderfeesten, I.T.P., Reijers, H.A., van der Aalst, W.M.P.: Product-based workflow support. Inf. Syst. 36(2), 517–535 (2011)
24. Vanhatalo, J., Völzer, H., Koehler, J.: The refined process structure tree. Data Knowl. Eng. 68(9), 793–818 (2009)
25. Varvoutas, K., Gounaris, A.: Evaluation of heuristics for product data models. In: Business Process Management BPM Workshops. pp. 355–366 (2020)
26. Varvoutas, K., Kougka, G., Gounaris, A.: Optimizing business processes through parallel task execution. In: Proceedings of the 14th International Conference on Management of Digital EcoSystems, MEDES. pp. 24–31. ACM (2022)
27. Vergidis, K., Tiwari, A., Majeed, B.: Business process analysis and optimization: Beyond reengineering. Trans. Sys. Man Cyber Part C 38(1), 69–82 (2008)
28. Yaghoubi, M., Zahedi, M.: Tuning concurrency of the business process by dynamic programming. pp. 1–5 (02 2018)

Konstantinos Varvoutas is a Ph.D. student at the Aristotle University of Thessaloniki. His main research interests lie in the fields of business process optimization and data intensive computing.

Georgia Kougka is a postdoc in Aristotle University of Thessaloniki and her research interests lie in the field of data science for industrial purposes, data-centric flow modeling, optimization and execution, but also in business process optimization. Moreover, she

has also participated in several research programs and initiatives for predictive maintenance purposes in Industry 4.0 scenarios. Finally, she deals with data analysis in smart agriculture and energy disaggregation scenarios.

Anastasios Gounaris is an associate professor at the Aristotle University of Thessaloniki, Greece. A. Gounaris received his PhD from the University of Manchester (UK) in 2005. His main research interests are in the areas of large-scale data management, massive parallelism, workflow and business process optimization, big data analytics, and data mining. More details can be found at `http://datalab.csd.auth.gr/gounaris/`

Received: April 01, 2023; Accepted: July 17, 2023.

A. TPSTs used in the experiments

We have already shown in Figure 6, the TPST corresponding to one of the three experimental settings. In Figures 11 and 12 the remaining two settings are presented.

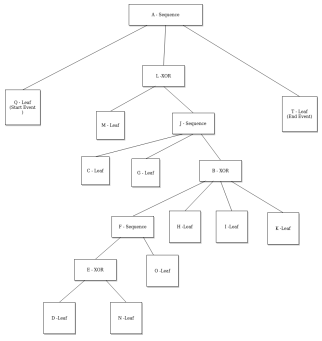

Fig. 11. The TPST of the first experimental setting

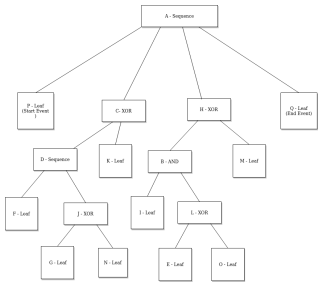

Fig. 12. The TPST of the third experimental setting

Computer Science and Information Systems 20(4):1687–1705 https://doi.org/10.2298/CSIS230320061F

Ownership Protection System for Partial Areas on Image Data using Ethereum Blockchain*

Natsuki Fujiwara and Shohei Yokoyama

Department of Computer Science, Faculty of Systems Design,
Tokyo Metropolitan University, Tokyo, Japan
fujiwara-natsuki@tmu.ac.jp
shohei@tmu.ac.jp

Abstract. Our proposed method utilizes blockchain technology to safeguard the ownership of specific regions within image data. In our approach, diverse values could be assigned to each region based on its importance, and only users with ownership rights can access these designated regions. This ensures the protection of ownership rights for individuals in any given region of an image. Identified regions are individually encrypted using an XOR cipher, and a corresponding key image is generated for decryption, thereby preserving the privacy of the encrypted region. Non-fungible tokens (NFTs) are employed to protect the key image and manage the ownership of each object in the image data. The NFT for the key image is generated by the key holder (who possesses the entire image), and the ownership NFT is acquired by the user who needs access to the key NFT. Furthermore, the ownership NFT and the key NFT are verified for a match by the judgment function, and only upon successful validation, the NFT is displayed on the screen. This method enables different values to be assigned to various parts of an image, facilitating the transfer and sharing of ownership. Additionally, the original image's owner can benefit financially based on the value of the image, thus enhancing the overall security of image data.

Keywords: Blockchain, Ownership, NFT.

1. Introduction

Image theft and ownership have skyrocketed with the increasing adaptation of the internet. Thus, ownership protection of image data has become critical. Blockchain is a decentralized database providing secure and transparent protection to records of all kinds. All transactions are recorded and stored in chronological order[1]. Also, blockchain can track and trace all recorded transactions. It is a useful and futuristic technology to improve data management and prove ownership of collected data such as digital art, music, and land. The main features of blockchain are as follows [2] [3]:

- **Immutability**: The ability of a blockchain ledger to remain unchanged, unaltered and indelible by cryptography and distributed consensus mechanisms. Centralized databases can be corrupted and rely on third parties to retain information.

* This is an extended version of the 14th International Conference on Management of Digital EcoSystems.

- **Decentralization**: The shift of control and decision-making from a centralized entity (an individual, organization, or group) to a decentralized network. Decentralization provides several benefits to blockchain network. One of example benefits is security since there is no central point of failure or attack that can be exploited by malicious actors. Also, it ensures scalability and robustness using the resources of participating nodes.
- **Integrity**:Integrity is important to ensure that all data stored on the blockchain is accurate and reliable, with no possibility of manipulation or corruption. Integrity is maintained through a combination of cryptography and decentralized consensus mechanisms. Each block in the chain contains a unique cryptographic hash created using a complex mathematical algorithm. This hash serves as a unique identifier for the block and is generated based on the data stored in the block, making it virtually impossible to alter the data in the block without being discovered by anyone.
- **Anonymity**: Allows anonymous transactions without registering user bank accounts or interacting with traditional financial gatekeepers. To prevent the true identity of the blockchain participants from being known, cryptographic functions are used to disguise or anonymize them, as appropriate. Public-private key cryptography is used for making it possible.

Recently many projects are creating a data management/tracking system, particularly in logistics and supply chain area, with blockchain [4] [5]. For instance, IBM's Food Trust [6] has been developed to enhance visibility and accountability across the food supply chain. Blockchain prevents tampering by allowing unalterable shared records of food origin, transaction details, and processing information. This study focuses on image management rather than developing those types of systems.

Non-fungible tokens (NFT) are commonly used to protect ownership of image data in blockchains. Opensea[1] is the world's first and largest NFT marketplace. It is similar to Amazon, but the listed items are digital collectibles in the form of NFTs. It is common for NFT marketplaces to see the whole image data without holding ownership. In addition, one image equals one ownership, and ownership cannot be split depending on the regions of an image.

NFTs is one of the contributions by smart contracts in Ethereum. NFTs are defined by smart contracts. Some blockchains have functions to execute and verify secure application code called a smart contract. The term smart contract was advocated by Nick Szabo in 1997 [7]. In 2008, bitcoin was proposed by Satoshi Nakamoto [8]. This was the first cryptocurrency based on the revolutionary technology of blockchain which until then had no distributed ledger. Because the blockchain contained only information about the transaction, it is challenging to stipulate the transaction conditions in a new block. Nevertheless, this technology was the catalyst for smart contracts.

Currently there are many different architectures and different user types of blockchain. An example is the Ethereum introduced by Vitalik Buterin [9], making it possible to use smart contracts. Ethereum has expanded upon Bitcoin's basic functions and smart contracts, which help to develop complex applications.

A smart contract is a set of agreements specified in digital form, including a protocol for the parties to execute these commitments. It consists of the value, address, functions,

[1] https://opensea.io/

and state. [10] Smart contracts in Ethereum make it possible to declare digital items as a non-fungible token (NFT) and add data about the creator and owner. Moreover, NFT ownership can be exchanged, transferred, or processed under the rules of smart contracts. A merit of using smart contracts is cost saving. Fees conventionally paid to intermediaries and third parties that guarantee reliability will become redundant. Moreover, the time required for a series of procedures is reduced, and intermediaries will fail to extract information.

We believe our proposed system could be applied to create new services at tourist and photogenic spots. For example, it could be applied to a commemorative photo service at tourist spots. We envision a situation in which a spherical camera is used to take a commemorative photo. The reason why we use the camera is because a 360◦ view of the landscape is shot at one time so that the image provides a sense of realism.

In this situation, the proposed method would be a practical new service that would allow users to purchase and view only specific image areas in which they have ownership rights. The ownership rights held by the system user are only for the user himself, and he does not hold the ownership rights of others. This service protects the privacy of passersby and people who do not want to be seen in the image. If a passerby appears in the photo, the mosaic cannot be removed by anyone who does not have ownership rights. In the future, the system will be integrated with the background scenery in areas where strangers, such as passersby, are present, and the person itself will be removed.

Another applicable case is for an image selling system. When buying a group photo, the current practice is to purchase one group photo. However, with this system, it is possible to give different ownership rights to each person in the image, so if users want images that show everyone in the photo, they must purchase ownership for everyone.

In our research, these specified regions have objects detected by an object detected model. We use You look only once(YOLO) [11] to detect objects. Images captured by spherical cameras are converted to panoramic images (Figure 1). It can be obtained over the entire 360◦ angular range in a plane with one shot. Panoramic images can be used similar to the normal images. The use situation envisioned for this research is a commemorative photo service at theme parks such as tourist attractions and amusement parks. Therefore, taking pictures of the entire scene, rather than a limited background, can create a more realistic feeling of presence, as well as the possibility of augmenting Augmented reality or Virtual reality.

In addition, if using a regular camera such as a smartphone, the scene is fixed, and the camera needs to be turned around to show other scenes. With a 360-degree camera, on the other hand, all scenes can be captured at once. Because of this feature, we thought it would be more efficient to use a 360-degree camera that can capture the entire scene at once, such as at a sightseeing spot, when you want to view the entire scene at once rather than just one spot. In this research, since the purpose of this research is to protect ownership for areas of an image, there is no problem with limited background scenes. In the future, however, we would like to apply this method to protect the ownership of arbitrary areas in video with real time processing. In this case, we believe that it is easier to track people when a larger area is captured efficiently by a single camera. With a camera such as a smartphone, it is necessary to physically orient the camera in relation to the moving person. However, if we used a 360-degree camera, we thought that since the entire background is being captured at once, the camera need only be fixed and tracking of the person can be done easily. This

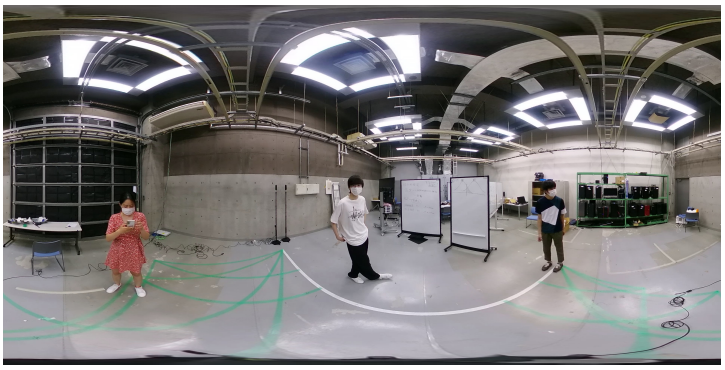

Fig. 1. Panoramic image

is because when tracking a person using a single ordinary camera such as a smartphone with a limited shooting range, if a person enters or exits the frame and then enters the frame again, he or she may be identified as a new person. To prevent this, multiple regular cameras can be installed so that there are no blind spots. However, we believe that using a 360-degree camera allows for efficient tracking, since only one camera captures images in all directions at once and it has less chance to detect the same person as a different person.

We encrypt detected object regions with XOR cipher and create key images corresponding to each area. Encryption converts the original image to a secure unpredictable image. We use the easiest image encryption method since this paper's main purpose is protecting ownership and giving a different value to selected regions of image data. Those key images would be required to decrypt. Crypted areas are shown as mosaic images and objects in this space cannot be identified. Those users having access to the right key images can see the original scenery under encrypted areas that support the key images.

The three main contributions of this study are as follows:

- **Sharability**: Our method makes it possible to give different values to each region and share ownership of a specified area with multiple people on one image data.
- **Affinity** Blockchain is affinity to payment method. Thus, key holders can make financial profit easily. Besides, ownership can be transferred through financial interactions.
- **Security**: Key to decryption is managed safety in the blockchain. They will be unlikely to re-write and leak out.

The remaining paper is organized as follows. The research related to the proposed system is introduced in Section 2. Section 3 describes the proposed method, including image processing and blockchain usage. Section 4 presents the result and outline of our user interface. Finally, Section 5 concludes this paper and reveals the future research directions.

2. Related Work

XOR operations[12], advanced encryption standard (AES) algorithm[13], RSA algorithm [14] and chaos-based algorithm [15] are commonly applied image encryption methods. Irfan et al. [16] suggested using RSA and Chaos-based algorithms. However, securing the image data through encryption may come at the risk of assailant interception in a centralized system. In addition, issues of ownership and copyright of original image data may also occur. To solve these issues, we focus on how and where to store the decryption key after encrypting the image data.

Pink[17] proposes a method to protect the integrity of digital images and verify their ownership. This embeds a digital watermark in the image. This watermark is a unique code that can be used to verify the authenticity and ownership of the image. A digital watermark is generated by combining the content of an image with a secret key to ensure that the image cannot be deleted or tampered without destroying it. To verify the integrity and ownership of an image, the watermark is extracted and compared to the original watermark generated when the image was created. Once the watermarks match, the image is considered authentic and owned by the person who generated the watermark. This method can reveal the owner and confirm whether a circulating image is genuine or not. However, in the proposed method, the encrypted image is leaked but the original image is leaked only to the person who holds the ownership. The emphasis is on protecting the privacy of the people in the image. In addition, our system can guarantee financial benefits to the original image holders.

R.Usha et al. [18] proposes a copyright management system that combines digital watermarking and blockchain technology to protect intellectual property rights. The proposed system uses digital watermarks that embed unique identifiers in digital assets such as images and videos as proof of ownership and copyright. It then leverages blockchain technology to create a distributed ledger of copyright ownership records protected by cryptography and distributed consensus mechanisms. This ledger provides an immutable and transparent record of ownership. It also uses smart contracts to automate copyright registration and licensing. The proposed copyright management system offers several advantages, including improved copyright protection, reduced infringement, and streamlined licensing and royalty management. This approach provides ownership protection for the entire image or video content. However, our research gives ownership respectively only to limited areas that need ownership protection, not to the entire image content. This makes it possible to manage a single image by giving different ownership rights to different areas of the image.

Ali et al.[19] proposes a copyright management system using blockchain and IPFS. The image and the copyright information of the image are registered in IPFS. After registering in IPFS, the hash value is created and registered in the blockchain. After that, when browsing with a web browser using the corresponding IPFS link, if the image is original, the ownership information will be displayed. This method uses IPFS and blockchain to verify whether copyright can be verified in a browser. In our study, after storing image data and other data in IPFS, we made it possible to buy and sell ownership by creating an NFT with IPFS links tied to it.

Waqas et al.[20] proposed securing image encryption based on blockchain. The proposed image encryption method uses the pixel change rate, unified averaged changed intensity, and information entropy analysis. Furthermore, to ensure decryption, each pixel

value of a key image is stored in the blockchain. However, the transaction speed reduces because each pixel data is stored in a blockchain. This research is like our work. However, we created NFT as key image data containing each pixel information to decrypt for improved transaction speed. Khan et al.[21] suggested a safe image-sharing framework using blockchain for medical applications. A list of the key owners with access to important images is stored. Moreover, it is impossible to share ownership depending on areas on the image since the key allows accessing one image or partial areas on the image.

Mohamed[22] suggested an image management system using an Ethereum network. They encrypted whole images, and decrypted keys are stored in the blockchain. Rashid et al. [23] proposed a blockchain-based framework for copyright protection by maintaining the integrity of the original content. Users can download content after verifying the programmed transaction contents. Khan et al.[24] introduced a blockchain system to guarantee the authenticity of stored recordings and allow authorities to verify that footage has not been tampered with. Metadata of images and videos are stored in the blockchain to prevent data forgery.

Wang et al.[25] explain NFTs and how they solve security issues like authenticity, integrity, non-reputability, confidentiality, availability, and authorization. Furthermore, they researched fields that can potentially use NFTs effectively. An example is protecting digital collectibles such as image data. The NFT creators can decide on the transaction contract details, for example, giving ownership and prices, making them an efficient way to manage and protect ownership.

Therefore, we use NFTs for our research because they allow image holders to decide on image value and show digital ownership. Furthermore, NFTs are more secure because of blockchain technology. It is unlikely to tamper with ownership or each image detail because those data are stored in each block and are almost impossible to re-write.

Moreover, most of the above studies focus on ownership protection of full image data. We extended it to facilitate protecting partial areas on images and ownership.

3. Proposed Method

We describe the object detection model and illustrate the image encryption method. In addition, we introduce the blockchain components. This section also explains creating ownership of image data as NFTs and outlines the user interface.

3.1. Spherical cameras

A spherical camera uses multiple lenses to combine all pictures taken by different lenses into a single image. This makes it possible to capture an omnidirectional space with a single camera and a single shoot. The captured images are converted to panoramic images by equirectangular projection before storage. Panoramic images allow dealing with the spherical images as normal images. In the converted image, latitude and longitude lines intersect at right angles and equal intervals. High and low latitude areas cause distortions.

Object Detection by Yolo We adopted YOLO, a state-of-the-art object detection algorithm using neural networks, as the object recognition model. This model outputs the coordinates and type of objects.

Previous traditional object recognition methods have classified each region by identifying multiple candidate object-like regions. However, YOLO does not list candidate object regions but uses a single convolutional neural network for prediction. It is also treated as a regression problem that directly predicts the coordinates and object size by training with a dataset containing the object's location and category. The region of the object is represented by establishing the class it belongs to under the condition that some object is present in a particular region. Moreover, it is faster to process and looks at the entire image, which improves accuracy. We use Yolo verison5 in our study.

In addition, we apply the trained model by Microsoft's Coco dataset. This model can detect 80 classes such as dogs, human beings, and cars. We chose humans because they are often seen around the mid-latitudes of image data, minimizing distortion effects from an omnidirectional camera.

3.2. Image encryption by XOR cipher

This section explains the XOR cipher followed by image encryption using it.

XOR cipher We use detected images and a coordinate list of each detected area to encrypt by XOR cipher. Because image encryption method is outside the scope of this study, we use one of the easiest image encryption methods, the exclusive OR (XOR) cipher, for each pixel value.

XOR is a bitwise operator. The result of xor operation is 1 if the two bits are different. The result is 0 if the two bits are the same. An example of calculating using the XOR operator on numbers 38 and 178 is as follows. The decimal value is first converted to the equivalent binary number. The binary equivalent of 38 and 178 is 10110010 and 00100110, respectively. The XOR operation returns the calculated value as 10010100, which is then converted back to the decimal equivalent 48.

Figure 2 shows an example of the encryption process. In step 1, we calculate the image size. Here, the image size is 2×2 and each RGB value is [55,136,244]. Moreover, we create a key sequence, a random number of the same size as the image to be encrypted. The key sequence is converted to a key image.

Image encryption Step 2 shows the results of the XOR operation on each RGB channel. The RGB values of the step 1 image are extracted. XOR cipher is performed separately for each RGB value and key sequence. For example, when the key sequence is 1, the XOR operation to key sequence and blue channel 244 returns 245. The calculation is repeated for each RGB channel and all pixels.

In step 3, the result of each RGB is merged to create encrypted color images. The XOR operation calculates the key and encrypted image to decrypt each region. The process is repeated for each detected area based on the text file of the object location.

3.3. Blockchain side

This section explains protecting ownership and managing key images using blockchain.

Ethereum We use Ethereum, a decentralized open source blockchain, to create NFTs and events such as transferring ownership under specified rules defined by smart contracts.

Smart contracts are digital self-executing contracts executed based on agreement terms between buyers and sellers. Firstly, we explain calling the deployed smart contract to the front.

Smart contracts are designed using a high-level language such as solidity. Compilation generates a JSON file including dates of both EVM bytecode and an application binary interface (ABI). ABI provides summary information needed to execute smart contracts and retrieve variables to invoke them outside Ethereum or from another contract. Then they are deployed to the blockchain network, and the contract address is published. A smart contract can be called and executed by calling those addresses to the front.

The currency used on Ethereum is called Ether (ETH). A transaction fee called gas fees is required to process and validate transactions, including deploying smart contracts or calling them on the Ethereum blockchain. In our research, we use MetaMask[2] as a wallet for ETH.

We use Hardhat[3] network as the test environment. Hardhat is a development environment for compiling, deploying, and testing smart contracts and debugging Ethereum software. It is possible to develop and connect a local or a specific blockchain network, such as a private blockchain. Moreover, fake ETH can be used to try our application since several accounts have fake 1000 ETH for the test net environment. The Hardhat network is connected to MetaMask in this study.

NFT NFTs serve two purposes. One is for ownership of key images, and another is for NFTs as key images. This method ensures that the key images cannot be accessed without ownership. The key image holder can assign different values to each key.

Our NFTs are designed by Ethereum Request for Comments 721 (ERC-721). This standard represents ownership of NFT. Image data is rarely stored on the blockchain because of the high gas fees. When creating image data as NFT, the data is uploaded to the interplanetary file system (IPFS), a protocol and peer-to-peer network for storing and sharing data in a distributed file system. [26]

[2] https://metamask.io/
[3] https://hardhat.org/

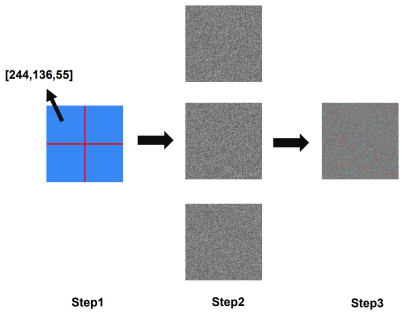

Fig. 2. Encryption method

IPFS relies on a distributed hash table (DHT) to retrieve file locations and node connection information.[27] It is a content address and assigns a unique hash to store files on the network. It also incorporates deduplication technology and is not constrained by a centralized server. In this research, IPFS desktop[4] is used. It assigns a specified ID corresponding to each uploaded image or content. This ID is written in the NFT metadata and stored in the blockchain.

NFTs are defined by smart contracts. We created four smart contracts, two to define the NFTs of ownership rights and key images. The other two specify actions such as obtaining and transferring NFTs.

Details of our smart contracts are as follows: The first two smart contracts have the same content, defining the token type created. This includes a counter function that would tell the number of NFTs created and the mint function. The mint function validates data, creates a new block, and records data into the blockchain. The function checks if the minted token is sent to the right contract to manage NFTs. These two smart contracts can not be converted into one smart contract since Key NFT and ownership NFT tokens are considered as different tokens and need to be defined separately.

The other two contracts define the data type of NFT name, image ID, price, and description as metadata. A smart contract defines two separate events: one for the ownership of NFTs and the other for keyNFTs. Regarding the ownership NFT event, the 'itemcount' value is updated when the ownership NFT is purchased. This value influences the determination and description of whether these contracts also include information about some actions. For example, it is an automatically executed transaction showing from the transfer of NFT ownership. In addition, some regulations to buy are written in the contract; for example, the minimum total amount in the wallet for the buyer is 1 ETH.

User interface Figure 3 shows pages created for different functions using React. We also use the ethers.js library, a complete and compact library for interacting with the Ethereum Blockchain.

Fig. 3. Page content

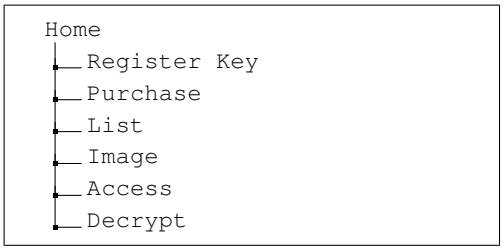

The home page asks users to connect with MetaMask. Once connected, all transactions are executed by the wallet. On the register key page, the key holder can mint key images and decide the cost of each image. A text box allows entering the name, price, and

[4] https://ipfs.io/

description to be stored in the blockchain. They will be required later to match ownership. On the Purchased page, key images would be added upon its purchase. The list page shows minted key images for key holders. If no key is mint, no image data is found.

The decrypted images are available from the Image page. There is an input box consisting of names and descriptions. This data will be stored in the blockchain and will be used to match ownership with the right key. This page is visible to all users. Ownership can be created here if the user wishes to decrypt each region. On the access page, a list of holding ownership will be shown with the corresponding ownership key images. If there is no ownership holding, they are no image.

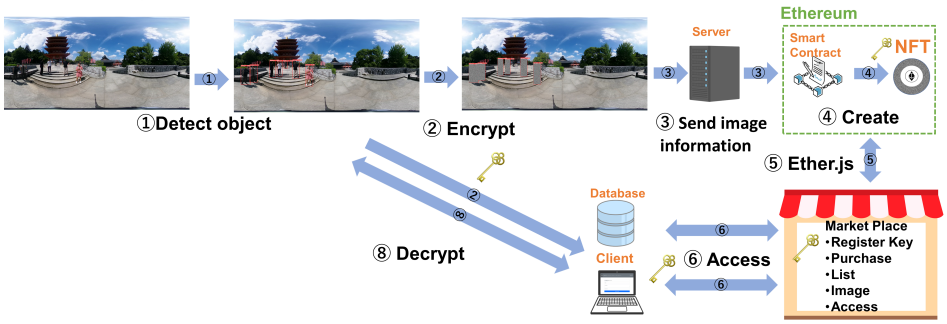

Fig. 4. Outline of our system

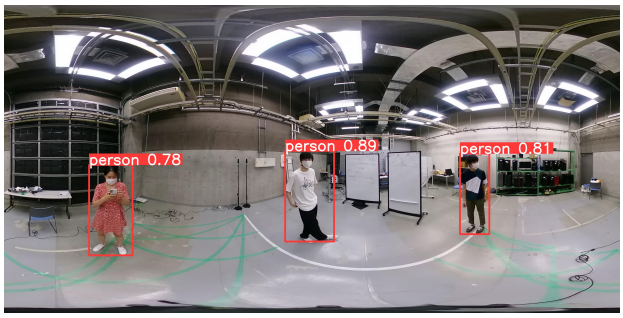

Fig. 5. Detected Object

4. Implementation

Figure 4 shows outline of our system. Server and client are not physically separated at this research. The first half are image processing sections such as detecting objects and

(a) Key **(b)** B **(c)** G **(d)** R **(e)** Merge

Fig. 6. Key and BGR images

encrypting the objects. The latter half shows how to create keys and ownership as NFTs as well as the flow of keys. Keys will move like the figure. Especially in the marketplace, it commands smart contracts as creating ownership of keys and key images. Besides, they ask for transferring ownership. We will describe each detailed process in the following section.

4.1. Object detection

We use a THETA Z1 from Ricoh as input images. The camera lens is focused on the center to avoid the influence of distortion at high and low latitudes when capturing an input image. Figure 5 shows the coordinate file and detected image generated by YOLOv5. Three people were detected accurately. However, objects at high and low latitudes are distorted.

4.2. Encryption

The process images to create an encrypted image for one detected person are depicted in Figure 6. The process is repeated for the other detected two persons. The detected areas are selected based on the coordinate file to create random sequences. The file contains information about the x and y coordinates in the upper left corner of the detected areas and the object's width and height. The size is the same as each detected area. These random sequences are converted into key images with only one channel because the sequences are based on a one-dimensional array. These images will become key NFTs in the next phase.

Besides key image generation, the red, green, and blue channel values are obtained from each object, and the XOR operation is performed for each channel and key image. We merged three encrypted images of each channel into one image and saved them as .png files because they can be compressed without any information loss. Thus, each pixel value can be fully restored when decrypting the images.

The image after successful encryption is shown in Figure 7. We also write ID numbers close to each detected area, such as key0, key1, and key2. These IDs will be used to check whether the held ownership corresponds to the key image.

Figure 8a is a successfully decrypted image with the right key. Figure 8b is decrypted image with the wrong key. When wrong key images are used, the incorrectly decrypted images cannot identify anything. Thus XOR cipher is the easiest way to image encryption and serves at least a minimum function.

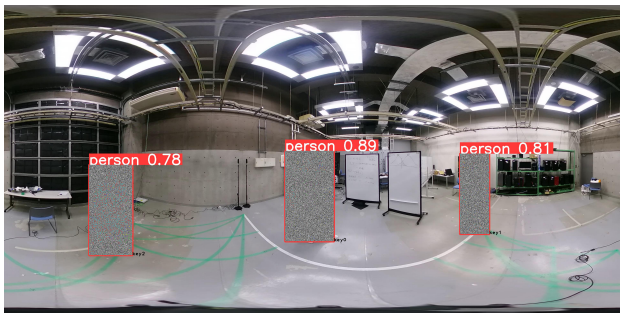

Fig. 7. Encrypted image

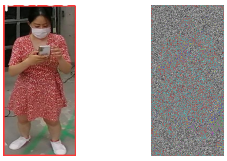

(a) Success **(b)** Fail

Fig. 8. Decryption

4.3. Database

During the encryption process, ImgID, KeyID, and the storage path of the encrypted image are registered in the relational database created by MySQL. Figure 9 shows example contents of these tables. ImgID is the image name, and KeyID is the ID assigned in Section4.2. Two tables are created using the ImgID as the primary key. Table accord includes detection coordinates (bbox data), ImgID, and KeyID. The table path is for storing the location of the encrypted image such as Fig.7. Bbox is the x and y coordinates in the upper left corner of the detected areas and the object's width and height. The detection coordinate values, and encrypted image paths stored in the database are utilized for decryption based on the input ImgID and KeyID information.

The first reason for using a database here is that encrypted images and detection coordinates do not require secure management. Secondly, blockchain is not good at inspecting information that has been registered in the past. Lastly, it leads to cost saving since issuing NFT of entire encryption images needs transaction fee. In addition, the reason for using the database and blockchain together this time is to simultaneously prove ownership and search and cite data. The blockchain makes it possible to clarify ownership and makes it difficult to tamper with whether ownership is retained. The database facilitates the search and citation of data registered in the past and enables the encryption and decryption of images.

4.4. WebSocket

In this research, WebSocket, a persistent connection between a client and server, is used for bridging process between Python and JavaScript. Python is used for image processing

Table path

ImgID	Path
0001	moji_0001.png
0002	moji_0002.png

Table accord

ImgID	KeyID	Accord
0001	0	2172 1077 40 91
0001	1	704 895 114 352
0001	2	1026 856 111 300
0001	3	567 931 205 448
0002	0	324 957 160 343
0002	1	145 060 195 380
0002	2	892 868 105 305

Fig. 9. Database table

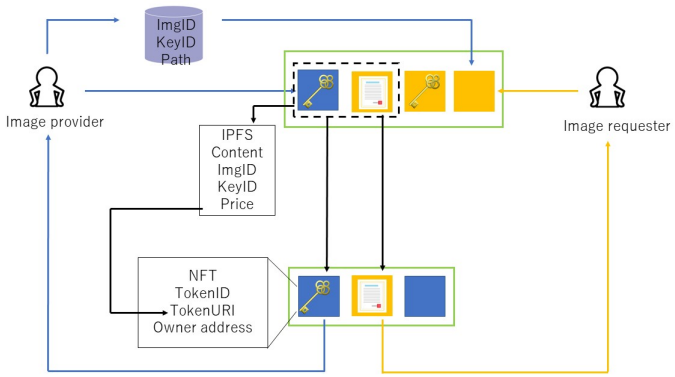

Fig. 10. Register

including object recognition, encryption and decryption. JavaScript is used for building the marketplace and connecting to Ethereum. The Python processing side would obtain related data such as ImgID and KeyID when marketplace asks for image decryption. Then, Python side will send back decryption image to marketplace.

4.5. Data flow

Figure 10 shows the data flow of a key image, key NFT and ownership NFT. This section shows the process by which a key image becomes a key NFT and how the key NFT is disseminated to users.

The image provider is the holder of the original image. The image requester is the user who wishes to obtain the original image. In step 1, the image provider converts the key image to NFT via the marketplace. Step 2 to step 4 is the data flow for the image requester side. The goal during these steps is that encrypted image is decrypted using the key NFT. Step 2 is the ownership creation for acquiring the key NFT. Step 1 and step 2 are the process of creating the NFT. Step 1 and step 2 are storing ImgID, KeyID and image contents which is for step 1 in IPFS.

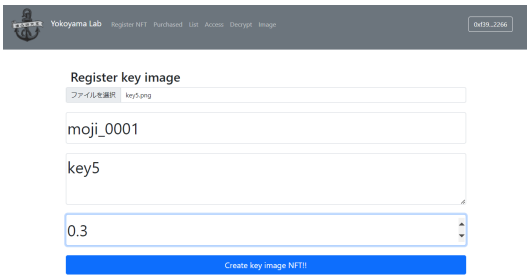

Fig. 11. Register

After the registration to IPFS is successfully completed, a URI is issued. This URI will be included in the metadata of the NFT. The owner address of the person who applied for the issuance of the NFT is also stored. When a key NFT is issued, it is the address of the image provider, and when an ownership NFT is issued, it is the address of the image requester. The address here is the address assigned to the MetaMask in this research.

Step 3 is the purchase of the key NFT. KeyID and ImgID information is obtained from the URI of the ownership NFT and the key NFT. The key NFT can be purchased only when the KeyID and ImgID of the two NFTs match.

In step 4, encryption processing is applied to the target area based on the purchased NFT. The KeyID and ImgID information is obtained from the URI of the purchased key NFT. Once those two IDs are obtained, the IDs are searched in the database and get data of path to an encrypted entire image and bbox. The decryption of the target area is performed based on the entire image and bbox value.

4.6. User interface

We will show the main features of our marketplace. In this research, we made a simple user interface to test the working of the proposed method.

Register Figure 11 is a register page. The function allows key holders to register key images as NFTs and input information to be stored in the blockchain upon completion of the transaction. The input includes name, description, and appropriate price value as information. However, there is no re-write option. Though the price field can vary, the key holders must input the right name (image name) and description (key ID) to access the key image. When successfully registered, the minted images will appear on the List page.

Image The list of partially encrypted images is shown in Figure 12. The locally stored encrypted images are manually added. Moreover, these images do not require storage in a secure environment and are, therefore, not registered as NFTs.

However, this page will create ownership as NFT once the transaction succeeds. A name (image) and description (key ID) are required to get ownership. People requiring

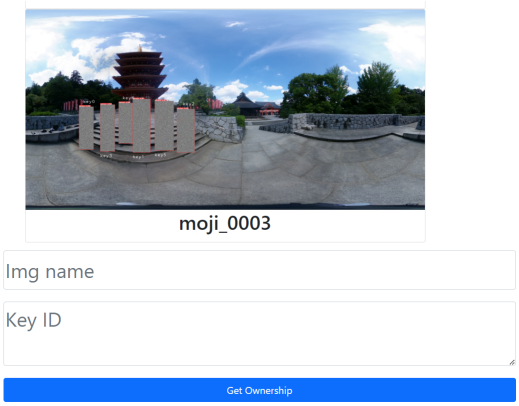

Fig. 12. Image

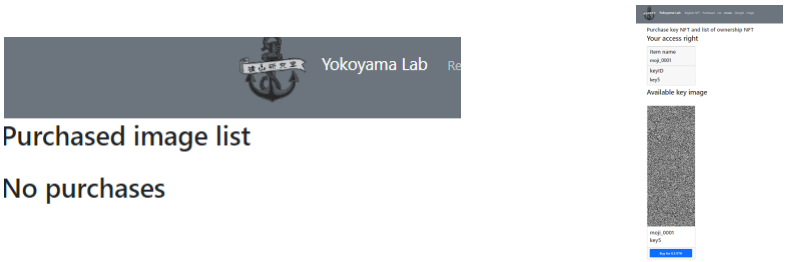

(a) No Key **(b)** Available key

Fig. 13. Access

ownership must input the name and description following the specific rules. For example, to acquire ownership of key0, the user needs to input img0 as name and key0 as description. The key will not be shown on another page if the wrong value is input.

Access The access page is shown in Figure 13.This page contains the ownership list and key images corresponding to the ownership. No images are screened when no ownership is obtained (Figure 13a). In contrast, key images appear when the name and description in ownership and key NFTs are matched (Figure 13b) using a linear search. The purchased key images are listed on the purchased list page. In this paper, connecting to the decryption page is overlooked. In the future, a new function that sends only purchased images to the decryption function will be designed. When users do not buy the key images, image decryption cannot be achieved.

Decrypt The decryption page is shown in Figure 14. This page shows entire images which obtained ownership areas are decrypted. Currently, the areas that are not owned to access are mosaic-like, but in the future those areas are assimilated with the background so that the photo is natural. For example, for application to video services, assimilation

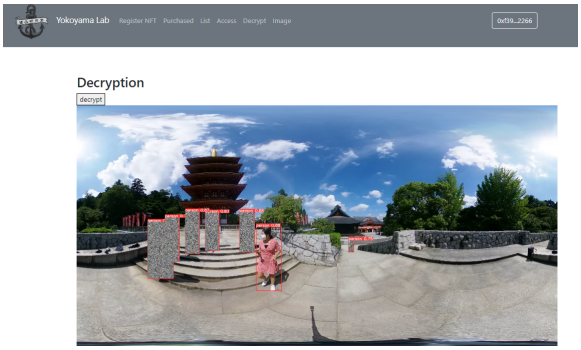

Fig. 14. Decrypt

by difference from the previous frame is being considered, and for difference in application to image services, assimilation methods that tconsider surrounding pixels are being considered.

5. Conclusion and Future Work

We proposed an ownership protection method for limited image regions by assigning different values to each area using blockchain. With this method, we achieve the following conditions.

- **Dividing**: Ownership to one image can be split corresponding to areas and each ownership can be shared with multiple people since users can apply for ownership on the image page. Besides, we can manage which key can be open to users on the register page.
- **Affinizing**: Key image holders can get financial profit by Eth every time a user buys the image. Besides, this earned Eth can be used to buy other keys or use different platforms. Moreover, as a merit for key holders, key holders can decide the value; for example, when the area is more valuable, key holders can set a higher price.
- **Protecting**: Ownership is controlled safety. This method prevents image theft because only limited people having ownership can access the key images to decrypt. The blockchain stores the key images, excluding the third party for saving images. Image ownership is protected because programmed smart contracts transfer ownership.

However, further improvements in usability and security are required. The discussion in this study centered on how to trade ownership. Considering that resale or hacking of keys can occur, we would like to move in the direction of using this system as proof of ownership. When key images are circulated via screenshots, etc., it is possible to determine if the owner is the correct owner by asking whether the ownership NFT is present. Ultimately, the goal is to allow users who wish to use the commemorative images/video

service at tourist spots to send signals to the proposed method's system on their smartphones. And it allows users to purchase ownership rights to their own areas and obtain images/videos. In the future, the following aspects will be considered.

- **Image Encryption methods**: Other image encryption methods might be considered for more secure operation. Though we generated a random sequence by a random function, it might predict rules since the random numbers are pseudorandom. Since the XOR operation used is very simple, we are considering the use of other cryptographic methods such as AES ciphers and the use of JPEG-style layered structures.
- **Matching algorithms**: This study uses a linear search algorithm. Other algorithms, such as binary search algorithm, with improved calculation speed and less memory usage will be used to match ownership and key.
- **key management**: We manually input an partial encrypted image data on image page. We are thinking of using database to save all the images and automatically call it to the front side. The images are not necessary to be stored in blockchain. It dose not need to refer to security aspect since all important regions are concealed. Besides, it leads to cost saving since storing data in blockchain costs Eth.
- **Video application**: We have examined whether the proposed method can provide ownership protection for a portion of an image. In the future, we are considering applying the same process to video type. It is necessary to consider how to manage keys when processing for video. In this research, since it was an image, a new key was issued each time. However, the same key should be used to encrypt the same person on all frames in the case of video since it is better for users to purchase only one key for decryption.
- **New network**: All images need to be reset after testing in the local blockchain. Therefore, we aim to create a private Ethereum blockchain using Geth. Geth is Go Ethereum's[5] standalone CLI client implemented in Go Language. Go Ethereum is one of the three original implementations of the Ethereum protocol.
- **Token standard**: Though ERC721 is common for NFTs, several smart contracts need to be created. However, by combining one smart contract with ERC1155, gas fees can be reduced because the contracts can contain some definition of tokens.
- **Real-time processing**: In the future, we aim to process all steps in real-time. YOLOv5 can immediately detect objects from the input images sent from a camera. However, the delay in sending real-time images to the blockchain and creating each NFT should be investigated.
- **Improving user interface**: With current user interface, a user and key holder need to input image name and key ID by hand. This is not a user-friendly interface. Because they have to input one by one. Besides, there might be a mistake to type wrong text and create incorrect NFTs. To avoid human error and improve user experience, we will change the interface. For example, Name and key ID are automatically input when a user clicks the desire areas.

[5] https://geth.ethereum.org/

– **Mobile access**:In this study, MetaMask login is done using the chrome extension. Currently, it is not possible to log in using the extension from a smartphone browser. Therefore, a login page for smartphone users will be created in the future to allow access from smartphones.

References

1. Wang, H., Zheng, Z., Xie, S., Dai, H.N., Chen, X.: Blockchain challenges and opportunities: a survey. International Journal of Web and Grid Services 14, 352 – 375 (10 2018)
2. de Haro Olmo, F., Varela Vaca, A., Álvarez Bermejo, J.: Blockchain from the perspective of privacy and anonymisation: A systematic literature review. Sensors 20 (12 2020)
3. Kumar, N.M., Mallick, P.K.: Blockchain technology for security issues and challenges in iot. Procedia Computer Science 132, 1815–1823 (2018), https://www.sciencedirect.com/science/article/pii/S187705091830872X, international Conference on Computational Intelligence and Data Science
4. Saberi, S., Kouhizadeh, M., Sarkis, J., Shen, L.: Blockchain technology and its relationships to sustainable supply chain management. International Journal of Production Research 57, 1–19 (10 2018)
5. Pal, K., Yasar, A.U.H.: Internet of things and blockchain technology in apparel manufacturing supply chain data management. Procedia Computer Science 170, 450–457 (01 2020)
6. IBM: About ibm food trust (2019), https://www.ibm.com/downloads/cas/8QABQBDR
7. Szabo, N.: Formalizing and securing relationships on public networks. First Monday 2(9) (Sep 1997)
8. Nakamoto, S.: Bitcoin: A Peer-to-Peer Electronic Cash System (Oct 2008)
9. Buterin, V.: Ethereum: A Next-Generation Smart Contract and Decentralized Application Platform (2014)
10. Bahga, A., Madisetti, V.: Blockchain platform for industrial internet of things. Journal of Software Engineering and Applications 09, 533–546 (01 2016)
11. Redmon, J., Divvala, S., Girshick, R., Farhadi, A.: You Only Look Once: Unified, Real-Time Object Detection (May 2016)
12. Han, J., Park, C.S., Ryu, D.H., Kim, E.S.: Optical image encryption based on XOR operations. Optical Engineering 38(1), 47 – 54 (1999)
13. Zhang, Q., Ding, Q.: Digital image encryption based on advanced encryption standard (aes). In: 2015 Fifth International Conference on Instrumentation and Measurement, Computer, Communication and Control (IMCCC). pp. 1218–1221 (2015)
14. Sahoo, A., Mohanty, P., Sethi, P.C.: Image encryption using rsa algorithm. In: Udgata, S.K., Sethi, S., Gao, X.Z. (eds.) Intelligent Systems. pp. 641–652. Springer Nature Singapore, Singapore (2022)
15. Guan, Z.H., Huang, F., Guan, W.: Chaos-based image encryption algorithm. Physics Letters A 346(1-3) (Oec 2015)
16. Irfan, P., Prayudi, Y., Riadi, I.: Image encryption using combination of chaotic system and rivers shamir adleman (rsa). Computer Applications 123(6) (Aug 2015)
17. Wong, P.W.: A watermark for image integrity and ownership verification. In: Image Processing, Image Quality, Image Capture Systems Conference (1998)
18. Meng, Z., Morizumi, T., Miyata, S., Kinoshita, H.: Design scheme of copyright management system based on digital watermarking and blockchain. In: 2018 IEEE 42nd Annual Computer Software and Applications Conference (COMPSAC). vol. 02, pp. 359–364 (2018)
19. Ali Muwafaq, Alchaqmaqchee, a.S.N.A.: Design scheme for copyright management system using blockchain and ipfs. Computer and Degital Systems 10(1) (2021)

20. Khan, P.W., Byun, Y.: A blockchain-based secure image encryption scheme for the industrial internet of things. Entropy 22(2) (2020), https://www.mdpi.com/1099-4300/22/2/175
21. Jabarulla, M.Y., Lee, H.N.: Blockchain-based distributed patient-centric image management system. Applied Sciences 11(1) (2021), https://www.mdpi.com/2076-3417/11/1/196
22. Dedge, O., Shingade, R., Jagtap, A., Yadav, A., Kamble, A.: Image copyright protection system using blockchain. BULLETIN MONUMENTAL 21(2) (2021)
23. Rashid, Mamunur, M., Lee, S.H., Kwon, K.R.: Blockchain technology for combating deepfake and protect video/image integrity. Journal of Korea Multimedia Societ 24(8) (2021)
24. Khan, P.W., Byun, Y.C., Park, N.: A data verification system for cctv surveillance cameras using blockchain technology in smart cities. Electronics 9(3) (2020)
25. Wang, Q., Li, R., Wang, Q., Chen, S.: Non-fungible token (nft): Overview, evaluation, opportunities and challenges 123(6) (Oct 2021)
26. Benet, J.: Ipfs - content addressed, versioned, p2p file system (07 2014)
27. Steichen, M., Fiz Pontiveros, B., Norvill, R., Shbair, W., State, R.: Blockchain-based, decentralized access control for ipfs (07 2018)

Natsuki Fujiwara is a master's student of computer science at Tokyo Metropolitan University. Her work focuses specifically on managing the ownership of image/video data on blockchain.

Shohei Yokoyama is an associate professor at Tokyo Metropolitan University, a visiting associate professor at the National Institute of Informatics, and a research fellow at the University of Tokyo, Japan. He received a Ph.D. degree in engineering from Tokyo Metropolitan University in 2006. As a postdoctoral fellow, he joined the National Institute of Advanced Industrial Science and Technology in 2006. From 2008 to 2018, he was an assistant professor, a lecturer, and an associate professor at Shizuoka University. Since 2018, he has been an associate professor at Tokyo Metropolitan University. His work focuses specifically on data engineering and data science. His research interests include data communication on 5G networks and geo-social big data analysis.

Received: March 20, 2023; Accepted: August 10, 2023.

Computer Science and Information Systems 20(4):1707–1728 https://doi.org/10.2298/CSIS221125027L

Generative Adversarial Network Based on LSTM and Convolutional Block Attention Module for Industrial Smoke Image Recognition

Dahai Li[1,⋆], Rui Yang[1], and Su Chen[2]

[1] School of Electronics and Electrical Engineering, Zhengzhou University of Science and Technology
Zhengzhou 450064, China
ldadahai@163.com
yangrui2233@163.com

[2] Department of Mechanical and Electrical Engineering, Henan Vocational College of Water Conservancy and Environment
Zhengzhou 450002, China
chensssu@163.com

Abstract. The industrial smoke scene is complex and diverse, and the cost of labeling a large number of smoke data is too high. Under the existing conditions, it is very challenging to efficiently use a large number of existing scene annotation data and network models to complete the image classification and recognition task in the industrial smoke scene. Traditional deep learn-based networks can be directly and efficiently applied to normal scene classification, but there will be a large loss of accuracy in industrial smoke scene. Therefore, we propose a novel generative adversarial network based on LSTM and convolutional block attention module for industrial smoke image recognition. In this paper, a low-cost data enhancement method is used to effectively reduce the difference in the pixel field of the image. The smoke image is input into the LSTM in generator and encoded as a hidden layer vector. This hidden layer vector is then entered into the discriminator. Meanwhile, a convolutional block attention module is integrated into the discriminator to improve the feature self-extraction ability of the discriminator model, so as to improve the performance of the whole smoke image recognition network. Experiments are carried out on real diversified industrial smoke scene data, and the results show that the proposed method achieves better image classification and recognition effect. In particular, the F scores are all above 89%, which is the best among all the results.

Keywords: industrial smoke image recognition, generative adversarial network, LSTM, convolutional block attention module, data enhancement.

1. Introduction

Bad weather conditions will have an impact on our production and life. If the weather can not be accurately identified, timely judged, it will lead to the threaten to human life and property. The weather can change very quickly sometimes. In particular, fog, rain, snow, smoke, sand and other extreme weather will affect all walks of life [1,2]. Industrial smoke

⋆ Corresponding author

weather, as an important scene, widely exists in the daily life of big cities, and various tasks for the smoke scene have become very urgent, and gradually become one of the hot spots in computer vision area. In order to successfully complete the classification and recognition task of smoke and dust image, it is necessary to provide a sufficient number of manually labeled images for each specific smoke and dust scene in advance [3]. However, in practice, it costs a lot of cost to acquire enough diverse smoke labeled data samples. With the emergence of large amount of labeled training data and large amount of computing resources, deep neural network can achieve satisfactory performance. These data and deep neural network models can be directly and widely applied to image classification in most scenarios. However, when dealing with the classification of smoke scene, there will be a huge classification error. In order to make use of the existing conditions for image recognition of smoke scene [4], it is necessary to solve the problem of data distribution difference. However, the data distribution of smoke scene is more different from that of other conventional situations. At the same time, data with such a difference in distribution also have a larger domain shift. Convolutional neural networks are difficult to learn invariance features of data.

In view of the above problems, existing research methods provide some solutions, which are mainly divided into two categories. On the one hand, based on the existing convolutional neural network, combined with data enhancement methods, for example, PM-SNet (Robust haze removal based on patch map for single images) [5], DCPDN (densely connected pyramid dehazing network) [6] remove haze to reduce the distribution difference between haze and normal scenario data. However, most fog removal algorithms require a large number of paired images for training. Due to the particularity of fog environment, fog scene images in the training data are mostly synthetic, so it is difficult to reduce the distribution difference in the pixel field. According to Huang et al, [7] data enhancement using fog removal algorithm has no significant gain in fog classification and recognition task in real scene. And collecting and generating more data will increase training time and cost. In addition, atmospheric degradation model is used to train the data. However, this method is difficult to apply to the true diversity of fog scenes.

On the other hand, it is difficult to extract invariable features in feature domain only by using data enhancement-based deep neural network due to different distribution between different data sets. The domain adaptive algorithm can reduce the domain offset and learn invariance features of different data. Existing domain adaptive algorithms use different feature alignment methods to align features extracted from convolutional neural networks, and some methods reduce domain offset based on maximum mean difference. For example, DANN (Domain Adaptive Neural Network) [8] used maximum mean difference measurement to reduce feature distribution between two hidden layers by samples extracted from different domains. Deep domain confusion (DDC) [9] used an adaptation layer to connect two parallel CNN (convolutional neural Network [10,11]) models, and utilized MMD (Maximum Mean Discrepancy) to define the loss function and narrow the domain offset of source domain and target domain. Based on CORAL method, the nonlinear transformation method was used to align the second-order statistical features of source domain and target domain distribution. Another adversarial approach, such as DANN-A (Domain-Adversarial Training of Neural Networks) [12], used adversarial networks to obtain domain-invariant features. Most of the existing domain adaptive algorithms focus on the edge distribution of aligning single feature. A single feature only represents the

characteristic information of a small part of data. Some adaptive algorithms will appear unstable training and poor robustness when there is a large field offset.

To solve the above problems, Zhao et al. [13] used CycleGAN (Unpaired image-to-image translation using Cycle-consistent Adversarial Networks) for data enhancement. On the one hand, data enhancement can be carried out in the normal scenario (source domain) to generate labeled data with a style similar to that in the fog scenario. Cycle-GAN used conventional data and foggy scene data (target domain) for antagonistic training, which could reduce the data distribution difference between them in pixel domain. Since Cycle-GAN did not need to use paired images and additional data, which greatly saved training time and training cost.

Chen et al. [14] proposed an effective adaptive network, namely multi-scale featuresand multi-adversarial network (MFMAN) and proposed an IAM (Inception adversarial) network to fully align data distribution in feature domain and reduce field offset (perceptual adversarial module). After feature extraction by convolutional neural network, IAM was used to extract multiple features of different scales to replace a single feature. Feature information extracted by convolutional neural network was fully utilized to form adversarial by multiple domain discriminators to reduce feature distribution differences. In order to make use of the complex multi-mode structure, Karnewar et al. [15] used multiple discriminators to learn the multi-mode structure of data distribution on the category, which increased the discriminant ability of the category, thus increasing the positive migration and reducing the negative migration. Features could reduce domain differences in each category and learn domain invariance features.

Our main contributions are as follows.

- We set up a new industrial smoke data set. a low-cost data enhancement method is used to effectively reduce the difference in the pixel field of the image.
- The smoke image is input into the LSTM in generator and encoded as a hidden layer vector. This hidden layer vector is then entered into the discriminator.
- Meanwhile, a convolutional block attention module is integrated into the discriminator to improve the feature self-extraction ability of the discriminator model, so as to improve the performance of the whole smoke image recognition network.

The remaining paper is shown as follows: Section 2 presents the related works in detail. Section 3 discusses the data sets used in this paper. Generator model based on encoder-decoder framework and Discriminator are stated for the proposed method in section 4 and section 5 respectively. In Section 6, experiments are conducted and analyzed. The paper is concluded in Section 7.

2. Related Works

Image segmentation is a basic computer vision technology. Its purpose is to divide an image into visually meaningful areas with similar properties, such as mountains and people, according to the features of color, texture, gray level and motion. Because of its fundamental role in the field of computer vision, image segmentation plays an important role in image understanding, content-based video compression and coding, content-based image and video retrieval, etc [16].

In recent years, scholars have carried out a large number of relevant researches on this task, which can be divided into traditional digital image processing method and deep learning method according to different research methods.

In image segmentation method, threshold technique [17] is a simple and effective method. The basic idea of threshold segmentation is as follows. First, it obtains the gray histogram corresponding to the image, and then determines a gray threshold value according to the histogram information as the basis of segmentation. Finally, pixel points in the image whose gray value is greater than the threshold value are classified into one class (such as the target region), while pixel points in the image whose gray value is less than or equal to the threshold value are classified into another class (such as the background region).

At present, there are two common threshold segmentation methods: bimodal method and maximum variance method [18]. Bimodal method means that the background and the object of concern in the image form a crest respectively on the gray histogram of the image, that is, the region corresponds to the crest one by one. In this way, as long as the gray value corresponding to the trough between the two wave peaks is selected as the threshold, the object and the background can be separated well. Bimodal method is applicable to the grayscale distribution of each object in the image is relatively regular, and many soot images do not conform to this situation. The maximum variance method can automatically select the threshold value without manual parameter setting, and the selected threshold value can obtain better segmentation effect in most cases.

The threshold segmentation algorithm of the maximum variance method is described as follows. It is assumed that the image to be segmented contains two types of regions: Region 1 and Region 2. t is set as the threshold for separating two regions, and according to histogram statistics, the area ratio of region 1 and region 2 separated by t to the whole image is θ_1 and θ_2:

$$\theta_1 = \sum_{j=0}^{t} \frac{n_j}{n} \tag{1}$$

$$\theta_2 = \sum_{j=t+1}^{G-1} \frac{n_j}{n} \tag{2}$$

Where n is the area of the whole image. n_j is the corresponding area when the gray level is j. The average gray level of Region 1, Region 2 and the whole image is μ_1, μ_2 and μ:

$$\mu_1 = \frac{1}{\theta_1} \sum_{j=0}^{t} (f_i \times \frac{n_j}{n}) \tag{3}$$

$$\mu_2 = \frac{1}{\theta_1} \sum_{j=t+1}^{G-1} (f_i \times \frac{n_j}{n}) \tag{4}$$

$$\mu = \sum_{j=0}^{G-1} (f_i \times \frac{n_j}{n}) \tag{5}$$

Where f is the gray value corresponding to gray j.

The variance between the two regions after the image is segmented by the threshold value is shown as follows:

$$\sigma_B^2(t) = \theta_1(\mu_1 - \mu) + \theta_2(\mu_2 - \mu) \tag{6}$$

When the variance between the two divided regions reaches the maximum, it is considered that the two regions have reached the best separation state, and the corresponding threshold t is the best threshold T to be found.

$$T = max\lfloor\sigma_B^2(t)\rfloor \tag{7}$$

At present, deep networks such as convolutional neural networks (CNN) are widely used in image classification, object detection and other tasks, and have achieved higher accuracy than traditional digital image processing methods. Although it requires a large amount of data to train the deep network, it has the advantage of better adaptability and provides an end-to-end solution, that is, the data from the input end can be directly obtained from the output end, avoiding multiple steps such as image preprocessing and result repair, which are often used in the process of digital image processing methods to divide smoke and dust. The method of using deep network model to detect soot in image includes target detection and semantic segmentation.

Object detection is a detection method based on candidate region. For example, Teng et al. [19] applied Faster R-CNN to video smoke detection, avoiding the complicated artificial feature extraction processing in traditional smoke detection methods. Firstly, the training data set was expanded by stitching smoke for forest and other scene images, so as to train the classifier to carry out target detection of smoke. Wu et al. [20] proposed a smoke detection method combining mixed Gaussian model and YOLOV2 network. Firstly, the mixed Gaussian algorithm was used to determine the approximate soot region, and on this basis, the YOLO network was trained to predict the final soot region. The result of target detection was to determine the soot area in the image with a rectangular frame, which leaded to the inevitable inclusion of a large number of background areas in the result, which would affect the subsequent calculation result of pollution level based on the Ringelmann smoke blackness level.

The semantic segmentation method classifies each pixel so as to achieve pixel level segmentation of image target area. Li et al. [21] used the fully convolutional network model for target segmentation of soot image. By manually marking the smoke region in the smoke image to make a data set, and then training the fully convolutional network, the trained model could predict the smoke image and give pixel-level smoke segmentation results. Wang et al. [22] designed a network model containing two branches of rough segmentation and fine segmentation, both adopted a fully convolutional network with encoding and decoding structure. Li et al. [23] adopted a conditional generation adversarial network model to segment smoke regions in continuous video frames. Although the method based on the fully convolutional network has achieved a high accuracy, the segmentation accuracy in complex scenes needs to be improved. For example, the interference of clouds with high similarity to soot in the background will affect the segmentation, and it is often a problem to judge a part of the area belonging to clouds as soot. Therefore, we propose a novel generative adversarial network based on LSTM and convolutional block attention module for industrial smoke image recognition.

3. Data Sets

According to experimental requirements, real industrial smoke scene classification data set and normal scene classification data set are needed for training and testing. Currently, some larger public datasets, such as Caltech-256, PASCALVOC (Pattern Analysis, Statistical Modeling and Computational Learning Visual Object Classes) and ImageNet are mainly normal image scenarios. Image data sets in normal scenarios used in this paper are mainly from these large open source datasets, and 12 categories are extracted to form a Normal-12 set. This data is usually easy to obtain and does not require annotation. Smoke images are mainly obtained from images and videos on the Internet, they are manually classified and labeled, and named as Smoke-12 set. Smoke image data sets cover most industrial scenes. Normal-12 has 4800 images including 3600 images for training set and 1200 images for test set. Smoke-12 has 2400 images as target domain data. Detailed information of images is shown in table 1, and Figure 1 shows partial images in the dataset.

Table 1. Samples in the data sets

Name	Normal-12 train	Normal-12 test	Smoke-12
truck	270	95	170
tree	300	103	200
train	307	100	220
streetlamp	290	95	180
people	300	100	195
car	301	100	210
bus	282	92	190
building	306	102	200
bridge	315	104	215
boat	300	100	200
bird	301	100	182
plane	328	111	238
total	3600	1200	2400

Cycle-GAN algorithm [24] is used for data enhancement, as shown in Figure 2. The structure consists of a pair of generator networks and a pair of discriminator networks. A group of unaligned images are input for training to learn the pixel-level mapping between input images and output images, and the images are converted from source domain A to target domain B. The goal is to learn a map G_AB: $A \rightarrow B$ and use the discriminator D_B to narrow the distribution between Fake_B and B. Similarly, in G_BA: $B \rightarrow A$, the discriminator D_A is used to narrow the distribution of Fake_A and A, and a cyclic consistency loss is introduced to enforce $F(G(A)) \approx B$. When cycle-GAN is used for processing data enhancement, Normal-12 is used as source domain A, Smoke-12 serves as the target domain B. Through such a cyclic adversarial network structure, labeled data similar to the smoke scene style, namely Fake_B, can be obtained, and at the same time, the distribution differences of data in the two scenes can be initially reduced in the pixel domain.

Fig. 1. Some samples in data sets

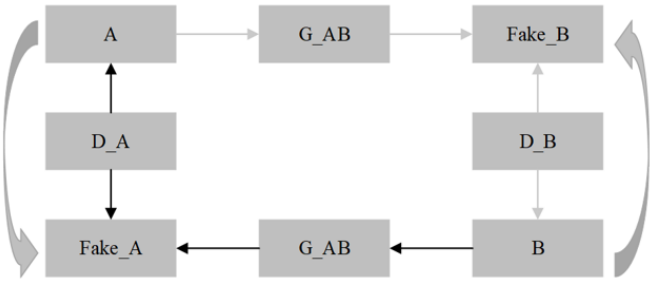

Fig. 2. Cycle-consistent adversarial network structure

4. Generator Model Based on Encoder-Decoder Framework

This section introduces the generator model G of Encoder-Decoder framework based on LSTM in detail. The purpose of the model is to learn the distribution function P_g of the generator on sample data. The distribution function of real samples is P_{data}. First, it inputs image S into LSTM (named EnLSTM) in Encoder stage, and obtains hidden layer vector with fixed dimension after encoding. Then, the hidden layer vector is input into LSTM (named DeLSTM) in Decoder stage [25]. The hidden layer vector at t moment is generated by combining the output at $t-1$ moment, and the generated sequence y is finally decoded. The mapping process is expressed as $G(S,\theta)$. θ is the parameter of LSTM. The generator model structure is shown in Figure 3. In the following, we give the detailed Encoder process and Decoder process in Generator.

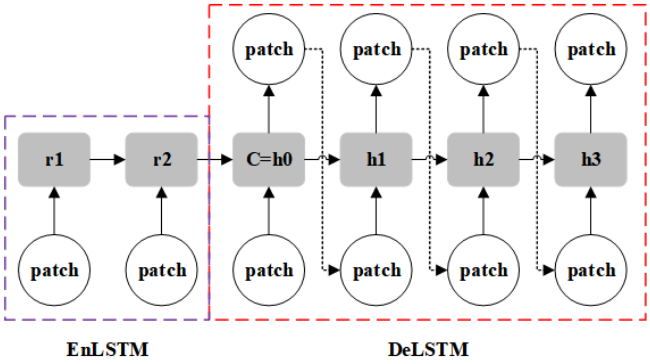

Fig. 3. Generator model

4.1. Encoder

As shown in Figure 3, the left purple box is the Encoder process. The $i-th$ image slice in S is denoted as s_i, slice sequence $S = s_1, s_2, \cdots, s_t$ is defined as EnSen. Then, the input is sequentially into EnLSTM, and a slice vector is input for each time step t. The hidden layer vector r_t at the current moment t is determined by the hidden layer vector r_{t-1} at the $t-1$ moment and the input s_t at the current moment. LSTM has the ability to remove or add information to a hidden state. LSTM includes three gate structures, namely, forgetting gate, input gate and output gate. First, the forgetting gate layer decides to discard some information:

$$f_t = \sigma(W_f \cdot [r_{t-1}, s_t] + b_f) \tag{8}$$

Where W_f is the weight that decides to forget the information and b_f is the bias value.

The input gate determines what information is to be updated. This step has two parts: First, the Sigmoid layer, called the input gate layer, determines what values are to be

updated. Then, it creates a new candidate value vector $\tilde{C}_t$ through tanh layer and adds it to the state, namely:

$$i_t = \sigma(W_i \cdot [r_{t-1}, s_t] + b_i) \tag{9}$$

$$\tilde{C}_t = tanh(W_c \cdot [r_{t-1}, s_t] + b_c) \tag{10}$$

W_i and W_c are the weights of Sigmoid layer and tanh layer respectively. b_i and b_c are the offset values. Based on the above calculation, the updated status information is:

$$C_t = f_t \cdot C_{t-1} + i_t \cdot \tilde{C}_t \tag{11}$$

Finally, the output information is determined through the output gate, and then the vector representation of the output information is obtained as shown in formula (12) and formula (13):

$$o_t = \sigma(W_o \cdot [r_{t-1}, S_t] + b_o) \tag{12}$$

$$r_t = o_t \cdot tanh(C_t) \tag{13}$$

W_o is the weight that determines the output information. b_o is the offset value. After the above coding, a hidden layer vector sequence $r = r_1 : r_t$ is obtained. When it is input to end flag (EOS), the final semantic vector r_c is generated. r_c is input to the decoder stage as the initial vector.

4.2. Decoder

The red box on the right in Figure 3 is the Decoder network structure diagram of the generator model. In this stage, the semantic vector r_c obtained in the Encoder stage is first input into DeLSTM, which is denoted as h_0 as the hidden layer vector at the initial t_1 moment. Then it is decoded to obtain the output y_0 at time t_1. At time t_1, the input of DeLSTM is the output y_1. Then the hidden layer vector h_2 at time t_2. We use the same method to obtain the each hidden layer vector at t moment. Then through the three gate operations of DeLSTM such as formulas (8)-(13), the implicit vector sequence $h = [h_0 : h_1]$ of DeLSTM is obtained. Then, the hidden layer vector at time t is input into a Softmax function to generate a probability distribution of N words in the image description dictionary C, so that each word in the dictionary at time t belongs to $n(1, \cdots, N)$ the probability of class words. For example, the dictionary size is $V :< W_{o1}^t, W_{o2}^t, \cdots, W_{oV}^t >$, so:

$$P(W_{oV}^t = n|EnSen, \theta) = \frac{exp(\omega_n^T h_t)}{\sum_{n=1}^{N} exp(\omega_n^T h_t)} \tag{14}$$

Where ω_c is the weight matrix of decoder LSTM from the hidden layer to the output sequence. These probability values can be further obtained by an Argmax function to obtain the output sequence $y_1, y_2, \cdots, y_t$, defined as DeSen. o is the parameter to generate the LSTMs in the model. This process predicts the image slice y_t of the next output according to the given semantic vector r_c and the previously generated output sequence $y_1, y_2, \cdots, y_{t-1}$, that is:

$$y_t = argmaxP(y_t|y_1, y_2, \cdots, y_{t-1}, r_c, h_t) \tag{15}$$

Equation (15) can be abbreviated as:

$$y_t = g(y_{t-1}, h_t, r_c) \tag{16}$$

Where h_t is the hidden layer vector of DeLSTM. y_{t-1} is the output of the previous moment. g is a nonlinear multilayer perceptron that generates the probability that each slice in dictionary C belongs to y_t.

5. Discriminator Based on Convolutional Block Attention Module (CBAM)

5.1. Generative Adversarial Network (GAN)

The traditional generative adversarial network (GAN) [26] consists of a generator (G) and a discriminator (D). G is to generate sample data similar to or even consistent with real samples according to the characteristics of real samples, so as to supplement the lack of sample types and achieve a balance of sample distribution. D is to supervise the quality of the generated samples and judge whether the generated samples are consistent with the characteristics of the real samples, so as to achieve the purpose of expanding the number of samples. For generator G, the data input only contains the generated sample, so the objective function of G is:

$$min_G L(G) = minE[logP(S = F_{fake}|X_{fake})] \tag{17}$$

Where S stands for data source. X_{fake} represents the sample generated by the generator. $P(S = F_{fake}|X_{fake})$ represents the probability that the generated sample belongs to the generated sample data source. E is the expectation calculation. According to Formula (10), the optimization goal of G is to make the probability of the generated sample being judged as "false sample" as small as possible. When enough samples are generated to "look like real", the optimization goal is completed. For D, data input includes both real samples and generated samples, and its objective function is shown in Equation (18).

$$min_D L(D, G) = maxE[logP(S = R_{real}|X_{real})] + E[logP(S = F_{fake}|X_{fake})] \tag{18}$$

Where X_{real} represents the real sample. $P(S = real|X_{real})$ represents the probability that the real sample belongs to the real sample data source. Its optimization objective is: whether the input is real sample or generated sample, the final result can give the correct judgment. In the process of training, GAN plays a game with each other through alternate optimization and finally achieves Nash equilibrium to complete the model training.

5.2. GAN-CBAM

The results of sample source and sample label judgment are output by D, and the performance of D determines the overall performance of GAN. Therefore, in this paper, CBAM [27] is added to the feature extraction network of D to focus on the detailed features in all kinds of transient SPM tracks, so as to improve the feature capture ability of the discriminator network and make it better calculate training errors.

CBAM can be divided into channel attention network and spatial attention network. Firstly, average pooling and maximum pooling are used to aggregate the whole channel information to generate two different spatial features F_{avg} and F_{max}. Then, the results are weighted through the multi-layer perceptron (MLP) [28] network containing a single implicit layer, and the parameter distribution weights of each channel are obtained. The calculation process is shown in Figure 4.

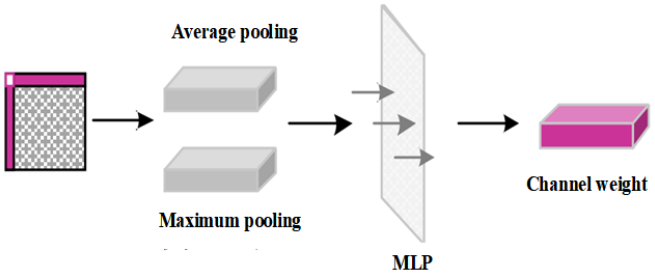

Fig. 4. Schematic diagram of channel attention

The calculation expression is shown below:

$$M_C(F) = \sigma(MLP(avgPool(F)) + MLP(maxPool(F))) \tag{19}$$

Where F represents the input convolution feature. σ stands for sigmoid function. MLP processes parameter sharing.

The output of channel attention is used as the input of spatial attention. As shown in Figure 5, maximum pooling and average pooling are performed for the data at each position in the feature matrix of each channel. And then convolution dimension reduction aggregation is performed for the two pooled results. Finally, sigmoid function is used to get spatial attention feature.

The expression of feature calculation is:

$$\begin{aligned} M_C(F) &= \sigma(f^{7\times7}([AvgPool(F); MaxPool(F)])) \\ &= \sigma(f^{7\times7}([F^S_{avg}\cdot; F^S_{max}])) \end{aligned} \tag{20}$$

f stands for dimensionality reduction convolution. In general, 7×7 convolution kernel dimension reduction convolution calculation is adopted (the size of the eigenmatrix before and after convolution remains unchanged by adding 0).

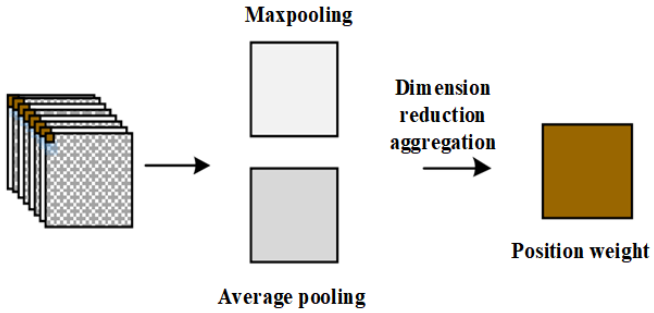

Fig. 5. Diagram of spatial attention

5.3. Loss Function and Training Process

The proposed GAN loss function in this paper consists of the global discriminator loss function, the local discriminator loss function and the tag predictor loss function, which is defined as:

$$L(\theta_f, \theta_m, \theta_y, \theta_d, \theta_d^c|_{c=1}^C) = L_y + \lambda(L_g + L_l) \tag{21}$$

Where θ_f is the backbone network parameter. θ_m is LSTM feature parameter. θ_y is tag classifier parameter. θ_d is global discriminator loss. θ_d^c is local discriminator loss. λ is the hyperparameter, which is used to determine the proportion of local loss and global loss in the total loss.

$$\theta_f \leftarrow \theta_f - \mu(\frac{\partial L_y}{\partial \theta_f} - \lambda(\frac{\partial L_g}{\partial \theta_f} - \frac{\partial L_l}{\partial \theta_f})) \tag{22}$$

$$\theta_m \leftarrow \theta_m - \mu(\frac{\partial L_y}{\partial \theta_m} - \lambda(\frac{\partial L_g}{\partial \theta_m} - \frac{\partial L_l}{\partial \theta_m})) \tag{23}$$

$$\theta_y \leftarrow \theta_y - \mu\frac{\partial L_y}{\partial \theta_y} \tag{24}$$

$$\theta_m \leftarrow \theta_m - \mu\frac{\partial L_m}{\partial \theta_m} \tag{25}$$

$$\theta_d \leftarrow \theta_d - \mu\frac{\partial L_g}{\partial \theta_d} \tag{26}$$

$$\theta_d^c \leftarrow \theta_c^c - \mu\frac{\partial L_l}{\partial \theta_d^c} \tag{27}$$

Where μ is the learning rate.

Stochastic gradient Descent (SGD) is used as the optimizer in the optimization process. However, in Formula (22), the discriminator loss is opposite to the label classifier sign loss. The discriminant loss will make the field offset of the two data bigger and bigger, the purpose of confrontation cannot be achieved. Similar some other optimizers, such

as Adagrad, Adaelta, cannot be optimized, so GRL(Gradient Reversal Layer) is added here. The network layer has no parameters related to it, so it is a normal connection layer in forward propagation and does not affect network propagation. During the back-propagation, the sign of the gradient will be changed, it is multiplied by -1, and then the back-propagation will continue. The purpose of reversing the gradient will be achieved through this network layer, so that optimization can be carried out using the optimizer.

6. Experiments and Analysis

The proposed dataset Normal-12 and Smoke-12 are used here, as shown in Figure 1 for a partial sample dataset. It contains a large number of industrial smoke scenes with different concentrations. The data set is diverse and industrial smoke images are mostly taken from common scenes in daily life. 3600 images in Normal-12 are selected as the original data. 1200 images are selected as the test set of data for training the basic classification network, and 2300 images in Smoke-12 are selected as the target data set of smoke classification and recognition.

The hardware configuration of the experimental platform is Intel(R) Xeon (R) Gold5118 CPU @ 2.30ghz, memory 256 GB, NVIDIATesla(16 GB) graphics card, software configuration is Centos7.5 using pytorch deep learning framework. Images are cropped to 256×256 pixels, and then it uses the Random Crop to randomly crop them to 224×224 pixels. Batch size is set to 128. The initial learning rate of the pre-trained backbone network is 0.001. The initial learning rate of other network layers is 0.01. The learning rate change strategy follows the existing work, the weight attenuation is 0.0005, the momentum is set as 0.9, and there are 50 training rounds in total. Based on the existing experience, grid search experiment is carried out with parameters ranging from 0 to 1. When λ is 0.3 on this data set, the convergence is faster and the accuracy is higher. The experiment mainly tests the ratio of the accurate prediction quantity of each category to the category quantity in the target domain as the category accuracy. The ratio of the number of accurate predictions of all categories to the number of smoke scene data is taken as the total accuracy.

In order to effectively evaluate the effectiveness of the proposed algorithm in smoke data set classification, the GAN is used as the basic classification network and the backbone network. In order to verify the effectiveness of adding CBAM and LSTM modules and the effectiveness of data enhancement, ablation experiments are conducted on the basic classification network for different data enhancement methods. The selected basic classification networks include GAN, MCW [29], ALSTM [30], KutralNext [31].

In order to verify that the new GAN is more effective than other image recognition algorithms in data enhancement, Normal-12 is used as the training set and Smoke-12 is as the test set. Firstly, data enhancement is performed on test set smoke-12. Classical and current mainstream recognition algorithms are used including EDL [32], DDCNN [33], EPHD [34]. In contrast, proposed GAN performs data enhancement [35] on training set Normal-12 and generates data similar to Smoke scenes for testing on Smoke-12.

To verify the segmentation effect of the method on smoke in different scenarios, the images of the test set are divided into five scenarios: easily distinguishable scene, the small-area smoke scene, the thin smoke scene, the multi-objective smoke scene, and the cloud interference scene, as shown in Figure 6.

Fig. 6. Scene classification scheme (from right to left: easily distinguishable scene, the small-area smoke scene, the thin smoke scene, the multi-objective smoke scene, and the cloud interference scene)

GAN is the result of using normal-12 as the training set and smoke-12 as the test set in Table 2. It can be seen from Table 2 that MCW, ALSTM, KutralNext algorithms have an increase of 0.8%, 1.5% and 1.9% in classification accuracy compared with GAN respectively. The DCP algorithm shows a 1.6% decrease. According to the experiment, it can be seen that it is difficult to achieve good results in the real diversified smoke scene by using the algorithm of defogging data enhancement. The recognition model developed from the synthetic smoke data set used by most recognition algorithms will over-fit on the synthetic data set and fail to narrow the distribution of the pixel field. Recognition algorithms will cause some information loss in the image. According to the results of proposed GAN in Table 2, the new GAN data enhancement can achieve the best results in three basic classification and recognition networks, and the accuracy is significantly improved compared with direct recognition of foggy images.

Table 2. Data enhancement with different methods/%

Method	GAN	MCW	ALSTM	KutralNext	Proposed
truck	58.5	53.9	53.3	55.0	65.5
tree	92.1	98.2	95.6	97.7	98.1
train	45.7	56.4	66.1	71.4	72.9
streetlamp	94.8	87.2	90.7	93.6	94.5
plane	81.4	79.7	88.8	81.9	91.8
car	51.8	54.7	49.8	41.2	62.5
bus	33.1	33.6	46.7	48.2	49.9
building	76.8	90.6	88.2	90.6	91.7
bridge	97.2	93.9	93.5	94.6	98.2

According to the experimental results in Table 3, the classification accuracy of CBAM module is improved by 3.3%. The dual channel can fully align the feature distribution in the feature domain and effectively reduce the field offset.

Figure 7 and table 4 shows the change curve of the proposed GAN loss in the industrial smoke data set. It can be seen from Figure 6 that the loss curve of the training set is ideal

Table 3. Classification accuracy after processing with proposed GAN/%

Method	GAN	EDL	DDCNN	EPHD	Proposed
truck	65.5	64.9	70.8	71.2	72.7
tree	94.1	95.6	95.8	96.2	97.3
train	72.4	78.2	81.6	80.2	96.1
streetlamp	94.2	88.9	89.5	91.3	95.5
plane	91.8	91.1	92.3	92.4	94.6
car	62.5	69.3	71.4	72.5	73.8
bus	54.6	46.5	53.8	58.1	62.2
building	91.6	91.8	92.3	92.7	94.1
bridge	98.2	99.1	97.2	98.5	99.1

and the network fitting speed is fast. In 10 epoches, the training is relatively stable, the network convergence speed is fast, and there is no fitting phenomenon.

Table 4. The training loss

epoch	0	10	20	30	40	50
loss	1.12	0.52	0.50	0.48	0.48	0.48

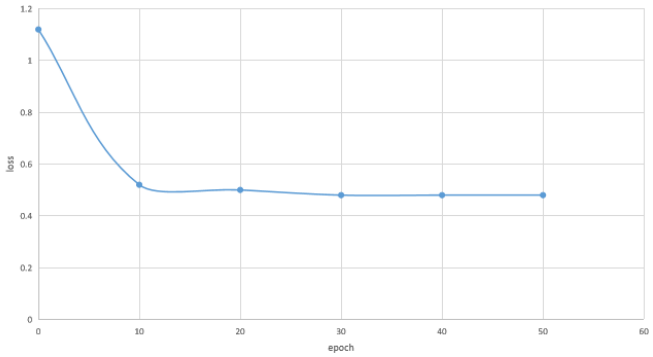

Fig. 7. The curve of training loss

In order to quantitatively analyze the recognition and segmentation results of industrial smoke, Precision, Recall, F-score, Accuracy [56] and Intersection over Union (IoU) [35] are selected as the evaluation indexes.

The same smoke data set and hyperparameter are used to train four models respectively, and then tested on the test sets with the five scenes. The comparison of recognition results is shown in figures 8-12. (a) is the original image, (b) is the result of manual marking, (c) is the EDL model, (d) is the result of DDCNN, (e) is the result of EPHD, and (f)

is the result of the Proposed method. The quantitative index pairs of test results are shown in Tables 5-9.

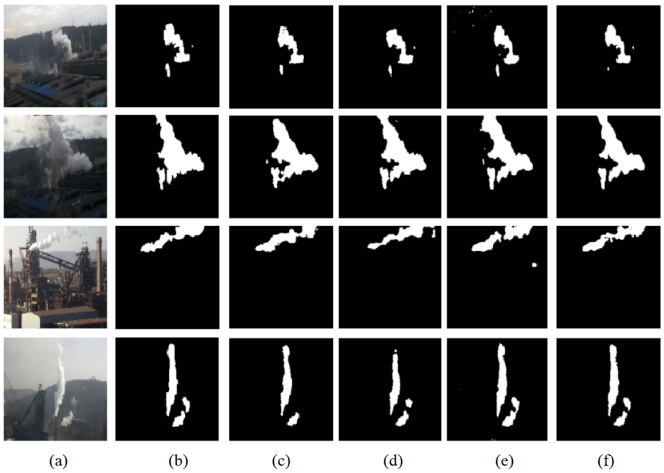

Fig. 8. Comparison on easily distinguishable scene

Table 5. Comparison result of easily distinguishable scene

Index	EDL	DDCNN	EPHD	Proposed
IoU/%	68.26	69.52	84.12	83.74
Precision/%	88.18	86.68	91.24	92.23
Recall/%	75.96	78.82	92.49	91.18
F1-score/%	81.61	84.98	91.86	91.70

6.1. Experimental Results and Discussion

1. In the comparison of distinguishable scene recognition results, interference points appear in the results of EDL, and a part of the background region is segmented. DDCNN has the problem of missing small areas, which leads to incomplete recognition results. There is a small amount of interference in EPHD results. The method presented in this paper is the most accurate.
2. In the comparison of small area smoke scene recognition results, a part of non-smoke area is segmented by EDL. The segmentation result of DDCNN is not accurate, the result is incomplete and the problem of false recognition occurs. EPHD also has some inaccurate results. The method in this paper is the most accurate.
3. In the comparison of thin smoke scene recognition results, EDL has the problem of identifying the background of small areas as smoke. DDCNN results are incomplete. The results of EPHD and the proposed method are relatively accurate.

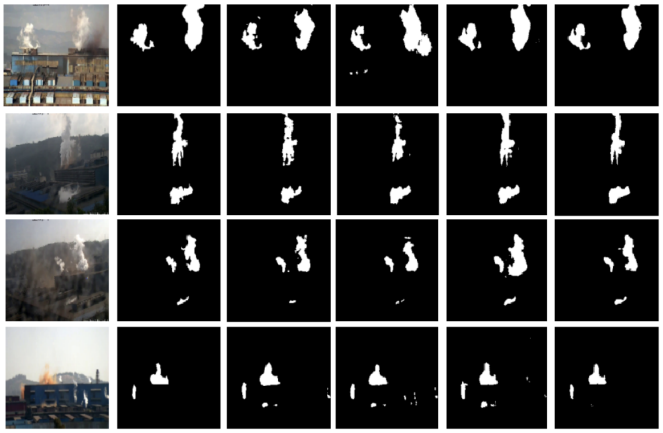

Fig. 9. Comparison on multi-objective smoke scene

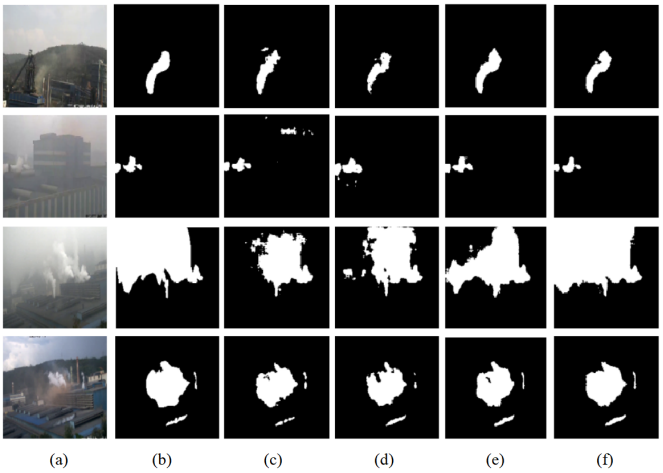

Fig. 10. Comparison on thin smoke scene

Table 6. Comparison result of small-area smoke scene

Index	EDL	DDCNN	EPHD	Proposed
IoU/%	58.22	60.48	77.22	78.86
Precision/%	77.24	81.76	83.55	89.28
Recall/%	68.22	69.09	92.28	87.30
F1-score/%	75.44	78.86	87.69	88.28

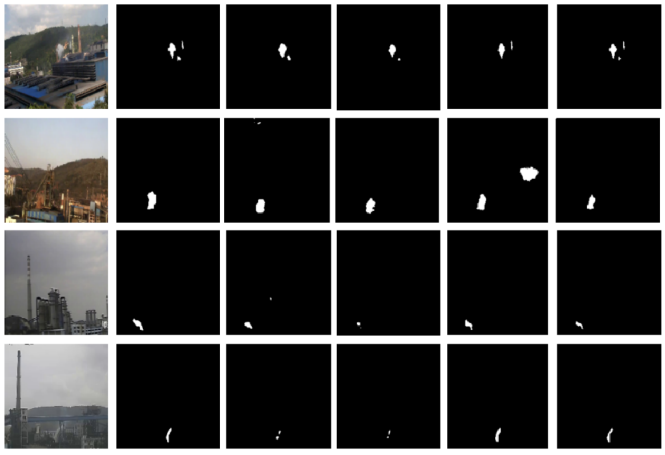

Fig. 11. Comparison on small-area smoke scene

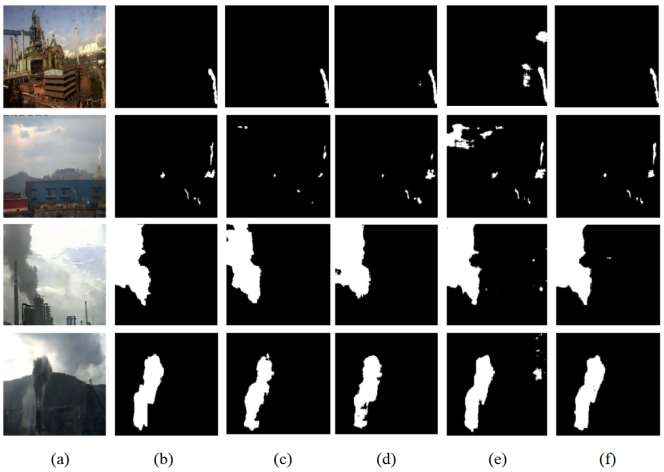

Fig. 12. Comparison on cloud interference scene

Table 7. Comparison result of multi-objective smoke scene

Index	EDL	DDCNN	EPHD	Proposed
IoU/%	72.04	70.21	79.66	80.05
Precision/%	88.61	86.94	87.80	90.19
Recall/%	81.14	80.44	90.93	88.89
F1-score/%	84.71	85.53	89.34	89.53

Table 8. Comparison result of cloud interference scene

Index	EDL	DDCNN	EPHD	Proposed
IoU/%	65.19	66.58	72.69	78.27
Precision/%	82.56	83.27	79.55	88.74
Recall/%	77.66	79.09	90.16	87.50
F1-score/%	80.04	82.40	84.52	88.12

Table 9. Comparison result of cloud interference scene

Index	EDL	DDCNN	EPHD	Proposed
IoU/%	69.21	67.85	76.41	75.75
Precision/%	85.94	85.52	84.79	89.29
Recall/%	79.97	78.62	89.71	89.98
F1-score/%	82.85	84.04	87.18	88.08

4. In the comparison of multi-object smoke scene recognition results, both EDL and DDCNN have the problem of excessive segmentation, and the edge of recognition results is not accurate. EPHD divides a small building area. EPHD fails to identify the darker soot. The new method has the best relative performance.
5. In the comparison of recognition results of interference scenes, EDL is greatly affected by cloud interference, and recognition results include areas belonging to clouds. DDCNN and EPHD have better anti-interference than EDL, but the results are not complete. The new method shows the best anti-interference performance.

To sum up, the anti-interference ability of EDL is poor, and it is easy to identify and segment the non-smoke area. Moreover, there is the problem of excessive segmentation, which is reflected in the inaccurate edge of the identification result. With the encoding and decoding structure adopted by DDCNN, the precision of the recognition results should be better than that of EDL. However, because the smoke edges are rough and the image resolution used in the experiment is not high, the edge improvement is not obvious from the results, but the anti-interference ability is obviously better than that of EDL, but the recognition results are incomplete. On the basis of DDCNN, EPHD adds a parallel shallow network to refine the results. As can be seen from the recognition results, EPHD has a certain degree of improvement in anti-interference compared with DDCNN, and also has a great improvement in the problem of missing small areas that DDCNN is prone to. The proposed method has the best anti-interference performance among all the methods. The multi-scale convolution operation adopted enhances the feature extraction ability of smoke. Compared with EDL, the test results can effectively distinguish the interference in soot and background, and the comparison results are closest to the manual labeling results.

In terms of quantitative indicators, DDCNN method has the lowest index, because the pre-trained network weight is not used in the initialization of the network parameters. In order to improve the accuracy of recognition results, a parallel branch is added. To compare the results of the new parallel network pair. During the training, it maintains the same parameter initialization mode as DDCNN. In terms of indicators, it has a certain improvement compared with DDCNN. The method adopted in this paper has significantly

improved the accuracy rate and intersection ratio index of test results in all scenarios compared with EDL, especially in the test set of interference scenes, which is also consistent with the performance of recognition results comparison.

7. Conclusion

Considering that it is difficult to achieve good classification and recognition effect for unlabeled smoke scene images under existing labeled data, this paper proposes a GAN model based on LSTM and CBAM. The existing data is enhanced to make it easily and effectively close to the smoke scene in the style and data distribution of the pixel field. And LSTM module is used to make full use of data feature information through multi-scale feature module to further align data distribution in feature domain effectively. Combined with CBAM, the accuracy of smoke classification and identification is greatly improved. Through experiments, the proposed framework has significantly improved the classification and recognition accuracy in smoke scenes compared with the basic classification network trained with existing labeled data. The current method still needs to be further improved in classification accuracy and structural optimization. The subsequent research will explore the fusion of algorithms in pixel domain and feature domain, improve the overall framework structure, further enrich the data set, and make the overall performance towards a more efficient direction.

Acknowledgments. This work was supported by Henan Province Science and Technology Project (212102210273).

References

1. Niero M, Ingvordsen C H, Peltonen-Sainio P, et al. "Eco-efficient production of spring barley in a changed climate: A Life Cycle Assessment including primary data from future climate scenarios," *Agricultural Systems,* vol. 136, pp. 46-60. (2015)
2. Arora N K. Impact of climate change on agriculture production and its sustainable solutions[J]. Environmental Sustainability, 2019, 2(2): 95-96.
3. Kumar V S, Muthukumaravel A. Seasonal forecasting of mobile data traffic in GSM networks with linear trend[J]. Journal of Applied Science and Engineering, 2020, 23(3): 469-474.
4. Ousmen A, Touraine C, Deliu N, et al. Distribution-and anchor-based methods to determine the minimally important difference on patient-reported outcome questionnaires in oncology: a structured review[J]. Health and quality of life outcomes, 2018, 16(1): 1-12.
5. Chen W T, Ding J J, Kuo S Y. PMS-net: Robust haze removal based on patch map for single images[C]//Proceedings of the IEEE/CVF Conference on Computer Vision and Pattern Recognition. 2019: 11681-11689.
6. Zhang H, Patel V M. Densely connected pyramid dehazing network[C]//Proceedings of the IEEE conference on computer vision and pattern recognition. 2018: 3194-3203.
7. Huang S, Liu Y, Wang Y, et al. A new haze removal algorithm for single urban remote sensing image[J]. IEEE Access, 2020, 8: 100870-100889.
8. Zhu Q, Du B, Yan P. Boundary-weighted domain adaptive neural network for prostate MR image segmentation[J]. IEEE transactions on medical imaging, 2019, 39(3): 753-763.
9. Chen C, Chen Z, Jiang B, et al. Joint domain alignment and discriminative feature learning for unsupervised deep domain adaptation[C]//Proceedings of the AAAI conference on artificial intelligence. 2019, 33(01): 3296-3303.

10. Liguo Wang, Yin Shoulin, Hashem Alyami, et al. A novel deep learning-based single shot multibox detector model for object detection in optical remote sensing images [J]. Geoscience Data Journal, 2022. https://doi.org/10.1002/gdj3.162
11. Man Jiang and Shoulin Yin. Facial expression recognition based on convolutional block attention module and multi-feature fusion [J]. Int. J. of Computational Vision and Robotics, 2021. DOI:10.1504/IJCVR.2022.10044018
12. Gallego A J, Calvo-Zaragoza J, Fisher R B. Incremental unsupervised domain-adversarial training of neural networks[J]. IEEE Transactions on Neural Networks and Learning Systems, 2020, 32(11): 4864-4878.
13. Zhao Y, Wu R, Dong H. Unpaired image-to-image translation using adversarial consistency loss[C]//European Conference on Computer Vision. Springer, Cham, 2020: 800-815.
14. Chen J, Chen L, Wang S, et al. A novel multi-scale adversarial networks for precise segmentation of x-ray breast mass[J]. IEEE Access, 2020, 8: 103772-103781.
15. Karnewar A, Wang O. Msg-gan: Multi-scale gradients for generative adversarial networks[C]//Proceedings of the IEEE/CVF conference on computer vision and pattern recognition. 2020: 7799-7808.
16. Zhang, J., Yu, X., Lei, X., Wu, C.: A Novel Deep LeNet-5 Convolutional Neural Network Model for Image Recognition. Computer Science and Information Systems, Vol. 19, No. 3, 1463-1480. (2022), https://doi.org/10.2298/CSIS220120036Z.
17. Sonekar S V, Pal M, Tote M, et al. Enhanced route optimization technique and design of threshold-T for malicious node detection in ad hoc networks[J]. International Journal of Information Technology, 2021, 13(3): 857-863.
18. de Oliveira Khn V, Lopes B C F L, Caicedo B, et al. Micro-structural and volumetric behaviour of bimodal artificial soils with aggregates[J]. Engineering Geology, 2021, 288: 106139.
19. Teng, L., Qiao, Y.: BiSeNet-oriented context attention model for image semantic segmentation. Computer Science and Information Systems, Vol. 19, No. 3, pp. 1409-1426. (2022), https://doi.org/10.2298/CSIS220321040T
20. Wu Z, Xue R, Li H. Real-Time Video Fire Detection via Modified YOLOv5 Network Model[J]. Fire Technology, 2022, 58(4): 2377-2403.
21. Li Y, Wen W, Guo X, et al. High-throughput phenotyping analysis of maize at the seedling stage using end-to-end segmentation network[J]. PLoS One, 2021, 16(1): e0241528.
22. Mazzia V, Angarano S, Salvetti F, et al. Action Transformer: A self-attention model for short-time pose-based human action recognition[J]. Pattern Recognition, 2022, 124: 108487.
23. Li Y, Ko Y, Lee W. RGB image-based hybrid model for automatic prediction of flashover in compartment fires[J]. Fire safety journal, 2022, 132: 103629.
24. Smagulova K, James A P. A survey on LSTM memristive neural network architectures and applications[J]. The European Physical Journal Special Topics, 2019, 228(10): 2313-2324.
25. Gui J, Sun Z, Wen Y, et al. A review on generative adversarial networks: Algorithms, theory, and applications[J]. IEEE Transactions on Knowledge and Data Engineering, 2021.
26. Woo S, Park J, Lee J Y, et al. Cbam: Convolutional block attention module[C]//Proceedings of the European conference on computer vision (ECCV). 2018: 3-19.
27. Yang F, Moayedi H, Mosavi A. Predicting the degree of dissolved oxygen using three types of multi-layer perceptron-based artificial neural networks[J]. Sustainability, 2021, 13(17): 9898.
28. Ju A, Wang Z. A novel fully convolutional network based on marker-controlled watershed segmentation algorithm for industrial soot robot target segmentation[J]. Evolutionary Intelligence, 2022: 1-18.
29. Cao Y, Yang F, Tang Q, et al. An attention enhanced bidirectional LSTM for early forest fire smoke recognition[J]. IEEE Access, 2019, 7: 154732-154742.
30. Ayala A, Macdo D, Zanchettin C, et al. KutralNext: An Efficient Multi-label Fire and Smoke Image Recognition Model[C]//Anais Estendidos do XXXIV Conference on Graphics, Patterns and Images. SBC, 2021: 7-13.

31. Yang Z, Wang T, Bu L, et al. Training with augmented data: Gan-based flame-burning image synthesis for fire segmentation in warehouse[J]. Fire Technology, 2022, 58(1): 183-215.
32. Namozov A, Im Cho Y. An efficient deep learning algorithm for fire and smoke detection with limited data[J]. Advances in Electrical and Computer Engineering, 2018, 18(4): 121-128.
33. Gu K, Xia Z, Qiao J, et al. Deep dual-channel neural network for image-based smoke detection[J]. IEEE Transactions on Multimedia, 2019, 22(2): 311-323.
34. Yuan F, Shi J, Xia X, et al. Encoding pairwise Hamming distances of Local Binary Patterns for visual smoke recognition[J]. Computer Vision and Image Understanding, 2019, 178: 43-53.
35. Y. Yuan, Z. Xu and G. Lu, "SPEDCCNN: Spatial Pyramid-Oriented Encoder-Decoder Cascade Convolution Neural Network for Crop Disease Leaf Segmentation," in IEEE Access, vol. 9, pp. 14849-14866, 2021, doi: 10.1109/ACCESS.2021.3052769.

Dahai Li is with the School of Electronics and Electrical Engineering, Zhengzhou University of Science and Technology. Research direction: Information security, image processing.

Yang Rui is with the School of Electronics and Electrical Engineering, Zhengzhou University of Science and Technology, Zhengzhou 450064, China. Research direction: Information security, image processing.

Su Chen is with the Department of Mechanical and Electrical Engineering, Henan Vocational College of Water Conservancy and Environment, Zhengzhou 450002, China. Research direction: image processing.

Received: November 25, 2022; Accepted: March 30, 2023.

Computer Science and Information Systems 20(4):1729–1748 https://doi.org/10.2298/CSIS221130028Z

A Novel Feature Fusion Model Based on Non-subsampled Shear-wave Transform for Retinal Blood Vessel Segmentation

Feng Lijuan[1] and Zhang Fan[2]

[1] School of Electronics and Electrical Engineering, Zhengzhou University of Science and Technology, Zhengzhou City, 450064, China
857003841@qq.com
[2] Zhengzhou University of Technology
Zhengzhou 450064, China
fanzhang0225@163.com

Abstract. Background: Fundus image is a projection of the inner surface of the eye, which can be used to analyze and judge the distribution of blood vessels on the retina due to its different shape, bifurcation and elongation. Vascular trees are the most stable features in medical images and can be used for biometrics. Ophthalmologists can effectively screen and determine the ophthalmic conditions of diabetic retinopathy, glaucoma and microaneurysms by the morphology of blood vessels presented in the fundus images. Traditional unsupervised learning methods include matched filtering method, morphological processing method, deformation model method, etc. However, due to the great difference in the feature complexity of different fundus image morphology, the traditional methods are relatively simple in coding, poor in the extraction degree of vascular features, poor in segmentation effect, and unable to meet the needs of practical clinical assistance. Methods: In this paper, we propose a new feature fusion model based on non-subsampled shear-wave transform for retinal blood vessel segmentation. The contrast between blood vessels and background is enhanced by pre-processing. The vascular contour features and detailed features are extracted under the multi-scale framework, and then the image is postprocessed. The fundus images are decomposed into low frequency sub-band and high frequency sub-band by non-subsampled shear-wave transform. The two feature images are fused by regional definition weighting and guided filtering respectively, and the vascular detection image is obtained by calculating the maximum value of the corresponding pixels at each scale. Finally, the Otsu method is used for segmentation. Results: The experimental results on DRIVE data set show that the proposed method can accurately segment the vascular contour while retaining a large number of small vascular branches with high accuracy. Conclusion: The proposed method has a high accuracy and can perform vascular segmentation well on the premise of ensuring sensitivity.

Keywords: Retinal blood vessel segmentation, non-subsampled shear-wave transform, feature fusion, regional definition weighting, guided filtering, Otsu method.

1. Introduction

Retinal vascular disease detection is the main method to assist in the diagnosis of hypertension, diabetes and many other diseases. Regular retinal vascular disease detection

can detect vascular abnormalities in time and help patients find the disease early, thereby preventing the further development and deterioration of the disease. The blood vessels of the retina in the fundus are very complicated, with small blood vessels, fuzzy outlines and intertwined distribution, so it is more difficult to segment blood vessels. Therefore, accurate and rapid segmentation of blood vessels is of great significance for the detection of retinal blood vessels [1-3].

Vessel segmentation methods mainly include supervised and unsupervised methods. The supervised method distinguishes the blood vessel and the background through a trained classifier, and the unsupervised method mainly detects the blood vessel by maximizing the filter response on the gray profile of the blood vessel cross-section. Liang et al. [4] proposed a u-shaped retinal vessel segmentation algorithm with adaptive vascular morphology and scale information, it used u-shaped segmentation model to perform end-to-end training on preprocessed images, and used local information entropy sampling for data enhancement. Wang et al. [5] proposed a multiple vessel segmentation (MVP) algorithm, which segmented retinal vessels into well-constrained subsets, and grouped blood vessel pixels with similar geometric characteristics in the subsets. Parallel training was performed on a group of homogeneous classifiers to form a discriminative decision for each group. Yan et al. [6] proposed a three-stage deep learning model, which separately segmented thick and thin blood vessels, further identified non-vascular pixels through vascular fusion, and improved the results by improving the overall blood vessel thickness consistency. Odstrcilik et al. [7] designed five different kernels based on the typical cross-sectional profile of blood vessels, and considered the five width categories of retinal blood vessels, and rotated the kernels to 12 different directions to cover all directions of the blood vessels. Dharmawan et al. [8] proposed a new retinal vessel segmentation framework based on the best adaptive filter. Rodrigues et al. [9] proposed a new optic disc detection algorithm based on wavelet transform and mathematical morphology, and used the tubular characteristics of blood vessels to segment retinal arteries and veins. Aguirre et al. [10] proposed a method that used Gabor filter and Gaussian fractional derivative to significantly enhance the structure and contour of blood vessels, and applied thresholds and a series of morphological-based decision rules to separate blood vessels.

Most of the existing methods perform well in blood vessel segmentation on the fundus retinal image, but they will lose the contour information of the blood vessel to a certain extent or produce more false positive pixels at the blood vessel contour. It is difficult to be more accurate. The small branches of the blood vessel are segmented, which leads to the decrease of the blood vessel integrity and the segmentation accuracy. This paper considers the segmentation of blood vessel contours and small branches, and proposes a new feature fusion model based on non-subsampled shear-wave transform (NSST) for retinal blood vessel segmentation with fusing blood vessel contour feature information and detailed feature information in a multi-scale framework. The fundus images are decomposed into low frequency sub-band and high frequency sub-band by NSST. The two feature images are fused by regional definition weighting and guided filtering respectively, and the vascular detection image is obtained by calculating the maximum value of the corresponding pixels at each scale. Finally, the Otsu method is used for segmentation, which solves the problem of vessel contour and detail information loss on a single scale, thus effectively improving the accuracy of vessel segmentation.

The remaining paper is settled as follows: Section 2 presents the related works in de-

tail. Section 3 discusses the proposed method. Then, experiments are provided in Section 4. Finally, the paper is concluded in Section 5.

2. Related Works

Blood vessels are one of the most important components of the retina. Retinal vascular segmentation and the division of vascular morphological attributes, such as length, width, tortuosity and angle, can be used for the diagnosis, screening, treatment and evaluation of a variety of cardiovascular and ophthalmic diseases, such as diabetes, glaucoma, hard exudate and hypertension and other systemic diseases [11].

However, the segmentation of retinal blood vessels by an ophthalmologist is time-poor and lacks accuracy. Therefore, the research on the automatic segmentation of blood vessels and automatic recognition [12] of blood vessel morphological attributes becomes a crucial step to assist medical diagnosis.

Existing retinal segmentation methods can be roughly divided into unsupervised and supervised methods [13]. The unsupervised learning retinal blood vessel segmentation methods can be divided into matching filtering, mathematical morphology, blood vessel tracking and clustering. Reference [14] proposed an improved Top-Hat transformation, which was applied to retinal blood vessel segmentation, it used circular structural elements of different radii to detect blood vessels of different widths, further improving the segmentation rate of tiny blood vessels, but it was more sensitive to noise. Reference [15] proposed a blood vessel tracking method based on Bayesian probability, which combined the information of blood vessel connectivity and gray level to fit the blood vessel structure. This method could better solve the problem of segmentation and fracture at the intersection of blood vessels, but had low segmentation accuracy for small blood vessels. In reference [16], principal component analysis (PCA) was used to extract features of blood vessels, and threshold value was used for segmentation. It had low segmentation of small blood vessels and segmentation rupture at the intersection of blood vessels.

Supervised learning requires experts to provide gold standard retinal images with tags, use a set of features based on local or global images to train the classifier, act as prior knowledge and guide training. Reference [17] proposed a random forest classifier integrating multiple features, which could well solve the situation of segmentation and fracture at the intersection of blood vessels, but there was a phenomenon of mis-segmentation of optic disc into blood vessels. In reference [18], the vascular segmentation algorithm integrating phase characteristics better solved the problem of insufficient detection of vascular phase consistency features, but there was still a problem of insufficient microvascular segmentation. In reference [19], blood vessel segmentation was regarded as a binary classification problem, and a hybrid 5D feature based on support vector machine (SVM) was proposed to distinguish blood vessel pixels from non-blood vessel pixels, which had strong adaptability to noise and solved the problem of optic disc being misdivided into blood vessels, but there was the problem of small blood vessels being easily broken. Therefore, this paper proposes a new feature fusion model based on non-subsampled shear-wave transform (NSST) for retinal blood vessel segmentation with fusing blood vessel contour feature information and detailed feature information in a multi-scale framework.

3. Proposed Retinal Blood Vessel Segmentation Method

The retinal blood vessel segmentation method based on NSST is mainly divided into three stages: image preprocessing, blood vessel feature information extraction, and blood vessel detection and segmentation. The contrast-limited adaptive histogram equalization (CLAHE) method is used to enhance the contrast of the green channel image of the original image and reduce noise. The contour feature information of the blood vessel is obtained by calculating the gradient amplitude of the retinal image, and the detailed feature information of the blood vessel is obtained by calculating the maximum principal curvature. The contour and the detailed information are processed for feature image post-processing respectively. Finally, the NSST is used to fuse the image containing the contour and detail information of the blood vessel to obtain the blood vessel detection information at multiple scales, and the Otsu method is used for segmentation. The flowchart of multi-scale blood vessel segmentation is shown in figure 1.

3.1. Image Pre-processing

In the fundus retinal image, the contrast of the green channel image is relatively high, so the green channel image is selected as the initial image for subsequent operations. The retinal blood vessel area is a low-contrast dark area, and the CLAHE algorithm can enhance the image while suppressing noise. The CLAHE is simple to calculate, only the amplitude limiting parameter is determined, so the CLAHE method can be used to enhance the retinal image [20]. The preprocessing of the original image is shown in figure 2.

3.2. Vessel Feature Information Extraction

The blood vessels in the retinal image of fundus show a network structure, and the diameter of the blood vessels is different, so it is difficult to accurately detect the blood vessel information using the information of a single scale. In this paper, vascular information is extracted and detected in a multi-scale framework. In general, the original image $I(x, y)$ and Gaussian kernel $G(x, y; \sigma)$ with variance σ^2 to define information at different scales [12-14]:

$$I_\sigma(x, y, \sigma) = I(x, y) \times G(x, y; \sigma) \tag{1}$$

Where $(x, y; \sigma) = \frac{1}{2\pi\sigma^2} exp(-\frac{x^2+y^2}{2\sigma^2})$.

The derivative of the image can be approximated numerically as the convolution of the image with the derivative of the scale-normalized Gaussian kernel, so the first and second derivatives of the image can be expressed as:

$$\partial I_\sigma(x, y; \sigma) = I(x, y) \times \sigma \partial G(x, y; \sigma) \tag{2}$$

$$\partial^2 I_\sigma(x, y; \sigma) = I(x, y) \times \sigma^2 \partial^2 G(x, y; \sigma) \tag{3}$$

Where $I(x, y)$ denotes the original image. σ is the scale factor.

A. Contour information extraction

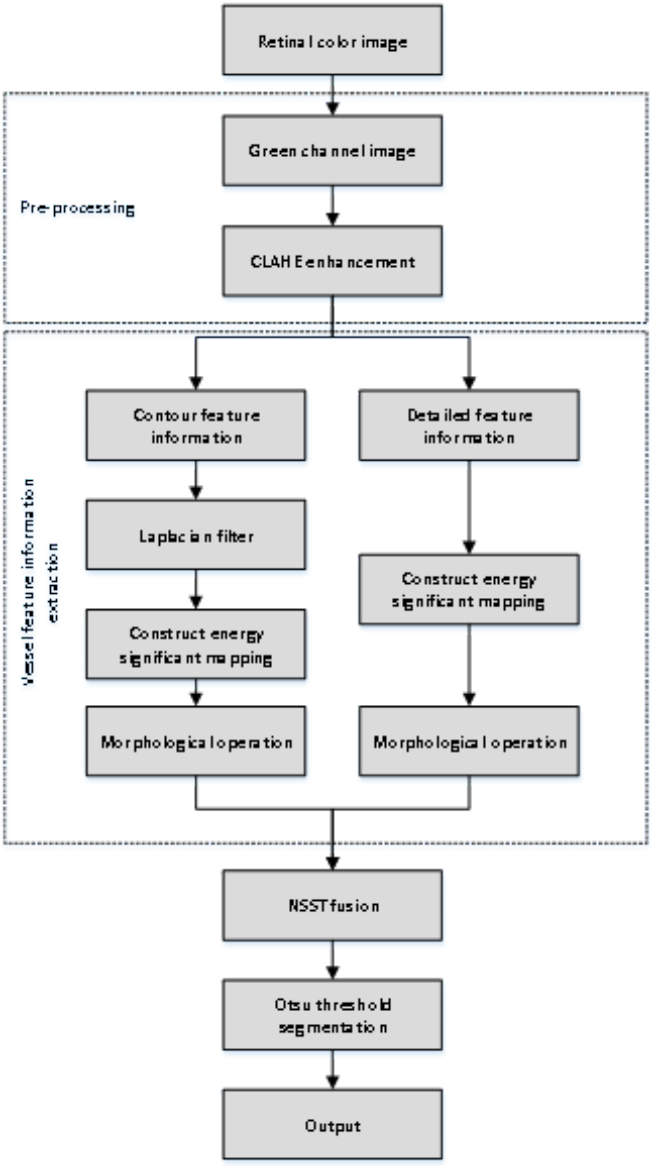

Fig. 1. Flow chart of proposed blood vessel segmentation

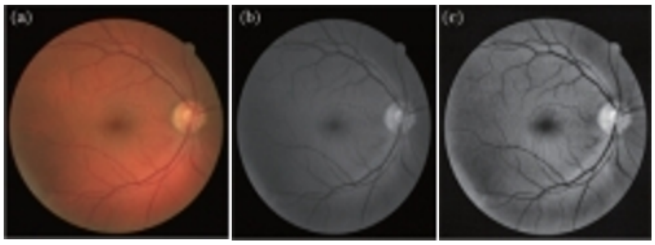

Fig. 2. Preprocessed images. (a) Original color image; (b) green channel image; (c) contrast enhanced image by CLAHE

The gradient amplitude describes the change in image intensity near the pixels. The image obtained by convolution of the original image $I(x, y)$ with Gaussian kernel $G(x, y; \sigma)$ is $I_\sigma(x, y; \sigma)$, and the gradient at point (x, y) can be defined as a vector:

$$grad[I(x, y)] = [\partial_x I_\sigma \quad \partial_y I_\sigma]^T \tag{4}$$

We can see from the definition of gradient that: 1) The vector $grad[I(x, y)]$ points to the direction with the maximum increase rate of $I(x, y)$, and the direction of the image edge is perpendicular to this gradient direction; 2) If $G[I(x, y)]$ is used to represent the amplitude of $grad[I(x, y)]$, then there is:

$$G[I(x, y)] = \sqrt{(\partial_x I_\sigma)^2 + (\partial_y I_\sigma)^2} \tag{5}$$

In the multi-scale framework, $G[I(x, y)]$ represents the slope of image intensity at a specific scale σ. The gradient amplitude images at scale σ=1,2, and 4 pixels are shown in figure 3.

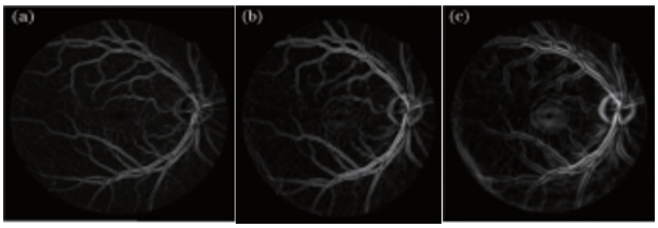

Fig. 3. Gradient amplitudes values. (a) σ=1 (b) σ=2 (c) σ=4

When scale σ is 1, 2, and 4 pixels respectively, most of the vascular contour information in the retinal images can be obtained by extracting the gradient amplitude information of the images. Convolution with Gaussian for image will suppress most structures whose feature length is smaller than scale σ, and the image will become blurred gradually with the increase of scale.

B. Detail information extraction

The second order directional derivative describes the change of image gradient intensity near the pixel point. The main curvature information of blood vessels in image $I(x, y)$ can be obtained by Hessian matrix. The Hessian matrix can be expressed as:

$$H = [\partial_{xx} I_\sigma \quad \partial_{xy} I_\sigma, \partial_{yx} I_\sigma \quad \partial_{yy} I_\sigma]^T \tag{6}$$

In a two-dimensional image, the Hessian matrix is a two-dimensional positive definite matrix with two eigenvalues, each of which has a corresponding eigenvector. When blood vessel relative to the background of low dark tubular structure, the blood vessels in pixel Hessian matrix has a larger eigenvalue λ_1 and a smaller eigenvalue λ_2, $\lambda_1 \geq \lambda_1$. The maximum eigenvalue λ_1 corresponds to the maximum principal curvature of the Hessian matrix, so if $\lambda_1 \geq 1$, the pixels belonging to the vascular region in the image will be weighted as vascular pixels. Figure 4 shows the maximum principal curvature image when scale σ is 1,2, and 4 pixels respectively.

The results of figure 4 show that with the increase of the scale factor, vessels with a radius similar to the scale factor are more obvious, while the information of vessels with a radius smaller than the scale factor is suppressed. With small scale, the maximum principal curvature image can well reflect the information of each small branch of the vessel. With large scale, the maximum principal curvature image can fully reflect the main artery information.

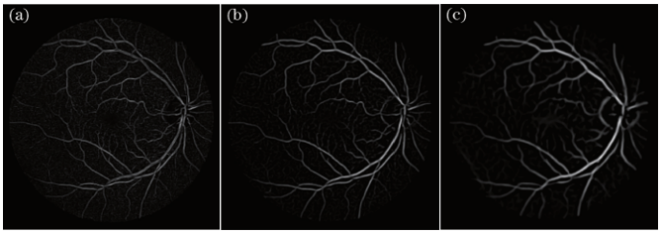

Fig. 4. Maximum principal curvature images. (a) σ=1 (b) σ=2 (c) σ=4

C. Feature image post-processing

The gradient amplitude image describes the contour information in the original image, while the maximum principal curvature image captures the details in the original image. Therefore, before image fusion, the two images are post-processed respectively to achieve better fusion effect.

1. Contour feature image post-processing
   Assuming that the fundus retinal image is $I(x, y)$, its gradient amplitude image can be expressed as $G[I(x, y)]$. First, The Gradient amplitude image is processed by Laplacian filter, and the high-pass image is obtained as shown in figure 5(a):

$$U^G = G \times L_{ap} \tag{7}$$

   Where L_{ap} is Laplace filter with size 3×3.

Then the local average value of the absolute value of the high-pass image is taken to construct the energy significant mapping image [21].

$$S^G = |U^G \times A_{vg}| \tag{8}$$

Where A_{vg} is the average filter of size 3×3.
The energy significant mapping image S^G is shown in figure 5(b), which contains the contour information of small vessels, but there are many noises around them. Therefore, the mathematical morphology is used to remove these noises. Since the blood vessels in retinal images are tubular structures, linear structures are selected as structural elements. The structure element takes two parameters: length and Angle. First, the length of the linear structural element is increased from the minimum diameter of the vessel to the maximum diameter with stride=1 pixel based on the diameter of the vessel. The angles of linear structural elements are selected from 0 to 170, the interval is 10 [22], and 198 linear structural element templates are obtained. The result of morphological open operation can be calculated with 198 element templates. Assume that the gray value of the open operation result of the $l-th$ template at pixel point (x, y) is $I_{open_l}(x, y)$, then the gray value of each pixel after final morphological processing should be the maximum value of the corresponding position among 198 operation results, namely,

$$I_R = \max_l I_{open_l}(x, y) \tag{9}$$

Where I_R is the image processed by mathematical morphology, and the result is shown in figure 5(c).

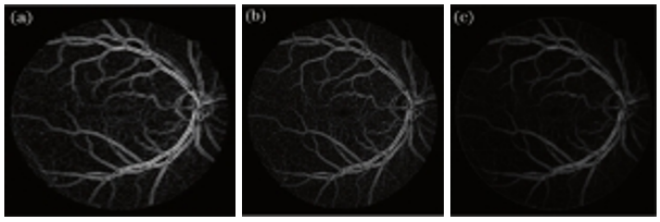

Fig. 5. Results of post-processing for contour feature image. (a) Laplacian filtered image; (b) energy significant mapping image; (c) mathematical morphology processing

2. Detail feature image post-processing
The detailed feature image is $F[I(x, y)]$, and a similar approach is adopted for post-processing. Since the detail feature image inherits the high frequency information of the original image, it is unnecessary to use Laplace filter to obtain the high pass image. The absolute value of the detail feature image $F[I(x, y)]$ is directly averaged locally to construct the energy significant mapping image $S^F = |F \times A_{vg}$, and then the noise around the small vessels is removed by mathematical morphology processing. The post-processing results of detail feature images are shown in figure 6.

The results of figure 5(c) and figure 6(b) show that after the post-processing of contour feature image and detail feature image respectively, the contour and detail information in the image are clearer, and the post-processing effectively reduces the noise, which provides a good foundation for the subsequent fusion.

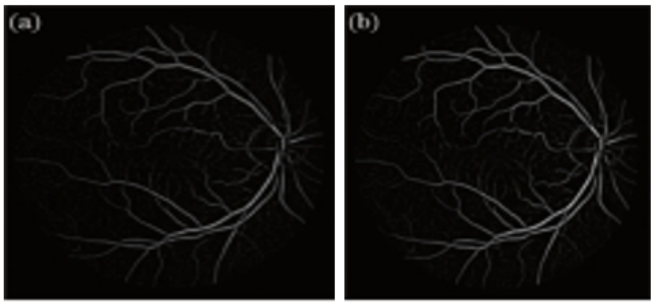

Fig. 6. Results of post-processing for detail feature image. (a) Energy significant mapping image; (b) image obtained by mathematical morphology processing

3.3. NSST-based image fusions

After post-processing, the noise in contour feature image and detail feature image is significantly reduced. The contour information and detail information contained in these two images are more prominent respectively. Therefore, NSST is used to fuse these two images [23-26]. The process of using NSST to fuse contour feature images and detail feature images is shown in figure 7. Wavelet coefficients are fused by regional definition weighting for low frequency and guided filtering for high frequency.

A. Low frequency component fusion rule

The purpose of low frequency sub-band fusion of fundus vascular image is to obtain a clearer fundus image. Logically, image blur is caused by the fact that the contour of the object in the image is not obvious, the grayscale change of the contour edge is not strong, and the sense of hierarchy is not strong. On the contrary, if the gray level of the contour edge changes significantly and the hierarchy is strong, the image will be clear. For an image, we can regard the image as a two-dimensional function $f(x, y)$. According to calculus, the sharpness of the image can be expressed by the gradient of the image.

For low frequency components, a fusion strategy based on region definition weighting is designed. As an evaluation index of clarity, energy of gradient (EOG) has clear physical meaning in spatial domain, good time performance and high sensitivity [27,28]. EOG uses the difference between adjacent points to calculate a gradient at a point, as defined below:

$$E = \sum_{x} \sum_{y} [f(x+1, y) - f(x, y)]^2 + [f(x, y+1) - f(x, y)]^2 \tag{10}$$

c_1, c_2 and c are used to represent the low-frequency coefficients of image A, image B and fusion image F in the same sub-band, the same direction and the same position, respectively. r_1 and r_2 represent the EOG of low-frequency sub-band coefficients of image

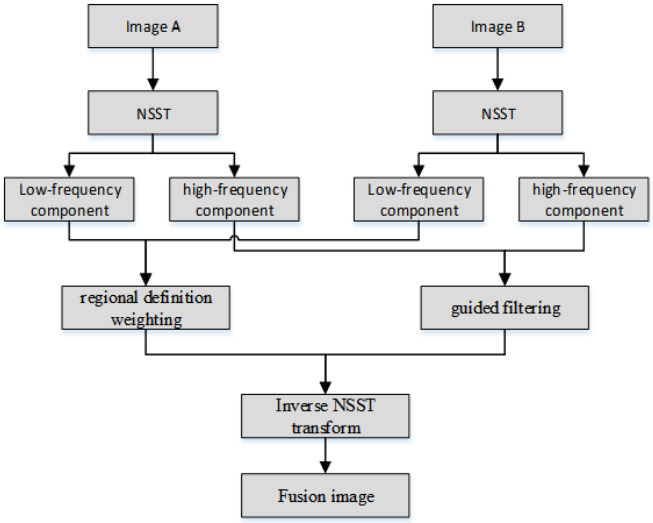

Fig. 7. Fusion process of NSST

A and image B in the same sub-band, direction and position in the NSST region, then the fusion strategy can be expressed as:

$$c = w_1 c_1 + w_2 c_2 \tag{11}$$

Where $w_1 = \frac{r_1}{r_1+r_2}$, $w_2 = \frac{r_2}{r_2+r_2}$

B. High-frequency component fusion rule

For high-frequency sub-band fusion, the aim is to preserve as much spatial detail, edge, and contour as possible. The high frequency sub-band of fundus vascular image A after NSST decomposition is taken as the input image, the high frequency sub-band of fundus vascular image B after NSST decomposition is taken as the guide image, and the output image is the high frequency sub-band image after fusion. In addition, the input image and the guided image must be on the same level and in the same direction. The fusion strategy can be expressed as:

$$H_F^{l,k} = G_{r,\varepsilon}(H_A^{l,k}, H_B^{l,k}) \tag{12}$$

$H_A^{l,k}$ and $H_B^{l,k}$ represent the high frequency sub-band of image A and image B in the k direction of the $l-th$ decomposition layer respectively, while $H_F^{l,k}$ represents the high frequency fusion sub-band in the k direction of the $l-th$ decomposition layer.

The results of NSST fusion for contour feature image and detail feature image are shown in figure 8. Figure 8 shows that the NSST fuses the image detail and contour information, which significantly improves the image quality. The outline of blood vessels and the information of thicker blood vessels are retained completely. At the same time, small vessels are retained to a large extent and non-vascular pixel interference around them is reduced, but some vascular information smaller than the current scale is lost in this process.

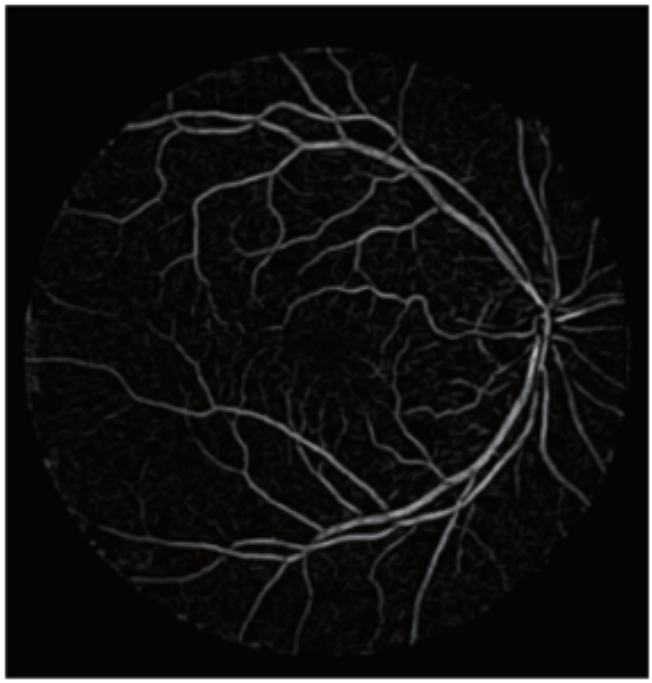

Fig. 8. Fusion image with NSST when $\sigma = 1$

3.4. Multi-scale Vascular Detection

Vessel detection at a single scale σ can only ensure that the vessel information corresponding to the radius of the current scale can be completely detected, while the vessel information smaller than this scale may be lost. So it needs to compute all feature information within a certain range $\sigma(\sigma_{min} \leq \sigma \leq \sigma_{max})$, where σ_{min} and σ_{max} are the minimum and maximum radius of blood vessels in retinal images to be detected. These two parameters must be known in advance and depend on the pixel resolution of the original image and the field of view of the fundus camera. In DRIVE data sets, σ_{min} and σ_{max} are usually set as 1 and 6 respectively [29-31].

First, at every scale $\sigma(\sigma_{min} \leq \sigma \leq \sigma_{max})$, the contour feature images G_k and detail feature images F_k are obtained respectively:

$$G_k = \sqrt{(\partial_x I_{\sigma_k})^2 + (\partial_y I_{\sigma_k})^2} \tag{13}$$

$$F_k = f(p_0, \sigma_k) = \lambda_1 \tag{14}$$

Then, G_k and F_k are post-processed respectively.

- The High pass image $U_k^G = G_k \times L_{ap}$ is obtained by Laplace transform of gradient amplitude image G_k. Reconstruction of energy significant mapping image $S_k^G = U_k^G \times A_{vg}$. Finally, the mathematical morphology processing image $I_{R_k}^G$ is obtained.
- The energy significant mapping image $S_k^F = F_k \times A_{vg}$ of detail feature image F_k is directly constructed, and then the image $I_{R_k}^F$ is obtained by mathematical morphology processing.

Finally, NSST is used to fuse the post-processing images of contour features and detail features at each scale, and the fusion image $R_k = fusion(I_{R_k}^G, I_{R_k}^F)$ at each scale is obtained. Then, it is corresponding to the multi-scale, and the maximum value of pixels corresponding to each scale is calculated to obtain the multi-scale vascular detection image:

$$M_k = \max_{\sigma_{min} \leq \sigma_k \leq \sigma_{max}} R_k \tag{15}$$

The images obtained by multiscale vascular detection are shown in figure 9. Figure 10 shows the contrast of image details obtained from multi-scale vascular detection.

Figure 10 shows that the contour feature image can retain the edge contour information of the image well and accurately describe the boundary of blood vessels (figure 10(b)). The detailed feature image retains the information of the central area of the vessels and the small vessels (figure 10(c)). As shown in figure 10(d), fusion of the two images can preserve as much as possible the information of small branches of blood vessels on the premise of accurately describing image boundaries. However, in a single scale, the limitation of scale will lead to thinning of blood vessels, and part of blood vessel information not corresponding to the current scale will be lost in the image. The corresponding scale of figure 10(d) is σ=1 pixel, figure 10(e) is σ=2 pixel, and figure 10(f) is σ=4 pixel. When the scale is σ=1 pixel, many small branching vessels are retained, but the main and branching vessels are thinner than the original vessels. When the scale gradually increasing, as shown in figure 10(e) and (f), the width of main vessels gradually becomes normal,

Fig. 9. Image obtained by multi-scale vascular detection

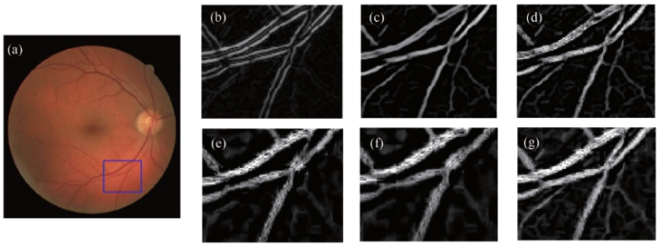

Fig. 10. Comparison of detail images obtained by multi-scale blood vessel detection.?(a) Original color image;?(b) contour feature.(c) detail feature, and (d) detail image of wavelet transform fusion at σ=1 pixel;?detail images obtained by blood vessel detection when (e) σ=2 pixel and (f) σ=4 pixel;?(g) detail image obtained by multi-scale blood vessel detection

but the information of small vessel branches will be lost. Therefore, this paper adopts the method of vascular detection under the multi-scale framework to ensure the equality and consistency of all pixels and all scales in the detection image. As can be seen from figures 8-10, the vascular information in the image is relatively intact. The contour of all the larger vessels is clear, and the vascular information at the edge is not lost. Most of the fine vessels are also well preserved, and the interference of surrounding non-vascular pixels is reduced.

4. Experiments and Analysis

4.1. Data Set

Color fundus retinal images from DRIVE dataset are used in this paper. The dataset consists of 20 training images and 20 testing images. These images are taken with a Canon CR5 non-dilated camera with a field of $45°$. The field of view (FOV) of each image is round, with a diameter of about 540 pixels. Each image has a corresponding mask image depicting FOV and two expert manual segmentation results. Image size is 768×584pixels and an 8-bit color channel is used in the RGB model.

4.2. Evaluation Index

In order to quantitatively evaluate the segmentation results of blood vessels, three indicators are used to evaluate the segmentation results including accuracy (ACC), sensitivity (SE) and specificity (SP) [32]. The calculation formulas are shown in formulas (16)-(18). ACC represents the ratio of all correctly classified pixels to all the pixels in the retinal images. SE represents the proportion of vascular pixels correctly identified in the segmentation result. SP represents the proportion of non-vascular pixels correctly identified in the segmentation result. TP represents the number of vessel pixels judged as vessels in the results. FP represents the number of background pixels judged as blood vessels in the results. FN represents the number of blood vessel pixels judged as background in the algorithm results. TN represents the number of background pixels judged as background in the algorithm result.

$$ACC = (TP + TN)/(TP + FP + TN + FN) \tag{16}$$

$$SE = TP/(TP + FN) \tag{17}$$

$$SP = TN(TN + FP) \tag{18}$$

4.3. Results and Analysis

The edge of the field of view of fundus camera can be misjudged as vascular pixel by vascular detection in fundus retinal images. Therefore, in order to ensure the segmentation results and the accuracy of evaluation index calculation, the given mask is first used to remove the interference of the edge, and then the classical Otsu algorithm is used to

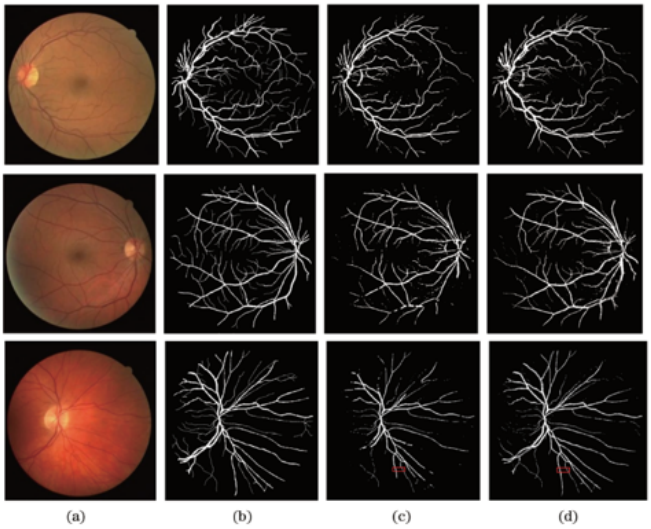

Fig. 11. Comparison of retinal vascular segmentation.(a) Original color fundus retinal images; (b) Gold standard images; (c) Results of vascular segmentation with single scale; (d) Vascular segmentation results with multiple scales.

perform segmentation directly. DRIVE test set is used to test the proposed method, and comparative analysis is conducted with gold standard images. The comparison of retinal vascular segmentation effect is shown in figure 11.

Figure 11 compares the segmentation effects of the two methods on three randomly selected retinal images in the DRIVE test set. Figure 11(a) is the original color retinal fundus image, figure 11(b) is the gold standard image, figure 11(c) is the result of blood vessel segmentation with single scale, and figure 11(d) is the result of blood vessel segmentation with the multi-scale framework. The third image in figure 11 shows the 1D cross section of the middle row marking the sub-area as shown in figure 12. The comparison results show that the proposed method can effectively reduce the influence of optic disc on vascular segmentation and reduce the possibility of many false positive pixels around blood vessels. The proposed method can ensure the accuracy of vascular segmentation, while retaining most of the small vessels, and has good segmentation performance.

The detail segmentation results with fusing vascular contour information and detail information under multi-scale and single-scale frameworks is shown in figure 13. Figure 13 is the obtained conclusion by comparing the segmentation results at different scales. In figure 13, only the corresponding good results are listed in figure 13(c) (i.e., the corresponding scale is 4 pixel). By comparing figure 13 (b) (d), it can be found that a large number of small vessel structures are lost in the vessel segmentation result of fusion under the single-scale framework, and the information of some main vessels is also lost in the image of the second row, resulting in incomplete vascular structure and poor connectivity. The vessel segmentation obtained by using the multi-scale framework is shown in figure 13(d). This new method retains more information about small vessels while ensuring the

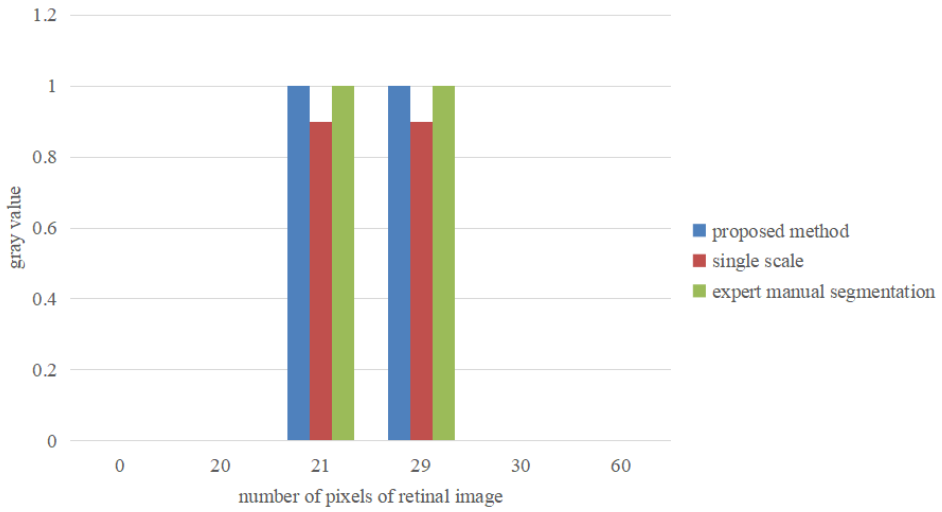

Fig. 12. The 1D cross section of the middle row of the marked area in the third image in figures 11(c) and (d)

integrity of the main vessel, and the structure of vessels is relatively complete and the connectivity is good.

In order to reflect the fusion effect of the vascular wheel information and detail information with NSST transform on the vascular contour area in retinal images, the fusion results of the vascular contour information and detail information and the unfusion results of the vascular contour information and detail information are compared and analyzed in a multi-scale framework. Vascular segmentation results of fused and unfused contour information and detail information at multiple scales are shown in figure 14.

Figure 14 compares the fusion results of vascular contour information and detail information with those of unfusion contour information and detail information using NSST in a multi-scale framework. It can be seen that, when vascular contour information and detailed information are not fused, contour features are very vague in the segmentation results where vascular branches and multiple vessels are intertwined, which leads to a lot of vascular information that cannot be accurately segmented. The fusion of vascular contour information and detailed information can ensure the accuracy and integrity of vascular contour at the intersection of vascular branches and multiple vessels.

4.4. Discussion

In order to more intuitively compare the performance of the proposed algorithm with other classical algorithms, the ACC, SE and SP are compared and analyzed. The performance comparison is shown in Table 1.

The sensitivity of M-GAN in Table 1 is the highest, slightly higher than 0. 0103 of the proposed algorithm in this paper. However, the accuracy of the proposed algorithm is 0.0119 higher than that of M-GAN. Compared with other methods, the proposed method has the highest accuracy and it is 0. 0117 higher than other methods. The sensitivity of

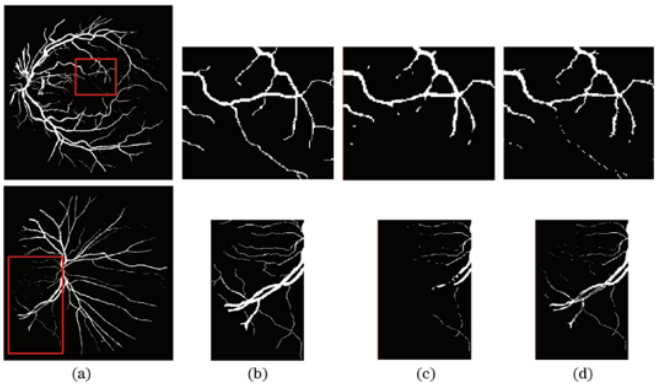

Fig. 13. Vascular segmentation results with contour information and detail information fusion in multi-scale and single-scale frames. (a) Fusion result with multi-scale framework; (b) Gold standard image details; (c) Detailed diagram of fusion results in a single-scale framework; (d) Detailed diagram of fusion results in a multi-scale framework.

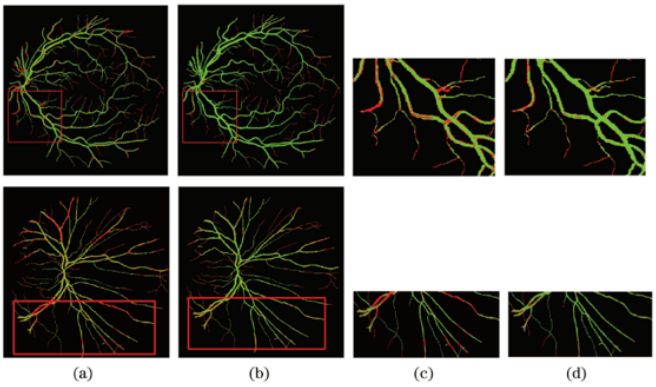

Fig. 14. Vessel segmentation results of fused and unfused contour information and detail information at multiple scales. (a) Unfused vascular contour information and detailed information; (b) Fusion of vascular contour information and detailed information; (c) Marked detailed diagram in figure 14(a); (d) Marked detailed diagram in figure 14 (b).

Table 1. Performance comparison of retinal vessel segmentation methods

Method	ACC	SE	SP
Sine-Net [33]	0.9351	0.7071	0.9704
UNMU [34]	0.9431	0.6781	0.9821
M-GAN [35]	0.9474	0.7199	0.9804
EOA [36]	0.9476	0.7176	0.9812
Proposed	0.9593	0.7097	0.9817

the proposed method in this paper is higher than that of Sine-Net and UNMU, and only slightly lower than that of M-GAN and EOA. The accuracy and sensitivity of the proposed method are higher than the average values of other methods. The above performance comparison results show that the proposed method has a high accuracy and can perform vascular segmentation well on the premise of ensuring sensitivity.

5. Conclusion

A multi-scale NSST transform fusion method for retinal vessel segmentation is proposed. The proposed method combines the contour and detail features of retinal vessels with multiple scales, and keeps the fine branches of retinal vessels well while ensuring the accurate contour of retinal vessels. The average accuracy, sensitivity and specificity were 0.9593, 0.7097 and 0.9817 respectively. On the premise of ensuring the sensitivity, the proposed method has high accuracy and good overall performance, while keeping a certain balance between sensitivity and accuracy indexes. However, in order to further improve the accuracy of vascular segmentation, the interference of optic disc on vascular segmentation needs to be solved. In the future,this proposed method will be utilized in the clinical trials.

Acknowledgments. The author is very grateful to the anonymous expert review, which provides valuable guidance to the paper.

References

1. Tchinda B S, Tchiotsop D, Noubom M, et al. Retinal blood vessels segmentation using classical edge detection filters and the neural network[J]. Informatics in Medicine Unlocked, 2021, 23(3):100521.
2. Mohammedhasan M, Uguz H. A New Deeply Convolutional Neural Network Architecture for Retinal Blood Vessels Segmentation[J]. International Journal of Pattern Recognition and Artificial Intelligence, 2020.
3. Francia G A, Pedraza C, Aceves M, et al. "Chaining a U-Net With a Residual U-Net for Retinal Blood Vessels Segmentation," *IEEE Access*, vol. 8, pp. 38493-38500., (2020).
4. Liang LM, Sheng XQ, Lan ZM, et al. U-Shaped Retinal Vessel Segmentation Algorithm Based on Adaptive Scale Information[J]. Acta Optica Sinica, 2019, 39(8):0810004.
5. Wang X, Jiang X. Retinal vessel segmentation by a divide-and-conquer funnel-structured classification framework[J]. Signal processing, 2019, 165(Dec.):104-114.
6. Yan Z, Yang X, Cheng K T. A Three-Stage Deep Learning Model for Accurate Retinal Vessel Segmentation[J]. Biomedical and Health Informatics, IEEE Journal of, 2019, 23(4):1427-1436.
7. Odstrcilik J, Kolar R, Budai A, et al. Retinal vessel segmentation by improved matched filtering: Evaluation on a new high-resolution fundus image database[J]. IET Image Processing, 2013, 7(4):373-383.
8. D. A. Dharmawan, B. P. Ng and N. Borijindargoon. Design of Optimal Adaptive Filters for Two-Dimensional Filamentary Structures Segmentation. IEEE Signal Processing Letters, vol. 26, no. 10, pp. 1511-1515, Oct. 2019, doi: 10.1109/LSP.2019.2938631.
9. Rodrigues LC, Marengoni M, et al. Segmentation of optic disc and blood vessels in retinal images using wavelets, mathematical morphology and Hessian-based multi-scale filtering[J]. Biomedical signal processing and control, 2017: 36, 39-49.
10. Hugo A R, Gabriel A, Ivan C A, et al. Blood vessel segmentation in retinal fundus images using Gabor filters, fractional derivatives, and Expectation Maximization[J]. Applied Mathematics and Computation, 2018, 339:568-587.

11. Moosavi A, Figueiredo N, Prasanna P, et al. Imaging features of vessels and leakage patterns predict extended interval aflibercept dosing using ultra-widefield angiography in retinal vascular disease: findings from the PERMEATE study[J]. IEEE Transactions on Biomedical Engineering, 2020, 68(6): 1777-1786.
12. Bhuvana, J., Mirnalinee, T. T., Bharathi, B., Sneha, I.: Efficient Generative transfer learning framework for the detection of COVID-19. Computer Science and Information Systems, Vol. 19, No. 3, 1241-1259. (2022), https://doi.org/10.2298/CSIS220207033B
13. Chen C, Chuah J H, Ali R, et al. Retinal vessel segmentation using deep learning: a review[J]. IEEE Access, 2021, 9: 111985-112004.
14. Arhami M, Desiani A, Yahdin S, et al. Contrast enhancement for improved blood vessels retinal segmentation using top-hat transformation and otsu thresholding[J]. International Journal of Advances in Intelligent Informatics, 2022, 8(2): 210-223.
15. Lee C. LSTM-CRF models for named entity recognition[J]. IEICE transactions on information and systems, 2017, 100(4): 882-887.
16. J. Jiang, J. Ma, C. Chen, Z. Wang, Z. Cai and L. Wang, "SuperPCA: A Superpixelwise PCA Approach for Unsupervised Feature Extraction of Hyperspectral Imagery," in IEEE Transactions on Geoscience and Remote Sensing, vol. 56, no. 8, pp. 4581-4593, Aug. 2018, doi: 10.1109/TGRS.2018.2828029.
17. Mookiah M R K, Hogg S, MacGillivray T J, et al. A review of machine learning methods for retinal blood vessel segmentation and artery/vein classification[J]. Medical Image Analysis, 2021, 68: 101905.
18. Dong H, Zhang T, Zhang T, et al. Supervised learning-based retinal vascular segmentation by m-unet full convolutional neural network[J]. Signal, Image and Video Processing, 2022, 16(7): 1755-1761.
19. Aguirre-Ramos H, Avina-Cervantes J G, Cruz-Aceves I, et al. Blood vessel segmentation in retinal fundus images using Gabor filters, fractional derivatives, and Expectation Maximization[J]. Applied Mathematics and Computation, 2018, 339: 568-587.
20. Fu Q, Celenk M, Wu A. An improved algorithm based on CLAHE for ultrasonic well logging image enhancement[J]. Cluster Computing, 2019, 22(5): 12609-12618.
21. Qingwu Shi, Shoulin Yin, Kun Wang, et al.?Multichannel convolutional neural network-based fuzzy active contour model for medical image segmentation.?Evolving Systems?(2021). https://doi.org/10.1007/s12530-021-09392-3
22. Lee M, Lee J G, Kim N, et al. Hybrid Airway Segmentation Using Multi-Scale Tubular Structure Filters and Texture Analysis on 3D Chest CT Scans[J]. Journal of Digital Imaging, 2018, 32(5):1-14.
23. Shoulin Yin, Hang Li, Desheng Liu and Shahid Karim. Active Contour Modal Based on Density-oriented BIRCH Clustering Method for Medical Image Segmentation [J]. Multimedia Tools and Applications. Vol. 79,?pp. 31049-31068, 2020.
24. Yang H, Wu X T, He B G, et al. Image fusion based on multiscale guided filters[J]. Guangdianzi Jiguang/Journal of Optoelectronics Laser, 2015, 26(1):170-176.
25. Ding B, Wen G, Ma C, et al. Target recognition in synthetic aperture radar images using binary morphological operations[J]. Journal of Applied Remote Sensing, 2016, 10(4):046006.
26. Gai D, Shen X, Chen H, et al. Medical image fusion using the PCNN based on IQPSO in NSST domain[J]. IET Image Processing, 2020(5).
27. Zhang Z, Xi X, Luo X, et al. Multimodal image fusion based on global-regional-local rule in NSST domain[J]. Multimedia Tools and Applications, 2020(5):1-27.
28. R Yang, Du B, Duan P, et al. Electromagnetic Induction Heating and Image Fusion of Silicon Photovoltaic Cell Electrothermography and Electroluminescence[J]. IEEE Transactions on Industrial Informatics, 2020, 16(7):4413-4422.
29. Jing Yu, Hang Li, Shoulin Yin. Dynamic Gesture Recognition Based on Deep Learning in Human-to-Computer Interfaces [J]. Journal of Applied Science and Engineering, vol. 23, no. 1, pp.31-38, 2020.

30. Wang Z, Wang L, Elimelech M. Viability of Harvesting Salinity Gradient (Blue) Energy by Nanopore-Based Osmotic Power Generation[J]. Engineering, 2021.
31. Premjith B, Soman K P. Deep learning approach for the morphological synthesis in malayalam and tamil at the character level[J]. Transactions on Asian and Low-Resource Language Information Processing, 2021, 20(6): 1-17.
32. Y. Yuan, Z. Xu and G. Lu, "SPEDCCNN: Spatial Pyramid-Oriented Encoder-Decoder Cascade Convolution Neural Network for Crop Disease Leaf Segmentation," in IEEE Access, vol. 9, pp. 14849-14866, 2021, doi: 10.1109/ACCESS.2021.3052769.
33. Atli B, Gedik O S. Sine-Net: A fully convolutional deep learning architecture for retinal blood vessel segmentation[J]. Engineering Science and Technology an International Journal, 2021, 24(2): 271-283.
34. Upadhyay K, Agrawal M, Vashist P. Unsupervised multiscale retinal blood vessel segmentation using fundus images[J]. IET Image Processing, 2020, 14(11).
35. K. -B. Park, S. H. Choi and J. Y. Lee, "M-GAN: Retinal Blood Vessel Segmentation by Balancing Losses Through Stacked Deep Fully Convolutional Networks," in IEEE Access, vol. 8, pp. 146308-146322, 2020, doi: 10.1109/ACCESS.2020.3015108.
36. Rezaee K, Haddadnia J, Ashkan T. Optimized clinical segmentation of retinal blood vessels by using combination of adaptive filtering, fuzzy entropy and skeletonization[J]. Applied Soft Computing, vol. 52, pp. 937-951, 2017. doi: 10.1016/j.asoc.2016.09.033.

Feng Lijuan is with School of Electronics and Electrical Engineering, Zhengzhou University of Science and Technology.

Fan Zhang is with the Zhengzhou University of Technology, Zhengzhou 450000, China. Research direction: Information security, image processing and cloud computing.

Received: November 20, 2022; Accepted: April 12, 2023.

Computer Science and Information Systems 20(4):1749–1770 https://doi.org/10.2298/CSIS221205029Z

LUN-BiSeNetV2: A Lightweight Unstructured Network Based on BiSeNetV2 for Road Scene Segmentation

Yachao Zhang[1] and Min Zhang[2]

[1] School of Electronics and Electrical Engineering, Zhengzhou University of Science and Technology
Zhengzhou 450064, China
zhangychaoc@163.com
[2] Zhengzhou Commercial Technician College
Zhengzhou 450064, China
zhangminmin@126.com

Abstract. With the continuous introduction of automatic driving technology, the research of road scene segmentation algorithm in machine vision has become very important. In traditional methods, most researchers use machine learning methods to segment thresholds. However, the introduction of deep learning in recent years makes convolutional neural networks widely used in this field. Aiming at the problem that the traditional threshold segmentation method is difficult to effectively extract the threshold value of road image in multiple scenes and the serious problem of over-segmentation caused by deep neural network training data directly, this paper proposes a road scene segmentation method based on a lightweight unstructured network based on BiSeNetV2. The network contains backbone segmentation network and BiSeNetV2 network. The Mobilenetv2 network is used in the backbone network to replace the Xception feature extraction network in the decoder. In addition, grouping convolution is used to replace common convolution in Mobilenetv2 network. And it selects the batch specification layer to reduce the number of parameters, without affecting the accuracy and improving the efficiency of segmentation. At the same time, due to the relatively fixed distribution position of unstructured roads in the image, attention mechanism is introduced to process advanced semantic features, so as to improve the sensitivity and accuracy of the network. The BiSeNetV2 network enhances the dominant relationship between channel features by adding a compression excitation module based on channel attention mechanism after the detail branch, so as to perceive key areas and highlight local features. The lightweight feature pyramid attention mechanism is used to optimize semantic branches, improve the feature integration between contexts, extract high-level road semantic information more efficiently and retain spatial location information to the maximum extent. Finally, local semantic features and high-level semantic features are fused to improve the effect of unstructured road detection. The experiment is trained on the open data set. The results show that compared with other state-of-the-art networks, the accuracy and real-time performance of proposed LUN-BiSeNetV2 in this paper are good, and the false segmentation and edge clarity are better. Compared with the classical algorithm, the average intersection is improved by 2.2% compared with mIoU, the average pixel accuracy is improved by 7.6%, and the frame rate is improved by 24.5%.

Keywords: Road Scene Segmentation, BiSeNetV2, lightweight unstructured network, attention mechanism.

1. Introduction

Image segmentation in driverless cars has become a hot topic in the society. Driverless driving is defined as the realization of highly autonomous driving behavior through environmental perception: starting, braking, lane line tracking, lane change, collision avoidance, parking, etc. Road scene image segmentation plays an important role in this technology [1]. It is of great significance for the development of unmanned driving technology to study how to obtain efficient scene segmentation image in complex scene and serious noise environment [2].

The traditional road segmentation method is based on binocular stereo vision and motion index. Rajendar et al. [3] proposed pedestrian detection based on binocular stereo vision and support vector machine (SVM) algorithm, and determined the coordinate position of moving target by threshold segmentation. In view of the diversity of motion indicators, Raipuria et al. [4] segmented the road with multiple motion indicators such as projected surface direction, object height and feature tracking density. However, the above methods have high requirements on computing resources. In view of the practical requirements of unmanned driving at the present stage, a more simple method with lower resource occupancy rate is needed.

Recently, deep learning has been gradually introduced into road scene segmentation. Teng et al. [5] studied on intelligent vehicle steering based on end-to-end deep learning. Good road feature coding was obtained by pre-training self-encoding. In recent years, AI technology has attracted the attention from many scholars [6]. With the continuous research and development of GPU parallel running, computing acceleration, storage space compression and other technologies, the environmental requirements of excessive data and computation have gradually ceased to be the limitation. Convolutional neural network (CNN) has become a research hotspot of the public again and has been widely used. Kong et al. [7] learned high-order features in the scene based on deep learning algorithm to achieve road scene segmentation. Although the calculation intensity was reduced to a certain extent, the problem of over-segmentation in some complex scenes still existed. Abdalla et al. [8] proposed a method to measure feature similarity in source-target scenes with feature auto-encoder based on the feature automatic extraction capability of deep convolutional neural network (DCNN) depth structure for complex scenes. Zhu et al. [9] proposed image object segmentation by integrating T-node cues, considering that image boundaries could be effectively maintained in the process of image segmentation. However, the segmentation accuracy of these algorithms for road signs, vehicles and pedestrians has not reached the ideal result. The segmentation phenomenon often occurs on the road surface in cloudy and rainy days, snowy days and high temperature days.

Wang et al. [10] used the parallel linear edges of lanes in structured traffic environment as the basis for the detection of passable areas, and proposed a recognition method based on gray features. In order to reduce the impact of light changes and shadows on detection results, Yuji et al. [11] proposed a segmentation method based on lane marker lines by taking advantage of the fact that most edge points towards the expansion center of road boundaries were located at road boundaries. However, the above methods are not applicable to unstructured road detection. The reason is that unstructured roads lack identifiable lane lines, clear road edges and large background differences [12], making it difficult to complete the detection task. Fully Convolutional Networks (FCN) [13] realized end-to-end semantic segmentation, which greatly improved the generalization

ability of convolutional neural networks. In order to improve the segmentation accuracy, scholars have made a series of improvements based on FCN. SegNet [14] improved the up-sampling process by using the recorded maximum pooled index for up-sampling processing, which greatly improved the segmentation accuracy. DeepLabv1 [15] optimized the boundary details by processing the segmentation results using Conditional Random Field (CRF)[16]. DeepLabv2 used dilated convolution to replace the up-sampling method in the original Deeplabv1, and proposed the Atrous Spatial Pyramid Pooling (ASPP) module, which could reduce the number of parameters and increase the accuracy. DeepLabv3 [17] optimized the hollow space pyramid module to better capture multi-scale information. DeepLab3 introduced an encoder-decoder structure based on DeepLabv3 to better integrate low-level semantic features with high-level semantic features. PSPNet [18] proposed pyramid pool module, which could make full use of context information. UNet [19] proposed the U-shaped structure, which could use a smaller number of data sets without reducing the segmentation accuracy.

Since unstructured roads are characterized by many features, wide distribution range, large regional differences, and sensitivity to environmental factors [20]. If the above semantic segmentation network is used for identification, not only a large number of unstructured road data sets with rich types are needed, but also targeted modifications to the network structure are required. Otherwise, too deep network will lead to poor real-time performance and over-fitting phenomenon. DeepLabv3+ network with high segmentation accuracy, strong robustness and relatively simple structure is selected for improvement in this paper. The specific contributions of this paper are as follows.

1. The backbone Xception [21] in DeepLabv3+ network is replaced by MobileNetv2 [22], which can reduce the network structure, improve the feature extraction speed, and prevent over-fitting phenomenon.
2. In MobileNetv2 and dilated space pyramid module, grouping convolution [23] is used to replace traditional convolution, and batch specification layer is deleted, so as to reduce the number of parameters and computation without affecting the accuracy, and improve the segmentation efficiency.
3. The attention module is added to the dilated space pyramid module to improve the speed and accuracy of network recognition.
4. The BiSeNetV2 network enhances the dominant relationship between channel features by adding a compression excitation module based on channel attention mechanism after the detail branch, so as to perceive key areas and highlight local features.

The remaining paper is managed as follows: Section 2 presents the related works in detail. Section 3 discusses the proposed road scene segmentation. Then, in Section 4, experiments and results are provided. Lastly, the paper is concluded in Section 5.

2. Related Works

With the popularization of intelligent transportation and the rapid development of unmanned driving technology, high-precision detection and segmentation of multi-class targets in road scenes based on computer vision is becoming increasingly important. Currently, road scene segmentation based on deep learning method is the most widely used. In mainstream segmentation networks, many factors affect the robustness and richness

of features, and there are various methods to optimize feature performance, including multi-scale feature extraction, spatial context, attention mechanism, etc. One of the novel methods is to train features against interference.

The mainstream road segmentation networks start from the fully convolutional neural networks (FCN). Deconvolution was first proposed in FCN to replace the fully connected structure in convolutional neural network. The fully connected layer was removed, the ability of sharing convolution features was improved, and the prediction of road position pixel level was realized. However, with the increase of network pooling times, the problem of feature loss in encoder structure becomes more and more serious. In order to deal with the problem, SegNet was proposed to improve the image quality of up-sampling by introducing anti-pooling layer. Fan et al. [24] used the residual module on the basis of FCN, which could deepen the depth of the network and increase the propagation path of feature information at the same time, thus improving the detection accuracy and convergence speed of the network respectively. Wang et al. [25] put forward a pyramid pooling module in PSPNet, which used multi-scale pooling operation to output feature graphs of four sizes and carry out convolution operation to obtain image features under different receptive fields. In reference [26], a pyramid pool module of void space was introduced into DeepLabV3, and void convolution with different expansion multiples was used to obtain information of different sensitivity fields, which increased the diversity of extracted features. Kazerouni et al. [27] proposed a U-shaped network structure, which constructed multiple skip connection (SC) between encoder and decoder to realize the combination of low-level features and high-level features, reduce the loss of features during down-sampling, and improve the accuracy of segmentation results.

The above semantic segmentation network improves the segmentation accuracy of the target to a certain extent, and obtains good extraction effect. But it is slightly insufficient in the ability of anti-interference, which may come from the input image or from the features extracted by the network. Xu et al. [28] proposed the denoising convolutional neural network. Firstly, Gaussian noise was artificially added to the input image, and the convolutional network with residual structure was used to remove the noise, so as to achieve the denoising function. However, these noises were artificially added and natural real noise image had a certain difference. In order to simulate the possible interference information more truly, Ding et al. [29] proposed a pseudo-feature generator and linearly superimposed the generated pseudo-features into the intermediate feature layer of the detection network. Through the training method of generating antagonism [30], the constantly changing pseudo-features were obtained, so that the pseudo-features were similar to the real features. However, the detection network needed to overcome these feature interference and obtain the capability of anti-feature interference, which improved the accuracy of road detection. This training method of introducing confrontation to the encoder of detection network belongs to self-supervised learning [31], which indirectly improves the ability of encoder to filter interference by combining two supervised learning methods in training.

The advantage of self-supervised learning compared with supervised learning is that it does not have to rely on a large number of human-annotated labels. In recent years, the contrast learning method [32] has further improved self-supervised learning. The measure function is used to enhance the positive correlation and reduce the negative correlation, so as to improve the ability of the network to distinguish between positive and negative

samples. The contrast learning method pays more attention to the ability of learning feature extraction, and can achieve higher detection accuracy by fine-tuning training with a small amount of labeled data in specific tasks, improve the generalization performance of the network, and effectively reduce the phenomenon of over-fitting.

Since there is a certain correlation between global information and local information in the road scene. For example, the lane often appears in the middle of the image, it learns the attribution relationship between the them that is helpful to improve the prediction ability of the network. Zhu et al. [33] established the attribution relationship between global information and local information by maximizing mutual information between global and local features. Therefore, this paper proposes a novel road scene segmentation method based on a lightweight unstructured network and BiSeNetV2 to improve the robustness of the overall network.

3. Proposed Road Scene Segmentation

DeepLabv3+ network has good semantic segmentation, simple structure and fast segmentation speed. Because the original Xception network will appear over-fitting phenomenon when performing the tasks in this paper, and the speed cannot meet the real-time requirement, so the backbone is replaced by the lightweight transformation of MobileNetv2 network, which avoids the phenomenon of over-fitting phenomenon in the network depth and improves the efficiency of feature extraction. In order to improve the segmentation efficiency, the dilated space pyramid pool structure is improved by lightweight. At the same time, in order to improve the decoder's sensitivity to the target region, the attention module is introduced after the hollow space pyramid structure of the encoder. Then, the BiSeNetV2 network is used to improve the decoder, and the high-level and low-level feature graphs are fused and the pixels are classified. The complete network structure is shown in Figure 1.

3.1. Grouping Convolution

In order to reduce the number of parameters and improve the network efficiency, this paper, inspired by reference [34], uses grouping convolution to replace the common convolution operation in MobileNetv2 and spatial pyramid structure. Grouping convolution operation refers to grouping feature graphs and then convolving them when convolving feature graphs. The principle is shown in Figure 2. For an un-grouped network, the input feature graph size is $C \times W \times H$, the number of groups of convolution kernel is N, and the size of convolution kernel is $C \times K \times K$. To output N groups of feature graphs, it needs to learn $C \times K \times K \times N$ parameters. If the feature graph is divided into G groups, only $(C/G) \times K \times K \times N$ parameters need to be learned, and the total number of parameters is reduced to $1/G$. At the same time, the grouping convolution can also be regarded as making an dropout on the original feature graph, which has the regularization effect and avoids the phenomenon of over-fitting.

3.2. Lightweight Backbone

In this paper, the backbone of the new network adopts the structure of MobiletNetv2, and the specific structure is shown in Table 1.

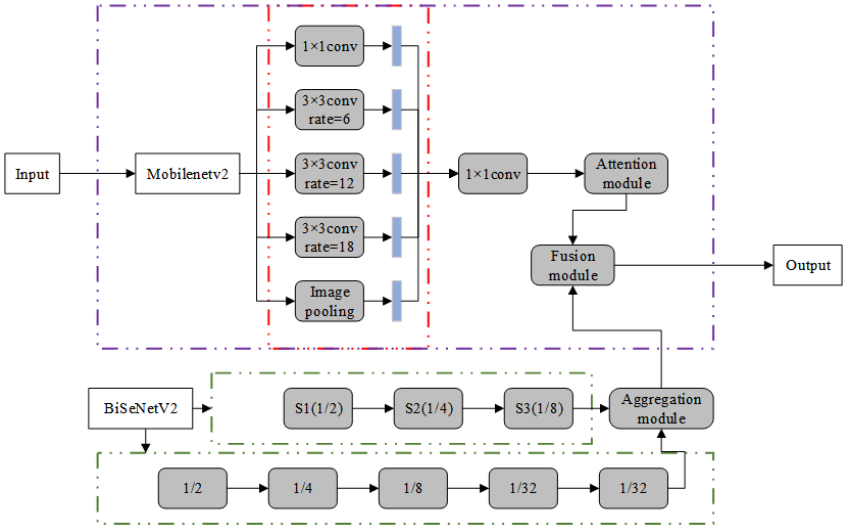

Fig. 1. The overall of proposed model framework

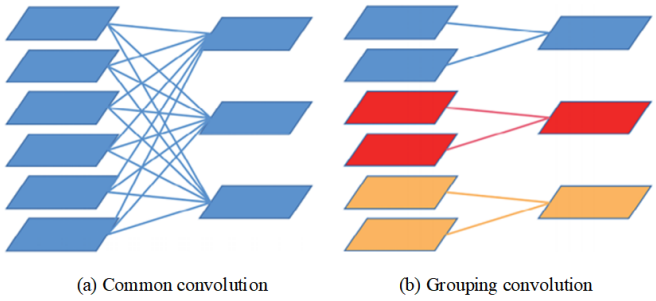

Fig. 2. The schematic diagram of groups convolution

Table 1. Parameters in the main backbone network

Input size ($H^2 \times C$)	Operator	t	c	n	s
$512^2 \times 3$	Conv2d	none	32	1	2
$256^2 \times 32$	Lite-bottleneck	6	16	1	1
$256^2 \times 16$	Lite-bottleneck	6	24	2	2
$128^2 \times 24$	Lite-bottleneck	6	32	3	2
$64^2 \times 32$	Lite-bottleneck	6	64	4	2
$32^2 \times 642$	Lite-bottleneck	6	96	3	1
$32^2 \times 96$	Lite-bottleneck	6	160	3	2
$16^2 \times 160$	Lite-bottleneck	6	320	1	1

In Table 1, H^2 is the number of pixels in the input image. C is the number of input channels. t is the multiplication factor of the input channel. n The number of repetitions of Lite-bottleneck of this size. s is the convolution step length of each Lite-bottleneck module.

In this structure, Lite-bottleneck is a bottleneck that is a lightweight improvement over its previous bottleneck. Lite-bottleneck has the same mechanism as its original bottleneck, and it can be divided into increasing dimension layer, convolutional layer, and dimension reduction layer. First, 1×1 convolution in the increasing dimension layer is used to raise the spatial dimension of the feature graph. Then, the feature of each channel feature graph is extracted by the depth separable convolution of 3×3 in the convolutional layer. Finally, the dimension is reduced by 1×1 convolution. Among them, the activation function of "dimension enhancement layer" and "convolution layer" is ReLU function. In order to prevent ReLU function from destroying the compressed features, the activation function after "dimension reduction layer" uses Linear function, as shown in Figure 3. Lite-bottleneck replaces the common convolution in "dimension raising layer" and "dimension reducing layer" by a block convolution with a bottleneck number of 2, which reduces the number of parameters. At the same time, because grouping convolution prevents over-fitting in shallow networks, it removes batch specification layers in Lite-bottleneck to reduce the computation amount. In the process of feature extraction, the feature map output with the size of 1282×24 is input into the decoder as low-level semantic features, and the feature map is input into the hollow space pyramid pool structure. The specific algorithm of network is shown in **Algorithm 1**. If the input image is bottleneck X and has a total of N layers, the following operation procedure occurs.

Algorithm 1 Lightweight MobileNetv2 algorithm

Input: X

$X_t = Conv(X)$
$X_R = ReLU(X_c)$
for $n = 1$ to N **do**
  $X_1 = ExpandedConv(X_n, groups = 2, noBN)$
  $X_2 = DepthwiseConv(X_1)$
  $X_3 = ProjectConv(X_2, groups = 2, noBN)$
end for
if $n == 2$ **then**
  $X_{LowLevel-Feature} = X_n$
end if
Output: $X_{LowLevel-Feature}, X_n$

Compared with the original Xception of DeepLabv3+, the new structure greatly reduces the network depth and the number of parameters, which is more suitable for the real-time unstructured road detection task in this paper.

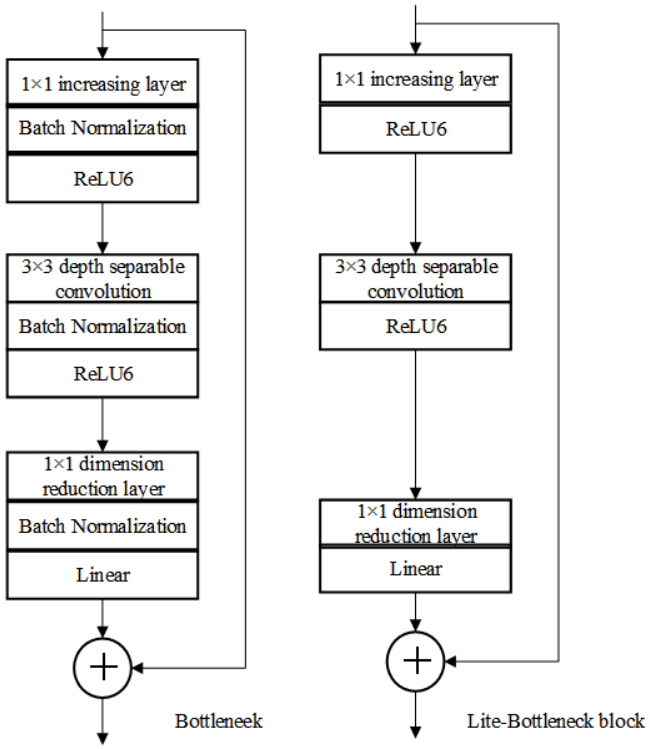

Fig. 3. Structure comparison of original bottleneck and Lite bottleneck

3.3. A lightweight dilated space pyramid pool module integrating attention mechanism

In order to enlarge the receptive field and extract multi-scale feature maps, DeepLabv3+ network adopts dilated space pyramid structure. The convolution with different dilated rates is used, and the large feature maps of different scales are extracted with the same number of parameters, which can better detect large targets like roads. At the same time, multi-scale context information can be captured to locate the target more accurately. After the image is transformed into a space pyramid pool, the feature map with unified dimensions and sufficient information is output. In order to accelerate the segmentation process and realize the function of real-time detection, a lightweight dilated space pyramid pool module is proposed in this paper. The dilated convolution is replaced by the dilated grouping convolution with group number of 2, which can reduce the number of parameters and act as the batch specification layer. Then it deletes the batch specification layer to reduce computation. The feature graphs of the lightweight void space pyramid pooling module are fused together, and the number of channels is adjusted by 1×1 convolution, and then the attention module is passed.

By assigning different weights to pixels, the attention module can adjust the attention focus of the whole network and improve the recognition effect and efficiency. The attention module in this paper is composed of channel attention module and space attention module in series. The channel attention module can focus on the meaningful part of the input feature, while the spatial attention module can obtain the global information in the scene [35].

The structure of the channel attention module is shown in Figure 4. After global average pooling and global maximum pooling, two groups of 1×1 feature maps X^c_{avg} and X^c_{max} are obtained for input feature X, which are then sent into two layers in fully connected neural networks respectively. The two-layer fully connected neural network shares parameters for the two groups of feature graphs, and then adds the two groups of feature graphs to get the weight coefficient between 0 and 1 by Sigmoid function, and multiplies it with the feature graphs to get the optimized feature graph. W_0 and W_1 are used to represent the two parameters of the shared network hiding layer (SharedMLP). The Sigmoid function is represented by σ. The channel attention can be calculated by the following formula.

$$M_c(X) = \sigma(W_1(W_0(X^c_{avg})) + W_1(W_0(X^c_{max}))) \tag{1}$$

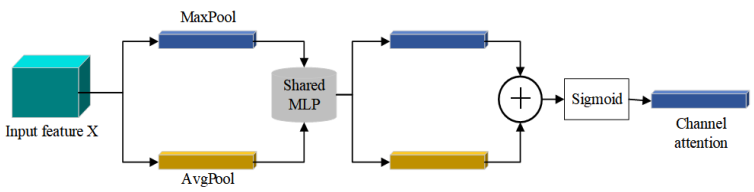

Fig. 4. Channel attention module

The structure of spatial attention module is shown in Figure 5. The optimized feature graph X' by the channel attention module is input. First, after maximum pooling and average pooling with only one channel dimension, the two obtained feature graphs X^s_{avg} and X^s_{max} are spliced together. After another convolution layer, it adopts a 7×7 convolution kernel for convolution operation. At the same time, it keeps the feature map size unchanged. The obtained feature graph is generated by using the Sigmoid function to generate the spatial weight coefficient, which is multiplied with the input feature graph to obtain the final feature graph. The calculation formula is as follows.

$$M_s(X') = \sigma(f^{7\times7}([AvgPool(X'); MaxPool(X')])) = \sigma(f^{7\times7}([X^s_{avg}; X^s_{max}])) \quad (2)$$

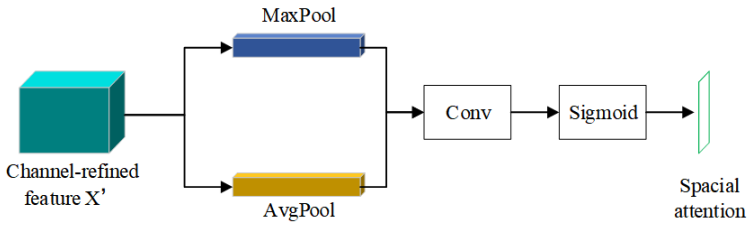

Fig. 5. Spacial attention module

3.4. Detail Branch Network Model Design

In road detection, due to the complexity and importance of road edge details, the network model in this paper uses detail branch with shallow high-channel convolution structure to extract road features. The shallow convolution structure can extract the detailed information, reduce the memory access cost, and improve the model reasoning speed. A higher number of channels can encode a variety of local information. This branch uses S1, S2 and S3 to represent the three sub-sampling stages, as shown in Table 2.

Table 2. Structure of Detail Branch

Stage	Operation	Kernel	Size	repetition	Output size
S1	Conv2D	$64 \times 3 \times 3$	2	1	256×256
S1	Conv2D	$64 \times 3 \times 3$	1	1	256×256
S2	Conv2D	$64 \times 3 \times 3$	2	1	128×128
S2	Conv2D	$64 \times 3 \times 3$	1	2	128×128
S3	Conv2D	$128 \times 3 \times 3$	2	1	64×64
S3	Conv2D	$128 \times 3 \times 3$	1	2	64×64

Each stage consists of 2 to 3 Conv2D convolution blocks, wherein Conv2D operation is shown in Equation (3).

$$O = g_s^{3\times3} = \delta(BN(f_s^{3\times3}(I))) \tag{3}$$

Where, O is the output feature map of Conv2D. $g_s^{3\times3}$ represents Conv2D with convolution kernel of 3×3 and step size of s. I is the input feature map of Conv2D. $f_s^{3\times3}$ is the convolution operation with convolution kernel 3×3 and step size s. BN is batch normalization. δ is the ReLu activation function. After three stages of Conv2D, the final output feature map extracted by the branch is $1/8$ of the original input image.

In road detection, although pooling operation is not carried out in this branch, convolution processing with step size of 2 is used to reduce dimension and reduce the size of the output feature map. In addition, compared with pooling operation, this dimension reduction method can retain more local road feature information through parameter fitting, and the shallow structure does not increase the complexity of the network too much, thus improving the speed of road feature detection.

3.5. Semantic branch network model design

When extracting features from roads, semantic branches are designed to extract advanced semantic features from roads. It is mainly divided into three stages S1, S2 and S3, which represent three stages of Stem block, gather-and-expansion (GE) block and context embedding (CE) block respectively, as shown in Table 3. Extracting high-level semantic information requires a large receptive field, so this branch adopts fast down-sampling strategy to improve the expression level of road features, rapidly expand receptive field, and uses global average pooling to obtain context relations.

Table 3. Structure of Semantic Branch

Stage	Operation	Kernel	Size	repetition	Output size
S1	Stem	$16 \times 3 \times 3$	4	1	128×128
S2	GE	$32 \times 3 \times 3$	2	1	64×64
S2	GE	$32 \times 3 \times 3$	1	1	64×64
S2	GE	$64 \times 3 \times 3$	2	1	64×64
S2	GE	$64 \times 3 \times 3$	1	1	32×32
S2	GE	$128 \times 3 \times 3$	2	1	32×32
S2	GE	$128 \times 3 \times 3$	1	3	16×16
S3	CE	$128 \times 3 \times 3$	1	1	16×16

Stem blocks are adopted in S1 stage, and the structure is shown in Figure 6. The module first convolves the original input image, down-samples the original image, and then uses two different down-sampling methods to reduce the feature representation. Finally, the output features of the two branches are connected as outputs, and a feature graph of 1/4 size is obtained. Due to the using of Stem modules for convolution and pooling operations to narrow the feature map, the structure has efficient computational cost and effective road feature representation capability.

In phase S2, multiple GE blocks are used. This stage belongs to the semantic integration stage of semantic branches, and the structure of each GE block is shown in Figure 7.

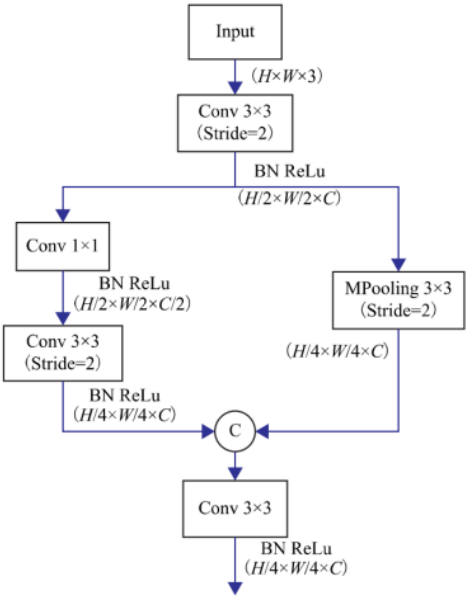

Fig. 6. Architecture of Stem Block

In this module, two 3×3 depth separable convolutions are independently used on each channel for feature extraction. Compared with one 5×5 depth separable convolution, they have the same receptive field. However, the complexity of the module is reduced.

The CE block is used in the S3 phase to integrate contextual information, and the structure is shown in Figure 8. In this module, global average pooling and residual connection are used to effectively extract global context information, so as to achieve the integration of road context information of GE layer. However, the structure of residual-linked will slow down the overall reasoning speed of the model.

3.6. Design of aggregation network model

After the details branch and semantic branch extract the features of different levels of the road, the extracted features need to be fused in the aggregation module to improve the accuracy of feature extraction. The network model design of the aggregation module is shown in Figure 9.

Since the feature graph of semantic branch output is 1/4 of the feature graph size of detail branch output, the detail branch is divided into two parts in this paper. One part uses conventional convolution with step size 2 and convolution kernel size 3×3 and 3×3 average pooling operation with step size 2, and the other part uses depth-separable convolution and 1×1 convolution. The semantic branch is also divided into two parts for processing. One part only uses conventional convolution and four up-sampling operation, while the other uses deep separable convolution with convolution kernel of 3×3 and convolution operation of 1×1. The final detail branch and semantic branch are divided into four branches, and the fusion method is shown in Formula (4).

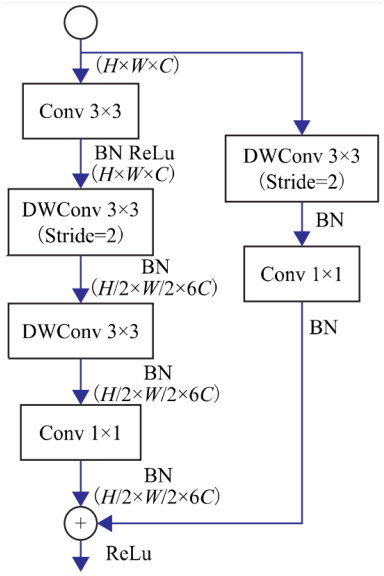

Fig. 7. Architecture of GE Block

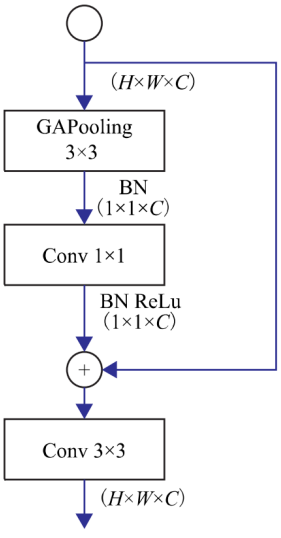

Fig. 8. Architecture of CE Block

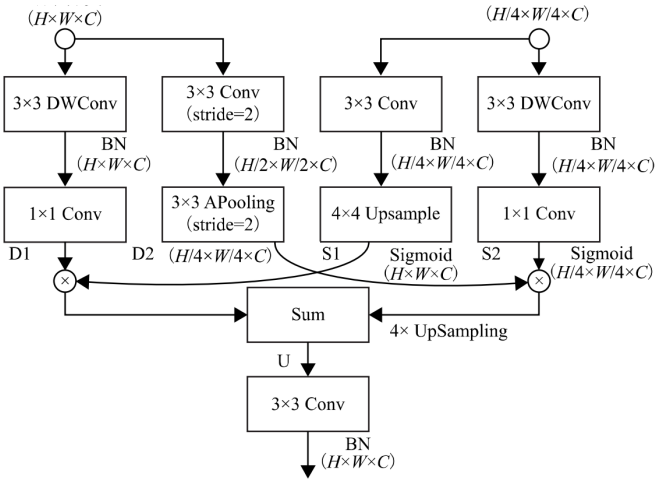

Fig. 9. Aggregation module

$$U = f_2(D_1 \otimes \sigma(S_1), f_1(D_2 \otimes \sigma(S_2) \tag{4}$$

Where, S_1, S_2, D_1 and D_2 are the feature graphs of detail branch and semantic branch processed in the first stage in the aggregation module respectively. U is the fusion feature graph obtained in Sum block. $\otimes$ represents the multiplication of corresponding elements in the feature graph. σ means Sigmoid function. f_1 means to perform 4 times up-sampling operations on the feature graph. f_2 represents the sum of the corresponding elements of the feature graph.

The feature fusion method adopted in this paper pays more attention to the diversity of the upper level road feature and the lower level road feature information in the two branches. By using different scale guidance, different feature representations can be captured, so that multi-scale information can be encoded, so that local information and high-level semantic information can be integrated more effectively, and thus improve the performance of road detection.

4. Experimental results and analysis

The unstructured road detection task is different from the structured road detection task with clear road markers such as expressways and urban arterial roads, which can simplify the detection task into lane lines or road boundary detection without obvious lane lines or clear road boundaries. Traditional urban street view semantic segmentation data sets are not suitable for unstructured road recognition. After comparing with other street view semantic segmentation data sets such as Cityscapes, India Driving Dataset (IDD) is more suitable for the training task of unstructured road detection [36]. The Indian road driving dataset contains 34 categories with a pixel size of 1920×1080. 6792 Street View images that meet the requirements are selected, as shown in Figure 10. As there are many types

of road driving data set in India, targeted transformation is carried out on it. Road and parking are divided into passable areas, and the remaining 32 categories are divided into impassable areas. The selected 6792 images were randomly divided into training set, verification set and test set according to the ratio of 8:1:1. The training set is used to train the network parameters, the verification set is used to feedback the training results and adjust the network parameters in time, and the test set is used to evaluate the quality of the trained network.

(a) (b)

Fig. 10. Selected IDD dataset example

4.1. Network Parameters

The training environment of this network is as follows: Windows11 operating system, CPU Intel(R) Core(TM) i5-10400F, 16GB Memory, Ge Force RTX 3060 GPU, 12GB video memory. We use PyTorch deep learning framework. An adaptive learning rate algorithm named Adam is used to update the weight of the neural network. In training stage, batchsize=8, initial learning rate=1.2×10^{-6}, weight attenuation=5.3×10^{-4}.

4.2. Evaluation Index

In this paper, the Dice similarity coefficient is used as the evaluation index of network model detection accuracy. In order to evaluate the road test results as comprehensively as possible, this paper also uses the recall rate and accuracy rate as evaluation indexes. The calculation formulas of Dice coefficient, Recall and Precision are shown in Equations(5) (7).

$$Dice = \frac{2TP}{FP + 2TP + FN} \tag{5}$$

$$Recall = \frac{TP}{TP + FN} \tag{6}$$

$$Precision = \frac{TP}{TP + FP} \tag{7}$$

Where, TP is the number of pixels in the predicted and actual road areas. FP is the number of pixels predicted to be road area but actually non-road area. TN is the number of pixels in the predicted and actual non-road area. FN is the number of pixel points predicted to be non-road area, but actually is road area.

On the other hand, frames per second (FPS) is used as the evaluation index for road detection speed in road area.

$$v = \frac{N}{\sum_i^N t_i} \tag{8}$$

Where N is the number of test images. t is the time required to process the $i - th$ image. v is the number of images processed per second by the semantic segmentation network model.

4.3. Optimized network results comparison

In order to analyze the performance of the network model proposed in this paper and verify the stability of the optimization module, experiments are carried out on the road data set for the road detection task in the open-pit mining area. Four groups of ablation experiments were set up here to compare the performance of BiSeNetV2, BiSeNetV2+SE, BiSeNetV2+FPA and DAM-BiSeNetV2, respectively. The loss function of the training process is shown in Figure 11, and the evaluation index is shown in Table 4.

Table 4. Font

Model	Parameter size/M	Dice/%	Recall/%	Precision/%	FPS/fps
BiSeNetV2	2.34	95.9	93.8	97.9	55
BiSeNetV2+SE	2.37	96.9	96.8	96.8	53
BiSeNetV2+FPA	2.30	97.4	97.3	96.7	69
DAM-BiSeNetV2	2.33	98.5	98.4	97.6	64

According to the analysis of loss function, the four models all reach convergence in the 60 generation times, and the DAM-BiSeNetV2 training loss can be reduced to a smaller loss value compared with other models. Then, the evaluation index of the model is analyzed. In terms of the number of parameters, FPA module adopts deep separable convolution, which reduces the number of parameters compared with ordinary convolution, and also reduces the number of parameters compared with the original CE module by 0.04 M. Combined with SE module, the complexity of the model can be reduced and

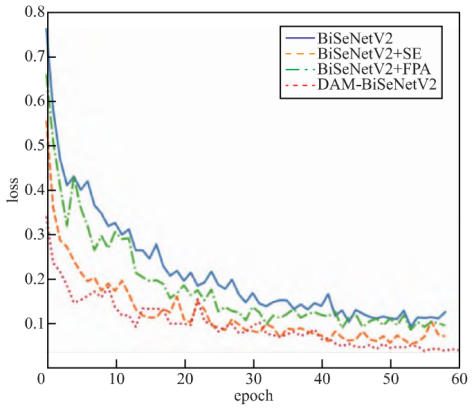

Fig. 11. Comparison of Loss Functions with Different Optimized Networks in Training Set

the reasoning speed of the model can be effectively improved. In terms of accuracy and detection rate, BiSeNetV2 can achieve good results in road detection, but in terms of Dice similarity coefficient and recall rate, it still needs to be further improved. BiSeNetV2+SE benefites from the SE module's ability to extract the dominant relationship between channels. Compared with BiSeNetV2, the Dice coefficient increased by 3.0%, and the tradeoff between recall rate and accuracy is achieved as far as possible. BiSeNetV2+FPA combined with lightweight FPA module can extract features of global concern and reduce model complexity. Compared with BiSeNetV2, the detection rate increases by 14fps and Dice similarity coefficient increases by 1.5%. DAM-BiSeNetV2 integrates SE module and FPA module reasonably. Due to the advantage of introducing multiple feature extraction modules without increasing the number of parameters, the Dice similarity coefficient increases by 2.6%, and the detection frame rate reaches 64fps, which is 9fps higher than BiSeNetV2. When the Dice similarity coefficient is improved, the detection rate of the model for the image is also improved. Therefore, the optimized DAM-BiSeNetV2 model can be better applied to road detection.

4.4. Comparison with other state-of-the-art methods

In order to further analyze the performance of the proposed model for road detection, the proposed method is compared with SSCNN [37], FNN [38], LWIR [39] and CODA [40] on road data sets. To keep the model lightweight, SSCNN and FNN use mobilenetv2 as the backbone, while LWIR and CODA use the backbone from the original network.

The experimental results are shown in Figure 12, where the first two behaviors detect the straight road scene and the last two behaviors detect the curve scene. SSCNN model is unable to detect crooked roads near mountain sides. FNN model will detect the sky or the slope along the road as the road area in some subtle places, and also cannot accurately detect the road area on some curved hillside roads. LWIR has poor detection effect on road images, and many hollowed out areas will appear, which cannot be accurately detected. CODA network model has a good detection effect on the road, but the detection is not

fine enough in the road edge area, and the slope will be mistakenly detected as a road. The method in this paper uses compression excitation module, so the model has the best detection results on the road. From the overall detection effect, the results of the proposed method are better than those of the lightweight LWIR and CODA semantic segmentation networks.

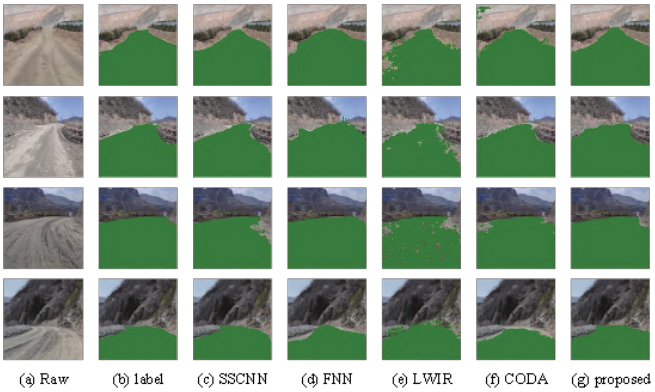

Fig. 12. Results of road detection by different segmentation models

The evaluation indicators obtained are shown in Table 5. The Dice similarity coefficient of the proposed model in this paper reaches 97.5%, and the detection speed reaches 65fps. As SSCNN uses dilated convolution, although the road detection effect is slightly better than that of the proposed model, the detection speed is far lower than that of the new model. Because FNN uses the feature pyramid pool module, it also has a serious impact on the reasoning speed of the model. When compared with LWIR, the proposed method is inferior to this network in terms of detection speed, but LWIR has poor effect on road detection and cannot meet the accuracy requirements. Compared with CODA, proposed method in this paper has 2.5% improvement in Dice similarity coefficient and 9fps improvement in reasoning speed. After the above analysis, the proposed model is superior to other mainstream models in road detection.

Table 5. Road detection results with different segmentation models

Model	Dice/%	Recall/%	Precision/%	FPS/fps
SSCNN	97.8	98.6	96.9	10
FNN	96.0	96.5	95.7	13
LWIR	93.8	91.8	94.4	71
CODA	95.0	93.1	98.9	56
Proposed	97.5	98.4	96.6	65

We also make a comparison on other images as shown in figure 13. By comparing the segmentation effect, it can be seen that the proposed method in this paper is closest to the label image. For the segmentation of the first three images, although the edge segmentation is better in reference [41], it is prone to false segmentation. As shown in the segmentation results of the first and second samples, small pieces of mis-segmentation appears on both vehicles, and the segmentation of the lower edge of vehicles in the segmentation results of the second sample is not very accurate. Although FNN is the fastest, the segmentation accuracy is relatively poor, and the edge details are lost more, which makes it impossible to accurately identify the passable area and the edge of obstacles. LWIR segmentation is more accurate, but the vehicle edge segmentation in the second sample is not accurate, and the segmentation speed is slow. For the fourth sample, except CODA, the other three algorithms can barely segment the left side of the pit contour. But for the right curb, different degrees of mis-segmentation appear in FNN, LWIR and CODA, while the proposed method avoids this phenomenon.

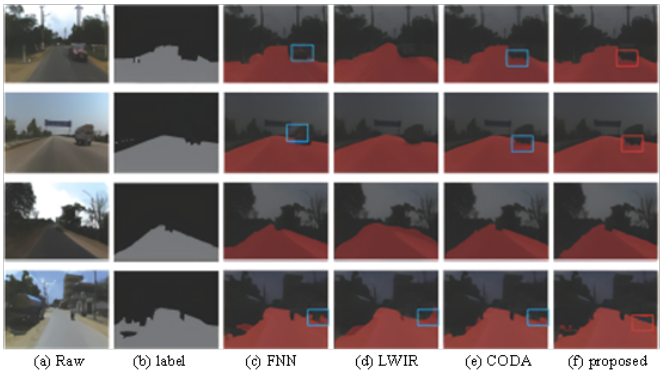

Fig. 13. Comparison of segmentation results

In the same environment and configuration, the selected Indian road driving data set is used to train the network in this paper, and the results are compared with the above networks, as shown in Table 6 (for figure 13). Due to the integration of attention mechanism and lightweight, the new network has improved the performance of average intersection ratio and passable area intersection ratio. The average pixel accuracy is increased to 98.7%, and the frame per second is increased to 72%, reaching 39.4 frames/s, which meets the real-time requirements of unstructured road segmentation task.

5. Conclusions

In order to better fulfill the task of unstructured road recognition, this paper uses selected Indian road driving data sets. Indian road driving data sets are very similar to the unstructured road condition in our country. After training, a semantic segmentation network model suitable for the unstructured road condition can be obtained. Aiming at the problem that structured road segmentation method cannot meet the real time and accuracy

Table 6. Road detection results with different segmentation models

Model	Dice/%	Recall/%	Precision/%	FPS/fps
FNN	96.3	97.4	97.5	32
CLWIR	95.7	92.5	93.8	53
CODA	95.4	94.6	95.2	61
Proposed	98.6	99.1	98.7	72

required by unstructured road segmentation in practical application, this paper proposes a lightweight unstructured network based on BiSeNetV2. To avoid the over-fitting phenomenon caused by too deep network and the low efficiency caused by too many parameters, MobileNetv2 is used to replace Xception as the feature extraction network. In addition, grouping convolution is used to replace common convolution in MobileNetv2 and dilated space pyramid pooling module. Their batch specification layer is rationally selected, which greatly reduces the number of network parameters. This method can improve the segmentation speed without affecting the accuracy of segmentation and meet the requirement of real-time performance. At the same time, in order to enlarge the common features of unstructured road image distribution to improve the segmentation accuracy, BiSeNetV2 is added to output advanced image features. Experiments show that the proposed network is superior to other advanced networks in terms of accuracy and efficiency. It provides some basis for improving the application of semantic segmentation in unstructured road recognition tasks. Future works will focus on more advanced deep learning method for road detection and apply them in real engineering applications.

Acknowledgments. This work was supported by "Project Name: Research on Road Scene Segmentation Technology Based on Convolutional Neural Network; Project Number: 222102210318".

References

1. Teng, L., Qiao, Y. "BiSeNet-oriented context attention model for image semantic segmentation," *Computer Science and Information Systems,* vol. 19, no. 3, pp. 1409-1426. (2022)
2. Liu, D., Yin, S., et al,. "Research on the online parameter identification method of train driving dynamic model," *International Journal of Computational Vision and Robotics*. (2022) doi:10.1504/IJCVR.2022.10047951
3. Rajendar, S., Rathinasamy, D., Pavithrao, R., et al,. "Prediction of stopping distance for autonomous emergency braking using stereo camera pedestrian detection," *Materials Today: Proceedings,* Vol. 51, pp. 1224-1228. (2022)
4. Raipuria. G., Gaisser. F., and Jonker. P.P. "Road infrastructure indicators for trajectory prediction," *2018 IEEE Intelligent Vehicles Symposium (IV). IEEE*, pp. 537-543. (2018)
5. S. Teng, L. Chen, Y. Ai, Y. Zhou, Z. Xuanyuan and X. Hu. "Hierarchical Interpretable Imitation Learning for End-to-End Autonomous Driving," *IEEE Transactions on Intelligent Vehicles,* vol. 8, no. 1, pp. 673-683. (2023) doi: 10.1109/TIV.2022.3225340.
6. Liguo Wang, Yin Shoulin, Hashem Alyami, et al. "A novel deep learning-based single shot multibox detector model for object detection in optical remote sensing images," *Geoscience Data Journal,* (2022). https://doi.org/10.1002/gdj3.162

7. Kong J, Yang C, Xiao Y, et al. "A graph-related high-order neural network architecture via feature aggregation enhancement for identification application of diseases and pests," *Computational Intelligence and Neuroscience,* vol. 2022, (2022).
8. Abdalla Y, Iqbal M T, Shehata M. "Copy-move forgery detection and localization using a generative adversarial network and convolutional neural-network," *Information,* vol. 10, no. 9, pp. 286 (2019).
9. Zhu J, Yang H, Lin W, et al. "Group re-identification with group context graph neural networks," *IEEE Transactions on Multimedia,* vol. 23, pp. 2614-2626 (2020).
10. Wang H, Wang Y, Zhao X, et al. "Lane detection of curving road for structural highway with straight-curve model on vision," *IEEE Transactions on Vehicular Technology,* vol. 68, no. 6, pp. 5321-5330 (2019).
11. Huang D Y, Chen C H, Chen T Y, et al. "Vehicle detection and inter-vehicle distance estimation using single-lens video camera on urban/suburb roads," *Journal of Visual Communication and Image Representation,* vol. 46, pp. 250-259 (2017).
12. Zhang, J., Yu, X., Lei, X., Wu, C. "A Novel Deep LeNet-5 Convolutional Neural Network Model for Image Recognition," *Computer Science and Information Systems,* Vol. 19, No. 3, pp. 1463-1480. (2022). https://doi.org/10.2298/CSIS220120036Z
13. Li Y, Zhao H, Qi X, et al. "Fully convolutional networks for panoptic segmentation," *Proceedings of the IEEE/CVF conference on computer vision and pattern recognition,* pp. 214-223, (2021).
14. Badrinarayanan V, Kendall A, Cipolla R. "Segnet: A deep convolutional encoder-decoder architecture for image segmentation," *IEEE transactions on pattern analysis and machine intelligence,* vol. 39, no. 12, pp. 2481-2495 (2017).
15. Harika A, Sivanpillai R, Variyar V V S, et al. Extracting Water Bodies in RGB Images Using DEEPLABV3+ Algorithm[J]. The International Archives of Photogrammetry, Remote Sensing and Spatial Information Sciences, 2022, 46: 97-101.
16. Li Y, Li C, Li X, et al. A comprehensive review of Markov random field and conditional random field approaches in pathology image analysis[J]. Archives of Computational Methods in Engineering, 2022, 29(1): 609-639.
17. Yurtkulu S C, ahin Y H, Unal G. Semantic segmentation with extended DeepLabv3 architecture[C]//2019 27th Signal Processing and Communications Applications Conference (SIU). IEEE, 2019: 1-4.
18. Zhou J, Hao M, Zhang D, et al. Fusion PSPnet image segmentation based method for multifocus image fusion[J]. IEEE Photonics Journal, 2019, 11(6): 1-12.
19. Ronneberger O, Fischer P, Brox T. U-net: Convolutional networks for biomedical image segmentation[C]//Medical Image Computing and Computer-Assisted InterventionCMICCAI 2015: 18th International Conference, Munich, Germany, October 5-9, 2015, Proceedings, Part III 18. Springer International Publishing, 2015: 234-241.
20. Yin Shoulin, Liu Jie, Teng Lin. A new krill herd algorithm based on SVM method for road feature extraction[J]. Journal of Information Hiding and Multimedia Signal Processing, vol. 9, no. 4, pp. 997-1005, July 2018.
21. Chollet F. Xception: Deep learning with depthwise separable convolutions[C]//Proceedings of the IEEE conference on computer vision and pattern recognition. 2017: 1251-1258.
22. Sandler M, Howard A, Zhu M, et al. Mobilenetv2: Inverted residuals and linear bottlenecks[C]//Proceedings of the IEEE conference on computer vision and pattern recognition. 2018: 4510-4520.
23. Guo Q, Wu X J, Kittler J, et al. Self-grouping convolutional neural networks[J]. Neural Networks, 2020, 132: 491-505.
24. Fan J, Hua Q, Li X, et al. Biomedical sensor image segmentation algorithm based on improved fully convolutional network[J]. Measurement, 2022, 197: 111307.
25. Wang W, Wang S, Li Y, et al. Adaptive multi-scale dual attention network for semantic segmentation[J]. Neurocomputing, 2021, 460: 39-49.

26. Chen Z, Rajamanickam L, Tian X, et al. Application of Optimized Convolution Neural Network Model in Mural Segmentation[J]. Applied Computational Intelligence and Soft Computing, 2022, 2022.
27. Kazerouni I A, Dooly G, Toal D. Ghost-UNet: An asymmetric encoder-decoder architecture for semantic segmentation from scratch[J]. IEEE Access, 2021, 9: 97457-97465.
28. Xu Q, Zhang C, Zhang L. Denoising convolutional neural network[C]//2015 IEEE International Conference on Information and Automation. IEEE, 2015: 1184-1187.
29. Zhou D, Wang N, Peng C, et al. Towards multi-domain face synthesis via domain-invariant representations and multi-level feature parts[J]. IEEE Transactions on Multimedia, 2021, 24: 3469-3479.
30. Lin G, Kong L, Liu T, et al. An antagonistic training algorithm for TFT-LCD module mura defect detection[J]. Signal Processing: Image Communication, 2022, 107: 116791.
31. Yin Shoulin, Liu Jie, Li Hang. A Self-Supervised Learning Method for Shadow Detection in Remote Sensing Imagery[J]. 3D Research, vol. 9, no. 4, December 1, 2018. https://doi.org/10.1007/s13319-018-0204-9
32. Li G, Yu Y. Deep contrast learning for salient object detection[C]//Proceedings of the IEEE conference on computer vision and pattern recognition. 2016: 478-487.
33. Zhu J, Li X, Gao C, et al. Unsupervised community detection in attributed networks based on mutual information maximization[J]. New Journal of Physics, 2021, 23(11): 113016.
34. Liao Y, Lu S, Yang Z, et al. Depthwise grouped convolution for object detection[J]. Machine Vision and Applications, 2021, 32: 1-13.
35. Wang S H, Zhou Q, Yang M, et al. ADVIAN: Alzheimer's disease VGG-inspired attention network based on convolutional block attention module and multiple way data augmentation[J]. Frontiers in Aging Neuroscience, 2021, 13: 687456.
36. Dokania S, Hafez A H, Subramanian A, et al. IDD-3D: Indian Driving Dataset for 3D Unstructured Road Scenes[C]//Proceedings of the IEEE/CVF Winter Conference on Applications of Computer Vision. 2023: 4482-4491.
37. Dewangan D K, Sahu S P. Road detection using semantic segmentation-based convolutional neural network for intelligent vehicle system[C]//Data Engineering and Communication Technology: Proceedings of ICDECT 2020. Springer Singapore, 2021: 629-637.
38. Mehtab S, Yan W Q. Flexible neural network for fast and accurate road scene perception[J]. Multimedia Tools and Applications, 2022, 81(5): 7169-7181.
39. Li N, Zhao Y, Pan Q, et al. Illumination-invariant road detection and tracking using LWIR polarization characteristics[J]. ISPRS Journal of Photogrammetry and Remote Sensing, 2021, 180: 357-369.
40. Li K, Chen K, Wang H, et al. Coda: A real-world road corner case dataset for object detection in autonomous driving[C]//Computer VisionCECCV 2022: 17th European Conference, Tel Aviv, Israel, October 23C27, 2022, Proceedings, Part XXXVIII. Cham: Springer Nature Switzerland, 2022: 406-423.
41. Y. Yuan, Z. Xu and G. Lu, "SPEDCCNN: Spatial Pyramid-Oriented Encoder-Decoder Cascade Convolution Neural Network for Crop Disease Leaf Segmentation," in IEEE Access, vol. 9, pp. 14849-14866, 2021, doi: 10.1109/ACCESS.2021.3052769.

Yachao Zhang is with the School of Electronics and Electrical Engineering, Zhengzhou University of Science and Technology. Research direction: Information security, image processing.

Min Zhang is with the Zhengzhou Commercial Technician College. Research direction: Information security, image processing.

Received: December 05, 2022; Accepted: May 10, 2023.

Computer Science and Information Systems 20(4):1771–1795 https://doi.org/10.2298/CSIS221210030D

A Novel Multilevel Stacked SqueezeNet Model for Handwritten Chinese Character Recognition

Yuankun Du[1], Fengping Liu[2], and Zhilong Liu[3]

[1] School of Big Data and Artificial Intelligence, Zhengzhou University of Science and Technology
450002 Zhengzhou, China
duyuankk@163.com
[2] School of Information Engineering, Zhengzhou University of Science and Technology
450002 Zhengzhou, China
liufengppp@163.com
[3] Library of Henan Institute of Animal Husbandry and Economics
450002 Zhengzhou, China
liuzhilonglo@163.com

Abstract. To solve the problems of large number of similar Chinese characters, difficult feature extraction and inaccurate recognition, we propose a novel multilevel stacked SqueezeNet model for handwritten Chinese character recognition. First, we design a deep convolutional neural network model for feature grouping extraction and fusion. The multilevel stacked feature group extraction module is used to extract the deep abstract feature information of the image and carry out the fusion between the different feature information modules. Secondly, we use the designed down-sampling and channel amplification modules to reduce the feature dimension while preserving the important information of the image. The feature information is refined and condensed to solve the overlapping and redundant problem of feature information. Thirdly, inter-layer feature fusion algorithm and Softmax classification function constrained by L2 norm are used. We further compress the parameter clipping to avoid the loss of too much accuracy due to the clipping of important parameters. The dynamic network surgery algorithm is used to ensure that the important parameters of the error deletion are reassembled. Experimental results on public data show that the designed recognition model in this paper can effectively improve the recognition rate of handwritten Chinese characters.

Keywords: Handwritten Chinese character recognition, multilevel stacked SqueezeNet model, inter-layer feature fusion, L2 norm.

1. Introduction

Handwritten Chinese character recognition (HCCR) is one of the most challenging problems in pattern recognition and machine learning [1,2]. Optical Character Recognition (OCR) involves many disciplines such as digital signal processing, pattern recognition and natural language processing, and it has been widely applied in computer and other related fields [3]. Handwritten Chinese character recognition being realized can be used for machine marking, mail automatic sorting, bill recognition, etc,. However, there are a large number of similar Chinese characters due to various categories of Chinese characters, complex font structure [4]. Handwritten Chinese characters are different from person

to person, resulting in handwritten Chinese character recognition difficulties, so handwritten Chinese character recognition has been a research difficulty and hotspot.

According to the collection method of handwritten Chinese characters data, it can be divided into off-line handwritten Chinese characters recognition and online handwritten Chinese characters recognition. The off-line handwritten Chinese character pictures are captured by cameras or scanners and other instruments [5]. Online handwritten Chinese character recognition collects handwritten Chinese characters by various hardware devices in real time. In this process, not only the characteristics of Chinese characters, but also the stroke track information of Chinese characters are collected [6]. Off-line handwritten Chinese characters inevitably add noise interference in the process of picture acquisition. Therefore, in general, off-line handwritten Chinese character recognition is more difficult than online handwritten Chinese character recognition. Traditional off-line handwritten Chinese character recognition mainly includes three steps: data preprocessing, feature extraction and recognition classification. Among them, data processing mainly involves smoothing and de-noising, whitening, shaping and transforming. Feature extraction mainly includes statistical features and structural features. The statistical features have better effects than structural features, which mainly include Gabor feature [7] and Gradient feature [8], etc. Support vector machine classifier and linear discriminant classifier are mainly used to identify the differences.

In recent years, the traditional "pre-processing+feature extraction+classifier" handwritten Chinese character recognition does not seem to have made great progress, and there are few breakthrough research reports. However, the rise of deep learning has brought new vitality and extremely effective solutions to handwritten Chinese character recognition problems, especially the introduction of Convolutional Neural Network (CNN), which makes breakthroughs in the field of image recognition. Deep convolutional neural network models such as VGGNet, improved Inception, ResNet and other models have achieved excellent results on the ImageNet data set [9]. These advanced technologies provide the basis and reference for off-line handwritten Chinese character recognition.

So far, many researchers have done a lot of researches on off-line handwritten Chinese character recognition. Some researchers conduct research based on traditional machine learning methods. For example, reference [10] adopts an improved affine propagation clustering algorithm. In reference [11], a multi-feature handwritten Chinese character recognition technology based on support vector machine SVM was proposed. On the basis of grid feature extraction, centroid features, stroke features and feature points of Chinese characters were extracted, and SVM classifier was adopted to realize handwritten Chinese character recognition. This kind of method requires data preprocessing and complex feature extraction, so it is difficult to extract accurate features comprehensively. In reference [12], a partial cascade feature classification scheme based on LS-SVM was adopted. The sampling results of low-threshold Hough space were used as coarse classification features, and the local two-branch distribution histogram was used as fine classification features for coarse classification. Sample classification was realized after coarse classification. Reference [13] used Modified Quadratic Discriminant Function (MQDF) and the Convolutional Neural Networks (CNN) to obtain a higher accuracy than the single CNN and MQDF. Reference [14] adopted the cascaded MQDF and Deep Belief Networks (DBN) to achieve higher accuracy. Based on deep learning algorithms, some researchers improve the recognition performance by improving the network structure or proposing

improved training methods. For example, Residual Networks (ResNet) were used in reference [15] to optimize network performance by improving the unit structure of residual learning module. In reference [16], iterative refinement was adopted in convolutional neural networks. Reference [17] applied the VGGNET model in convolutional neural network to Chinese character recognition. In reference [18], the center loss function proposed in face recognition was applied to the CNN network of handwritten Chinese characters to reduce the intra-class distance, increase the inter-class distance and improve the recognition performance. Wang et al. [19] used a deep CNN network, combined the printed and handwritten data sets to train the recognition network, and builded a service to expand the training data set and improved the adaptability to different writing styles.

Although the recognition accuracy of handwritten Chinese characters based on CNN model has been greatly improved, it requires large computing resources, power consumption and storage space, it has many parameters, and it is difficult to conduct distributed training. It is the greatest challenge for deploy the corresponding model in embedded platforms such as ARM board and FPGA with limited hardware resources [20]. In order to realize handwritten Chinese character recognition with limited resources, the size of the model is reduced as much as possible while the model prediction performance is guaranteed in this paper.

There are five commonly used methods to compress CNN model volume: network pruning, parameter sharing, quantization, network distillation and compact network design, all of them can obtain obvious compression effect. The compact network improves the convolution with more network parameters and computations. For example, SqueezeNet, ShuffleNet, MobileNet, and Xception all have reduced the convolution layer [21].

In the proposed multilevel stacked SqueezeNet, FireModule is introduced into AlexNet convolutional model, and the model is compressed 50 times with good accuracy, and is successfully applied to embedded platform. In this paper, the compression of handwritten Chinese character model is studied. After modifying the SqueezeNet model, the Dynamic Network Surgery model is added to compress the parameters of the model, including cutting and repairing, and the accuracy of the model is ensured at the same time.

This part is the organization structure. Section 2 introduce the related works of CNN. Section 3 shows the detailed multilevel stacked SqueezeNet model. The experiments and analysis are conducted in section 4. Section 5 concludes this paper.

2. Related Works

Convolutional neural network (CNN) is a structured and supervised multi-layer feed-forward neural network, which is mainly applied to two-dimensional data processing. It can automatically extract image features through learning, and finally achieve the purpose of image classification. It consists of alternating convolution layers, sampling layers and fully connection layers, each of which contains multiple convolution kernels. Each neuron in the convolutional layer is connected with the local region of the upper layer, and the feature information of two-dimensional data is extracted through the convolutional operation, and the interference of noise on the feature is reduced. The sampling layer samples two-dimensional data, reduces the resolution, saves the feature information of the image as much as possible, reduces the dimension of the data and the number of parameters,

then it improves the network operation speed. LetNet-5 is a classical convolutional neural network structure [22], and its structure diagram is shown in Figure 1.

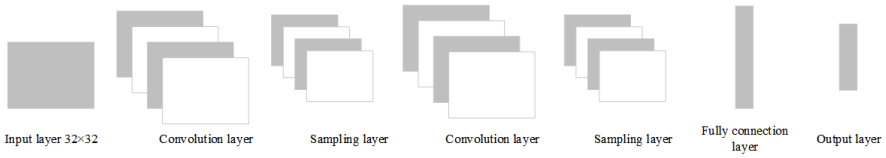

Fig. 1. Structure of LetNet-5

2.1. Convolutional Layer

For the convolutional layer, the convolutional kernel performs sliding convolution operation with the feature map of the previous layer, and the bias is added to get a net output, as shown in Formula (1). Finally, the result of convolution is obtained through the nonlinear action of activation function, namely, the output feature map, i.e.,

$$u_i^l = \sum_j^M x_j^{l-1} \times k_{ij}^l + b_i^l, i = 1, 2, \cdots, N \tag{1}$$

$$x_i^l = f(u_i^l) \tag{2}$$

Where, N represents the number of convolution kernels in the $l-th$ layer. M represents the number of feature maps at layer $l-1$. x_j^{l-1} is the $j-th$ feature graph in layer $l-1$. k_{ij}^l is the $j-th$ channel in the $i-th$ convolution kernel of the l layer. b_i^l is the bias of the $i-th$ convolution kernel. u_i^l is the net output of the $i-th$ convolution kernel in layer 1. The operation $\times$ stands for convolution operation. x_i^l is the $i-th$ feature graph of the $l-th$ layer. $f(\cdot)$ is the activation function, usually Sigmoid function. The Sigmoid function is shown in Formula (3):

$$S(x) = \frac{1}{1+e^{-x}} \tag{3}$$

2.2. Sampling Layer

In the sampling layer, the output feature map of the previous layer is down-sampled, and the input feature map is divided into multiple non-overlapping image blocks by sampling window, and then the maximum pooling or average pooling method is adopted for each image block. Assume that the size of the sampling window is $n \times n$, the size of the input

feature graph is $iS \times iS$, and the size of the output feature graph is shown in Formula (4). Maximum pooling and average pooling are shown in Equation (5) and Equation (6).

$$oS = \frac{iS}{n} \tag{4}$$

$$x_{kj}^{l} = max(x_{k1}^{l-1}, \cdots, x_{kn^2}^{l-1}), x_{ki}^{l-1} \in V_{kj}, k = 1, 2, \cdots, N \tag{5}$$

$$x_{kj}^{l} = \frac{1}{n \times n} \sum x_{ki}^{l-1} \tag{6}$$

Where l represents the current sampling layer. N represents the number of input feature maps, which is the same as the number of output feature maps. $V_{kj}, j = 1, 2, \cdots, oS^2$ represents the $j - th$ image block of the $k - th$ input feature graph. Each image block contains n^2 elements. x_{ki}^{l} is the $i - th$ element in V_{kj} image block. x_{kj}^{l} is the $j - th$ element on the $k - th$ output feature map of the current layer.

2.3. Fully Connection Output Layer

After the convolution layer and the down-sampling layer, the advanced features of the original image have been extracted. The purpose of the fully connection layer is to use these features to classify the original image. The fully connection layer does the weighted sum of these features, adds the bias quantity, and finally obtains the final output by activating the function, as shown in Equation (7). The output layer is also essentially a fully connection layer, except that the activation function is classified by the classification function [23].

$$y^{l} = f(w^{l} x^{l-1} + b^{l}) \tag{7}$$

Where, x^{l-1} is the output feature diagram of the previous layer, and the elements are high-level features extracted through convolution and down-sampling. w^{l} is the weight coefficient of the fully connection layer. b^{l} is the offset of the fully connection layer l.

The convolutional neural network is generally used in the case of multiple classifications, and the classification function usually adopts Softmax function, which normalizes the inactive output Z^{L} of the last layer L to the range of $(0, 1)$. Meanwhile, the sum of output values is 1 for classification. The calculation formula of Z^{L} is shown in Equation (8), and the function of Softmax is shown in Equation (9).

$$z^{L} = w^{L} x^{L-1} + b^{L} \tag{8}$$

$$a_i^{L} = \frac{e^{z_i^{L}}}{\sum_{j=1}^{n^{L}} e^{z_i^{L}}} \tag{9}$$

Where L represents the last output layer ($L-th$ layer). n^L denotes that there are n output neurons in layer L. a_i^L is the output of the $i-th$ category in n categories. z_i^L represents the $i-th$ inactive output. z_j^L represents the $j-th$ inactive output. e is a natural constant.

2.4. SqueezeNet Model

SqueezeNet is based on AlexNet model. It is with fewer parameters while achieving an accuracy close to AlexNet network [24]. The core of SqueezeNet lies in FireModule, where small convolution kernels replace partially large ones. When 5×5 and 3×3 convolutions are used for convoluted one $5 \times 5 \times 1$ image, the former will produce 25 parameters and 25 calculations, while the latter will produce 18 parameters and 90 computations. However, the memory reading speed of the computer is much slower than that of multiplication calculation, and the convolution speed of small convolution kernel with fewer parameters is faster. Therefore, in this paper, 1×1 is used to replace part 3×3, which will accelerate the convolution speed, and the remaining 3×3 convolution kernel guarantees the convergence speed. the convolution speed. The other 3×3 convolution kernels ensure the convergence speed.

As shown in Figure 2, SqueezeNet is divided into Squeeze layer and Expand layer. The Squeeze layer has S convolution layers with 1×1 kernel. The Expand layer is a convolution layer with e_1 1×1 and e_2 3×3 convolution kernels, and the activation layer is ReLU. The input feature map size of FireMoudle is $H \times W \times M$, and the output feature map size is $H \times W \times (e_1 + e_2)$. Only the dimension is changed, but its resolution is not changed. Firstly, the feature maps of $H \times W \times M$ are squeezed through the Squeeze layer, and S feature maps are obtained to achieve compression effect ($S < M$). In the Expand layer, $H \times W \times S$ is convolved with e_1 1×1 convolution kernels and e_2 3×3 convolution kernels respectively, and the convolution results of the two parts are fused to obtain the output result with $H \times W \times (e_1 + e_2)$ size. The value of $(e_1 + e_2)$ must be greater than M. So FireMoudle increases the dimension of the input. Where, S, e_1, and e_2 are adjustable parameters, which represent the number of convolution kernels and also reflect the dimension of the output feature graph. In this paper, $e_1 = e_2 = 4S$ is taken.

In addition, down-sampling operation is used in the module to ensure that the convolutional layer has a larger activation function, and the model accuracy is guaranteed under the condition of limited network parameters.

3. Multilevel Stacked SqueezeNet Model

Traditional convolutional neural networks have some problems, such as inadequate feature extraction and poor network learning ability. At the same time with the deepening of the network, it also has the information loss issue. In order to solve these problems, this paper uses the advantages of ResNet residual network to transfer information directly to the output results, thus protecting the integrity of information and alleviating the problem of information loss. The feature information is divided into groups, and then feature extraction is carried out respectively. Finally, the information of each group is integrated together to increase the diversity of online learning.

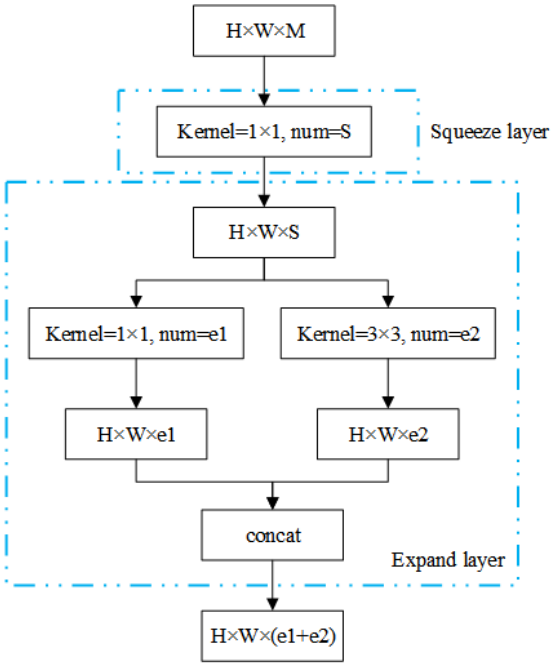

Fig. 2. FrieMoudle module

3.1. Feature group extraction module

The feature group extraction module designed in this paper is shown in Figure 3 and Figure 4. The number of input feature maps of the network module in Figure 3 is 129. Before the feature grouping, channel rearrangement of the feature information is performed to disrupt the order of input feature information.

As shown in Figure 5, taking three groups as an example, in order to increase the diversity of network learning, the feature information is grouped with different colors to represent different information. In the absence of channel rearrangement, the same feature information may be contained in the same group segment, but the information in different groups segment will be different. If features are directly grouped, the information in the group segmentation will be incomplete and the representation ability of the information will be reduced. It can be seen from the figure that rearrangement of channels enables different segments to exchange information, enriching the feature information of different segments. Through channel rearrangement, each group has the characteristic information of other groups. In this way, although there is no contact between groups after grouping, the information of each group is comprehensive and will not be lost. Then, 129 feature graphs are divided into three groups with 43 features in each group. In order to enhance the diversity of network extraction information, convolution kernels of different sizes are used for feature extraction in each group. After information extraction for each group, information exchange and fusion between groups are carried out. At this time, the number of feature maps for each group increased from 43 to 86. Then 86 feature maps of each

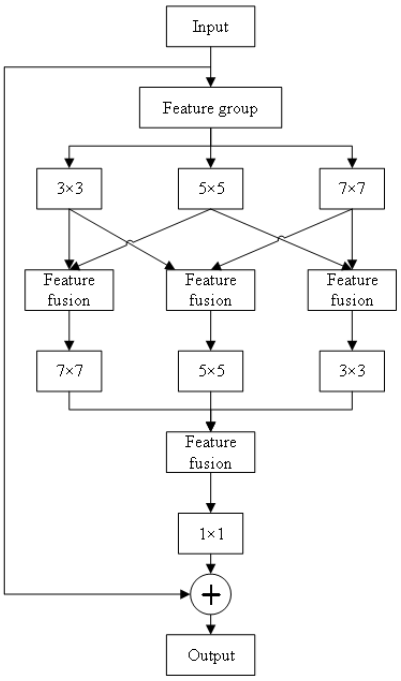

Fig. 3. Network module 1

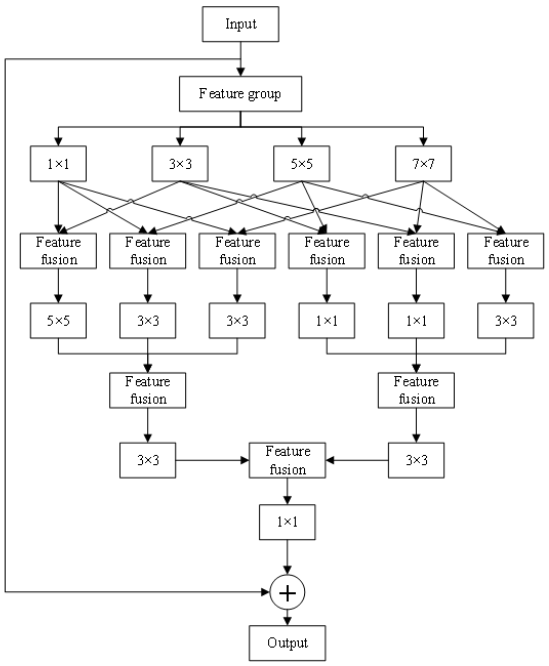

Fig. 4. Network module 2

group are extracted to further improve the learning ability of the network. Finally, the information of each group is merged and integrated, and the number of integrated feature channels is 258. In order to make them consistent with the input channel and facilitate the residual calculation with the original input information, 1×1 convolution is needed to reduce the dimension of the output channel. The number of input feature maps of the network module in Figure 4 is 256, which are divided into four groups with 64 feature maps in each group. The idea of information exchange combination is the same as that in Figure 3.

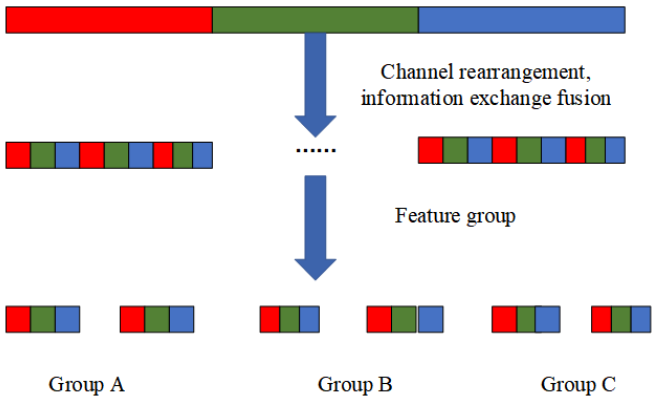

Fig. 5. Channel rearrangement

3.2. Down-sampling and channel amplification module

The traditional convolutional neural network usually adopts average pooling layer or maximum pooling layer for down-sampling, but this method ignores the importance and secondary of feature information, it does not consider the position information of the image, and regards the features of all positions as the same. For example, the receptive field information in the central area of an image is more complete and important than that in other areas, so different areas of an image correspond to different weights. In order to avoid the problem of decreasing accuracy due to the fuzzy effect of pooling layer, this paper uses 3×3 and 5×5 convolution kernels for down-sampling, so that the network learns the weights of different points by itself and combines them with the channel amplification process into a module. As shown in Figure 6, where the convolution step of 3×3 and 5×5 is 2, it is responsible for down-sampling. 1×1 (with step size 1) is responsible for raising and lowering dimensions of the channel.

3.3. Concentration and refining of feature information

After feature extraction of grouping module, the network can get rich feature information, but it is inevitable that there will be overlapping same information in these information. If

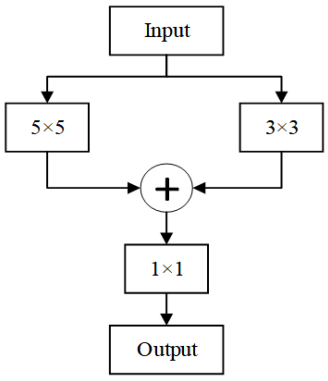

Fig. 6. Down-sampling module

all feature information is extracted and classified, the same information will be extracted repeatedly, resulting in a waste of computing resources. Therefore, a Feature Fusion and Concentration Convolution layer (FFCConv) is designed in this paper, which refines and condenses feature information by merging feature maps to solve the overlapping and redundant problems of feature information. The input of this layer is the feature map with $4 \times 4 \times 510$. Firstly, the feature information is rearranged through channels. After information exchange and fusion, the feature information is divided into A, B, C and D, and the number of feature maps in each group is 51, 102, 153 and 204, respectively. The specific process is shown in Figure 7. Convolution is carried out for each feature graph in Group A. For group B, two layers are combined into one for convolution; For group C, three layers are combined into one for convolution. For group D, four layers are convolved into one. The convolution mode is different from the conventional convolution mode, and the weighted mean convolution as shown in formula (1) is adopted. Where ω represents the weight of the corresponding position. Suppose that the weighted mean convolution calculation of the two feature graphs in group B is X_1 and X_2 respectively, then the calculation method of the feature combination result X_B in group B is shown in Formula (13). Similarly, the calculation method of the combined results of group C and group D is the same as that of group B. In this way, 51 1×1 feature maps are obtained for each group, and then 204 1×1 feature maps are obtained by integrating each group of channels. The number of information channels has been condensed and integrated from 510 to 204. In order to control the degree of information enrichment and prevent the loss of important feature information due to excessive information refining, this paper adopts the combination method as shown in Figure 7.

$$X_A = \frac{\omega_{11}x_{11} + \omega_{12}x_{12} + \cdots, \omega_{44}x_{44}}{16} \tag{10}$$

$$x_1 = \frac{\omega_{12}x_{12} + \omega_{13}x_{13} + \cdots, \omega_{44}x_{44}}{16} \times X_A \tag{11}$$

$$x_2 = \frac{\omega_{21}x_{21} + \omega_{22}x_{22} + \cdots, \omega_{44}x_{44}}{16} \times X_A \tag{12}$$

$$X_B = \frac{x_1 + x_2}{2} \tag{13}$$

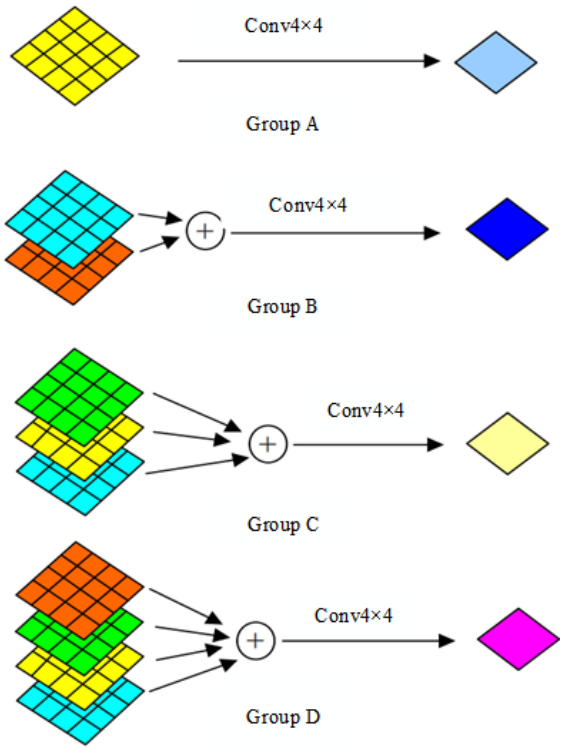

Fig. 7. Concentration and refining process

After many experiments, it is found that the network performance can be optimized by reusing Figure 4 module five times and Figure 5 module twice. The overall network configuration is shown in Table 1. Where c represents the number of channels and s represents the step size. The last down-sampling module in the network structure will keep the number of channels unchanged and only process the image size. Finally, the output of the network is fed into the full connection layer. Although the size of the image remains the same every time the network passes through a feature grouping extraction module, the image features extracted each time are different. These rich image features are helpful to improve the accuracy of image recognition.

$\omega_{11}x_{11}$	$\omega_{12}x_{12}$	$\omega_{13}x_{13}$	$\omega_{14}x_{14}$
$\omega_{21}x_{21}$	$\omega_{22}x_{22}$	$\omega_{23}x_{23}$	$\omega_{24}x_{24}$
$\omega_{31}x_{31}$	$\omega_{32}x_{32}$	$\omega_{33}x_{33}$	$\omega_{34}x_{34}$
$\omega_{41}x_{41}$	$\omega_{42}x_{42}$	$\omega_{43}x_{43}$	$\omega_{44}x_{44}$

Fig. 8. Feature map with 4×4 size

Table 1. Network configuration details

Input	Operator	c	s
$64 \times 64 \times 1$	$Conv3 \times 3$	64	1
$64 \times 64 \times 64$	Down-sampling module	129	2
$32 \times 32 \times 129$	[Network module 1]$\times$5	129	1
$32 \times 32 \times 129$	Down-sampling module	256	2
$16 \times 16 \times 256$	[Network module 2]$\times$2	256	1
$16 \times 16 \times 256$	Down-sampling module	510	2
$8 \times 8 \times 510$	Down-sampling module	510	2
$4 \times 4 \times 510$	FFCConv4$\times$4	204	4
$1 \times 1 \times 204$	$Conv1 \times 1$	1024	1

3.4. New SqueezeNet Framework

As shown in Figure 9, the network structure of SqueezeNet is similar to that of the traditional convolutional neural network, CNN IS implemented by stacking the convolutional operation, but SqueezeNet is stacked by FireMoudle.

In this paper, the SqueezeNet model is improved in several parts: 1) The maximum pooling layer is added to the lower FireMoudle layer for fusion, and the over-fitting problem of small convolution kernel is improved. In this process, the size of the maximum pooling layer feature map and the fused FireMoudle feature map are guaranteed to match; 2) For FireMoudle layer feature map parameters, dynamic compression network surgery algorithm is used to dynamically link pruning and reduce network complexity; 3) Softmax with L2 norm constraint [25] is used to replace the original Softmax for classification and achieve better constraint effect through regularization. The model parameters are shown in Table 2. Pruning and splicing belong to dynamic network surgery process.

3.5. Dynamic Network Surgery

The commonly used model parameter pruning algorithm is to delete unimportant parameters by threshold value to compress the CNN model, but the importance of parameters often changes with the network performance, which leads to two common problems: 1) Important parameters may be deleted, which can reduce the accuracy of the model; 2) It takes a long time and the convergence is too slow. Dynamic network surgery (DNS) compression model adjusts the parameters [26]. The process of DNS contains pruning and

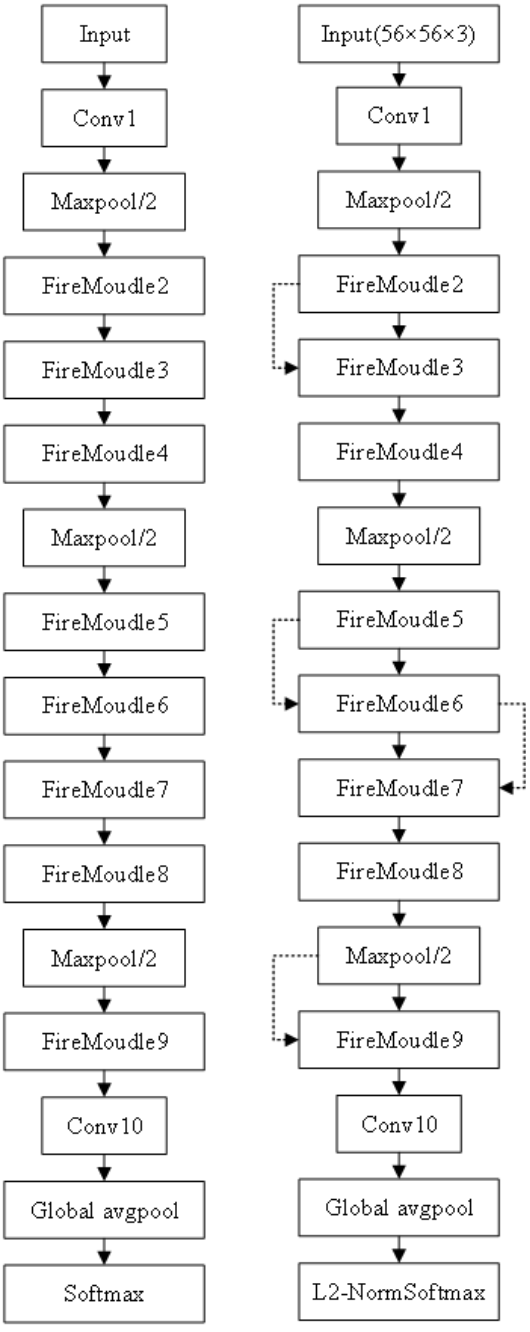

Fig. 9. Original and new SqueezeNet structure

Table 2. Improved SqueezeNet module parameters

Layer	Output size	step size	parameter	pruning	splicing
Input	$64 \times 64 \times 3$	none	none	none	none
Conv1	$64 \times 64 \times 96$	$1 \times 1 \times 96$	none	none	none
Maxpool1	$32 \times 32 \times 96$	$3 \times 3/2$	none	none	none
Fire2	$32 \times 32 \times 128$	none	11920	5746	7756
Fire3	$32 \times 32 \times 128$	none	12432	6258	8208
Fire4	$32 \times 32 \times 256$	none	45344	20646	25468
Maxpool4	$16 \times 16 \times 256$	$3 \times 3/2$	none	none	none
Fire5	$16 \times 16 \times 256$	none	49440	24742	32886
Fire6	$16 \times 16 \times 384$	none	104880	44700	63326
Fire7	$16 \times 16 \times 384$	none	111024	46236	73339
Fire8	$16 \times 16 \times 512$	none	188992	77581	10668
Maxpool8	$8 \times 8 \times 512$	$3 \times 3/2$	none	none	none
Fire9	$8 \times 8 \times 512$	none	197184	77581	10669
Conv10	$8 \times 8 \times 3755$	$1 \times 1 \times 3755$	513000	103400	24380
Avgpool10	$1 \times 1 \times 3755$	$8 \times 8 \times 1$	none	none	none

splicing, as shown in Figure 10. Training is synchronized with compression, which can reduce a large number of parameters while ensuring accuracy. Pruning is a compression network model. Splicing is to make up for the loss of precision caused by incorrect pruning and restore splicing of incorrect pruning. It not only improves the learning efficiency, but also better closes to the compression limit. For problem 2, there are two ways to accelerate the training speed: 1) reduce the deletion probability of parameters and improve the convergence speed; 2) separate FireMoudle and convolutional layer for parameter tailoring.

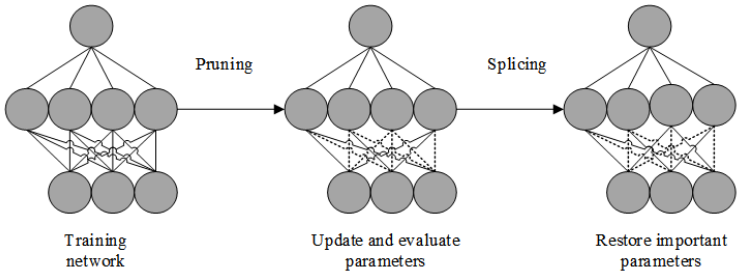

Fig. 10. Dynamic network surgery strategy

Formula (14) shows the loss function of the network.

$$\begin{cases} min_{W_k,T_k} L(W_k \odot T_k) \\ s.t. T_k^{(i,j)} = h_k(W_k^{(i,j)}), \forall (i,j) \in I \end{cases} \tag{14}$$

$L(W_k \odot T_k)$ is the network loss function. $\odot$ stands for matrix Hadamard product. $(h_k(w))$ is a classification function. If the judgment is important, it is 1; otherwise, it is 0. T_k is the 0-1 matrix, indicating the connection state of the network, whether it is pruned or not. I is a member of the matrix W_k.

Classification function $(h_k(w))$ is shown in Equation (15). The importance of parameters is based on the absolute value of weight, and two thresholds a_k, b_k are set, where $b_k = a_k + T_k$.

$$h_k(W_k^{(i,j)}) = \begin{cases} 1, b_k \leq |W_k^{(i,j)}| \\ T_k^{(i,j)}, a_k \leq |W_k^{(i,j)}| \prec b_k \\ 0, a_k > |W_k^{(i,j)}| \end{cases} \tag{15}$$

After W_k and T_k are determined, the value of W_k is updated by Formula (16). β is positive learning efficiency. Equation (16) not only updates important parameters, but also updates parameters that have been identified as unimportant or invalid to the loss reduction function, that is, the parameter set as 0 in T_k is still updated.

$$W_k^{(i,j)} \leftarrow W_k^{(i,j)} - \beta \frac{\partial L(W_k \odot T_k)}{\partial (W_k^{(i,j)} T_k^{(i,j)})}, \forall (i,j) \in I \tag{16}$$

Pruning and splicing in the algorithm is a iteration process, which is realized by constantly changing the values of the weight W_k and T_k of the connection until the iteration number $iter$ reaches a preset value. The dynamic network algorithm is shown in **Algorithm 1**.

Algorithm 1 Dynamic network surgery algorithm

Input: training set X**, related model** W_k**, learning rate** α**, learning strategy** f

Initializing $W_k = W_{k0}, T_k = 1, 0 \leq K \leq C, \beta = 1, iter = 0$
Select the network trained by X
Forward propagation and loss calculation are obtained from $W_0 \odot T_0$ to $W_c \odot T_c$
Back propagation yields model output and loss function gradient
for $k = 0$ to C **do**
    Update T_k with function h_k and existing W_k
    Update W_k through the formula and the existing loss function gradient
    $X_3 = ProjectConv(X_2, groups = 2, noBN)$
end for
Update $iter = iter + 1, \beta = f(\alpha, iter)$
Until $iter$ reaching the preset maximum value

Output: (W_k, T_k)

3.6. Network Optimization

The overall network has a Batch Normalization (BN) layer following the convolutional layer of each module. The distribution of input data is easy to change, and the change will be amplified with the deepening of the network. Therefore, in order to adapt to the

change, the network model has to learn the new data distribution of the change, which leads to slower and slower training convergence. BN layer can prevent the change of data distribution through normalization, and enlarge the influence factor of input on loss function, so that the gradient of back propagation becomes larger. To apply the data after BN normalization and increase the gradient, it is necessary to increase the learning rate to accelerate the convergence speed.

Assuming that the input of layer l of the network is $Z^{[l-1]}$, it is normalized and the superscript $[l-1]$ is ignored, then the normalization process is shown in formulas (17) (19):

$$\mu = \frac{1}{m}\sum_{i=1}^{m} Z_i \tag{17}$$

$$\delta^2 = \frac{1}{m}\sum_{i=1}^{m}(Z_i - \mu)^2 \tag{18}$$

$$Z_{norm}^i = \frac{Z_i - \mu}{\sqrt{\delta^2 + \epsilon}} \tag{19}$$

Where, m is the number of samples contained in a single training data set. ϵ is constant, $\epsilon = 10^{-7}$. The input value z_{norm}^i has a mean of 0 and a variance of 1. However, if the data is forced to be normalized, the original feature learning of the network will be affected, resulting in the decline of the network expression ability. By introducing two adjustable parameters γ and β, formula (20) can be obtained, namely:

$$Z = \gamma \times Z_{norm}^i + \beta \tag{20}$$

In the formula, γ and β are learnable parameters, similar to weight and bias, they are obtained by gradient descent algorithm. The value of Z can be changed by adjusting the values of γ and β. If $\gamma = \sqrt{\delta^2 + \epsilon}$, $\beta = \mu$, then $Z = Z_i$. Therefore, the introduction of parameters γ and β can enable the network to obtain the distribution of features to be learned and enhance the expression ability of the network.

3.7. Fusion Process

The fusion of the maximum pooling layer and the lower FireMoudle layer not only improves the over-fitting problem of small convolution kernel, but the bottom feature has a higher resolution and contains more location and detail information. However, there is a lot of noise, while the top feature has a lower resolution but poor perception of details. The fusion of high-level features and low-level features can improve the detection effect of small targets (points in handwritten Chinese characters). The feature map learned by the front layer can be accessed by the back layer, and the whole network shares some features, making the model more compact.

The feature map obtained by pooling layer and the feature map obtained by FireMoudle are fused to get a new feature map. The process is shown in Equation (21).

$$\begin{cases} x(n) = f[w^i down(x)^j + b^j] f(w^i x^i + b^i) \\ s.t. i + j = n \end{cases} \tag{21}$$

Where n, i and j represent the number of new feature maps, the number of feature maps extracted by pooling layer and the number of feature maps processed by FireMoudle respectively.

3.8. L2-Softmax

For the given test input, Softmax estimates and normalizes the probability value of each category through the hypothesis function, and obtains the normalized probability value of the category, as shown in Equation (22). In pattern recognition tasks, multiple categories can be separated effectively and easily implemented. But there are also obvious disadvantages: 1) If there are too many categories, there will be matching problems; 2) Limited by the processing method of maximizing conditional probability, it is more suitable for high-quality images than difficult and rare images.

$$L = -\frac{1}{M} \sum_{i=1}^{M} log \frac{e^{\varphi}}{\sum_{j=1}^{C} e^{\varphi}} \tag{22}$$

where $\varphi = W_{y_i}^T f_i$.

Feature visualization is achieved when the output of the last hidden layer is restricted to 2. Figure 11 shows the feature distribution obtained by Softmax and L2-Softmax [27] on the mnist data set. The accuracy of L2-Softmax is higher than that of Softmax.

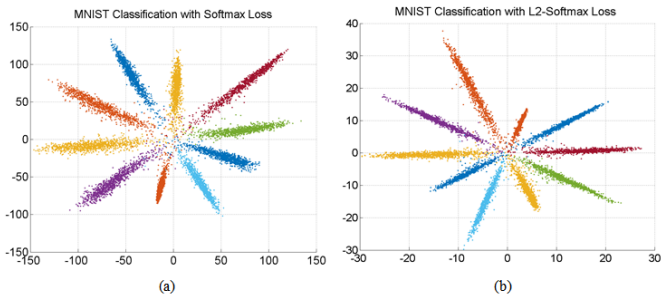

Fig. 11. Comparison of Softmax and L2-Softmax feature distributions in the mnist dataset

Since there are many categories of handwritten Chinese characters in this paper, Softmax constrained by L2-norm is adopted for classification. Based on the norm constraints, images of the same category are closer to each other in the normalized feature space, and images of different categories are farther apart. The attention given to sample averaging works well for poor quality samples.

Formula (23) is the normalization of L2-Softmax category probability values. Where $f(x_i)$ is an input image with size M. y_i represents the class description of the $i-th$ object,

where only one element is 1. $f(x_i)$ is the D-dimensional feature description before the final fully connected layer. C is the number of categories. W and b represent trainable weights and deviations in the network respectively.

$$\begin{cases} min(L) \\ s.t.||f(x_i)||_2 = \alpha, \forall i = 1, 2, \cdots, M \end{cases} \tag{23}$$

The implementation of L2 constraint in the network is shown in Figure 12. Softmax process directly normalizes Softmax loss to obtain probability values, while L2-Softmax introduces L2 formatting layer and Scale layer before Softmax output. L2 formatting layer normalizes the input feature x into a unit vector. The Scale layer scales the unit vector to a fixed radius according to the given parameter a. Given that the value obtained from the simultaneous training of parameter a and other network parameters is too large, this paper directly fixes a as a small constant, which has a better effect.

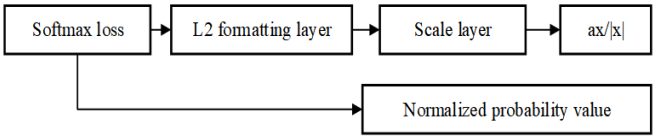

Fig. 12. L2-Softmax process

4. Experimental Results and Analysis

In this paper, CASIA-HWDB (V1.1) data set [28] and ICDAR-2013 data set [29] are selected to train and test the designed neural network model. The two data sets include 68645 first-level Chinese character samples. The collected data set is the original sample. In order to improve the performance of the neural network training model, it is necessary to perform data amplification and error selection processing on the training set. The training set plays an important role in the training of the model. In order to keep the original samples of the training set and improve the performance of the training model as much as possible, only the obvious errors are processed in this paper. At the same time, in order to train the test of the model and prevent over-fitting, the training set is only lightly processed, and the test set is not changed.

Due to the deepening of the network, there may be the risk of over-fitting. At this time, if the data set is small, it is easy to fit the characteristics of the data set. Therefore, data augmentation is introduced to protect against the risk of over-fitting. First, the original sample of the training set is randomly flipped up and down. The training set after processing has more than 500 sample images for each category of handwritten Chinese characters, which makes the training model be better.

The different handwriting depth of Chinese characters in the data set will affect the recognition accuracy, and the image contrast enhancement operation will be carried out.

$$D(x,y) = \frac{(I(x,y) - I_{min}) \times 255}{I_{max} - I_{min}} \tag{24}$$

In Formula (24), I_{max} and I_{min} are the maximum and minimum gray pixel values of the original image respectively. $I(x,y)$ is the pixel value of the original image. $D(x,y)$ is the pixel value of the target image.

If the image size is too large, the network burden will be increased, and if it is too small, the recognition performance will be reduced. The nearest neighbor interpolation method is used to normalize the image size to 56×56. The combination of gradient features can improve the effectiveness and accuracy of handwritten Chinese character recognition. The features of handwritten Chinese characters are extracted from the 8 directions of 0, $\pi/4$, $\pi/2$, $3\pi/4$, $3\pi/2$, $7\pi/4$, which can cover horizontal, vertical, skimming and curling strokes of Chinese characters. The horizontal and vertical gradients are obtained by Sobel operator, and the feature graphs of eight directions are obtained by parallelogram decomposition. Finally, the average gradient image is obtained by superposition.

In Figure 13, the upper left corner is one Chinese character of the original image, the middle is the image after image enhancement processing, the upper right corner is the average gradient image after gradient image superposition, and the following 8 images are gradient images in corresponding directions.

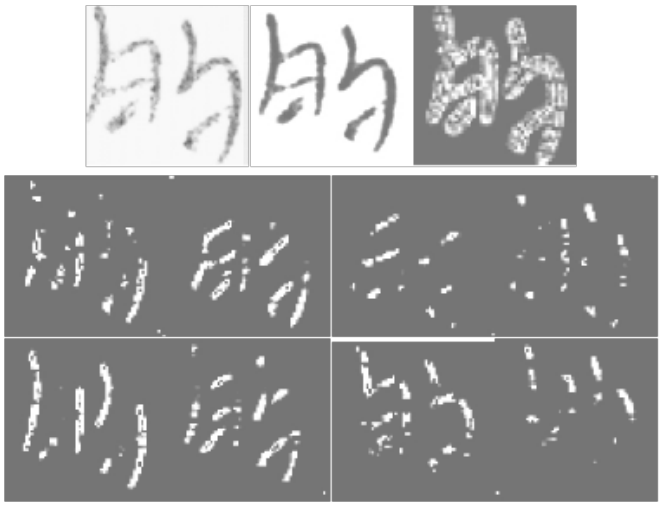

Fig. 13. Pretreatment of Chinese word

4.1. Experimental environment and implementation

All experiments in this paper used CUDA parallel computing architecture on Ubantu 18.04 system, and built PyTorch framework on the basis of CUDNN accelerated computing library [30]. The graphics card used in the experiment was NVIDIA GEForce

GTX3090 (24G) with 32.0GB of memory and Intel(R) Core(TM) i7-6950XCPU 3.00GHZ. We set network hyperparameters as shown in Table 3. FireMoudle sets the compression ratio to 0.5. The filter number of 3×3 accounts for 0.25 of the total filter number.

Table 3. Hyperparameters set

Parameter	Value
Loss function	L2-Softmax
Optimizer	Adadelta
Activation function	ReLU
Dropout	0.5
Iterations	20
Batch Size	128

4.2. Comparison analysis

The model has a total of 10^4 training iterations, and data is saved every 100 steps. Therefore, the loss and accuracy of model training and testing are shown in figures 14 17. In order to optimize the results of the training model, the whole experiment process is monitored and the parameters are adjusted timely according to the training situation. We set the learning rate to 0.1 to accelerate the convergence speed; When training step= 40000, the learning rate is reduced to 0.01 to stabilize the training; When training step=80000, the learning rate is reduced to 0.001. At the end of training, training loss and test loss converge stably to 0.48 and 0.17, respectively. The accuracy of training and testing is 0.9875 and 0.9716, respectively. Finally, top-5 experiments are carried out on the basis of the trained model, and the accuracy rate is as high as 99.37%.

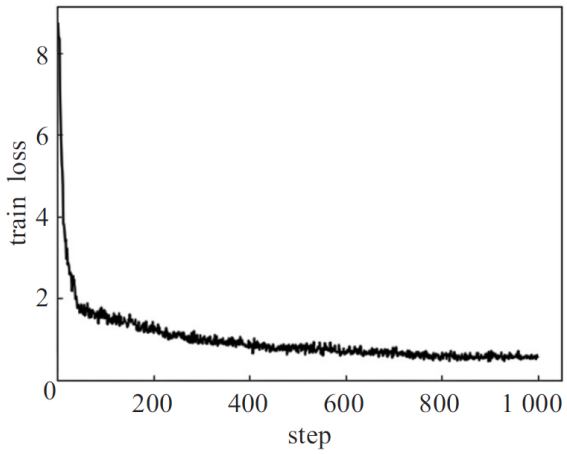

Fig. 14. Training loss

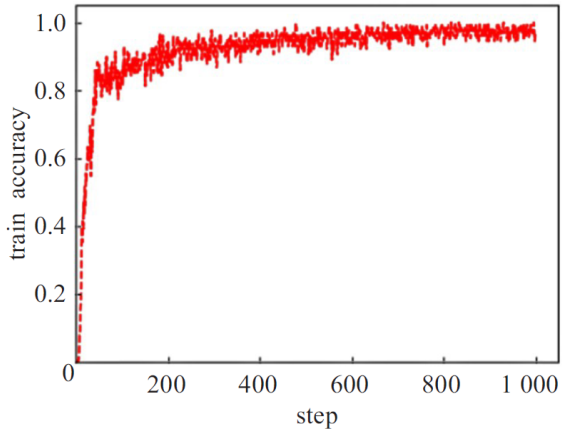

Fig. 15. Training accuracy

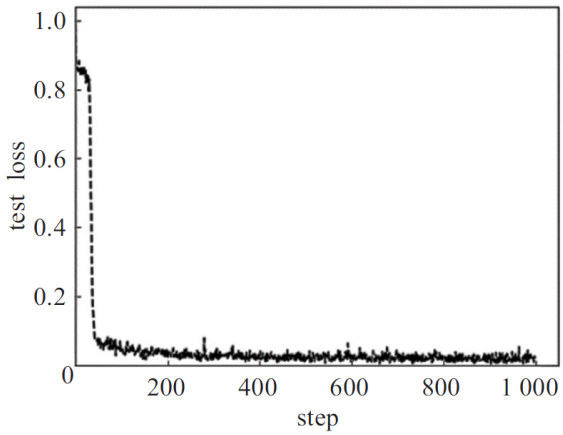

Fig. 16. Test loss

Table 4 shows the ablation results. The proposed method in this paper has higher accuracy in all tests than a single SqueezeNet model. For Top-1, Top-2 and Top-5, the accuracy values of proposed method are 98.65%, 99.72% and 99.84% respectively.

Table 5 shows the comparison results between the proposed method and other advanced methods including PageNet [31], SON [32], HHCR [33], ROA [34]. Compared with the original residual network, the accuracy of PageNet has obvious advantages, but it is much different from that of other advanced models. The SON model has only 5 convolutional layers, and the extraction of feature information is insufficient, which affects the classification effect. In HHCR, multiple neural networks are used for training, and then the average of these multiple results is taken. This method requires a lot of work

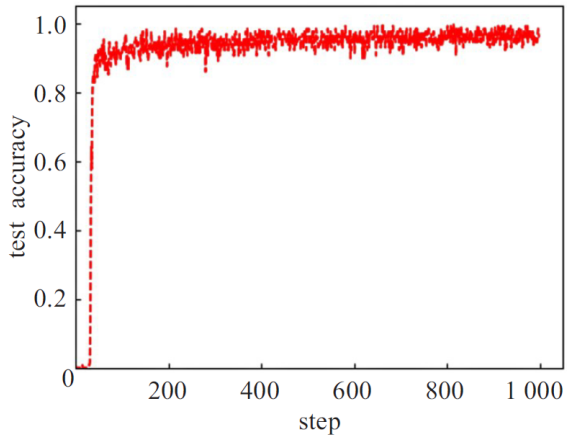

Fig. 17. Test accuracy

Table 4. Ablation result

Model	Top-1 accuracy %	Top-2 accuracy %	Top-5 accuracy %
SqueezeNet	95.43	98.18	97.25
Proposed	98.65	99.72	99.84

and time-consuming experiments. ROA improves the traditional convolution method and adopts the convolution method without shared weights, which achieves good results, but there is a problem of too large parameter volume. The results obtained by the new method are better than those obtained by other methods.

Table 5. Ablation result

Model	Top-1 accuracy %	Top-2 accuracy %	Top-5 accuracy %
PageNet	92.19	93.34	92.08
SON	93.45	92.67	93.84
HHCR	94.87	94.96	95.52
ROA	95.77	96.23	96.79
Proposed	98.65	99.72	99.84

5. Conclusions

Aiming at the problem of difficult recognition for handwritten Chinese characters, a multilevel stacked SqueezeNet model is proposed. By seeking an appropriate fusion comparison strategy and combining the advantages of SqueezeNet in handwritten Chinese character recognition, the multilevel stacked feature group extraction module is used to extract the deep abstract feature information of the image. Experimental results show that the

proposed fusion model achieves better recognition results than other advanced machine learning methods on open data sets. The next research direction is to further improve the network structure and explore better fusion ways. And handwritten Chinese character recognition is often used in some embedded devices, its resources limit the application of this method, so how to compress the network structure, save resources and speed up the calculation is also the focus of the research direction.

Acknowledgments. This work was supported by "Project Name: Image Processing based handwritten Chinese character recognition and correction scoring method and application research; Project number: 22B520044".

References

1. Li, Y., et al.: "Fast and Robust Online Handwritten Chinese Character Recognition with Deep Spatial & Contextual Information Fusion Network," *IEEE Transactions on Multimedia*, doi: 10.1109/TMM.2022.3143324.
2. Hu, M., Qu, X., Huang, J., et al.: "An End-to-End Classifier Based on CNN for In-Air Handwritten-Chinese-Character Recognition," *Applied Sciences,* Vol. 12, No. 14, 6862. (2022)
3. Li, P., Laghari, A., Rashid, M., Gao, J., Gadekallu, T., Javed, A., Yin, S.: "A Deep Multimodal Adversarial Cycle-Consistent Network for Smart Enterprise System," *IEEE Transactions on Industrial Informatics,* Vol. 19, No. 1, 693-702. (2023). doi: 10.1109/TII.2022.3197201.
4. Dan, Y., Zhu, Z., Jin, W., et al.: "S-Swin Transformer: simplified Swin Transformer model for offline handwritten Chinese character recognition," *PeerJ Computer Science,* Vol. 8, e1093. (2022)
5. Dan, Y., Zhu, Z., Jin, W., et al. "PF-ViT: Parallel and Fast Vision Transformer for Offline Handwritten Chinese Character Recognition," *Computational Intelligence and Neuroscience,* Vol. 2022. (2022)
6. Peng, D., et al.: "Recognition of Handwritten Chinese Text by Segmentation: A Segment-annotation-free Approach," *IEEE Transactions on Multimedia,* doi: 10.1109/TMM.2022.3146771.
7. Wang, L., Yin, S., Hashem, Alyami., et al.: "A novel deep learning-based single shot multibox detector model for object detection in optical remote sensing images," *Geoscience Data Journal,* (2022). https://doi.org/10.1002/gdj3.162
8. Teng, L., Qiao, Y.: "BiSeNet-oriented context attention model for image semantic segmentation," *Computer Science and Information Systems,* Vol. 19, No. 3, pp. 1409-1426. (2022)
9. Zhang, K., Zuo, W., Chen, Y., et al.: "Beyond a gaussian denoiser: Residual learning of deep cnn for image denoising," *IEEE transactions on image processing,* 2017, 26(7): 3142-3155.
10. Zhu, Y., Zhang, H., Huang, X., et al.: "Visual normalization of handwritten Chinese characters based on generative adversarial networks," *International Journal of Pattern Recognition and Artificial Intelligence*, Vol. 36, No. 3, 2253002. (2022)
11. Hu, S., Wang, Q., Huang, K., et al.: "Retrieval-based language model adaptation for handwritten Chinese text recognition," *International Journal on Document Analysis and Recognition (IJDAR)*, 1-11. (2022)
12. Yan, K., Guo, J., Zhou, W.: "A Novel Method for Offline Handwritten Chinese Character Recognition Under the Guidance of Print," *Advances in Knowledge Discovery and Data Mining: 25th Pacific-Asia Conference, PAKDD 2021, Virtual Event, May 11C14, 2021, Proceedings, Part II. Cham: Springer International Publishing*, 106-117. (2021)
13. Zhou, M., Zhang, X., Yin, F., et al.: "Discriminative quadratic feature learning for handwritten Chinese character recognition," *Pattern Recognition*, Vol. 49, 7-18. (2016)

14. Qu, X., Wang, W., Lu, K., et al.: "Data augmentation and directional feature maps extraction for in-air handwritten Chinese character recognition based on convolutional neural network," *Pattern recognition letters*, Vol. 111, 9-15. (2018)
15. Diao, H., Chen, C., Yuan, W., et al.: "Deep residual networks for sleep posture recognition with unobtrusive miniature scale smart mat system," *IEEE Transactions on Biomedical Circuits and Systems*, Vol. 15, No. 1, 111-121. (2021)
16. Cui, R., Liu, H., Zhang C.: "A deep neural framework for continuous sign language recognition by iterative training," *IEEE Transactions on Multimedia*, Vol. 21, No. 7, 1880-1891. (2019)
17. Guo, Z., Zhou, Z., Liu, B., et al.: "An Improved Neural Network Model Based on Inception-v3 for Oracle Bone Inscription Character Recognition," *Scientific Programming*, Vol. 2022. (2022)
18. Heo, Y.: "Loss function optimization for cnn-based fingerprint anti-spoofing," *International Journal of Computer and Information Engineering*, Vol. 15, No. 6, 344-348. (2021)
19. Wang, Z., Du, J.: "Fast writer adaptation with style extractor network for handwritten text recognition," *Neural Networks*, Vol. 147, 42-52. (2022)
20. Wu, Y., Yin, F., Liu, C.: "Improving handwritten Chinese text recognition using neural network language models and convolutional neural network shape models," *Pattern Recognition*, Vol. 65, 251-264. (2017)
21. Greco, A., Saggese, A., Vento, M., et al.: "Gender recognition in the wild: a robustness evaluation over corrupted images," *Journal of Ambient Intelligence and Humanized Computing*, Vol. 12, 10461-10472. (2021)
22. McGuire, M., Moore, T.: "Prediction of tornado days in the United States with deep convolutional neural networks," *Computers & Geosciences*, Vol. 159, 104990. (2022)
23. Kohler, M., Langer, S.: "On the rate of convergence of fully connected deep neural network regression estimates," *The Annals of Statistics*, Vol. 49, No. 4, 2231-2249. (2021)
24. Baaran, E.: "Classification of white blood cells with SVM by selecting SqueezeNet and LIME properties by mRMR method," *Signal, Image and Video Processing*, Vol. 16, No. 7, 1821-1829. (2022)
25. Yang, M., Tjuawinata, I., and Lam, K.: "K-Means Clustering With Local d?-Privacy for Privacy-Preserving Data Analysis," *IEEE Transactions on Information Forensics and Security*, Vol. 17, 2524-2537. (2022) doi: 10.1109/TIFS.2022.3189532.
26. Guo, Y., Yao, A., Chen, Y.: "Dynamic network surgery for efficient dnns," *Advances in neural information processing systems*, Vol. 29. (2016)
27. Sun, L., Li, W., Ning, X., et al.: "Gradient-enhanced softmax for face recognition," *IEICE TRANSACTIONS on Information and Systems*, Vol. 103, No. 5, 1185-1189. (2020)
28. Wu, Y., Yin, F., Liu, C.: "Improving handwritten Chinese text recognition using neural network language models and convolutional neural network shape models," *Pattern Recognition*, Vol. 65, 251-264. (2017)
29. Karatzas, D., Shafait, F., Uchida, S., et al.: "ICDAR 2013 robust reading competition," *2013 12th international conference on document analysis and recognition. IEEE*, 1484-1493. (2013)
30. Yuan, Y., Xu, Z., and Lu, G.: "SPEDCCNN: Spatial Pyramid-Oriented Encoder-Decoder Cascade Convolution Neural Network for Crop Disease Leaf Segmentation," *IEEE Access*, Vol. 9, 14849-14866.(2021) doi: 10.1109/ACCESS.2021.3052769.
31. Peng, D., Jin, L., Liu, Y., et al.: "PageNet: Towards End-to-End Weakly Supervised Page-Level Handwritten Chinese Text Recognition," *International Journal of Computer Vision*, Vol. 130, No. 11, 2623-2645. (2022)
32. Xu, X., Yang, C., Wang, L., et al.: "A sophisticated offline network developed for recognizing handwritten Chinese character efficiently," *Computers and Electrical Engineering*, Vol. 100, 107857. (2022)
33. Huang, G., Luo, X., Wang, S., et al.: "Hippocampus-heuristic character recognition network for zero-shot learning in Chinese character recognition," *Pattern Recognition*, Vol. 130, 108818. (2022)

34. Wang, Y., Yang, Y., Ding, W., et al.: "A residual-attention offline handwritten Chinese text recognition based on fully convolutional neural networks," *IEEE Access*, Vol. 9, 132301-132310. (2021)

Yuankun Du is with the School of Big Data and Artificial Intelligence, Zhengzhou University of Science and Technology, Associate Professor, research direction: Artificial Intelligence, Big data analysis.

Fengping Liu (Senior Engineer) is with the School of Information Engineering, Zhengzhou University of Science and Technology, Research interests: Software development, Information management and information system.

Zhilong Liu (Lecturer) is with the Library of Henan Institute of Animal Husbandry Economics, Research interests: computer network, information system.

Received: December 10, 2022; Accepted: April 28, 2023.

Computer Science and Information Systems 20(4):1797–1817 https://doi.org/10.2298/CSIS221212031C

Deep Adversarial Neural Network Model Based on Information Fusion for Music Sentiment Analysis

Wenwen Chen

College of Music, Jimei University
21 Yindou Road, Jimei District, Xiamen City, Fujian Province, China
chenwwencww@163.com

Abstract. Natural language processing (NLP) is a computer-based technology used to process natural language information in written and spoken form that is unique to human society. In the process of mining massive text information, a variety of technologies and research directions in the field of NLP have gradually emerged. And sentiment analysis is an important research direction, which has important research value and practical application value for enterprises and social life. Sentiment analysis is basically a single mining of semantic or grammatical information without establishing the correlation between semantic information and grammatical information. In addition, previous models simply embed the relative distance or grammatical distance of words into the model, ignoring the joint influence of relative distance and grammatical distance on the aspect words. In this paper, we propose a new model that combines deep adversarial neural network model based on information fusion for music sentiment analysis. Firstly, the information of music text sequence is captured by the bidirectional short and long time memory network. Then the sequence information is updated according to the tree structure of dependency syntactic tree. Then, the relative distance and syntactic distance position information are embedded into the music text sequence. Thirdly, the adversarial training is used to expand the alignment boundary of the field distribution and effectively alleviate the problem of fuzzy features leading to misclassification. Semantic information and syntactic information are optimized by attention mechanism. Finally, the fused information is input into the Softmax classifier for music sentiment classification. Experimental results on open data sets show that compared with other advanced methods, the recognition accuracy of the proposed method is more than 90%.

Keywords: Natural language processing, deep adversarial neural network, information fusion, music sentiment analysis, attention mechanism.

1. Introduction

Text information on the Internet is growing day by day, and a large number of texts with sentiment information are generated on social media and e-commerce platforms. Sentiment analysis is an important task in natural language processing. Sentiment analysis has attracted wide attention in industry and academia in recent years [1,2].

Aspect level sentiment analysis, also known as target-specific sentiment analysis or fine-grained sentiment analysis, refers to the analysis of the sentiment polarity of the aspects (goals) involved in the text when given a paragraph and specific aspect words [3]. In

sentiment expression sentences, different aspects may express different sentiments. Song et al. [4] proposed an attention-based Long Short-Term Memory (LSTM) network, adding aspect words to the sentence. The sentence representation that generates aspect perception predicts the textual sentiment polarity of a given aspect word using an attention-mechanism-based LSTM. Chen et al. [5] used convolutional neural network to extract sentiment features and selectively outputted features related to aspect words through gating mechanism for sentiment classification. Li et al. [6] introduced multiple attention mechanism to obtain more comprehensive attention information, integrate contextual self-attention and specific aspect of word attention, and predict specific aspect of sentiment polarity. A lot of works had been done to obtain better performance of aspect-level emotion classification tasks by constructing different attention networks.

Sentiment expression is highly related to the field. The same music sentiment word may express the same or similar sentiment in different fields, but also may express opposite sentiment. When dealing with such samples, it is relatively easy for sentiment classifiers to carry out domain migration [7]. Without a classifier to carry out domain adaptation to the target domain, it is difficult to correctly distinguish the sentiment polarity of statements containing such words. Traditional music sentiment classification methods require sufficient labeled training data, and require the same distribution of training set and test set [8]. Emerging fields often lack sufficient labeled data. How to use the rich source domain of aspect-level music sentiment category labels to judge the polarity of music sentiment for the specified aspect words in the target domain is a widely concerned issue in the field of sentiment analysis. The cross-domain music sentiment classification task makes full use of the large-scale data labeled in the source domain and migrates it to the new domain with few labeled data by using some algorithms [9], so as to realize the classification of music sentiment in the new domain.

In terms of cross-domain aspect-level sentiment classification task, Zhang et al. [10] proposed Interactive Attention Transfer Network (IATN) to integrate the influence of aspect words into the representation learning of cross-domain sentiment classification model. Tian et al. [11] proposed to extract domain-invariant sentiment features with the assistance of aspect word detection to conduct cross-domain aspect level sentiment classification. Cao et al. [12] jointly extracted aspect words and affective features, carried out unsupervised domain adaptation setting, and aligned automatically captured correlation vectors through selective adversarial learning method to achieve adaptability between domains at the word level.

Recently, with the proposal of Graph Convolutional Network (GCN) [13], GCN has been widely used in sentiment analysis tasks. Huang et al. [14] used GCN for text classification, and then combined it with dependency syntax tree for aspect level sentiment analysis. This method combining dependency tree and graph convolution could shorten the distance between aspect words and sentiment words and used graph convolution network to learn grammatical information. Zhang et al. [15] used the dependency relationships of sentences to construct the adjacency matrix, and used the graph convolutional network to learn the grammatical relations in sentences, proving that the graph convolutional neural network could correctly capture syntactic information and remote word dependencies. Zhao et al. [16] proposed a new network architecture to connect sentiment feature words with aspect words by using multi-layer graph attention network. Xue et al. [17] believed that the common adjacency matrix lacked the dependency and co-occurrence relationship

between words, and proposed hierarchical syntactic graph and hierarchical lexical graph to replace the common adjacency matrix for grammar learning. For example, the word ”nothing special” pair in the sentence ”food was okay, nothing special.” appeared five times in the training set, and the word pair indicated negative emotional polarity. In this case, if the word ”food” was to be predicted correctly, other information was needed to counteract the positive appearance of ”okay” in the sentence.

Therefore, we propose a new model that combines deep adversarial neural network model based on information fusion for music sentiment analysis. The new model learns semantic information and syntactic information at the same time. Hierarchical vocabulary is used to replace common dependency syntax tree for syntactic information learning, and hierarchical word frequency graph is used to replace common dependency syntax tree for syntactic information learning of graph convolutional network. In addition, relative distance and syntactic distance information are fused and embedded into the model. Contributions of this paper are as follows:

1. The new model integrates relative distance and grammatical distance into the model, that is, the influence of relative distance of words on aspect words is taken into account, as well as the influence of grammatical distance of words on aspect words.
2. The influence of the position of a word in the dependency syntactic tree is proposed, and the importance of the height of a word in the syntactic tree and the degree of the word node in the text sequence is considered.
3. At the same time, the semantic information and grammatical information are studied, and the information contained in the text sequence is fully considered to make it contain richer information, so as to improve the extraction of aspect word information.
4. The hierarchical lexical graph is introduced to replace the common dependency syntax tree, which can not only capture grammatical information, but also pay attention to the co-occurrence relationship between words, so as to improve the efficiency of grammar learning.

The rest of this paper is organized as follows. In the second section, related works are introduced. The third section introduces the proposed work in detail. The fourth part introduces the experiments and results. Finally, the fifth section concludes this paper.

2. Related Works

The neural network model is used as an aspect level sentiment analysis task, and most of them use the word embedding layer [18] as the starting layer of the model. The main reason is that word embedding layer can map text sequence information to low-dimensional vector space one by one, and then it can learn the information mapped to low-dimensional vector space through various deep learning models. Convolutional Neural Network (CNN) is initially used in image processing tasks, mainly by convolutional kernel to extract the local information of the image. Since CNNs have been used in natural language processing tasks [19], researchers have further extracted feature information by combining CNN with other models. Zhang et al. [20] used multiple layers of CNN to model the context in parallel, and then used the attention mechanism to associate the information between context and aspect words. Wang et al. [21] proposed a model of convolutional neural network combined with gating mechanism, which could filter sentiment features unrelated

to aspect word information, so as to selectively output relevant sentiment features based on aspect word.

Studies have shown that, in the task of aspect level sentiment analysis, each word in a sentence has a different degree of influence on aspect words. The farther away the word is from aspect words, the smaller the influence on aspect words. Therefore, distance can be divided into relative distance and grammatical distance. Sun et al. [22] used the weighted convolutional network to explore the relative position relation and grammatical distance relation, and the research results proved that the grammatical distance relation was more conducive to the classification of aspect words than the relative distance relation. Zhang et al. [23] integrated the syntactic location information into the model, and the experimental results proved that the syntactic location could help the model better understand the relationship between context and aspect words.

With the continuous in-depth study of sentiment analysis, grammatical information is constantly being mined. For example, by using a grammar parsing tool, The sentence "The music was excellent as well as service, however, I left the four seasons very disappointed" is resolved into a dependency syntax tree with syntactic information. There are three aspects in the sentence: music, service and seasons. Clauses infer that the aspect words "music" and "service" are positive, and "seasons" is negative. Many models in the past focused on the wrong word in some cases [24]. For the word "service" shown in Figure 1, many models mistakenly focus on "well", but from the whole sentence, the emotional polarity of the word "service" depends on "excellent" rather than "well". From the dependency syntax tree, "service" connects with "excellent" through the dependency relationship "attr" and "acomp", reducing the influence of "well" on the aspect word.

The advantage of graph convolutional network is that it can capture the structure information of dependency syntactic tree very well, which makes up the defect that other models can not capture syntactic information. Zheng et al. [25] could selectively utilize dependent information through key-value memory network, and finally weighted different dependent information according to memory mechanism to effectively screen useless information. Zhao et al. [26] proposed to use hierarchical syntactic graph and hierarchical lexical graph to learn grammatical information. Hierarchical lexical graph (HLG) uses the frequency of two words in the corpus as connecting factors to construct hierarchical lexical graph for each sentence, as shown in Figure 1.

3. Proposed Music Sentiment Analysis Model

Given a music text sequence $s = w_1, w_2, \cdots, w_n$ and an aspect word sequence $a = w_t, w_{t+1}, \cdots, w_{t+m-1}$. Wherein, the music text sequence contains n words, the aspect word sequence contains m words, and the aspect word sequence a is a subsequence of the text sequence s. The model in this paper is shown in Figure 2. The model consists of seven layers, namely, word deep adversarial layer, hidden layer, location embedding layer, learning layer, attention layer, feature extraction layer and pooling layer. Among them, the learning layer is divided into two modules, namely semantic learning module and grammar learning module. The attention layer is also divided into two parts, namely semantic optimization attention and syntactic optimization attention.

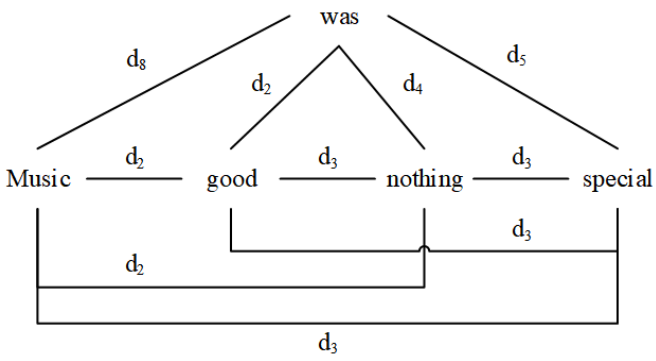

Fig. 1. Hierarchical Lexical Graph

3.1. Deep Adversarial Layer

The expression of music text has various meanings and distributed representation can better express the semantic information of music text. In this paper, the pre-trained Word Vector (Global Vector for Word Representation) [27] is used to generate distributed representations for each word in the text data. The word Embedding search matrix $L \in R^{d_e \times |V|}$ is first generated. Where, d_e represents the dimension size of the word vector. $|V|$ is the vocabulary size. During data preprocessing, each word in the vocabulary is assigned a unique index corresponding to the index number of L, and the required word embedding can be generated for each word in the data set through the mapping relationship. For a given input data:

$$x = [w_1, w_2, \cdots, w_n] \tag{1}$$

Input can be mapped to music context embedding.

$$\hat{E}^c = [e_1, e_2, \cdots, e_n]^T \in R^{n \times d_e} \tag{2}$$

At the same time, a given input aspect word $a = [e_1, e_2, \cdots, e_m]$ is mapped to an aspect word embedded representation.

$$E^a = [e_1, e_2, \cdots, e_m]^T \in R^{m \times d_e} \tag{3}$$

The task of cross-domain aspect level emotion classification needs to make full use of the given aspect word information and establish the relationship between aspect word and emotion information of music text. In music texts, the feature words that usually express emotion are close to their related aspect words. In this paper, location information is integrated to enrich the embedded representation information, which is helpful to improve the performance of aspect-level sentiment classification. For the embedded sentence representation $\hat{E}^c$, the position information of each word in the input data x is incorporated

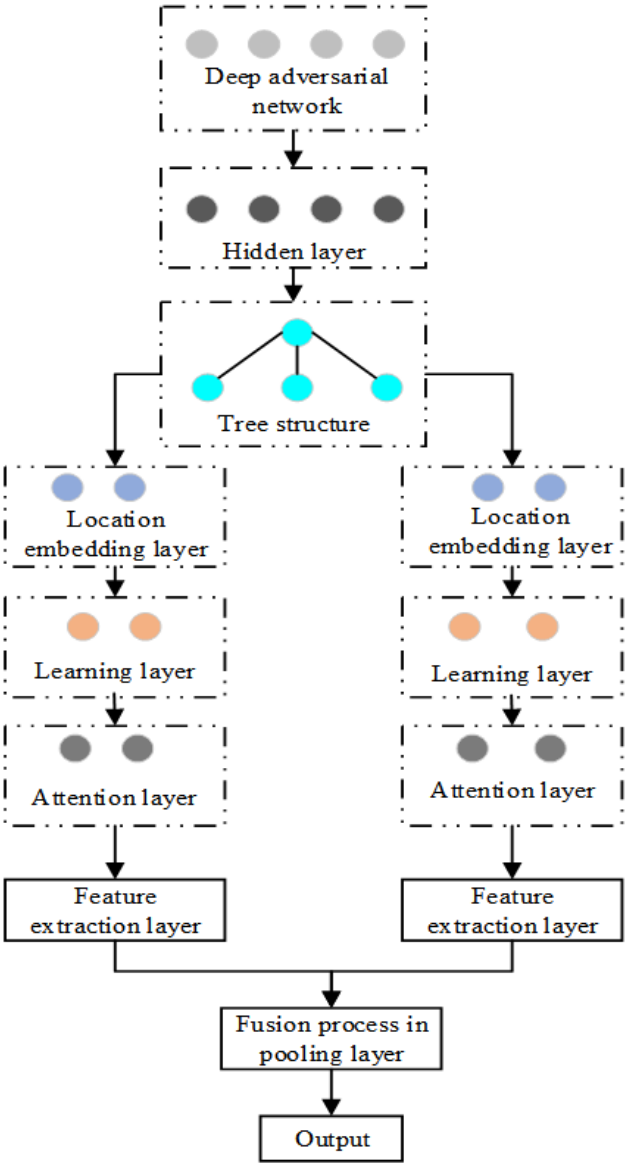

Fig. 2. The overall of proposed model

into $\hat{E}^c$ to obtain the final context-embedded representation E^c. Here, the location encoding method [28] is adopted:

$$PE(pos, 2i) = sin(\frac{pos}{10^{8i/d_e}}) \tag{4}$$

$$PE(pos, 2i+1) = cos(\frac{pos}{10^{8i/d_e}}) \tag{5}$$

$$E^c = \hat{E}^c + PE \tag{6}$$

Where, pos is the position of the word in the sentence, and i stands for the $i-th$ dimension of the corresponding vector at position pos in PE.

Since the aspect words of each domain in a music text may contain more than one word, the characteristics of long-distance dependence need to be learned. For context sentence embedded representation E^c and aspect word embedded representation E^a, feature extraction is carried out using Bidirectional Gated Recurrent Unit (BiGRU) respectively to generate context-rich semantic representations H^c and H^a:

$$H^c = [\overrightarrow{GRU}(E^c); \overleftarrow{GRU}(E^c)] \tag{7}$$

$$H^a = [\overrightarrow{GRU}(E^a); \overleftarrow{GRU}(E^a)] \tag{8}$$

For the context feature representation H^c and aspect word feature representation H^a, the weight of Attention is calculated through the Interaction Attention (IA) layer, and the interaction relationship between context and aspect words is established, so that the context representation can pay more attention to the features with high correlation with aspect words, and the interaction matrix represented by the two features is calculated:

$$I = H^c H^a \tag{9}$$

Through I with column softmax and row softmax, α and β are obtained. Then, the context attention γ, which is closely related to aspect words, is obtained.

$$\gamma = \frac{1}{n} \sum_i \alpha \times \beta^T \tag{10}$$

yγ is applied to the context to represent H^c, focusing on the features closely related to aspect words, and the final feature representation is obtained:

$$H = H^c \gamma \tag{11}$$

3.2. Learning Layer

A music sentence contains semantic and grammatical information, both of which play a role in determining the emotion polarity of aspect words. Two modules are designed to learn semantic information and syntactic information respectively.

A. Grammar learning module

Graph convolution is an improvement on the traditional convolutional neural network. It mainly manipulates graph structure. For each node in the graph structure, the graph convolution should consider the feature information of the node itself as well as the feature information of all neighbors, so that the information between two connected nodes can be obtained effectively. When performing aspect-level sentiment analysis task, it can transfer and obtain information according to the edges in dependency syntax tree. For example, in Figure 3, the aspect word ”service” connects to the ”was” node in the dependency syntax tree, and the ”was” node connects to the ”excellent ”node. Therefore, to obtain information, the ”excellent” node information will pass the feature information to the ”was” node first, and then the feature information to the ”service” node. In the process of information acquisition, the distance of information transmission in the relative position is shortened, and the noise in the process of transmission is effectively reduced.

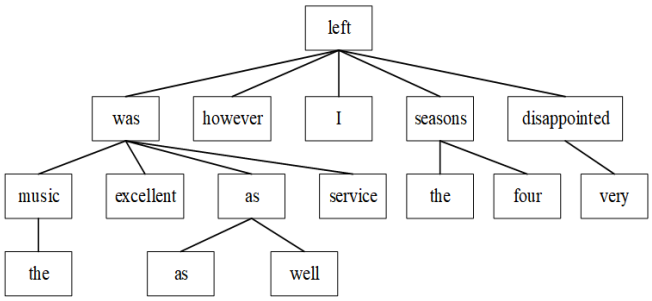

Fig. 3. Simplified dependency syntax tree

Since the common graph convolution operation does not contain graphs with marked edges, this paper uses the hierarchical lexical graph for grammar learning. The graph contains not only the syntactic tree structure, but also the co-occurrence relation between words. Through this graph convolution, words with the same co-occurrence relationship can be merged into virtual nodes, and then all the merged virtual nodes can be updated. Virtual node information update is shown in Formula (12):

$$h_i^l = ReLU(w_l(\oplus_r h_i^{l,r})) \tag{12}$$

Where, $\oplus_r$ represents connections of different co-occurrence relationship types. l indicates the number of layers. w_l is the weight in the $l-th$ layer. $h_i^{l,r}$ represents the representation of each co-occurrence relation r.

B. Semantic learning module

Before graph convolution was proposed, most models used semantic learning to improve the judgment of emotion polarity of aspect words. In this paper, multi-layer convolutional neural networks are used to learn semantic information. Convolutional neural network extracts information between adjacent words by means of sliding window from the matrix corresponding to a music text sequence through convolution kernel. The high pass permanent of the convolution kernel is 3, and the length is the dimension of the word vector. Therefore, the convolution operation is often affected by some noise words. Before semantic learning, the model in this paper weakens the noise words in location encoding. Therefore, this paper reduces some operations on noisy words in semantic learning. We use Formula (13) to learn semantic information:

$$h_i^{c,l} = CNN(h_i^p) \tag{13}$$

Where, CNN represents the convolutional operation, and l represents the layer number of the convolutional neural network.

3.3. Attention Layer

After the semantic and grammatical learning in the learning layer, the two parts of information need to be optimized and integrated. Because there are some differences between semantic information and grammatical information, direct integration of the two will lead to inadequate integration. Therefore, in order to better integrate these two types of information, semantic information and syntactic information are optimized by using tree structured information. The attention layer is divided into two parts: semantic optimization attention and syntactic optimization attention.

A. Semantic optimization attention

Semantic optimization focuses on interactive optimization of information learned by semantic learning modules and structured tree information, as shown in equations (14)-(16).

$$\tilde{\alpha}_i = h_i^t h_i^{c,l} \tag{14}$$

$$\alpha_i = \frac{exp(\tilde{\alpha}_i)}{\sum_{i=1}^{n}(\tilde{\alpha}_i)} \tag{15}$$

$$S_i^{\alpha} = \sum_{i=1}^{n} \alpha_i h_i^{c,l} \tag{16}$$

S_i^{α} represents the output of semantically optimized attention.

B. Syntactic optimization attention

The syntactic optimization attention is to optimize the interaction between the grammar information learned by the grammar learning module and the structured tree information, as shown in equations (17)-(19).

$$\tilde{\beta}_i = h_i^t h_i^l \tag{17}$$

$$\beta_i = \frac{exp(\tilde{\beta}_i)}{\sum_{i=1}^{n}(\tilde{\beta}_i)} \tag{18}$$

$$G_i^{\beta} = \sum_{i=1}^{n} \beta_i h_i^l \tag{19}$$

Where, G_i^{β} represents the output of syntactic optimization attention.

3.4. Feature Extraction Layer

The information of aspect words is particularly important for the judgment of the emotion polarity of aspect words. The feature extraction layer is to extract the information of aspect words from semantic information and grammatical information respectively. Aspect word extraction information is shown in Formula (20).

$$a = h_i, t \leq i < t + m \tag{20}$$

If $1 \leq i < t$ or $t + m \leq i \leq n$, then $a = 0$. Where, a represents aspect word information. Formula (20) is used to extract aspect word information in semantic information and aspect word information in grammatical information, denoted as a_s and a_g respectively.

3.5. Pooling Layer

After extracting aspect word information, the extracted aspect word information is integrated, that is, a_s and a_g are spliced. The information integration formula of aspect words is shown as follows:

$$o_a = [a_g, a_s]. \tag{21}$$

The integrated aspect word information is carried out the maximum pooling operation through the pooling layer to further screen the effective information of the aspect word.

$$o_p = max - pooling(o_a) \tag{22}$$

Here $max - pooling$ indicates maximum pooling.

3.6. Classification Module

For the feature representation H obtained by the previous layers of source domain data and target domain data, gradient inversion is performed using GRL_d based on gradient inversion layer:

$$GRL_d(x) = x, \frac{\partial GRL_d(x)}{\partial x} = -\lambda I \tag{23}$$

The domain classifier is trained by reversing the gradient direction so that the representation of source domain and target domain can be mapped to the same distribution space for edge alignment. Here, domain edge refers to the distribution boundary of samples from two different domains when the features of samples from two different domains are mapped to the same vector space. Domain edge alignment or feature alignment means that the feature distributions of samples from different domains are close in the same vector space, so that the classifier can better distinguish the emotional polarity of samples from different domains. Through the domain classifier, it can predict the domain category label:

$$y_d = softmax(W_d GRL_d(H) + b_d) \tag{24}$$

When the domain classifier and feature extractor are trained, the source domain representation and target domain representation are mapped into the same distribution space to narrow the distance between the two domain feature representation. However, there may be fuzzy features near the decision boundary formed by music emotion classifier, which make the samples easy to be wrongly classified. In order to better carry out domain adaptation and solve the problem of misclassification of decision boundary samples, two emotion classifiers C_1 and C_2 are trained to detect the sample points near these decision boundaries that are prone to misclassification. The feature extraction is further trained to generate better features so that the sample points are far away from the decision boundary.

As shown in Figure 4, black represents source domain data, gray represents target domain data, circle represents positive samples, and square represents negative samples.

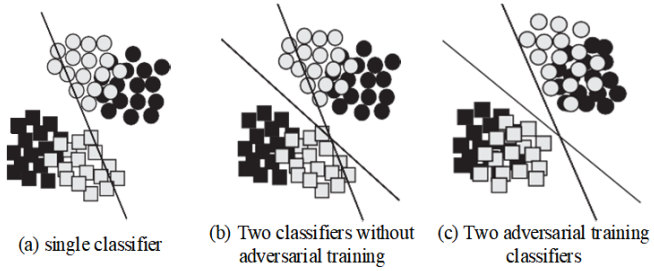

Fig. 4. Decision boundaries formed by different classifiers

It can be observed from Figure 4(a) that part of the target domain samples near the decision boundary are misclassified. When a different emotion classifier is trained to form another different decision plane as shown in Figure 4(b). The effect shown in Figure 4(c) will eventually be achieved after training, alleviating the problem of sample misclassification near the decision plane to a greater extent.

The feature representation H^s is obtained from the source domain label data through the feature extraction module G, which is passed through two emotion classifiers C_1 and C_2 respectively to predict the emotion category label. It minimizes the emotion classification loss to optimize parameters and emotion classification loss is:

$$L_{cls} = -\frac{1}{N_s}\sum_{i=1}^{N_s}\sum_{j=1}^{K} M1 - \frac{1}{N_s}\sum_{i=1}^{N_s}\sum_{j=1}^{K} M2 \tag{25}$$

$$M1 = y_i^s(j) log_2 \tilde{y}_{1i}^s(j) \tag{26}$$

$$M2 = y_i^s(j) log_2 \tilde{y}_{2i}^s(j) \tag{27}$$

$$\tilde{y}_{1i} = C_1(H^s) \tag{28}$$

$$\tilde{y}_{2i} = C_2(H^s) \tag{29}$$

K represents the number of categories of affective polarity categories.

If the decision boundary defined by emotion classifiers C_1 and C_2 is changed, the samples close to the decision boundary will change accordingly. In order to make C_1 and C_2 provide different guidance for these boundary samples and form different decision boundaries for the alignment of feature representations, the difference functions of the two emotion classifiers need to be defined first. Probabilistic output of two emotion classifiers is:

$$p_1 = (y|x), p_2 = (y|x) \tag{30}$$

Defining difference loss:

$$L_{dis} = E_{x \in D_s \cup D_t}[d(p_1 = (y|x), p_2 = (y|x))] \tag{31}$$

The difference function $d(p_1 = (y|x), p_2 = (y|x))$ is realized by calculating the mean value of the absolute value difference of the output probabilities of C_1 and C_2 in each category, i.e.,

$$d(p_1 = (y|x), p_2 = (y|x)) = \frac{1}{K}\sum_{i=1}^{K}|p_{1i} = (y|x) - p_{2i} = (y|x)| \tag{32}$$

Emotion classifiers C_1 and C_2 are trained in the way of adversarial training to align feature distribution representations. In order to make the point close to the decision boundary far away from the decision boundary, it is necessary to maximize the difference loss of the two emotion classifiers. The parameters of other modules are fixed, and only the parameters of two emotion classifiers C_1 and C_2 are trained, and the points near the decision boundary are detected by maximizing the difference function. The training objectives are as follows:

$$max(C_1, C_2)E_{x\in D_s\cup D_t}[\frac{1}{K}\sum_{i=1}^{K}|p_{1i} = (y|x) - p_{2i} = (y|x)|] \tag{33}$$

In order to reclassify the misclassified points near the original decision plane, it is necessary to make them far away from the new decision boundary constructed by two different emotion classifiers. Therefore, the parameters of two emotion classifiers C_1 and C_2 are fixed, and the parameters of part G of feature extractor are trained to minimize the differences. The optimization objectives are as follows:

$$max(G)E_{x\in D_s\cup D_t}[\frac{1}{K}\sum_{i=1}^{K}|p_{1i} = (y|x) - p_{2i} = (y|x)|] \tag{34}$$

Repetitive adversarial training enables the model to locate the misclassified sample points near the original decision plane, further making it far away from the newly formed decision plane for correct classification, rather than simply field edge alignment.

3.7. Training Process

The model uses standard gradient descent algorithm to learn and train parameters. The training algorithm is cross entropy loss function and L2 regularization term.

$$\zeta(\theta) = \sum_{i=1}^{c}\hat{y}_i log y_i + \lambda\sum_{\theta\in\Theta}\theta^2 \tag{35}$$

Where, C represents the number of emotional labels. $\hat{y}_i$ represents the output emotion value of the model. y_i represents the true value in the tag. λ stands for L2 regularization parameter. Θ represents the parameter used in the model.

4. Experiments and Analysis

The new model in this paper is run on the CPU with Intel(R) Xeon(R) W2123 3.60GHz and GPU server with NVIDIA GeForce RTX3060Ti. In this experiment, python language

is used for programming. The python version is Python 3.8.8, the programming tool is PyCharm Community Edition.

The model in this paper uses GloVel [14] as the word embedding layer to initialize the music text, and initializes the dimension of the word vector as 300. The hidden layer dimension of the bidirectional short and long time memory network is the same as the word vector dimension, which is set to 300. Adam is selected as the optimizer for the model. The model learning rate is 10^{-4}. The coefficient of L2 regularization term is 10^{-6}. Batch size is 32.

4.1. Experiment Data Set

The data sets used in this experiment are five public English music aspect word sentiment analysis data sets. They are Twitter, RES14, LAP14 in SemEval-2014 Task 4, Res15 in SemEval-2015 Task 12 and Res16 [29] in SemEval-2016 Task 5. The data set label distribution is shown in Table 1.

Table 1. Data sets

Data	Positive	Positive	Neutral	Neutral	Negative	Negative
Class	train	test	train	test	train	test
Twitter	1572	184	3138	357	1571	184
LAP14	995	352	475	181	882	139
RES14	2175	739	648	207	818	207
Res15	923	337	39	38	267	193
Res16	1271	480	72	32	468	128

4.2. Evaluation Index

In order to verify the validity of this experiment, two evaluation indexes are adopted in this paper, one is accuracy (Acc), the other is F1. Acc represents the proportion of samples with correct classification, calculated as shown in Equation (37). F1 is the harmonic average of accuracy rate and recall rate, calculated as shown in equations (38)-(40).

$$Acc = \frac{TP + TN}{TP + TN + FP + FN} \tag{36}$$

$$F1 = \frac{2P \times R}{P + R} \tag{37}$$

$$P = \frac{1}{c} \sum_{i=1}^{c} \frac{TP_i}{TP_i + FN_i} \tag{38}$$

$$R = \frac{1}{c}\sum_{i=1}^{c}\frac{TP_i}{TP_i + FP_i} \tag{39}$$

Where TP represents the sample number of correctly classified positive tags. TN represents the sample number of correctly classified negative tags. FP represents the sample number of misclassified positive labels, and FN represents the sample number of misclassified negative labels. C represents the number of label types of emotion categories.

4.3. Comparison Experiments and Analysis

In order to evaluate the effectiveness of the proposed model, we make comparison with some state-of-the-art methods.

SVM: The support vector machine method is used to classify music emotion.

AKSM [30]: This model combines text sequences with aspect words to fuse information, and classifies emotion polarity through LSTM and attention mechanism.

GCNN [31]: This model uses convolutional neural network to extract feature information, then filters emotion features unrelated to aspect word information through gating mechanism, and then selectively outputs relevant emotion features.

LSTM-GAN [32]: This model uses LSTM to model music text sequences and aspect words respectively, uses interactive attention to cross-fuse text sequences and aspect word information, and generates specific music text sequences and aspect word information.

GCNBA [33]: This model uses the attention mechanism to focus on the characteristics of important information, modeling aspect words and sentences in a joint way, and then capturing the interactive information between aspect words and sentences.

HOIE [34] : This model uses dependency syntax tree to build a dependency syntax graph, and then learns syntax information through the graph convolution operation.

DIMM [35]: This model uses the dependency relationship between words to transmit emotional features.

GCNNHM [36] : This model proposes hierarchical syntactic graph and hierarchical lexical graph in dependency syntax tree, and learns syntactic information through double-layer interactive graph convolutional network.

The first five models carry out semantic information learning based on the models in machine learning and deep learning. These models do not learn grammatical information. The last three models learn sentence grammar through dependency syntactic relations. The results of each model on the data set are shown in Tables 2-6.

As can be seen from the above tables, deep learning is generally better than machine learning. This is because deep learning can independently learn the feature information in music sentences and capture richer and more complete information. By comparing the first five models with the last four models, it can be seen from the data in the table that the values of the first five models are significantly less than those of the last four models. This is mainly because the last four models take into account syntactic information, while the first five models do not. It also verifies that the grammatical information of the sentence can effectively help the model identify the emotion polarity of the aspect words.

There is little difference between the HOIE model and the DIMM model in the five data sets, and they all have their own levels. In the Twitter data set, the accuracy rate and

Table 2. Results on Twitter

Model	Acc	F1
SVM	64.51	64.41
AKSM	70.76	68.51
GCNN	72.75	70.99
LSTM-GAN	73.61	71.92
GCNBA	73.41	71.31
HOIE	73.29	71.52
DIMM	73.31	71.56
GCNNHM	75.27	74.46
Proposed	75.39	74.25

Table 3. Results on LAP14

Model	Acc	F1
SVM	71.60	70.39
AKSM	70.25	64.29
GCNN	71.01	66.82
LSTM-GAN	73.16	68.49
GCNBA	73.73	68.63
HOIE	76.66	72.16
DIMM	76.74	71.85
GCNNHM	75.70	72.95
Proposed	78.85	75.38

Table 4. Results on RES14

Model	Acc	F1
SVM	81.27	81.11
AKSM	78.43	66.68
GCNN	79.68	69.17
LSTM-GAN	80.37	71.20
GCNBA	81.08	71.53
HOIE	81.88	73.13
DIMM	82.43	72.83
GCNNHM	83.08	74.59
Proposed	83.61	75.65

Table 5. Results on RES15

Model	Acc	F1
SVM	69.34	56.21
AKSM	76.54	57.45
GCNN	78.96	60.74
LSTM-GAN	79.65	53.76
GCNBA	79.28	58.13
HOIE	81.01	63.02
DIMM	81.49	61.61
GCNNHM	82.27	65.90
Proposed	82.84	67.26

Table 6. Results on RES16

Model	Acc	F1
SVM	73.54	62.37
AKSM	84.36	64.96
GCNN	87.40	66.98
LSTM-GAN	85.85	56.32
GCNBA	88.61	67.32
HOIE	90.10	68.59
DIMM	88.82	68.98
GCNNHM	90.07	71.95
Proposed	90.72	72.68

F1 value of the DIMM model are higher than that of the HOIE model, but the difference is not significant. In Lap14, Res14 and Res15 data sets, the accuracy of the DIMM model is higher than that of the HOIE model, but the accuracy of F1 model is lower than that of the HOIE model. In Res16 data set, although the accuracy of DIMM is lower than that of HOIE, the F1 value is higher than that of HOIE. Therefore, it is difficult to improve the result of learning syntactic information only through dependency trees. Therefore, GCNNHM adds the connection relationship between words in the dependency graph. It can be seen from the data in the table that the value of GCNNHM after adding the connection relationship is significantly higher than that of the previous two models.

Compared with HOIE and DIMM, the accuracy and F1 of the proposed model in this paper are better than those of the two models in the five data sets, which indicates that the new model cannot ignore semantic information when considering grammatical information. This shows that both semantic information and grammatical information are important for the judgment of the affective polarity of aspect words.

Compared with the GCNNHM model, the results of the proposed model in the five data sets are almost improved. All results are higher than GCNNHM except that F1 is lower than GCNNHM on the Twitter dataset. In the other four data sets, F1 values increases by 2.43%, 1.06%, 1.36% and 0.73%, respectively. Among them, the accuracy of five data sets increases by 0.11%, 3.15%, 0.53%, 0.57% and 0.65%, respectively. This also verifies that the new model is meaningful for learning semantic and syntactic information of music text sequences.

4.4. Ablation Experiment

In order to verify the importance of each component in the proposed model in this paper, a series of ablation experiments are set up for verification. The experimental results are shown in Table 7 and table 8. A represents the ablation of position information. B indicates that tree structured information is dissolved. C represents the ablation of the attention layer. D represents the ablation of grammar learning module. E represents the ablation of semantic learning module. F represents the ablation of the feature extraction layer.

As can be seen from the ablation experimental data in Table 7 and table 8, after the ablation of position information and tree structure information, experimental results of A and B declines sharply, indicating that the position information and tree structure information of each word would have an impact on the judgment of related words. Compared

Table 7. Ablation Experiment Results on Twitter, LAP14 and RES14

Model	Twitter	Twitter	LAP14	LAP14	RES14	RES14
Value	Acc	F1	Acc	F1	Acc	F1
A	74.66	73.01	77.59	73.23	82.09	73.76
B	74.37	72.60	76.65	72.99	83.34	75.29
C	75.24	73.67	79.95	76.18	81.73	72.10
D	74.66	72.68	76.81	73.23	82.53	74.91
E	74.23	72.79	75.71	70.46	81.11	71.91
F	74.80	73.03	75.56	72.06	80.75	71.52
Proposed	75.38	74.25	78.85	75.38	83.61	75.65

Table 8. Ablation Experiment Results on RES15 and RES16

Model	RES15	RES15	RES16	RES16
Value	Acc	F1	Acc	F1
A	81.55	67.14	90.07	71.12
B	81.36	66.78	89.25	71.82
C	81.18	66.10	89.90	71.06
D	81.36	65.78	90.23	74.45
E	80.81	67.17	89.58	71.70
F	80.81	63.52	90.39	70.97
Proposed	82.84	67.26	90.72	72.68

with the experimental results of the five data sets, the decline amplitude of A in Res14 data set is greater than that of B, and the decline amplitude of B in the other four data sets is greater, indicating that the influence of tree structure information on aspect word is greater than that of location information. After the ablation of the attention layer, the experimental results increases in Lap14 data set, while decreases in other data sets, indicating that the semantic and grammatical information learned in Lap14 data set can express the emotion polarity of the aspect words. However, the excessive focus of attention mechanism on information, on the contrary, inhibits the fusion of semantic information and grammatical information. In the other four data sets, the attention mechanism effectively fuses semantic and syntactic information. After the ablation of the syntactic learning module and the semantic learning module, the results of both C and D show a decrease trend, but the decrease of the results of E is a little larger than that of E, indicating that the semantic learning module and the grammatical learning module are equally important in the new model, but the new model has a higher dependence on the learning of semantic information. Finally, after the ablation of the feature extraction layer, the result of F experiment decreases, indicating that it is necessary to extract the feature of aspect words at the end. From the whole data, the experimental results of the model decreases significantly after the ablation of some components in the model, indicating that every part of the model is very important and cannot be absent. The magnitude of the decline in the results after the ablation of each component also is varied, indicating that each component is sensitive to different data sets to varying degrees, which is limited by the completeness and length of the sentences in each data set.

5. Conclusions

The proposed model in this paper combines semantics and syntax for simultaneous learning. Before the model learning semantic and syntactic information, the music text sequence is updated through the position information of the music text sequence in the dependency syntax tree as well as the relative position information and grammatical position information of the text sequence, which not only effectively reduces the influence of some noise words in the text sequence, but also makes the original text sequence contain grammatically related information before information learning. The experimental results show that the proposed model can effectively learn semantic and grammatical information, and each part of the model is very important. In the task of music-level emotion analysis, the learning of semantic and grammatical information is very important for the judgment of emotion polarity of aspect words, neither of which can be ignored. In the future works, we will research more advanced algorithms and apply them in real engineering application.

Acknowledgments. This work was supported by "2022 Fujian Education System Philosophy and Social Science Research Project "Young and middle-aged Teachers Education Research Project" Research results of Fujian and Taiwan Intangible Cultural Heritage in Ethnic instrumental Music Education in Colleges and Universities, project number: JAS22059".

References

1. Birjali, M., Kasri, M., Beni-Hssane, A.: "A comprehensive survey on sentiment analysis: Approaches, challenges and trends," *Knowledge-Based Systems*, Vol. 226, 107134. (2021)
2. Yadav, A., Vishwakarma, D.: "Sentiment analysis using deep learning architectures: a review," *Artificial Intelligence Review*, Vol. 53, No. 6, 4335-4385. (2020)
3. Jiang, D., Li, H., and Yin, S.: "Speech Emotion Recognition Method Based on Improved Long Short-term Memory Networks," *International Journal of Electronics and Information Engineering*, Vol. 12, No. 4, 147-154. (2020)
4. Song, M., Park, H., Shin, K.: "Attention-based long short-term memory network using sentiment lexicon embedding for aspect-level sentiment analysis in Korean," *Information Processing & Management*, Vol. 56, No. 3, 637-653. (2019)
5. Chen, Y., Zhuang, T., Guo, K.: "Memory network with hierarchical multi-head attention for aspect-based sentiment analysis," *Applied Intelligence*, Vol. 51, 4287-4304. (2021)
6. Li, W., Qi, F., Tang, M., et al.: "Bidirectional LSTM with self-attention mechanism and multi-channel features for sentiment classification," *Neurocomputing*, Vol. 387, 63-77. (2020)
7. Xu, X., Zhu, G., Wu, H., Zhang, S., Li, K.: "SEE-3D: Sentiment-driven Emotion-Cause Pair Extraction Based on 3D-CNN," *Computer Science and Information Systems*, Vol. 20, No. 1, 77C93. (2023), https://doi.org/10.2298/CSIS220303047X
8. Zhao, Y., Li, H., Yin, S.: "A Multi-channel Character Relationship Classification Model Based on Attention Mechanism," *International Journal of Mathematical Sciences and Computing(IJMSC)*, vol. 8, no. 1, 28-36. (2022)
9. Yang, M., Tjuawinata, I., Lam, K., Zhu, T., and Zhao, J.: "Differentially Private Distributed Frequency Estimation," *IEEE Transactions on Dependable and Secure Computing*, doi: 10.1109/TDSC.2022.3227654.
10. Zhang, K., Zhang, H., Liu, Q., et al.: "Interactive attention transfer network for cross-domain sentiment classification," *Proceedings of the AAAI Conference on Artificial Intelligence*, Vol. 33, No. 01, 5773-5780. (2019)

11. Tian, Y., Yang, L., Sun, Y., et al.: "Cross-domain end-to-end aspect-based sentiment analysis with domain-dependent embeddings," *Complexity*, Vol. 2021, 1-11. (2021)
12. Cao, Z., Zhou, Y., Yang, A., et al.: "Deep transfer learning mechanism for fine-grained cross-domain sentiment classification," *Connection Science*, Vol. 33, No. 4, 911-928. (2021)
13. Liang, B., Su, H., Gui, L., et al.: "Aspect-based sentiment analysis via affective knowledge enhanced graph convolutional networks," *Knowledge-Based Systems*, Vol. 235, 107643. (2022)
14. Huang, B., Zhang, J., Ju, J., et al.: "CRF-GCN: An effective syntactic dependency model for aspect-level sentiment analysis," *Knowledge-Based Systems*, Vol. 260, 110125. (2023)
15. Zhang, Z., Hu, C., Pan, H., et al.: "Aspect-Dependent Heterogeneous Graph Convolutional Network for Aspect-Level Sentiment Analysis," *2022 International Joint Conference on Neural Networks (IJCNN). IEEE*, 1-8. (2022)
16. Zhao, A., Yu, Y.: "Knowledge-enabled BERT for aspect-based sentiment analysis," *Knowledge-Based Systems*, Vol. 227, 107220. (2021)
17. Xue, B., Zhu, C., Wang, X., et al.: "The Study on the Text Classification Based on Graph Convolutional Network and BiLSTM," *Proceedings of the 8th International Conference on Computing and Artificial Intelligence*, 323-331. (2022)
18. Wang, L., Yin, S., Hashem, A., et al.: "A novel deep learning-based single shot multibox detector model for object detection in optical remote sensing images," *Geoscience Data Journal*, (2022). https://doi.org/10.1002/gdj3.162
19. Chen, H., Nemni, E., Vallecorsa, S., Li, X., Wu, C., Bromley, L.: "Dual-Tasks Siamese Transformer Framework for Building Damage Assessment," *IGARSS 2022 - 2022 IEEE International Geoscience and Remote Sensing Symposium, Kuala Lumpur, Malaysia*, 1600-1603, (2022). doi: 10.1109/IGARSS46834.2022.9883139.
20. Wu, Y., Li, W.: "Aspect-level sentiment classification based on location and hybrid multi attention mechanism," *Applied Intelligence*, Vol. 52, No. 10, 11539-11554. (2022)
21. Wang, Y., Chen, Q., Ahmed, M., et al.: "Joint inference for aspect-level sentiment analysis by deep neural networks and linguistic hints," *IEEE transactions on knowledge and data engineering*, Vol. 33, No. 5, 2002-2014. (2019)
22. Sun, K., Zhang, R., Mao, Y., et al.: "Relation extraction with convolutional network over learnable syntax-transport graph," *Proceedings of the AAAI Conference on Artificial Intelligence*, Vol. 34, No. 05, 8928-8935. (2020)
23. Zhang, R., Chen, Q., Zheng, Y., et al.: "Aspect-Level Sentiment Analysis via a Syntax-Based Neural Network," *IEEE/ACM Transactions on Audio, Speech, and Language Processing*, Vol. 30, 2568-2583. (2022)
24. Yang, L., Li, Y., Wang, J., et al., "Sentiment analysis for E-commerce product reviews in Chinese based on sentiment lexicon and deep learning," *IEEE access*, Vol. 8, 23522-23530. (2020)
25. Zheng, Y., Gao, Z., Shen, J., et al., "Optimising Automatic Text Classification Approach in Adaptive Online Collaborative Discussion-A perspective of Attention Mechanism-Based Bi-LSTM," *IEEE Transactions on Learning Technologies*, 1-14. (2022)
26. Zhao, G., Yang, P.: "Pretrained embeddings for stance detection with hierarchical capsule network on social media," *ACM Transactions on Information Systems (TOIS)*, Vol. 39, No. 1, 1-32. (2020)
27. Pennington, J., Socher, R., Manning, C.: "Glove: Global vectors for word representation," *Proceedings of the 2014 conference on empirical methods in natural language processing (EMNLP)*, 1532-1543. (2014)
28. Xue, Y., Li, Y., Liu, S., et al.: "Oriented localization of surgical tools by location encoding," *IEEE Transactions on Biomedical Engineering*, Vol. 69, No. 4, 1469-1480. (2021)
29. Pontiki, M., Galanis, D., Papageorgiou, H., et al.: "Semeval-2015 task 12: Aspect based sentiment analysis," *Proceedings of the 9th international workshop on semantic evaluation (SemEval 2015)*, 486-495. (2015)
30. Sindhu, C., Vadivu, G.: "Fine grained sentiment polarity classification using augmented knowledge sequence-attention mechanism," *Microprocessors and Microsystems*, 81, 103365. (2021)

31. Zhang, J., Liu, F., Xu, W., et al.: "Feature fusion text classification model combining CNN and BiGRU with multi-attention mechanism," *Future Internet*, Vol. 11, No. 11, 237. (2019)
32. Yu, Y., Srivastava, A., Canales, S.: "Conditional lstm-gan for melody generation from lyrics," *ACM Transactions on Multimedia Computing, Communications, and Applications (TOMM)*, Vol. 17, No. 1, 1-20. (2021)
33. Liu, J., Liu, P., Zhu, Z., et al.: "Graph convolutional networks with bidirectional attention for aspect-based sentiment classification," *Applied Sciences*, Vol. 11, No. 4, 1528. (2021)
34. Li, B., Fan, Y., Sataer, Y., et al.: "Improving semantic dependency parsing with higher-order information encoded by graph neural networks," *Applied Sciences*, Vol. 12, No. 8, 4089. (2022)
35. Wen, J., Jiang, D., Tu, G., et al.: "Dynamic interactive multiview memory network for emotion recognition in conversation," *Information Fusion*, Vol. 91, 123-133. (2023)
36. Li, X., Lu, R., Liu, P., et al.: "Graph convolutional networks with hierarchical multi-head attention for aspect-level sentiment classification," *The Journal of Supercomputing*, Vol. 78, No. 13, 14846-14865. (2022)

Wenwen Chen is with the Jimei University School of Music. She has published several papers and won several awards. Her research direction: Emotion recognition, artistic feature extraction.

Received: December 12, 2022; Accepted: May 05, 2023.

Computer Science and Information Systems 20(4):1819–1843 https://doi.org/10.2298/CSIS221218032H

A Novel Single Shot-multibox Detector Based on Multiple Gaussian Mixture Model for Urban Fire Smoke Detection

Hao Han

Guizhou Fire and Rescue Brigade
Department of Natural Resources of Guizhou Province
hanhaovip0@163.com

Abstract. Under complex scenes, the traditional smoke detection methods cannot satisfy the real-time and accuracy requirements. Therefore, this paper proposes a novel single shot-multibox detector based on a multiple Gaussian mixture model for urban fire smoke detection. Multiple Gaussian models are used to represent the features of each pixel in the moving object image. The Gaussian mixture model is updated based on the principle that each pixel in the image is regarded as a background point if it matches the Gaussian mixture model. Otherwise, if it matches the Gaussian mixture model, it is regarded as the foreground point. By updating the foreground model and calculating the short-term stability index, the detection effect of moving objects is improved. By determining the relationship between Gaussian distribution and pixel, a new parameter is set to construct the background model to eliminate the influence caused by illumination mutation. Aiming at the problems of smoke detection efficiency and network over-fitting, we present an InceptionV3-feature fusion single shot-multibox detector. The new neural network is trained and tested by smoke positive and negative sample images. At the same time, Multibox Loss function is replaced by the Focal Loss function, which reduces the detector misdetection caused by the imbalance of positive and negative samples. Experimental results show that the proposed method is feasible and effective. The average accuracy of smoke detection is 97.5%, and the average response time of the smoke alarm is 4.57s, which can meet the requirements of real-time smoke detection in complex scenes.

Keywords: urban fire smoke detection, multiple Gaussian mixture model, single shot-multibox detector, InceptionV3-feature fusion.

1. Introduction

Smoke is an important symbol of the early stage of fire. Accurate detection and recognition of smoke are helpful for early warning of fire. Traditional smoke detection methods mainly use smoke detectors, the detection range is small, and the detection accuracy is susceptible to temperature, humidity, airflow, and other factors [1,2]. In recent years, smoke detection technology has been widely used in fire warning, fire detection and other fields because of its advantages of wide monitoring range, sensitive response and low environmental requirements [3].

In recent years, the research on smoke detection mainly focuses on the static characteristics of smoke, such as color, shape and texture, and the dynamic characteristics of smoke, such as motion and diffusion. Generally, the flow of smoke detection algorithm

can be divided into three stages: extraction of smoke proposal area, extraction of smoke features, and smoke recognition. Millan-garcia et al. [4] used the color space features of smoke to process video images and exclude non-smoke areas. The shortcoming of this method was that the color information was sensitive to threshold setting. Favorskaya et al. [5] regarded the smoke as dynamic texture, and used different local binary mode (LBP) histograms to classify and identify dense smoke, transparent smoke and non-smoke areas. For remote fire smoke images, Zhou et al. [6] realized smoke recognition based on the local extremal region segmentation method, but this method had a high false positive rate for the areas with thick fog. Dimitropoulos et al. [7] proposed a high-order linear dynamic system (H-LDS) to describe the feature operator and analyzed the dynamic texture of smoke, thus improving the recognition rate of smoke features. Jia et al. [8] first performed enhanced color transformation on the smoke image, then segmented the smoke proposal area, and finally detected the smoke area by establishing static and dynamic criteria of smoke. Vijayalakshmi et al. [9] established a saliency smoke detection model based on the color and motion characteristics of smoke and realized the segmentation of smoke area. Starting from the tone of the image, Cruz et al. [10] compared the pixel tonal distribution of the area containing smoke and the area without smoke, and proposed the concept of fire detection index, which was used to extract the smoke area. Ye et al. [11] used the motion characteristics of smoke to extract the smoke proposal movement area in the video, and further realized the identification of smoke based on space-time wavelet transform, Weber contrast analysis and color space segmentation.

After the above video smoke detection methods extract the features of the smoke proposal area, it is generally necessary to set certain thresholds for the relevant features, and then form a rule criterion to identify the smoke. In this process, most of the smoke feature extraction operators are manually designed, which may not reflect the essential characteristics of the smoke. The selection of threshold values mostly depends on personal experience, and the rationality of threshold value greatly affects the effect of smoke identification [12]. Therefore, based on the above traditional video smoke detection, some scholars have studied smoke recognition based on support vector machine (SVM), AdaBoost algorithm and other methods. Kim et al. [13] used SVM to identify the smoke in the video based on the optical flow characteristics of the smoke by analyzing its diffusivity, color and opacity. Prema et al. [14] extracted the suspected smoke area by YUV color model (Y is the brightness value of black and white, U and V are the chroma value), and realized the smoke identification based on the extracted space-time, contrast and other multi-features and SVM. Zhao et al. [15] identified smoke based on the Adaboost algorithm by taking advantage of the color and other characteristics of smoke, which could also effectively distinguish fog from smoke. Yuan et al. [16] proposed a smoke recognition method based on dual-threshold Adaboost to recognize black smoke and white smoke with bimodal distribution characteristics. However, SVM, AdaBoost and other traditional classifiers still have some limitations. When the amount of smoke image features is small, these classifiers perform well. When the amount of smoke image features is large, the classification accuracy of this classifier needs to be improved.

At present, deep learning [17,18] has been successfully applied in image classification, pattern recognition and other fields. Wei et al. [19] integrated static and dynamic smoke texture information and proposed a smoke texture recognition framework based on the cascaded convolutional neural network (CNN)[20,21], which could improve the

accuracy of smoke recognition. However, the static and dynamic texture information was processed separately in this method, which increased the complexity of the algorithm and affected the real-time performance of smoke detection. Xu et al. [22] used synthetic smoke images and real smoke images to train the CNN model based on the domain adaptability method [23]. Although this method could reduce the false detection rate of smoke recognition, the use of the synthetic smoke images would affect the performance of the training model in the actual scene. On the whole, the current video smoke detection methods have strong scene pertinence. In a fixed scene, these video smoke detection methods can achieve a high recognition accuracy, but in the face of the change of weather, light and other interference factors, these smoke detection false alarm rate is high.

Aiming at the above problems, on the basis of summarizing the current smoke detection methods, this paper proposes an urban fire smoke detection method combining multiple Gaussian mixture model and a modified single shot-multibox detector (MSSD) to satisfy the requirements of anti-interference, real-time smoke detection.

This paper is organized as follows. Section 2 is the related works for the smoke recognition. We detailed show the proposed smoke recognition method in section 3. The experiments are displayed in section 4. Section 5 concluded this paper.

2. Related Works

As an important means of fire detection, smoke detection has been widely used in fire and explosion detection and early warning. The traditional detection technology based on smoke sensor has a small monitoring range, high cost of laying in factories, warehouses, forests and other large areas, and such sensors are easy to age and reduce sensitivity. In recent years, video smoke detection technology has attracted much attention from researchers at home and abroad because of its advantages such as short response time, high sensitivity and large coverage area.

Current video smoke detection methods mainly rely on visual features such as motion, color, shape, transparency and texture. Reference [24] proposed a detection method using smoke color and motion characteristics. Firstly, background extraction and color filtering were used to obtain candidate smoke regions. The light flow was then characterized by the mean and variance of its speed and direction. Finally, BP neural network was used to complete the classification and recognition. The dimension of the obtained eigenvector was too low to effectively describe the different manifestations of smoke in complex environment. Reference [25] proposed a cumulative motion model and used integral graph to rapidly estimate the direction of smoke motion. This method assumed that smoke moved upward, and its application scope was limited. Subsequently, reference [26] proposed a smoke detection method combining the dual mapping frame feature and AdaBoost. The first layer mapped each frame into blocks and extracted the edge direction histogram, edge intensity histogram, LBP histogram, edge intensity density, color and saturation density and other features of each image block. The second layer mapped the image into partitions and calculated the mean value, variance, peak state and skewness of each block feature. These statistics were eventually used to train and classify the AdaBoost model. Reference [27] proposed a smoke detection method based on contour and wavelet transform for fixed camera video. The Hidden Markov model (HMM) was used to analyze the periodic change of smoke profile in time domain. Smoke usually had a certain transparency,

and its visual features were affected by background. If background interference could be overcome, the difficulty of smoke identification could be effectively improved. Aiming at this problem, reference [28] analyzed the mixing mechanism of smoke and background, built a set of smoke foreground extraction method, and solved the mixing coefficient by using sparse expression, local smoothing and other constraints. This method could reduce background interference to some extent and improve the accuracy of smoke recognition.

In the aspect of smoke texture feature extraction, GLCM, LBP, Wavelet are the most widely used. Reference [29] implemented a set of real-time flame and smoke detection system based on GLCM analysis of smoke texture. Reference [30] proposed a smoke detection method based on pyramid histogram sequence. Firstly, the pyramid sampling was a three-layer multi-scale structure, and the LBP and LBPV features of different modes were extracted from each layer. Finally, the LBP and LBPV feature sequences were spliced together as smoke texture features, and the BP neural network was used for classification. However, there are many false detections in the existing methods in practical application, mainly for the following reasons: 1) Smoke presents various states under different environments. The data set selected in the existing references is small, so it is difficult to train a stable and reliable classifier to fit its complex manifestations. 2) Smoke visual feature extraction has always been a difficulty in video smoke detection. Relying only on static features is insufficient to distinguish smoke from some smoke-like objects (such as clouds, fountains, etc.). How to construct a stable and efficient feature extraction algorithm to integrate static and dynamic information in video becomes the key to reduce false smoke detection.

Traditional classifiers such as SVM and decision tree perform well in small data sets, but it is difficult to improve the classification accuracy when the amount of data is large. In recent years, deep neural network (DNN) has been successfully applied in the field of computer vision. By establishing a hierarchical network model structure similar to human brain, DNN extracts features from the input data step by step from the bottom level to the top level, so as to better obtain the mapping relationship from the bottom level signal to the top level semantic. Convolutional neural networks (CNN), as one of the most important network models, have made breakthroughs in face recognition and image classification, driven by big data and high-performance computing. In 2012, reference [31] used deeper CNN on the famous ImageNet image data set to obtain the best results in the world, reducing the recognition error rate from 26% to 15%, and greatly improving the accuracy of large-scale image recognition. Deep convolutional neural networks can take the original image as input to learn features from the bottom pixel level to the top representation level, transforming the mode of manual feature extraction to the mode of automatic feature learning from data. Moreover, the model is more effective on big data.

In this paper, CNN is introduced into smoke texture feature extraction and a cascaded CNN smoke texture recognition framework is proposed to integrate static and dynamic texture information. The original image is used as input in the static texture and the optical flow sequence of the original image is used as input in the dynamic texture. The final experimental results show that the proposed method achieves better performance in the accuracy and false detection rate of smoke recognition.

3. Proposed Smoke Detection Method

The urban smoke detection algorithm flow is shown in figure 1. Firstly, the image of urban smoke scene is obtained by the camera. Secondly, the background subtraction method is used to process the collected sequence images, and the foreground image of moving object is extracted preliminarily. Further, the noise in the foreground image is removed by morphology operation. Finally, the trained SSD model [32] is used to classify and identify the moving object area. If it is judged as smoke, smoke alarm will be issued.

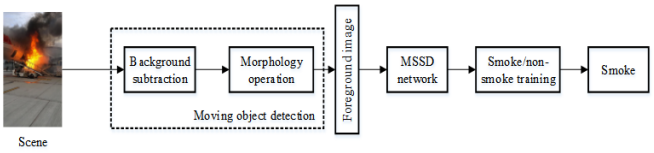

Fig. 1. Flowchart of the smoke detection algorithm

3.1. Moving Object Detection

In complex scenes, clouds, fogs and other objects similar to smoke will interfere with smoke detection. In video stream sequence images, moving object extraction can effectively filter out the interference of static objects, and then reduce the false positive rate of CNN recognition. In addition, the filtering of non-smoke areas in video images can reduce the running time of subsequent smoke detection algorithms and further improve the efficiency of smoke detection.

A. Gaussian mixture model (GMM) The features of each pixel in the moving object image are represented by N Gaussian models. The Gaussian mixture model is updated with each frame of the image [33]. The Gaussian mixture model is matched with each pixel in the current image. If there is no match, it determines that the pixel is the foreground point. If a match can be made, the pixel is the background point. Set the gray value of a pixel in the image as g, and the pixel gray value from time 1 to time t is expressed as $(a_1, a_2, \cdots, a_i, \cdots, a_t)$. A detailed description of pixel gray values requires N Gaussian distributions. In the description, N Gaussian distributions need to be mixed by weighting, so as to obtain the probability density function:

$$g(a_t) = \sum_{i=1}^{t} \lambda_{t,i} \times \gamma(a_i, v_{t,i}\Sigma_{t,i}) \tag{1}$$

Where $\gamma(a_i, v_{t,i}\Sigma_{t,i})$ represents the probability density function of Gaussian distribution. $v_{t,i}$ is the mean value of the Gaussian distribution. $\lambda_{t,i}$ is the weight. $\Sigma_{t,i}$ is the covariance matrix of the Gaussian distribution. The probability density function of Gaussian distribution is calculated as follows:

$$\gamma(a_i, v_{t,i}\Sigma_{t,i}) = \frac{1}{2\pi(d/2)|\Sigma_{t,i}|^{0.5}} s^{-0.5(a_t - v_{t,i})\sum_{i=1}^{t}(a_t - v_{t,i})} \tag{2}$$

Where, the dimension of a_t is d. When the observation point is updated as a_{t+1}, the pixel values and the mean value $\tau_{t,i}$ of N Gaussian function distributions are compared respectively. Formula (3) is used as the judgment rule to select Gaussian function.

$$|a_{t+1} - \tau_{t,i}| < o \times \varepsilon_{t,i}^2, i = 1, 2, \cdots, N \tag{3}$$

In the formula, o represents a user-defined parameter, whose value is usually 2.5. When equation (3) is satisfied, the $i-th$ Gaussian matches a_{t+1}.

In the absence of a Gaussian match, the variance and mean remain the same. Equations (4) to (6) represent the generated parameters after the Gaussian function is matched with a_t, they are updated by:

$$\tau_{t,i} = (1 - \vartheta) \times \tau_{t-1,i} + \vartheta \times a_t \tag{4}$$

$$\varepsilon_{t,i}^2 = (1 - \vartheta) \times \varepsilon_{t-1,i}^2 + \vartheta \times (a_t - \tau_{t,i})^2 \tag{5}$$

$$\vartheta = \delta \times \lambda_{t,i} \tag{6}$$

In the formula, ϑ is the parameter learning rate. N Gaussian distribution weights are updated through equation (7):

$$\lambda_{t,i} = (1 - \delta) \times \lambda_{t-1,i} + \vartheta \times E \tag{7}$$

In the formula, the updating rate of the Gaussian distribution weight is expressed as $\delta \in [0, 1]$. When $E = 1$, the matching distribution is satisfied. When $E = 0$, it satisfies $N - 1$ distribution.

In order to improve the reliability of the background model, the weight is normalized. After normalization, we can get $\bar{\lambda}_{t,i} = \lambda_{t,i} / \sum_{i=1}^{n} \lambda_{t,i}$. The descending order of each distribution should follow the ratio $\bar{\lambda}_{t,i}/\varepsilon_{t,i}$. The reliable background part is selected as the first x distribution, and the number of background distribution needs to be controlled by H_1, where $x = \underset{x'}{argmin}(\sum_{i=1}^{x'} \bar{\lambda}_{t,i} > H_1)$. The reliability of the background distribution needs to be expressed by the ratio $\bar{\lambda}_{t,i}/\varepsilon_{t,i}$. When the weight is inversely proportional to the variance, it can be concluded that the samples belonging to this distribution are affected by the probability of sample occurrence. The higher probability denotes the more concentrated the samples. The probability is higher of the distribution belonging to the background distribution.

B. Improved GMM In common moving object detection and tracking methods, foreground model is seldom used, it is only used as auxiliary. However, in the modeling of improved Gaussian mixture model, the generated foreground model when background matching fails is used to make a comprehensive judgment of foreground combined with

short-term stability index [34]. Based on the Gaussian mixture model, if all the corresponding N background models fail to match the current pixel value, the variance and mean of the model with the minimum weight will be replaced by the larger value and the current pixel value. The generated model at this time is the foreground model $\gamma(\tau_f, \varepsilon_f)$. If the threshold value H_f is greater than the difference between the mean value of the prospect model and the subsequent points, formula (8) is needed to update the prospect model and Formula (9) is used to calculate the short-term stability:

$$R = \frac{P\sum_{i=0}^{P} a_{t+1}^2 - \sum_{i=0}^{P} a_{t+i}}{P(P-1)} \tag{8}$$

$$\tau_{f,t+1} = (1 - v_f)\tau_{f,t} + v_f a_{t+1} \tag{9}$$

Where $v_f \in [0, 1]$ represents the learning rate of the prospect model. P represents the range of sliding window frames. When matching the current pixel, the foreground model is preferred, which can reduce the decision risk caused by the error of matching background model and foreground point.

The shapes of moving objects are different, and the calculation window length P value of short-term stability of moving objects with uniform colors is set in the range of 2-5. If the color of the moving object is rich, the change time of pixel value is too short, which will cause the object to be mistaken for the background [35]. At this point, P value should be controlled within 5-20, and there is a positive correlation between P value and detection effect. However, if the P value is too large, the response speed of the index will be slow. After the stability is obtained through formula (9), the threshold R_{th} of judgment can be obtained as:

$$R_{th} = R_{min} + \frac{R_{max} - R_{min}}{L} \tag{10}$$

The maximum stability of the current L frame is R_{max} and the minimum stability is R_{min}. L is a constant. The condition that the current pixel is judged to be a foreground point is that all the current pixels in the range of consecutive L frames exceed the short-term stability threshold.

The change of stability is positively correlated with the relation of pixel value. Therefore, the stability can fully describe the emergence and persistence of prospects. If the pixels in the moving object area change in a short time, it is easy to detect the background incorrectly. This situation can be effectively avoided by using the short-term stability index to improve the Gaussian mixture function. When the traditional Gaussian model detects the object's motion speed is too slow, it cannot be detected. In this paper, the method of combining short-term stability index and prospect model is adopted to solve the common problems of Gaussian mixture model and improve the detection effect of object's motion.

C. Elimination of light mutation The improved Gaussian mixture model can improve the background extraction due to the slow motion of the detected object. However, pixels will be wrongly detected as foreground pixels, once it is disturbed by light mutation.

The movement of the object and the change of illumination will lead to the mutation of pixel gray scale, and the mutation caused by the change of illumination is larger than that caused by the movement of the object [36]. Therefore, in order to achieve better detection and tracking effect, it is necessary to eliminate light mutation. The specific methods are as follows.

In order to determine whether the Gaussian distribution in the current frame matches the pixel, a new parameter w needs to be set for each pixel in the image. The value of w is set to improve the background estimation. If N Gaussian functions and pixels can be matched with each other, then $w = 0$. If not, the value of w is 1. If the pixel mutation area is large, it is caused by illumination mutation. The number of $w = 1$ in the image is counted. If formula (11) is satisfied, it indicates that the background illumination mutation occurs in this time.

$$\frac{\sum_{i=1}^{K} w_i}{K} > H_1 \tag{11}$$

When illumination mutation occurs, the proportion of pixel area with gray mutation occurs in the image is the threshold value, which is represented by H_1. In the actual experiment, $H_1 = 0.66$. If the image can conform to formula (11), the background pixel is determined to be a pixel block with $w = 1$. In this case, the background model is updated by improving the background model, and the one with the smallest weight among the first N distributions is replaced by the Gaussian distribution based on the gray value of pixel blocks as the mean value, and it becomes the background model.

3.2. Morphological Processing

Isolated noises, small gaps and holes still exist in foreground images extracted by improved GMM background subtraction method. In order to realize the complete extraction of moving object, the foreground image is further processed by morphological method. Let O be the object to be processed, S be the structural element. It uses S to perform open and close operations on O respectively, i.e,

$$OPEN(O, S) = (O \Theta S) \oplus S \tag{12}$$

$$CLOSE(O, S) = (O \oplus S) \Theta S \tag{13}$$

Where, Θ is the corrosion operation on the image. $\oplus$ is the expansion operation of the image. Firstly, the open operation is performed on each image, then the gaps and holes in the image are filled by closed operation after the noise is eliminated. Finally, the processed results are obtained.

3.3. Network Design for Smoke Detection

A. InceptionV3 network InceptionV3 is one of the Google Inception series networks. Based on InceptionV2, this network proposed a new Network in Network (NIN) structure

[37]. InceptionV3 is a new network constructed according to the NIN architecture of the Inception module. The Inception module for InceptionV3 is shown in figure 2.

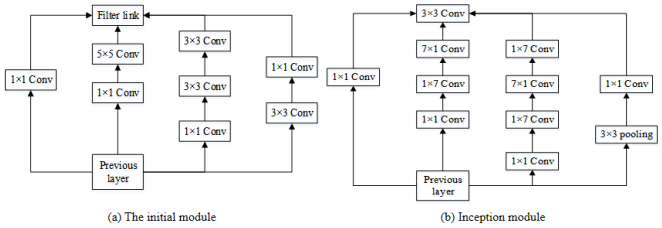

Fig. 2. Structure of InceptionV3 Inception module

As shown in figure 2, InceptionV3 module reduces the parameter number of the model by extracting features of different scales [38]. At the same time, multi-scale features can improve the recognition ability of the model. Studies have proved that the convolution layer with 1×1 convolution kernel can realize feature conversion, improve network recognition ability and change the number of channels output by the convolution module through a small amount of computation. The fifth ninth modules of InceptionV3 use a larger convolution kernel to capture more abstract features. For the convolution layer with 7×7 convolution kernel and prone to generate a large number of parameters, InceptionV3 uses 1×7 convolution layer and 7×1 convolution layer to improve the efficiency and reduce the over-fitting. Experiments show that this asymmetric convolution structure can deal with more and more spatial features and increase feature diversity.

B. SSD and MSSD InceptionV3 network model is mainly used to classify smoke. There is a limitation that there can only be one smoke in each image and the background cannot be too complicated. To solve this problem, many object detection methods have been proposed, such as using color and texture features to detect smoke. The accuracy of smoke detection is greatly reduced because of overlapping and false detection.

At present, there are many deep learning methods for object detection that are widely used in urban areas, such as towards real-time object detection with region proposal networks (Faster-RCNN) [39], Object-detection via region-based fully convolutional networks (RFCN) [40], Single shotmultibox detector (SSD), You only look once (YOLO) [41] and RetinaNet [42]. In addition, smoke detection has higher requirements on the real-time performance of the algorithm, so it is necessary to choose a more efficient algorithm as far as possible under the condition that the accuracy meets the requirements.

SSD is an algorithm that uses the same deep neural network to detect and identify detected objects in images. SSD generates a series of candidate boxes of different sizes. The offset value of the labeled box and the candidate box is calculated to match them. Typically, each annotation box will match multiple candidate boxes. SSD considers candidate boxes with IoU greater than 0.5 as positive samples, and sets other boxes as negative samples.

SSD uses VGG16 as the backbone network to form multi-scale detection by extracting feature maps with different sizes from Conv4_3, FC7, Conv7_2, Conv6_2, Conv8_2 and Pool6. The network structure diagram of SSD is shown in figure 3.

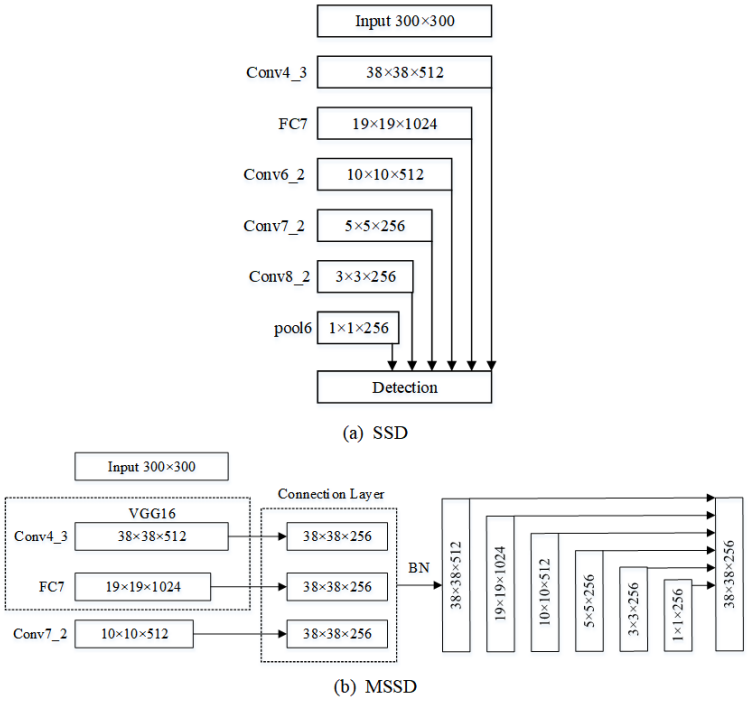

Fig. 3. Model structure of SSD and MSSD

The sizes of feature map are 5×5 pixels, 3×3 pixels and 1×1 pixels, respectively. Low-level feature maps are beneficial to small object detection, while advanced feature maps with the size of 38×38 pixels, 19×19 pixels and 10×10 pixels are beneficial to large object detection. SSD uses 3×3 convolution layer and 1×1 convolution layer with 1024 channels to replace full connection layer and lose layer to reduce model parameters, improve computational efficiency and effectively prevent over-fitting. The loss function of SSD is:

$$L(x, c, l, g) = \frac{1}{N}(L_{conf}(x, c) + \alpha L_{loc}(x, l, g)) \tag{14}$$

Where $L(x, c, l, g)$ is the total loss value. x is the convolution eigenvalue. c is the real class. l is the predicted box position coordinate value. g is the real box position coordinate value. L_{loc} is the smoothing loss between the prediction box and the real box. N is the number of candidate boxes. L_{conf} is the softmax loss under multi-class confidence. α is the weight of L_{loc}. Multibox Loss is composed of two parts. The former uses Softmax to calculate the classification loss, and the latter predicts the position through local loss.

SSD provides a solid foundation for smoke detection tasks, with the primary benefit of fast detection. However, experiments have shown that SSD has the following problems: small objects are difficult to identify; Some background regions are identified as object objects, and objects are repeatedly identified. To solve these problems, the SSD model is modified to the MSSD model without increasing the number of model parameters and reducing the detection speed.

The relationship between each layer used for prediction in the SSD model is independent of each other. The MSSD model fuses these layers with feature maps of different proportions so that they communicate with each other and improve accuracy. However, this approach is not suitable for fusing feature maps less than 10×10 in the MSSD model, because there is little information to merge. Feature graphs of three larger layers are combined to generate feature graphs of 3838 pixels. Feature pyramid network (FPN) is generated [43]. Finally, the FSSD model extracts features from FPN.

The structure of the MSSD model is shown in figure 3b. The MSSD model uses VGG16 as the main backbone network. The feature map of Conv7_2 becomes 10×10. FC7 and Conv7_2 use bilinear interpolation to adjust the feature maps to 38×38 pixels and then connect them to Conv4_3, in which the number of channels in the fusion layer is 768(256+256+256). BN acts on the fusion layer, the number of channels in this layer is reduced to 512, and 5 convolution layers are used to reduce the size of the feature graph. Finally, six feature maps of different sizes (38×38 pixels, 19×19 pixels, 10×10 pixels, 5×5 pixels, 3×3 pixels and 1×1 pixel) are obtained and used for multi-scale prediction. This method can combine shallow detail features with high-level semantic features to identify small objects better than SSD models and reduce false detection rates. However, the speed of MSSD model is slightly lower than that of SSD model.

The loss function partially satisfies the following equations:

$$L = L_{cls} + L_{reg} \tag{15}$$

$$L_{cls} = \lambda_1 L_{tr} + \lambda_2 L_{tcl} \tag{16}$$

$$L_{reg} = \lambda_3 L_r + \lambda_4 L_{sin} + \lambda_5 L_{cos} \tag{17}$$

Where L_{cls} represents the classification loss of TR and TCL. L_{reg} represents the regression loss of r, $cos\theta$ and $sin\theta$. L_{tr} and L_{tcl} are the cross drop losses of tr and tcl respectively. L_r, L_{sin} and L_{cos} are smooth-L1 losses. Set λ_1, λ_2, λ_3, λ_4 and λ_5 to 1, satisfying the following formula:

$$[L_r, L_{cos}, L_{sin}]^T = SmoothedL_1[(\hat{r} - r)/r, \hat{cos\theta} - cos\theta, \hat{sin\theta} - sin\theta]^T \tag{18}$$

C. Optimized MSSD In this paper, it is only necessary to determine whether the detection object is smoke or not, without multi-category classification. Optimized MSSD is simplified as IFSSD. The IFSSD model structure is shown in figure 4.

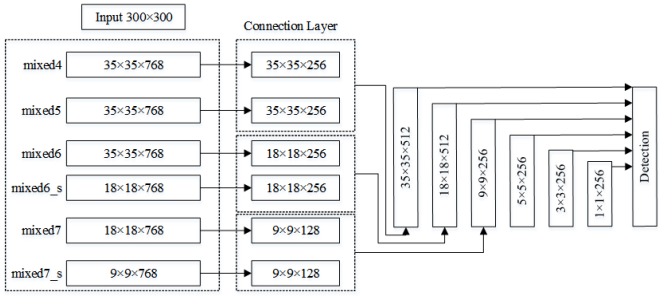

Fig. 4. IFFSD-based smoke detection structure

In order to reduce the parameter number and improve the detection effect of small objects, InceptionV3 is adjusted in this paper to achieve multi-scale detection based on different receptive fields. The mixed7 layer has been removed in this article. IFSSD model adds 1×1 convolution after mixed6 layer with step size of 2 and channel number of 768, and then conducts batch normalization. The feature map of the newly added layer mix6_s is 18×18 pixels. The feature map size of mixed7 layer has been changed from 35×35 pixels to 18×18 pixels. After mixed7, the convolution layer with convolution kernel 1×1, step size 2 and channel number 768 is added. The feature map of mixed7_s is 99 pixels.

The IFSSD model is similar to the FSSD model in that large feature maps are combined. In InceptionV3 of IFSSD model, four layer modules with different feature graph sizes are selected respectively, namely mixed4, mixed5, mixed6_s and mixed7_s. In the first connection layer, the convolution layer with convolution kernel of 1×1, step size of 1 and channel number of 256 is applied to mixed4 and mixed5. The purpose of this method is to reduce the model parameters without changing the size of the feature graph, so as to reduce the number of parameters in the model and enhance the nonlinear recognition ability of the model. The size of the feature graph generated after convolution is

35×35 pixels, and then the feature graph generated by convolution of mixed4 and mixed5 is fused together. In the second connection layer, a convolution layer with 11 convolution kernel, 2 step size and 256 channels are added after mixed5 module, and the size of the generated feature map is 18×18 pixels. After mixed6_s, it adds a convolution layer with 1×1 convolution kernel, 1 step size and 256 channels. The generated feature map is 1818 pixels.

Then, the two feature maps are combined. In the third connection layer, a convolutional layer with 1×1 convolution kernel, step size 2 and channel number 128 is added to mixed6_s to generate a feature graph of $9 \times 9 \times 128$. Finally, the convolution layer with convolution kernel of 1×1, step size of 1 and channel number of 128 are added to mixed7_s to generate a feature graph of $9 \times 9 \times 128$, and the two feature graphs are combined.

In the IFSSD model, $35 \times 35 \times 512$, $18 \times 18 \times 512$ and $9 \times 9 \times 256$ connection layers are used to generate FPN. After the connection layer of $9 \times 9 \times 256$, it adds a SAME convolution layer with a convolution kernel of 3×3, step size of 2 and channel number of 256, and generates a feature map with a size of 5×5 pixels. Then, it adds a convolution kernel of 3×3, step size of 1×1, channel number of 256 and uses VALID convolution layer to generate feature graph size of 3×3 pixels. Finally, after layer $3 \times 3 \times 256$, it adds a VALID convolution layer with convolution kernel 3×3, step size 1 and channel number 256, and generates feature graph size 1×1 pixel.

It can be seen that, the MSSD model uses bilinear interpolation to get the same dimensions from three different layers in VGG16 and fuses them together to get an output layer and generate FPN. IFSSD model uses 1×1 convolution to modify the channel number and image size of mixed4, mixed5, mixed6_s, and mixed7_s layers in InceptionV3, and fuses the above modified convolution layers in pairs to obtain three different layers, and then generates FPN based on these three layers.

The difference in performance between one-stage and two-stage algorithms is mainly caused by the imbalance of a large number of foreground background categories. In the two-stage algorithm, in the candidate box stage, score and non-maximum suppression (NMS) [44] are adopted to filter out a large number of negative samples. Then it fixes the proportion of positive and negative samples in the classification and regression stage to make foreground and background relatively balanced. The one-stage algorithm needs to generate about 100kb candidate locations. Despite repeated sampling, training is still dominated by a large number of negative samples. The IFSSD model used in this paper belongs to the one-stage model, and Focal Loss is used to replace the original loss function.

Focal Loss is mainly to solve the problem of serious imbalance of positive and negative sample ratio in one-stage object detection. The loss function is reduced, and the weight of a large number of simple negative samples in training can also be understood as a kind of difficult sample mining. Focal Loss is modified based on the cross entropy Loss function. The cross entropy loss of dichotomies can be calculated as:

$$L = \begin{cases} -lg(y') & y = 1 \\ -lg(1 - y') & y = 0 \end{cases} \tag{19}$$

In the formula, L is the loss value of cross entropy. y is the true classification. y' is the prediction classification. y' is the output of the activation function, and the value is between 0 and 1. It can be seen that for the positive cross entropy, the larger output probability denotes the smaller loss. For negative samples, the smaller output probability denotes the smaller loss. At this time, the loss function is slow and may not be optimized in the iterative process of a large number of simple samples.

Focal Loss adds a constant factor γ to the original basis to reduce the Loss and focus more on difficult and misclassified samples. In addition, the balance factor a_t is added to balance the uneven proportion of positive and negative samples. The specific formula is as follows:

$$F_L(p_i) = -a_t(1-p_i)^{\gamma} lg(p_i) \tag{20}$$

p_i is the probability of different categories. a_t is the ratio of positive samples to negative samples. If the foreground category is a_t, the corresponding background category is $1 - a_t$.

For the data set of single target detection, Anchor can be reasonably set according to the size of target object identified in the data set and the width to height ratio of real frame, which cannot only better detect the location of target, but also improve the detection speed and detection accuracy of network model. In order to obtain the specific aspect ratio of smoke in the experimental sample, 50 images are randomly selected from the sample data set, and then about 200 single fire images are manually intercepted, and the width and height of single smoke images are recorded at the same time.

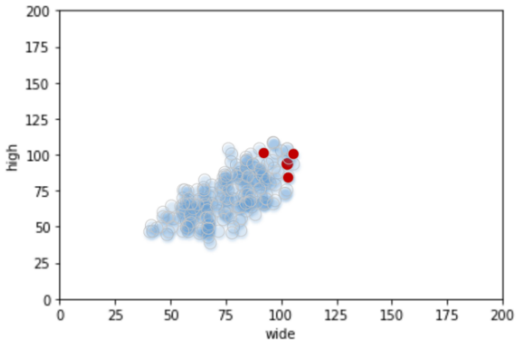

Fig. 5. Wide and high scatter diagram

It can be seen from figure 5 that the smoke scatter plot of width and height is relatively concentrated. It generally presents a linear distribution. This is because in the wild, smoke varies little in aspect ratio, so it is more concentrated. The aspect ratio of the Anchor of the initial lightweight SSD is set as 1/3, 1/2, 1, 2 and 3. By drawing these five straight lines in the aspect scatter plot, the setting of the aspect ratio of Anchor can be more intuitively understood. In figure 6, 1/3, 1/2, 1, 2 and 3 correspond to the red, black, pink, blue and green lines in the figure respectively.

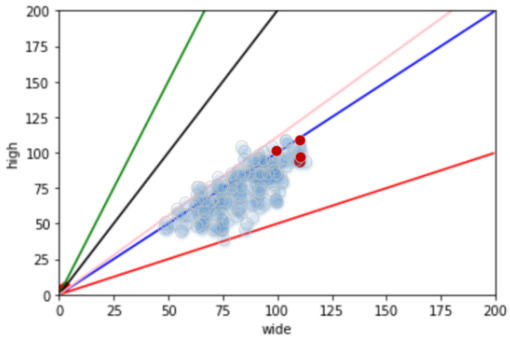

Fig. 6. Anchor setup for the original lightweight SSD

It can be seen that the original aspect/height ratio setting of Anchor is not reasonable, so this paper resets the aspect/height ratio parameters of Anchor. Firstly, the aspect ratio of all single smoke images obtained from the sample database is calculated, and then the new aspect ratio parameters are analyzed.

D. Training stage The Blending strategy in the training stage consists of two prediction parts: base learner and meta learner. Firstly, the data sets are divided (training set, validation set, test set) and input into each base learner in the first layer of the model. Each base learner will produce a prediction result in the validation set and the test set. Secondly, the historical load values corresponding to the prediction results, validation, set and samples in the test set of the first layer are recombined into a new sample set, which is used as the input of the meta-learner model in the second layer. Finally, the meta-learner fits the prediction results of the validation set, predicts the prediction results of the test set, and obtains the final prediction results. Blending models can make full use of the differences of prediction principles of different models, so as to achieve complementary advantages among them. The specific training method is:

- Step 1. For a data set $S = (y_n, x_n), n = 1, 2, \cdots, N$, where x_n is the feature vector of n-th sample. y_n is the load value corresponding to the $n - th$ sample. n is the number of features, that is, each feature vector is $[x_1, x_2, \cdots, x_n]$. Firstly, the data is divided into training set $S_1 = (y_v, x_v), v = 1, 2, \cdots, V$, and validation set $S_2 = (y_i, x_i), i = 1, 2, \cdots, I$. The size of the data set after partitioning is $S_1 < S_2 < S$. The test set to be predicted in this paper is $S_3 = (y_t, x_t), t = 1, 2, \cdots, T$. It selects K different models as the base learner, fits the K base learners on S_1, makes prediction on S_2 and S_3, and gets the predicted value of S_2 as A_{ik}. The predicted value on S_3 is B_{tk}. A_{ik} and B_{tk} are combined with target values corresponding to S_2 and S_3 respectively to constitute the new training set $D_1 = (A_{ik}, y_i), k = 1, 2, \cdots, K$, testing set $D_2 = (A_{tk}, y_t), k = 1, 2, \cdots, K$.
- Step 2. The newly generated data sets D1 and D2 are taken as the input data of the second layer, and the meta-learner model of the second layer is used to fit on D1 and predict on D2 to obtain the final prediction result.

XGBoost algorithm adds penalty term and second-order Taylor expansion on the basis of gradient lifting tree (GBDT). The objective f_k is obtained by reducing the loss function. The loss function is shown in Equation (21):

$$L^{(t)} = \sum_{i=1}^{n} l(y_i, \hat{y}_i) + \sum_{k=1}^{K} \Omega(f_k) \tag{21}$$

Where, the first part is the sum of training errors, where $\hat{y}_i$ is the predicted value. y_i is the target value, t is the iteration number. The second part is the sum of regularization coefficients, that is, the sum of tree depth T and leaf node weight w is:

$$\Omega(f) = \gamma T + 0.5\lambda ||w||^2 \tag{22}$$

Where, γ and λ represent the penalty coefficient of the model. Second order Taylor expansion is carried out for Equation (22):

$$\begin{aligned} L^{(t)} &\cong \sum_{i=1}^{n} (g_i f_t(x_i) + 0.5 h_i f_t^2(x_i)) + \Omega(f_t) \\ &\cong \sum_{i=1}^{n} (g_i f_t(x_i) + 0.5 h_i f_t^2(x_i)) + \gamma T + 0.5\lambda \sum_{j=1}^{T} w_j^2 \\ &\cong \sum_{j=1}^{T} [(\sum_{i \in I_j} g_i) w_j + 0.5 (\sum_{i \in I_j} h_i + \lambda)] + \gamma T \end{aligned} \tag{23}$$

Where $g_i = \partial_{\hat{y}_i^{(i-1)}} l(y_i, \hat{y}_i^{(t-1)})$, $h_i = \partial^2_{\hat{y}_i^{(i-1)}} l(y_i, \hat{y}_i^{(t-1)})$ are first and second derivatives of the loss function. Define $G_j = \sum_{i \in I_j} g_i$, $H_j = \sum_{i \in I_j} h_i$, so formula (23) can be written as:

$$L^{(t)} \cong \sum_{j=1}^{T} [G_j w_j + 0.5 (H_j + \lambda) w_j^2] + \gamma T \tag{24}$$

Taking the partial derivative with respect to w and substituting it into the objective function, we can obtain:

$$L^{(t)} \cong -0.5 \sum_{j=1}^{T} \frac{G_j^2}{H_j + \lambda} + \gamma T \tag{25}$$

In XGBoost model, the smaller loss function denotes the better model effect. Through the greedy algorithm, the model traverses all the different tree structures, splits nodes, and calculates the gain of each split node. The gain L_{Gain} is:

$$L_{Gain} \cong 0.5 (\frac{G_L^2}{H_L + \lambda} + \frac{G_R^2}{H_R + \lambda} - \frac{G_L + G_R}{H_L + H_R + \lambda}) - \gamma \tag{26}$$

Where, the first two terms are the gains after left and right segmentation, and the third term is the overall segmentation gain.
The training pseudocode based on Bagging-blending multiple models fusion method is shown in **Algorithm 1**.

Algorithm 1 Bagging-blending fusion method

Input: Image set $M = (x_n, y_n), n = 1, 2, \cdots, N$;
Output: Bagging-blending fusion model;

Step 1. The data is divided into L identical training sets $M_{1L} = (x_v, y_v), v = 1, 2, \cdots, V$ validation set $M_{2L} = (x_i, y_i), i = 1, 2, \cdots, I$, the testing set $M_{3L} = (x_t, y_t), i = t, \cdots, T$.
Step 2. L single models are trained and predicted.
for all $l = 1$ to L **do**
    The prediction error ∂_l is obtained by fitting M_{1L} prediction on M_{2L}.
end for
Step 3. Pearson correlation coefficient algorithm is used to analyze the correlation r_{xy} between model prediction error ∂_l, and L_1 single models with large differences are selected, where $L_1 \leq L$.
Step 4. Embed L_1 in the Bagging ensemble algorithm.
for all $l = 1$ to L_1 **do**
    Using l_1 as the base learner of Bagging ensemble model, the integrated model L_2 is obtained.
end for
Step 5. The grid search G is used to optimize L_2.
for all $l_2 = 1$ to L_2 **do**
    G_{l_2} is used to search for the optimal hyperparameter of the model.
end for
Step 6. The L_2 model with adjusted superparameters is trained as the base learner at layer 1.
for all $l = 1$ to L_2 **do**
    s is used to fit on the training set M_{ls}, and the prediction is made on the validation set M_{2s} and training set M_{3s} respectively, and the prediction result is P_{is} and Q_{ts}.
end for
Step 7. Constitute a new training set $M_{1new} = (P_{is}, y_i), s = 1, 2, \cdots, L_2$, testing set $M_{2new} = (Q_{ts}, y_t), s = 1, 2, \cdots, L_2$.
Step 8. The XGBoost model of Blending Layer 2 meta-learner is used to fit on the new training set and predict on the new test set.

4. Experiments and Analysis

The CPU used in the experiment is Intel Core I7-6700, main frequency 3.4GHz, 16G memory, NVIDIA graphics TX1060, video memory is 64GB under Windows10 operating system. The smoke detection network model is built and trained by TensorFlow.

4.1. Training and Testing Data Sets

The data set used in the experiment contains 15000 images with 128×128pixels containing positive and negative samples. Combined with the common moving object in-

terference items in the actual smoke scene, the negative samples are divided into four categories: people, cars, motorcycles and buses, with about 3000 images in each category. Smoke sample data are from the Bilkent, Visor and KLFS. Smoke area images are extracted from different videos. It can guarantee the diversity of smoke images to prevent over-fitting of training network. Part of positive smoke samples are shown in figure 7(a). Negative samples come from ImageNet data set and network search, and some negative samples are shown in figure 7(b).

Fig. 7. Data set. (a) Positive samples; (b) Negative samples

In this paper, 70% of the positive and negative samples are used as the training set and 30% as the test set. GPU is used to train and test the proposed network model in figure 8.

In this paper, different parameters are set for the model, and the optimal parameters are selected through cross-validation. The initial learning rate is 0.001. After several iterations, it is fine-tuned to 10^{-4}. The minimum normalized boundary is set to 0.0001, the redecay is 5×10^{-4}, and the image batch is 16. The detection rate of the model in this paper for 128×128 pixel images is 29f/s. The change curve of loss value in the training process is shown in figure 8. As the number of iterations increases, the loss value of IFFSD model decreases continuously. After 100 iterations, the decline tends to flatten and it is stable after 200 iterations.

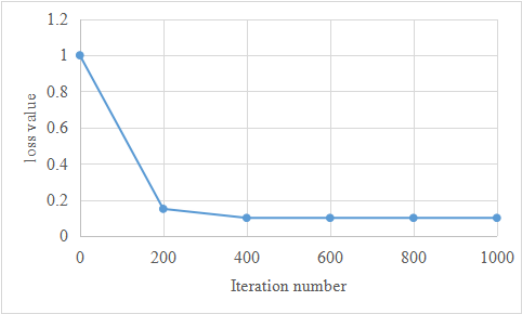

Fig. 8. Change of loss value during IFSSD training

4.2. Smoke Recognition Results

Based on the moving object extraction method and the image processing function of OpenCV, the contour of each moving area detected in the smoke scene is extracted by using the minimum rectangle box. Furthermore, the moving areas extracted from each rectangular frame label are uniformly converted into images with 128×128 fixed size. The smoke discrimination of each moving object is carried out by the network model after training and testing.

In this paper, IFFSD, SSD and MSSD models are used to detect smoke data sets respectively. Table 1 shows the average detection results, in which detected objects are regarded as positive samples and undetected objects as negative samples. The IoU (Intersection over Union) threshold is 0.5. Figure 9 shows the intuitive result. There are four test results, namely, IoU value is less than or equal to 0.5 (FP), IoU value is greater than 0.5 (TP), and without real object FN and TN. TN samples are not counted in this paper. The accuracy rate can be calculated by:

$$P = \frac{T_P}{T_P + F_P} \times 100\% \tag{27}$$

Where T_P is the detected positive sample. F_P is the detected negative sample.

Table 1. Detection results with different models

Model	Accuracy/%	Model size/MB	Detection time per image/s
SSD	5.4	28.1	36
MSSD	92.6	28.1	39
IFFSD	94.8	19.5	21

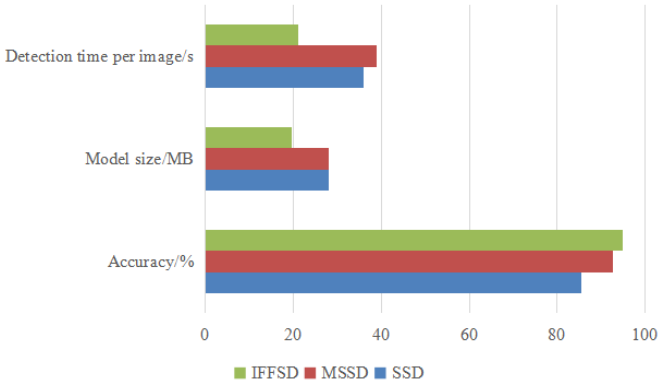

Fig. 9. Detection results with different models

In terms of detection accuracy, the accuracy of IFFSD model is 94.8%, which is 9.4% higher than SSD model and 2.2% higher than FSSD model. In terms of image detection rate, the detection time of IFFSD model is 21s, which is lower than 36s of SSD model and 39s of MSSD model.

As shown in table 2 and figure 10, the accuracy of IFFSD model is higher than that of Histogram of Oriented gradient (HOG)+Support Vector Machine (SVM) and Deformable Parts Model (DPM)+SVM [45], it is increased by 14.1% and 16.4% respectively. This is because the traditional object detection algorithm is only suitable for the image with obvious features and simple background. However, in practical application, the background is complex and changeable, and the object to be detected is complex and changeable, so it is difficult to complete the object detection through general abstract features. However, deep learning can extract rich features of the same object to complete object detection. However, IFFSD model is larger than HOG+SVM and DPM+SVM in model size, because IFFSD model has more parameters. In terms of efficiency, the IFFSD model is close to the traditional method.

Table 2. Comparison of IFSSD and other detection methods

Model	Accuracy/%	Model size/MB	Detection time per image/s
HOG+SVM	80.7	20.8	28
DPM+SVM	78.4	3.6	26
Faster RCNN	87.0	53.1	29
YOLOv2-DarkNet-19	85.4	24.6	20
IFFSD	94.8	20.8	28

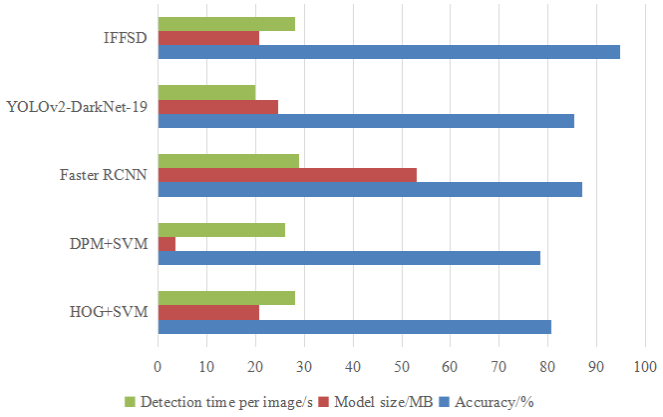

Fig. 10. Comparison of IFSSD and other detection methods

Compared with Faster RCNN and YOLOv2-Darknet19, the accuracy of IFFSD model is increased by 7.8% and 9.4% respectively due to the addition of FPN structure and

Inception backbone network. In terms of detection time, IFFSD model is close to Faster RCNN model.

For all input foreground images, the IFFSD model should be able to identify smoke and non-smoke moving objects. However, in practice, due to the limited training sample data, it is difficult for the negative sample to cover all non-smoke motion interference items, which makes some out-of-sample moving objects cause false positives to smoke detection. Figure 11 is the detection result.

Fig. 11. The detection result with proposed method.

In order to further verify the effectiveness of the urban smoke detection algorithm proposed in this paper, 120 videos of different scenes are obtained through self-shooting and Internet downloading, in which 72 images are smoke videos as shown in figure 12(a). There are 48 smoke-free videos as shown in figure 12(b).

Fig. 12. Video set. (a) Examples of smoke videos; (b) Examples of non-smoke videos

The response time from outbreak of fire to fire alarm signal should not exceed 20s. On this basis, in the video with smoke, if the smoke alarm is issued within 20s after the smoke breaking, the proposed method in this paper is considered to meet the requirements of smoke detection. If there is no smoke alarm in 20s, it is judged to be missed detection. In the smoke-free video, if the non-smoke area is identified as the smoke area, it will be judged as a false positive. Some experimental results are shown in table 3.

In the 72 videos with smoke, only No. 18 and No. 43 have the smoke alarm response more than 20s, with a missed alarm rate of 2.7%. In the 48 smoke-free videos, only the

Table 3. Model performance of smoke detection

Video sequence	Video type	Response time/s	Type of alarm
1	smoke	4.31	true
2	smoke	7.42	true
11	smoke	0.17	true
18	smoke	23.83	missed
43	smoke	25.60	missed
52	smoke	8.52	true
71	smoke	5.68	true
72	smoke	1.83	true
73	Non-smoke	–	–
74	Non-smoke	–	–
93	Non-smoke	–	false
119	Non-smoke	–	–
120	Non-smoke	–	–

No. 93 video has false positive, with a false rate of 2.0%. Overall, the smoke detection accuracy of 120 videos is 97.5%. In the smoke alarm video with smoke (except No.18 and 43), the longest response time is 8.52s of No. 52 video, and the shortest response time is 0.17s of No. 11 video. According to statistics, the average response time of smoke alarm is 4.58s, which is far lower than the specified 20s. The above experimental results show that under the current experimental conditions, the urban video smoke detection algorithm proposed in this paper can meet the real-time and accuracy requirements of most actual smoke detection.

The main factors affecting the accuracy of smoke detection include: 1) the number of positive samples used for SSD model training is limited, and smoke items not covered by positive samples may cause missing reports; 2) The negative sample data is limited, such as water fog with similar color and movement of smoke, white automobile exhaust and other interference items not covered by the negative sample, will cause certain false positives. By increasing the diversity of positive and negative samples, the accuracy of video smoke detection can be further improved.

5. Conclusions

An urban smoke detection method based on MGMM and improved SSD is proposed. This method does not need to judge and recognize all the objects in the video, but only input the moving objects in the foreground image into the IFFSD model for smoke recognition after filtering the static objects in the video image by the improved Gaussian mixture model. This method can not only reduce the interference of static objects, but also improve the efficiency of smoke detection. Experimental results show that this method is feasible and effective in many complex environments. The early fire smoke is mostly gray due to low temperature, so the positive samples selected in this paper are mainly gray smoke, aiming to solve the problems of real-time and accuracy of video smoke detection in complex scenes. In order to make the smoke detection method more general, the diversity of positive and negative samples can be increased in the subsequent work to meet the smoke

detection requirements with more scenes and further improve the accuracy of smoke detection. In the future, more advanced deep learning method will be adopted to improve the detection rate.

Acknowledgments. The author greatly appreciates the expert review comments.

References

1. Lh, A., Xg, A., Sz, A., et al.: "Efficient attention based deep fusion CNN for smoke detection in fog environment-ScienceDirect," *Neurocomputing*, 434, 224-238. (2021)
2. Saponara, S., Elhanashi, A., Gagliardi, A.: "Real-time video fire/smoke detection based on CNN in antifire surveillance systems," *Journal of Real-Time Image Processing*, 18, 889-900. (2021)
3. Liu, H., Lei, F., Tong, C., et al.: "Visual smoke detection based on ensemble deep cnns," *Displays*, 69, 102020. (2021)
4. Millan-Garcia, L., Sanchez-Perez, G., Nakano, M., et al.: "An early fire detection algorithm using IP cameras," *Sensors*, Vol. 12, No. 5, 5670-5686. (2012)
5. Favorskaya, M., Pyataeva, A., Popov, A.: "Verification of Smoke Detection in Video Sequences Based on Spatio-temporal Local Binary Patterns," *Procedia Computer Science*, Vol. 60, No. 1, 671-680. (2015)
6. Zhou, Z., Shi, Y., Gao, Z., et al.: "Wildfire smoke detection based on local extremal region segmentation and surveillance," *Fire Safety Journal*, 85, 50-58. (2016)
7. Dimitropoulos, K., Barmpoutis, P., Grammalidis, N.: "Higher order linear dynamical systems for smoke detection in video surveillance applications," *IEEE Transactions on Circuits and Systems for Video Technology*, Vol. 27, No. 5, 1143-1154. (2016)
8. Jia, Y., Chen, W., Yang, M., et al.: "Video Smoke Detection with Domain Knowledge and Transfer Learning from Deep Convolutional Neural Networks," *Optik-International Journal for Light and Electron Optics*, Vol. 240, No. 8, 166947. (2021)
9. Vijayalakshmi, S., Muruganand, S.: "Smoke detection in video images using background subtraction method for early fire alarm system," *2017 2nd International Conference on Communication and Electronics Systems (ICCES). IEEE*, 167-171. (2017)
10. Cruz, H., Eckert, M., Meneses, J., et al.: "Efficient Forest Fire Detection Index for Application in Unmanned Aerial Systems (UASs)," *Sensors*, Vol. 16, No. 6, 893. (2016)
11. Ye, S., Bai, Z., Chen, H., et al.: "An effective algorithm to detect both smoke and flame using color and wavelet analysis," *Pattern Recognition and Image Analysis*, Vol. 27, No. 1, 131-138. (2017)
12. Shi, J., Wang, W., Gao, Y., et al.: "Optimal placement and intelligent smoke detection algorithm for wildfire-monitoring cameras," *IEEE Access*, Vol. 8, 72326-72339. (2020)
13. Kim, J., Bae, S.: "Smoke Detection Method Using Local Binary Pattern Variance in RGB Contrast Imag," *Journal of Korea Multimedia Society*, Vol. 18, No. 10, 1197-1204. (2015)
14. Prema, C., Vinsley, S., Suresh, S.: "Multi Feature Analysis of Smoke in YUV Color Space for Early Forest Fire Detection," *Fire Technology*, Vol. 52, No. 5, 1319-1342. (2016)
15. Zhao, Y., Li, Q., Gu, Z.: "Early smoke detection of forest fire video using CS Adaboost algorithm," *Optik -International Journal for Light and Electron Optics*, Vol. 126, No. 19, 2121-2124. (2015)
16. Yuan, F., Fang, Z., Wu, S., et al.: "Real-time image smoke detection using staircase searching-based dual threshold AdaBoost and dynamic analysis," *IET Image Processing*, Vol. 9, No. 10, 849-856. (2015)
17. Maguire, G., Chen, H., Schnall, R., et al.: "Smoking cessation system for preemptive smoking detection," *IEEE Internet of Things Journal*, Vol. 9, No. 5, 3204-3214. (2021)

18. Yuan, Y., Xu, Z., Lu, G.: "SPEDCCNN: Spatial Pyramid-Oriented Encoder-Decoder Cascade Convolution Neural Network for Crop Disease Leaf Segmentation," *IEEE Access*, vol. 9, 14849-14866. (2021) doi: 10.1109/ACCESS.2021.3052769. (2021)
19. Ye, W., Zhao, J., Zhao, Y., et al.: "Smoke detection based on Surfacelet transform and dynamic texture," *Comput. Eng.*, Vol. 41, No. 2, 203-208. (2015)
20. Almeida, J., Huang, C., Nogueira, F., et al.: "EdgeFireSmoke: A Novel Lightweight CNN Model for Real-Time Video FireCSmoke Detection," *IEEE Transactions on Industrial Informatics*, Vol. 18, No. 11, 7889-7898. (2022)
21. Yang, M., Tjuawinata, I., Lam, K.: "K-Means Clustering With Local d_X-Privacy for Privacy-Preserving Data Analysis," *IEEE Transactions on Information Forensics and Security*, vol. 17, 2524-2537. (2022) doi: 10.1109/TIFS.2022.3189532. (2022)
22. Xu, G., Zhang, Y., Zhang, Q., et al.: "Deep Domain Adaptation Based Video Smoke Detection using Synthetic Smoke Images," *Fire Safety Journal*, Vol. 93, 53-59. (2017)
23. Jang, H., Lee, J.: "Machine learning versus econometric jump models in predictability and domain adaptability of index options," *Physica A: Statistical Mechanics and its Applications*, Vol. 513, 74-86. (2019)
24. Wang, S., Guo, Q., Xu, S., et al.: "A moving target detection and localization strategy based on optical flow and pin-hole imaging methods using monocular vision," *2021 IEEE International Conference on Real-time Computing and Robotics (RCAR). IEEE*, 147-152. (2021)
25. Esfahlani, S.: "Mixed reality and remote sensing application of unmanned aerial vehicle in fire and smoke detection," *Journal of Industrial Information Integration*, Vol. 15, 42-49. (2019)
26. Liu, B., Sun, B., Cheng, P., et al.: "An embedded portable lightweight platform for real-time early smoke detection," *Sensors*, Vol. 22, No. 12, 4655. (2022)
27. Kaabi, R., Bouchouicha, M., Mouelhi, A., et al.: "An efficient smoke detection algorithm based on deep belief network classifier using energy and intensity features," *Electronics*, Vol. 9, No. 9, 1390. (2020)
28. Tao, H., Zheng, P., Xie, C., et al.: "A three-stage framework for smoky vehicle detection in traffic surveillance videos," *Information Sciences*, Vol. 522, 17-34. (2020)
29. Martins, L., Guede-Fernndez, F., Valente de Almeida R, et al.: "Real-Time Integration of Segmentation Techniques for Reduction of False Positive Rates in Fire Plume Detection Systems during Forest Fires," *Remote Sensing*, Vol. 14, No. 11, 2701. (2022)
30. Dong, Y., Wu, H., Li, X., et al.: "Multiscale symmetric dense micro-block difference for texture classification," *IEEE Transactions on Circuits and Systems for Video Technology*, Vol. 29, No. 12, 3583-3594. (2018)
31. Krizhevsky, A., Sutskever, I., Hinton, G.: "ImageNet Classification with Deep Convolutional Neural Networks," *Advances in neural information processing systems*, Vol. 25, No. 2. (2012)
32. Yang, J., He, W., Zhang, T., et al.: "Research on Subway Pedestrian Detection Algorithms Based on SSD Model," *IET Intelligent Transport Systems*, Vol. 14, 7553. (2020)
33. Yin, S., Zhang, Y., Karim, S.: "Large scale remote sensing image segmentation based on fuzzy region competition and Gaussian mixture model," *IEEE Access*, Vol. 6, 26069-26080. (20181)
34. Zhang, X., Hill, D.: "Load stability index for short-term voltage stability assessment," *2019 IEEE Power & Energy Society General Meeting (PESGM). IEEE*, 1-5. (2019)
35. Zhang, D., Shafiq, M., Wang, L., et al.: "Privacy-preserving remote sensing images recognition based on limited visual cryptography," *CAAI Transactions on Intelligence Technology*, (2023). https://doi.org/10.1049/cit2.12164
36. Yin, S., Wang, L., Shafiq, M., Teng, L., Laghari, A., Khan, F.: "G2Grad-CAMRL: An Object Detection and Interpretation Model Based on Gradient-Weighted Class Activation Mapping and Reinforcement Learning in Remote Sensing Images," *IEEE Journal of Selected Topics in Applied Earth Observations and Remote Sensing*, vol. 16, 3583-3598. (2023) doi: 10.1109/JSTARS.2023.3241405

37. Suzuki, S., Shouno, H.: "A study on visual interpretation of network in network," *2017 International Joint Conference on Neural Networks (IJCNN)*, 903-910. (2017) doi: 10.1109/IJCNN.2017.7965948.
38. Zhao, Y., Xie, K., Zou, Z., He, J.: "Intelligent Recognition of Fatigue and Sleepiness Based on InceptionV3-LSTM via Multi-Feature Fusion," *IEEE Access*, vol. 8, 144205-144217. (2020)
39. Yin, S., Li, H.: "Hot Region Selection Based on Selective Search and Modified Fuzzy C-Means in Remote Sensing Images," *IEEE Journal of Selected Topics in Applied Earth Observations and Remote Sensing*, vol. 13, 5862-5871. (2020) doi: 10.1109/JSTARS.2020.3025582.
40. Xu, C., Hong, X., Yao, Y., et al.: "Multi-Scale Region-based Fully Convolutional Networks," *Neurocomputing*, 500-505. (2020)
41. V. E.K. and C. Ramachandran.: "Real-time Gender Identification from Face Images using you only look once (yolo)," *2020 4th International Conference on Trends in Electronics and Informatics (ICOEI)(48184)*, 1074-1077. (2020)
42. Zhu, M., et al.: "Arbitrary-Oriented Ship Detection Based on RetinaNet for Remote Sensing Images," *IEEE Journal of Selected Topics in Applied Earth Observations and Remote Sensing*, vol. 14, 6694-6706. (2021) doi: 10.1109/JSTARS.2021.3082526.
43. Tan, Y., Wu, P., Zhou, G., et al.: "Combining Residual Neural Networks and Feature Pyramid Networks to Estimate Poverty Using Multisource Remote Sensing Data," *IEEE Journal of Selected Topics in Applied Earth Observations and Remote Sensing*, Vol. 13, No. 99, 553-565. (2020)
44. Tao, H., Lu, X.: "Smoke Vehicle Detection Based on Spatiotemporal Bag-Of-Features and Professional Convolutional Neural Network," *IEEE Transactions on Circuits and Systems for Video Technology*, vol. 30, no. 10, 3301-3316. (2020) doi: 10.1109/TCSVT.2019.2920657.
45. Hebbalaguppe, R., Garg, G., Hassan, E., Ghosh, H., Verma, A.: "Telecom Inventory Management via Object Recognition and Localisation on Google Street View Images," *2017 IEEE Winter Conference on Applications of Computer Vision (WACV)*, 725-733. (2017) doi: 10.1109/WACV.2017.86.

Hao Han is with the Guizhou Fire and Rescue Brigade and Department of Natural Resources of Guizhou Province. He has published several papers and won several awards. His research direction: Image processing, big data analysis.

Received: December 18, 2022; Accepted: May 20, 2023.

Computer Science and Information Systems 20(4):1845–1868 https://doi.org/10.2298/CSIS221222033H

A^{2}FWPO: Anti-aliasing Filter Based on Whale Parameter Optimization Method for Feature Extraction and Recognition of Dance Motor Imagery EEG

Tianliang Huang[1,⋆], Ziyue Luo[1], and Yin Lyu[2]

[1] School of Art, Hunan University of Information Technology
Maotang Industrial Park, Changsha Economic and Technological Development Zone (410151) China
tlhuang2023@163.com
luoziyue77@163.com
[2] College of Music, Huaiyin Normal University
Huai'an, China
8201711037@hytc.edu.cn

Abstract. The classification accuracy of EEG signals based on traditional machine learning methods is low. Therefore, this paper proposes a new model for the feature extraction and recognition of dance motor imagery EEG, which makes full use of the advantage of anti-aliasing filter based on whale parameter optimization method. The anti-aliasing filter is used for preprocessing, and the filtered signal is extracted by two-dimensional empirical wavelet transform. The extracted feature is input to the robust support matrix machine to complete pattern recognition. In pattern recognition process, an improved whale algorithm is used to dynamically adjust the optimal parameters of individual subjects. Experiments are carried out on two public data sets to verify that anti-aliasing filter-based preprocessing can improve signal feature discrimination. The improved whale algorithm can find the optimal parameters of robust support matrix machine classification for individuals. This presented method can improve the recognition rate of dance motion image. Compared with other advanced methods, the proposed method requires less samples and computing resources, and it is suitable for the practical application of brain-computer interface.

Keywords: EEG signals classification, Dance motor imagery, Anti-aliasing filter, Whale parameter optimization, Two-dimensional empirical wavelet transform, Robust support matrix machine.

1. Introduction

Brain Computer Interface (BCI) technology aims to bypass the pathway between the brain and muscles by creating a signal transmission interface between the human brain and the machine [1]. It allows the user to control the external device directly through the brain, instead of using the traditional method of muscle movement. Therefore, BCI technology has a broad application prospect in patients with paralysis and confinement, as well as in extreme environments such as space. BCI technology involves signal processing, machine

⋆ Corresponding author

learning, cognitive neuroscience and other disciplines [2].

In so many BCI technologies, Electroencephalogram (EEG) is collected in the cerebral cortex in a non-invasive way, thus becoming a brain-computer interface technology suitable for ordinary people to participate in without ethical constraints and invasive brain operation [3]. In EEG based brain-computer interface technology, event-related potential, steady-state visual potential and sensory motor rhythm are the three main application methods. Here, the perceptual Motor rhythm is induced by Motor Imagery BCI (MI-BCI) [4]. MI-BCI mainly changes the energy of specific rhythm of EEG on the opposite side of the brain, and these energy changes are recorded by EEG, known as Event Related desynchronization phenomenon (ERD) [5]. Sensorimotor rhythm in the brain is widely distributed and controlled by different brain regions. However, due to the topological organization of motor neurons, EEG signals collected by the cerebral cortex are usually aliases of multiple motor sensing neurons, resulting in poor spatial resolution of the original EEG signal and affecting the pattern recognition results of the motor imagination EEG signal.

In order to improve the spatial resolution of ERD phenomenon in EEG, ensure pattern recognition accuracy of MI-BCI, commonly used feature extraction methods include spectral analysis, auto-regression, source reconstruction and Common Spatial Pattern (CSP) [6]. CSP brings spatial resolution advantage to ERD phenomenon, so it is widely used in the recognition of perceptual motor rhythm. Although CSP can distinguish signal maximization differences according to different tasks, the distinguishable characteristics often depend on the selection of frequency bands. Therefore, the frequency bands are divided into several sub-band Filter Bank CSPS (FB-CSP) to improve the recognition performance [7].

Researchers have successively proposed a large number of improved algorithms for CSP, including the CSP-based spatio-temporal filtering, the co-sparse spectral space mode, the regularization CSP and the regularization CSP-based probability model. All these methods achieve better results on the basis of traditional CSP characteristics. It is difficult to select the optimal frequency band because of the great difference of perception-motor rhythm of different objects. Zhang et al. [8] introduced sparse Bayesian learning method on the basis of CSP, and the selected frequency band could improve the classification performance. A large number of relevant studies have shown that CSP relies more on the frequency band range of energy changes generated by motion imagination in the process of feature extraction, so it is necessary to further study the frequency band range of CSP filtering to ensure better distinguishable features extracted by CSP.

After feature extraction, pattern recognition is usually accomplished by classifier. In early pattern recognition, mainstream shallow classifiers such as linear discriminant analysis or support vector machine were directly adopted [9]. In recent years, the wide application of deep learning in small sample classification has led to more applications of deep learning in pattern recognition of motor imagination EEG signals. Gao et al. [10] adopted deep self-coding network to reduce the dimensionality of time series of high-dimensional EEG signals, achieving better recognition effect. After introducing the Convolutional Neural Network (CNN) structure, Ahmed et al. [11] still carried out convolutional operations in the time domain and the space, respectively, to form the combined features and complete the classification. Apicella et al. [12] regarded the time domain of signals as different time segments, carried out convolution respectively, simulated FB-CSP by

neural network model, and obtained the current optimal effect on the brain-computer interface competition data set. On this basis, the further CNN classification structure and 3 Dimension CNN (3DCNN) classification structure have both achieved performance improvement on motion imagination data sets. Recurrent Neural Network (RNN) has also made initial progress [13]. Researchers regard FB-CSP features as time series and use RNN to identify feature sequences to achieve better results on different data sets.

Although the deep learning architecture represented by CNN can directly complete the recognition of motor imagination on the EEG signal, without the traditional feature extraction process. However, the training process of deep learning requires the support of a large number of samples and computing resources, so it is not applicable to the field of BCI where it is difficult to obtain a large number of EEG samples. In addition, the application of BCI usually requires real-time and free environment, which cannot match the fixed environment of a large number of computing resources [14]. Therefore, scholars began to use machine learning to process the whole multi-dimensional EEG matrix, and Support Matrix Machine (SMM) [15] and Robust SMM (RSMM) [16] are successful in recognizing small samples of EEG. This kind of algorithm adopts the idea of Support Vector Machine (SVM) to directly process the multidimensional EEG matrix, and regards the EEG as the superposition of real EEG and noise signals. In the process of iterative optimization, the original EEG signals are corrected through the separated noise signals, so as to improve the classification accuracy of EEG signals.

However, the parameters of RSMM classifier have a great influence on the pattern recognition results, and the parameters of different subjects are different. Thus, the anti-aliasing filter based on whale parameter optimization (A^{2}FWPO) method has been proposed in this paper for feature extraction and recognition of dance motor imagery EEG. In this method, anti-aliasing filter is used to obtain the deep-band features, and the filtered signals are extracted by two-dimensional empirical wavelet transform. RSMM completes the feature recognition. In the process of recognition, the improved whale algorithm is used to find the optimal RSMM parameters for different subjects, so that the EEG classification accuracy of each subject can be achieved.

The organizational structure of this article is as follows. Section 2 gives related works for this paper. In section 3, we detailed show the proposed method. Experiments and analysis are given in section 4. There is a conclusion in section 5.

2. Related Works

Brain-computer interface is a new type of information transmission channel between the brain and external electronic devices, which does not rely on muscle tissue and peripheral nerves. EEG has become one of the most effective data sources for decoding the cognitive activity of the brain due to its high temporal resolution, good portability and non-invasive nature. EEG motor imagination brain-computer interface belongs to the category of spontaneous brain-computer interface, whose purpose is to accurately identify the user's intention of body movement, which commonly includes the imagination of left hand, right hand, feet and tongue movement [17], it is of great significance for medical rehabilitation, leisure and entertainment and other fields.

The traditional research methods of motor imaging EEG recognition task first need to preprocess EEG signals, then select appropriate methods to extract EEG features under

different cognitive states and select the most recognizable feature subset, and finally complete the recognition of motor imaging EEG signals through machine learning method. Through in-depth analysis of the manifestations and mechanisms of EEG features, we can see that the control of limb movement is controlled by the cross movement consciousness of contralateral brain region during the process of right-right movement imagination, which makes EEG present typical neurophysiological features. The mu rhythm and beta band amplitude of the corresponding EEG region on the opposite side decrease (event-related desynchronization (ERD), while the mu rhythm and beta band amplitude of the corresponding EEG region on the same side increase (event-related synchronization (ERS)). Therefore, the presence of motor awareness on the left or right side of the body can be judged based on the above ERD and ERS phenomena. However, there is no significant difference in ERD/ERS phenomenon and no clear distribution of corresponding EEG band in the motion imaging EEG of the body under different motion modes (especially unilateral body motion only), and it has nonlinear and non-stationary transient characteristics. Therefore, EEG feature extraction and unilateral motion intention recognition are relatively difficult to achieve under different motion modes. At present, there are few researches in this field at home and abroad.

Based on linear discriminant analysis of EEG, Xiao et al. [18] realized the intention recognition of hand stretching in patients with stroke paralysis. Wang et al. [19] identified the grasping movement imagination of stroke patients based on power spectrum analysis and brain topographic map information. The above methods are based on traditional analysis methods to achieve motion intention recognition under a single hand movement. In order to further accurately depict and effectively classify EEG motion image features under different motion modes, further research is needed to quantitatively describe EEG transient nonlinear features. Lin et al. [20] obtained an average recognition accuracy of 92.8% on the BCI Competition III IVa dataset by using the high-order statistical features extracted from the wavelet packet decomposition sub-band and multi-scale principal component analysis (MSPCA) denoising method. Baig et al. firstly used the Common Spatial Pattern (CSP) algorithm to extract the feature sets under the left- and right-handed motion imagination state, and then used the differential evolution optimization algorithm to extract the optimal feature subsets of each subject. Finally, it was sent into the Support Vector Machine (SVM) to build the classification model. The average classification accuracy of BCICompetition III dataset IVa was more than 95%. Faced with complex and unstructured data, traditional machine learning and statistical methods often require a certain feature engineering ability to extract more effective features or select more appropriate model parameters, while deep learning can train more abstract and effective features to complete end-to-end learning tasks.

Lopes et al. [21] used Short-Time Fourier Transform (STFT) to extract the time-frequency information of and rhythm in each channel, and combined them into 2D information as the input of the network. The Network was a deep network formed by the combination of Convolutional Neural Network (CNN) and Stacked Auto-Encoder (SAE), and classified the features extracted by CNN through SAE. The Kappa value of the proposed method on the dataset BCI Competition V dataset 2b was 0.547. Ma et al. [22] proposed a novel convolutional neural network for pattern recognition of motion imagery EEG. In this network, two convolution layers were set to extract the spatial and temporal features of signal sequences respectively.

3. Proposed Method

3.1. Feature Extraction Strategy

Task recognition of dance motor imagery EEG consists of two parts: signal feature extraction and pattern recognition. In this paper, anti-aliasing filter is used to extract the frequency-domain features of EEG signals, and two-dimensional empirical wavelet transform is used to extract the spatial features, which are composed of frequency-spatial features for pattern recognition of dance motion imagery tasks. In pattern recognition, the matrix form of EEG frequency domain-spatial characteristics is retained, and RSMM is used to complete the classification of motion imagination tasks. Due to the great difference of EEG in different individuals, the parameters used by RSMM in actual classification are different. Therefore, whale algorithm is adopted to automatically find the optimal classification parameters according to the characteristics of different individual signals, so as to achieve the highest recognition rate of the motion imagination EEG patterns of each individual.

The main principle of motion image pattern recognition is the event-related desynchronization phenomenon (ERD) in the process of imagination, which is reflected as the energy suppression of μ rhythm (8-12Hz) and β rhythm (18-24Hz) of EEG signal. In order to recognize the pattern of energy suppression, EEG pretreatment is needed. Common EEG acquisition devices generally collect signals between 0.1 and 100 Hz, but the signals generated by the discharge of neurons in the cerebral cortex are concentrated between 4 and 40 Hz. Therefore, the primary task of pre-processing is to keep the EEG frequency band between 4 and 40 Hz through band-pass filter. However, the detailed energy suppression caused by ERD cannot be obtained in a wide band, so the pattern recognition results are not ideal [23].

If no aliasing occurs in the sampled signal, down-conversion is performed to convert the sampled signal into base-band signal, and each signal in the multi-band communication signal is separated one by one. If two signals in the same frequency domain are aliased after sampling, the following analysis is carried out.

The two signals with aliasing after sampling are defined as $R_0(f)$ and $R_1(f)$. The delay difference between the first and second sample streams is T. The spectrum of the two signals after the first sampling flow is $R_A(f)$, and the spectrum after the second sampling flow is $R_B(f)$. $R_A(f)$ and $R_B(f)$ satisfy the relationship:

$$\begin{cases} R_A(f) = R_{0A}(f) + R_{1A}(f) \\ R_B(f) = R_{0B}(f) + R_{1B}(f) \\ R_B(f) = R_{0A}(f)e^a + R_{1A}(f)e^b \end{cases} \tag{1}$$

Assuming that the communication number of the RF band to be sampled is $R(f)$ and its bandwidth is B. The sampling frequency f_s is adopted, which is $f_s = 2B$. Where $a = e^{-j2\pi\Delta T f_s n_0}$, $b = e^{-j2\pi\Delta T}$. $((n+1)/2)f_s < |f| < ((n+1)/2)f_s$.

The two digital signals obtained by the second order sampling module are aliased by an anti-aliasing filter. Anti-aliasing filters $S_A(f)$ and $S_B(f)$ are designed and applied to channel A and channel B respectively. The recovered signal spectrum then becomes:

$$R(f) = B \times [S_A(f) \cdot R_A(f) + S_B(f) \cdot R_B(f)] \tag{2}$$

By splitting the normal spectrum and secondary spectrum of the signal, Equation (2) takes the transformation as:

$$R(f) = B \times [S_A(f) \cdot (R_{A+}(f) + R_{A-}(f)) + S_B(f) \cdot (R_{B+}(f) + R_{B-}(f))] \quad (3)$$

For each channel, there are signals from frequency positions a and b, so Formula (2) is further decomposed as:

$$\begin{aligned} R(f) =& B \times [S_A(f) \cdot (R_{0A+}(f) + R_{1A+}(f) + (R_{0A-}(R_{1A+}(f)) \\ &+ S_B(f) \cdot (R_{0B+}(f) + R_{1B+}(f) + R_{0B-}(f) + R_{1B-}(f)] \end{aligned} \quad (4)$$

Filters $S_A(f)$ and $S_B^0(f)$ are designed to restore $R_0(f)$ and eliminate $R_1(f)$. Therefore, the filters $S_A(f)$ and $S_B^0(f)$ should satisfy the follows:

$$B \times [S_A(f) \cdot R_{0A+}(f) + S_B^0(f) \cdot R_{0B+}(f)] = C \cdot R_{0A+}(f - 2aB) \quad (5)$$

$$B \times [S_A(f) \cdot R_{0A-}(f) + S_B^0(f) \cdot R_{0B-}(f)] = C \cdot R_{0A-}(f - 2aB) \quad (6)$$

$$B \times [S_A(f) \cdot R_{1A+}(f) + S_B^0(f) \cdot R_{1B+}(f)] = 0 \quad (7)$$

$$B \times [S_A(f) \cdot R_{1A-}(f) + S_B^0(f) \cdot R_{1B-}(f)] = 0 \quad (8)$$

Where C is the amplitude gain of the signal. Here, $S_A(f)$ is chosen as the simplest form, i.e.,

$$S_A(f) = \begin{cases} 1/B & |f| < B \\ 0 & otherwise \end{cases} \quad (9)$$

Therefore, by solving equations (7) and (8), $S_B^0(f)$ can be obtained as follows.

$$S_B^0(f) = \begin{cases} -\dfrac{\beta^{-b}}{B} & -B < f < 0 \\ -\dfrac{\beta^{b}}{B} & 0 < f < B \\ 0 & otherwise \end{cases} \quad (10)$$

Equations (8)-(10) are expressions of filters in the frequency domain. Their impulse response can be obtained through equations (8)-(10), and the filter impulse response can be written as:

$$S_A(t) = \int_{f_t}^{f_h} S_A(f) e^{j2\pi ft} dt \tag{11}$$

$$S_B^0(t) = \int_{f_t}^{f_h} S_B^0(f) e^{j2\pi ft} dt \tag{12}$$

$$S_B^1(t) = \int_{f_t}^{f_h} S_B^1(f) e^{j2\pi ft} dt \tag{13}$$

f_t and f_h are the lowest and highest frequencies of the anti-aliasing filter, respectively. By sampling the sampled signal with $f_s = 2B$, the sampled value can be used as the parameter of anti-aliasing filter. When the signal position index changes, the same S_A can still be used. However, for S_B, when the position index changes, the filter parameters need to be adjusted according to the position index.

Due to the anti-aliasing filter, the restored signal has a certain amplitude difference from the original signal. By substituting equations (8) and (9) into equation (6), the expression of amplitude gain can be obtained, as shown in Equation (14).

$$|C| = |1 - \beta^{\pm(b-a)}| = \sqrt{2 \cdot 1 - cos[2\pi T_\Delta f_s |b-a|]} \tag{14}$$

As can be seen from Equation (14), better gain effect can be obtained by adjusting T_Δ value in real time according to the position of a and b.

3.2. Constraint Condition

The sampling frequency of the second-order band-pass sampling module should follow the following formula.

$$\begin{cases} n_k \cdot f_s - f_s/2 < f_{lk} < f_{uk} < n_k \cdot f_s + f_s/2 \\ |f_{Ncb} - f_{Nca}| \geq \dfrac{B_a + B_b}{2} \end{cases} \tag{15}$$

In $n_k \cdot f_s - f_s/2 < f_{lk} < f_{uk} < n_k \cdot f_s + f_s/2$, n_k is the position index of the $k-th$ signal in the multi-band RF band communication signal. f_s is the sampling frequency. f_{lk} and f_{uk} are the lowest and highest frequencies with communication number k, respectively. This formula limits aliasing of sampled signal images. At the same time, the multi-band communication number should also satisfy $|f_{Ncb} - f_{Nca}| \geq \frac{B_a+B_b}{2}$. This formula can be used to avoid overlapping of more than two signals after sampling. B_a and B_b are the processing bandwidths of the two sampled RF bands. f_{Ncb} and f_{Nca} are the signal center frequencies of the sampled two-way tape signal in the first Nyquist region.

In fact, due to the nonlinear and non-stationary characteristics of EEG signals, the feedback of different subjects and the same subjects to motor imagination in different

stages of motor imagination has a floating range in different sub-bands [24]. Some subjects may have rhythms in the 6-11Hz range, while others may have rhythms in the 20-28Hz range. The floating range of rhythm and rhythm in the sub-band cannot be dealt with by simply dividing multiple sub-bands with the range of 4Hz. This paper proposes that anti-aliasing filter can be divided into different sub-bands according to different overlapping range combinations.

3.3. Two-Dimensional Empirical Wavelet Transform

Two-dimensional empirical wavelet transform is an improvement on the classical two-dimensional Littlewood Paley wavelet transform. Its filter bank has a ring support in Fourier domain, and the inner and outer radii of the support are fixed on the binary decomposition plane of Fourier domain, namely the scale factor [25]. Here, empirical analysis method is applied to detect each ring supported by the ring. The detection is carried out in Fourier's pseudo-polar plane, so the boundary can be represented by the frequency modulus $|\omega|$. In order to solve the construction problem of Fourier transform of pseudo-poles, references [26,27] put forward some methods, and provided an operator $F_p(f)(\theta, |\omega|)$ to construct it. In the Fourier support, the one-dimensional Fourier spectrum exists in each Angle θ. However, under tensor transformation, if Fourier boundary detection is performed separately for each Angle θ, there will be some discontinuities in the output spectrum. In order to avoid this influence, two-dimensional empirical wavelet transform adopts the idea of tensor transformation to calculate the average spectrum, namely,

$$\tilde{F}(|\omega|) = \frac{1}{N_\theta} \sum_{i=0}^{N_\theta - 1} F_p(f)(\theta_i, |\omega|) \tag{16}$$

Where, N_θ is the number of discrete angles. Then, the spectrum $\tilde{F}(|\omega|)$ is boundary detected, and the set ω^n. This set is used to construct a set of two-dimensional experiential Littlewood Paley wavelets.

$$B^{ELP} = \varphi_1(X), \phi_n(X)_{n=1}^{N-1} \tag{17}$$

Where, $\phi_n(X)$ is the empirical wavelet function. $\varphi_1(X)$ is the empirical scale function. B^{ELP} is established for a set of two-dimensional empirical wavelets. This definition is a direct extension of one-dimensional empirical wavelet. Since the extension of the ring over $\omega^{N-1} \leq |\omega| \leq \omega^N$ is to preserve the "Angle" of the Fourier domain, it is defined as shown in equations (18)-(20), except for the last ring.

$$F_2(\varphi_1)(\omega) = \begin{cases} 1 \quad |\omega| \leq (1-\gamma)\omega^1 \cdot A \\ if(1-\gamma)\omega^1 \leq \omega \leq (1+\gamma)\omega^1 \\ 0 \quad otherwise \end{cases} \tag{18}$$

If $n \neq N-1$, then

$$F_2(\varphi_n)(\omega) = \begin{cases} 1 \quad if(1-\gamma)\omega^n \le \omega \le (1+\gamma)\omega^{n+1} \cdot A \\ if(1-\gamma)\omega^{n+1} \le \omega \le (1+\gamma)\omega^{n+1} \cdot B \\ if(1-\gamma)\omega^n \le \omega \le (1+\gamma)\omega^n \\ 0 \quad otherwise \end{cases} \tag{19}$$

$$F_2(\varphi_{n-1})(\omega) = \begin{cases} 1 \quad if(1+\gamma)\omega^{N-1} \le |\omega| \cdot B \\ if(1-\gamma)\omega^{N-1} \le \omega \le (1+\gamma)\omega^{N-1} \\ 0 \quad otherwise \end{cases} \tag{20}$$

Here, $A = cos[\frac{\pi}{2}\beta(\frac{1}{2\gamma\omega^1}(|\omega| - (1-\gamma)\omega^1))]$ and $B = sin[\frac{\pi}{2}\beta(\frac{1}{2\gamma\omega^n}(|\omega| - (1-\gamma)\omega^n))]$. The detail coefficient of the two-dimensional empirical wavelet transform of signal f is defined as:

$$W_f^{ELP}(n, X) = F_2^*(F_2(f)\omega)\overline{F_2(\phi_n)(\omega)} \tag{21}$$

The approximate coefficient (conventionally expressed by $W_f^{ELP}(0, X)$) is:

$$W_f^{ELP}(0, X) = F_2^*(F_2(f)\omega)\overline{F_2(\phi_1)(\omega)} \tag{22}$$

Its inverse transformation is:

$$f(x) = F_2^*(F_2(W_f^{ELP})(0,\omega)F_2(\varphi_1(\omega)) + \sum_{n=1}^{N-1} F_2(W_f^{ELP})(n,\omega)F_2(\phi_n)(\omega)) \tag{23}$$

From the above analysis, the algorithm flow of 2D-EWT image processing can be obtained as **Algorithm 1**.

3.4. Robust Support Matrix Machine Pattern Recognition Method

After anti-aliasing filtering in frequency domain and two-dimensional empirical wavelet transform filtering in spatial domain, a stable frequency-spatial characteristic matrix can be generated. In the traditional machine learning model, the pattern recognition of frequency domain-spatial eigenmatrix usually needs to be transformed into vector form, such as linear discriminant analysis and support vector machine. The vector form does not retain the spatial geometric relationship of the original EEG signal, and the accuracy of pattern recognition is not high. The deep learning model is directly carried out on the frequency-spatial eigenmatrix. Due to the ”black box” property of convolutional neural network, accurate optimization strategy cannot be given. Experiments show that EEG recognition performance can be better if the model is not deeper, which is usually due to the nonlinear and non-stationary characteristics of EEG. Therefore, the classification of EEG frequency domain-spatial characteristic matrix should be completed by accurate and

Algorithm 1 2D-EWT process

Input: signal $f(x)$, filter number N.

1: Step 1. Calculate $F_p(f)(\theta, |\omega|)$ and find the average spectrum.

$$\tilde{f}(|\omega|) = \frac{1}{N} \sum_{i=0}^{N_\theta - 1} |F_p(f)(\theta_i, |\omega|)|$$

2: Step 2. The Fourier boundary is detected by Equations (18)-(20), and the spectral radius set and the corresponding filter banks are obtained.

$$B = \varphi_1(X), \phi_n(X)_{n=1}^{N-1}$$

3: Step 3. The original signal is filtered by equations (21) and (22), and the target signal f is obtained. **Output: B^{ELP} and $W_f^{ELP}(n, X)$**

stable optimization strategy on the basis of preserving the geometric characteristics of the matrix.

In this paper, robust support matrix machine (RSMM) is introduced to complete the identification of dance EEG frequence-spatial characteristic matrix. Suppose two categories of dance motor imagination training set are represented as $x_t, y_t{}_{t=1}^{T}$. Where, $X_t \in R^{d_1 \times d_2}$ represents the extracted feature of the $t-th$ signal sample. d_1 represents the frequency-spatial dimension. d_2 represents the time domain dimension. $y_t \in -1, 1$ represents the true label of the $t-th$ signal sample.

Pattern recognition for multiple categories of dance motion imagination can still be used in One versus All (OVA) way. RSMM regards the anti-aliasing filter two-dimensional empirical wavelet transform (AF-TDEWF) feature matrix as the sum of low-rank noiseless feature matrix $L_t \in R^{d_1 \times d_2}$ and noise feature matrix $S_t \in R^{d_1 \times d_2}$:

$$X_t = L_t + S_t \tag{24}$$

In the training process, the noiseless low-rank brain feature matrix is used to replace the original feature matrix to complete the pattern recognition problem of dance motion imagination. According to the maximum interval theory of SVM, RSMM regards the pattern recognition problem as the minimum maximum interval with regular term:

$$\underset{W,b}{Min} \sum_{t=1}^{T} 1 - y_t[tr(W^T L_t) + b]_+ + \lambda_1 ||W||_* + \sum_{t=1}^{T} (\lambda_2 ||L_t||_* + \lambda_3 ||L_t||_1) \tag{25}$$

Where, W and b represent the classification hyperplane and bias of the two categories of dance motion imagination. $\lambda_1 ||W||_*$ represents the regular term of hyperplane pair optimization. $\lambda_2 ||L_t||_*$ represents that the address noiseless eigenmatrix adopts kernel norm for the regular term of the optimization function. $\lambda_3 ||L_t||_1$ represents the regular term of the noise characteristic matrix against the optimization function, using the l_1-norm.

Since this optimization problem cannot be directly transformed into a vector, the optimization process of SVM cannot be adopted, and there are 4 variables and the joint minimization problem of kernel norm and norm, so the iterative optimization process with alternating optimization directions can only be adopted. In the RSMM solution process, the interval is rewritten as:

$$h(W, b, L_t) = 1 - y_t[tr(W^T L_t) + b]_+ \tag{26}$$

The hyperplane regular term is rewritten as $W = Z$, then we introduce augmented Lagrange multiplier V, $X_t \in R^{d_1 \times d_2}$, the augmented Lagrange function of Equation (25) can be given to solve the optimization problem with restrictive conditions:

$$\begin{aligned} h(W, Z, b, L_t, S_t, V, M_t) = & \sum_{t=1}^{T} h(W, b, L_t) + \lambda_1 ||Z||_* \\ & + tr[V^T(Z - W)] + \frac{\mu_1}{2}||Z - W||_F^2 \\ & + \sum_{t=1}^{T} \lambda_2 ||L_t||_* + \lambda_3 ||S_t||_1 \\ & + \sum_{t=1}^{T} tr[M_t^T(X_t - L_t - S_t)] \\ & + \sum_{t=1}^{T} \frac{\mu_2}{2}||X_t - L_t - S_t||_F^2 \end{aligned} \tag{27}$$

Where, μ_1 and μ_2 are the two penalty parameters of the augmented Lagrange multiplier respectively, and both are positive numbers. Given appropriate Lagrangian multipliers V, $X_t \in R^{d_1 \times d_2}$ and the corresponding penalty parameters μ_1 and μ_2 (large positive numbers), the Lagrangian multipliers are augmented to optimize Equation (27) by iterative optimization in alternating optimization directions, and the minimization result of Equation (27) is the same as that of Equation (25) with constraints.

3.5. Parameter Optimization

In the minimization function constructed by RSMM, there are three regular term parameters λ_1, λ_2, λ_3, which are usually set as $\lambda_1 = 1$, $\lambda_2 = 0.1$, $\lambda_3 = 0.01$ by default in dance motion imaginary pattern recognition. In fact, due to the sensitivity of EEG electrodes, the EEG stability of different subjects is different, and the noise introduced in the acquisition process is also different. Therefore, it is not reasonable to adopt the same regularization parameters to correct and optimize the process for all test subjects, and different subjects have regularization parameters more suitable for EEG morphology. Therefore, the modified whale algorithm is introduced into the parameter optimization of RSMM to provide more scientific and reasonable regularization parameters for EEG of different test subjects.

Whale Optimization algorithm (WOA) is an algorithm proposed by Mirjalili et al to simulate humpback whale bubble net feeding [28]. This algorithm is essentially a meta-heuristic algorithm based on swarm intelligence simulation.

A. Surrounding the prey WOA considers prey location as the optimal target or approximate optimal solution, and individuals in other populations update their positions based on this process. The mathematical model of this process can be expressed by the following formula:

$$\begin{cases} D = |C \times X^*(t) - X(t)| \\ X(t+1) = X^*(t) - A \cdot D \\ A = 2ar - a \\ C = 2r \end{cases} \tag{28}$$

Where t represents the number of iterations. A and C represent the coefficient vector. X^* is the current best whale position. X is the current whale position. a decreases linearly from 2 to 0 during iteration. r represents the random number in the interval [0-1].

B. Bubble net attack mode Bubble net attack can be divided into two strategies: shrink surround and spiral update position.

1)shrink surround.

This is achieved by the a value in the formula. a is reduced from 2 to 0 during the iteration, and A is a random number in the interval ($-a$,a), that is, a is a random value in (-2, 2). When A is set from -1 to 1, the whale's new position can be defined as anywhere between the original position and the prey position.

2)spiral update position.

Firstly, the distance between the whale and the prey position is calculated, and then the spiral equation is established between the two positions to simulate the spiral motion of the whale:

$$\begin{cases} X(t+1) = D \cdot e^{bl} \cdot cos(2\pi l) + X^*(t) \\ D = |X^*(t) - X(t)| \end{cases} \tag{29}$$

Where D is the distance between the whale and its prey. b represents spiral shape constant. l is the random number in the interval [-1,1].

While shrinking to encircle prey, the whale hunts prey in a spiral orbit. In order to simulate this simultaneous behavior, suppose that there is a probability of 0.5 to make a choice between shrinking to encircle the prey and the spiral model to update the whale position, then the mathematical model is as follows:

$$X(t+1) = \begin{cases} X^*(t) - A \cdot D & p < 0.5 \\ D \cdot e^{bl} \cdot cos(2\pi l) + X^*(t) & p \geq 0.5 \end{cases} \tag{30}$$

C. Hunt for prey Whales look for prey based on each other's positions. When $|A| > 1$, the whale position is updated by random selection. The mathematical model is as follows:

$$\begin{cases} X(t+1) = Xrand(t) - A \cdot D \\ D = |C \cdot Xrand(t) - X(t)| \end{cases} \tag{31}$$

Where $Xrand(t)$ represents the location of random whales.

3.6. Process of Proposed Method

Finally, the feature matrix is first extracted from the dance motion imaging EEG signal, the improved whale algorithm is used to obtain the optimal parameters for each test object, and the RSMM of the optimal parameters is used for pattern recognition of the extracted feature matrix. In the proposed method, the three parameters λ_1, λ_2, λ_3 of RSMM initialization vary greatly according to the EEG of different individuals. Since there are only 4 overlapping ranges, the suitable overlapping ranges of EEG signals from different individuals can be determined by pre-experiment. However, the value range of the three parameters of RSMM is:

$$1 \leq \lambda_1 \leq 10, 0.11 \leq \lambda_2 \leq 1, 0.01 \leq \lambda_3 \leq 0.1 \tag{32}$$

Therefore, whale algorithm is used to select appropriate parameters for EEG signals of different subjects. The negative recognition rate of dance motion image is taken as the fitness function of whale algorithm:

$$fitness(i) = RSMM(AF - TDEW, L, \lambda_1, \lambda_2, \lambda_3) \tag{33}$$

Where, i is the number of iterations. $fitness(i)$ is the fitness function. L is the dance motor imagination task tag.

By minimizing the fitness function of the whale algorithm, the parameters with the highest recognition rate of each individual EEG signal can be found, and the optimal recognition parameters of individual dynamic adjustment can be formed. The specific process of the method in this paper is shown in Figure 1.

The time complexity of the proposed method consists of three parts: feature extraction, RSMM classifier iterating, WOA to find the optimal parameters, and form a robust pattern recognition method for supporting matrix machine. Suppose that the training samples are n EEG matrices of size $d_1 \times d_2$. d_1 is the number of electrodes. d_2 is the number of signal sampling points. AF-TDEW generates f frequency bands, and the signal matrix of each band needs to calculate feature decomposition. The time complexity is as follows:

$$O(min(fd_1^2 d_2, fd_1 d_2^2)) \tag{34}$$

In the RSMM classifier training iteration process, eigenvalue decomposition of Z and L should also be calculated, and the time complexity is respectively:

$$O(min(d_1^2 d_2, d_1 d_2^2)) \tag{35}$$

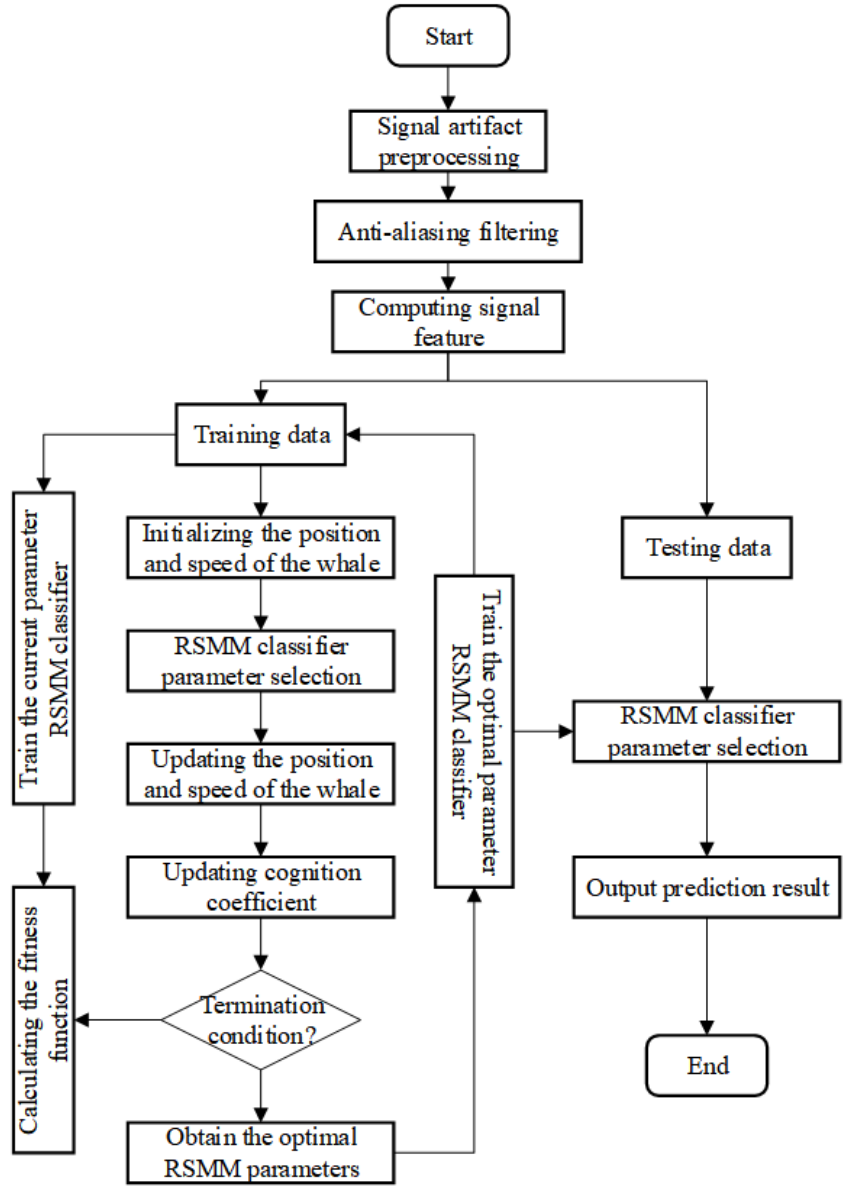

Fig. 1. The flow chart of proposed method in this paper

$$O(min(nd_1^2d_2, nd_1d_2^2)) \tag{36}$$

In addition, RSMM also needs to solve the weight W through quadratic programming, and the time complexity is $O(n^2d_1d_2)$. AF-TDEW only modifies c_1 and c_2 parameters on the basis of WOA. Theoretically, the time complexity is the same as WOA, but the iterative convergence process of parameters reduces the number of iterations for obtaining the optimal solution of AF-TDEW. Because the number of EEG electrodes and the number of signal sampling points are usually small, $d_1 \ll d_2 < 1000$. The value ranges of the three parameters optimized by AF-TDEW are all small. Therefore, assuming that the number of iterations of RSMM is K_1, the iteration number of AF-TDEW is K_2, and the number of whale population is m, the time complexity of the proposed method is:

$$O(K_1(n^2d_1d_2) + mK_2 \tag{37}$$

4. Experiments and Analysis

4.1. Data Set and Preprocessing

In this paper, BCI Competition II dataset III exercise imagination dataset is selected, which records 300 random left and right hand exercise imagination experiments of a normal female subject. Some samples are shown in figure 2. 150 experiments are selected in a random way as the training set and the remaining 150 experiments as the test set [29]. The training set consists of 75 left hand visuals and 75 right hand visuals. During the whole collection process, the EEG signal is recorded at the sampling frequency of 128 Hz, and the band pass filtering is performed at 0.5-30Hz. The time flow of each experiment in the process of data acquisition is shown in Figure 3.

The duration of each experiment is 9s, and there will be 2s preparation time after the beginning of the experiment. At the beginning of the third second, there will be a short sound indicating that the subjects are about to perform the dance motion imagination task, and at the same time, the screen shows a cross "+" lasting 1s. From the fourth second, an arrow will appear on the screen, and the subjects drags the feedback bar to move in the direction indicated by the arrow through motion imagination. And it holds until the end of the ninth second.

There are regular electrical changes in the motor sensory cortex of the brain when people imagine body movements. When the subjects imagined unilateral limb movement, the intensity of μ rhythm (8-12Hz) in the contralateral cortex decreased, while the intensity of β rhythm (12-25Hz) in the ipsilateral cortex increased. These are called Event Related Desynchronization (ERD) and Event Related Synchronization (ERS) phenomena. These two phenomena are important basis for distinguishing different types of EEG signals, among which time-frequency domain analysis is one of the most efficient analysis methods.

Fig. 2. Samples in dataset

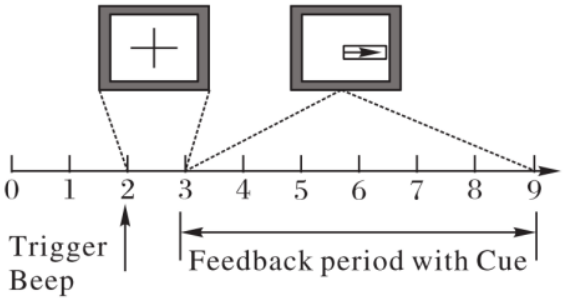

Fig. 3. Time sequence diagram of single dance motion imagination task

4.2. Experimental Environment and Implementation

In the process of dance motor imagination paradigm, EEG extraction of dance motor imagination is concentrated in the time range of 3-6s, and 3.5-6s time period is selected for pattern recognition of dance motor imagination when verifying the method. We split the data set in two sets: Dataset 2a and Dataset 2b. Dataset 2a data sets have 4 labels. OVA is used for pattern recognition to compare one category with the other three categories. Dataset 2b data sets have 2 labels and are completed using a common binary classification.

Parameters are set as follows: $d_1 = 25$, $d_2 = 630$. In Dataset 2a $n = 288$, in Dataset 2b $n = 400$. Parameters of WOA are initialized as $c_1 = 2$, $c_2 = 0$, $w = 1$, and the maximum population number $m = 50$. The iteration number of RSMM is set to $K_2 = 500$. The iteration number of RSMM is set to $K_1 = 10$ and $K_2 = 50$ in Dataset 2a and Dataset 2b respectively.

The simulation platform of the experiment is Matlab R2017a with Intel i7-9700 CPU, 64 GB memory and 64-bit Windows 11 operating system. EEG data sets from the BCI Competition IV are in GDF format and accessed through the Biosig toolbox (http://biosig.sourceforge.net).

4.3. Experimental Results of Feature Extraction

In order to verify the extraction results of AF-TDEW features, session 1 and session 4 of S_6 on Dataset2b data set are taken as examples. Three different overlapping ranges of anti-aliasing filter A^{2}F=0,1,2,3,4 are set, and AF-TDEW features are extracted after filter preprocessing. Table 1 shows the best and second-best features of AF-TDEW in five overlapping ranges.

Table 1. The proportion of the best and second-best features of AF-TDEW in five overlapping ranges/%

A^{2}F	Best	Second-best
0	88.7	89.1
1	89.3	90.2
2	85.6	87.8
3	82.9	83.3
4	78.5	79.4

As can be seen from Table 1, anti-aliasing filtering can affect the features of two-dimensional empirical wavelet transform, especially the best features and second-best features. According to the calculation process of two-dimensional empirical wavelet transform feature, the feature needs to find the feature with the maximum distinction between the two categories, so as to ensure that the feature can be used to identify different motion imagination modes to the maximum extent. According to the best features and second-best features displayed by the two class training sets and test sets, the best features and second-best features extracted by two-dimensional empirical wavelet transform can be separated according to the class after anti-aliasing filtering. The separation occurs in both the training set and the test set. The smaller the overlap range is, the more detailed band

energy the filter banks can obtain. Therefore, compared with A^2F=0,2,3,4, A^2F=1 can distinguish different categories of two-dimensional empirical wavelet transform features more greatly.

In dance motion image pattern recognition, SVM, RSMM and AF-TDEW+RSMM are used respectively to compare the extracted features. SVM uses polynomial kernel function parameters $C = 2.5$, $g = 0.02$. RSMM parameter: $\lambda_1 = 1$, $\lambda_2 = 0.1$, $\lambda_3 = 0.01$.

Table 2 and Table 3 show the results of dance motion image pattern recognition of AF-TDEW features in different classifiers.

Table 2. When A^2F=1, recognition accuracy with different classifiers on Dataset 2a/%

Subject	SVM	RSMM	AF-TDEW+RSMM
S1	83.75	84.44	85.11
S2	54.58	49.72	55.99
S3	80.28	86.18	86.49
S4	59.44	53.54	61.27
S5	41.04	41.96	42.92
S6	50.76	51.86	53.24
S7	84.79	85.49	87.92
S8	72.97	71.25	73.38
S9	71.60	69.39	72.84

Table 3. When A^2F=1, recognition accuracy with different classifiers on Dataset 2b/%

Subject	SVM	RSMM	AF-TDEW+RSMM
S1	64.55	69.56	73.92
S2	57.90	58.21	60.32
S3	54.55	57.36	59.63
S4	91.42	94.23	96.43
S5	76.42	77.51	76.65
S6	77.36	81.67	83.92
S7	75.80	76.95	77.92
S8	81.12	84.86	87.67
S9	75.81	76.74	78.92

It can be seen from Table 2 and Table 3 that, on the two dance motion imagination data sets, AF-TDEW+RSMM has higher pattern recognition accuracy.

4.4. Pattern Recognition Result

In order to verify the role of WOA in RSMM parameter optimization, Genetic Algorithm (GA) [30], Quantum Immune GA (QIGA) [31] and PSO are adopted to conduct comparison experiments. The comparison of the four algorithms is carried out on the basis

A^{2}F=1, and tables 4,5 show the pattern recognition results of RSMM based on the four algorithms.

Table 4. Recognition accuracy by different parameter optimization methods on Dataset 2a/%

Subject	GA	QIGA	PSO	WOA
S1	80.2	81.7	84.1	85.6
S2	54.8	56.4	57.3	58.9
S3	84.7	86.5	87.3	89.6
S4	55.6	57.9	59.1	60.2
S5	48.3	52.7	54.2	55.7
S6	54.5	56.3	58.4	59.1
S7	87.4	89.6	91.1	92.3
S8	74.7	76.9	78.4	80.5
S9	68.7	70.6	72.5	73.5

Table 5. Recognition accuracy by different parameter optimization methods on Dataset 2b/%

Subject	GA	QIGA	PSO	WOA
S1	65.4	67.2	68.7	69.2
S2	52.8	54.6	56.4	58.7
S3	56.7	57.1	58.2	59.4
S4	92.1	94.5	96.5	98.8
S5	79.6	81.1	82.1	83.6
S6	77.5	78.9	80.7	82.4
S7	78.3	80.2	81.6	82.9
S8	82.9	84.3	86.2	88.3
S9	76.7	77.1	78.5	79.6

As can be seen from Table 4 and 5, the overall improved WOA better optimizes the pattern recognition results of RSMM. According to the classification accuracy of 9 subjects in Dataset 2a and Dataset 2b, WOA is superior to GA, QIGA, PSO in parameter optimization of RSMM classifier.

In addition, in terms of the provided experimental simulation platform parameters, Table 6 shows the comparison of the running time of the four algorithms on the two data sets. As can be seen from the table 6, WOA and QIGA need more computing steps than PSO and GA, thus generating greater time complexity. Compared with QIGA, WOA not only achieves higher classification accuracy, but also requires more iterations and corresponding optimization time.

Combined with the above experimental results, using AF-TDEW+RSMM pattern recognition method, the optimal recognition results on the two data sets are presented

Table 6. Running time comparison with four algorithms on two data sets/s

Method	Dataset 2a	Dataset 2b
GA	498.97	2497.87
QIGA	503.78	2519.39
PSO	280.58	1497.49
WOA	519.34	2769.60

in Table 7 and Table 8 respectively. The iteration number of RSMM in Dataset 2a and Dataset 2b is set to 10 and 50 respectively.

Table 7. The optimal recognition results of the proposed method on Dataset 2a

Subject	Training time/s	Test time/s	Best accuracy/%
S1	98.67	17.68	86.53
S2	242.70	40.63	54.33
S3	80.24	14.04	87.32
S4	203.40	37.21	60.37
S5	201.03	35.18	48.26
S6	95.57	16.07	56.19
S7	198.84	35.30	89.96
S8	195.31	32.86	74.42
S9	105.87	17.01	70.67

Table 8. The optimal recognition results of the proposed method on Dataset 2b

Subject	Training time/s	Test time/s	Best accuracy/%
S1	78.20	44.11	70.74
S2	87.31	51.71	57.61
S3	83.71	51.34	57.62
S4	11.77	5.21	96.86
S5	164.25	72.38	83.24
S6	63.92	39.74	79.49
S7	142.84	64.73	76.99
S8	11.61	4.99	88.24
S9	75.38	41.14	78.86

It can be seen from the statistical data in Table 7 and Table 8 that the classification accuracy of Dataset 2a and Dataset 2b is greatly improved. When the sample size is 288 (Dataset 2a) and 320(Dataset 2b), the ratio of training time to testing time is about 6 times. The training time and test time of the proposed method are relatively stable, which is suitable for the application scenario of brain-computer interface. The influence time is only affected by different overlap parameters.

In order to compare the proposed method, the optimal recognition results of the proposed method are compared with other state-of-the-art methods including MSCNN [32], CNN-LSTM [33], DANN [34], and LFFN [35]. Table 9 shows the optimal recognition accuracy of each method. Table 10 shows the p-value values of the new method in this paper and other methods.

Table 9. The optimal recognition results of each method/%

Method	Dataset 2a	Dataset 2b
MSCNN	66.58	74.79
CNN-LSTM	68.38	77.23
DANN	68.69	77.63
LFFN	69.84	78.21
Proposed	75.49	79.87

Table 10. The p-value results of each method

Method	Dataset 2a	Dataset 2b
MSCNN	0.862	0.986
CNN-LSTM	0.778	0.845
DANN	0.729	0.763
LFFN	0.684	0.541
Proposed	p¡0.01	p¡0.01

As can be seen from Table 9 and Table 10, the pattern recognition accuracy of this method is higher than that of other methods on Dataset 2a and Dataset 2b. In fact, deep learning methods require a large number of samples and training calculations, and are not applicable in the field of brain-computer interfaces. The proposed method requires only a small amount of samples and computation, and can obtain the pattern recognition results of motion imagination similar to deep learning, which has wider applicability in the application field of brain computer interface. Compared with TSVM, which needs to solve the optimization problem of two SVMS, RSMM only needs to solve the optimization problem of one SMM, and the calculation amount in the optimization calculation process is significantly reduced. Therefore, the proposed method has better practicability in motion image pattern recognition.

5. Conclusions

In this paper, the non-stationary and nonlinear high-dimensional characteristics of the dance motion image EEG signals are analyzed, and the anti-aliasing filtering strategy and parameter optimization method are proposed to achieve pattern recognition of the dance motion image EEG signals. In view of the low spatial resolution of the original EEG signal, the anti-aliasing filtering process can ensure the better resolution of the

two-dimensional empirical wavelet transform features. In addition, according to the variable EEG distribution of different subjects, AF-TDEW can automatically provide suitable RSMM parameters for different EEG distribution for pattern recognition. Compared with traditional methods, the proposed method can improve the recognition accuracy of dance motion imagination. Compared with the deep learning methods, the proposed method achieves almost the same recognition accuracy and requires fewer computational samples and resources, which is more suitable for the application of BCI in the actual environment. The future work will focus on applying the proposed method to actual MI-BCI, further discussing the feature extraction and pattern recognition results of the proposed method according to actual experience, and updating the method and parameters according to the results to make it more suitable for actual application environment.

Acknowledgments. This research received funding by "Study on Inheritance and Development of Yao Umbrella Dance in Lanshan from the perspective of Cultural Ecology. Project number: 22B1029. Project Name: 2022 Scientific Research Project of Education Department of Hunan Province".

References

1. Lecuyer, A., George, L., Marchal, M.: "Toward adaptive VR simulators combining visual, haptic, and brain-computer interfaces," *IEEE computer graphics and applications*, Vol. 33, No. 5, 18-23. (2013)
2. Yin, S., Wang, L., Shafiq, M., et al.: "G2Grad-CAMRL: An Object Detection and Interpretation Model Based on Gradient-weighted Class Activation Mapping and Reinforcement Learning in Remote Sensing Images," *IEEE Journal of Selected Topics in Applied Earth Observations and Remote Sensing*. (2023) doi: 10.1109/JSTARS.2023.3241405.
3. Chen, X., Li, C., Liu, A., et al.: "Toward open-world electroencephalogram decoding via deep learning: A comprehensive survey," *IEEE Signal Processing Magazine*, Vol. 39, No. 2, 117-134. (2022)
4. T. Yu et al., "Enhanced Motor Imagery Training Using a Hybrid BCI With Feedback," in IEEE Transactions on Biomedical Engineering, vol. 62, no. 7, pp. 1706-1717, July 2015, doi: 10.1109/TBME.2015.2402283.
5. L. Yao, N. Jiang, N. Mrachacz-Kersting, X. Zhu, D. Farina and Y. Wang, "Reducing the Calibration Time in Somatosensory BCI by Using Tactile ERD," in IEEE Transactions on Neural Systems and Rehabilitation Engineering, vol. 30, pp. 1870-1876, 2022, doi: 10.1109/TNSRE.2022.3184402.
6. Li H, Ding M, Zhang R, et al. Motor imagery EEG classification algorithm based on CNN-LSTM feature fusion network[J]. Biomedical signal processing and control, 2022, 72: 103342.
7. Liao S C, Wu C T, Huang H C, et al. Major depression detection from EEG signals using kernel eigen-filter-bank common spatial patterns[J]. Sensors, 2017, 17(6): 1385.
8. Zhang Y, Wang Y, Jin J, et al. Sparse Bayesian learning for obtaining sparsity of EEG frequency bands based feature vectors in motor imagery classification[J]. International journal of neural systems, 2017, 27(02): 1650032.
9. Nkengfack L C D, Tchiotsop D, Atangana R, et al. EEG signals analysis for epileptic seizures detection using polynomial transforms, linear discriminant analysis and support vector machines[J]. Biomedical Signal Processing and Control, 2020, 62: 102141.
10. Gao Q, Yang Y, Kang Q, et al. EEG-based emotion recognition with feature fusion networks[J]. International journal of machine learning and cybernetics, 2022, 13(2): 421-429

11. T. Ahmed and L. Longo, "Examining the Size of the Latent Space of Convolutional Variational Autoencoders Trained With Spectral Topographic Maps of EEG Frequency Bands," in IEEE Access, vol. 10, pp. 107575-107586, 2022, doi: 10.1109/ACCESS.2022.3212777.
12. Apicella A, Arpaia P, Mastrati G, et al. EEG-based detection of emotional valence towards a reproducible measurement of emotions[J]. Scientific Reports, 2021, 11(1): 21615.
13. S. Zhang et al., "An Explainable and Generalizable Recurrent Neural Network Approach for Differentiating Human Brain States on EEG Dataset," in IEEE Transactions on Neural Networks and Learning Systems, 2022, doi: 10.1109/TNNLS.2022.3214225.
14. Yuhao Zhao, Hang Li, Shoulin Yin. A Multi-channel Character Relationship Classification Model Based on Attention Mechanism[J]. International Journal of Mathematical Sciences and Computing(IJMSC). vol. 8, no. 1, pp. 28-36, 2022.
15. I. Razzak, M. Blumenstein and G. Xu, "Multiclass Support Matrix Machines by Maximizing the Inter-Class Margin for Single Trial EEG Classification," in IEEE Transactions on Neural Systems and Rehabilitation Engineering, vol. 27, no. 6, pp. 1117-1127, June 2019, doi: 10.1109/TNSRE.2019.2913142.
16. Pan H, Xu H, Zheng J, et al. Multi-class fuzzy support matrix machine for classification in roller bearing fault diagnosis[J]. Advanced Engineering Informatics, 2022, 51: 101445.
17. Houssein E H, Hammad A, Ali A A. Human emotion recognition from EEG-based brainC-computer interface using machine learning: a comprehensive review[J]. Neural Computing and Applications, 2022, 34(15): 12527-12557.
18. Xiao F, Gu L, Ma W, et al. Real time motion intention recognition method with limited number of surface electromyography sensors for A 7-DOF hand/wrist rehabilitation exoskeleton[J]. Mechatronics, 2021, 79:102642.
19. P. Wang, P. Gong, Y. Zhou, X. Wen and D. Zhang, "Decoding the Continuous Motion Imagery Trajectories of Upper Limb Skeleton Points for EEG-Based BrainCComputer Interface," in IEEE Transactions on Instrumentation and Measurement, vol. 72, pp. 1-12, 2023, Art no. 2503212, doi: 10.1109/TIM.2022.3224991.
20. Y. Lin, R. Palaniappan, P. De Wilde and L. Li, "A normalisation approach improves the performance of inter-subject sEMG-based hand gesture recognition with a ConvNet," 2020 42nd Annual International Conference of the IEEE Engineering in Medicine & Biology Society (EMBC), Montreal, QC, Canada, 2020, pp. 649-652, doi: 10.1109/EMBC44109.2020.9175156.
21. Lopes W N, Junior P O C, Aguiar P R, et al. An efficient short-time Fourier transform algorithm for grinding wheel condition monitoring through acoustic emission[J]. The International Journal of Advanced Manufacturing Technology, 2021, 113: 585-603.
22. Ma W, Xue H, Sun X, et al. A novel multi-branch hybrid neural network for motor imagery EEG signal classification[J]. Biomedical Signal Processing and Control, 2022, 77: 103718.
23. Zhang X, Wang T, Xiong Q, et al. A Dense Long Short-Term Memory Model for Enhancing the Imagery-Based Brain-Computer Interface[J]. Computational Intelligence and Neuroscience, 2021, 2021: 1-10.
24. C. Liang and C. Chen, "Generalized Composite Multiscale Diversity Entropy and Its Application for Fault Diagnosis of Rolling Bearing in Automotive Production Line," in IEEE Access, vol. 9, pp. 84545-84558, 2021, doi: 10.1109/ACCESS.2021.3063322.
25. Padmashree A, Krishnamoorthi M. Decision Tree with Pearson Correlation-based Recursive Feature Elimination Model for Attack Detection in IoT Environment[J]. Information Technology and Control, 2022, 51(4): 771-785.
26. Al-Shami T M, Mhemdi A. Approximation operators and accuracy measures of rough sets from an infra-topology view[J]. Soft Computing, 2023, 27(3): 1317-1330.
27. Wang S, Wang H, Perdikaris P. Learning the solution operator of parametric partial differential equations with physics-informed deeponets[J]. Science advances, 2021, 7(40): eabi8605.
28. Mirjalili S, Lewis A. The whale optimization algorithm[J]. Advances in engineering software, 2016, 95: 51-67.

29. https://www.bbci.de/competition/ii/
30. Mirjalili S, Mirjalili S. Genetic algorithm[J]. Evolutionary Algorithms and Neural Networks: Theory and Applications, 2019: 43-55.
31. R. M. Bichara, F. A. Asadallah, M. Awad and J. Costantine, "Quantum Genetic Algorithm for the Design of Miniaturized and Reconfigurable IoT Antennas," in IEEE Transactions on Antennas and Propagation, doi: 10.1109/TAP.2023.3245199.
32. Roy A M. An efficient multi-scale CNN model with intrinsic feature integration for motor imagery EEG subject classification in brain-machine interfaces[J]. Biomedical Signal Processing and Control, 2022, 74: 103496.
33. Li H, Ding M, Zhang R, et al. Motor imagery EEG classification algorithm based on CNN-LSTM feature fusion network[J]. Biomedical signal processing and control, 2022, 72: 103342.
34. Hwaidi J F, Chen T M. Classification of motor imagery EEG signals based on deep autoencoder and convolutional neural network approach[J]. IEEE access, 2022, 10: 48071-48081.
35. Yu Z, Chen W, Zhang T. Motor imagery EEG classification algorithm based on improved lightweight feature fusion network[J]. Biomedical Signal Processing and Control, 2022, 75: 1036

Tianliang Huang is with the School of Art; Hunan University of Information Technology; Maotang Industrial Park, Changsha Economic and Technological Development Zone (410151). Research direction: Research on folk dance, image processing.

Ziyue Luo is with the School of Art; Hunan University of Information Technology; Maotang Industrial Park, Changsha Economic and Technological Development Zone (410151). Research direction: Research on folk dance, image processing.

Yin Lyu is with College of Music, Huaiyin Normal University, Huaian, China. His research direction is musical emotion analysis.

Received: December 22, 2022; Accepted: June 01, 2023.

Computer Science and Information Systems 20(4):1869–1883 https://doi.org/10.2298/CSIS221228034J

Heterogenous-view Occluded Expression Data Recognition Based on Cycle-Consistent Adversarial Network and K-SVD Dictionary Learning Under Intelligent Cooperative Robot Environment

Yu Jiang[1] and Shoulin Yin[2,⋆]

[1] College of Fine Art and Design, Shenyang Normal University
Shenyang, 110034 China
zsshanln@163.com
[2] Software College, Shenyang Normal University
Shenyang, 110034 China
yslin@synu.edu.cn

Abstract. In space art design, the recognition of expression is of great help to the understanding of art. It is very difficult to obtain occlusion expression data from robot environment. In particular, it is very challenging to recognize the occluded expression. In the case of facial occlusion, it is difficult to extract the features of occluded expressions by traditional methods. In order to reduce the dependence of expression recognition on individuals, this paper proposes a cycle-consistent adversarial network and K-SVD dictionary learning method for occluded expression recognition in education management under robot environment. Firstly, the new method uses the cyclic-consistent generation adversarial network as the skeleton model, which can generate the un-occluded expression image without the need of paired data sets. Meanwhile, in order to improve the discriminant ability and image generation ability of the network, a multi-scale discriminator is used to construct the discriminant network. Then, the least squares and cyclic sensing loss are used to strengthen the constraints on the network model and improve the image quality. By subtracting the error matrix from the test sample, a clear image of the expression classification stage can be recovered. The clear image samples are decomposed into identity features and expression features by using the collaborative representation of two dictionaries. Finally, it is classified according to the contribution of each expression feature to the joint sparse representation. Experiments conducted on CK+, RAF-DB and SFEW datasets, the results show that the average accuracy of the new model is 98.44%, 87.12% and 62.17%, respectively. Compared with the traditional convolutional neural network models and advanced methods, this model effectively improves the accuracy of facial recognition in the case of facial occlusion.

Keywords: Heterogenous-view data, Intelligent Cooperative Robot, cyclic-consistent generation adversarial network, K-SVD dictionary learning.

1. Introduction

In recent years, Facial Expression Recognition (FER) has been widely used in human-computer interaction, automatic driving and mental health assessment. As a cross-domain

⋆ Corresponding author

technology, the development of facial expression recognition can promote the progress of face detection technology [1,2], face recombination technology [3], animation simulation technology [4] and other related technical fields. At the same time, it is also very important for the development of robotics, which can be applied in the robot face recognition, reduce costs and reduce the risk of personnel outstanding under the COVID-19 pandemic. Although existing facial expression recognition systems have a high recognition rate, most of them are obtained based on laboratory database systems, such as CK+, JAFFE, MMI, etc. Most of these face images are positive face images without any occlusion, so they are not universal in practical application. In order to improve the recognition rate of facial expressions in real scenes, researchers collected a large number of facial images to build an expression database [5-7], and proposed novel algorithms [8,9] and optimized network architecture [10]. However, according to the performance of the existing models in the database, the facial expression recognition technology in the real scene is still in its infancy. One of the biggest factors affecting the recognition rate is the occlusion problem. In the real scene, occlusion is inevitable. It may be caused by itself, such as self-occlusion caused by posture, hair, arms, etc., or by external objects, such as glasses, scarves, masks, food and other people's occlusion. This will inevitably lead to the decline of identification accuracy.

In the aspect of occluded facial expression recognition, researchers have proposed many methods to reduce the impact of occluded factors on facial expression recognition. The most commonly used methods include feature reconstruction, sub-region analysis, sparse representation, deep learning and so on. XBellamkonda et al. [11] jointly applied Robust PCA (RPCA) and significance detection to occlusion expression recognition. Firstly, significance detection was used to locate occlusions, and then RPCA was used to reconstruct the occlusive area of the image. Khan et al. [12] reconstructed 54 reference points in the occluded face image by combining the nearest point selection and fuzzy C-Means (FCM) algorithm. This feature recovery of the occluded area based on facial contour features relied heavily on reliable face detection and facial feature tracking, and required pre-positioning of the occluded area and accurate facial alignment, which was difficult to achieve in practical applications. Dapogny et al. [13] proposed a local expression prediction algorithm (LEPs) for expression classification prediction and AU prediction under the condition of local occlusion to reduce the negative impact brought by occlusion. Göre et al. [14] used the geometric features of face point displacement to predict the AU unit under oral occlusion. Gaussian mixture model (GMM) was used to model the gray pixel distribution of the face area to detect the occlusion area. Subarea analysis methods assume that the occlusion occurs in only a small part of the face. These methods usually produce satisfactory performance for small areas of occlusion. However, the granularity of subdividing a face into local areas and its effect on performance remains an open problem, especially for random occlusion without fixed location, shape, and size. At the same time, the method based on sub-region is sensitive to noise because of the inaccuracy of face location, alignment and normalization. Saka et al. [15] proposed a deep generative model, which used Markov Random Field (MRF) with gates as the first layer of DBN for expression recognition under occlusion. Houshmand et al. [16] proposed a deep neural network structure under the condition of partial occlusion, which used Gabor filters to extract multi-scale and multi-direction Gabor features from face images and input them into a three-layer Deep Boltzmann Machine (DBM) for emotion classification.

Yao et al. proposed that Wasserstein generative adversarial network could be used to complete the occlusion area of face image, which alleviated the impact caused by the loss of local expression information.

Deep learning techniques can automatically learn the most discriminative facial expression feature patterns from raw facial data, often without the need for a separate occlusion detection or reconstruction process [17-19]. However, using deep architectures requires large amounts of training data to ensure proper feature learning, the difficulty of adjusting large numbers of system parameters, and the need for expensive computations. Cen et al. [20] obtained various levels of occlusion base images by partitioning images, and constructed a non-orthogonal occlusion dictionary by using these images. Then the coefficients were obtained by sparse decomposition of the image to be measured and the expression category was determined in the subspace of the image to be measured. Wang et al. [21] proposed a robust regularized coding random occlusion expression recognition. By assigning different weights to each pixel of the expression image, the weight converged to the threshold through continuous generation selection. Finally, the sparse representation of the image to be measured was calculated by the optimal weight matrix. This method achieved good recognition effect. However, this method did not avoid the interference of identity characteristics on expression classification. The biggest advantage of sparse representation is that it is not only robust to occlusion and damage, but also can be used to estimate the occluded or damaged part of the face. The traditional sparse representation methods sparse representation (SRC) and collaborative representation (CRC) separate each dictionary atom and process it independently [22]. The relationships between atoms are not considered, and the resulting sparse representation is unstructured. Meanwhile, both SRC and CRC use the original training data set as the classification dictionary. When the training samples are damaged, blocked or deformed, the algorithm lacks robustness and the classification effect is poor. In low-rank algorithms, kernel norm is generally used to replace rank function, but kernel norm may not be able to effectively estimate the rank of matrix, and kernel norm is sensitive to Gaussian noise.

Our main contributions are as follows. This paper analyzes the occlusion problem in expression recognition and proposes a cycle-consistent adversarial network and K-SVD dictionary learning method with occlusion perception ability to extract facial expression features under robotic environment. The new method uses the cyclic-consistent generation adversarial network as the skeleton model, which can generate the un-occluded expression image without the need of paired data sets. Then, the least squares and cyclic sensing loss are used to strengthen the constraints on the network model and improve the image quality. By subtracting the error matrix from the test sample, a clear image of the expression classification stage can be recovered. The clear image samples are decomposed into identity features and expression features by using the collaborative representation of two dictionaries.

The structure of this paper is organized as follows. Section 2 introduces the related works. Section 3 detailed shows the facial expression method. Rich experiments are conducted in section 4. There is a conclusion in section 5.

2. Related Works

2.1. Generative Adversarial Network

Generative Adversarial Network (GAN) [23] is a deeply generative neural network model. The network model is composed of two functional modules, generator and discriminator. The structure of GAN is shown in Figure 1.

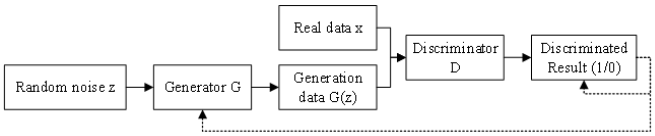

Fig. 1. Structure of GAN

The generator receives random noise z, gets the data distribution from the real sample and maps it to the new data space. It tries to generate a false sample $G(x)$ that can deceive the discriminator. The input of the discriminator consists of two parts, namely the data $G(x)$ generated by the generator and the real data x. The discriminator tries its best to determine whether the input sample is a generator generated sample or a real sample. If the test input is a real sample, the output is 1, otherwise it is 0. The generator and discriminator are constantly fighting and optimizing until the sample generated by the generator is fake and the discriminator has the lowest probability of discriminating wrong.

The training process of GAN can be regarded as a game between generator and discriminator. The training will first fix the generator G to update the parameters of the discriminator D. Then it fixes the discriminator D and updates the parameters of the generator G. The two models are iterated alternately and the optimal solution is finally reached. The antagonistic relationship between generator and discriminator is shown as follows:

$$\min_{G}\max_{D} V(D,G) = E_{x\sim p_{data}(x)}[lgD(x)] + E_{z\sim p_z(z)}[lg(1-D(G(z)))] \quad (1)$$

In order to minimize the error probability of discriminant model D, it is necessary to maximize the discriminant model when training the discriminant. When the input to the discriminator is the real sample x, $D(x)$ is expected to approach 1. When the input is a false sample $G(z)$, $D(G(z))$ is expected to approach 0, that is, $(1-D(G(z)))$ is expected to approach 1. For the generation model G, minimization is required, and the input of the generator is only random noise z. In this case, $D(G(z))$ is expected to approach 1, that is, $(1-D(G(z)))$ is expected to approach 0. The generated sample $G(z)$ is judged by the discriminator to be true with a probability value of 1. Only when $p_z = p_{data}$, the generator can learn the distribution of real sample p_{data}, and the discriminator's accuracy is stable at 0.5. At this time, the model can get the global optimal solution.

2.2. Sparse Representation Classification

Suppose n training samples can be divided into c categories, then the training set $D = [D_1, \cdots, D_c] \in R^{m \times n}$. In the sparse representation, test sample y can be approximately represented as a combination of feature vectors of training samples:

$$y = D_1 x_1 + D_2 x_2 + \cdots + D_c x_c \tag{2}$$

The sparse representation problem is to solve the coefficient vector under the constraint conditions of Equation (2) and minimize the L0 norm of x. According to the knowledge of compression theory, when Equation (2) is sparse enough, the minimization of L1 norm and L0 norm are equivalent, and the approximate solution of coefficient x can be obtained by solving the convex relaxation optimization problem in Equation (3).

$$\min_x ||x||_1, s.t. y = Dx \tag{3}$$

Sparse representation classification is more robust than traditional classifiers such as SVM, and abnormal noise points have less interference on classification.

3. Proposed Occluded Expression Recognition

Our proposed method is shown in figure 2. It mainly includes two parts: Cycle-Consistent Adversarial Network and K-SVD dictionary learning.

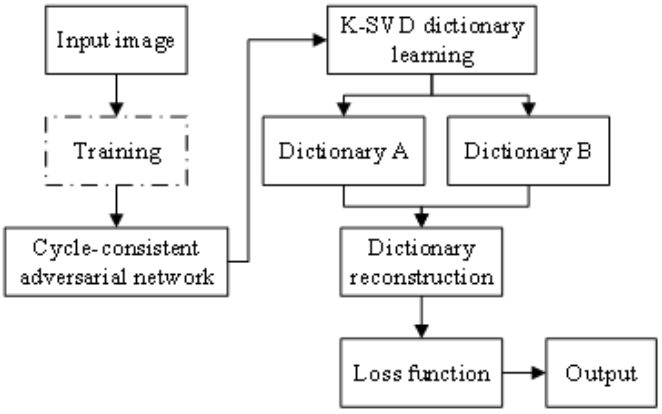

Fig. 2. Proposed occluded expression recognition framework

3.1. Cycle-Consistent Adversarial Network

CycleGAN (Cycle-Consistent Adversarial Network) is an unsupervised generative adversarial network based on the GAN network [24]. The network structure with two generators

and two discriminators is obtained by the mirror symmetry of traditional GAN. Because of this cyclic network structure, the CycleGAN model can convert images from two domains to each other without the need for paired image data sets. Its schematic diagram is shown in Figure 3. Where X and Y are the original domain X and target domain Y respectively. G and F are the generators of $X \rightarrow Y$ mapping and $Y \rightarrow X$ mapping respectively. D_X and D_Y are the corresponding discriminators. G converts the image in X domain to the image $G(x)$ in Y domain, and then the discriminator D_Y determines whether the image is true or false. Similarly, F converts the image in the X domain to the image $F(y)$ in the Y domain, and then the discriminator D_X determines whether the image is true or false.

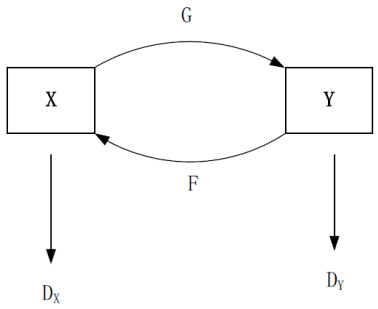

Fig. 3. Structure of CycleGAN

The generator G generates an image $G(x)$, and the discriminator D_Y determines if $G(x)$ is a real image. This process is a standard one-way GAN model training process. Therefore, the adversarial loss function of CycleGAN is consistent with that of GAN. The anti-loss function of G and D_Y is expressed as follows:

$$L_{GAN}(G, D_Y, X, Y) = E_{x \sim p_{data}(x)}[lgD_Y(y)] + E_{x \sim p_{data}(x)}[lg(1 - D_Y(G(x)))] \quad (4)$$

$$L_{GAN}(F, D_Y, Y, X) = E_{x \sim p_{data}(x)}[lgD_X(x)] + E_{y \sim p_{data}(y)}[lg(1 - D_X(F(y)))] \quad (5)$$

After the generator G converts the image x to $G(x)$ and then from F to $F(G(x))$, in order to ensure the consistency of the image after two networks as much as possible, that is, it tries to make $F(G(x)) \approx x$ and $F(F(y)) \approx y$, it needs to calculate the loss between the original image and $F(G(x))$. The cyclic uniform loss is calculated by the L1 norm of the original image and the mapped image, and its function expression is as follows:

$$L_{cyc}(G, F) = E_{x \sim p_{data}(x)}[||F(G(x)) - x||_1 + E_{y \sim p_{data}(y)}[||G(F(y)) - y||_1]] \quad (6)$$

Finally, the loss function of CycleGAN consists of the above three parts, and its total objective function is shown as follows:

$$L(G, F, D_X, D_Y) = L_{GAN}(G, D_Y, X, Y) + L_{GAN}(F, D_Y, Y, X) + \lambda L_{cyc}(G, F) \quad (7)$$

Where L_{GAN} is the counter loss. L_{cyc} is cyclic consistency loss. λ is the weight coefficient of cyclic consistency loss.

3.2. K-SVD Construction Based on Non-convex Logarithm Function Low-rank Decomposition

In expression recognition, there are similar features among the same expressions of different people, but there are also differences in identity, illumination, occlusion and so on. These details are not the key to determining categories. Adding these factors will reduce the classification accuracy of sparse representation. Therefore, the expression features and identity features of the expression images are separated by the non-convex logarithm function low-rank matrix decomposition. The dictionary learning is carried out respectively to obtain the double dictionary pattern of the in-class related dictionary and the differentially structured dictionary. The accuracy of sparse representation can be improved and the robustness of recognition can be enhanced by the decomposition of the internal structure information features of the image.

Given a training sample $X = [X_1, X_2, \cdots, X_c]$, it is assumed that it can be decomposed into a low-rank matrix L and a sparse matrix S. The objective function is as follows:

$$\min_{L,S}(rank(L) + \gamma||S||_{2,1}), s.t. X = L + S \quad (8)$$

In Equation (8), $rank(*)$ is the rank function. To prevent over-fitting, the constant $\gamma > 0$ is the weight factor used to balance the rank of the matrix and the sparsity of the noise matrix.

The rank function has non-convexity and discontinuity, and its minimization is an NP problem. Under certain conditions, the rank of matrix is replaced by the kernel norm convex approximation. The rank of the matrix is only related to the value of the largest non-zero singular value, whereas the kernel norm simply adds all the singular values of the matrix. When there are some large singular values, the kernel norm is too loose, so that the final calculation result will deviate from the real rank. Compared with the kernel norm, the non-convex approximation function can approximate the real rank of the matrix more accurately. In reference [25], when solving the subspace clustering problem, the logarithmic determinant function was used for non-convex approximation of the matrix rank function, and the experimental effect of cluster analysis in Yale B face Library was better than that of the kernel norm. It showed that using logarithmic determinant function to approximate the rank function of matrix was better, and had the advantages of strong anti-interference ability and small deviation.

The logarithmic approximation function is defined as formula (9).

$$||x||_d = logdet(I + (x^T x)^{0.5}) = \sum_{i=1}^{minm,n} log(1 + \sigma_i(x)) \quad (9)$$

In Equation (9), I is the identity matrix. σ_i is the singular value of matrix x. m and n are the dimensions of matrix x. The square root of $x^T x$ is taken to facilitate optimization.

Algorithm 1 Solving Lagrange function

Input: Training matrix X, parameter μ, γ, ε.
Output: L, S.

1: Fixed other values, update L.

$$L_{K+1} = \underset{L}{argmin} \sum_{i}^{minm,n} log(1+\sigma_i(L)) + \frac{\mu}{2}||\frac{Y_K}{\mu} + X - L - S^K||_F^2$$

2: Fixed other values, update S.

$$S_{K+1} = \underset{S}{argmin}\, \gamma||S||_{2,1} + \frac{\mu}{2}||\frac{Y_K}{\mu} + X - L - S^K||_F^2$$

3: Fixed other values, update Y.

$$Y_{K+1} = Y_K \gamma\mu(X - L_{K+1} - S_{K+1})$$

4: Check whether the convergence conditions satisfies:

$$||X - L_{K+1} - S_{K+1}||_F < \varepsilon$$

5: If it does not converge, the cycle continues until the convergence ends.

$$\underset{L,S}{min}\, ||L||_d + \gamma||S||_{2,1}, s.t. X = L + S \tag{10}$$

Formula (10) is solved by the augmented Lagrange multiplier method. The auxiliary variable Y is introduced for ease of calculation. Then the Lagrange function of Equation (10) is shown as follows:

$$L(L,S,Y,\mu) = \sum_{i=1}^{minm,n} log(\sigma_i(L)) + \gamma||S||_{2,1} + < Y, X - L - S > + \frac{\mu}{2}||X - L - S||_F^2 \tag{11}$$

In formula (11), Y is the Lagrange multiplier, and the initial value is 0. $< \cdot >$ represents the Euclidean inner product of a matrix. The specific solution steps are described as Algorithm 1.

Low-rank decomposition is carried out for each type of training sample. L and S are obtained after decomposition. L represents facial feature and S represents identity feature.

$$L = [L_1, L_2, \cdots, L_c] \in R^{n \times mc} \tag{12}$$

$$L = [S_1, S_2, \cdots, S_c] \in R^{n \times mc} \tag{13}$$

Where L represents the expression feature matrix. S stands for identity eigenmatrix. c is the number of emotion categories. Then the K-SVD dictionary learning algorithm is used to learn L and S to get dictionary A that can capture the discriminant features of the class and dictionary B that reflects the changes within the class. The K-SVD algorithm mainly improves the dictionary updating speed and reduces the complexity.

4. Experiments and Analysis

4.1. Datasets

In this paper, the experimental evaluation is conducted on three public databases, namely a laboratory image database CK+ [26] and two real scene databases, including RAF-DB [27] and SFEW [28].

The CK+ database is the most widely used database of laboratory collected images. CK+ consists of 593 video sequence items from 123 participants. These sequences range in duration from 10 to 60 frames and contain the transition of facial expressions from natural to peak. In the videos, 327 sequences from 118 gatherers are labeled with seven basic expressions based on the Facial Expression Action Coding System (FACS), including anger, contempt, disgust, fear, happiness, sadness and surprise. Because CK+ does not provide a specified training, validation, and test set, so the algorithm evaluation is not uniform on this database. Based on the static recognition method, the most commonly used data selection method is to extract the peak expression from the natural expression in the first frame to the last frame, and divide the subjects into n groups for n cross-validation experiments, in which n values are usually selected as 5, 8 and 10.

RAF-DB is the real world emotional face database, a large facial expression database, which has downloaded about 30,000 various facial images from the Internet. Each image is individually annotated about 40 times on the basis of crowd-sourcing. Subjects in the database vary greatly in age, gender, race, head posture, lighting conditions, occlusion (such as glasses, facial hair or self-occlusion), and post-processing operations (such as various filters and special effects). RAF-DB is characterized by diversity, large quantity and abundant annotation. The database contains two distinct subsets: the single-tag subset and the double-tag subset. The single label subset includes 7 types of basic emotions and boundary frames. The double-labeled subset includes 12 types of compound emotions, 5 accurate landmark locations, 37 automatic landmark locations, boundary boxes, races, age ranges, and each image gender attribute is annotated. Baseline classifiers are used to output basic emotions and compound emotions. In order to evaluate the performance of the test system objectively, the database is divided into training set and test set, in which the size of the training set is 5 times that of the test set, and the distribution of the two groups of expressions is almost the same.

SFEW database is a very challenging database of static frame pictures selected from actual expressions in real scenes. The SFEW database contains different levels of facial expression, unconstrained head postures, different shading, different age ranges, and different lighting variations. The sample database is an emotion tag with seven expressions: anger disgust, fear, happiness, sadness, surprise and nature. There are 95 topics in the database, of which there are 663 clearly labeled images. The database has been classified into training, validation, and test sets. SFEW 2.0 is divided into three groups: the training set with 958 samples, the verification set with 436 samples, and the test set with 372 samples. Each image in the database is classified into one of seven expressions, namely anger, disgust, fear, nature, happiness, sadness and surprise. The labels for the test and validation sets of the expression are public.

The decision unit training data set is the training occlusion decision unit. 100 facial images are selected from the open database for occlusion synthesis and used as training samples.

Occlusions are selected according to their frequency in daily life, such as fruit, hair, hats, books, cups, glasses, etc. In addition, another 100 natural occlusion images were selected as training samples. After consistent marking and inspection by team members, the database finally contains 200 training samples. In this paper, the threshold of area occlusion rate is set as 0.5, that is, when the area occlusion rate exceeds 1/2, the label is set as 0. As a result, the database is easy to tag and train. During the training process, the data expansion strategy is used to enhance the samples for 7 times, and the final accuracy rate reaches 85.4% through training.

4.2. Configuration of Experiment

The model proposed in this paper is based on Keras framework and runs on Ubuntu operating system. Experimental data obtained on NVIDIA CUDA framework 6.5 and NVIDIA GTX 1080GPU is used for experiments. In addition, GAN is used as the backbone network of proposed network. Firstly, the image data on ImageNet is used to initialize the network parameters. In the experiment, the small batch random gradient descent method is used to optimize the model. The initial value of the basic learning rate was set at 0.001, and the polynomial strategy was used to reduce it to 0.1. The momentum is set to 0.9 and the weight loss is set to 0.000 5. In the training phase, it sets the value of the actual batch size to 64 and selects the generation 10,000 times. When training the cyclic adversarial network, the face images on ImageNet are also used to pre-train the convolution layer, and all the parameters of the convolution layer are initialized. Then the parameters of the convolution layer are fixed and the fine-tuning training of the final fully connected layer is carried out. In the training process, the value of learning rate is set as 0.01. After 20,000 times of generation selection, the value of learning rate is adjusted to 0.0001 in the fine-tuning stage, and the iteration is continued for 10,000 times. The whole model training take 5 days, and after the parameters are fixed, the time for the model to process a single image is 1.2s.

4.3. Evaluation of Weight

This paper evaluates the weight factor α on three benchmark databases. During the test, the initial value of α is set to 0 and the increment was set to 0.1. When $\alpha = 0$, it means that only the output of the occlusion awareness network is used as the classification result. When $\alpha = 1$, it means that only the output of the generated adversarial network is used as the classification result. As shown in Table 1, the evaluation results are presented respectively on CK+, RAFDB and SFEW databases. In these three databases, when α values are 0.5, 0.7 and 0.6 respectively, the model achieves the best performance. Then, the value of α is further tested, and the results showed that when the value of α is 0.6, the overall performance of the model on the three databases is the best. Therefore, the value of α is finally set to 0.6 manually.

4.4. Experimental Results

The confusion matrix results of the proposed model on the three public databases are shown in Figure 4. Figure 4(a) shows the experimental results on the database CK+. For

Table 1. Evaluations on different datasets/%

α value	CK+	RAF-DB	SFEW
0	95.5	83.2	57.1
0.1	95.0	84.0	58.0
0.2	95.3	84.1	57.8
0.3	95.6	84.9	58.0
0.4	96.2	85.1	59.0
0.5	97.6	85.9	59.1

the 6 expressions, the recognition accuracy is above 95%, which is similar to the recognition rate of human beings. In particular, it is 99 percent accurate for the expressions with obvious changing features, such as happiness and anger. This means that the laboratory image database is no longer challenging for existing models. So researchers need to focus more on solving facial expression recognition problems in real situations. Figure 4(b) shows the confusion matrix in the database RAF-DB. For happy and angry expressions with obvious changing characteristics, the accuracy of the experimental model reaches more than 90%, which is within the acceptable range. For expressions that are not obvious in appearance, such as disgust and sadness, the recognition rate remains below 85%. The analysis of the experimental results shows that the main reason is that these expressions are not significantly different in the real scene. Even for humans, it is difficult to distinguish these two expressions accurately. Figure 4(c) shows the experimental results on the database SFEW, which is the most challenging database in the evaluation experiment. The experimental results show that only 2 emojis have a recognition rate of more than 80%, and all the other emojis have a recognition rate of less than 70%, or even only 49%. The analysis shows that the main reason for the low recognition rate of expression "disgust" is that the change of expression is not obvious; In addition, there are two pairs of expressions that are frequently mixed, including "sad" and "fearful," "surprised" and "happy." In reality these expressions are often associated with sex. For example, sadness caused by fear and surprise mixed with joy are expressions that are difficult for humans to distinguish from a single static image even in real situations.

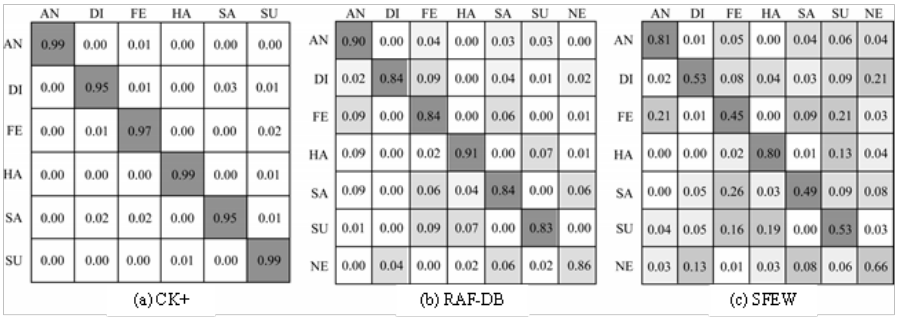

Fig. 4. Confusion matrices on three public databases

4.5. Comparison Results

In this paper, the experimental results of the proposed model are compared with those of similar models and widely used models including OFR [30], GMLA [31], DACS [32]. Tables 2 4 are the comparison results between the new model in this paper and other models in three different databases.

Table 2. Comparative evaluation of experiments on CK+ database

Model	Recognition rate/%	Time/s
OFR	92.15	12.5
GMLA	94.68	8.9
DACS	95.23	7.8
Proposed	97.44	3.5

Table 3. Comparative evaluation of experiments on RAF-DB database

Model	Recognition rate/%	Time/s
OFR	80.97	10.5
GMLA	82.94	9.1
DACS	84.64	5.7
Proposed	86.12	2.8

Table 4. Comparative evaluation of experiments on SFEW database

Model	Recognition rate/%	Time/s
OFR	55.41	12.7
GMLA	57.28	9.7
DACS	59.14	5.5
Proposed	62.17	3.8

Table 2 shows the comparison results on the database CK+. The analysis shows that the average accuracy of the model proposed in this paper is 97.33%. The images in CK+ database are all unshielded frontal face photos collected in the laboratory, and no specified training set and test set are provided. Therefore, different classification results will lead to different experimental results. It can also be seen from Table 2 that the recognition rate of most models in the laboratory database has achieved a satisfactory accuracy rate, achieving a recognition level comparable to that of human beings.

Table 3 shows the comparison results on RAF-DB database. The results show that the average accuracy of the proposed model is 86.12% and its accuracy is 0.93% higher than that of the OFR. Compared with GMLA, the model in this paper uses the sliding partition

selection method to partition in the drive domain, which does not depend on the accuracy of key points. The selection method is similar to the filter in the convolutional neural network, so that the network can retain more effective features. In addition, the single occlusion decision unit in this paper only needs to determine the occlusion threshold of the subarea, but does not need to calculate the precise occlusion proportion of the subarea, which makes the single occlusion decision unit easier to train. In the output fusion mode, the single factor mode is used for fusion, which further improves the performance of the model. In addition, compared with network B, it increases by 2.16%. The experimental results show that adding the zone occlusion decision unit and optimizing the network structure can improve the network performance.

Table 4 shows the comparison on the SFEW database. Through the analysis of the results of two real scene expression databases, RAFDB and SFEW, it can be seen that for the SFEW database with greater challenges, the performance improvement brought by the addition of occlusion decision unit is more obvious than that on the RAF-DB database, which confirms the practical application potential of occlusion awareness network. From the performance of the model in three open databases and the comparison results with the existing methods, the model has practical application value. Also the time consumption is the lowest with proposed method.

5. Conclusion

In this paper, we propose a cycle-consistent adversarial network and K-SVD dictionary learning method for occluded expression recognition in education management under robot environment. This method uses the low-rank decomposition of non-convex logarithm approximate rank function to separate the identity features from the facial features, and then carries on the dictionary learning to get a double dictionary. The identity features and expression features of the test images are reconstructed by using double dictionaries. And it introduces the cyclic generative adversarial network as the basic network model. The multi-scale discriminator is used to replace a single discriminator to improve the quality of the generated images, so that the generated images are more natural and closer to the real face images, so that the impact caused by local occlusion can be reduced during recognition. Finally, the classification is realized according to the contribution of each facial feature in the joint sparse representation. The experimental data in CK+ and KDEF show that the algorithm in this paper can overcome the negative effects brought by individual differences to a certain extent, which not only improves the robustness of sparse representation, but also has strong robustness to face recognition with different regions and different degrees of occlusion. The next step will be to process and recognize multi-pose facial images.

Acknowledgments. This work was supported by ”Horizontal project: Appearance design of intelligent cooperative robot SCR series”. The authors gratefully acknowledge the anonymous reviewers for their valuable comments.

References

1. Kumar A, Kaur A, Kumar M. Face detection techniques: a review[J]. Artificial Intelligence Review, 2019, 52(2): 927-948.

2. Jiang M, Yin S. Facial expression recognition based on convolutional block attention module and multi-feature fusion[J]. International Journal of Computational Vision and Robotics, 2023, 13(1): 21-37.
3. Chi C, Zhang S, Xing J, et al. Selective refinement network for high performance face detection[C]//Proceedings of the AAAI conference on artificial intelligence. 2019, 33(01): 8231-8238.
4. Li X, Lai S, Qian X. Dbcface: Towards pure convolutional neural network face detection[J]. IEEE Transactions on Circuits and Systems for Video Technology, 2021, 32(4): 1792-1804.
5. Zhang S, Wen L, Shi H, et al. Single-shot scale-aware network for real-time face detection[J]. International Journal of Computer Vision, 2019, 127(6): 537-559.
6. Jisi A and Shoulin Yin. A New Feature Fusion Network for Student Behavior Recognition in Education[J]. Journal of Applied Science and Engineering. vol. 24, no. 2, pp.133-140, 2021.
7. Tang X, Du D K, He Z, et al. Pyramidbox: A context-assisted single shot face detector[C]//Proceedings of the European conference on computer vision (ECCV). 2018: 797-813.
8. Zhang S, Wang X, Lei Z, et al. Faceboxes: A CPU real-time and accurate unconstrained face detector[J]. Neurocomputing, 2019, 364: 297-309.
9. Wang X. Crowd Density Estimation Based On Multi-scale Information Fusion And Matching Network In Scenic Spots[J]. Journal of Applied Science and Engineering, 2022, 26(6): 865-875.
10. Singh P, Chaudhury S, Panigrahi B K. Hybrid MPSO-CNN: Multi-level particle swarm optimized hyperparameters of convolutional neural network[J]. Swarm and Evolutionary Computation, 2021, 63: 100863.
11. Bellamkonda S, Gopalan N P, Mala C, et al. Facial expression recognition on partially occluded faces using component based ensemble stacked CNN[J]. Cognitive Neurodynamics, 2022: 1-24.
12. Khan M A, Arshad H, Nisar W, et al. An integrated design of fuzzy C-means and NCA-based multi-properties feature reduction for brain tumor recognition[M]//Signal and image processing techniques for the development of intelligent healthcare systems. Springer, Singapore, 2021: 1-28.
13. Dapogny A, Bailly K, Dubuisson S. Confidence-weighted local expression predictions for occlusion handling in expression recognition and action unit detection[J]. International Journal of Computer Vision, 2018, 126(2): 255-271.
14. Göre E, Evlioğlu G. Assessment of the effect of two occlusal concepts for implant-supported fixed prostheses by finite element analysis in patients with bruxism[J]. Journal of Oral Implantology, 2014, 40(1): 68-75.
15. Saka K, Kakuzaki T, Metsugi S, et al. Antibody design using LSTM based deep generative model from phage display library for affinity maturation[J]. Scientific reports, 2021, 11(1): 1-13.
16. Houshmand B, Khan N M. Facial expression recognition under partial occlusion from virtual reality headsets based on transfer learning[C]//2020 IEEE Sixth International Conference on Multimedia Big Data (BigMM). IEEE, 2020: 70-75.
17. Shi Q, Yin S, Wang K, et al. Multichannel convolutional neural network-based fuzzy active contour model for medical image segmentation[J]. Evolving Systems, 2022, 13(4): 535-549.
18. Shen W. A Novel Conditional Generative Adversarial Network Based On Graph Attention Network For Moving Image Denoising[J]. Journal of Applied Science and Engineering, 2022, 26(6): 831-841.
19. Gao S. A two-channel attention mechanism-based MobileNetV2 and bidirectional long short memory network for multi-modal dimension dance emotion recognition[J]. Journal of Applied Science and Engineering, 2022, 26(4): 455-464.
20. Cen F, Zhao X, Li W, et al. Deep feature augmentation for occluded image classification[J]. Pattern Recognition, 2021, 111: 107737.
21. Wang K, Peng X, Yang J, et al. Region attention networks for pose and occlusion robust facial expression recognition[J]. IEEE Transactions on Image Processing, 2020, 29: 4057-4069.
22. Rubinstein R, Bruckstein A M, Elad M. Dictionaries for sparse representation modeling[J]. Proceedings of the IEEE, 2010, 98(6): 1045-1057.

23. Goodfellow I, Pouget-Abadie J, Mirza M, et al. Generative adversarial networks[J]. Communications of the ACM, 2020, 63(11): 139-144.
24. Wen L, Wang Y, Li X. A new Cycle-consistent adversarial networks with attention mechanism for surface defect classification with small samples[J]. IEEE Transactions on Industrial Informatics, 2022, 18(12): 8988-8998.
25. Peng C, Kang Z, Li H, et al. Subspace clustering using log-determinant rank approximation[C]//Proceedings of the 21th ACM SIGKDD international conference on Knowledge Discovery and Data Mining. 2015: 925-934.
26. Chen W. A novel long short-term memory network model for multimodal music emotion analysis in affective computing[J]. Journal of Applied Science and Engineering, 2022, 26(3): 367-376.
27. Li S, Deng W, Du J P. Reliable crowdsourcing and deep locality-preserving learning for expression recognition in the wild[C]//Proceedings of the IEEE conference on computer vision and pattern recognition. 2017: 2852-2861.
28. Wang K, Peng X, Yang J, et al. Region attention networks for pose and occlusion robust facial expression recognition[J]. IEEE Transactions on Image Processing, 2020, 29: 4057-4069.
29. Poux D, Allaert B, Ihaddadene N, et al. Dynamic facial expression recognition under partial occlusion with optical flow reconstruction[J]. IEEE Transactions on Image Processing, 2021, 31: 446-457.
30. Zhao Z, Liu Q, Wang S. Learning deep global multi-scale and local attention features for facial expression recognition in the wild[J]. IEEE Transactions on Image Processing, 2021, 30: 6544-6556.
31. Farzaneh A H, Qi X. Facial expression recognition in the wild via deep attentive center loss[C]//Proceedings of the IEEE/CVF winter conference on applications of computer vision. 2021: 2402-2411.

Yu Jiang, female, associate professor, postgraduate student, visiting scholar in Sheffield Hallam University in April 2012, CEA graphic Designer, (double professional) National Vocational Skills Appraisal of decorative art assessment. Researchr direction: Environmental art design.

Shoulin Yin is with Software College, Shenyang Normal University, Shenyang 110034, China. Research direction: image processing and AI.

Received: December 28, 2022; Accepted: June 04, 2023.